IODP-ICDP Kolloquium 2009 in Potsdam

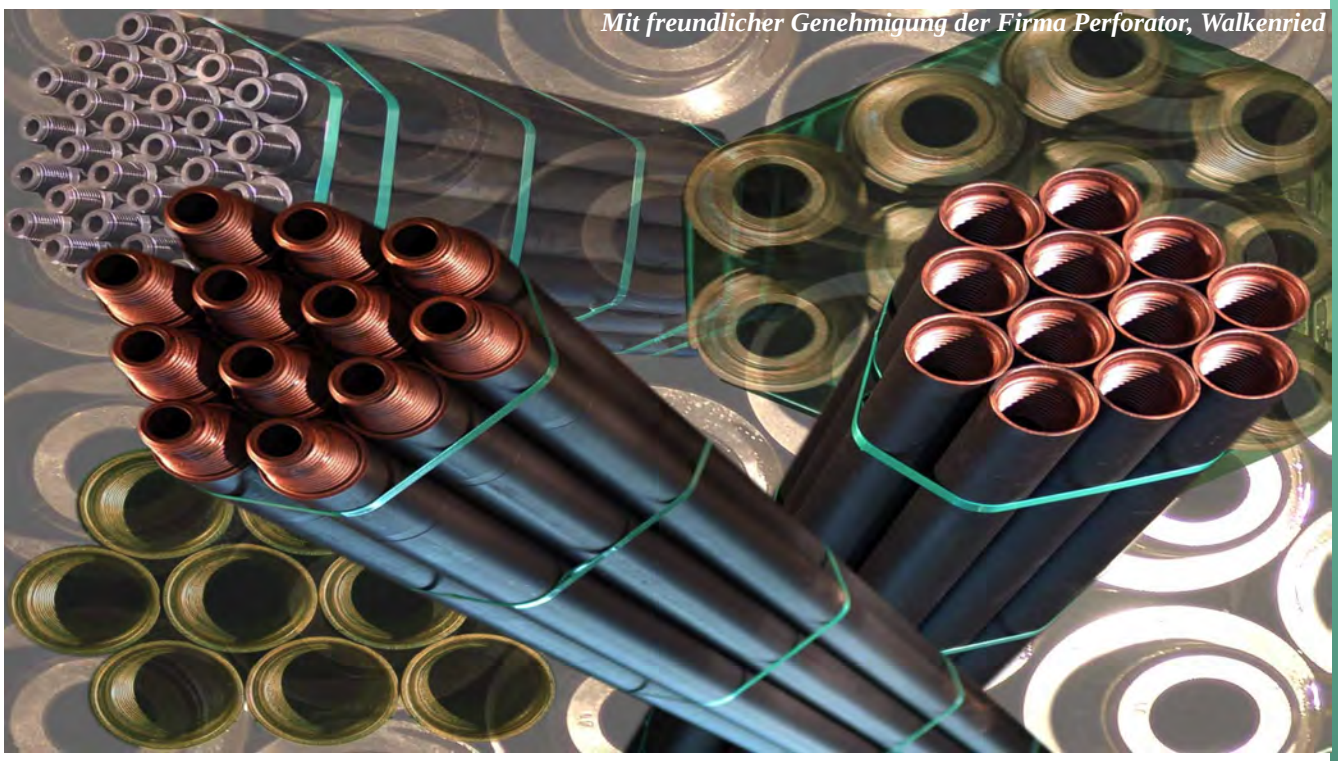

Mit freundlicher Genehmigung der Firma Perforator, Walkenried

16. - 18. März 2009

Universität Potsdam

GFZ Potsdam

Deutsche Forschungsgemeinschaft

DFG

Hinweis: Der Tagungsband ist als pdf File (Tagungsbeiträge 2009) mit farbigen Abbildungen auf der Internetseite
http://www.geo.uni-potsdam.de/icdp_homepage/tagung09/index.html#tagungsprogramm
für Sie bereitgestellt.

Tagungsort: Haus H

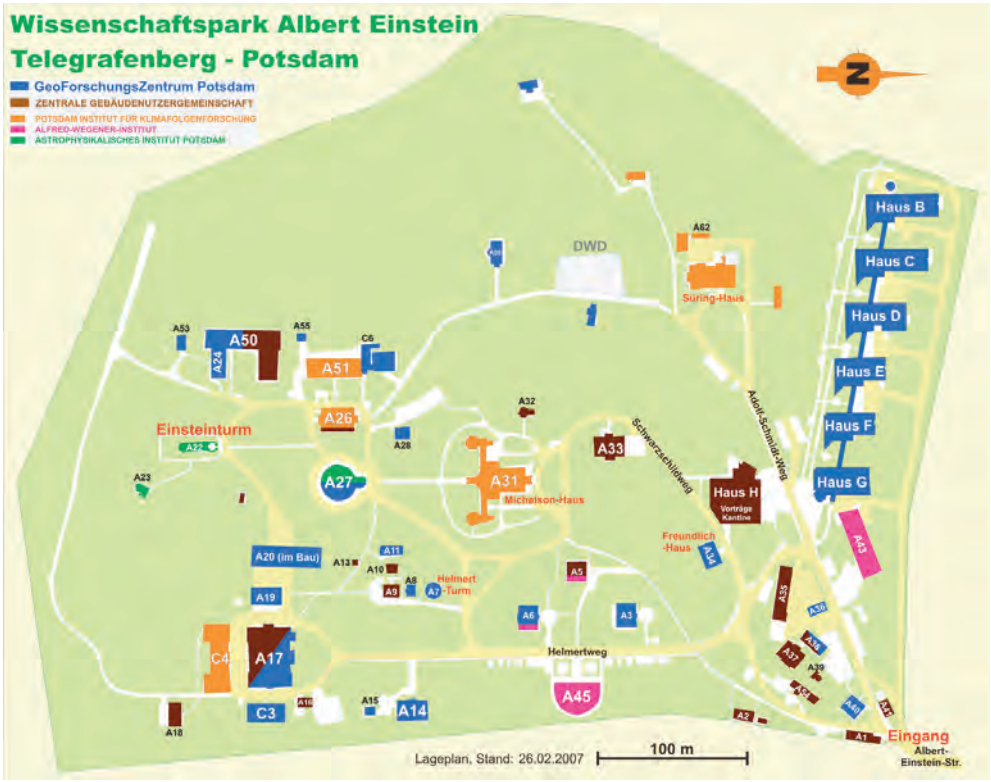

Lageplan des Deutschen GeoForschunszentrums

Fußweg: Gehen Sie in Richtung Süden über die Friedrich-Engels-Straße und die Heinrich-Mann-Allee zur Albert-Einstein-Straße in Richtung Landtag. Folgen Sie der Albert-Einstein-Straße bis zum Wissenschaftspark "Albert-Einstein".

Bus: Nehmen Sie die Linie 691 vom Potsdamer Hauptbahnhof direkt zum Wissenschaftspark "Albert-Einstein".

Montag, 16. März 2009		
11:00	13:00	**Registrierung**
13:00	13:40	**Eröffnung** Prof. Dr. Dr. h.c. R. F. J. Hüttl, Hausherr GFZ Prof. Dr.-Ing. habil. Dr. phil. S. Kunst, Präsidentin Uni Potsdam S. Dürr, G. Lüniger DFG, Programmdirektoren J. Erbacher, R. Oberhänsli, Koordinatoren
Berichte / Entwicklungen		
13:40	14:00	R. EMMERMANN ICDP Current Status & Perspectives
14:00	14:20	R. OBERHÄNSLI ICDP Deutschland – Wie geht es weiter?
14:20	14:35	J. BEHRMANN, J. ERBACHER IODP / ECORD Status und Perspektiven
14:35	14:50	J. ERBACHER IODP Deutschland Rückblick auf 2008 – Wie geht es weiter?
14:50	15:00	R. OBERHÄNSLI GESEP Status Report
15:00	15:20	B. ZOLITSCHKA, F. ANSELMETTI, D. ARUZTEGUI, H. CORBELLA, P. FRANCUS, C. GEBHARDT, A. HAHN, P. KLIEM, A. LÜCKE, C. OHLENDORF, F. SCHÄBITZ, AND THE PASADO SCIENCE TEAM PASADO Report about the ICDP Lake Drilling at Laguna Potrok Aike, Argentina
15:20 bis	16:30	**Posterpräsentation: Berichte / Entwicklungen (7), Seismogene Zonen / Impaktstrukturen (2)** **Kaffeepause**
16:30	16:50	G. KUHN, F. NIESSEN Antarctic Geologic Drilling ANDRILL Results and Plans
16:50	17:00	T. BEILECKE Forschungsbohrungen des Leibniz-Instituts für Angewandte Geophysik (LIAG) – Kristallisationspunkt für die Geowissenschaften
Impaktstrukturen / Störungszonen		
17:00	17:20	STEPHAN V. SOBOLEV, ANTON POPOV, AND M.D. ZOBACK Numerical model of Cenozoic evolution of the San Andreas Fault system constrained by geo-observations and SAFOD-drilling data
17:20	17:40	A. DEUTSCH, J. BERNDT, K. MEZGER, P. SCHULTE The Chicxulub ejecta layer in ODP 207 drill sites: analysis of the geochemical anaomalies at the µm-scale
17:40		**Posterpräsentation: Berichte / Entwicklungen (7), Impaktstrukturen / Störungszonen (2)** **Ice Breaker**
Ab 19:30 Gemeinsames Abendessen: Kutschstall, Am Neuen Markt		

Dienstag, 17. März 2009		
Faults / Seismogene Zonen		
9:00	9:20	A. KOPF Why are some faults weak, some strong, and many seismogenic? Results from deformation tests in a combined ICDP – IODP study
9:20	9:40	M. STRASSER, G.F. MOORE, A.J. KOPF Nankai Trough submarine landslide history: Results from IODP NanTroSEIZE drilling and presentation of a new IODP APL-proposal
9:40	10:00	G. DRESEN, M. BOHNHOFF, M. AKTAR, H. EYIDOGAN, H. ITO GONAF – a deep Geophysical Observatory at the North Anatolian Fault
10:00 bis 11:00		**<u>Posterpräsentation:</u> Tiefe Biosphäre (3), Gashydrate / Gase / Fluide (4), Magmatische Petrol., Metamorphose (5)** **Kaffeepause**
Tiefe Biosphäre / Fluide		
11:00	11:20	JENS KALLMEYER, KAI MANGELSDORF AND BRIAN HORSFIELD BUGLab – A new mobile geomicrobiology and biogeochemistry laboratory for exploring the deep biosphere
11:20	11:40	B. ENGELEN, T. ENGELHARDT, M. SAHLBERG, H. CYPIONKA Viral infections as controlling factors of the deep biosphere
11:40	12:00	S. BERTHOLD, F. BÖRNER Identification of vertical convection in boreholes - preliminary results for the KTB-MH
Magmatische Petrologie, Metamorphose		
12:00	12:20	N. A. STRONCIK, T. KRÜSMANN, S. NIEDERMANN, J. ERZINGER Geochemical surface patterns and the structure of mantle plumes – news from Ne isotopes and noble gas abundance ratios from Hawaii
12:20	12:40	W. BACH, F. KLEIN, N. JÖNS Ocean floor metasomatism re-examined: insights from thermodynamic modeling
12:40	13:00	S.B. CICHY, R.E. BOTCHARNIKOV, F. HOLTZ, H. BEHRENS, H. SATO Experimental simulation of vesiculation and microlite crystallization on ascent of rhyodacitic magma at Unzen Volcano
13:00	13:20	B. NASH, CATHEY, H., VALLEY, J., ALLEN, C., ALMEEV, R., HOLTZ, F. Geochemical and petrologic constraints on rhyolite magma genesis, Yellowstone hotspot track, Snacke River Plain, U.S.A.
13:20 bis 14:20		Mittagspause
Paläozeanographie/ Paläoklima		
14:20	14:40	REUSCHEL, M., STRAUSS, H., MELEZHIK, V.A., LEPLAND, A. Sulphur isotope variation in Paleoproterozoic strata from Fennoscandia
14:40	15:00	C. MONTOYA PINO, S. WEYER, B. VAN DE SCHOOTBRUGGE, A.D. ANBAR, H.W. ARZ, W. OSCHMANN, J. PROSS Global versus regional ocean anoxia during OAE-2 and the T-OAE
15:00 bis 16:30		**<u>Posterpräsentation:</u> Paläozeanographie, Paläoklima (1)** **Kaffeepause**
16:30	16:50	P. HOFMANN, B. BECKMANN, S. FLÖGEL, T. WAGNER Effects of orbital-scale fluctuations of the ITCZ on continental hydrology and marine carbon burial in the mid Cretaceous tropical Atlantic region
16:50	17:10	S. STEINKE, J. GROENEVELD, H.J.H. JOHNSTONE East Asian summer monsoon evolution and variability during the Late Miocene
17:10	17:30	J. GROENEVELD , H. DEBEY, E.C. HATHORNE, S. STEINKE Marine Isotope Stages (MIS) 100-101: The first modern glacial – interglacial cycle?
17:30 bis 18:30		Poster und Snack
19:00 Öffentlicher Vortrag: D.B. Dingwell: Explosive Vulkanausbrüche: Experimentelle Erkenntnisse		

Mittwoch, 18. März 2009		
Paläoklima / Seenforschung		
8:30	8:50	A. RÜGGEBERG, V. LIEBETRAU, J. RADDATZ, S. FLÖGEL, W.-CHR. DULLO, AND THE IODP EXP. 307 SCIENTIFIC PARTY A. Cold-water coral reef development on carbonate mounds in relation to paleo-density estimates
8:50	9:10	H. VOGEL, B. WAGNER, G. ZANCHETTA, R. SULPIZIO, S. SCHOUTEN, M.J. LENG A paleoclimate record with tephrochronological age control for the last climatic cycle from Lake Ohrid, Albania and Macedonia
9:10	9:30	M. E. WEBER, G. KUHN, W. RICKEN, L. REICHELT Weddell Sea bottom-water production and ice-sheet dynamics during the Last Glacial Maximum – seasonal- to centennial-scale variability
9:30	9:50	M. MELLES, J. BRIGHAM-GRETTE, P. MINYUK, C. KOEBERL, B. WAGNER, AND EL'GYGYTGYN SCIENTIFIC PARTY Lake El´gygytgyn Drilling under way: state of the operation and first results
9:50 bis 11: 00		**Posterpräsentation: Paläozeaonographie / Paläoklima (1), Neue Projekte / Projektvorschläge (6)** **Kaffeepause**
11:00	11:20	U. KOTTHOFF, J. PROSS, U. MÜLLER, G. SSCHMIEDL, I. DORMOY, O. PEYRON, A. BORDON Climate dynamics in the Aegean region from 17 to 7 ka BP deduced from combined marine and terrestrial palynological records
11:20	11:40	T. LITT, S. KRASTEL, M. STURM ,R. KIPFER, S. ÖRCEN, N. CAGATAY Lake Van Drilling Project 'PaleoVan'International Continental Scientific Drilling Program (ICDP): Upcoming Deep Drilling Campaign and Scientific Goals
Neue Projekte / Projektvorschläge		
11:40	12:00	TRWALTER, M SHIRZAEI, A MANCONI, R LANARI, B LÜHR, H WOITH, J ZSCHAU, T WIERSBERG, J ERZINGER Deformation and stress transfer at Vusuvius and Campi Flegrei
12:00	12:20	T. ANDREN, S. BJÖRCK, J. HARFF , J. B. JENSEN, B. B. JØRGENSEN , A. KOTILAINEN Paleoenvironmental Evolution of the Baltic Sea through the Last Glacial Cycle
12:20		Posterprämierung und Schlussworte
Ca. 13 Uhr		Tagungsende

Mittwoch, 18. März 2009	
Im Anschluß an das IODP/ICDP Kolloquium	
Ca. 14:00	GESEP WORKSHOP: EARTH PROBING SCHOOL
Organisiert von GESEP, 24 Teilnehmer aus 10 Instituten Der modulare Kurs wird von Ingenieuren und Wissenschaftlern aus Bremen, Bremerhaven, Hannover, Kiel und Potsdam mit langer Erfahrung in IODP und ICDP gehalten und wird jungen Wissenschaftlern Grundkenntnisse in Bohrtechnik, Bohrlochgeophysik und Monitoring, Antragstellung und Management vermitteln.	
Ende: Donnerstag, 19. März, gegen 13 Uhr	

Teilnehmerliste

Name	Vorname	Institution & Ort
Almeev	Renat	Institut für Mineralogie, Leibniz Universität Hannover
Andreev	Andrej	Alfred Wegener Institute, for Polar and Marine Research Potsdam
Andreula	Roberto	Marum - Universität Bremen
Bach	Wolfgang	Fachbereich Geowissenschaften, Universität Bremen
Bachmann	Gerhard	Institut für Geowissenschaften , Martin-Luther-Universität Halle-Wittenberg
Bahlburg	Heinrich	Geologisch-Paläontologisches Institut, WWU Münster
Baumann	Karl-Heinz	FB Geowissenschaften Universität Bremen
Becken	Michael	GFZ Deutsches GeoForschungsZentrum
Beckmann	Britta	Bundesanstalt für Geowissenschaften und Rohstoffe (BGR), Hannover
Behrens	Harald	Institut für Mineralogie, Leibniz Universität Hannover
Beilecke	Thies	LIAG, Hannover
Berthold	Susann	DGFZ Dresdner Grundwasserforschungszentrum e.V.
Betzler	Christian	Geologisch-Paläontologisches Institut, Hamburg
Blazejak	Anna	Bundesanstalt für Geowissenschaften und Rohstoffe (BGR), Hannover
Bock	Barbara	Universität Potsdam
Böhm	Florian	Leibniz-Institut für Meereswissenschaften, IFM-GEOMAR, Kiel
Bornemann	André	Institut für Geophysik und Gelogie, Universität Leipzig
Bosch	Frank	E.ON Energy Research Center, RWTH Aachen University
Botcharnikov	Roman	Institut für Mineralogie, Leibniz Universität Hannover
Böttcher	Michael	Leibniz Institute for Baltic Sea Research, Rostock
Bräuer	Karin	Helmholtz-Zentrum für Umweltforschung - UFZ, Halle
Breuker	Anja	Bundesanstalt für Geowissenschaften und Rohstoffe (BGR), Hannover
Brückmann	Warner	Leibniz Institut für Meereswissenschaften, IFM-GEOMAR, Kiel
Brumsack	Hans-J.	ICBM Oldenburg
Bücker	Christian	RWE Dea AG, Hamburg
Buske	Stefan	FU Berlin
Cichy	Sarah B.	Institut für Mineralogie, Leibniz Universität Hannover
Conze	Ronald	GFZ Deutsches GeoForschungsZentrum
Cordonnier	Benoît	Earth and Environmental Sciences, LMU München
Dersch-Hansmann	Michaela	Hessisches Landesamt für Umwelt und Geologie, Wiesbaden
Desbois	Guillaume	Geologie - Endogene Dynamik, RWTH, Aachen University
De Schepper	Stijn	Universität Bremen, Fachbereich Geowissenschaften
Deutsch	Alex	Institut für Planetologie, Universität Münster
Diester-Haass	Liselotte	Universität des Saarlandes, Saarbrücken
Dietze	Frank	Geologisches Institut, Universität Karlsruhe
Dingwell	Donald B.	Earth and Environmental Sciences, LMU München
Doose	Heidi	Bundesanstalt für Geowissenschaften und Rohstoffe (BGR), Hannover
Drath	Gabriela	Bundesanstalt für Geowissenschaften und Rohstoffe (BGR), Hannover
Dresen	Georg	GFZ Deutsches GeoForschungsZentrum
Duggen	Svend	IFM-GEOMAR, Leibniz-Institut für Meereswissenschaften, Kiel
Dultz	Stefan	Institut für Bodenkunde, Leibniz Universität Hannover
Dümmong	Stefan	Institute for Geophysics, University of Hamburg
Dupont	Lydie	Marum, Universität Bremen
Dürbaum	Hans-Jürgen	Isernhagen
Dürr	Sören	DFG, Bonn
Dziony	Wanja	Institut für Mineralogie, Leibniz Universität Hannover
Eckert	Sebastian	ICBM Oldenburg
Eder	Franz Wolfgang	Dept. Earth Sciences, Geology, Univ. Muenchen
Eisenhauer	Anton	Leibniz Institut für Meereswissenschaften, IFM-GEOMAR, Kiel
Emeis	Kay-Christian	IfBM, Hamburg
Emmermann	Rolf	GFZ Deutsches GeoForschungsZentrum
Engelen	Bert	ICBM Oldenburg
Engelhardt	Tim	ICBM Oldenburg
Erbacher	Jochen	Bundesanstalt für Geowissenschaften und Rohstoffe (BGR), Hannover
Erzinger	Jörg	GFZ Deutsches GeoForschungsZentrum
Flaws	Asher	
Flechsig	Christina	Universität Leipzig, Institut für Geophysik und Geologie
Förster	Verena	Universität Köln - Seminar für Geographie und ihre Didaktik
Gärtner	Claudia	Geologisch-Paläontologisches Institut, Universität Münster
Grieß	Juliane	AWI Potsdam
Grimmer	Jens C.	Struct. Geol. & Tectonophysics, Geological Institute, Universität Karlsruhe (TH)
Groeneveld	Jeroen	Institute of Marine Environmental Sciences, University Bremen
Gutjahr	Stine	Freie Universität Berlin Fachrichtung Geophysik
Hahn	Annette	GEOPOLAR, Institut für Geographie, Universität Bremen
Handiani	Dian	Marum - Universität Bremen
Harff	Jan	Leibniz Institut for Baltic Sea Research, Rostock
Harjes	Hans-Peter	Ruhr-Universität Bochum
Harms	Ulrich	GFZ Deutsches GeoForschungsZentrum

Hathorne	Ed	Marum - Zentrum für Marine Umweltwissenschaften, Universität Bremen
Heide	Klaus	Universität Jena
Heidinger	Philipp	Geophysikalisches Institut der Universität Karlsruhe
Hensen	Christian	Leibniz-Institut für Meereswissenschaften, IFM-GEOMAR, Kiel
Hepp	Daniel A.	Marum, Universität Bremen
Hess	Kai-Uwe	Earth and Environmental Sciences, LMU München
Hesse	Reinhard	Dept. Geo- und Umweltwissenschaften, Ludwig Maximilians Universität München
Heßler	Ines	Marum - Universität Bremen
Heuer	Verena	Fachbereich Geowissenschaften, Universität Bremen
Hinrichs	Kai-Uwe	Marum – Universität Bremen
Hoefs	Jochen	
Hoffmann	Nadine	Neotectonics and Natural Hazards Group, RWTH Aachen University
Hofmann	Peter	Universität zu Köln, Institut für Geologie und Mineralogie
Holtz	Francois	Institut für Mineralogie, Universität Hannover
Hördt	Andreas	Institut für Geophysik und extraterrestrische Physik, TU Braunschweig
Hüpers	Andre	Marum - Zentrum für Marine Umweltwissenschaften, Universität Bremen
Janssen	Christoph	GFZ Deutsches GeoForschungsZentrum
Jöns	Niels	Fachbereich Geowissenschaften, Universität Bremen
Kämpf	Horst	GFZ Deutsches GeoForschungsZentrum
Kallmeyer	Jens	Universität Potsdam, Institut für Geowissenschaften
Karas	Cyrus	Leibniz-Institut für Meereswissenschaften, IFM-GEOMAR, Kiel
Kastner	Stephanie	AG Geopolar, Institut für Geographie, Universität Bremen
Kessels	Winfried	Institut für Geowissenschaftliche Gemeinschaftsaufgaben, Hannover
Khelifi	Nabil	IfG - Kiel University
Kitamura	Yujin	Leibniz-Institut für Meereswissenschaften, IFM-GEOMAR, Kiel
Klein	Torsten	Institut für Geophysik und extraterrestrische Physik, TU Braunschweig
Kliem	Pierre	GEOPOLAR, Institut für Geographie, Universität Bremen
Klügel	Andreas	Universität Bremen, Fachbereich 5 - Geowissenschaften
Knies	Jochen	Geological Survey of Norway, Trondheim
Koepke	Jürgen	Institut für Mineralogie, Leibniz Universität Hannover
Kontny	Agnes	Institut für Angewandte Geowissenschaften der Universität Karlsruhe
Kopf	Achim	Marum - Universität Bremen
Köweker	Gerrit	Bundesanstalt für Geowissenschaften und Rohstoffe (BGR), Hannover
Kotthoff	Ulrich	Department of Geosciences, Universität Hamburg
Kück	Jochem	GFZ Deutsches GeoForschungsZentrum
Kudraß	Hermann-Rudolf	Bundesanstalt für Geowissenschaften und Rohstoffe (BGR), Hannover
Kuhn	Gerhard	AWI Bremerhaven
Langenkamp	Oliver	Universität Köln - Seminar für Geographie und ihre Didaktik
Lavallee	Yan	LMU München
Lazarus	David	Museum für Naturkunde, Berlin
Leuschner	Dirk	
Lindhorst	Katja	Leibniz-Institut für Meereswissenschaften, IFM-GEOMAR, Kiel
Lischka	Martin	Institut für Geographie und Geologie, Universität Greifswald
Litt	Thomas	Steinmann-Institut für Geologie, Mineralogie und Paläontologie, Uni Bonn
Lodemann	Manuela	Geowissenschaftliches Zentrum der Universität Göttingen
Lückge	Andreas	Bundesanstalt für Geowissenschaften und Rohstoffe (BGR), Hannover
Lüniger	Guido	DFG, Bonn
Mang	Christoph	Institut für Angewandte Geowissenschaften der Universität Karlsruhe
Mangelsdorf	Kai	GFZ Deutsches GeoForschungsZentrum
Maronde	Dietrich	Bonn
März	Christian	ICBM, Universität Oldenburg
Matthiessen	Jens	Alfred Wegener Institute for Polar and Marine Research, Bremerhaven
Meister	Patrick	MPI for Marine Microbiology, Bremen
Meschede	Martin	Institut für Geographie und Geologie, Universität Greifswald
Meyers	Philip	University of Michigan
Mischke	Steffen	Institut für Geowissenschaften, FU Berlin
Mohr	Barbara	HU Berlin
Montoya-Pino	Carolina	Universität Frankfurt, Institut für Geowissenschaften
Müller	Frank	LIAG, Hannover
Mutterlose	Jörg	Institut für Geologie, Mineralogie und Geophysik, Ruhr-Universität Bochum
Naafs	David	Alfred-Wegener-Institut for Polar and Marine Research, Bremerhaven
Nash	Barbara	University of Utah
Niedermann	Samuel	GFZ Deutsches GeoForschungsZentrum
Niessen	Frank	AWI Bremerhaven
Nowak	Marcus	Institut für Geowissenschaften, Universität Tübingen
Oberhänsli	Roland	Institut für Geowissenschaften, Potsdam
Oberhänsli	Hedwig	GFZ Deutsches GeoForschungsZentrum
Ockert	Charlotte	Institut für Mineralogie, Westfälische Wilhelms-Universität Münster
Ohlendorf	Christian	Geopolar, Universität Bremen
Paul	André	Marum - Universität Bremen
Perez	Liseth	Instiut für Umweltgeologie, TU Braunschweig

Piribauer	Christoph	RWTH Aachen, Institut für Mineralogie und Lagerstättenlehre
Planert	Lars	Leibniz-Institut für Meereswissenschaften, IFM-GEOMAR, Kiel
Plenkers	Katrin	GFZ Deutsches GeoForschungsZentrum
Raddatz	Jacek	Leibniz-Institut für Meereswissenschaften, IFM-GEOMAR, Kiel
Raschke	Ulli	Naturkundemuseum, HU Berlin
Rausch	Svenja	Institut für Geowissenschaften, Universität Bremen
Reicherter	Klaus	Lehr- und Forschungsgebiet Neotektonik und Georisiken RWTH Aachen
Reimold	Wolf Uwe	Naturkundemuseum, HU Berlin
Reischmann	Thomas	Universität Mainz
Renaudie	Johan	
Reshetnikov	Anton	FU Berlin Fachrichtung Geophysik
Reuschel	Marlene	Westfälische Wilhelms Universität Münster, Geologisch-Paläontologisches Institut
Riedinger	Natascha	MPI for Marine Microbiology, Bremen
Riemann	Astrid	Institut für Geowissenschaften, Universität Potsdam
Röhl	Ursula	Marum - Zentrum für Marine Umweltwissenschaften, Universität Bremen
Rommerskirchen	Florian	Marum - Zentrum für Marine Umweltwissenschaften, Universität Bremen
Rosner	Martin	Federal Institute for Material Research & Testing, Berlin
Rücker	Carsten	Universität Leipzig
Rüggeberg	Andres	Leibniz-Institut für Meereswissenschaften, IFM-GEOMAR, Kiel
Sarnthein	Michael	Institut für Geowissenschaften, Universität Kiel
Schäbitz	Frank	Seminar für Geographie und ihre Didaktik, Universität Köln
Scheibner	Birgit	Forschungszentrum Jülich
Schleicher	Anja	University of Michigan/ Uni Erlangen
Schmidt-Schierhorn	Frederike	Geowissenschaften, Uni. Bremen
Schmincke	Hans-Ulrich	Leibniz-Institute of Marine Science, IFM-GEOMAR, Kiel
Schreck	Michael	Alfred Wegener Institute for Polar and Marine Research (AWI), Bremerhaven
Schulz	Hartmut	Institut für Geowissenschaften, Geobiol. & angew. Paläontol. Universität Tübingen
Schumann	Jens	GFZ Deutsches GeoForschungsZentrum
Schütze	Claudia	Universität Leipzig, Institut für Geophysik und Geologie
Schwalb	Antje	Institut für Umweltgeologie, TU Braunschweig
Schwamborn	Georg	Alfred-Wegener-Institut für Polar- und Meeresforschung, Potsdam
Sens-Schönfelder	Christoph	Institut für Geophysik und Geologie, Universität Leipzig
Shishkina	Tatiana	Institut für Mineralogie, Leibniz Universität Hannover
Simonyan	Anna	Institut für Mineralogie, Universität Hannover
Sindern	Sven	RWTH Aachen, Institut für Mineralogie und Lagerstättenlehre
Smolka	Peter P.	Universität Münster
Sobolev	Stephan	GFZ Deutsches GeoForschungsZentrum
Spiess	Volkhard	Marine Techn. & Environmental Res., Dept. of Earth Sciences, Bremen University
Stein	Rüdiger	Alfred-Wegener-Institut, Bremerhaven
Steinke	Stephan	Marum - Universität Bremen
Stosch	Heinz-Günter	Universität Karlsruhe
Strack	Dieter	International Oil & Gas Consultant, Ratingen
Strasser	Michael	Marum - Universität Bremen
Strauch	Gerhard	UFZ, Leipzig – Halle
Strauss	Harald	Geologisch-Paläontologisches Institut, WWU Münster
Stroncik	Nicole A.	GeoForschungsZentrum Potsdam
Sumita	Mari	Leibniz-Institute of Marine Science, IFM-GEOMAR, Kiel
Teichert	Barbara	Geologisch-Paläontologisches Institut, WWU Münster
Trampe	Anna F.	Institut für Geowissenschaften, Universität Bremen
Trauth	Martin	Institut für Geowissenschaften, Universität Potsdam
Urbat	Michael	Institut für Geologie und Mineralogie Universität zu Köln
Viehberg	Finn	TU Braunschweig
Viereck-Götte	Lothar	Institut für Geowissenschaften, Friedrich-Schiller-Universität Jena
Virgil	Christopher	Institut für Geophysik & Extraterrestrische Physik, TU-Braunschweig
Vogel	Hendrik	Institut für Geologie und Mineralogie, Universität Köln
Vogt	Christoph	Kristallographie, Geowissenschaften, Universität Bremen
Voigt	Silke	Leibniz-Institut für Meereswissenschaften, IFM-GEOMAR, Kiel
Wagner	Bernd	Institut für Geologie und Mineralogie, Universität Köln
Wagner	Thomas	Newcastle University
Walter	Thomas	GFZ Deutsches GeoForschungsZentrum
Weber	Michael E.	Institute of Geology and Mineralogy, University of Köln
Wefer	Gerold	Marum - Universität Bremen
Wellmer	Fr.-Wilhelm	Universität Hannover
Weyer	Stefan	Universität Frankfurt, Institut für Geowissenschaften
Wiersberg	Thomas	GeoForschungsZentrum Potsdam
Winkelmann	Daniel	IFM GEOMAR, Kiel
Wohlgemuth	Lothar	GFZ Deutsches GeoForschungsZentrum
Wonik	Thomas	LIAG, Hannover
Zolitschka	Bernd	GEOPOLAR, Institut für Geographie, Universität Bremen

Autor	Titel	SPP
Almeev, R., F. Holtz, L. Kuschel, H. Cathey, B. Nash	Pre-eruptive conditions of the Bruneau-Jarbidge Rhyolite, Snake River Plain-Yellowstone hotspot track	ICDP
Andreev, A. A.	Quaternary vegetation and climate dynamics inferred from palaeoecological records of the El'gygytgyn permafrost core	ICDP
Andren, T., S. Björck, J. Harff , J. B. Jensen, B. B. JØrgensen, A. Kotilainen	Paleoenvironmental Evolution of the Baltic Sea through the Last Glacial Cycle	IODP
Bach, W., F. Klein, N. Jöns	Ocean floor metasomatism re-examined: insights from thermodynamic modeling	IODP
Bachmann, G. H., R. Blakey, J. Geissman, D. Kent, W. Kürschner, P. Olsen, J. Sha	Colorado Plateau Coring Project (CPCP): 100 Million Years of Climatic, Tectonic, and Biotic Evolution in Continental Cores	ICDP
Baumann, K.-H., H. Meggers, J. Holtvoeth	Abrupt millennial-scale variations in North Atlantic surface-water circulation (ODP Site 980) during the last 20,000 years as revealed by coccolithophorid assemblages	IODP
Becken, M., O. Ritter, P.A. Bedrosian, U. Weckmann, G. Munoz	San Andreas Fault system: Implications for the structure and dynamics from lithospheric electrical conductivity ICDP project ELSAF (ELectrical conductivitiy structure of the San Andreas Fault)	ICDP
Beckmann, B., D. Birgel, J. Erbacher, A. Lückge	Ocean-continent interactions during mid Cretaceous Oceanic Anoxic Events in the western tropical Atlantic	IODP
Berthold, S., F. Börner	Identification of vertical convection in boreholes - preliminary results for the KTB-MH	ICDP
Betzler, C., J. Fürstenau, C. Hübscher & T. Lüdmann	Monsoonal impact on the Maldives carbonate platform (ODP Site 716)	IODP
Blazejak, A., A. Schippers	Cayre, O., Beaufort, L., and Vincent, E., 1999, Paleoproductivity in the Equatorial Indian Ocean for the last 260,000 yr: A transfer function Quantification of JS-1 and Chloroflexi related bacteria in shallow and subsurface marine sediments using real-time-PCR	IODP
Böhm, F. , A. Eisenhauer, S. Rausch, W. Bach, A. Klüge	Calcium Isotope Systematics of Low Temperature Alteration Carbonates in the Ocean Crust	IODP
Bornemann, A.	The Paleocene–Eocene transition in the Bay of Biscay (DSDP Site 401) – first micropaleontological and geochemical results	IODP
Bosch, F.P., R. Pechnig, C. Clauser	RWTH Aachen University as part of the European Petrophysics Consortium (EPC)	IODP
Botcharnikov, R.E., J. Koepke, B. Putlitz	Experimental study on evolution of gabbros from the ODP Legs 118/176 drilled at the Southwest Indian Ridge	ICDP
Bräuer, K., H. Kämpf, J. Schumann, G. Strauch	The different degassing behaviour of upper mantle-derived fluids in the western Eger rift area - a contribution to find an optimal ICDP location	ICDP
Cichy, S.B., R.E. Botcharnikv, F. Holtz, H. Behrens, H. Sato	Experimental simulation of vesiculation and microlite crystallization on ascent of rhyodacitic magma at Unzen Volcano	ICDP
Cordonnier, B., K.U. Hess, D. Dingwell	Brittleness and shear thinning: the explosive-effusive transition of Unzen lava dome experimentally investigated	ICDP
Desbois, G., J.L. Urai	Characterization of the pore space in SAFOD samples combining Ar-beam cross sectioning and SEM imaging: First results	ICDP
De Schepper, S., M.J. Head, J. Groeneveld	North Atlantic Current variability through Marine Isotope Stage MIS M2 (ca. 3.3 Ma) during the warm mid-Pliocene	IODP
Deutsch, A., J. Berndt, K. Mezger, P. Schulte	The Chicxulub ejecta layer in ODP 207 drill sites: analysis of the geochemical anomalies at the µm-scale	IODP
Diester-Haaß, L., M, Billups, K. Emeis	Orbital control on marine biological productivity and the positive carbon isotope shift at the Oligocene-Miocene transition	IODP
Dietze, F., C. Virgil, A. Kontny, M.-L. Airo	Rock magnetic properties and their anisotropy from the Outokumpu assemblage in the Outokumpu deep drilling, Finland	ICDP
Dresen, G., M. Bohnhoff, M. Aktar, H. Eyidogan, H. Ito	GONAF - a deep Geophysical Observatory at the North Anatolian Fault	ICDP
Dümmong, S., C. Hübscher, M. Beitz, L. Marlow	Stratigraphy and distribution of Messinian Evaporites in the Levantine basin	IODP
Duggen, S., K. Hoernle, F. Hauff, J. Geldmacher	High-precision Pb (double spike) and Sr-Nd-Hf-isotopic record of upper oceanic crust at Leg 206 (Site 1256, Eastern Central Pacific)	IODP
Dziony, W., J. Koepke, I. Horn, G. Steinhöfel, J. Schüßler, F. Holtz	In-situ iron isotope ratio determination and thermo-oxibarometry in Fe-Ti oxides of IODP Hole 1256D (ODP Leg206 and IODP Exp. 309 & 312, East Pacific Rise)	IODP
Eckert, S., B. Schnetger, H.-J. Brumsack	Trace metal patterns in Black Sea sapropels as a chemostratigraphic tool	IODP

Engelen, B., T. Engelhardt, M. Sahlberg, H. Cypionka	Viral infections as controlling factors of the deep biosphere	IODP
Flaws, A., K.-U. Hess B. Schillinger, D.B. Dingwell	Development of an ultra-high resolution neutron computed tomography system for the characterisation of drill cores	ICDP
Förster, V., O. Langenkamp	Die Pollensedimentation der Kleinen Eiszeit im Vergleich zur rezenten Pollensedimentation auf dem Seeboden der Laguna Potrok Aike, Südpatagonien, Argentinien	ICDP
Gärtner, C., H. Bahlburg, E. Kooijman, J. Berndt, V. Melezhik, A. Lepland	The Archean to Paleoproterozoic transition as recovered in the FAR DEEP cores: LA-ICP-MS U-Pb geochronology of detrital zircons and accompanying provenance analysis of siliciclastic sedimentary rocks	ICDP
Gebhardt, A. C., F. Niessen, M. De Batist, F. S. Anselmetti, D. Ariztegui, C. Kopsch, C. Ohlendorf, B. Zolitschka	Seismic data reveal origin and evolution of the Laguna Potrok Aike maar (Patagonia, Southern Argentina)	ICDP
Griess, J., K. Mangelsdorf, D. Wagner	Response of the Methane Cycle to Climate Changes in the Past and Present	ICDP
Grimmer, J.C., X.X. Qi, Z.Q. Xu	Magnetofabrics of ultrahigh-pressure gneisses from the Chinese Continental Scientific Drilling (CCSD) project: Evidence for a genetic link between ferromagnetic and paramagnetic gneisses	ICDP
Groeneveld, J., H. Debey, E.C. Hathorne, S. Steinke	Marine Isotope Stages (MIS) 100-101: The first modern glacial – interglacial cycle?	IODP
Hahn, A., P. Kliem, C. Ohlendorf, B. Zolitschka and the PASADO Science Team	PASADO deep drilling (southern Argentina) - first results reveal a climate record far back into the last glacial	ICDP
Handiani, D. N., A. Paul, L. M. Dupont	Comparing the tropical vegetation distribution of a Heinrich-like climate to that of a pre-industrial one	IODP
Hathorne, E. C., J. Groeneveld, S. Steinke, M. Kölling	Flow Through cleaning and sequential dissolution of Neogene planktonic foraminifera for Mg/Ca analyses	IODP
Heidinger, P., H. Wilhelm, Y. Popov, D. Miklashevskiy	Investigations of the Heat Flow Density at the Chesapeake Bay Area, Virginia, USA	ICDP
Hepp, D. A., T. Mörz, T. Frederichs, H.-J. Brumsack	Magnetic susceptibility loss at glacial-interglacial transitions in the early Pliocene sedimentary record of ODP Site 1095	IODP
Heßler, I., L.M. Dupont, A. Paul	Preliminary Results of Vegetation Development in Tropical Africa during Heinrich Event 3 (ODP 1078, off Angola)	IODP
Heuer, V.B., J.W. Pohlman, M.E. Torres, M.A. Lever, M. Elvert, K.-U. Hinrichs	The stable carbon isotope biogeochemistry of acetate in sediments from the NE Pacific: a synthesis	IODP
P. Hofmann, B. Beckmann, S. Flögel, T. Wagner	Effects of orbital-scale fluctuations of the itcz on continental hydrology and marine carbon burial in the mid Cretaceous tropical Atlantic region	IODP
Hofmann, P., C. L. Handly, H. Talbot, T. Wagner	Development of sea surface temperature across the lower Aptian Oceanic Event 1a in the Subtropical North Atlantic, Galicia Margin	IOPD
Hüpers, A., S. Kreiter, A.J. Kopf	Ramifications of high insitu temperatures for geotechnical testing at ambient temperature conditions – a case study from the Nankai margin	IODP
Janssen, C.	Fault zone damage and chemical reactions at dept in the San Andreas Fault Zone – A study of SAFOD drill core samples	ICDP
Jöns, N., W. Bach, M. Rosner, T. Schroeder	Melt-rock and fluid-rock interactions in serpentinized abyssal harzburgites (Mid-Atlantic Ridge, ODP Leg 209)	IODP
Kallmeyer, J., K. Mangelsdorf, B. Horsfield	BUGLab – A new mobile geomicrobiology and biogeochemistry laboratory for exploring the deep biosphere	IODP
Karas, C., D. Nürnberg, A. K. Gupta, K. Mohan, R. Tiedemann, T. Bickert	Rapid switch in Indonesian subsurface throughflow triggering climate change across the mid-Pliocene	IODP
Kastner, S., C. Ohlendorf, T. Haberzettl, A. Lücke, N. I. Maidana, C. Mayr, F. Schäbitz, B. Zolitschka	Climatically induced spatial sedimentation dynamics of late Holocene sediment infill in Laguna Potrok Aike (southern Patagonia, Argentina) – a preliminary study in the framework of the ICDP project PASADO	ICDP
Khélifi, N., M. Sarntheim	Increased aridity in the Mediterranean Sea 3.55 – 3.35 Ma: a trend without climatic analogue in the ocean?	IODP
Kitamura, Y., T. Kanamatsu, X. Zhao	Sediment deformation in accretionary prism toe: results from NanTroSEIZE Expedition 316, Sites C0006 and C0007	IODP
Klein, T., A. Hördt, M. Leven , C. Virgil	Messungen mit dem Göttinger Bohrlochmagnetometer (GBM) in der Bohrung Schotten/Sichenhausen im Vogelsberg	ICDP
Knies, J., K. Andreassen, K. Fabian, K. GrØsfjeld, M. Hald, K. Husum	The Arctic Chronology Project – Academia meets Industry	

Kopf, A.	Why are some faults weak, some strong, and many seismogenic? Results from deformation tests in a combined ICDP – IODP study	IODP
Kotthoff, U., J. Pross, U. Müller, G. Schmiedl, I. Dormoy, O. Peyron, A. Bordon	Climate dynamics in the Aegean region from 17 to 7 ka BP deduced from combined marine and terrestrial palynological records	IODP
Köweker, G., C. Höft, A. Schippers	Comparison of methods for the determination of total cell numbers in different sediments	IODP
Kuhn, G., F. Niessen	Antarctic geological drilling ANDRILL results and plans	
Lavallée, Y., D. B. Dingwell, K.-U. Hess, G. Andrews, K. J. Russell	Absolute healing of pyroclasts during rheomorphic welding of ignimbrites in the Snake River Plain, USA	ICDP
Lazarus, D., J. Renaudie	Synthesis and Analysis of Antarctic Neogene Radiolaria	IODP
Ledru, M.-P., W.U. Reimold, I. Bentaleb, A. Crosta, G. Ramstein, C. Riccomini	Quaternary Tertiary Tropics, Colônia Sediment Archive Project (QUE COISA)	ICDP
Lindhorst, K., S. Krastel-Gudegast, T. Schwenk, K. Reicherter, G. Daut, M. Wesels, B. Wagner	Seismic pre-site survey for the SCOPSCO ICDP-campaign in ancient Lake Ohrid	ICDP
Litt, T., S. Krastel, M. Sturm, R. Kipfer, S. Örcen, N. Cagatay	Lake Van Drilling Project 'PaleoVan' International Continental Scientific Drilling Program (ICDP): Upcoming Deep Drilling Campaign and Scientific Goals	ICDP
Lodemann, M., H. Erlenkeuser, M. Wolf, O. Stückrad, P.M. Grootes, P. Schmitt-Kopplin, J. Schwarzbauer, N. Hertkorn, S.A. Huber	DIC and DOM (dissolved inorganic carbon and dissolved organic matter) in deep fluids. Preliminary results from the KTB-VB site	ICDP
Marquardt, M., T. Henke, C. Hensen, C. Müller, R. Gehrmann, K. Wallmann	Derivation and application of a simple transfer function for submarine gas hydrate quantification	IODP
März, C., A. Stratmann, S. Eckert, B. Schnetger, H.-J. Brumsack	Manganese diagenesis in Arctic Ocean sediments – Stratigraphic and paleoenvironmental implications	IODP
März, C., B. Schnetger, H.-J. Brumsack	Major and minor element signatures and their paleoenvironmental significance in Central Arctic Ocean sediments (Lomonosov Ridge, IODP Leg 302)	IODP
Matthiessen, J., M. Schreck	The Arctic Ocean Sea-Ice Cover in the Neogene: Evidence from Marine Palynomorphs	IODP
Meggers, H., C. Vogt, K.-H. Baumann, T. Wagner	Millenial and shorter scale slowdown of North Atlantic Meridional	IODP
Meister, P., S. Freund, L. M. Wehrmann, B. Brunner, T. G. Ferdelman	Degree of pyritization and δ^{34}S-values record suboxic conditions in sediments of the Eastern Equatorial Pacific, ODP Site 1226	IODP
Melles, M. , J. Brigham-Grette, P. Minyuk, C. Koeberl, B. Wagner, and ELGYGYTGYN Scientific Party	Lake El´gygytgyn Drilling under way: state of the operation and first results	ICDP
Meschede, M., H. Ueda, Y. Ogawa, and shipboard scientific party of Yk08-05	Serpentinite schists in an intraoceanic island arc: exhumation by extension?	IODP
Mischke, S., I. Rajabov, N. Mustaeva, C. Zhang, I. Boomer, S.C. Sherlock, E.T. Brown, A. Myrbo, A. Noren, K. Brady, U. Herzschuh, M.E. Schudack, E. Ito	Lake Karakul in the Pamirs and its potential as a long-term climate archive	IODP
Montoya Pino, C., S. Weyer, B. Van De Schrootbrugge, A.D. Anbar, H. W. Arz, W. Oschmann, J. Pross	Global versus regional ocean anoxia during OAE-2 and the T-OAE	IODP
Müller, W.F., Z.Q. Xu, F.E. Brenker	Omphacite and other minerals in the eclogites from the Chinese Continental Scientific Drilling project (CCSD): A TEM study	ICDP
Naafs, B. D., R. Stein, G. Haug	WI Sea surface characteristics in the North Atlantic during the Pleistocene and Pliocene; a biomarker approach	IODP
Nash B., H. Cathey, J.Valley, C. Allen, R. Almeev, and F. Holtz	Constraints on rhyolite magma genesis, Yellowstone hotspot: evidence from mineral thermometry, Nd and O isotopes, and U-Th-Pb zircon geochronology	ICDP
Ockert, C., B.M.A. Teichert, S. Kaufhold, N. Gussone	Fractionation processes of Ca isotopes in interstitial waters of marine sediments	IODP

Pérez , L., B. Scharf, A. Schwalb	Living and fossil ostracode species assemblages from the Yucatán Península as indicators of environmental change - a contribution to the Lago Petén Itzá Drilling Project-	ICDP
Piribauer, C., F. M. Meyer, S. Sindern, T. W. Vennemann, W. Prochask	Fluid composition and Palaeofluid evolution in veins of the Outokumpu drilling site, Finland	ICDP
Planert, L., D. Klaeschen, C. Berndt, W. Brückmann, C. Hensen	Drilling into dewatering sites along the Costa Rica and Nicaragua margin (IODP proposal 633-Full2): first results from pre-site survey seismic data evaluation	IODP
Plenkers, K., Kwiatek, G; Nakatani, M.; Dresen, G.; Philipp, J.; Yabe, Y.; Jaguars-Group	Observation of high-frequency seismic events (100 Hz to 170,000Hz) in a deep gold mine, South Africa	ICDP
Raddatz, J., A. Rüggeberg, S. Margreth, W.-Chr. Dullo, and IODP EXP. 307 Scientific Party	Paleo-environment of cold-water coral initiation in the NE Atlantic: Implications from a deep-water carbonate mound drilling core	IODP
Rausch, S., F. Böhm, A. Klügel, W. Bach	Timing and magnitude of CO2 uptake by ocean crust through seawater interaction and carbonate veining	IODP
Reicherter, K., T. Fernández-Steeger, N.Hoffmann	Tectonic Evolution of the Ohrid Basin (Macedonia/Albania): preliminary results for a future ICDP deep drilling site	ICDP
Reshetnikov, A., S. Buske, S. Shapiro	Active seismic imaging using microseismic events – results from the San-Andreas-Fault system at SAFOD	ICDP
Reuschel, M., Strauss, H., Melezhik, V.A., Lepland, A.	Sulphur isotope variation in Paleoproterozoic strata from Fennoscandia	ICDP
Riedinger, N., B. Brunner, E. Solomon, L. Claesson Liljedahl, S. Kasten, T.G. Ferdelman, and IODP Expedition 314/315/316 Scientific Party	Iron and sulfur cycling in sediments from the Nankai Trough, Japan	IODP
Riemann, A., R. Oberhänsli, A. Möller, A. Gerdes	In situ dating of metasomatically controlled zircon growth during retrogression: a LA-SF-ICP-MS study of zircon from UHP eclogites (Sulu deep drill hole, CCSD)	ICDP
Rommerskirchen, F., L. Dupont, T. Condon, G. Mollenhauer, E. Schefuß	Southeast Atlantic upwelling intensity changes influencing late Miocene C4 plant expansion?	IODP
Rüggeberg, A., Liebetrau, V., Raddatz, J., Flögel, S., W.-Chr. Dullo, and the IODP Exp. 307 Scientific Party	Cold-water coral reef development on carbonate mounds in relation to paleo-density estimates	IODP
Scheibner, B., H.-G. Stosch	Chalcophile element budget in the oceanic crust: First results from the complete section of upper oceanic crust at borehole 1256D (ODP-Leg 206, Exp 309 and Exp 313)	IODP
Schleicher, A.M., B.A. Van Der Plujim, L.N. Warr	Clay nano-coatings and their role in fault-creep activity in the San Andreas Fault	ICDP
Schmidt-Schierhorn, F., R. Harris, M. Kinoshita	Preliminary heat flow results from NanTroSeize Expeditions 314/315/316 Nankai Trough, Japan	IODP
Schreck, M., J. Matthiessen	Palecology and Paleoenvironment of the Neogene Nordic Seas based on Dinocyst Assemblages	IODP
Schulte, P., A. Kontny, M. Joachimski	Pelagic red beds in ODP Leg 207 (Demerara Rise): Evidence for an Early Paleogene oxic event in the Western Atlantic?	IODP
Schütze, C., C. Rücker, Ch. Flechsig	Research study for a geoelectrical pre-site survey of the drilling location within the Eger Rift / NW-Bohemia: Investigation of the subsurface electrical conductivity distribution	ICDP
Schwamborn, G., G. Fedorov, B. Diekmann, L. Schirrmeister, H.-W. Hubberten	A record of permafrost conditions for Arctic Siberia from El'gygytgyn Impact Crater	ICDP
Shishkina, T., R. Botcharnikov, R. Almeev, F. Holtz	Storage conditions and degassing processes of low-K and high-Al tholeiitic island-arc magmas: Experimental constraints for Mutnovsky volcano, Kamchatka	ICDP
Simonyan, A., S. Dultz, H. Behrens, J. Pastrana, U. Schwarz-Schampera	Determination of porosity and diffusion transport in differently altered basalts of the oceanic crust	IODP
Smolka, P. P.	The Greenland–Scotland–Ridge needs to be revisited	IODP
Sobolev, S. V., A. Popov, M.D. Zoback	Numerical model of evolution of the San Andreas Fault system constrained by geo-observations and SAFOD-drilling data	ICDP
Spiess, V., J. Metzen, N. Fekete, L. Palamenghi, M. Sacchi	Experience with a Shallow Water Seismic Pre-Site Survey for combined IODP and ICDP Drilling Campaigns in the Gulf of Naples and Gulf of Pozzuoli, Tyrrhenian Sea	ICDP

Spiess, V., B. Preu, T. Schwenk, L. Palamenghi, R. Schneider, I. Hall, R. Zahn	Drilling in Current-Controlled Sedimentary Environments on the Southeast African Margin - The SAFARI Pre-Site Survey Challenges on the Madagascar, Mozambique and the South African Margin	IODP
Steinke, S., J. Groeneveld, H.J.H. Johnstone	East Asian summer monsoon evolution and variability during the Late Miocene	IODP
Strasser, M., G.F. Moore, A.J. Kopf	Nankai Trough submarine landslide history: Results from IODP NanTroSEIZE drilling and presentation of a new IODP APL-proposal	IODP
Stroncik, N. A., T. Krüsmann, S. Niedermann, J. Erzinger	Geochemical surface patterns and the structure of mantle plumes – news from Ne isotopes and noble gas abundance ratios from Hawaii	ICDP
Sumita, M., H.-U. Schmincke	Explosive volcanism during evolution of Lake Van	ICDP
Teichert, B.M.A., N. Gussone, M. E. Torres	Controls on Calcium Isotope Fractionation in Sedimentary Porewaters of ODP Expedition 204	IODP
Tiedemann, R., D. Rincon-Martinez, C. Saukel , F. Lamy, S. Steph, A. Sturm	The missing link to understand Plio-Pleistocene changes in southeast Pacific oceanography, productivity, and El Niño behavior – SE trade wind strength and its dust transport	IODP
Trampe, A. F., V. Spiess, S. Krastel, T. Andren, R. Endler, J.Harff	The quaternary depositional history of Anholt Loch Kattegat and Hanø Bay / Bornholm Basin: Results of a high resolution seismic IODP Pre-Site Survey	IODP
Viereck-Goette, L., J. Francis, A. Vaughan, S. Marenssi, B. Mohr, and The D-ANDRILL Members	Proposal to drill for the Cretaceous and Paleogene high latitude climate history, James Ross Basin, Antarctic Peninsula	ICDP
Virgil, C., F. Dietze, A. Hördt, T.Klein, M. Leven, E. Steveling	Three-Component Magnetic Logging in the Outokumpu Borehole	ICDP
Vogel, H., B. Wagner, G. Zanchetta, R. Sulpizio, S. Schouten, M.J. Leng	A paleoclimate record with tephrochronological age control for the last climatic cycle from Lake Ohrid, Albania and Macedonia	ICDP
Vogt, C., J. Matthiessen, C. März, H.-J. Brumsack, R. X. Fischer	Climate Cycles and Events in the Plio-/Pleistocene of the Yermak Plateau, Arctic Ocean: Causes and Consequences based on validated X-ray Fluorescence Scanner Data of ODP Sites 910 and 911: Towards Millenial Scale Resolution	IODP
Wagner, B., T. Wilke, A. Grazhdani, G. Kostoski, S. Krastel-Gudegast, K. Reicherter, G. Zanchetta	SCOPSCO – Scientific Collaboration On Past Speciation Condition in Lake Ohrid	ICDP
Wagner, T. H. Meggers, K.-H. Baumann, T. Eglinton, J. Holtvoeth, G. Mollenhauer	Millennial-to-centennial scale fluctuations in marine organic carbon export and burial since the Last Glacial Maximum in the Northeast Atlantic	IODP
Walter, T. R., Manconi, A., Shirzaei, M., Lanari, R., Lühr, B., Woith, H., Zschau, J., T. Wiersberg, J. Erzinger	Deformation and stress transfer at Vesuvius and Campi Flegrei	ICDP
Weber, M. E., G. Kuhn, W. Ricken, L. Reichelt	Weddell Sea bottom-water production and ice-sheet dynamics during the Last Glacial Maximum – seasonal- to centennial-scale variability	IODP
Westerhold, T., U. Röhl, H. K. McCarren, J. C. Zachos	Latest on the absolute age of the Paleocene – Eocene Thermal Maximum (PETM): new insights from exact stratigraphic position of key ash layers +19 and -17	IODP
Wiersberg, T. & Erzinger, J.	Gas migration and permeability structure of the San Andreas Fault at SAFOD deduced from drill-mud gas monitoring data	ICDP
Zolitschka, B., F. Anselmetti, D. Ariztegui, H. Corbella, P. Francus, C. Gebhardt, A. Hahn, P. Kliem, A. Lücke, C. Ohlendorf, F. Schäbitz, and the PASADO Science Team	PASADO: Report about the ICDP lake drilling at Laguna Potrok Aike, Argentina	ICDP

Pre-eruptive conditions of the Bruneau-Jarbidge Rhyolite, Snake River Plain-Yellowstone hotspot track

R. ALMEEV[1], F. HOLTZ[1], L. KUSCHEL[1], H. CATHEY[2], B. NASH[2]

[1]Institute of Mineralogy, Leibniz University of Hannover
[2]Department of Geology and Geophysics, University of Utah

Introduction

The Snake River Plain – Yellowstone (SRPY) bimodal volcanism of the western United States is related to migration of the North America plate over the Yellowstone hotspot. Silicic volcanism generally predates basaltic activity and age relationships show a north-eastward migration of the rhyolite caldera complexes and associated ignimbrites from SW Idaho to Island Park-Yellowstone eruptive center, which is the current locus of recent volcanic activity and deep thermal source. The proposed ICDP drilling in the Snake River Plain volcanic province is aimed to trace the interaction of the Yellowstone hotspot with continental lithosphere and to provide new data on chemical evolution and pre-eruptive conditions of the basaltic and rhyolitic magmas with time and space. This requires information on the origin and peculiarity of the contrasting magmatism, the evolution of chemistry, sources, differentiation and storage conditions of both the rhyolitic and basaltic magmas. In the frame of this drilling program and in the course of our research project (Project Ho 1337/17) we performed an experimental investigations of differentiation paths and pre-eruptive conditions of the typical rhyolite magmas from Bruneau-Jarbidge silicic eruptive center.

The Cougar Point Tuff

The Cougar Point Tuff (CPT) consists of 10 large-volume (> 102-103 km^3 each) rhyolitic ash-flow tuffs erupted from the Bruneau-Jarbidge volcanic center (12.5-10.5 Ma). CPT magmas are generally crystal poor (5-25%) metaluminous ferroan rhyolites, characterized by anhydrous phenocryst assemblage which includes plagioclase, feldspar (sanidine), augite, pigeonite, quartz, titanomagnetite, ilmenite, fayalite, and accessory zircon and apatite (Figure 1). Previous investigations (e.g. Honjo et al., 1992; Perkins & Nash, 2002) favored relatively high pre-eruptive temperatures (900-1000°C) and low fO_2 (~QFM) and aH_2O for CPT magmas. Recent studies on rhyolitic airfall glasses (Cathey and Nash, 2004) confirm high temperature storage conditions over long periods implying the existence of a dynamically evolving magma reservoir that was chemically and thermally zoned and periodically recharged, leading to successive eruptive units.

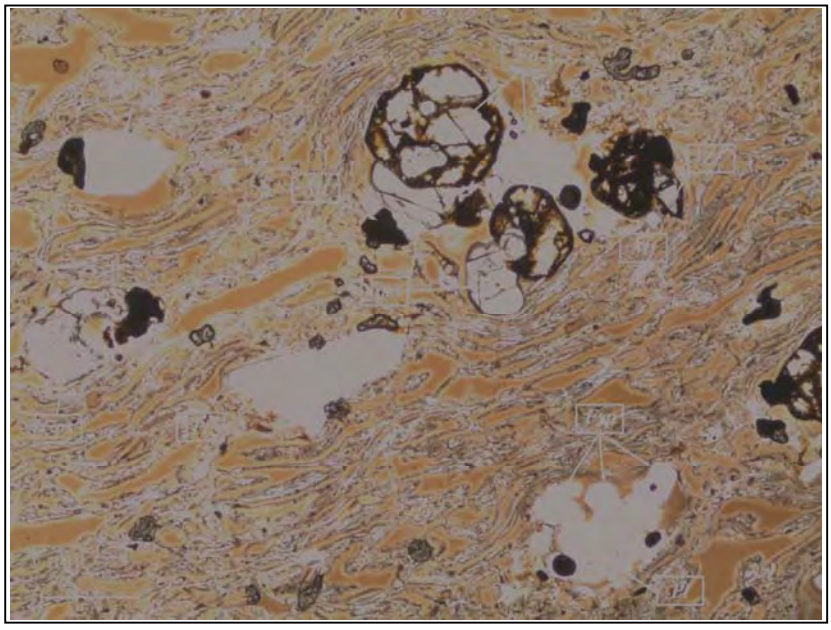

Fig. 1. Photomicrograph of the Cougar Point Tuff ignimbrite (sample BJR-4, Unit 9j, after Cathey and Nash, 2004) showing typical phenocryst assemblage: plagioclase (Pl), feldspar (Fsp), clinopyroxene (Cpx), quartz (Qtz), fayalite (Fa), titanomagnetite (Mt) and accessory zircon (Zr). Pigeonite and ilmenite (not shown) were also found in this sample. The sample was used in crystallization experiments as a starting material.

Crystallisation experiments

We investigated phase relations in the rhyolitic ignimbrite BJR-4 (Fig. 1) from the Cougar Point Tuff, Bruno-Jarbidge eruptive center (Unit 9j after Cathey and Nash, 2004). The starting glass was prepared from the powder of whole-rock rhyolitic ignimbrite by two-times fusion at 1600 °C and 1 atm in air. The major element composition of the obtained glass was determined by electron microprobe (N=60; in wt %): 73.55 ± 0.31 (SiO_2), 0.46 ± 0.04(TiO_2), 11.81 ± 0.14 (Al_2O_3), 3.92 ± 0.23 (FeO_{total}), 0.07 ± 0.06 (MnO), 0.23 ± 0.03 (MgO), 1.12 ± 0.07 (CaO), 2.34 ± 0.12 (Na_2O), 6.13 ± 0.08 (K_2O), 0.10 ± 0.06 (P_2O_5), 0.28 ± 0.09 (BaO). Crystallization experiments were performed at 200 MPa in cold seal pressure vessel (CSPV) at temperatures 800 and 850°C, and in internally heated pressure vessel (IHPV) at temperatures 900, 950 and 1000°C. The water activity (aH_2O) of the experimental charges was varied by adding a fluid composed of a mixture of H_2O and CO_2. Experimental charges at dry conditions were prepared without adding H_2O and CO_2. In CSPV the oxygen fugacity was monitored by adding a solid Ni-NiO oxygen buffer (NNO). In IHPV all experiments were conducted at intrinsic oxygen conditions, corresponding to the NNO+2.6 oxygen buffer under H_2O-saturated conditions and ~QFM at (nominally) dry conditions. The run duration varied with temperature: 14 to 25 days for runs at 850 and 800°C, and 7 to 21 days for runs at 1000 and 900°C. Results of these crystallization experiments are summarized in the Fig. 2, where phase relations for rhyolite BJR-4 are shown as a function of

temperature and water concentration in the residual melt (H_2O^m, in wt %). The water concentrations in the experimental glasses have been determined using infrared spectroscopy (FTIR). For FTIR, the linear absorbance of the band at 3500 cm^{-1} was determined using a tangential background correction. The H_2O concentrations were calculated using a molar absorptivity (ε) of 67 L/mol·cm for ε_{3500} (Stolper 1982) and the Lambert Beer's Law (for details on the apparatus and procedure used, see e.g., Behrens and Stuke 2003). The density of the glass was estimated using a density–water content relationship proposed by Ohlhorst et al. (2001). The reproducibility of the method is always better than 5% relative. Karl-Fischer titration (Behrens and Stuke, 2003) was also adopted for samples with low crystal contents and high water concentration. The uncertainty of the KFT analyses is less than ± 0.1 wt % H_2O (absolute value). The composition of the run products were characterized by electron microprobe (Cameca SX100). The data for the crystalline phases and glasses were acquired with an accelerating voltage of 15 kV / 15 nA and 15 kV / 4 nA, respectively. Counting times for Na and K were 5 s for minerals and 2 s for glasses. For the other elements, the counting times were 10 s for minerals and 5 s for glasses. For glasses, the beam size was defocused to 10 - 20 μm.

Fig. 2. Phase relations for composition BJR-4 as a function of temperature and water concentration (wt %) in the melt (H_2O^m). Symbols represent experimental charges and stable mineral phases at given run conditions. Stability curves are labeled with mineral names; the fields of stability are always to the left of the curves. Mineral abbreviations are similar to those in Figure 1. Note the change of oxygen conditions in experimental runs as a function of H_2O concentration in residual melt. The shaded zone bracket the experimental crystallisation where the

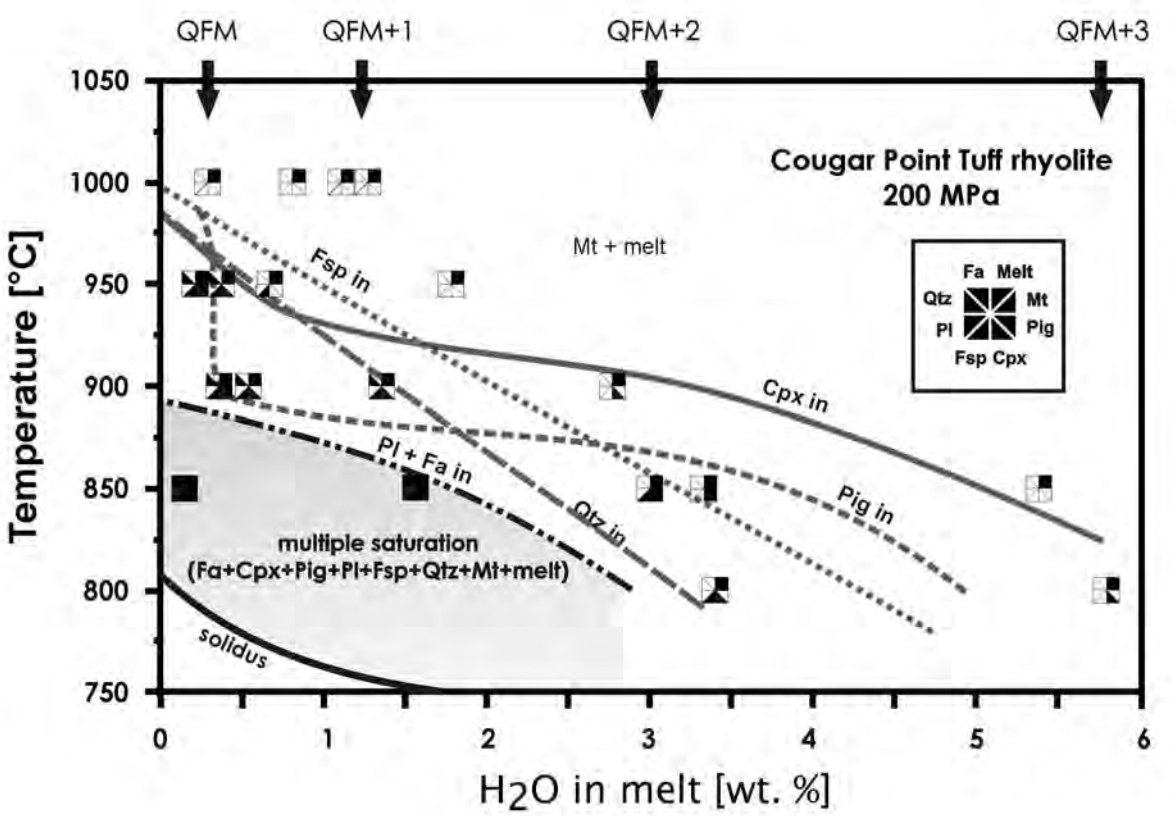

maximal number of mineral phases have been reproduced (multiple saturation). These conditions can be interpreted as pre-eruptive conditions of the natural rhyolitic ignimbrite BJR-4 (Fig. 1).

At 1000°C rhyolitic melt was coexisting with magnetite in the range of all studied melt H_2O concentrations. With decreasing temperature magnetite was followed by the crystallization of sanidine up to ~ 1 wt % H_2O^m. In nominally dry run (< 0.5 wt % H_2O^m) at 950°C and in the runs with H_2O^m < 1.4 wt % at 900°C quartz and pigeonite and clinopyroxene were observed. Fayalite and plagioclase were stable at temperatures below 900°C and H_2O^m < 1.5-2.0 wt %. In these two experimental runs (T=850°C, H_2O^m = 0.3 wt %, H_2O^m = 1.5 wt %) the maximum number of minerals was crystallized corresponding to multiple saturation conditions of the investigated rhyolite composition.

Interpretation of results

The phase relationships determined experimentally can be used to bracket the conditions of crystallization of natural CPT rhyolitic magmas. The natural mineral assemblage Pl+Fsp+Cpx+Pig+Mt+Qtz±Fa in the studied sample (Fig. 1) was experimentally reproduced only in the runs with low water concentration in the melt (< 1.5 wt%) at a temperature of 850°C. The low water contents required in our experiments to reproduce natural mineral association of the CPT rhyolite are in agreement with previous ideas (Honjo et al., 1992; Perkins & Nash, 2002; Cathey and Nash, 2004) on the nearly anhydrous character of the SRPY silicic magmatism. However, from the results at 200 MPa in this study, the temperature at which the natural mineral assemblage is reproduced (conditions of multiple saturation in CPT rhyolite) can not be higher than 900 °C,

contradicting with the relatively high (950-1000°C) pre-eruptive temperatures obtained as a result of mineral thermometry in previous studies (Honjo et al., 1992; Cathey and Nash, 2004). The main probem to reproduce the high temperatures predicted from geothermometry is the absence of plagioclase in the phase asemblage at such conditions, even at nearly dry conditions.

There are different possible explanations for the discrepancy between data from geothermometry and from the experimental dataset. It is possible that part of the mineral assemblage is not in equilibrium with the magma. In this case plagioclase would be inherited from another source (e.g., low temperature magma tapped during ascent) or the mineral assemblage could result from a mixture of different portions of magmas in a chemically and thermally zoned magmatic reservoir. On the other hand ilmenite which is present in some of the natural rocks has not been reproduced in our experiments, indicating that the experimental conditions may be too oxydizing. A change of the redox conditions may affect the stability of magnetite, which would in turn affect the stability field of clinopyroxene and plagioclase. Preliminary calculations and data obtained for other compositions show that the stability of pigeonite is strongly dependent on oxygen fugacity at low water concentrations.

Further objectives

Rhyolites: the conditions at which the Cougar Point Tuff rhyolites have been generated is a priority in the research program. It appears extremely important to check if the temperature of the rhyolites is as high as postulated in previous studies. The experimental conditions will be varied to check (1) if pressure may play a role (experiments are in progress at 500 MPa, and it is already clear that pressure influences strongly the pyroxene and quartz stability fields), (2) to which extent the oxygen fugacity influences the stability of ferromagnesian phases and of plagioclase and (3) to which extent small compositional changes of the bulk composition may affect the plagioclase stability field. Dissolution experiments are also in progress to check if kinetic problems may have affected the crystallization of plagioclase and other phases at low water contents (the crystallization kinetics are slow in such water-poor rhyolitic melts). Prof. B. Nash is going to visit Hannover for a sabbatical period of several months (2 to 4 months, depending on a submitted proposal for financial support) and the experimental strategies will be discussed with her. We also plan to use the recently proposed Ti-in-quartz thermometer and try to calibrate it for the investigated compositions.

Basalts: Considering that the heat source for rhyolite generation is related to the emplacement of basalts in the lower crust, we also planed to determine the magma storage conditions of some basaltic eruptions of the SRPY. The COMAGMAT program was used to evaluate crystallization conditions of the McKinney basaltic suite, a composite unit, covering nearly 300 km^2 in the Snake River Plain (Leeman and Vitaliano, 1976). We performed a series of fractional crystallization calculations along the QFM oxygen buffer using a primitive sample s72-3B as starting composition with various initial H_2O contents. The results of these calculations indicate that a polybaric fractionation must be assumed and that differentiation may have occurred up to a depth of 200 MPa. Thus basaltic magma chambers may have been located at this depth in the crust. Calculations of the conditions of crystallization for the Crater of the Moon basalts (Leeman et al., 1976) and the Graveyard Point differentiated mafic intrusion (White, 2007) are in progress in cooperation with J. Shervais and E. Christiansen.

Behrens, H., and Stuke, A. (2003) Quantification of H2O contents in silicate glasses using IR spectroscopy - a calibration based on hydrous glasses analyzed by Karl-Fischer titration. Glass Science Technology, 76(4), 176-189.

Cathey, H.E., and Nash, B.P. (2004) The Cougar Point Tuff: Implications for Thermochemical Zonation and Longevity of High-Temperature, Large-Volume Silicic Magmas of the Miocene Yellowstone Hotspot. Journal of Petrology, 45(1), 27-58.

Honjo, N., Bonnichsen, B., Leeman, W.P., and Stormer, J.C. (1992) Mineralogy and Geothermometry of High-Temperature Rhyolites from the Central and Western Snake River Plain. Bulletin of Volcanology, 54(3), 220-237.

Ohlhorst, S., Behrens, H., and Holtz, F. (2001) Compositional dependence of molar absorptivities of near-infrared OH- and H2O bands in rhyolitic to basaltic glasses. Chemical Geology, 174(1-3), 5-20.

Leeman, W.P., and Vitaliano, C.J. (1976) Petrology of Mckinney-Basalt, Snake-River-Plain, Idaho. Geological Society of America Bulletin, 87(12), 1777-1792.

Leeman, W.P., Vitaliano, C.J., and Prinz, M. (1976) Evolved Lavas from Snake-River Plain - Craters of Moon-National-Monument, Idaho. Contributions to Mineralogy and Petrology, 56(1), 35-60.

Perkins, M.E., and Nash, B.P. (2002) Explosive silicic volcanism of the Yellowstone hotspot: The ash fall tuff record. Geological Society of America Bulletin, 114(3), 367-381.

Stolper, E.M. (1982) Water in silicate glasses: an infrared spectroscopic study. Contributions to Mineralogy and Petrology, 81, 1-17.

White, C.M. (2007) The Graveyard Point Intrusion: an Example of Extreme Differentiation of Snake River Plain Basalt in a Shallow Crustal Pluton. Journal of Petrology, 48(2), 303-325.

Quaternary vegetation and climate dynamics inferred from palaeoecological records of the El'gygytgyn permafrost core

A.A. ANDREEV

Alfred Wegener Institute for Polar and Marine Research Telegrafenberg A43, D-14473 Potsdam, Germany

The planned proposal focuses on long-term palaeoenvironmental reconstructions from a 140 m permafrost core from the El'gygytgyn Impact Crater (NE Siberia). The drilling in the frame of the ICDP funded project (ICDP-01/05) occurred in November 2008 provides an excellent opportunity to obtain a unique record of palaeoenvironmental evolution in NE Siberia. Of particular interest is vegetation and climate history inferred from frozen deposits. Such deposits are an excellent archive providing the basis for palaeoenvironmental reconstructions on local and regional scales. The preliminary data show that the crater lake sediments currently represent the longest terrestrial archive for the Siberian Arctic. The permafrost core study will provide highly valuable data from the El'gygytgyn catchment reflecting environmental dynamics. The sediments will be studied mainly for pollen and non-pollen-palynomorphs. Pollen is a primary source of palaeoenvironmental information archived in the Quaternary sediments, which is easy to extract and study. Other found bio-remains (non-pollen-palynomorphs, plant macrofossils, rhizopods, and chironomids) will be studied to compliment the pollen results. The results will play a key role in the long-term regional to global-scale palaeoenvironmental reconstructions syntheses and in data-model comparisons, which can be viewed as scenarios of future climate changes.

Paleoenvironmental Evolution of the Baltic Sea through the Last Glacial Cycle

T. ANDREN[1], S. BJÖRCK[2], J. HARFF [3], J. B. JENSEN[4], B. B. JØRGENSEN [5], A. KOTILAINEN[6]

[1]School of Life Sciences, Södertörn University, SE-141 89 Huddinge, Sweden
[2]Geobiosphere Science Center, Quaternary Sciences, Lund University, Sölveg. 12, 223 62 Lund, Sweden.
[3]Leibniz-Institute for Baltic Sea Research Warnemünde / Szczecin University, Seestr. 15, D-18273 Rostock, Germany
[4]Geological Survey of Denmark and Greenland, Øster Voldgade 10, DK-1350, Copenhagen K, Denmark
[5]Aarhus University, Nordre Ringgade 1. DK-8000 Aarhus C, Denmark
[6]Geological Survey of Finland, P.O.Box 96, 02151 Espoo, Finland

The Baltic Sea Basin hosts high resolution sedimentary records of the Last Glacial Cycle. Coring the sediments and a multi-proxy based interpretation of its litho- and biostratigraphy and sedimentary facies would increase our knowledge and understanding of the environmental and climatic development in respect to (1) the transition from glacial to interglacial periods and vice versa, and its regional driving forces, (2) periodicities in Fennoscandian Ice Sheet dynamics and its possible feedback to the North Atlantic meridional overturning circulation (MOC), (3) varved Holocene BSB sediments as detailed archives of changes in Holocene atmospheric circulation patterns, including variations in the Arctic Oscillation (AO) and the North Atlantic Oscillation (NAO), and (4) influence of glacial/interglacial change on microbial communities. A full proposal for a Baltic Sea drilling initiative within the frame of the IODP program is being prepared by a team of scientists from Denmark, Estonia, Finland, Germany, Latvia, Lithuania, Poland, Russia, and Sweden.

Ocean floor metasomatism re-examined: insights from thermodynamic modeling

W. BACH[1], F. KLEIN[1], N. JÖNS[1]

[1]Fachbereich Geowissenschaften, Universität Bremen, Klagenfurter Str., 28359 Bremen

One of the great benefits of ocean drilling is the recovery of rocks that are unaffected by seafloor weathering so that the phase relations established during hydrothermal alteration are preserved. We use thermodynamic reaction path models coupled with detailed petrographic characterization to gain insights into the formation of metasomatic rocks recovered by ocean drilling (see list of recent references). In this paper we focus on the formation of rodingites and steatites at mafic/ultramafic boundaries.

Rodingites: The computations were set up to investigate the shifts in fluid-rock equilibria as fluids move from peridotite undergoing serpentinization into a gabbroic body. Phase relations were investigated in the direction of increasing extent of reaction of the serpentinization fluid with gabbro at 200°C, 300°C, and 400°C. Phase assemblages typical of rodingite (grossular+diopside±chlorite) are predicted to form at 200°C and 300°C, but only in areas where the fluid is essentially unaffected by reactions with gabbro, i.e, near the contact with ultramafic rock or adjacent to a fissure filled with serpentinization fluid. As the fluid becomes more affected by reactions with the gabbro, prehnite or epidote-ss replace garnet, while tremolite replaces clinopyroxene. Once the fluid chemistry is completely reset by reactions with gabbro, the predicted assemblage is typical of greenschist facies: albitic plagioclase, actinolite, chlorite, and epidote-ss. These transitions predicted in the model are very similar to what is observed in natural rodingites recovered by ocean drilling in different settings. Our model results hence support the hypothesis that rodingites form during serpentinization and only in areas where fluids

controlled by serpentinization reactions are present. Mass transfer of Ca is likely by diffusion of the $CaOH^+$ species, which is predicted to show a very steep concentration gradient across a mafic-ultramafic boundary. Rodingitization is most likely a result of diffusional metasomatism. The activity gradients in pore waters equilibrated with ultramafics on one side and mafics on the other is greatest in protons and silica. The activity gradient in Ca^{2+} is virtually nil. Diffusive mass transfer of Ca into the rodingite is likely related to diffusion of hydroxo species. Ca is not added to the rock by large fluxes of infiltrating Ca-bearing solutions. On the contrary, large fluid fluxes are likely to wipe out the steep activity gradients required to drive rodingitization and will result in whole sale depletion of Ca from the system.

Steatites: Steatitization is another common metasomatic process near the contact of mafic and ultramafic lithologies. Here serpentinite is turned into talc and both dynamic and static recrystallization of serpentinite to talc have been reported from ultramafic massifs in the oceans. Talc appears in blackwalls at the contact to small (<10 m) gabbroic units, but steatite is also formed by static replacement of serpentinite by talc, which starts along anastomosing vein networks and continues to pervasive steatitization, during which the serpentine hourglass texture is preserved. Thermodynamic reaction path models suggest that olivine is stable at T>350°C and that hydration of pyroxenes imposes high silica activities to the fluids. Low aqueous silica activities can only develop at temperatures <<350°C, in particular when fluid pH is high due to the hydrolysis of olivine. Brucite-bearing serpentinite as well as rodingite are expected to form under those conditions. Steatitization, in contrast, requires high silica activities so is inconsistent with peridotite-seawater interactions at T<350°C.

We propose two possible explanations for the variability in phase relations at mafic-ultramafic contacts. (1) They are a result of the variable proportions of mafic and ultramafic lithologies, where one dominates the fluid composition, or (2) they are a consequence of the temperature-dependent reaction sequences taking place along the fluid flow path. Examining the CMASH system (i.e., gabbro) phase relations along with the MSH system (i.e., peridotite) phase relations in activity–activity and temperature–activity diagrams provides some plausible answers for the extreme variability in the reaction pathways. At T<300°C, the fluid interacting with peridotite will be buffered by serpentine-diopside-brucite. Encountering gabbroic rocks, this fluid will transform the gabbro into rodingite, composed of diopside, grossular, and chlorite. In contrast, at T around 400°C, the fluid interacting with peridotite is buffered by tremolite, serpentine, and talc; it will transform gabbro to talc and tremolite. The same phase relations reveal that any serpentine interacting with fluids that are controlled by interactions with gabbro should turn into talc. Indeed, talc is common in serpentinite at the contact with gabbroic dikes that are not fully altered and do not show assemblages characteristic of rodingite. Serpentinite in contact with rodingite, on the other hand, never exhibits talc-alteration. Furthermore, brucite is absent in immediate contact with rodingite, unless the rodingite is entirely composed of diopside and garnet.

Bach W, Klein F (2008) Petrology of rodingites: Insights from geochemical reaction path modeling, *Lithos*, doi:10.1016/j.lithos.2008.10.022

Jöns N, Bach W, Schroeder T (2008) Formation and alteration of plagiogranites in an ultramafic-hosted detachment fault at the Mid-Atlantic Ridge (ODP Leg 209), *Contribution to Mineralogy and Petrology* doi:10.1007/s00410-008-0357-2

Klein F, Bach W (2009) Fe-Ni-Co-O-S phase relations in peridotite-seawater interactions, *Journal of Petrology*, doi:10.1093/petrology/egn071

McCollom TM, Bach W (2008) Thermodynamic constraints on hydrogen generation during serpentinization, *Geochimica et Cosmochimica Acta* doi:10.1016/j.gca.2008. 10.032

Colorado Plateau Coring Project (CPCP): 100 Million Years of Climatic, Tectonic, and Biotic Evolution in Continental Cores

G. H. BACHMANN[1], R. BLAKEY[2], J. GEISSMAN[3], D. KENT[4], W. KÜRSCHNER[5], P. OLSEN[6], J. SHA[7]

[1]Institut für Geowissenschaften, Martin-Luther-Universität Halle-Wittenberg, Von-Seckendorff-Platz 3, D-06120 Halle (Saale), gerhard.bachmann@geo.uni-halle.de
[2]Northern Arizona University, Flagstaff, [3]University of New Mexico, Albuquerque, [4]Rutgers University, Piscataway, NJ, [5]Utrecht University, NL [6]LDEO, Columbia University, Palisades, NY, [7]Chinese Academy of Sciences, Nanjing

The goal of the CPCP is to recover the complete Triassic and Jurassic section of this classic area to decipher the climatic, biotic, and tectonic evolution of western equatorial to temperate Pangea and derivative Laurasia. Cores will provide quintessential continuous reference sections placing 100 million years of climatic, biotic, and tectonic evolution into a more precise and globally relevant chronostratigraphic and paleogeographic context. The drilling concept is to obtain three long (~1 km) cores and two shorter cores. The drilling areas were chosen to optimize the quality of data from the stratigraphic record for geochronologic, paleoclimatic, and tectonic analyses of the critical Early Mesozoic transitions in clear superposition. The end result of the CPCP will be a synoptic view, in appropriate geochronologic context, of one of the largest and arguably most data-rich epicontinental basins in the world. A first planning CPCP Workshop with 45 international researchers was held in St. George, Utah in November 2008. The next Workshop with the goal of forming an international science team is planned on May 8–11, 2009 in Albuquerque, New Mexico. Central to the project are hypothesis-driven questions that require a scientific drilling experiment to answer: 1) What are the global or regional climate trends vs. plate position changes in “hot house” Pangea and subsequent Laurasia? 2) How do largely fluvial systems respond to cyclical climate change? 3) What are the rates and magnitudes of the transition from the Paleozoic to essentially modern terrestrial ecosystems? 4) How does the stratigraphy of the basin sections reflect the interplay between spatially dynamic growth in accommodation space, uplift, and eustatic fluctuations in this epicontinental basin? Some of the further scientific outcomes of the CPCP are expected to be: 1) The highest attainable resolution magnetic polarity stratigraphy for the Triassic and Jurassic

epicontinental sediments on the Colorado Plateau which is essential for regional and especially global chronostratigraphic correlations to other continental (e.g., Newark basins, Germanic basin) as well as marine (e.g., Tethyan) sections; 2) Refinement of the paleogeography, particularly changes in paleolatitude, of western Pangea during the Triassic and Jurassic and the relationship to the expression of paleoclimate in the sedimentary record, especially the apparent aridification in the Triassic and Early Jurassic; 3) Comparison of this well-calibrated paleoclimate record against other parts of Pangea for tests of climate models; 4) Refinement of lithostratigraphic and biostratigraphic correlations, including pinning down the ages and extents of proposed regional unconformities and their possible relationship to eustatic fluctuations; 5) Development of a chemostratigraphic reference section for the American Southwest for the early Mesozoic; 6) Developing a sufficiently detailed stratigraphic framework to establish teleconnections between the Colorado Plateau sedimentary record and rifting of Pangea, the emplacement of the Central Atlantic Magmatic Province, and the opening of the Atlantic Ocean, and other large igneous provinces, notably the Karoo-Ferrar and possibly the Siberian traps.

Abrupt millennial-scale variations in North Atlantic surface-water circulation (ODP Site 980) during the last 20,000 years as revealed by coccolithophorid assemblages

K.-H. BAUMANN[1], H. MEGGERS[1], J. HOLTVOETH[2]

[1] FB Geowissenschaften, Univ. Bremen, Postfach 330440, D-28334 Bremen, Germany, baumann@uni-bremen.de
[1] FB Geowissenschaften, Univ. Bremen, Postfach 330440, D-28334 Bremen, Germany, meggers@uni-bremen.de
[2] Dept. Earth & Ocean Sciences, University of Liverpool, UK, holtvoeth@liverpool.ac.uk

A coccolith-based micropalaeontological investigation of ODP Site 980 from the Feni contour drift of the northern North Atlantic was conducted in order to reconstruct the pattern and timing of surface circulation changes in the area during the last 20,000 years. In addition, sea-surface paleotemperature records from both sites were generated at high resolution based on the widely used alkenone paleothermometer.

It is a well-established fact that millennial-scale climatic shifts occurred repeatedly in most parts of the northern hemisphere during the last glacial period (e.g., Bond et al., 1993). These repetitive climatic instabilities at millennial and orbital time scales resulted in rapid oscillations in the atmospheric temperature over Greenland in the order of 5-10°C and associated fluctuations of ~4°C in surface-water temperature (SST) in the northern ocean (e.g., Bond et al., 1993; Oppo et al., 2003). A number of North Atlantic records confirm that the beat of millennial-scale climate variability continued through the last Deglacial and the Holocene (e.g., Bond et al., 2001; Oppo et al., 2003), notably at times at the same magnitude as during full glacial conditions.

The down-core variation in coccolith assemblage composition indicate that changes in properties of surface waters in the northern North Atlantic occurred stepwise during the Termination I. Sparse occurrences of coccolithophores before about 16,000 yrs BP indicate harsh environmental conditions and a relatively massive influence of melt-water. The following successive increase in absolute numbers of coccolithophores in the whole area indicates an increasing influence of North Atlantic Drift water till about 10,500 yrs BP.

High coccolith numbers are observed in the early Holocene, which coincide well with maximum Northern Hemisphere summer insolation, although not all of the observed species respond to the increased insolation. However, Site 980 seems to be furthermore influenced by drastic, short-termed variations in productivity. In particular, successive decreases in the numbers of coccolithophores, and in particular of *E. huxleyi* as previously described by Giraudeau et al. (2000), demonstrate that advection of cool, possibly ice-bearing waters from the Greenland-Iceland Seas to the North Atlantic occurred throughout the Holocene. These events correspond well with previously described ice-rafting episodes during the Holocene (Bond et al., 2001).

Superimposed on this, another successive cooling of the surface waters, accompanied by an increase in perturbations of the surface hydrology during the last ca. 5000 yrs is documented by changes in the total numbers of the species and is also reflected by a change in the relative abundances of the dominant coccolith species. In particular, the numbers of the cold-adapted species *Coccolithus pelagicus* increased considerably after about 5000 yrs BP. These long-term reorganisations of the surface hydrology are interpreted as the response of the North Atlantic to the combined forces of the solar insolation and the waning Laurentide ice sheet.

Bond, G., Broecker, W. S., Johnsen, S., McManus, J. F., Labeyrie, L., Jouzel, J., and Bonani, G. (1993). Correlations between climate records from North Atlantic sediments and Greenland ice. Nature 365, 143-147.

Bond, G., Kromer, B., Beer, J., Muscheler, R., Evans, M. N., Showers, W., Hoffmann, S., Lotti-Bond, R., Hajdas, I., and Bonani, G. (2001). Persistent solar influence on North Atlantic climate during the Holocene. Science 294.

Dansgaard et al., 1993

Giraudeau, J., Cremer, M., Manthe, S., Labeyrie, L., and Bond, G. (2000). Coccolith evidence for instabilities in surface circulation south of Iceland during Holocene times. Earth and Planetary Science Letters 179, 257-268.

Oppo, D. W., McManus, J. F., and Cullen, J. L. (2003). Deepwater variability in the Holocene epoch. Nature 422, 277-278.

San Andreas Fault system: Implications for the structure and dynamics from lithospheric electrical conductivity

ICDP project ELSAF (ELectrical conductivitiy structure of the San Andreas Fault)

M. BECKEN[1], O. RITTER[1], P.A. BEDROSIAN[2], U. WECKMANN[1,3], G. MUNOZ[1]

[1] Helmholtz Centre Potsdam - German Research Centre for Geosciences (GFZ), Telegrafenberg, Potsdam, 14473, Germany
[2] US Geological Survey, MS 964, Box 25046, Bldg 20 Denver Federal Center, Denver, CO 80225, United States
[3] University of Potsdam, Institute of Geosciences, Karl-Liebknecht-Strasse 24, Potsdam, 14476, Germany

Deep non-volcanic tremor (NVT) has been observed SW of the San Andreas Fault Observatory at Depth (SAFOD), where the San Andreas Fault (SAF) zone changes its mechanical behavior from creeping farther north to being locked farther south (Nadeau and Dolenc, 2005). Recent seismological array observations confirm a depth range of approximately 30-50 km for the NVT but suggest that the source region is offset from the surface trace of the SAF by about 15 km to the SW. The cause of NVT at transform faults is not fully understood yet (to date), but it has been suggested that fluids play an important role in their genesis. Electrical conductivity is highly sensitive to the presence of fluids and/or partial melts. The only geophysical technique capable of probing the earth at lower crustal and upper mantle depths for its electrical conductivity structure is the magnetotelluric (MT) method.

Over the last four years we deployed in a series of three large field experiments (DeepRoot - ICDP/GFZ/NSF funded, TremorMT – GFZ-funded and ELSAF – ICDP/GFZ funded) more than 250 MT sites to study the deep roots of the SAF, to image deep structural 'along-strike' variations of the transitional segment of the SAF near Parkfield, and to image for the first time the source region of NVTs with MT. The initial DeepRoot experiment focused on the crustal structure in the vicinity of the SAFOD, while the TremorMT and ELSAF experiments extended the DeepRoot measurements to a more regional scale covering the entire transitional segment of the fault, including the SAFOD to the NW and the source region of NVT near Cholame to the SE. In total, we measured seven profiles covering 130 km across-strike and 60 km along-strike. In early 2009, our onshore profiles have been extended offshore in a collaborative research effort with our colleagues from Scripps Institution of Oceanography, UCSD.

Two-dimensional inversion of land MT data along profiles across the transitional-to-creeping segment of the SAF reveal a sub-vertical channel connecting a high conductivity region in the upper mantle and lower crust with the upper-crustal, brittle deformation zone of the SAF. We interpret this high conductivity as a zone where fluids can migrate into the SAF system (Becken et al., 2008). Interestingly, the crustal fluid channel is absent at the transitional-to-locked segment of the SAF. Along the locked segment, the zone of high mantle conductivity correlates with the source region of NVT. We speculate that these observations could be related with a confined region of locally trapped fluids at mantle depth. Depending on the permeability state of the crust, fluid migration and pressure release into the SAF system may only be possible where the fault exhibits creep. This release of fluids finds its expression in a sub-vertical channel of high conductivity and generally low or lacking tremor activity. Whether this along-strike variability in the deep hydraulic system depends on or controls the changing dynamics of the SAF is an open question.

Another interesting observation is a lateral correlation between the upper mantle conductor, 20-60 km offset to the W from the surface expression of the SAF, and the axis of Coast Range heat-flow anomaly. The latter defines a 50-100 km wide zone where heat flux is significantly higher than background values and where dissipative shear heating in combination with a "slab window effect" has been suggested to occur at upper mantle depths (e.g. Lachenbruch and Sass, 1981). As high temperatures are often the explanation for high electrical conductivity this could imply a common source for both observations in the upper mantle. This would have important implications for the dynamics of the SAF. The conductive zone in the mantle could be associated with a broad zone of ductile deformation caused by shear-heating along a lower-crustal or sub-crustal detachment zone. This detachment could represent the southwesterly offset ductile root of the SAF. For the transitional-to-creeping segment of the SAF, the sub-vertical zones of high electrical conductivity appear to directly link the deep detachment zone with the brittle SAF system in the upper crust, "lubricating" the SAF by providing a continuous supply of mantle derived fluids.

Becken, M.; Ritter, O.; Park, S. K.; Bedrosian, P. A.; Weckmann, U.; Weber, M., 2008. A deep crustal fluid channel into the San Andreas Fault system near Parkfield, California, Geophysical Journal International, 173, 2, 718-732.

Lachenbruch, A.H., and Sass, J.H. 1980. Heat flow and energetics of the San Andreas fault zone, *J. Geophys. Res.*, v. 85, 6185-6222.

Nadeau, M. N., and Dolenc, D., 2005, Nonvolcanic Tremors Deep Beneath the San Andreas Fault. *Science*, *307*, *389*.

Ocean-continent interactions during mid Cretaceous Oceanic Anoxic Events in the western tropical Atlantic

B. BECKMANN[1], D. BIRGEL[2], J. ERBACHER[1], A. LÜCKGE[1]

[1]Federal Institute for Geosciences and Resources, Stilleweg 2, 30655 Hannover, Germany (Britta.Beckmann@bgr.de)
[2]MARUM Center for Marine Environmental Sciences, University of Bremen, Organic Geochemistry Group, PO Box 330440, 28334 Bremen, Germany

The mid Cretaceous represents one of the most prominent episodes of greenhouse climate with high atmospheric CO_2 levels, much higher global temperatures (including a lack of permanent ice caps at the poles) and lower latitudinal temperature gradients than today. During this "super-greenhouse", massive and widespread deposition of organic carbon occurred during several oceanic anoxic events (OAEs). The OAEs are associated with significant turnover within numerous biotic groups and prominent shifts in carbon isotopes and thus represent major disturbances in the ocean system and the global carbon cycle. As such, OAEs played a fundamental role in the evolution of Earth's climatic and biotic history. In the past, research on the dynamics of the mid Cretaceous greenhouse world was almost exclusively based on marine proxy data, while upt to now, only few information is available on environmental dynamics and atmosphere/biosphere interactions in terrestrial settings.

We investigate two sites (1258 and 1260), drilled approx. 350 km off Suriname at the Demerara Rise during ODP Leg 207, recovering 56 and 96 m thick sequences of late Albian to Santonian sediments (Erbacher et al. 2004). These black shales were deposited in a proximal position relative to the tropical South American mainland and provide the unique opportunity to link terrestrial environmental information with a wide range of marine paleoclimatic and paleoceanographic proxy data, thus allowing a direct land/sea correlation. One of our goals is to trace runoff variations and terrestrial climate change during the late Albian to early Turonian in general and during exceptional paleoceanographic events, including the estimation of terrigenous input to the Demerara Rise. Further on, we will test the model of arid climates and saline bottom water formation in the tropical Atlantic during the late Cenomanian as proposed by Friedrich et al. (2008) and investigate linkages between marine paleotemperatures and terrestrial climate. This project allows us to estimate changes in large-scale hydrology and evaluate consequences for the accumulation of organic-rich sediments. Here we show first results from our multi-parameter study along a stratigraphic splice from the mid Cenomanian to early Turonian, covering two exceptional paleoceanographic events, the OAE2 and the Mid Cenomanian Event (MCE) which is smaller in magnitude and is characterized by double spike in $\delta^{13}C_{org}$ values. Friedrich et al (2008) suggest the MCE as being an important paleoceanographic turning point towards lower bottom-water oxygenation in the proto-North Atlantic Ocean based on a high-resolution study of benthic foraminiferal faunas and stable carbon and oxygen isotopes of planktic and benthic foraminifers.

Our working strategy combines XRF-core scanning with microscopic investigation (maceral analysis), biomarker analysis and subsequently determination of isotopic composition of specific terrestrial organic compounds (long-chain *n*-alkanes derived from plant waxes). Samples from the investigated interval cover a large range of total organic carbon (TOC) concentration, the organic material proves to be thermally immature. For the OAE2, values vary between approx. 1.5 % TOC after the maximum isotope excursion and approx. 23 % TOC within the maximum excursion; the amount of extractable organic matter (OM) varies between 1 mg OM/g sediment before the OAE2 and 19 mg OM/g sediment within the maximum isotope excursion at site 1258 and fluctuates between 1mg OM/g sediment and 31 mg OM/g sediment at site 1260 (strikingly, the peak value occurs before the onset of the OAE2).

Our current focus is on samples from the MCE, which are characterized by generally lower organic carbon variability compared to samples from the Cenomanian/Turonian boundary. At site 1258, values lie around 6% TOC before the MCE, rising to approx. 10% right before the begin of the isotope excursion and maximum values of 14 % TOC within the event, leveling off around 10 % TOC after the MCE (see Fig. 1). Carbonate and TOC content do not correlate in the investigated interval. During the MCE, organic carbon content somewhat follws the $\delta^{13}C_{org}$ values (data from Friedrich et al., 2008), however no correlation is observed when the entire investigated interval is taken into account. The $\delta^{13}C_{org}$ signal shows background values of approx. –29.3 ‰ with maximum values during the MCE of – 27.3‰. The amount of extractable organic matter varies between 3 mg OM/g sediment and 13 mg OM/g sediment, well within the range of OAE2 values. Based on our XRF-core scanning results, we suggest that all major terrestrial elements (Potassium, Zirconium, Titanium, Aluminium) derive from one source, possibly with the exception of Silicium, which could represent additional input of biogenous silicate into the sediment. Only a slight co-variation can be observed between redox-sensitive elements such as Zinc and Molybdenum, and Sulfur. While the overall pattern is somewhat comparable, the intensities of shifts are not, nor do the detected intensities of the redox-sensitive elements correlate with TOC content.

At site 1260, background values are around 6-7 % TOC with maxima reaching 18 % TOC during the isotope excursion. The shift in the isotope signal is much stronger than at site 1258; values rise from –28.5 ‰ before the MCE to –24 ‰ during the initial phase of the event and return to background ratios of approx. –28.5 ‰ (Friedrich et al.; 2008); according to their data, onset and first maximum excursion of the carbon isotopes occured some thousand years earlier than at site 1258. The amount of extractable organic matter fluctuates between 4 mg OM/g sediment and 12 mg OM/g sediment, generally slightly lower values and showing smaller variability than at site 1258. XRF-core scanning results display a good to very good correlation between all major terrestrial elements (including Silicium), it appears that all these elements derive from one source. No correlation can be observed among redox-sensitive elements, nor do they correlate with Sulfur or Iron. There is, however, a correlation between Sulfur and TOC content (r^2=0.73) suggesting that at least some Sulfur might be fixed as sulfurized organic matter.

Judging from XRF data, site 1260 might have been under a considerate influence from terrestrial input and the development of anoxia appears to have been of less importance. First results from maceral analysis support the impression of relatively high contribution of terrigenous OM to site 1260. Additionally to the high amount of amorphous marine OM, either as cloudy mass or as spherical aggregates and frequent algal remnants, samples from the MCE at site 1260 display some vitrinites and inertinites as well as sometimes large bituminites. Framboidal pyrites seem to be less frequent in samples from site 1260 than from site 1258, but pyrites are mostly restricted to microenvironments such as foraminifer shells at both sites. in general

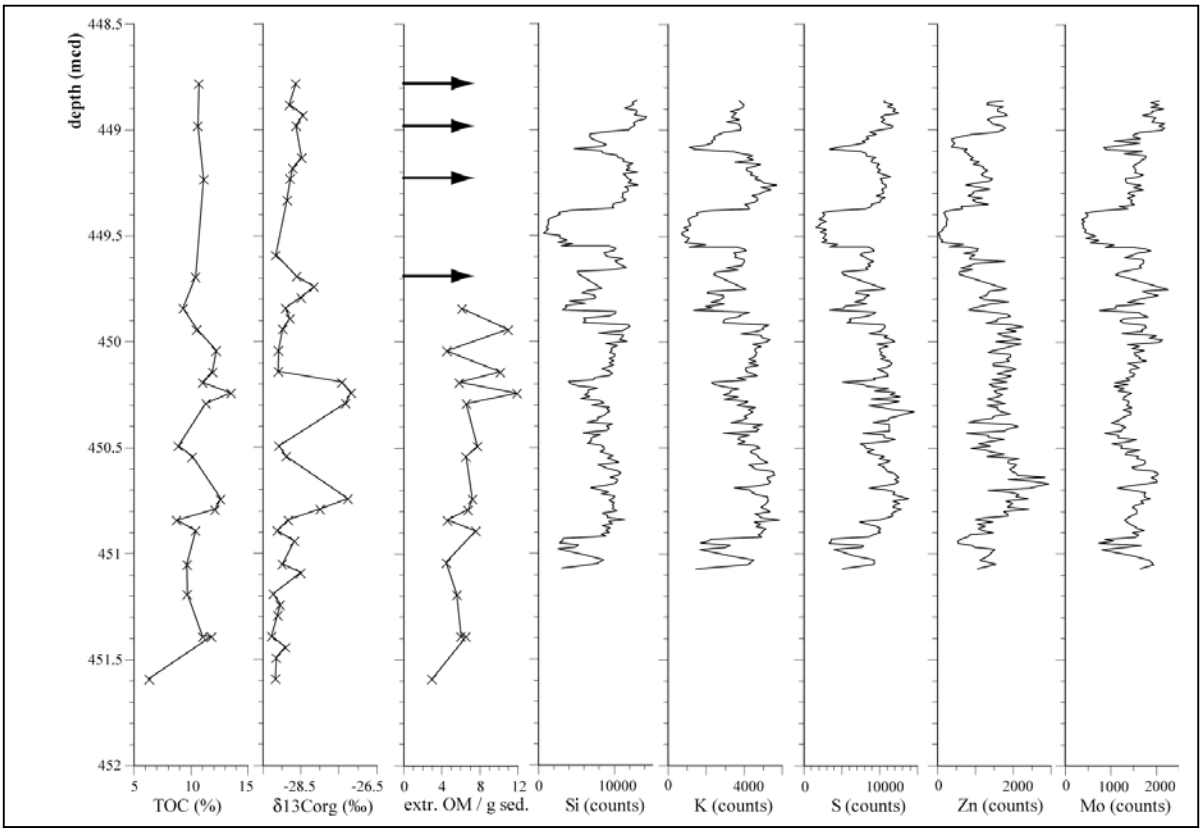

Figure 1: Organic carbon and XRF-core scanner data from mid Cenomanian at ODP Site 1258 (1258A46R1-3). Isotope values taken from Friedrich et al. (2008); mcd is meters composite depth, extr. OM/g sed. is extracted organic matter (mg) per g sediment, elements from XRF-core scanner are reported in counts; arrows indicate biomarker samples without extract weight was determined. Significant drop in all elements around 449.5 mcd is related to strong increase in Calcium counts, representing a carbonate-rich layer.

Along with maceral analysis, biomarker investigations are currently in progress. First biomarker results allow the identification of samples showing an almost exclusive marine distribution pattern of molecular markers as well as samples with a considerate input of terrigenous organic matter into the sediment. The latter are particularly suited for our anticipated molecular-isotopic approach to investigate carbon and hydrogen isotope signatures of plant wax lipids. Bulk $\delta^{13}C_{org}$ values from Friedrich et al (2008) imply an earlier onset and first maximum at the shallower site 1260, however, this might be due to some variations in compostion of the bulk organic matter between both sites. We therefore anticipate to use compound-specific carbon isotope data to possibly help to identify if the begin of the MCE isotope excursion occurred at the same time at sites 1258 and 1260. Where possible, we intend to determine hydrogen isotopes of the plant wax lipids. Especially long chain n-alkanes are preferred for Deuterium/Hydrogen (D/H) investigation because they behave isotopically conservative (Schimmelmann et al., 2006). Photosynthetic organisms are useful for monitoring changes in the hydrological circulation over time as they utilize water as main hydrogen source; deuterium concentration in the source is generally reflected by the deuterium composition of the organism. While moisture-loss leads to deuterium enrichment in plants and soil-waters become deuterium-enriched by evaporation under arid conditions (Sauer et al., 2001), D*H* values from leaf waxes reflect the balance of precipitation and evaporation and thus allow to address changes in runoff variations and changes in the hydrological cycle. We currently prepare samples for carbon and hydrogen isotope measurements and will compare the resulting isotope ratios with first counting data from maceral analysis.

Erbacher, J., Mosher, D. C., Malone, M.J. et al. (2004): Proceedings of the Ocean Drilling Program, Initial Reports, 207, College Station, TX (Ocean Drilling Program)

Friedrich, O. , Erbacher, J., Moriya, K., Wilson, P.A., Kuhnert, H. (2008): Warm saline intermediate waters in the Cretaceous tropical Atlantic Ocean. Nature Geoscience, 1, p. 453-457.

Sauer, P.E., Eglinton, T.I., Hayes, J.M., Schimmelmann, A., Sessions, A.L. (2001) : Compound-specific D/H ratios of lipid biomarkers from sediments as a proxy for environmental and climatic conditions. Geochimica et Cosmochimica Acta, 65, 213-222.

Schimmelmann, A., Sessions, A.L., Mastalerz, M. (2006) :Hydrogen isotopic (D/H) composition of organic matter during diagenesis and thermal maturation. Annual Review of Earth and Planetetary Science, 34, 501-533.

Identification of vertical convection in boreholes - preliminary results for the KTB-MH

S. BERTHOLD, F. BÖRNER

DGFZ Dresdner Grundwasserforschungszentrum e.V., Meraner Str. 10, 01217 Dresden, Germany

Vertical convections in the fluid column of boreholes can cause transport of heat and mass (Börner and Berthold 2009). Strong convective flow within the fluid column may adversely affect water samples. Gases, as well as other substances are possibly transported into new depths, where varying chemical processes may arise. So, knowing about the existence of vertical flows in fluid columns is important for hydrological investigations (e.g. determining points of in- and outflow) and for borehole geophysics (e.g. finding leakages in casings).

Furthermore, temperatures in fluid columns that are subject to vertical convection may depart significantly from the ones in the surrounding rock. Thus, understanding convective flow within the borehole is also crucial for geothermics and subsurface water movement investigations (e.g. determining reliable rock thermal properties and heat-flow densities using temperature profiles).

The main objective of this research project is the further development of an interpretation method for the detection, differentiation and quantification of such vertical flows in deep boreholes. The interpretation method to adapt was developed in an earlier project which dealt with the investigation of vertical convections in groundwater monitoring wells (Berthold and Börner 2008).

Besides the well-known forced convection, the project's focal point is especially the detection of free convection with its various density-driven transport processes and their differentiation. Outcome of the interpretation method is a so-called Synthetic convection log that is based on two independent algorithms. One allows for the detection of causes (driving forces) and the other one for the detection of effects (free convection or double diffusion) of vertical transport processes based on geophysical borehole measurements (temperature and fluid conductivity). The combination of both algorithms improves the reliability of the interpretation.

The application of the new interpretation method to deep boreholes is presented here based on preliminary results for the KTB main hole (KTB-MH).

In the KTB-MH combined temperature and electrical conductivity measurements were conducted in October 2008. Due to equipment-related limitations (cabel length) maximum measurement depth was 525 m below surface. The probe was lowered with a velocity of 2 m/min using a sampling interval of 1 cm. As regards the KTB-MH, such high-resolved temperature and electrical conductivity measurements were conducted for the first time.

Analysis of the measurement data concerning density-driven vertical flows revealed that at measurement time the entire investigated fluid column of the KTB-MH was subject to free convective flow. The existence of revolving flows was confirmed by both interpretation algorithms: cause- and effect-oriented interpretation. According to the Synthetic convection log, the main part of the fluid column is influenced by thermosolutal convection. That means temperature as well as salinity gradients have a destabilizing effect resulting in a distinct, intensive flow. Based on the analysis it can be assumed that a constant upward directed heat flow and a constant downward directed salt flow exist in the investigated part of the fluid column. To what extent the heat flow induced in the borehole affects, for example, the determination of reliable heat flow densities of the surrounding rock formation, remains to be clarifyed. However, this is beyond the scope of the project.

The KTB-borehole and the infrastructure of the KTB-field laboratory were provided by the Helmholtz Centre Potsdam GFZ German Research Centre for Geosciences.

Berthold S., Börner F. (2008): Detection of free vertical convection and double-diffusion in groundwater monitoring wells with geophysical borehole measurements, *Environmental Geology* 54(7), S. 1547-1566, DOI: 10.1007/s00254-007-0936-y.

Börner F., Berthold S. (2009): Vertical flows in groundwater monitoring wells, In: Kirsch, R. (ed.), *Groundwater Geophysics – A Tool for Hydrogeology*, 2nd ed., Springer-Verlag, Berlin, Heidelberg, S. 367-389.

Monsoonal impact on the Maldives carbonate platform (ODP Site 716)

C. BETZLER[1], J. FÜRSTENAU[1], C. HÜBSCHER[2] & T. LÜDMANN[3]

[1]Institute of Geology and Paleontology, University of Hamburg, Bundesstr. 55, 20146 Hamburg, Germany
[2]Institute of Geophysics, University of Hamburg, Bundesstr. 55, 20146 Hamburg, Germany
[3]Institute of Biogeochemistry and Marine Chemistry, University of Hamburg, Bundesstr. 55, 20146 Hamburg, Germany

The Maldives archipelago in the Indian Ocean is among the world's largest carbonate platforms. The platform is the remnant of a much larger bank, which underwent partial drowning during the time interval from the late Miocene to the early Pliocene, and has a unique geometry with a double row of atolls enclosing the Inner Sea with water depths of up to 500 m. To the Inner Sea side atolls are lined by active giant drift bodies. It is hypothesized, that the Maldives are a current-controlled carbonate platform and that its geometry is directly linked to the oceanographic setting. This implies that the platform deposits probably represent an excellent archive of the climatically-induced Cenozoic palaeoceanographic evolution.

The overall goal of this study is to develop a model for the evolution of a carbonate platform controlled by the monsoon. This will be achieved by an interdisciplinary analysis of ODP Site 716, involving sedimentological, geophysical, micropaleontological, and geochemical methods. The rationale for this goal arises from geophysical, hydroacoustic and piston core data acquired during Meteor Cruise M74/4 in December 2007. The aquired data set questions the hypothesis of a pure sea-level control on the middle Miocene to Recent platform evolution (e.g. Belopolsky and Droxler, 2004) revealing a strong impact of monsoonal triggered currents on platform evolution, beginning at latest during the late Miocene.

One focus of the research will be on the answer of the question of how sea-level changes and currents impacted and interacted on the carbonate platform during the past 7 Myrs. It will be addressed by a sedimentological re-description and sampling of ODP Site 716 (holes A and B), and a correlation of the lithostratigraphy and sedimentology with Meteor cruise M74/4 PARASOUND data and seismics, given for the first time a high resolution and thus, the opportunity to study sedimentary geometries in detail. The proposed lithostratigraphy of ODP Site 716, which shows no significant variations for a 264 m thick succession (Backmann et al., 1988) (Initial Results, ODP Leg 115) is challenged, as new high-resolution seismics as well as existing time series indicate changes in the prevailing sedimentary regime. This comprises ceasing of migration of megadunes occurring at the toe of slope of a prograding clinoform complex during the late Miocene, which is accompanied by partial drowning of the platform, followed by flat lying deposits with several packages of submarine dunes intercalated in the younger part of the succession. The preliminary interpretation of this stratigraphic architecture is that it reflects a pronounced control of monsoon-generated bottom currents on sediment deposition.

The other research theme deals with the sedimentary cyclicity at ODP Site 716 and its relation to fluctuations in monsoonal intensity as preserved in the succession, and its periodicities through time. Deciphering of relationships will be examined through grain-size analysis, and a refining and extending of existing time series of Site ODP 716 to develop a proxy for orbital forcing which is independent of early diagenesis. The approach is based on changes in amplitude fluctuations observed in existing carbonate content time series of ODP Site 716 and on findings of piston core M74/4 1143, which is situated in mid-slope position of the giant drift body lining the leeward side, with respect to the open ocean, of a Maledivian atoll. A photospectrometric color scan, p-wave, density and laser-diffraction grain-size measurements were performed for core M74/4 1143. Grain-size distribution and derivative parameters are calculated for a sample interval of 5 cm. Down to 9 m the mud-sand ratio of core M74/4 1143 visually correlates well with glacial-interglacial periodicities estimated from lightness variations. Wavelet power spectra of a depth series of each, sediment lightness and mud-sand ratio show significant power in a *c.*320 cm band periodicity down to *c.*10 m. Weaker, *c.*130 cm and a *c.*70 cm bands are also present. It is assumed that the frequency bands observed in the depth series are related to orbital forcing, as their ratio approximates the typical milankovitch scale frequency range of 100:40:20. Most of the grain-size measurements show a bimodal grain-size distribution with modes in the 125-250 µm and in the 355-500 µm range – the latter being mostly the weaker mode. In a tentative estimation, the 125-250 µm fraction consists mainly of smaller planktic foraminifera (e.g. *Globigerinoides ruber*), pteropods and foraminifera and pteropod debris whereas the 355-500 µm fraction shows mainly well preserved larger planktic foraminifera with *Neogloboquadrina dutertrei* as major constituent of the foraminiferal assemblage. Regarding the 125-250 µm content of the fraction containing both modes, only minor power of low frequency cyclicities is preserved downcore with respect to inferred glacial-interglacial periodicities. Instead, a higher-frequency variance is observed, which is assumed to be associated with the precessional band. As *N. dutertrei* is believed to be an indicator of primary production intensity (e.g. Cayre et al., 1999) it is proposed that relative abundance rates would be a valuable proxy for monsoonal variability.

The following analyses will be performed: in-depth sedimentological analysis of ODP Site 716 cores A and B, measurements of grain-size, carbonate content, and X-ray diffractometry, as well as time series analysis. Sedimentological core data will be merged with newly acquired PARASOUND and high-resolution seismic data in order to link sedimentological changes to breaks and changes in the stratigraphic architecture.

Backman, J. et al., 1988, Proc. ODP, Init. Repts., 115: College Station, TX (Ocean Drilling Program).
Belopolsky, A.V., and Droxler, A.W., 2004, Seismic Expressions of Prograding Carbonate Bank Margins: Middle Miocene Progradation in the Maldives, Indian Ocean, Atlas on Seismic Carbonate Reservoirs: AAPG Memoir: Tulsa, OK, p. 267-290.
Cayre, O., Beaufort, L., and Vincent, E., 1999, Paleoproductivity in the Equatorial Indian Ocean for the last 260,000 yr: A transfer function

Quantification of JS-1 and Chloroflexi related bacteria in shallow and subsurface marine sediments using real-time-PCR

A. BLAZEJAK, A. SCHIPPERS

Federal Institute for Geosciences and Natural Resources (BGR), Hannover

Particular interest of the deep biosphere research is to get insights into the microbial community structure. Recent studies have shown that microbial life which is taking place in this extreme environment is widespread and is representing one-tenth to one-third of living biomass on Earth (1). To investigate what kind of different microbial phyla populate the deep subsurface molecular techniques based on the 16S rRNA gene were applied. Comprehensive 16S rRNA clone libraries from subsurface sediments show a diverse microbial community with members of distinct, uncultured bacterial and archaeal lineages. Within the domain Bacteria in particular members of to the candidate division JS-1 and the Chloroflexi have been frequently identified. Sequences of the JS-1 group were first isolated from sediments of the Japan Sea giving the group its name. Although these bacteria appear to be widespread so far no representatives of this bacterial group could be cultivated and thus their metabolisms remains unexplored. Another bacterial group that is well represented in 16S clone libraries from subsurface sediments is Chloroflexi. This phylum is a deep-branching lineage of the Bacteria and can be divided into at least five major subdivisions. In particular in the subdivision 2 sequences isolated from different subsurface sediments are frequently present. Within this subphylum only one relative, the chlorinated hydrocarbon-reducing *Dehalococcoides ethenogenes*, could be cultivated. Molecular studies based on the 16S rRNA gene clone libraries showed that bacteria of the JS-1 division and Chloroflexi subdivision 2 are widespread in subsurface sediments. But how abundant they are?

To quantify these two important bacterial groups we used the molecular technique real-time polymerase chain reaction (Q-PCR) that enables the detection of their 16S rRNA genes. Four different marine sediment stations were chosen for the analysis: deeply buried sediments from the Peru margin (Station 1227, ODP Leg 201) and sediments with depths up to 12 mbsf from the Peru margin (Station 2, SO147), the Black Sea (Station 20, M72-5), and from a forearc basin off Sumatra (Station 3 and 6, SO189-2). Sediment samples provided for molecular analysis were taken aseptically from the centre of the cores and were stored at least at -20°C till further processing in the lab. DNA was isolated from 0.5 - 4 g sediment using a minor modified FastDNA Spin Kit protocol. Quantification of the 16S rRNA gene of Bacteria in total and the bacterial groups JS-1 and Chloroflexi subphylum 2 was performed by Q-PCR (ABI Prism 7000, Applied Biosystems). The Q-PCR assay for Bacteria was carried out as previously described (2). To quantify JS-1 and Chloroflexi subphylum 2 bacteria the forward primer 519F, designed with the ARB software (www.arb-home.de), and the reverse primer 655R (3) was applied. Specific amplification of the 16S rRNA gene using this primer pair was checked with DNA isolated from Bacteria of different phyla and by cloning using the same PCR conditions as for the Q-PCR assay.

Quantification of JS-1 and Chloroflexi subphylum 2 related bacteria could be succeeded in marine sediments from all analyzed stations: on the Peru continental margin, in the Black Sea, and in the forearc basin off Sumatra (Fig. 1). At the Peru Margin two sites of different depths were investigated, surface sediment with a depth between 0 - 0.35 mbsf (SO147, site 2MC) and deeply buried sediment with a depth between 0 - 121 mbsf (ODP Leg 201, site 1227). In the surface sediment the 16S rRNA gene from the bacterial groups JS-1 and Chloroflexi subphylum 2 was detected with 10^8 - 10^7 gene copies per gram sediment which is one to one and a half order of magnitude lower than the number of the Bacteria in total. The gradient of these two profiles is almost similar to each other showing a slight decrease with depth. This data indicate that in upper sediment layers (top 35 cm) at this station the bacterial groups JS-1 and Chloroflexi subphylum 2 are present in high numbers, but they are however not a dominant group within the detected Bacteria in a total. In contrast bacteria of the JS-1 and Chloroflexi subphylum 2 and the Bacteria in total occurred in almost identical gene copy numbers in the deply buried sediment (up to 121.4 mbsf) on the Peru Margin (Fig. 1). In these sediments a nearly identical depth gradient of the 16S rRNA genes was observed. Both, gene copy numbers of the bacterial groups JS-1 and Chloroflexi subphylum 2 and of the Bacteria in total, decreased strongly within the upper 9 mbsf sediment from $2.0 * 10^7$ to $1.3 * 10^6$ and $2.7 * 10^7$ to $1.9 * 10^6$ DNA copies g^-, respectively. After a further decline to about 10^6 DNA copies g^- in the adjacent sediment layers (9 - 45 mbsf) again a strong decrease between 45 and 55 mbsf was noted. Detection of the Bacteria in a total dropped to 10^4 DNA copies g- and kept this range of magnitude up to 121 mbsf. DNA copy numbers of the bacterial groups JS-1 and Chloroflexi subphylum 2 decreased also to 10^4 DNA copies g^- at 55 mbsf but dropped further to 10^3 gene copies g^- at the depth of 75 mbsf and were not detectable below 102 mbsf. Except for depths below 75 mbsf the 16S rRNA gene from the bacterial groups JS-1 and Chloroflexi subphylum 2 was observed for most of the samples with only slightly lower or similar copy numbers than those from the Bacteria in a total indicating that these bacterial groups appear to be abundant in these sediments. A high abundance of Bacteria affiliated to Chloroflexi or to the uncultured group JS-1 in subsurface sediments from the Peru margin (Site 1227) was also observed by 16S rRNA clone library analyses (4). In the upper sediment layers (<50 mbsf) nearly 90% of clones were associated either with Chloroflexi or the uncultured group JS-1. Because no 16S rRNA clone library analyses were done in sediment layers below 50 mbsf it remained unknown if these both bacterial groups would be also frequently present in clone libraries from the deeper buried sediments. Both molecular techniques, quantification of the bacterial groups JS-1 and Chloroflexi subphylum 2 in this study using Q-PCR and 16S rRNA clone library analyses (4) argue for a high abundance of these bacteria in sediments from the Peru margin (site 1227).

To test if JS-1 and Chloroflexi affiliated bacteria occur also in high numbers in marine sediments from other locations two further stations, in a forearc basin off Sumatra, and in the Black Sea, were investigated. In the southern Bengkulu basin off Sumatra a sediment core of circa 12 m depth was taken by a piston corer together with an adjacent multi corer during the cruise 189-2 of RV Sonne. In the Black Sea eastern of Crimea a sediment core of about 6 m depth was taken by a gravity

corer during the RV Meteor cruise M72-5. At these two sites JS-1 and Chloroflexi subphylum 2 affiliated bacteria could be successfully quantified showing similar profiles along the depth (Fig. 1). In near-surface sediments gene copy numbers of these Bacteria were lower as of the Bacteria in total with up to one order of magnitude difference. Similar values of the two groups were however observed in adjacent deeper sediments, demonstrating an important role of JS-1 and Chloroflexi subphylum 2 affiliated bacteria.

The present study demonstrates that quantification of the JS-1 and Chloroflexi subphylum 2 related bacteria using a newly developed Q-PCR assay could be successfully applied to marine sediments from different locations. In near-surface sediments in particular of the Peru margin these bacteria were identified with clearly lower gene copy numbers than the Bacteria in total indicating that in these sediments JS-1 and Chloroflexi subphylum 2 related bacteria are present in high numbers but do not dominate the bacterial community. In contrast to the near-surface sediments these bacteria appear to be abundant in the bacterial community from deeply-buried sediments at various locations in the sea worldwide.

1. Whitman, W. B., D. C. Coleman, and W. J. Wiebe. 1998. Prokaryotes: the unseen majority. PNAS USA 95: 6578-6583.
2. Nadkarni, M. A., F. E. Martin, N. A. Jacques, and N. Hunter. 2002. Determination of bacterial load by real-time PCR using a broad-range (universal) probe and primers set. Microbiology 148:257-266.
3. Webster, G., R. J. Parkes, J. C. Fry, and A. J. Weightman. 2004. Widespread Occurrence of a Novel Division of Bacteria Identified by 16S rRNA Gene Sequences Originally Found in Deep Marine Sediments. Appl. Environ. Microbiol. 70:5708-5713.
4. Inagaki, F., T. Nunoura, S. Nakagawa, A. Teske, M. Lever, A. Lauer, M. Suzuki, K. Takai, M. Delwiche, F. S. Colwell, K. H. Nealson, K. Horikoshi, S. D´Hondt, and B. B. Jørgensen. 2006. Biogeographical distribution and diversity of microbes in methane hydrate-bearing deep marine sediments on the Pacific Ocean Margin. PNAS USA 103:2815-2820.

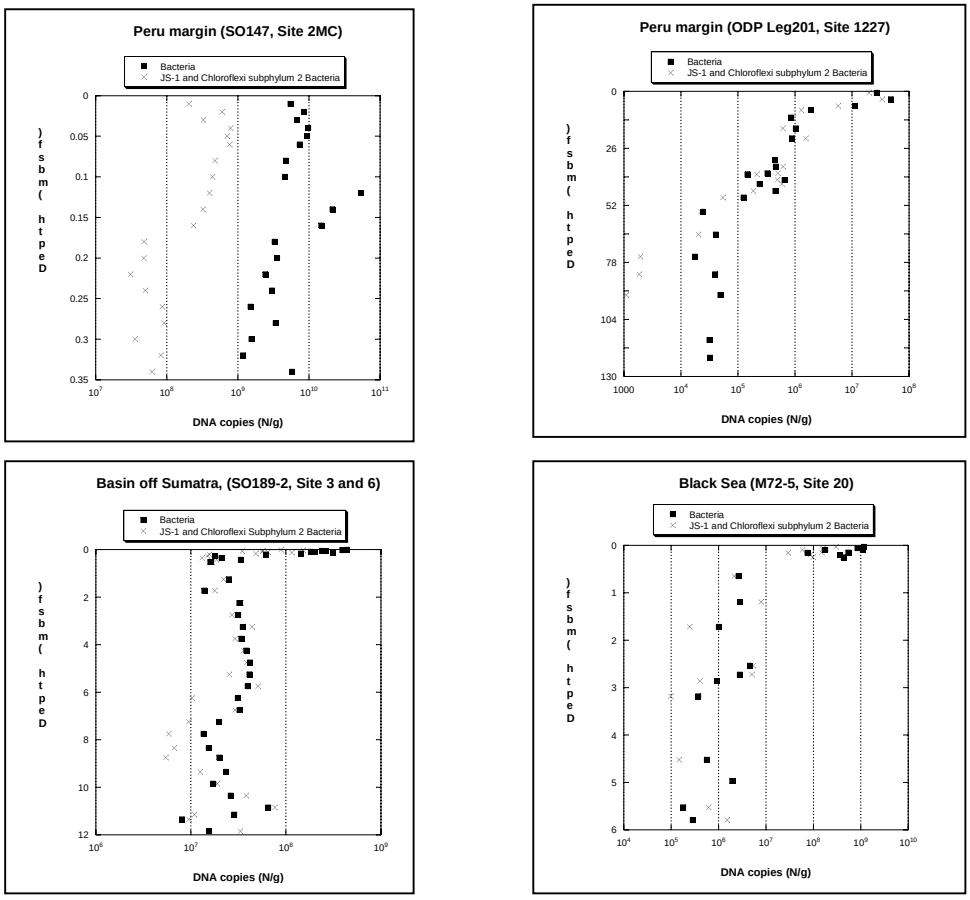

Fig.1. DNA copy numbers of the 16S rRNA genes from the Bacteria and JS-1 and Chloroflexi subphylum 2 related Bacteria in sediments from the Peru margin (ODP Leg 201 and SO147), a forearc basin off Sumatra (SO189-2), and the Black Sea (M72-5).
based on planktonic foraminifera: Quat. Sci. Rev., v. 18, p. 839-857.

Calcium Isotope Systematics of Low Temperature Alteration Carbonates in the Ocean Crust

F. BÖHM[1], A. EISENHAUER[1], S. RAUSCH[2], W. BACH[2], A. KLÜGEL[2]

[1]Leibniz-Institut für Meereswissenschaften, IFM-GEOMAR, Wischhofstr. 1-3, D-24148 Kiel, Germany
[2]Fachbereich Geowissenschaften, Universität Bremen, Klagenfurter Str. 2, D-28359 Bremen, Germany

During low temperature alteration of the ocean crust calcium carbonate is precipitated, mainly as calcite and aragonite cements filling vugs, veins and vesicles. Estimates of the $CaCO_3$ concentration in altered ocean crust (Alt & Teagle 1999) indicate that the Ca flux from seawater into the basaltic crust represents about 10% of the total calcium ouput flux from the oceans. Calcium isotopes can be strongly fractionated during precipitation of low temperature $CaCO_3$ minerals (Amini et al. 2008). Therefore, the low temperature alteration (LTA) carbonates may represent a significant factor in the global ocean calcium isotope budget. Calcium carbonate minerals in altered ocean crust are probably mostly transported to the upper mantle during subduction (Kelley et al. 2005). On very long time scales this flux may therefore lead to a Ca isotope fractionation between the Earth's crust and mantle.

We collected basement samples from DSDP and ODP drill cores from the Atlantic and Pacific Oceans (Sites 332, 333, 335, 395, 396, 407, 409, 417, 418, 597, 801, 1149, 1224). We measured Sr/Ca and Mg/Ca concentration ratios, $\delta^{18}O$, $\delta^{13}C$, $^{87}Sr/^{86}Sr$ and $\delta^{44/40}Ca$ of aragonite, calcite and dolomite powders collected from the core samples with a hand-held microdrill. Elemental ratios were measured by ICP-OES with a precision of 5% and 3% (2 rsd) for Mg/Ca and Sr/Ca, respectively, based on repeated measurements of standards. Oxygen and carbon isotopes were analyzed on a Finnigan MAT 252 equipped with a Kiel II device. Reproducibility for $\delta^{18}O$ and $\delta^{13}C$ is ±0.06‰ (2sd). Values are reported relative to V-PDB. Formation temperatures for the carbonate samples were estimated from $\delta^{18}O$ using calibrations of Friedman & O'Neil (1977) for calcite and Böhm et al. (2000) for aragonite and assuming isotopic equilibrium with seawater with a $\delta^{18}O$ of -0.5 ‰ (V-SMOW) for samples younger than 15 Ma and -1 ‰ (V-SMOW) for all older samples. Dolomite $\delta^{18}O$ values were corrected for acid fractionation (-0.8 ‰, Sharma & Clayton, 1965) and a dolomite-calcite fractionation of -2.6 ‰ (Vasconcelos et al. 2005). Strontium and calcium isotope compositions were determined by thermal ionisation mass spectrometry (TIMS) with a Finnigan Triton TI. The Sr isotope standard NIST SRM987, normalized to a $^{86}Sr/^{88}Sr$ ratio of 0.11940, was measured with a $^{87}Sr/^{86}Sr$ ratio of 0.710216(14) (2sd, n=15). The measured $^{87}Sr/^{86}Sr$ ratios were corrected to a SRM987 value of 0.710248 to allow direct comparison with the Strontium Isotope Stratigraphy (McArthur & Howarth 2004). Basement ages for all sites were compiled from the published magnetostratigraphic and biostratigraphic age data and converted to the GTS04 timescale (Gradstein et al. 2004) for comparison with the strontium isotope stratigraphy ages. Calcium isotopes were measured with a double spike technique (Heuser et al. 2002, Tang et al. 2008) and are reported as $\delta^{44/40}Ca$ relative to the standard NIST SRM915a.. All Ca isotope samples were at least measured two times. Average precision for $\delta^{44/40}Ca$ was ±0.13‰ (2 sem) based on repeated measurements of samples.

A comparison between the $^{87}Sr/^{86}Sr$ ratios of our samples and the strontium isotope stratigraphy of McArthur & Howarth (2004) allows to estimate the formation ages of the LTA carbonates (Fig. 1). The basement age of each site represents the maximum age for the formation of the respective LTA carbonates. We calculated Sr isotope residuals, i. e. the differences between the seawater $^{87}Sr/^{86}Sr$ ratio at the time of basement formation and the sample $^{87}Sr/^{86}Sr$ ratio (Fig. 1). Most residuals are positive, indicating that the LTA carbonates formed significantly later (up to 20 Ma) than the basement (Fig. 1). This interpretation is based on the reasonable assumption that no significant input of Sr with an isotope signature more radiogenic than seawater occurred at these mid ocean sites. Any Sr input from rock alteration would be less radiogenic than seawater as mid ocean basalts have $^{87}Sr/^{86}Sr$ ratios of about 0.7035 (Palmer & Edmond 1989). Some sites show negative residuals (Fig. 1), pointing to input of strontium from the ocean crust. However, only one sample shows a $^{87}Sr/^{86}Sr$ residual $<-4.10^{-4}$. The latter value corresponds to a crustal influence on the order of 5-10% (Amini et al. 2008). The Sr isotope ratios therefore point to only minor input of mantle Sr and a predominance of seawater as the source for strontium and probably also for calcium. This interpretation is further corroborated by the generally low formation temperatures of the carbonates, which are close to bottom water temperatures for most sites (Fig. 2). In addition carbon isotope values of most samples lie in the normal marine range (0.5 to 3.9 ‰; average $\delta^{13}C$ of calcite 1.7 ‰, of aragonite 3.4 ‰).

Calcium isotope values show a very large variation with $\delta^{44/40}Ca$ ranging from -0.7 ‰ to 1.8 ‰. The site averaged mean value is 1.1 ‰. The $\delta^{44/40}Ca$ values do not depend on the depth of formation in the basement. There is a negative correlation with temperature and a clear dependence on the crystal structure (Fig. 2). Aragonite has $\delta^{44/40}Ca$ values between -0.7 and +0.3 ‰. Calcite shows values between 0.9 and 1.8 ‰. The isotopic aragonite-calcite offset is in good agreement with the observations of Gussone et al. (2005) and Amini et al. (2008). The negative temperature correlation, however, disagrees with published observations.

Comparing $\delta^{44/40}Ca$ with $^{87}Sr/^{86}Sr$ residuals (Fig. 3) shows that calcites with negative residuals, which indicate input of Sr and Ca from basement rocks, generally have lower $\delta^{44/40}Ca$ values (average $\delta^{44/40}Ca$ 1.1 ‰) than calcites with positive residuals (average $\delta^{44/40}Ca$ 1.6 ‰). The lower $\delta^{44/40}Ca$ may be explained by precipitation from a rock dominated fluid composition. Amini et al. (2008) measured the same mean $\delta^{44/40}Ca$ of 1.1 ‰ in high temperature calcites at ODP Site 1271. The Sr isotope ratios of these samples (0.7039, ^{87}Sr residual=-0.005) pointed to precipitation from a pure hydrothermal fluid. Compared to this, the ^{87}Sr residuals observed in our samples (> -0.0008) point to very limited basaltic influence on the Sr of our calcites, and probably also on their Ca isotope composition. Therefore the low Ca isotopic composition of these samples needs a different explanation.

As almost all of these calcites come from sites with crustal ages between 125 and 165 Ma, two other explanations are possible. First, the $\delta^{44/40}$Ca of seawater was about 0.5 ‰ lighter during this time. Second, the calcites recrystallized in a fluid with a low $\delta^{44/40}$Ca derived from overlying carbonate sediments. It was shown by Fantle & DePaolo (2007) that pore waters in deep-sea carbonate ooze adopted the Ca isotopic composition of the carbonates within a few million years. These sediments, and consequently the pore waters, typically have $\delta^{44/40}$Ca values of about 0.6 ‰. Circulation of such pore fluids through the basaltic basement could have lowered the $\delta^{44/40}$Ca of our calcites to the observed values. However, this explanation is unlikely for Site 801, where the basement is overlain by cherts and clay sediments with a very low carbonate content. A seawater $\delta^{44/40}$Ca up to 0.5 ‰ lower than modern values during the Cretaceous and Jurassic is therefore a more likely explanation and would be roughly in agreement with the observations of Farkas et al. (2007).

Only a part of the observed variations can be explained by secular changes in the Ca isotopic composition of the oceans. There is substantial variations in $\delta^{44/40}$Ca values even at sites with crustal ages of 1-10 Ma, a period of rather constant seawater $\delta^{44/40}$Ca (Griffith et al. 2008). Comparing $\delta^{44/40}$Ca of calcites from these sites with their Sr/Ca ratios we find an explanation of the variations in the growth kinetics of the crystals (Fig. 4). Tang et al. (2008) explained covariations of $\delta^{44/40}$Ca and Sr/Ca ratios in inorganic calcite by the kinetic effect of surface entrapment. Only at very low crystal growth rates the isotopic and elemental composition of a crystal approach an equilibrium with the precipitating fluid. The calcite data in Fig. 4 can be grouped in three clusters: a young cluster (>12 Ma) in the upper right, an old cluster (>120 Ma) in the lower left, and an intermediate cluster (15-30 Ma) between the two. An extrapolation of the $\delta^{44/40}$Ca - Sr/Ca trend line from Tang et al. (2008) can explain a significant part of the variation in the young cluster. Assuming that seawater $\delta^{44/40}$Ca was about 0.4 ‰ lower for the old cluster, and/or seawater Sr/Ca was lower than today, a parallel trend line can be plotted through the old cluster with a reasonable fit. As temperatures in each cluster were rather constant they had only a minor influence on calcite $\delta^{44/40}$Ca and Sr/Ca. The major controlling factor therefore was precipitation rate. The calcite samples with the highest $\delta^{44/40}$Ca and the lowest Sr/Ca can be assumed to be closest to equilibrium. This is in good agreement with the highest measured calcite $\delta^{44/40}$Ca of 1.8 ‰, which is very close to the modern seawater value (i.e. equilibrium sensu Fantle & DePaolo 2007, Tang et al. 2008). Precipitation rates of the ocean crust calcites can be estimated from the data given in Tang et al. (2008) to be in the order of $<10^{-2}$ to 10^{2} µmol/m^2/h.

In conclusion the Ca isotopic composition of calcium carbonates formed in ocean crust basalts is controlled by the mineralogy, by growth rate and by the isotopic composition of the pore fluids. The latter probably at least partly reflects the $\delta^{44/40}$Ca of contemporaneous seawater. The $\delta^{44/40}$Ca values of the calcites are very high compared to biogenic carbonates: the average $\delta^{44/40}$Ca is 1.6 ‰ for Cenozoic LTA calcite compared to 0.6 ‰ for average modern biogenic carbonates. Aragonite shows lower $\delta^{44/40}$Ca values, but was found only at a few sites. Therefore LTA carbonates represent a sink for heavy Ca isotopes, both with respect to the land-ocean calcium cycle and to the crust-mantle Ca exchange.

Alt J.C., Teagle D.A.H. (1999) *Geochim. Cosmochim. Acta*., **63**, 1527-1535
Amini M., Eisenhauer A., Böhm F., Fietzke J., Bach W., Garbe-Schönberg D., Rosner M., Bock B., Lackschewitz K. S. , Hauff F. (2008) *Geochim. Cosmochim. Acta*, **72**, 4107-4122.
Böhm F., Joachimski M. M., Dullo W. C., Eisenhauer A., Lehnert H., Reitner J., Wörheide G. (2000) *Geochim. Cosmochim. Acta*, **64**, 1695–1703.
Fantle, M.S., DePaolo, D.J. (2007) *Geochim. Cosmochim. Acta*, **71**, 2524-2546.
Farkaš J., Böhm F., Wallmann K., Blenkinsop J., Eisenhauer A., van Geldern R., Munnecke A., Voigt S., Veizer J. (2007) *Geochim. Cosmochim. Acta*, **71**, 5117-5134.
Friedman I., O'Neil J. R. (1977) *Geol. Surv. Prof. Pap*. **440**–KK. US Govt. Printing Office.
Gradstein F., Ogg J., Smith A.(2004) A Geologic Time Scale 2004, 589p, Cambridge University Press, Cambridge.
Griffith E.M., Paytan A., Caldeira K., Bullen T.D., Thomas E. (2008) *Science*, **322**, 1671-1674.
Gussone, N., F. Böhm, A. Eisenhauer, M. Dietzel, A. Heuser, B.M.A. Teichert, J. Reitner, G. Wörheide, W.-Chr. Dullo (2005) *Geochim. Cosmochim. Acta*, **69**, 4485-4494.
Heuser A., A. Eisenhauer, N. Gussone, B. Bock, B.T. Hansen, and Th.F Nägler (2002) *Internat. J. Mass Spectr*., **220**, 387-399.
Kelley K.A., Plank T., Farr L., Ludden J., Staudigel H. (2005) *Earth Planet. Sci. Lett*., **234**, 369-383.
McArthur J.M., Howarth R.J. (2004) Strontium isotope stratigraphy. In Gradstein F., Ogg J., Smith A. (eds.) A Geologic Time Scale 2004, 96-105, Cambridge University Press, Cambridge.
Palmer M.R., Edmond J.M. (1989) *Earth Planet. Sci. Lett*., **92**, 11-26.
Sharma T., Clayton R.N. (1965) *Geochim. Cosmochim. Acta*, **29**, 1374-1353.
Tang J., Dietzel M., Böhm F., Köhler S.J., Eisenhauer A. (2008) *Geochim. Cosmochim. Acta*, **72**, 3733-3745.
Vasconcelos C., McKenzie J.A., Warthmann R., Bernasconi S.M. (2005) *Geology*, **33**, 317-320.

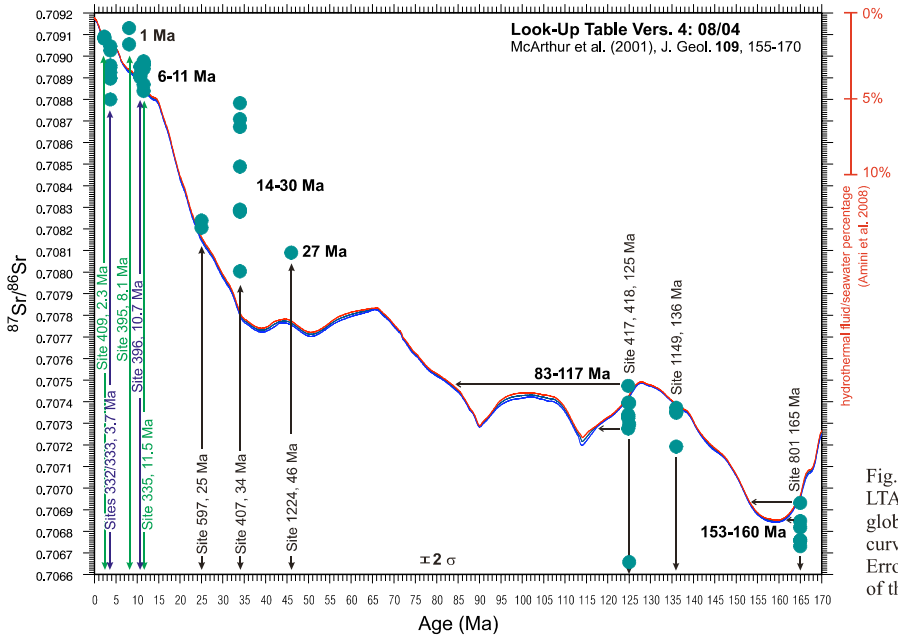

Fig. 1: Sr isotope vaules of LTA carbonates compared to global seawater $^{87}Sr/^{86}Sr$ curve (McArthur et al. 2004). Error bars are about the size of the symbols.

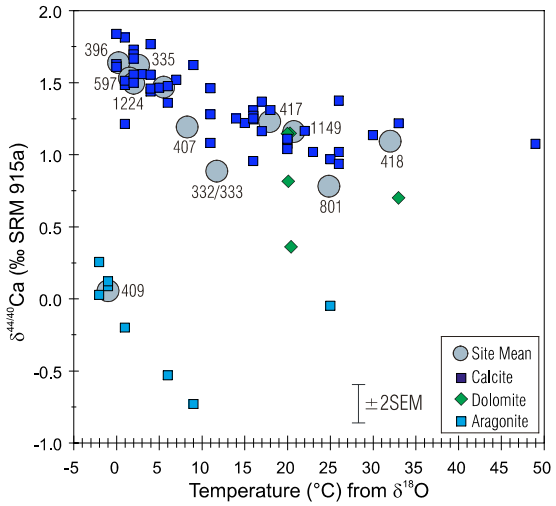

Fig. 2: Calcium isotope values of LTA carbonates and their temperature of formation calculated from $\delta^{18}O$ values.

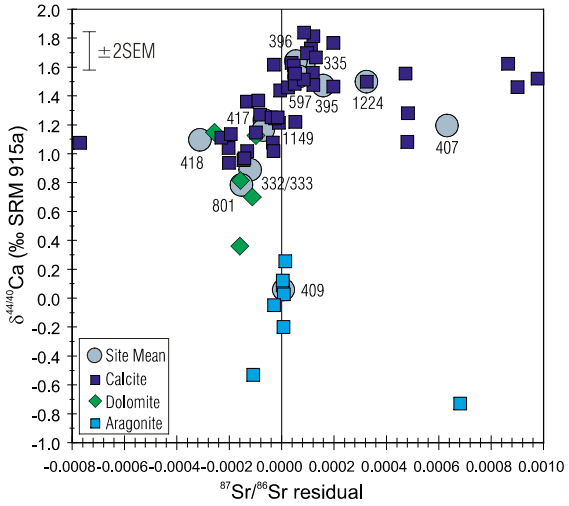

Fig. 3: Calcium isotope values of LTA carbonates and their $^{87}Sr/^{86}Sr$ deviation from seawater Sr isotope values at the time of basement formation.

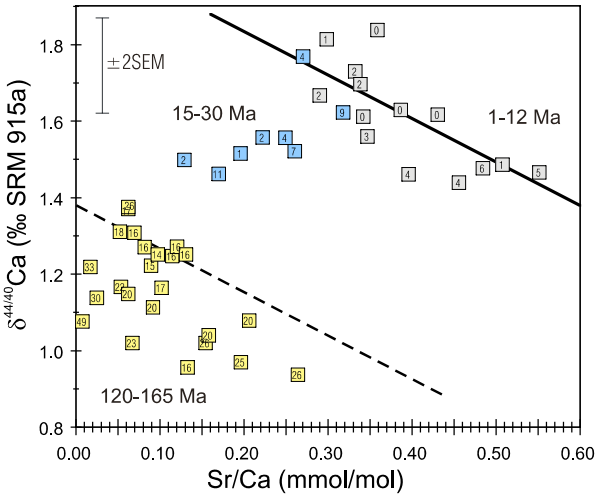

Fig. 4: Calcium isotope values of LTA calcites and their Sr/Ca ratios. Numbers in symbols are temperatures from Fig. 2. Grey, blue and yellow colours indicate the 3 age clusters described in the text. Solid trend line is the extrapolated trend from Tang et al. (2008). The dashed line is shifted by -0.5 ‰.

The Paleocene–Eocene transition in the Bay of Biscay (DSDP Site 401) – first micropaleontological and geochemical results

A. BORNEMANN

Institut für Geophysik & Geologie, Universität Leipzig, Talstrasse 35, 04103 Leipzig (E-Mail: a.bornemann@uni-leipzig.de)

DSDP Site 401 is situated on the edge of a tilted fault block, which underlies the southern edge of the Meriadzek terrace on the North Biscay margin (47°25.65'N; 08°0.62'W), and represents thereby, besides DSDP Site 550, one of the most northern locations, which provide pelagic carbonates of early and middle Paleogene age. This site has been drilled in a water depth of 2495 m (Montadert et al., 1979), while the paleo-water depth for the Eocene has been estimated at ~1800 m based on the benthic foraminiferal faunal composition (Schnitker, 1979), and consists of a nearly continuous sedimentary record through the latest Paleocene to Middle Eocene. Only in the uppermost Middle Eocene succession some larger recovery gaps occur. A 100-m-thick sedimentary succession covering the study interval is currently studied with respect to calcareous plankton assemblages (calcareous nannofossils, planktic foraminifera), and the oxygen and carbon isotopic composition of planktic and benthic foraminiferal tests.

Globally, the early Paleogene is characterized by a greenhouse climate mode, which is punctuated by at least two short-termed hyperthermal events and the longer lasting Early Eocene Climatic Optimum (EECO, peak temperatures ~51 Ma). The hyperthermal events cover the Paleocene–Eocene Thermal Maximum (PETM; ~55.5 Ma; duration: ~170 kyrs; Röhl et al., 2007) and the more recently discovered Elmo event (duration: <100 kyrs; Lourens et al., 2005), which took place about 1.8 Myrs after the PETM (Westerhold et al., 2007). In addition to these two transient warming events the number of further potential hyperthermal candidates is rapidly increasing. Whereas the PETM has been intensively studied during the last two decades only little is known about the ELMO and other similar events. Following the EECO a gradual long-term cooling commenced finally leading to the Oligocene icehouse as indicated by benthic foraminiferal oxygen isotope records (Zachos et al., 2001).

The overall aim of this study is to characterize the long-term and short-term climate variability as reflected by surface water conditions, which are recorded in the studied microfossils. At the moment only less is known about the long-term changes in the surface waters during this interval, because only few sites have been studied with respect to calcareous nannofossils and planktic foraminifera, yet. In order to achieve this goal it is intended in a first step to provide a biostratigraphic framework, in a second one to decipher the response of planktic organisms to the long-term Paleogene climate changes and finally if a further candidate for a hyperthermal event beside the PETM is recognized, this one will be studied at a higher-resolution. For the latter two steps multi-species planktic foraminiferal isotope records will be compiled for DSDP Site 401, which will supply us with information on the hydrographical situation, and compared to changes in the calcareous plankton communities.

First results provide a very detailed calcareous nannofossil biostratigraphy, which suggest that the study interval cover the biozones from NP9/CP8 to NP16/CP14a (according to Martini, 1970, and Okada and Bukry, 1980, respectively), all zones are present, although NP14/CP12 are quite condensed suggesting either very low sedimentation rates or a hiatus across the Early to Middle Eocene transition. While studying planktic foraminifera all biozones between P5 and E13 have been recognized (following Berggren and Pearson, 2005), however, the planktic foraminifera stratigraphy has not been finalized yet.

One-hundred-and-fifty samples are currently studied with respect to their content in calcareous nannofossils and benthic foraminifera, in addition geochemical parameters like TOC and $CaCO_3$ have already been analyzed. $CaCO_3$ values fluctuate strongly during the latest Paleocene and early Eocene with minima as low as 26 wt% during the PETM interval (core 14) and during the slightly below the proposed Early to Middle Eocene in core 11. Highest $CaCO_3$ values (>90 wt%) occur at NP10/NP11 boundary (core 13) and during the upper part of core 11 (lower Middle Eocene). The 70-m-thick middle Eocene succession is more uniform showing values beween 40 and 65 wt%. This interval is also characterized by an increase silica production as indicated by high abundances of radiolaria (mainly spumellaria) and diatoms in the 125 to 250 µm fraction. As expected the TOC values are very low through the entire study interval rarely exceeding 0.2 wt% without any lithogical related changes. Stable isotope (oxygen, carbon) measurements from well preserved, unfilled planktic and some benthic foraminifera (*Accarinina*, *Subbotina*, *Morozovella*, *Cibicidoides* and *Nuttallides truempyi*) is planned. A first set of latest Paleocene and Early Eocene samples is currently analyzed at the University of Erlangen.

High-resolution sampling of NP11 (core sections 13-1 to 13-3) show a well developed cyclitiy in the sediment color, which is also reflected in the $CaCO_3$ values which vary between 60 and 80 wt%. Darker, carbonate-poor horizons are also characterized by bulk-rock negative carbon isotope excursions of ~0.7 per mil and lighter oxygen isotope values, making them to potential candidates for Eocene hyperthermals. A better charaterization of this interval including the benthic fauna is currently in progress in cooperation with colleagues from the K.U. Leuven.

Berggren, W.A. and Pearson, P.N., 2005, Journal of Foraminiferal Research, 35, 279-298.
Martini, E., 1970, Nature, 226, 560.
Montadert, L. et al., 1979, Initial Reports DSDP, 48, 73-124.
Lourens, L.J. et al., 2005, Nature, 435, 1083-1087.
Okada, H. and Bukry, D., 1980, Marine Micropaleontology, 5, 321-325.
Röhl, U. et al. 2007, Geochemistry Geophysics Geosystems, 8, doi:10.1029/2007GC001784.
Schnitker, D., 1979, Initial Reports DSDP, 48, 377-414.
Westerhold, T. et al., 2007, Paleoceanography, 22, doi:10.1029/2006PA001322.
Zachos et al., 2001, Science, 292, 686-693.

RWTH Aachen University as part of the European Petrophysics Consortium (EPC)

F.P.BOSCH, R. PECHNIG C. CLAUSER

Applied Geophysics and Geothermal Energy, E.ON Energy Research Center, RWTH Aachen University

The European Petrophysics Consortium (EPC) involves three European universities performing petrophysics research, in particular, combining borehole geophysics and geology:

- Leicester (UK),
- Montpellier (France) and
- Aachen (Germany)

All three institutions have a history of involvement with ocean drilling, particularly in relation to downhole logging. The EPC central office is located at the University of Leicester and is responsible for management of the consortium. Leicester represents the EPC within ECORD (European Consortium for Ocean Research Drilling) and IODP (Integrated Ocean Drilling Programme). With the Borehole Research Group (BRG) from Lamont-Doherty Earth-Observatory (LDEO), Columbia University, NY, USA, which works within the IODP-US Implementing Organisation, EPC is part of the International Scientific Logging Consortium.

The EPC structure offers high-level scientific and technical support to the international IODP and ECORD. This comprises logging in highly variable environments drilled by the non-riser and mission specific platforms and addressing a range of scientific objectives. At each University, the EPC provides a petrophysical expertise base which is available to all scientists in the IODP:

- Development and revision of drilling proposals
- Development of tailored logging and core petrophysics programs for the expedition prospectus
- Evaluation and interpretation of petrophysical data from IODP expeditions and for scientists using legacy petrophysical data.

EPC provides ECORD Science Operator (ESO) with appropriate staff and facilities to enable and integrate all aspects of acquisition, management and distribution of petrophysical measurements from both core and downhole logging.

The institute for Applied Geophysics and Geothermal Energy, E.ON Energy Research Center of RWTH Aachen University provides equipment and staff for EPC activities concerning downhole logging measurements and interpretation as well as core analysis with Core Scanner devices. Additionally, the spatial thermal conductivity distribution can be measured with a portable contactless optical scanning system.

The work within EPC provides the consortium partners a valuable basis for academic research within IODP and additional programs.

Experimental study on evolution of gabbros from the ODP Legs 118/176 drilled at the Southwest Indian Ridge

R.E. BOTCHARNIKOV [1], J. KOEPKE [1], B. PUTLITZ [2]

[1]Institut für Mineralogie, Leibniz Universität Hannover, Callinstr. 3, 30167 Hannover
[2]Institute of Mineralogy and Geochemistry, University of Lausanne, Anthropole, CH-1015 Lausanne,Switzerland
R.Botcharnikov@mineralogie.uni-hannover.de

Gabbroic rocks from Hole 735B at the Southwest Indian Ridge (SWIR; Legs 118 and 176) represent the longest continuous section of oceanic lower crust ever drilled by ODP (Ocean Drilling Program). The drilling provides an insight into interactive processes of crustal accretion, igneous differentiation, high-temperature crystal-plastic deformation, and cooler static hydrothermal alteration of the lower ocean crust at a very slowly spreading ridge (Natland et al., 2002). About 25% of the core is strongly influenced by late-stage magmatic processes leading to Fe-rich (ferrogabbros) and Si-rich (plagiogranites) compositions as end-members. Presumably two different major processes in the little-investigated interface between igneous and hydrothermal conditions were active during the late-stage evolution of the deep SWIR crust: crystallization from a percolating Fe-Ti-rich late-stage melts and hydrous partial melting of solidified gabbro. For a comprehensive understanding of the late magmatic processes, occurring in the deep oceanic crust, we present here an approach combining three experimental subprojects focusing on natural gabbros from the ~ 1500 m long section drilled at SWIR.

A typical late-stage composition as starting material for our experiments was avaluated considering fresh Fe-Ti-rich glasses from mid-ocean ridges (MOR) which can be regarded as frozen liquids generated by late-stage MORB differentiation occurring in the eruptive sequence of the oceanic crust. For this purpose, analyses of MORB-type, fresh glasses from the "PETDB" database (Lehnert et al., 2000) from oceanic ridges all over the world were used, including all glasses from "normal" spreading centers but excluding all data from back-arc spreading centers which resulted in more than 14 000 datapoints. The late-stage composition (LS) of interest, representative for a MORB late-stage system for our experimental study, lies "at the end" of the ferrobasaltic trends with high amounts of FeO, TiO_2, and P_2O_5 (Table 1). In additon, the Si-rich composition (plagiogranite) for immiscibility experiments was evaluated as an average of 25 compositions analyzed in felsic veins from SWIR gabbro (Table 1).

Table 1. Starting late-stage compositions based on the PETDB and analyses of natural samples from SWIR.

Composition	SiO_2	TiO_2	Al_2O_3	FeO	MnO	MgO	CaO	Na_2O	K_2O	P_2O_5	S, ppm	Total
LS	49.56	3.73	11.42	17.92	0.31	3.89	8.93	2.85	0.28	0.40	2200	99.28
	0.33	0.08	0.15	0.33	0.11	0.14	0.22	0.20	0.04	0.10	0.00	
Felsic	61.61	0.92	17.16	4.04	0.09	3.09	6.03	6.54	0.30	0.16	----	99.95
	0.34	0.04	0.23	0.16	0.07	0.12	0.14	0.25	0.03	0.02		

(1) Phase relations and phase compositions in a typical late-stage system

In order to understand the late-stage processes within the deep oceanic crust, we have produced experimental data on the phase relations and liquid lines of descent in a late-stage silicate system under conditions prevailing at depth. We have conducted a phase-equilibria study in a typical LS system at 200 MPa with a special focus on the role of water, oxygen fugacity, and sulphur. The crystallization experiments were done in a range of temperatures from 850 to 1050°C and water activities (aH_2O) from 0.1 to 1 at two different fixed fH_2 (corresponding to the nominal oxygen buffers QFM+4 and QFM+1, at aH_2O=1). The main phases are magnetite (MT), ilmenite (ILM), clinopyroxene (CPX), plagioclase (PL), apatite (AP) and amphibole (AMPH). Figure 1 illustrates the differentiation trends of LS liquids in comparison with the expected differentiation of gabbro (Feig et al., 2006).

Figure1. Experimentally determined liquid lines of descent for the late-stage composition (blue circles) in comparison with the data for gabbroic composition after Feig et al., 2006 (green squares). Crosses in blue and green squares represent starting compositions of LS and gabbro, respectively. Red dashes are the compositions of melts after percolation experiments between LS melts and gabbro (see part 3).

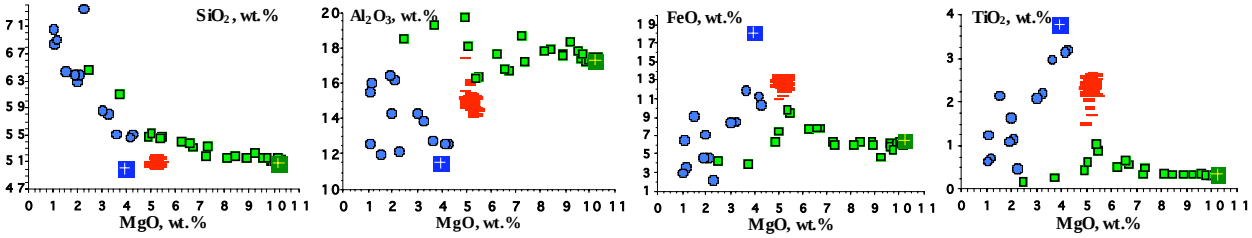

The results show that in this Fe- and Ti-rich late-stage system, Fe-Ti-oxides are the liquidus phases at both investigated redox conditions. The oxides are followed by CPX, AP and PL, which is more stable at low water activity in the system. The AP crystallizes at temperature <1000°C and its stability is almost independent on aH_2O (it must be noted that in the system with enhanced amount of phosporous >2 wt.% P_2O_5, AP is stable also at 1050°C). At reduced conditions, ILM appears at lower temperatures than CPX, whereas MT remains the liquidus phase. Amphibole is stable at high aH_2O and at temperatures

lower than 900°C, which is surprisingly low compared with the temperatures of AMPH crystallization in Fe-rich basaltic systems (i.e., <1000°C, Botcharnikov et al., 2008). The evolution of the melt composition with decreasing T and aH_2O follows in general the liquid lines of descent observed in the experiments on ferrobasaltic compositions (Toplis&Carroll, 1995; Thy et al., 2006; Botcharnikov et al, 2008) but shows trends that are significantly different from the expected trends which can be produced by cystallization of melts with gabbroic composition (Feig et al., 2006). It must be noted that orthopyroxene is not stable in all investigated Fe-rich systems at studied experimental conditions. Experiments in S-bearing system (1 wt.% bulk S) show formation of additional S-bearing phase: anhydrite (ANH) at oxidizing conditions and pyrhotite (PYR) at reduced conditions. Remarkable is that the phase stability and composition of the main mineral assemblage (MT, ILM, CPX, AP, AMPH) is not significantly affected by added S.

(2) Experimental liquid immiscibility

In the experiemental approach aimed to understand whether liquid immiscibility does occur in natural hydrous tholeiitic systems under crustal pressure we do not reveal any traces of immiscible liquids in experimental products. It must be noted, however, that recent experimental work of Veksler et al. (2007) showed that the separation of Fe-rich and Si-rich liquids might be controlled by kinetic nucleation barriers at the time-scale of laboratory experiments and coexistence of two liquids can be visible in some cases as fine emulsions at nanoscale only. Thus, although our experiments are probably unable to reproduce unmixing in natural systems, we can not exclude liquid separation occuring at the time-scale on natural geological processes in deep oceanic crust.

(3) Experimental percolation of late-stage melts through normal gabbro

It is believed that a considerable part of the deep oceanic crust at SWIR was modified by a permeable flow of late Fe-rich melts through the just solidified gabbro pile, causing both dissolution-precipitation reactions and diffusion-controlled processes in the primary mineral assemblages. We have conducted an experimental simulation of these processes, by performing percolation experiments using a synthetic LS melt and a natural "pure" microgabbro from Hole 735B. In the first run, the LS melt was pre-saturated with H_2O at 1200°C and 200 MPa in $Au_{80}Pd_{20}$ capsule. The capsule was cut in several pieces (cylinders). The H_2O-saturated cylinder of LS composition was placed under the drilled cylinder of natural gabbro and the resulting pair was closed shut in Au capsule, simulating scenario where hot gabbro interacts with H_2O-rich late-stage melt. In the second approach, the dry powder of LS was placed in the capsule, followed by ~5 wt.% bulk H_2O and finally the cylinder of natural gabbro. Such an assembladge simulated an ineraction between partly crystallized LS magma, gabbro and free fluid phase present at the interface between LS melt and gabbro. Both capsules were run at 200 MPa, 1050°C and fO_2~QFM+1 for 48 hours.

Fig 2. CT image of a product from percolation experiments: Shown are one length section (a; ca. 5 mm) and two cross sections at different heights (b, c). Three different zones are visible: (1) an inner core of unreacted gabbro; (2) a diffuse reaction zone surrounding the gabbroic core; (3) the frozen late-stage melt, now glass. Different phases can be recognized by their different gray levels.

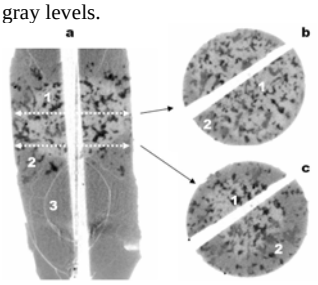

For studying the three-dimensional distribution of the percolating melt within in the host gabbro, we applied an innovative new tool: High-resolution X-ray computed tomography (CT; collaboration with L. Baumgartner in Lausanne, Switzerland). First rough CT analyses are shown in Fig. 2, further analysis with higher resolution is in progress. This method must be used before destroying the experimental product for microprobe preparation, and only after CT measurements microanalytical analysis of the involved phases can be done. The CT images show one length section and two cross sections in different heights of the cylinder; the processing of the composite 3-D computer model of the whole cylinder is in progress. Our results show three different zones: (1) an inner core of unreacted gabbro; (2) a diffuse, some hundred microns broad reaction zone surrounding the gabbroic core; (3) the frozen late-stage melt which was initially placed only at one side of the capsule and which is now surrounding the whole inner, gabbroic part of the cylinder. In the reaction zone at least four different phases can be recognized by their different gray levels. We assume that in addition to the three phases of the primary gabbro (PL, Cpx, Ol) one or more new phases, produced by melt reaction were generated. The microprobe analyses of experimental products show significant changes in the composition of the LS melts (see Fig.1) and minerals after percolation reactions. In the reaction zone PL, Ol and Cpx remain the main phases even crystallizing from the LS melt. However, the composition of new phases is different

Fig 3. Back-scattered electron image (ca. 600 μm in size) of the reaction zone between gabbro protolith and LS melt (A). The compositions of relict and new mineral phases: Olivine (B) and Plagioclase (C).

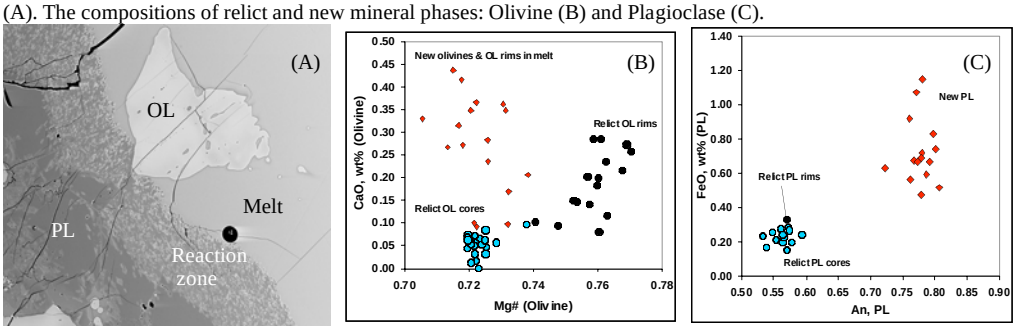

(Fig.3). New PL is enriched in Ca and Fe, new OL has higher Ca content, while Cpx is enriched in Al when compared with protolith mineral compositions. Orthopyroxene and amphibole are probably not stable at the experimental conditions. The rims of PLs from the reaction zone are composed of wide anorthite-rich zones with simplectite texture (such a zone is probably discovered as an additional phase in CT analysis). The width of the reaction rims is more than 100 μm in PL crystals and it can reach in about 30 μm Cpx crystals. The anorthite content inceases from 55 in relict PL to 80 in PL from simplectites (Fig.3C).

Additional infromation about geochemical aspects of percolation process was derived using Laser Ablation ICPMS (cooperation with K. Simon, Universität Göttingen). The dissolution/recrystallization of relict natural minerals caused exchange reactions for major elements between minerals and melt and produced a flux of trace elements from natural gabbro into a coexisting synthetic melt. We have analysed both the gabbroic minerals and reacted melts and the results are shown in Fig.4 as apparent distribution coefficients of elements for OL-melt, Cpx-melt and PL-melt pairs. Although the observed apparent values do not represent equilibrium trace element partition coefficients, they illustrate that percolation of late stage liquids through just solidified gabroic piles may significantly influence the geochemical signatures of rocks from lower oceanic crust.

Fig 4. View of the experimental products under the microscope (A) and apparent distribution coefficients of elements between gabbroic minerals and percolating late stage liquids (data obtained using LA ICPMS), (B) Ol-melt; (C) Cpx-melt and (D) Pl-melt.

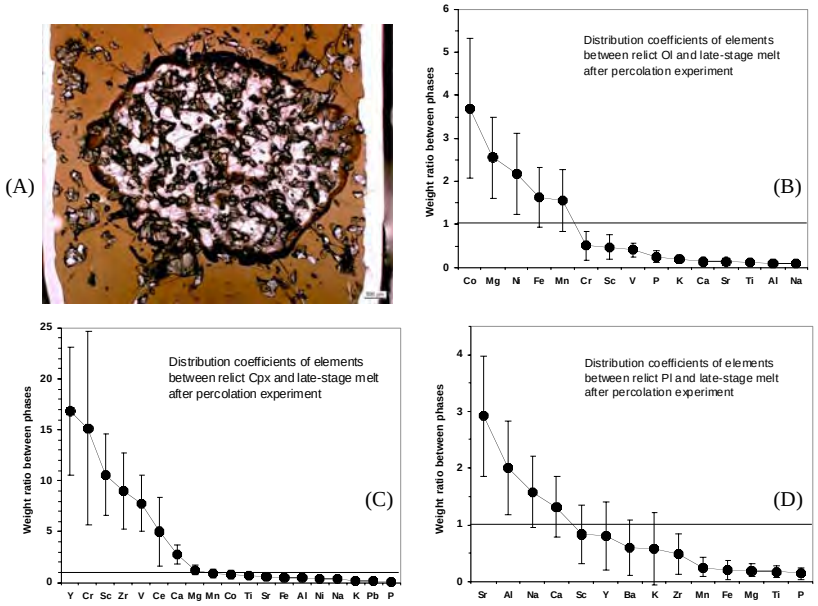

Botcharnikov R.E. et al. (2008) Experimental phase relations, mineral-melt equilibria and liquid lines of descent in a hydrous ferrobasalt - Implications for the Skaergaard intrusion and Columbia River flood basalts. J.Petrol. 49, 1687-1727.

Feig, S. T., Koepke, J. & Snow, J. (2006). Effect of water on tholeiitic basalt phase equilibria - an experimental study under oxidizing conditions. Contribution to Mineralogy and Petrology 152, 611-638.

Lehnert K., Su Y., Langmuir C.H., Sarbas B., Nohl U. (2000) A global geochemical database structure for rocks. Geochem Geophys Geosyst 1: 1999GC000026.

Natland J.H., Dick H..J.B., Miller D.J., Von Herzen R.P., (Eds.), 2002. Proc. ODP, Sci. Results, 176 [CD-ROM]. Available: Ocean Drilling Program, Texas A&M University, College Station TX 77845-9547, USA.

Thy P. et al. (2006) Experimental constraints on the Skaergaard liquid line of descent. Lithos 92(1-2), 154-180.

Toplis M. J. & Carroll M. R. (1995) An experimental study of the influence of oxygen fugacity on Fe-Ti oxide stability, phase relations, and mineral-melt equilibra in ferro-basaltic systems. J. Petrol. 36(5), 1137-1170.

Veksler IV, Dorfman AM, Borisov AA, et al. (2007) Liquid immiscibility and the evolution of basaltic magma. J. Petrol. 48, 2187-2210.

The different degassing behaviour of upper mantle-derived fluids in the western Eger rift area - a contribution to find an optimal ICDP location

K. BRÄUER[1], H. KÄMPF[2], J. SCHUMANN[2], G. STRAUCH[1]

[1]Helmholtz Centre for Environmental Reserach - UFZ
[2]Helmholtz Centre Potsdam GFZ German Research Centre for Geosciences

The western the Eger rift area is actual the most active part of the European Cenozoic Rift System. This statement is based on the repeated occurrence of earthquake swarms as well as the progressive increase of the mantle-derived helium at locations in the eastern part of the Cheb basin close to the Nový Kostel focal zone. Inside of the European Cenozoic Rift System the highest $^{3}He/^{4}He$ ratio are measured at the free gas phase of degassing locations in the eastern part of the Cheb basin (Bräuer et al., 2005, 2008). Two separated locations in the western Eger rift area would be interesting for an optimal ICDP location, the Nový Kostel focal zone and the major degassing field between Bublák and Hartoušov (Fig. 1; Fig. 4). Drilling at the first one would supply information about the crustal structure above (at the top) the focal zone and amongst others information about permeability barriers which prevent the mantle-derived fluid flux. In the second case the crustal structure related to fluid migration path take centre stage. In every case a lot of new information about fluid-driven processes from the upper mantle through the crust is to expect.

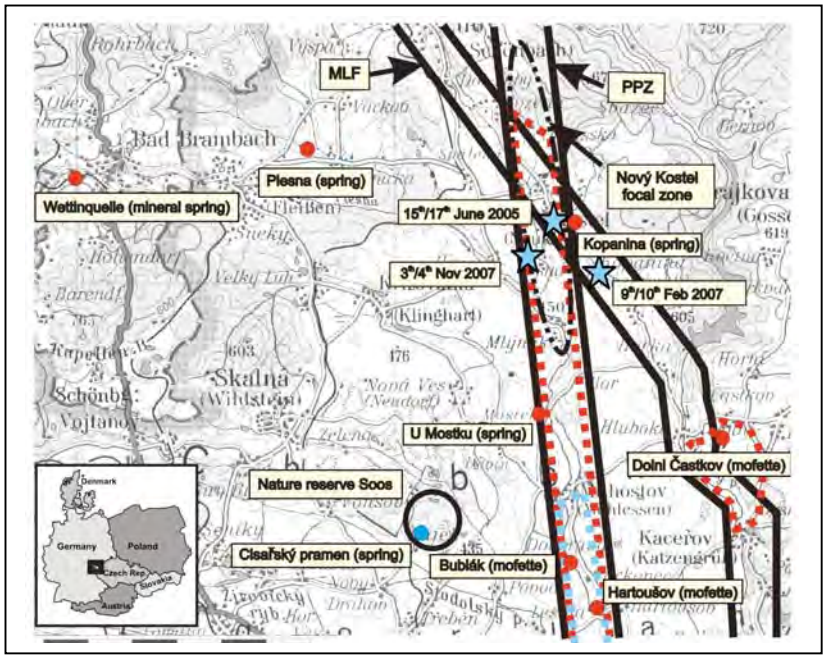

Fig. 1Sampling locations in relation to major faults (MLF = Mariánské Lázně fault zone; PPZ = Počatky-Plesná fault zone) and to the Nový Kostel focal zone. The blue stars mark the June 2005 and February 2007 and the November 2007 micro-swarms. Dashed red are the CO_2-mapped areas. The blue pointed area marks a mofette field that has been characterised by measurements of CO_2-soil gas, gas flux,$\delta^{13}C$ and $^3He/^4He$ ratios. The coloured points (red/blue) mark sampling locations.

Figure 1 summarised the situation in the western Eger rift area. To evaluate changes of fluid migration path due to the drilling process we select three degassing locations with high MORB-Type He contents close to the Nový Kostel focal zone (Kopanina, U Mostku, Fig.1). The first phase of the project has included the gas and isotope geochemical characterization as well as the study of seasonal and seismo-hydrological influences at these locations as well as to follow the rising $^3He/^4He$ ratios in the Cheb basin at least since 2000 which point to an increasing magmatic activity beneath the Cheb basin.

The monthly monitoring of the gas and isotope composition at the locations Bublák, U Mostku, Kopanina and Dolni Častkov has been carried out until June 2008. The sampling locations in relation to the major fault zones and the epicentral areas of the occurred micro-swarms (blue stars). The focal depth of the February swarm was at approximately 10000 m, whereas the focal zone of micro-swarm in November 2007 was 12500 m deep. All in all the year 2007 is marked by the repeated occurrence of seismicity related to the Nový Kostel focal zone. As an example for the geodynamic activity since 2005 the time-series of the $^3He/^4He$ ratios is shown (Fig. 2).

Due to occurred micro earthquake swarms repeatedly at all locations a decrease of the $^3He/^4He$ ratios have been observed. Such shifts of the $^3He/^4He$ have been already observed during the strong three months lasting period of seismicity 2000 (Bräuer et al., 2008) and have been interpreted as indication of seismically triggered release of crustal helium which may be admixed to the steady fluid flux from the upper mantle. In addition, based on the monthly sampling we have to taken into account that most likely not all anomalies could be recorded. More interesting than the repeatedly decrease of the $^3He/^4He$ ratios is the three month lasting increase of mantle-derived helium in spring 2006. Ascending of fresh magma from

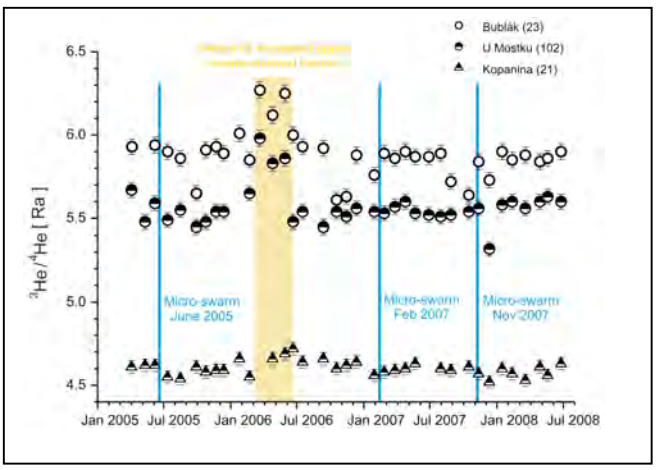

Fig. 2 presents the the time series of the 3He/4He ratios between April 2005 and June 2008 in relation to occurred micro swarm seismicity

the sub-continental mantle into the crust may be responsible for this anomaly. Addition to this anomaly of the time-series in spring 2006 at all locations in the eastern part of the Cheb basin a temporary increase has been observed (Fig. 3).

As a whole the detailed study of the isotope composition shows that the level of mantle helium is clearly higher along the PPZ than along the MLF. The increase of mantle-derived helium is limited at both faults zone. At the Cisařský pramen -a gas-rich mineral spring – in the nature reserve Soos the $^3He/^4He$ ratios have the same level like 1993 (Fig. 3). The increase of the mantle-derived helium level acts as progressive process and was observed first at the mofettes between

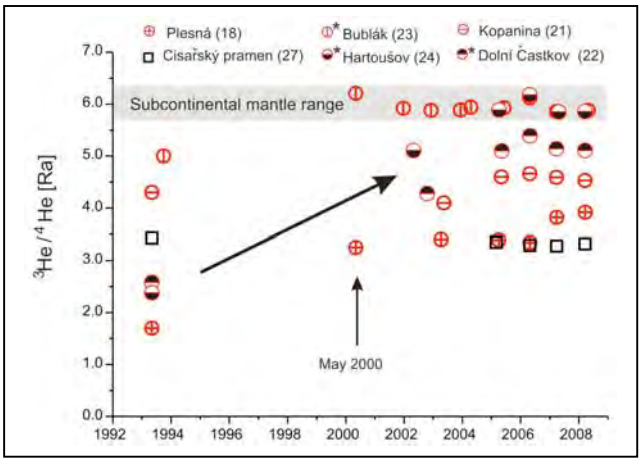

Fig. 3 shows the progressive increase of the $^3He/^4He$ ratios at locations in the eastern part of the Cheb basin.

Bublák and Hartoušov along the PPZ, thereafter at Dolni Častkov at the MLF, and during the last two years at the Plesná spring to the north of the Cheb basin, too (Fig. 3). The high gas flux together with the subcontinental helium signature indicates that the isotope patterns of the 'Bublák' gas are close to the signature of the magmatic reservoir at the crust/mantle boundary (Bräuer et al., 2008). Since 2005 the $^3He/^4He$ ratios at the mofette Hartoušov south of Bublák and close to the Počatky Plesná fault zone cover the sub-continental mantle range, too.

Figures 4 summarises all CO_2 soil gas and the flux measurements at the wet degassing locations. The outcome of CO_2 soil and gas flux measurements points to two isolated Diffuse Degassing Structures (DDS) into the Počatky-Plesná fault zone (each ca. 1 km in length and up to 300m in width). The two main Diffuse Degassing Structures in the surroundings of Bublák and Hartoušov are highly permeable sub-structures of the PPZ and act as mantle-fluid injection zones (Fig. 4a).

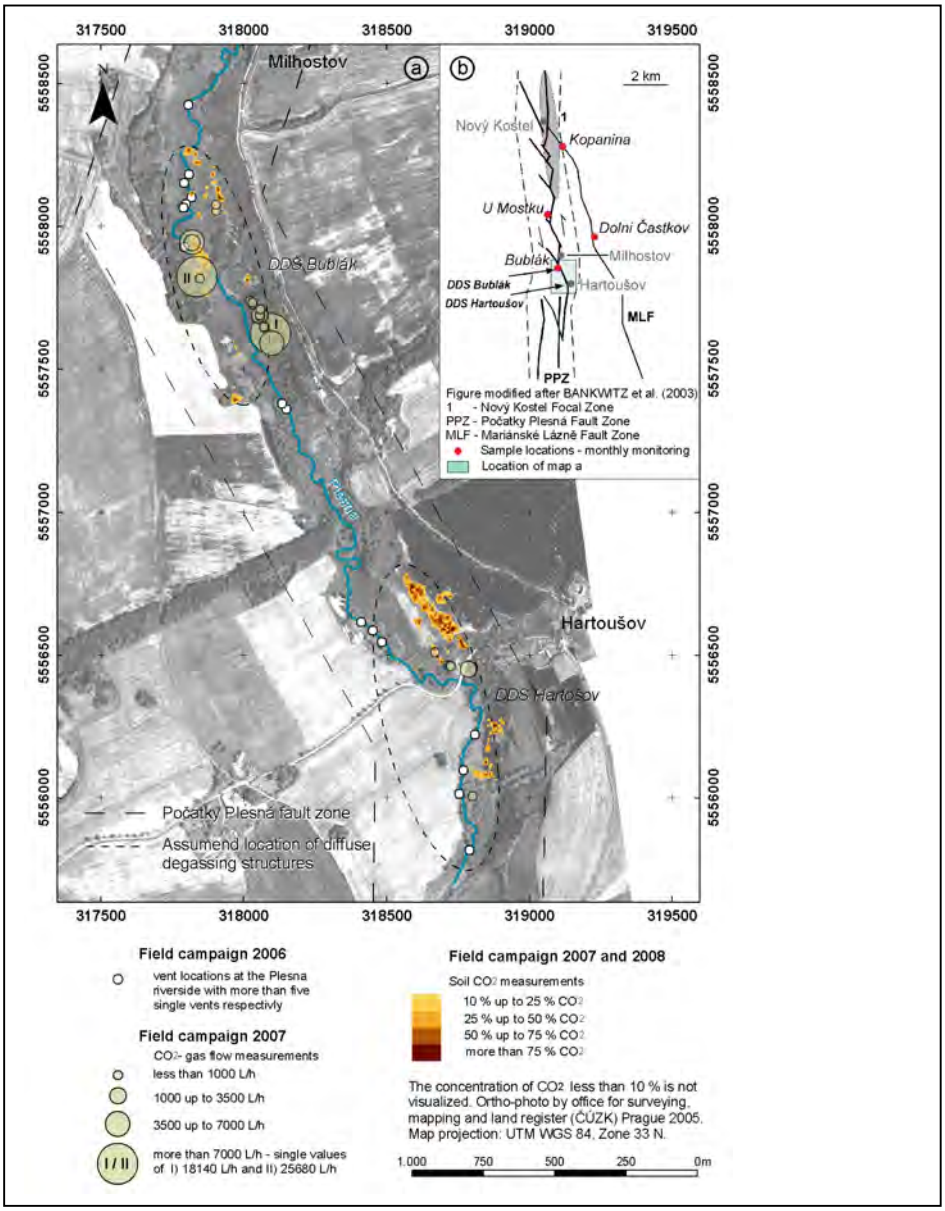

Fig. 4 Compiled results of fluid mapping and flux measurements (2006-2008) a: field indications; b: tectonic scheme

Outlook:

Drilling in the western Eger rift will give progress in the understanding of fluid-coupled geoprocesses in the lithosphere of an intra-continental rift area because following **features** exist:

- An active fluid system up to the lithospheric mantle
- Fault-related fluid transport from the upper mantle through the whole crust
- Fliud triggered earthquake swarms are driven by long-lasting hidden magmatic activity beneath the Cheb basin.

Open questions:

a. How is the temporal and spatial scale of the hidden magmatic activity?
b. Where is the magmatic source located beneath the Eger rift?
c. Are there intermediate magmatic accumulations in the lithosphere above the magmatic source?
d. Is there an increase of the geothermal gradient as a consequence of the hidden magmatic activity in the upper crust?

Not at least the **features** are the result of long-time detailed fluid studies. Particularly isotope geochemical time series have been proved as unique tool to verify such geodynamic processes. Further fluid studies would give useful contributions to solve the open questions.

Bräuer, K., Kämpf, H., Niedermann, S. & Strauch, G. Evidence for ascending upper mantle-derived melt beneath the Cheb basin, Central Europe. *Geophys. Res. Lett.* **32**, doi:10.1029/2004GL022205 (2005).

Bräuer, K., Kämpf, H., Niedermann, S., Strauch, G. & Tesar, J. The natural laboratory NW Bohemia – Comprehensive fluid studies between 1992 and 2005 used to trace geodynamic processes. *Geochem., Geophys., Geosys.* **9**, Q04018, doi: 10.1029/2007GC001921 (2008).

Experimental simulation of vesiculation and microlite crystallization on ascent of rhyodacitic magma at Unzen Volcano

S.B. CICHY[1], R.E. BOTCHARNIKOV[1], F. HOLTZ[1], H. BEHRENS[1], H. SATO[2]

[1]Institut fuer Mineralogie, Leibniz Universitaet Hannover, Callinstr. 3, 30167 Hannover, Germany, (s.cichy@mineralogie.uni-hannover.de)
[2]Dept. of Earth and Planetary Science, Kobe University, Japan

This project focuses on the physical and chemical processes that occured during the 1991-1995 eruption of Unzen volcano. Our approach is to reproduce experimentally the vesicularity, texture, mineral assemblage and mineral composition that were analyzed in the groundmass of Unzen volcanic rocks sampled at the surface and at depth (core samples from ICDP-drilling). In order to simulate the magma ascent from ca. 10 to 1.5 km depth (below ICDP target), two main experimental approaches have been used: (i) crystallization experiments in a broad range of temperatures and pressures to reproduce the equilibrium phase relations in rhyodacitic magmas; (ii) isothermal decompression experiments conducted at different decompression rates to investigate kinetic processes of magma degassing and crystallization, occuring on magma ascent. To provide a better insight into the bubble and microlite nucleation and growth processes at different stages (=depths) during magma ascent, it is necessary to conduct decompression experiments that are terminated/quenched at different pressures.

Here we report our results on two sets of isothermal decompression experiments (850°C) performed to simulate magma ascend in the deeper Unzen conduit, starting at 300 MPa and decompressing down to either (I) 50 MPa or down to (II) 200 MPa. Experiments conducted with decomression rates $\geq$ 0.1 MPa/s were decompressed continuously, while at decompression rates $\leq$ 0.1 MPa/s we used a multi-step decompression method. Decompression rates varied from 0.0002 to 20 MPa/s. For the set (I) experiments, we have duplicated runs with intermediate decompression rates (0.01 to 1 MPa/s). The experiments were fluid saturated either containing only water as a fluid component (H_2O) or containing water and carbon dioxide (H_2O+CO_2; mole fraction of H_2O in the fluid ~0.6). Additionally, we also present first results of our phase stability experiments at low temperatures (800-850°C).

The set (I) experiments were designed to reproduce the physical and chemical conditions of the Unzen magmas. The results of isobaric experiments and equilibrium phase assemblage along the decompression path for set (I) experiments at water-saturated conditions are shown in Fig. 1. Therefore, for set (I) experiments (grey arrow in Fig. 1a) plagioclase (Pl) was not part of microlite assemblage for the starting conditions (300 MPa) but was stable at equilibrium conditions at 50 MPa. In contrast, amphibole (Amph) was stable at 300 MPa but was not part of mineral assemblage at equilibrium conditions at 50 MPa. One important aspect in the decompression experiments was a reproduction of Pl microlites with lengths up to 100-300 μm as those that were observed in the groundmass of natural Unzen lavas by Noguchi et al. (2008).

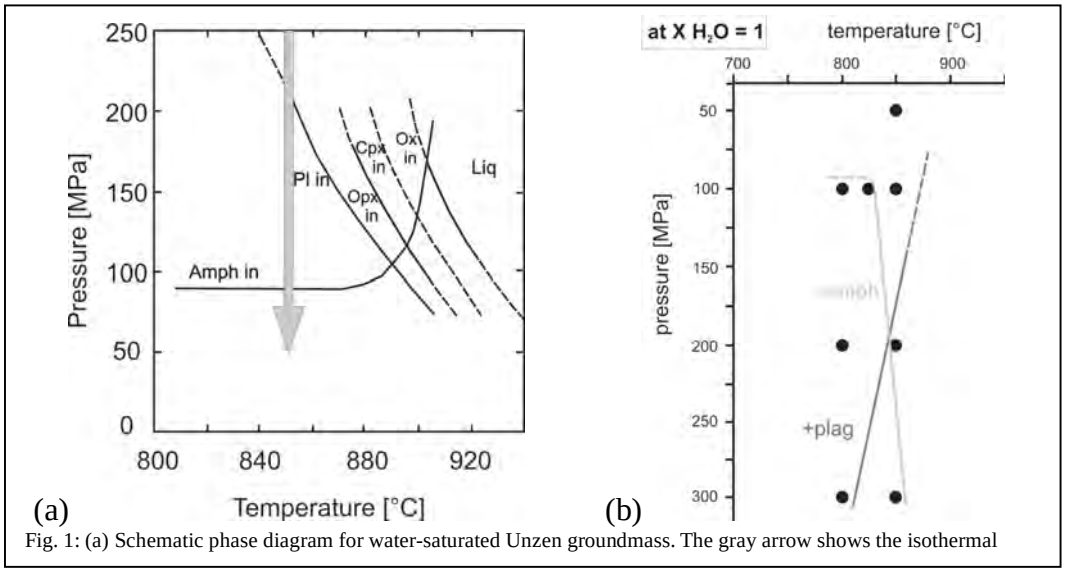

Fig. 1: (a) Schematic phase diagram for water-saturated Unzen groundmass. The gray arrow shows the isothermal

The experimental products of set (I) consist of pyroxenes, ± amphiboles, ± plagioclases, oxides and glass, where Pl microlites only occur in experiments with the two lowest decompression rates (0.0005 and 0.0002 MPa/s) in the H_2O-system. The length of those experimentally grown Pl in the water-bearing system reaches up to 200-250 µm which is consistent with Pl sizes in natural samples (Noguchi et al., 2008). But the lengths of Pl microlites produced in the H_2O+CO_2-system are not larger than ~80 µm (see Fig. 2).

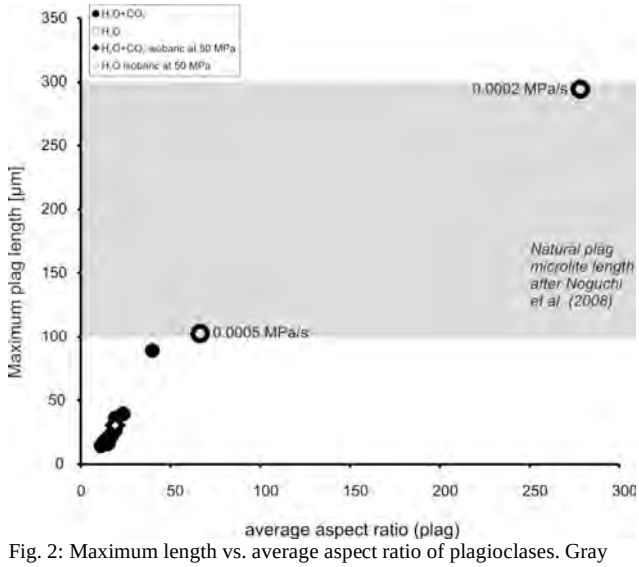

Fig. 2: Maximum length vs. average aspect ratio of plagioclases. Gray shaded area represents the natural groundmass plag lengths after Noguchi et al. (2008).

Chemical analysis of the residual melt of all experimental products shows that the SiO_2-content of the H_2O+CO_2-system increases with decreasing decompression rate (<0.1 MPa/s), becoming similar to the natural groundmass composition with SiO_2=78-80 wt% (Nakada and Motomura, 1999), whereas the silica content of the glasses in the water-bearing system remains nearly constant. Similar observations can be made for FeO and Al_2O_3 contents of the residual melts. In the H_2O-system, there is so significant change in the iron and alumina content with decreasing decompression rates. Chemical analyses of our experimental products of set-(II) are in progress.

For set (I), our determined bubble number density (BND) values range from $10^{11.5}$ m^{-3} to 10^{14} m^{-3} in both the H_2O-bearing and the H_2O+CO_2-bearing systems (Fig. 3). The analysis of the experimental data in the most recent experiments in the H_2O-bearing system is under progress. The BSE pictures illustrate two generations of bubbles (one with diameters > 50µm and a second with diameters <5µm) in H_2O+CO_2-bearing system decompressed at the highest decompression rate in both sets of experiments whereas only one bubble generation is observed in H_2O-bearing magmas. This observation points to a possible delay in nucleation of CO_2-rich bubbles due to lower rate of CO_2 diffusion in silicate melts compared to that of H_2O. In the H_2O+CO_2 system (set I), we can cleary see a trend of decreasing logBND with decreasing decompression rate (Fig. 3). Such a trend can be attributed to the increasing influence of bubble growth and coalescence on the processes of volatile exsolution from magmas with decreasing rate of decompression. In other words, the contribution of bubble growth becomes dominant over the contribution of the bubble nucleation with decreasing decompression rate. The logBND values for the H_2O+CO_2-bearing system of set (II), marked by triangles in Fig. 3, show no significant dependence (within uncertainty) on the decompression rate. This presumably indicates that for the pressure drop from 300 to 200 MPa the processes of bubble nucleation and growth might compensate each other. The discrepancy between set (I) and set (II) experiments can be probably explained by significant difference in viscosities of residual melts due to exsolution of volatiles on decompression to 50 and 200 MPa. The melts decompressed slowly to 50 MPa should have much higher viscosities (~2 orders of magnitude, Giordano et al, 2008) than melts decompressed to 200 MPa, resulting in lower mobility of H_2O and CO_2 in the melt and higher nucleation barrier for bubbles.

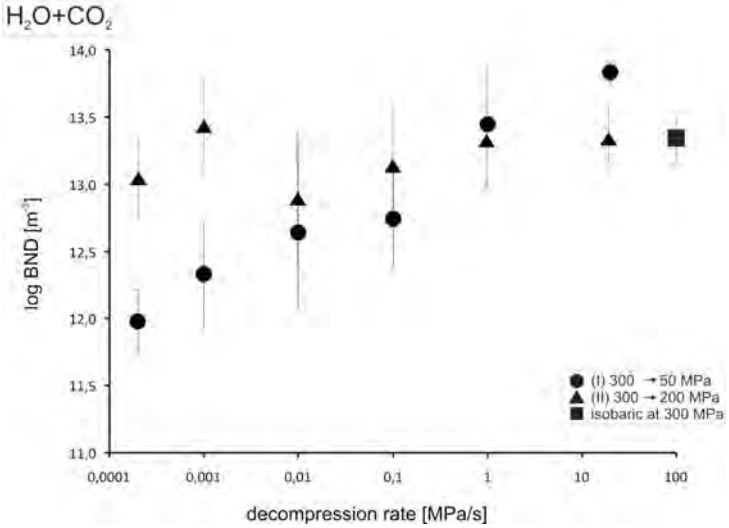

Fig. 3: Log BND values in dependence on the decompression rate for H_2O+CO_2 saturated samples. Two different series were already conducted both starting at a pressure of 300 MPa, which is equal to the natural Unzen magma chamber prior to the eruption (e.g. Sato et al., 1999; Holtz et al., 2005). The melts in set (I) experiments were decompressed to a final pressure of 50 MPa (circles) while the melts in set (II) runs were decompressed to a final pressure of 200 MPa (triangles).

It has to be pointed out that Pl microlites are not present in any products of the H_2O-bearing system in the experimental set-(II), in agreement with isobaric phase relation experiments where Pl microlites crystallize at pressures lower 200 MPa at a temperature of 850°C.

Our microlite number density (MND) values range from $10^{2.4}$ mm^{-3} to $10^{3.0}$ mm^{-3}. The experimental MND values obtained at slow decompression are at least one order of magnitude lower than that from natural samples (MND=10^5-10^6 mm^{-3}; Noguchi et al., 2008). In both sets (I) and (II) there is no clear variation of the MND value as a function of the decompression rate. But it should be noted that MND values for set (II) are lower than the values for set (I) experiments at same decompression rates in both fluid system. The difference between both sets in the water-bearing system (Fig. 4a) is in most cases within the experimental error. On the other hand, the significant difference in MND values for set I and set II experiments in H_2O-CO_2-bearing melts points to possible nucleation of microlites in systems decompressed to lower pressure and, hence having higher degree of undercooling.

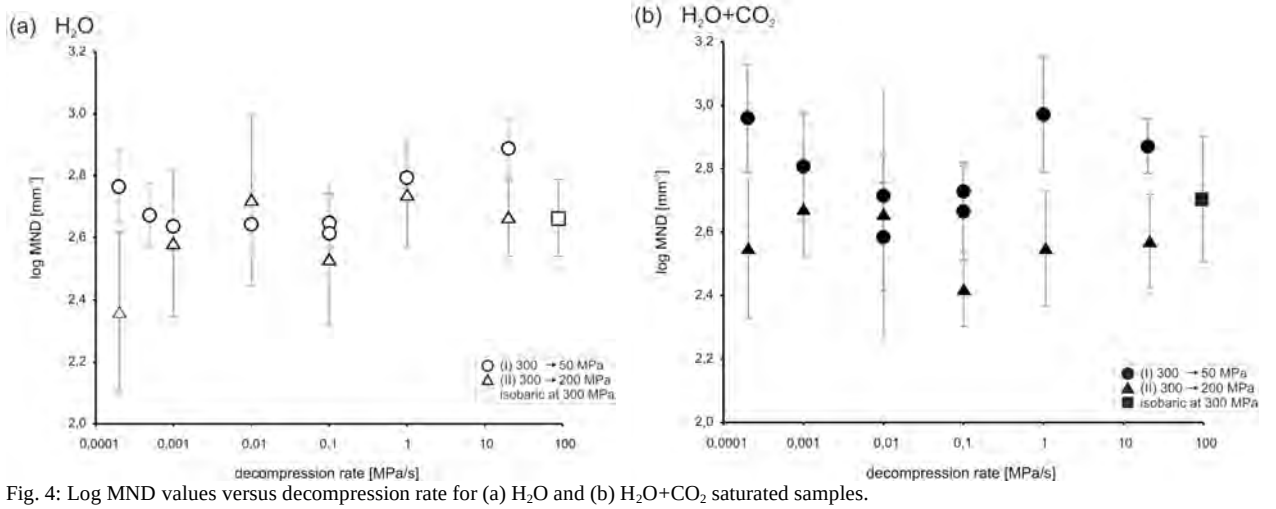

Fig. 4: Log MND values versus decompression rate for (a) H_2O and (b) H_2O+CO_2 saturated samples.

At this stage of our experimental work, we can state that the length of Pl microlites that are already present at 300 MPa will not exeed lengths larger than 50-80 µm during magma ascent at decompression rates from 0.0002 to 20 MPa/s, which was the case in our H_2O+CO_2-bearing system. But if Pl microlites are not stable at 300 MPa and if they crystallize during the magma ascent, the Pl lengths can reach values as large as 100-300 µm, corresponding to the lengths of natural Pl microlites observed in the Unzen groundmass. Such a case could be experimentally reproduced only in H_2O-bearing rhyodacitic magmas decompressed from 300 to 50 MPa at decompression rates $\leq$ 0.0005 MPa. Thus, the experimental results indicate that the ascent rates of Unzen magmas were close to or lower than ~ 6 m/hour. These values are in the same order of magnitude as the estimated magma ascent rate of 12-30 m/hour (Nakada and Motomura, 1999). However, it has to be noted that ascent rates are probably not constant over the whole conduit and that the experimental dataset needs to be completed to better bracket the possible range of natural conditions.

Further decompression experiments for lower pressures (from initial 50 MPa to final 10 and to 5 MPa) are planed to reproduce the conditions at shallower depths in magmatic conduit of Unzen volcano. Decompression experiments to final pressures of 100 MPa, corresponding to deeper conduit, are in progress. In addition, we will perform similar decompression experiments at temperature of 930°C which is close to the pre-eruptive temperature of Unzen magmas. Those experiments shall be conducted in internal heated pressure vessels (IHPV), equipped with a special decompression valve allowing continuous pressure release in the experiment. Further investigations of the stabilities of Amph and Pl will be performed in isobaric experiments at 300, 200, 100 and 50 MPa, at different temperatures (850-950°C) and with different composition of the fluid (H_2O+CO_2). This will provide better understanding and background information necessary to interpret our decompression experiments.

Nakada S., Motomura Y. (1999) Petrology of the 1991-95 eruption at Unzen: effusion pulsation and groundmass crystallization. J. Volc. Geotherm. Res, 89, 173-196

Sato, H., Nakada, S., Fujii, T., Nakamura, M., and Suzuki-Kamata, K. (1999). Groundmass pargasite in the 1991-1995 dacite of Unzen volcano: phase stability experiments and volcanological implications. J. Volc. Geoth. Res, 89, 197-212.

Holtz F., Sato H., Lewis J., Behrens H., Nakada S. (2005) Experimental petrology of the 1991-1995 Unzen Dacite, Japan. Part I: phase relations, phase composition and preeruptive conditions. J. Petrol, 46, 319-337.

Giordano D, Russell JK, & Dingwell DB (2008) Viscosity of Magmatic Liquids: A Model. EPSL, Accepted 3/08

Noguchi S., Toramaru A. and Nakada S. (2008) Relation between microlite textures and discharge rate during the 1991-1995 eruptions at Unzen, Japan. J Volc Geotherm Res., doi: 10.1016/j.jvolgeores.2008.03.037

Brittleness and shear thinning: the explosive-effusive transition of Unzen lava dome experimentally investigated.

B. CORDONNIER[1], K.U. HESS[1], D. DINGWELL[1]

[1]Department of Earth and Environmental Sciences LMU MUNICH

The results presented here are complementary to the recently performed study on Unzen volcano (ICDP- HE 4565/1-2). They synthetize the results obtained, integrate the last observations and give an overview on the remaining important investigations needed to characterize unzen volanic conduit rheology.

High-silica volcanic systems are considered to be the most devastating. Their highly viscous properties create a high pressurized non fluent system which consequently relaxes only by exploding through the brittle regime. In other words, such volcanoes have an explosive nature and often generate catastrophic pyroclastic flows.

The dome building eruptions in Unzen generate repeated dome failure and pyroclastic flows. They vary in character and behavior from effusive domes to brittle pyroclastic events. The deformation of highly crystallized dome lavas is key to understanding their rheology and to fixing their failure onset. In this study we investigate the stress and strain-rate dependence on several glasses and Mt Unzen dome lavas. Their rheology has been determined for temperatures from 900 to 1010°C and stresses from 2 to 60 MPa in uniaxial compression (Hess & al. 2007a). Additionally, tensile tests were performed on several volcanic products to track down the porosity effect.

This survey aims to distinguish the Non-Newtonian effects affecting magmatic melts also known as indicators of the brittle field. Towards our experiments we observed three majors viscosity decrease types. Two were dependant and typical of the solid fraction (IAVD & DAVD). The first is instantaneous and on the whole recovered during stress release. The second is time dependent and non-recoverable (Cordonnier & al. 2009). The third and last effect observed is attributed to the melt fraction and its self heating under stress (VHE).

The IAVD is typical of that observed in previous experiments on crystal-bearing melts (Lavallee & al. 2007). On crystal free melts, this viscosity decrease is observed at much lower magnitude. We infer that the crystal phase responds elastically to the stress applied and relaxes once the load is withdrawn. The DAVD appears more complex and this regime depends on the stress (and/or strain-rate) history. We distinguish four different domains: Newtonian, non-Newtonian, crack propagation and failure domains. Each of these domains expresses itself as a different regime of viscosity decrease. Due to stress localization, cracking appears in crystal-bearing melts (intra-phenocryst and/or the in the melt matrix) earlier than in crystal-free melts. For low stresses, the apparent viscosity is higher for crystal-bearing melts (as predicted by Einstein-Roscoe equations). However, while the stress (or strain rate) increases, the apparent viscosity is decreasing to that of the crystal-free melt and could be even lower if viscous heating effects are involved (Hess & al. 2007b).

Through this survey we distinguished apparent viscosity variations linked to the crystal network and/or the glass. Most of them are becoming relevant close the relaxation time scale of the material and may initiate the material failure (Lavallee & al. 2008).

More important, the crystalline phase is commonly believed to increase the viscosity according to the Einstein-Roscoe equations. Indeed, those equations are confirmed here for low stresses and strain rates. However, more importantly, the presence of the crystalline phases results in an apparent viscosity that becomes strongly stress and strain-rate dependent. Einstein-Roscoe overestimates this apparent viscosity by several orders of magnitude. Here a new model is proposed to forecast melt rheology evolution (Cordonnier & al. 2009). This study demonstrates the dominance of non-Newtonian rheology in understanding the extrusion of dome lavas at Mt Unzen.

Cordonnier, B., Hess, K. U., Lavallee, Y., Dingwell, D. B., 2009. Rheological properties of dome lavas: case study of Unzen volcano. Earth and Planetary Science Letters. Article revised: 6-DEC-2008 Article accepted for publication: 2-JAN-2009 Expected dispatch of proofs: 29-JAN-2009

Hess, K. U., Cordonnier, B., Lavallee, Y., Dingwell, D. B., 2007a. High-load, high-temperature deformation apparatus for synthetic and natural silicate melts. Review of Scientic Instruments 78 (7), 075102-075106.

Hess, K. U., Cordonnier, B., Lavallee, Y., Dingwell, D. B., 2007b. Viscous heating in rhyolite: An in situ experimental determination. Earth and Planetary Science Letters 275 (7), 121-126.

Lavallee, Y., Hess, K. U., Cordonnier, B., Dingwell, D., 2007. Non-newtonian rheological law for highly crystalline dome lavas. Geology 35 (9), 843-846.

Lavallee, Y., Meredith, P. G., Dingwell, D. B., Hess, K. U., Wassermann, J., Cordonnier, B., Gerik, A., Kruhl, J. H., 2008. Seismogenic lavas and explosive eruption forecasting. Nature 453 (7194), 507-510.

Characterization of the pore space in SAFOD samples combining Ar-beam cross sectioning and SEM imaging: First results

G. DESBOIS & J.L. URAI

Structural geology, Tectonics and Geomechanisms, RWTH Aachen University, Lochnerstrasse 4-20, 52056 Aachen, Germany

Porosity plays an important role in the evolution of the active fault zones but it is difficult to study due to the fine pore size and difficult sample preparation.

Studies of porosity include usually metal injection methods (Hildenbrand and Urai, 2003; Esteban et al., 2006), magnetic susceptibility measurement (Esteban et al., 2007), SEM imaging of broken surfaces (Hildenbrand, 2005) and CT scanner computing (Taud et al., 2005). However, observations and interpretations remain difficult because none of these approaches is able to directly characterize the in-situ porosity at the pore scale. Thus, much is still unknown and fundamental information is missing for a complete understanding of the fault gauges.

We are developing a new alternative (Desbois et al., 2008; Desbois et al., submitted) for the in-situ investigation of the pore space microstructures in geo-materials. The BIB-cryo-SEM method can combine the vitrification of the pore fluids by very rapid cooling and the excavation of the sample by argon beam (BIB, Broad Ion Beam) to prepare smooth and large (up to 2-3 mm^2) surfaces for high resolution imaging of the pore microstructures and the in-situ fluids. By this approach, we are able to investigate pores down to 10 nm in size and reconstruct the pore network in 3D applying serial cross sectioning procedure. In addition, micro-chemical analysis is also possible using an EDX system directly embedded in the SEM chamber.

The SAFOD drilling project committee gives us recently the unique opportunity to apply the BIB-cryo-SEM techniques on preserved samples from the active San Andreas Fault Gauge in order to make clearer the role of the porosity in the mechanical behavior of this active fault zone.

At the current time, we applied the combination of BIB cross sectioning and SEM imaging on two types of SAFOD samples (Hole E, Run 1, section 2: 37-39cm and Hole G, Run 4, section 2: 8-10cm). Our first investigations are very promising and demonstrate that the BIB-SEM methods' combination is powerful to get unprecedented high quality images at pore scale as well as rich detailed structural information like the distribution and morphologies of the pores in relation with the fabric and mineralogy.

At longer term, we will performed our investigations at cryo-temperature to quench the in-situ fluids and used serial cross-sectioning with the aim to study the distribution of fluid occupying the pore space and the connectivity of the pore network.

Desbois G. And Urai J.L. (submitted). In-situ morphology of meso-porosity in Boom clay (Mol site, Belgium) inferred by the innovative FIB-cryo-SEM method. E-earth.

Desbois G., Urai J.L., Burkhardt C., Drury M., Hayles M. and Humbel B. (2008). Cryogenic vitrification and 3D serial sectioning using high resolution cryo-FIB-SEM technology for brine-filled grain boundaries in halite: first results. Geofluids, 8: 60-72

Esteban L., Géraud Y. And Bouchez J.L. (2006). Pore network geometry in low permeability argillites from magnetic fabric data and oriented mercury injections. Geophysical Research Letters, vol. 33, L18311, doi : 10.1029/2006GL026908.

Esteban L., Géraud Y. And Bouchez J.L. (2007). Pore network connectivity anisotropy in Jurassic argillite specimens from eastern Paris Basin (France). Physics and Chemistry of the Earth, 32(1) :161-169.

Hildenbrand A., Krooss B. M. and Urai J. L. (2005). Relationship between pore structure and fluid transport in argillaceous rocks. Solid Mechanics and Its Applications, IUTAM Symposium on Physicochemical and Electromechanical Interactions in Porous Media, 125 : 231-237, doi : 10.1007/1-4020-3865-8_26.

Hildenbrand A. and Urai J.L. (2003) Investigation of the morphology of pore space in mudstones—first results. Marine and Petroleum Geology, 20(10):1185-1200.

H. Taud H., Martinez-Angeles R., Parrot J.F., Hernandez-Escobedo L. (2005). Porosity estimation method by X-ray computed tomography. Journal of Petroleum Science and Engineering, (47), 3-4, 30: 209-217

North Atlantic Current variability through Marine Isotope Stage MIS M2 (ca. 3.3 Ma) during the warm mid-Pliocene

S. DE SCHEPPER[1], M.J. HEAD[2], J. GROENEVELD[3]

[1] Fachbereich Geowissenschaften, Universität Bremen, Postfach 330 440, D-28334 Bremen <sdeschepper@uni-bremen.de>
[2] Department of Earth Sciences, Brock University, 500 Glenridge Avenue, St. Catharines, Ontario L2S 3A1
[3] Marum, Universität Bremen, Leobener Strasse, D-28359 Bremen. Now at: Alfred Wegener Institute, Columbusstrasse, D-27570 Bremerhaven

The mid-Pliocene was an episode of prolonged global warmth and strong North Atlantic thermohaline circulation, interrupted briefly at 3.30 Ma by a global cooling event corresponding to Marine Isotope Stage (MIS) M2. By integrating foraminiferal Mg/Ca and oxygen isotope ratios from *Globigerina bulloides* with the dinoflagellate cyst record from two sites (DSDP 610 and IODP 1308) in the eastern North Atlantic, we have tracked North Atlantic Current variability and polar front movement between ca. 3.40 and 3.20 Ma (Piacenzian). Our sea-surface temperature data support an active North Atlantic Current immediately before and after MIS M2, and a cooling of ca. 2–3˚C during MIS M2. A dinoflagellate cyst assemblage overturn, characterized by a significant decline in *Operculodinium centrocarpum*, points to a switch from an active to weakened North Atlantic Current. By comparing with records of ice-rafted debris, we show that this switch occurred >10 kyrs before fully glacial conditions had become established at MIS M2. This rules out fresh water input via icebergs as a

cause of North Atlantic Current slowdown. Weakening of the North Atlantic Current at our study sites is attributed to the southward advance of the polar front. The North Atlantic Current became reactivated in less than 6000 years with a return to warmer Pliocene conditions likely after passing an insolation or temperature threshold.

The Chicxulub ejecta layer in ODP 207 drill sites: analysis of the geochemical anomalies at the µm-scale

A. DEUTSCH[1], J. BERNDT[2], K. MEZGER[2], P. SCHULTE[3]

[1]Institut f. Planetologie, WWU Münster, D-48149 Muenster, Germany (deutsca@uni-muenster.de)
[2]Institut f. Mineralogie, WWU Münster, Corrensstr. 24, D-48149 Muenster
[3]GeoZentrum Nordbayern, Universität Erlangen, D-91054 Erlangen

Introduction: An up to 2-cm-thick Chicxulub ejecta deposit (Fig. 1) was recovered in 6 holes drilled during ODP Leg 207 (Demerara Rise, tropical western Atlantic [1-3]). This spherule deposit is the first dual-layer K/T boundary found in in marine settings [2, 3]. The most exciting feature of ths layer is the presence of carbonate clasts (Fig. 1 left) with exotic textures that are most probably of shock-metamorphic origin [3]. As this deposit totally lacks bioturbation, it is an ideal place to dissect the "iridium anomaly", and other geochemical peculiarities that have been reported in numerous studies at K/T sites world-wide (for review, see [4]). We have performed a detailed survey on the distribution of 40 trace elements in five, up to 7200-µm-long profiles across the K/T boundary (Fig. 1 right) with a very high spatial resolution, supplemented by a Sr-Nd isotope study on handpicked separates from this ejecta layer [3].

Analytical techniques: The trace elements were measured with the Element 2 La-ICP-MS (235 µm spot Ø) at the Inst. f. Mineralogie, WWU Münster. ^{29}Si concentrations determined by electron microprobe were used as internal standard for quantification of the trace element data. NIST 612 glass was used as standard for rare earth elements [REE], high field strength elements ([HFSE] – titanium, zirconium, hafnium, niobium, tantalum) and platinum; iridium was measured using a yet not certified laboratory standard with 12 ppm Ir. Standard materials BIR1-G and BHVO-2G served as monitors for precision and accuracy during La-ICP-MS analysis

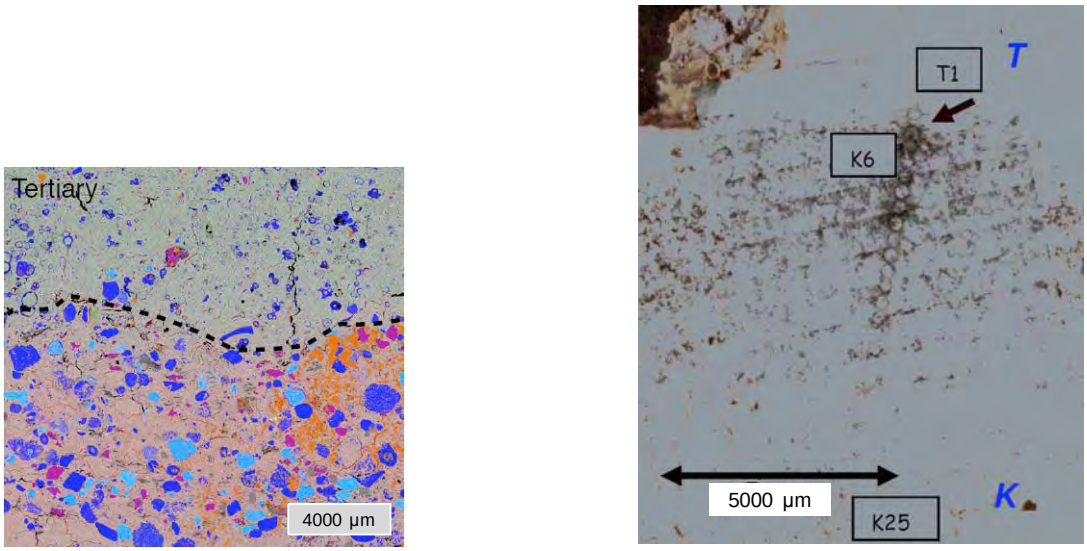

Fig. 1. (*left*) Combined BSE image and EDS maps (Quantax EDS system including a XFlash 4030 EDS silicon drift detector; BRUKER AXS Microanalysis GmbH, Berlin) showing the relative abundance of Ca, Mg, Si, Al, Fe in the uppermost part of the spherule deposit in ODP 207 Site 1259B and the transition (marked by the hatched line) to the early Paleogene claystone. Note the presence of large smectite spherules in the lower third and the occurrence of calcite and dolomite clasts as well as tectosilicates in the uppermost 0.5-0.7 mm of the K/T sequence. The local orange tinting is due to the presence of Fe-sulfides; (*right*) micrograph of the polished upper part of the K/T section in ODP 207 Site 1259C displaying the traces of one La-ICP-MS profile. T1, K6, and K25 are ablation spots mentioned in Fig. 2; red arrow corresponds to "K-T boundary" in Fig. 3.

Results: *Nickel - Chromium*. Ni/Cr ratios range in the Danian from 2.97 to 3.52 (mean ± 1σ is 3.24 ± 0.22; N = 5, one profile), and in the spherule layer from 2.31 to 2.84 (mean 2.64 ± 0.14; N = 20). The low Ni/Cr ratios are in contrast to what was expected, namely a contribution from the projectile, supposed to be a type CM2 chondrite [5] with a Ni/Cr ratio of 4.053 [6].

REE (Fig. 2). The REE concentrations differ by a factor of 3 to 5, with generally lower amounts in the spherule layer; some of this scatter reflects simply the high spatial resolution. The La_{CN}/Yb_{CN} ratio in the lowermost Danian ranges from 13.3 to 9.5 (mean 11.6 ± 1.5); again a sharp drop occurs at the topmost spherule layer to 6.2. In the spherule bed La_{CN}/Yb_{CN} varies from 6.05 to 11 (8.96 ± 1.7), with the lower values dominating in upper part. The rather flat REE_{CN} patterns with just a

minor Eu anomaly (e.g., Eu/Eu* = 0.88, K6 in Fig. 2) point to a mafic component, whereas, the REE_{CN} distribution in the lowermost Paleogene (spot T 1) and about 5 mm below K6 (spot K25) are typical for upper crustal material

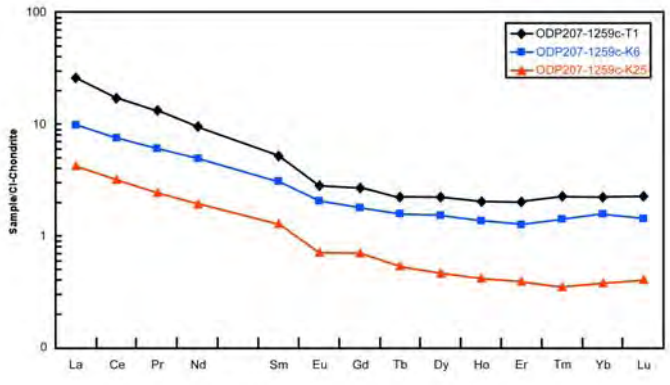

Fig. 2. CI chondrite-normalized REE distribution patterns for three spot analyses in the K/T boundary profile ODP 207 Site 1259C. T1 and K25 (cf. Fig. 1 right) display a negative Eu anomaly as typical for upper crustal rocks. This anomaly is less pronounced in the uppermost spherule layer (spot K6).

Platinum group elements (PGE). The Pt concentrations in the lowermost Danian (0 – 1000 µm in Fig. 3) range from 0.0034 to 0.01 ppm, followed by a sharp increase to a maximum value of ~0.1 ppm in the uppermost spherule layer, and a smooth decrease to ~0.0073 ppm about 6 mm below. The $^{195}Pt/^{194}Pt$ ratio (Fig. 3) shows slight variations (mean ± 1 σ_{SD} = 0.9737 ± 0.2705) compared to the certified reference value (0.9855 ± 0.0029 [7]), which we interpret to reflect the very small size of the PGE-carrying particles. The Ir concentrations also increase towards the top, reaching there a maximum of 0.04 ppm Ir.

HFSE. Already during documentation of the spherule layer with the scanning electron microscope we have noticed the presence of Ti-rich phases, some occurring as infilling of foraminifera shells [3]. The spherule bed has the following concentrations (in ppm): Ti >4000, Zr 44 - 67, Nb 0.90 - 10.6, Hf 2.36 - 3.26, and Ta 0.23 - 0.70. A Cretaceous reference sample collected 10 to 12 cm below the spherule bed contains: Zr 75 - 117, Nb 7.51 - 11.0, Hf 2.26 - 3.10, and Ta 0.57 - 0.78, and the Danian reference sample from 40 cm above the bed: Zr 83 – 105, Nb 10.5 – 13.8, Hf 2.10 – 2.61, Ta 0.63 – 0.94.

The *Nb/Ta ratio* drops in the lowermost Danian in five consecutive spots from 13.9 to 7.03, and is exceptionally low in the spherule layer (5.43 ± 0.81; Fig. 4). Three analyses of the Danian reference sample resulted in a "normal crustal value" of 15.4 ± 1.1 (N = 3); identical to the value for the Cretaceous reference sample (15.0 ± 2.4, N = 3). The *Zr/Hf ratio* drops also in the five consecutive spots from 26 to 20.4, and remains fairly constant in the spherule layer at a very low value of 20.5 ± 0.95. The Danian reference sample yielded a "normal crustal value" of 39.2 ± 1.4; similar to the value for the Cretaceous reference sample (35.5 ± 2.3). The Nb/Ta and Zr/Hf ratios for the standards BIR1-G and BHVO-2G measured in the course of this study correspond within errors to published values.

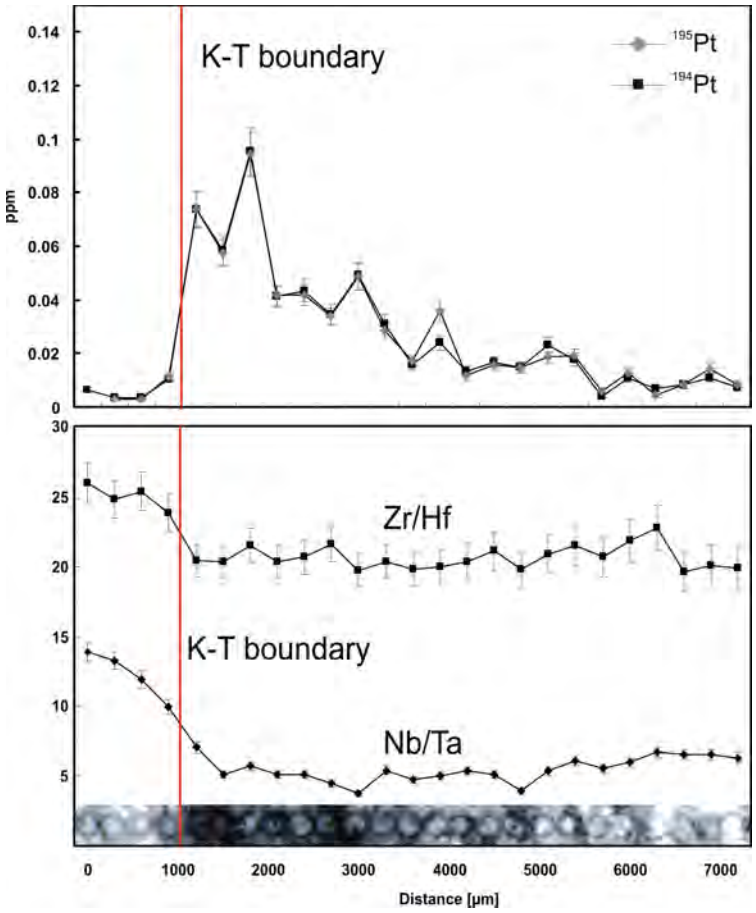

Fig. 3: Variation in (*upper*) platinum concentrations, calculated from counts measured for ^{195}Pt and ^{194}Pt, and (*lower*) in Zr/Hf and Nb/Ta ratios across the over the K-Pg profil, ODP Leg, Site 1259C. Chondritic values are 34.3 for Zr/Hf, and 19.9 for Nb/Ta [4]. The reference samples yielded Zr/Hf of 39.2, and Nb/Ta of 15.4 for the Danian, and Zr/Hf of 35.5, and Nb/Ta of 15.0 for the Cretaceous.

Tentative conclusions: Our high-resolution micro-chemical study clearly shows that various components contributed to the uppermost 5 mm of the K/T boundary at site 1259C. These are (i) Projectile matter, (ii) mafic ejecta, (iii) carbonates, (iv) local influx from the nearby continent, and (v) the contemporaneous seawater.

(i) The presence of *projectile matter* is documented by high PGE concentrations in the topmost mm. The PGE-carrying

particles are assumed to be in the nm-size range. As such particles would never reach the seafloor, they might have stuck to larger ejected clasts or glass spherules.

(ii) The *mafic component* is forming most probably *part of the ejecta*; this view is supported by EMP data for individual spherules in the uppermost mm of the ejecta layer [3]. The rather low Ni/Cr ratios in combination with the rather flat REE_{CN} patterns indicate that this mafic component is not related to an enhanced contribution of the projectile.

(iii) *Carbonate* clasts with various shock features, and probably back-reacted "shock-devolatilized" carbonates settled out of the ejecta, and occur only in the uppermost mm of the spherule layer.

(iv) The presence of the *local component* is the cause for the very exotic Zr/Hf and Nb/Ta ratios, and the low Nb/La ratio (i.e., ≥0.25) in the spots K6 to K10. Smectite, and altered glass spherules in the ejecta layer have, in addition, neodymium model ages T^{Nd}_{DM} around 1.9 Ga, and strongly negative $\varepsilon_{Nd}^{T=65Ma}$ of -17 [3]. Given the very short residence time of Nd in the ocean (≥200 yrs. [8]), and the probably even shorter residence time of HFSE in the ocean, this material was washed off obviously from the nearby Guayana craton [9].

(iv) The *contemporaneous seawater* is the source for the rather radiogenic Sr, analyzed in different separates from the spherule layer [3]. It is yet not constrained, to which proportions components (ii) to (v) have contributed to the geochemistry of the uppermost spherule layer in Site 1259C.

Outlook: We consider the spherule bed in the ODP 207 sites as key for understanding the mode of deposition and preservation of the various components that now compose this remarkable K/T boundary. Using minimum times for settling of 100-µm-sized glass spherules through the water column (i.e., Stoke's law), and estimates for the deposition of the continental influx, the spherule bed may cover a time span of 2 days to a few 100 years after the Chicxulub impact event.

[1] Proc. ODP Vol 207 Initial reports; doi:10.2973/odp.proc.ir.207.105.2004; doi:10.2973/odp.proc.ir.207.106.2004.
[2] MacLeod K.G. et al. (2007) GSA Bull. 119, 101-115.
[3] Schulte P. et al. (2009) GCA in press.
[4] Smit J. (1999) Ann. Rev. Earth Planet. Sci. 27**,** 75-113.
[5] Trinquier A. et al. (2006) EPSL 241, 780-788.
[6] Tagle R. and Berlin J. (2008) Meteoritics Planet. Sci. 43, 541-559.
[7] Briche et al. (1997) Anal. Chem. 69, 791-793.
[8] Tachikawa K. et al. (1999) EPSL 170, 433–446 [9] Goldstein S. L. et al. (1997) Chem. Geology 139, 271-286.

Acknowledgements: This research used samples provided by the Ocean Drilling Program (ODP). We acknowledge J. Erbacher, H. Brinkhuis and the ODP curators for making the samples available. U. Heitmann and T. Grund (WWU) are thanked for technical support and N. Artemieva (RAS Moscow) for very fruitful discussions.This research is supported by grants DE 401/13, and SCHU 2248/2 (Deutsche Forschungsgemeinschaft).

Orbital control on marine biological productivity and the positive carbon isotope shift at the Oligocene-Miocene transition

L.DIESTER-HAAß[1], K.BILLUPS[2], K.-C. EMEIS[3]

l.haass@mx.uni-saarland.de[1], kbillups@udel.edu[2], kay.emeis@zmaw.de[3]

The late Oligocene is marked by 400 kyrs cycles in the marine benthic $\delta^{13}C$ records with increasing amplitude, and by a 1‰ positive shift in carbon isotopes at 23.1 Ma simultaneous with a 1‰ positive oxygen isotope shift that marks a concomitant increase in Antarctic ice growth.

Which factors control the 400 kyrs carbon isotope cycles? Preliminary results from our project (which started in September 2008) show that at Site 926 (Ceara Rise, 3600 m water depth) marine biological productivity, as established from benthic foraminifer accumulation rates, increases in parallel with the $\delta^{13}C$ record from 25.3 to 23.5 Ma. Productivity maxima coincide with maxima in $\delta^{13}C$, whereas productivity is two times lower during the $\delta^{13}C$ minima.

First results from the 23.5 to 22.8 Ma time interval suggest that $\delta^{13}C$ lags the productivity changes. What is puzzling is that productivity during the maximum in $\delta^{13}C$ and $\delta^{18}O$ at 23.1 Ma is not higher than during the earlier and smaller, late Oligocene maxima.

We postulate, based on these preliminary results from one location (which have to be confirmed by studies at four additional locations), that variations in marine biological productivity are to a first approximation forced by insolation due to variations in orbital parameters and that marine productivity variations in turn control the marine $\delta^{13}C$ record. The apparent mismatch between productivity and $\delta^{13}C$ at 23.1 Ma calls for other influences that will be identified once our data base is complete.

Rock magnetic properties and their anisotropy from the Outokumpu assemblage in the Outokumpu deep drilling, Finland

F. DIETZE[1], C. VIRGIL[2], A. KONTNY[1], M.-L. AIRO[3]

[1] Geologisches Institut, Universität Karlsruhe, Germany
[2] Institut für Geophysik und Extraterrestrische Physik, Technische Universität Braunschweig, Germany
[3] Geological Survey of Finland, Espoo, Finland

Within the Outokumpu Deep Drilling Project, a 2516 m deep borehole into a strongly magnetic anomaly zone within Paleoproterozoic rocks in eastern Finland was drilled in 2004-2005 by the Geological Survey of Finland (GTK). Mainly paramagnetic mica schist and black schist interlayer units dominate until 2013 m, which are intercalated by a serpentinite sequence from 1314 - 1515 m. Below 2013 m dia- to paramagnetic pegmatitic granite was found. The focus of our study relates to the Outokumpu assemblage, which mainly consists of serpentinites, calc-silicate rocks, fine-grained quartz rocks and black schist (black schist = metasedimentary rock containing more than 1% of organic carbon), whereby quartz rock, cal-silicate rock and black schist are the host rocks of the Outokumpu-type Cu-Co-Zn sulfide deposits. Magnetic susceptibility measurements every 20 cm along the cores revealed that the rocks of the Outokumpu assemblage vary significantly from dia- and paramagnetic behaviour with values below $1*10^{-3}$ SI to ferrimagnetic behaviour with values above $10*10^{-3}$ SI. We measured a significant scattering of magnetic susceptibility within the serpentinite, which is interpreted to indicate variable degrees of serpentinization. Curie temperatures of 580°C indicate magnetite, which has been formed as a reaction product during serpentinization process. Secondary magnetite occurs along veins together with sulphide and oxide minerals, nickelite and chlorite. But there are also relics of pyrite-magnetite grains embedded in secondary pyrite.

NRM values of mica schist, calc-silicate rocks and black schist are generally weak (0.1 mA/m) and rarely increase to 6 mA/m in black schist due to increasing content of pyrrhotite. Some serpentinites show notable high remanence values up to 45 A/m. Generally a positive correlation between susceptibility and NRM of the ferromagnetic serpentinites can be observed, suggesting that the amount of magnetite controls strength of the magnetic anomalies.

AMS measurements of paramagnetic serpentinites, calc-silicate rocks, mica and black schist indicate up to 30% anisotropies of magnetic susceptibility (P' < 1.3) and a scattering of the shape factor from prolate to oblate ellipsoids. Only the black schist interlayer at 1513 m depth shows values of higher anisotropy (P' > 2). Ferrimagnetic serpentinites indicate a trend to more oblate shapes with increasing magnetic susceptibility and P' values. Especially the serpentinite layers at 1414 m and 1470 m – 1478 m have notable high degrees of magnetic anisotropie (P' > 3) and magnetic susceptibility values (up to $160*10^{-3}$ SI), due to high contents of magnetite. The dip of magnetic inclination scatters from 10 to 80° possibly indicating a fold structure in the Outokumpu assemblage.

Generally the rocks of the Outokumpu assemblage have none or just a weak field dependence of magnetic susceptibility, except for the black schist layer at 1508.5 m – 1514.3 m with values up to 37% due to pyrrhotite.

We observed no clear correlation between magnetic properties and density of the serpentinites, but there is a strong relationship between the formation of secondary magnetite and the degree of serpentinization. We will further study this relationship between mineralogy / geophysics and rock magnetic properties in our project.

GONAF - a deep Geophysical Observatory at the North Anatolian Fault

G. DRESEN, M. BOHNHOFF, MUSTAFA AKTAR, HALUK EYIDOGAN AND HISAO ITO

The North Anatolian Fault Zone (NAFZ) is the most active plate-bounding strike-slip fault in Europe that follows an EW trend offshore through the Sea of Marmara within less than 20 km south of Istanbul. The fault has produced a series of large and devastating earthquakes during the 20^th century starting in 1939 in eastern Anatolia and then systematically propagating westwards. The most recent M>7 earthquakes occurred in 1999 near Izmit and Düzce and produced accelerated seismic activity along the NAFZ south of the greater Istanbul area below the Sea of Marmara. Recent estimates indicate a 35-70% probability for the occurrence of a M>7 earthquake close to the population center of Istanbul by 2034. Here, we propose the installation of a deep borehole observatory in a 1000 m deep borehole at the offshore part of the North Anatolian Fault Zone (Geophysical Observatory at the North Anatolian Fault -- GONAF). The suggested borehole location is on Sivriada, the outermost spot of the Princes Islands, in direct vicinity to the major branch of the fault zone and the mega-city of Istanbul. GONAF is focussed on the installation of a deep borehole geophysical observatory with the aim to monitor microseismic activity and measure stress, heat and fluid flow. The location of the observatory is unique representing the only possible long-term monitoring site that is onshore and in close proximity to the NAFZ and the city of Istanbul. It is located at the transition between the western end of the 1999 Izmit rupture and an up to 150 km long seismic gap of the NAFZ below the Sea of Marmara that has repeatedly produced large (M>7) earthquakes and that may have accumulated a 4-5 m slip deficit since the last event in 1766.

GONAF will allow studying microearthquake activity close to the seismically active part of the fault zone, which is between 4-15 km depth. The deep borehole observatory will involve a vertical chain of downhole seismometers that will be combined with existing surface and planned shallow borehole seismometers to enhance the resolution and magnitude-detection threshold for seismological observations by several orders of magnitude. This allows studying the rupture process and interaction of small-magnitude events close to the source region of the expected Marmara earthquake with unprecedented detail. Heat and fluid flow close to the NAFZ will be monitored. The orientation and magnitude of local stresses and strains at the fault can be determined. This will allow estimating the in-situ strength at one of the major plate boundary faults. GONAF will allow to monitor seismicity and temporal changes of physical properties close to the NAFZ prior to an expected large earthquake.

Stratigraphy and distribution of Messinian Evaporites in the Levantine basin

S. DÜMMONG[1], C. HÜBSCHER[1], M. BEITZ[1] AND L. MARLOW[2]

[1]Institute of Geophysics, University of Hamburg
[2]Large Lakes Observatory, University of Minnesota

The semi-enclosed Levantine Basin in the easternmost Mediterranean is considered to represent the best natural laboratory for an investigation of the structural evolution of a young salt giant. This salt giant is virtually free of a major tectonic overprint. The impact on salt dynamics on differential sediment loading (e.g., lateral salt flow) can, therefore, be studied under well-constrained conditions. In this paper we present 2D prestack depth migrated seismic sections, corresponding depth maps, and isochrone maps of individual evaporitic sequences. Based on the interpretation and the analysis of these results it can be shown that a single, preferably continuous, drill core through the ~2 km-thick Messinian evaporite sequence in the Levantine Basin would allow the evolution of a salt giant to be unraveled and that this would shed important new light on fundamental aspects of the earth system. Further more, since our present understanding of the Messinian paleo-environment is almost entirely based on the study of exposures in the uplifted peripheral basins, those drilling results will serve as a fundamental data base which is crucial to unravel the fast and extreme environmental changes during the Messinian Salinity Crisis.

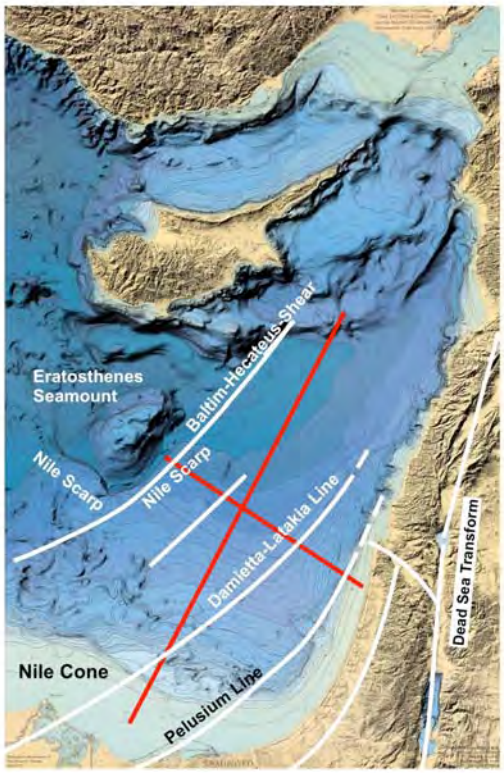

Figure 1: Geological setting in the Eastern Mediterranean. In red approximate profile directions are imaged, in white tectonic fault systems. (Map: Courtesy John K. Hall)

According to the chronostratigraphic scheme of Clauzon et al. (1996) or Krijgsman et al. (1999) the precipitation of the MU started around 5.6Ma during the Messinian Salinity Crisis (MSC). The duration of the MU formation and the rapidity with which the Mediterranean basin was refilled at the end of the MSC are still a matter of debate.

Recent publications showed a complex seismic stratigraphy of the MU in the Levantine Basin (Gradmann et al., 2005; Netzeband et al., 2006a; Bertoni and Cartwright, 2006), which can be divided into six sequences (Hübscher et al., 2007; Hübscher and Netzeband, 2007). Sequences ME-I, II, IV, and VI are seismically transparent and sequences ME-III and ME-V reveal several internal and subparallel reflections (Hübscher and Netzeband, 2007). The internal reflections have been interpreted as intercalated (and presumably overpressurized) clastics by Garfunkel et al. (1979) and Gradmann et al. (2005). However, 3D-seismic data analysis proved a high lateral continuity of seismic reflection characters and identified polarity changes, which are more indicative of chemical sedimentation processes, i.e., alternating evaporitic facies (Bertoni and Cartwright, 2007).

The deformation pattern of the intra-evaporitic sequences include folds and thrust faulting, which gives evidence for extensive salt tectonics and shortening, respectively, during the depositional phase. Both, the identified evaporitic facies of the individual intra-evaporitic sequences and the driving forces for the syn-depositional shortening remain unclear.

Prestack depth migrated seismic sections will serve as pre-site survey data for a future IODP-proposal. Industry seismic data sets were used to obtain depth migration results, which allow for the first time in detail the internal structure of the basinal Mobile Unit (MU) of the Messinian Evaporites. According to Hübscher et al. (2007) a future IODP proposal can make statements about the mechanical properties of the basinal MU of the Messinian Evaporites, as well as indications about extreme environmental changes, i.e., the Messinian salinity crisis, and about the possibility of the MU as an extreme habitat.

The processed data sets cover the basinal succession or Mobile Unit of the Messinian Evaporites, the Pliocene-Quaternary overburden, and the upper pre-Messinian succession. An exemplary illustration of the geological setting can be seen in Figure 2. 2D seismic lines were acquired with 25m shot, 12.5 receiver spacing, and with maximum offsets of 7325m. The interpretation of the vast industrial and academic seismic data allows basin-wide mapping of individual evaporitic facies.

Finishing the depth imaging processing of the data allowed, for the first time, the estimation of the thicknesses of single layers of the MU in the Eastern Mediterranean. Seismically transparent sequences ME-I, II, IV, and VI revealed interval velocities of 4.3 to 4.5 km/s (transparent sequences) and sequences ME-III and ME-V revealed interval velocities of 3.9 to

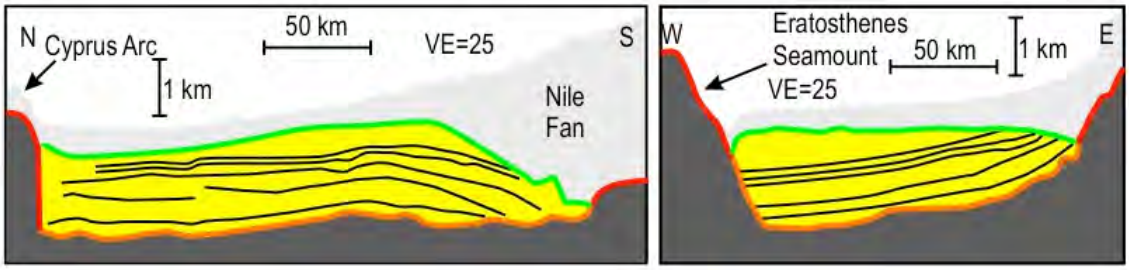

Figure 2: Schematic illustration of the geological situation in the Eastern Mediterranean. In yellow the mobile unit (MU) of the Messinian Evaporites with its basic geometrical characteristics. Six intra-evaporitic sequences can be traced throughout the basin.

4.1 km/s (Beitz, 2008; Dümmong et al, 2008), which are significantly lower and support the interpretation of intercalated clastics by Garfunkel et al. (1979) and Gradmann et al. (2005) (high reflective sequences). These interval velocities of young evaporites are also significantly lower than estimations of laboratory experiments for paleo-mesozoic evaporates, e.g., Zechstein salt, and indicate an even more complex evaporite mechanical behaviour as assumed before.

Figure 3 shows a representative East-West striking prestack depth migrated seismic section. It can be seen that the upper most layers of the MU (ME-VI to ME-III) are characterized by a toplap against the top of the Messian Evaporites (TES) with enlarging distance from the basin edges. ME-III pinches out next to the edges of the basin, where ME-VI already terminates in the middle part of the section in Figure 3. The geometry of the salt layers can be seen as a 'bulleye structure' with ongoing subsidence during deposition. This process normally forms evaporite deposits with the lowest salinity concentration first and the one with the highest concentration last. In this case we can only speak about individual evaporitic facies that are precipitated, due to refilling processes of the Eastern Mediterranean during the Messinian salinity crisis. But nevertheless the later sequences still form smaller layers, concentrating in the basin centre. This is the reason why we still stick to the term 'bulleye structure'. Ongoing subsidence even more deformed the individual layers after deposition.

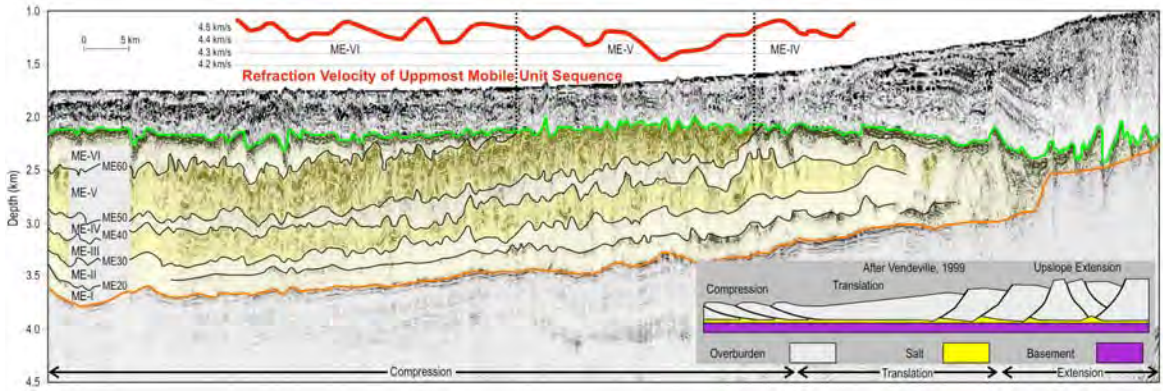

Figure 3: Prestack depth migration result of a West-East striking profile. The toplap of the individual layers (ME-VI to ME-III) of the MU against the top of the salt can be easily identified (after Dümmong and Hübscher, 2009).

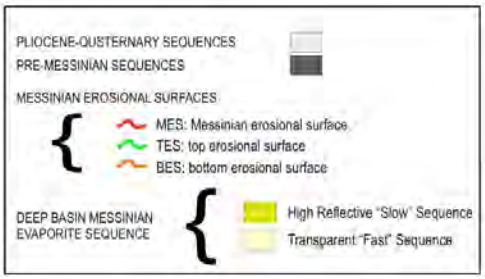

Additionally to the geometrical characteristics and the velocities obtained from the seismic model building process of ME-VI to ME-III the velocity of refracted waves from TES also supports the interpretation as layers with higher and lower velocities. As can be seen in Figure 3 when an individual sequence pinches out against the TES, the velocity of the refracted waves also varies corresponding to the interpretation as lower or higher velocity layer. The velocity of the refracted waves varies from approximately 4.5 km/s for sequence ME-VI to 4.2 km/s for ME-V and to 4.5 km/s for ME-IV. The obtained refracted velocities do not completely correspond to velocities obtained from seismic model building processes. But due to fact that refracted wave manly propagate in the horizontal direction and the structure of TES is quite rough, the velocities of refracted and reflected waves are not comparable in this case. Nevertheless they still support the interpretation of different composition of the individual sequences.

Typical models of thin skinned-salt tectonics include extensive parts at the edges of a basin, in the basin a compressive regime and in between a deformed area (translation) (after Vendeville (1999), see in Figure 3). In this case we can show that

the deformation pattern is dependend on the corresponding layer at the top of the salt body. The transparent sequences show a smoother erosional unconformity (ME-VI and ME-IV) than the high reflective sequence ME-V (see Figure 3). Especially in the areas, where ME-V toplaps, the top of salt is very rough. Two possibilities could explain this, one by different erosional behaviour at the TES and second by different rock mechanical behaviour. Additionally a combination of these two processes has to be taken into account. According to this observation we conclude that the deformation of the MU and the overburden is not only determined by lateral or vertical movements, but also by erosional/subrosional process of the upper MU and their corresponding sequences.

According to many authors (e.g., Neev, 1975) NE-SW striking strike slip faults have been proposed. However according to our processing results many of these sub-salt faults are apparent, due to processing artefacts, e.g., velocity pull-ups or pull-downs. But careful investigating and interpretation of the Damietta-Latakia fault, shows an overprint on the MU and the overburden, indicating a more or less recent activity.

The mapping and description of six intra evaporite sequences (ME-VI to ME-I) based on inline (East-West) and crossline (North-South) prestack depth migrated seismic sections is finished throughout the whole Levantine basin. It could be shown that the stratigraphy described in Hübscher et al. (2007) is representative for the whole Levantine basin between the Cyprus arc in the North, the Nile Cone in the South, and the Levantine coast in the East. The proposed stratigraphy could be traced on all seismic sections and forms a so called 'bulleye' structure. There are also clear evidences that this stratigraphic model can be extended towards the north in the shallower basins of the Cyprus arc area.

The most important conclusion from this study.is, that the stratigraphic model from Hübscher et al. (2007), including all evaporitic sequences (ME-IV to ME-I), can be calibrated by just one continuous well, which captures all evaporitic sequences in Eastern Mediterranean / Levantine basin. Based on this, the composition and, consequently, the mechanical properties of the Messinian Evaporites can predicted for the whole basin, since the stratigraphic model holds true for all areas related to this geological situation.

Further more, since our present understanding of the Messinian paleo-environment is almost entirely based on the study of exposures in the uplifted peripheral basins, those drilling results will serve as a fundamental data base which is crucial to unravel the fast and extreme environmental changes during the Messinian Salinity Crisis.

Acknowledgement:
The authors like to thank:

- IDOP Germany
- DFG grant Hu698/14
- Wave Inversion technology consortium (WIT)
- TGS-NOPEC

Bertoni, C. and J. Cartwright, 2006, Controls on the basinwide architecture of late Miocene (Messinian) Evaporites on the Levant margin (Eastern Mediterranean): Sedimentary Geology, 188-189, 93–114.

Bertoni, C. and J. Cartwright, 2007, Major erosion a the end of the Messinian Salinity crisis: evidence from the Levant Basin/ Eastern Mediterranean: Basin Research, 19, 1–18.

Clauzon, G., J. Suc, F. Gautier, A. Berger, and M. Loutre, 1996, Alternate interpretation of the messinian salinity crisis: controversy resolved?: Geology, 24, 363–366.

Garfunkel, Z., A. Arad, and A. Almagor, 1979, The Palmahim Disturbance and its regional setting: Geological Survey of Israel Bulletin, 72, 56.

Gradmann, S., C. Hübscher, Z. Ben-Avraham, D. Gajewski, and G. Netzeband, 2005, Salt tectonics of northern israel: Marine and Petroleum Geology, 22, 597–611.

Dümmong, S., Meier, K., Gajewski, D. and Hübscher, C., 2008, Comparison of prestack stereotomography and NIP-wave tomography for velocity model building: Instances from the Messinian Evaporites. Geophysics 73, VE291-VE302

Dümmong, S. and Hübscher, C., 2009, Salt-Atlas, in press

Beitz, M., 2008, Seismic processing of complex salt structures with model-based methods, Diploma thesis University of Hamburg

Hübscher, C., J. Cartwright, H. Cypionka, G. De Lange, A. Robertson, J. Suc, and J. Urai, 2007, Global look at salt giants: EOS, 88, 177–179.

Hübscher, C. and G. Netzeband, 2007, Evolution of a young salt giant: The example of the Messinian evaporites in the Levante basin: In: Wallner, M.; Lux, K.-H.; Minkley, W.; Hardy, Jr., H.R. (Eds.) The Mechanical behaviour of Salt - Understanding of THMC Processes of Salt, Taylor and Francis Group, London, 175–184.

Krijgsman, W., F. Hilgen, I. Raffi, F. Sierro, and D. Wilson, 1999, Chronology, causes and progression of the messinian salinity crisis: Nature, 400, 652–655.

Neev D., 1975, Tectonic evolution of the Middle East and the Levantine basin (easternmost Mediterranean), Geology 3, 683-686.

Netzeband, G., K. Gohl, H. C., Z. Ben-Avraham, A. Dehghani, D. Ga jewski, and P. Liersch, 2006a, The Levantine Basin - crustal structure and origin: Tectonophysics, 418, 178–188.

Vendeville, B. C., Mart, Y., and Vigneresse, J. L., 1999, Salt Shale and Igneous Diapirs in and around Europe, Geological Society Special Publications No. 174

High-precision Pb (double spike) and Sr-Nd-Hf-isotopic record of upper oceanic crust at Leg 206 (Site 1256, Eastern Central Pacific)

S. DUGGEN[1], K. HOERNLE[1], F. HAUFF[1], J. GELDMACHER[2]

[1] IFM-GEOMAR, Leibniz-Institute of Marine Sciences, Research Division 4, Division Dynamics of the Ocean Floor, Department of Magmatic and Hydrothermal Systems, Wischhofstrasse 1-3, 24148 Kiel, Germany
[2] Integrated Ocean Drilling Program, Texas A&M University, 1000 Discovery Drive, College Station, TX 77845-9547, USA

About half of the recent oceanic crust was generated on mid-ocean ridges at relatively fast spreading rates (> 80 mm/y full rate). The most complete section of oceanic crust has so far been drilled at IODP Site 1256 in the Eastern Central Pacific ocean (Cocos Plate). Site 1256 ocean crust was formed ca. 15 m.y. ago during a phase of superfast spreading at the East Pacific Rise. It is considered one of the most important reference drill holes for oceanic crust. So far three expeditions penetrated ca. 1,500 m of oceanic crust at this site and a proposal for further deepening is presently residing with the Operations Task Force of IODP awaiting scheduling (D. Teagle, pers. comm.). Currently, the deeper, mainly intrusive part of Hole 1256D below 750 mbsf, drilled during IODP Expeditions 309 and 312, is intensely studied (e.g. (Duggen et al., accepted pending revision)). The upper half of the Site 1256D above 750 mbsf, however, drilled during ODP Leg 206, which includes ca. 250 m of marine sediments followed by ca. 500 m of lava flows, has so far gained much less attention by geochemists. Relatively few geochemical data therefore exist in the literature for Leg 206 material (some first data, however, was recently published by our group (Sadofsky et al., 2008).

In the course of a new project that started September 2009, our group investigates the down-hole geochemical variation of Leg 206 sediments, lavas and alteration minerals, in order to contribute to establishing a complete and detailed record of the Sr-Nd-Hf-Pb (DS) isotope ratios and relevant trace element variations of the entire oceanic crust drilled at Site 1256. Based on these data, we aim at providing new constraints on: 1) magma genesis at superfast spreading ridges (East Pacific Rise); 2) the effects and timing of subsequent alteration including element fluxes in oceanic crust formed at superfast spreading rates (compared to slower rates); 3) element cycles in subduction zones, and 4) the contribution of ocean crust to the chemical evolution of the mantle and sources of magmatism at ocean islands (OIB). In September 2009 SD travelled to the Gulf Coast Repository (GCR) at College Station in Texas to sample the Leg 206 core material. The Leg 206 samples (sediments and lavas) are currently prepared for to major and trace element and stable and radiogenic isotope analysis in collaboration with a student assistant as scheduled. During the IODP Colloquium in Potsdam we plan to present the goals of the project and the first preliminary geochemical data.

Duggen, S., Hoernle, K., Hauff, F., and Geldmacher, J.: Geochemistry of basalts across the lava-dike transition zone in ocean crust of Hole 1256D (Eastern Pacific): Constraints on temporal changes of sub-ridge mantle heterogeneity and subsequent style and timing of alteration, Geochemistry Geophysics Geosystems, accepted pending revision.

Sadofsky, S., Hoernle, K., Duggen, S., Hauff, F., Werner, R., and Garbe-Schönberg, D.: Geochemical variations in the Cocos plate subducting beneath Central America: implications for the composition of arc volcanism and the extent of the Galápagos hotspot influence on the Cocos oceanic crust, International Journal of Earth Sciences, DOI: 10.1007/s00531-007-0289-5, 2008.

In-situ iron isotope ratio determination and thermo-oxibarometry in Fe-Ti oxides of IODP Hole 1256D (ODP Leg206 and IODP Exp. 309 & 312, East Pacific Rise)

W. DZIONY[1], J. KOEPKE[1], I. HORN[1], G. STEINHÖFEL[1], J. SCHÜßLER[1], F. HOLTZ[1]

[1] Institut für Mineralogie, Leibniz Universität Hannover

IODP multi-cruise mission "Superfast Spreading Crust" drilled successfully a complete section of the upper oceanic crust into the underlying gabbros (Site 1256; eastern equatorial Pacific; 15 Ma crust formed at the East Pacific Rise). The recovered rocks, now representing the first reference profile through fast-spreading upper oceanic crust, reveal a complex interaction between magmatic and metamorphic processes: Primary crystallization; low- and high-temperature alteration; contact-metamorphism; partial melting/assimilation; magma mixing. The petrographic record of the whole section reveals that all processes involve the formation of, or the reaction with, Fe-Ti oxides, which can consequently be used as suitable proxies for monitoring the different stages in the magmatic-metamorphic evolution of fast-spreading oceanic crust. In this report we present results on formation conditions of the Fe-Ti oxides and preliminary results on Fe isotopes distribution in these minerals.

Thermo-oxibarometry

Chemical data of the oxide minerals based on several thousands of microprobe analyses (Dziony et al., 2008, Koepke et al, 2007) were applied to reconstruct the redox and temperature conditions during the evolution of the oceanic crust at Site 1256D. We applied an improved two-oxide geothermo-oxibarometer of Sauerzapf et al. (2008) to the rocks of IODP Hole 1256D. For fresh basalt and most gabbros we estimated more reducing redox conditions (Delta NNO ~ -1, with NNO corresponding to the Nickel-Nickeloxide oxygen buffer) as expected for the MOR petrogenesis. For the lowermost dikes ("granoblastic dikes"), which suffered a contactmetamorphic overprint due to the thermal imprint of the magma chamber below (Koepke et al., 2008) and for most gabbros close to the dike/gabbro contact, a dramatic shift of the $f(O_2)$ (nearly 4

orders of magnitude) towards more oxidizing conditions (Fig. 1) was observed. This indicates that most gabbro samples were also overprinted at temperatures of ~ 600 °C and oxidizing conditions.

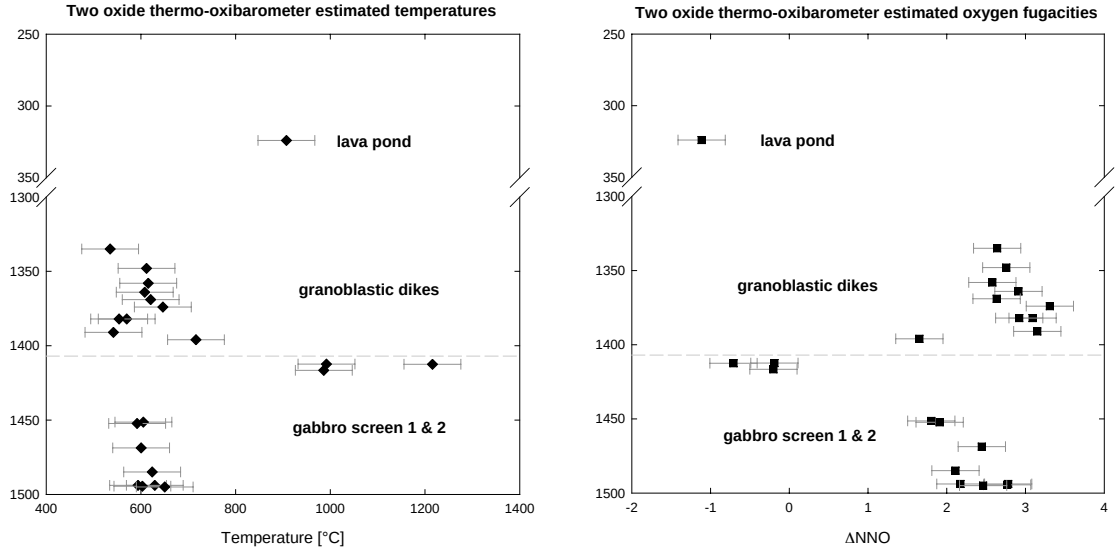

Fig. 1: Temperature and oxygen fugacity estimations by using the magnetite / ilmenite geothermo-oxibarometer by Sauerzapf et al. (2007). The dashed line corresponds to the dike/gabbro transition. mbsf=meters below sea floor; ΔNNO=f(O_2) in log units compared to the Ni/NiO oxygen buffer

In situ iron isotope determination

Recently, we analyzed iron isotopes in different Fe-bearing phases (magnetite, ilmenite, sulphides) using a UV-femtosecond laser ablation system coupled to a MC-ICP-MS (multiple-collector inductively coupled plasma mass spectrometer) in order to unravel the complex interplay between alteration/metamorphism and magmatic processes at fast-spreading mid-ocean ridges. This system has been recently developed at the Leibniz University Hannover. To test the reliability of this method, several studies have been done by Horn et al., (2006) and within this project. It has been shown that there is no influence of the matrix on the calibration of the $\delta^{56}Fe$ values ($\delta^{56}Fe=(^{56}Fe/^{54}Fe_{sample}/^{56}Fe/^{54}Fe_{IRMM\text{-}14}\text{-}1)*1000$) by comparing them to those obtained by analyzing a nebulized aqueous solution of the sample in the same MC-ICP-MS. Analytical and methodical techniques are given by Horn et al. (2006).

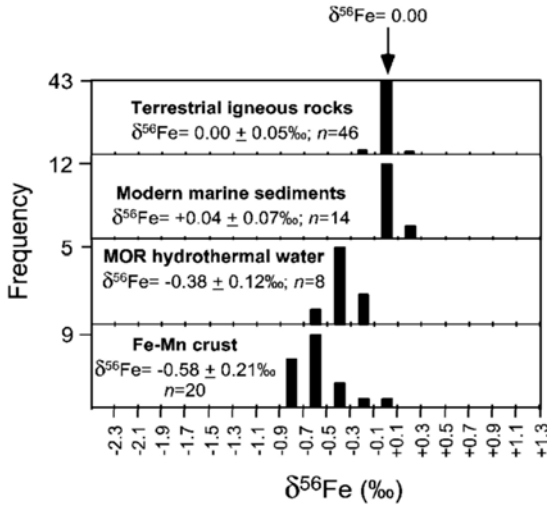

Fig. 2: Histogram plot of Fe isotope compositions of igneous rocks, marine sedimentary rocks, MOR hydrothermal water and oceanic Fe-Mn crust modified after Beard et al, (2003).

Terrestrial igneous rocks are very homogenous in Fe isotope compositions. All igneous rocks, ranging in composition from peridotite to high-silica rhyolite, show nearly identical $^{56}Fe/^{54}Fe$ ratios within an error of ±0.05‰ (1σ). In contrast, the Fe isotope compositions of hot fluids (> 300 °C) from mid-ocean-ridge spreading centers define a narrow range that is shifted to lower $\delta^{56}Fe$ values by 0.2‰–0.5‰ as compared to igneous rocks (Fig. 2, see Beard et al., 2003; Rouxel et al., 2003; Beard and Johnson, 2004). This relationship implies that hydrothermal alteration may influence the fractionation behavior of iron isotopes. Thus, if the formation of Fe-Ti-phases is related to hydrothermal alteration, a characteristic fingerprint in iron isotopes should be detected by in-situ isotope analysis.

First measurements show that we can distinguish between primary magmatic magnetites and those formed by secondary hydrothermal alteration by their $\delta^{56}Fe$ values with a precision of ±0.1 ‰. A sample taken from Gabbro screen 2 of the 1256D core shows both primary magmatic magnetite and obviously secondary magnetite nodules associated within an alteration patch. In this sample, primary oxide grains, now composed of an exsolution of magnetite and ilmenite, we measured an average $\delta^{56}Fe$ of ±0.0 ‰, but the $\delta^{56}Fe$ in the exsolved magnetite is in the range +0.2 to +0.3 ‰ and the $\delta^{56}Fe$ in the exsolved ilmenite is in the range -0.3 to -0.4 ‰ (Fig. 3). The secondary magnetite reveals a $\delta^{56}Fe$ of -0.3 ‰. In a sample of the uppermost unit of Hole 1256D (lava pond), which is completely unaltered, we found a $\delta^{56}Fe$ value of ±0.0 ‰ for magnetite.

Further isotope analyses of 1256D rocks and other samples are in progress in order to improve the understanding of the relationship between fractionation of iron isotopes in different phases and hydrothermal overprint.

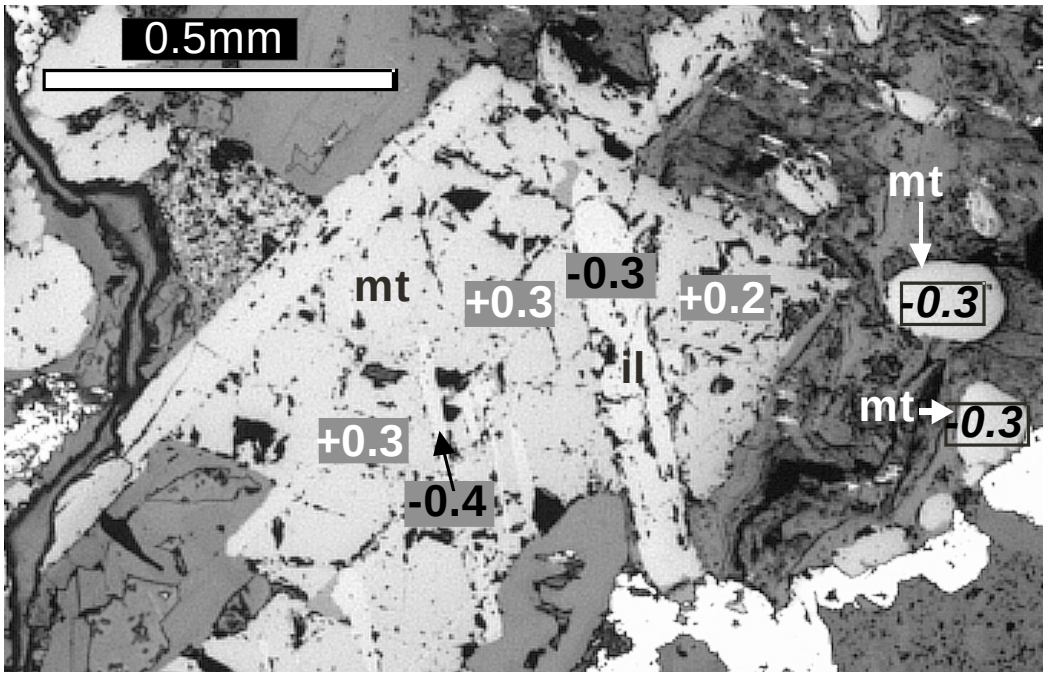

Fig. 3: Microphotography of a primary magmatic magnetite with exsolutions of ilmenite within a gabbro (sample 1256-312-232R2,1-3cm). On the right side two rounded grains of secondary magnetite are visible, embedded in a matrix of alteration minerals. δ^{56}Fe values are given for primary magnetite in white, for ilmenite exsolutions in black, for secondary magnetite in black italic. The average δ^{56}Fe value of the primary crystal (taking into account the proportions and composition of magnetite and exsolved ilmenite) leads to an initial δ^{56}Fe value of ±0.0‰.

Future objectives

It is planned to extend the analytical work on Fe-Ti oxides and Fe-sulphides and to complete the investigations on iron isotopes, in order to confirm or reject our hypothesis based on our priliminary data, that an hydrothermal overprint can be traced by in-situ measurements of δ^{56}Fe values. Furthermore, we plan to apply a second in-situ laser ablation method, designed for the analysis of oxygen isotopes.

Beard, B.L., Johnson, C.M., Von Damm, K.L., Poulson, R.L., 2003. Iron isotope constraints on Fe cycling and mass balance in oxygenated Earth oceans. Geology 31, 629-632.

Beard, B.L., Johnson, C.M., 2004. Fe isotope variations in the modern and ancient earth and other planetary bodies. Rev. Mineralogy & Geochemistry 55, 319-357.

Dziony, W., Koepke, J., and Holtz, F., 2008. Data report: petrography and phase analyses in lavas and dikes from Hole 1256D (ODP Leg 206 and IODP Expedition 309, East Pacific Rise). In Teagle, D.A.H., Alt, J.C., Umino, S., Miyashita, S., Banerjee, N.R., Wilson, D.S., and the Expedition 309/312 Scientists, Proc. IODP, 309/312: College Station, TX (Integrated Ocean Drilling Program Management International, Inc.)(doi:10.2204/iodp.proc.309312.201.2008)

Koepke, J., D. M. Christie, W. Dziony, F. Holtz, D. Lattard, J. Maclennan, S. Park, B. Scheibner, T. Yamasaki, and S. Yamazaki (2008), Petrography of the dike-gabbro transition at IODP Site 1256 (equatorial Pacific): The evolution of the granoblastic dikes, Geochem. Geophys.Geosyst.,9,Q07O09.(doi:10.1029/2008GC001939)

Horn, I., von Blanckenburg, F., Schoenberg, R., Steinhoefel, G., Markl, G., 2006. In situ iron isotope ratio determination using UV-femtosecond laser ablation with application to hydrothermal ore formation processes. Geochim. Cosmochim. Acta 70, 3677–3688.

Rouxel, O., Dobbek, N., Ludden, J., Fouquet, Y., 2003. Iron isotope fractionation during oceanic crust alteration. Chem. Geol. 202, 155-182.

Sauerzapf, U, Lattard, D, Burchard, M, Engelmann, R., 2008. The titanomagnetite-ilmenite equilibrium; new experimental data and thermo-oxybarometric application to the crystallization of basic to intermediate rocks. Journal of Petrology 49(6):1161-1185

Trace metal patterns in Black Sea sapropels as a chemostratigraphic tool

S. ECKERT[1], B. SCHNETGER[1], H.-J. BRUMSACK[1]

[1] Institut für Chemie und Biologie des Meeres (ICBM), AG Mikrobiogeochemie, Carl von Ossietzky Universität Oldenburg, Postfach 2503, D-26111 Oldenburg, Germany (sebastian.eckert@uni-oldenburg.de)

During DSDP Leg 42B (Site 379A), which was carried out in 1975, D/V *Glomar Challenger* recovered the only example of an Eemian sapropel in the Black Sea (Ross et al. 1978). This organic carbon-rich layer documents an earlier anoxic stage of the Black Sea presumably comparable to the Holocene situation. Up to date this Eemian setting has never been investigated in detail, in part owing to the lack of samples. To our knowledge the only geochemical data of this layer were published by Calvert and Batchelor (1978) and consist of one single composite sample. We intend to investigate this interval

in more detail based on re-sampling the archive half of the core which is kept at the Bremen Core Repository. During R/V *Meteor* expedition M72/5 in 2007 the Eemian sapropel unexpectedly was recovered in two gravity cores 7 m beneath the recent (Holocene) one. This offers the unique opportunity to compare the Holocene and Eemian development of anoxic conditions in this type locality based on geochemical proxies.

So far we have generated high-resolution geochemical data on well-preserved Holocene samples which were retrieved by several gravity cores and multicorer cores during R/V *Meteor* expeditions M51/4 (2001) and M72/5 (2007). These sediments comprise the last glacial/limnic stage (Unit III), the transition to the interglacial/marine stage (Unit II) and the recent sapropel (Unit I), which represents the today's marine/brackish stage. The sapropels were sub-sampled on a millimeter scale and analyzed by XRF and ICP-AES for major and minor elements. Ages of surface sediments were estimated by ^{210}Pb, verified by ^{137}Cs, and served to calculate sedimentation rates, which vary from 0.02 to 0.15 cm/yr. We detected well defined peaks in enrichments patterns of redoxsensitive elements (e.g. Co, Cr, Cu, Fe, Mo, Ni, U, and V) during deposition of sapropels documenting the paleoenvironmental history of the Black Sea. For example, Fe/Al depth profiles show several independent peaks above the Unit III-Unit II-boundary, indicating the rise and descent of the redoxcline in the Black Sea basin during the transition from the limnic to the marine stage. High Fe/Al ratios seem to document that the redoxcline was impinging the broad shelf area, where Fe may be mobilized from the sediment. A low Fe/Al ratio on the other hand implies that the redoxcline was situated at a deeper level at the slope, thus preventing significant Fe mobilization and creation of Fe-peaks. The Fe-peaks may serve as chemostratigraphic age markers for the Unit II sapropel because they are present in almost all cores we investigated so far. Our geochemical data as well show increasing trace metal enrichments with increasing water depth during Unit I, but almost constant basin-wide enrichments in several trace metals in Unit II. On the basis of Ca_{xs}, bulk Sr/Ca and Ti/Ca the paleoclimatic development was reconstructed and shows the alternating cold and warm events during the glacial period and the transition to the Holocene interglacial in the Black Sea. This is paralleled by enhanced paleoproductivity, as represented by TOC, Ba, P, Ni and Cu, which leads to increased deposition/preservation of organic matter during the warmer periods in the Black Sea.

Ross, D. A., 1978. *Initial reports of the Deep-Sea Drilling Project Vol. XLII*. U.S. Government Printing office, Washington D.C.
Calvert, S. E. & Batchelor, C. H., 1978. Major and minor element geochemistry of sediments from Hole 379A, Leg 42B, Deep Sea Drilling Project. *Initial reports of the Deep-Sea Drilling Project Vol. XLII*. U.S. Government Printing office, Washington D.C., p. 527-541.

Viral infections as controlling factors of the deep biosphere

B. ENGELEN, T. ENGELHARDT, M. SAHLBERG, H. CYPIONKA

Institut für Chemie und Biologie des Meeres, Universität Oldenburg, Carl-von-Ossietzky Straße 9-11, D-26111 Oldenburg, Germany, http://www.icbm.de/pmbio

The marine deep biosphere represents the largest biotope on Earth. Throughout the last years, we have obtained interesting insights into its microbial community composition. However, one component that was completely overlooked so far is the viral inventory of deep-subsurface sediments. While viral infections were identified to have a major impact on the benthic microflora of deep-sea surface sediments (Danavaro et al. 2008), no studies were performed on deep-biosphere samples, so far. As grazers probably play only a minor role in anoxic and highly compressed deep sediments, viruses might be the main "predators" for indigenous microorganisms. Furthermore, the release of cell components, called "the viral shunt", could have a major impact on the deep biosphere in providing labile organic compounds to non-infected microorganisms in these generally nutrient depleted sediments. However, direct counting of viruses in sediments is highly challenging due to the small size of viruses and the high background of small particles. Even molecular surveys using "universal" PCR primers that target phage-specific genes fail due to the vast phage diversity.

One solution for this problem is the lysogenic viral life cycle as many bacteriophages integrate their DNA into the host genome. It is estimated that up to 70% of cultivated bacteria contain prophages within their genome. Therefore, culture collections represent an archive of the viral composition within the respective habitat. These prophages can be induced to become free phage particles in stimulation experiments in which the host cells are set under certain stress situations such as a treatment with UV exposure or DNA-damaging antibiotics.

In our first phage-induction experiments, representative isolates from our ODP Leg 201 culture collection (Batzke et al. 2007) were screened for the presence of lysogenic phages using the antibiotic mitomycin C. Six out of thirteen cultures from various phylogenetic groups, sampling sites and sediment depths showed a drop in cell density due to viral lysis. After the treatment, the growth curves of the induced cultures declined significantly in comparison to the controls. At the end of the experiment, the number of virus-like particles (VLP) turned out to be up to 3×10^{10} VLP/ml. The phage morphology was visualized by transmission electron microscopy (TEM).

The study of the viral component within the deep biosphere offers to answer the following questions: To which extent are deep-biosphere populations controlled by viral infections? What is the inter- and intra-specific diversity and the host-specific viral biogeography? Can viral infections tell us something about the physiological state of indigenous microorganisms? Finally, we will obtain estimates for the viral shunt as an important factor for sustaining the deep biosphere.

Batzke A, Engelen B, Sass H, Cypionka H (2007) Phylogenetic and physiological diversity of cultured deep-biosphere bacteria from Equatorial Pacific Ocean and Peru Margin sediments. Geomicrobiology J 24:261-273
Danovaro R, Dell'Anno A, Corinaldesi C, Magagnini M, Noble R, Tamburini C, Weinbauer M (2008) Major viral impact on the functioning of benthic deep-sea ecosystems. Nature 454: 1084-U1027.

Development of an ultra-high resolution neutron computed tomography system for the characterisation of drill cores

A. FLAWS[1], K.-U. HESS[1], B. SCHILLINGER[2], D.B. DINGWELL[1]

[1] Department für Geo- und Umweltwissenschaften, LMU, Theresienstr. 41/III, 80333 München
[2] Forschungsreaktor FRM-II, Technische Universität München, 85747 Garching

The aim of this project (started at 01.03.09) is to further develop neutron computed tomography (NCT) as a non-destructive tool for the analysis of drill cores and other geological samples. We will apply this method to analyse crystal phases in drill cores and dome material taken from the Unzen volcano. The physics of non-Newtonian rheology of Unzen type dome lavas needs to be adequately understood in order to generate appropriate eruptions and forecast models. Acoustic emission and post deformation experimental texture analyses reveal that cracking is very important across the ductile-brittle transition. Textural analyses of our experiments show a crack distribution more or less parallel to the maximum stress field, as expected for deformation of a homogeneous cylinder in compression. The crystals, in particular, appear to influence crack propagation and in some cases strong, intact crystals may deviate crack propagation. Moreover, there was a tendency for the plagioclase crystals to be partially fragmented during the deformation. At high stresses, macroscopic cracks propagated across the crystals and shear zones developed in which crystals were completely crushed and pulverized to powder. Plagioclase crystals were especially susceptible to such crushing and the crystals which were most extensively pulverized were unfortunately rarely preserved during thin section preparation. The description of the effects of crystals in flowing lavas and the generation of cracking across the ductile-brittle transition is essential to understand effusive and explosive eruptions.

Here we propose to couple our unique experimental setup with a sequence of neutron tomography to track in situ the evolution of crystals and cracks during lavas deformation. We aim to study the differences between altered and unaltered samples in terms of the development of shear zones and their seismogenic character. The ultimate goal of this research is to observe the evolution of shear zones within the samples and thereby understand the processes involved. It is hoped this will lead to a deterministic model of failure, which in turn can lead to a prediction model of explosive eruptions. Decade volcanos, a group to which Unzen belongs, are a highly dangerous class of volcano. Such a prediction model could allow for hazard mitigation on the timescale of seconds to minutes, potentially shutting down gas; power, road bridges and other vulnerable systems in the event of an explosive eruption.

Die Pollensedimentation der Kleinen Eiszeit im Vergleich zur rezenten Pollensedimentation auf dem Seeboden der Laguna Potrok Aike, Südpatagonien, Argentinien

V. FÖRSTER, O. LANGKAMP

[1] Seminar für Geographie und ihre Didaktik, Universität Köln, Gronewaldstr. 2, D-50931 Köln, Deutschland

Anhand von ausgewählten Proben aus 46 Kurzkernen der Laguna Potrok Aike in Südpatagonien werden diese für den Sedimentationszeitraum der Kleinen Eiszeit auf Pollen untersucht, und in Vergleich zu den Ergebnissen der rezenten Pollenniederschlagsmuster gesetzt. Faktoren wie Windverhältnisse, Lufttemperatur und Niederschlag beeinflussten Strömungsverhältnisse und Pollenproduktion den Pollenniederschlag und die Sedimentation. Die prozentuale Verteilung und die absolute Konzentration der Taxa lassen Rückschlüsse auf die Umweltbedingungen zur Kleinen Eiszeit für den Sedimentationsraum der Laguna Potrok Aike zu.

The Archean to Paleoproterozoic transition as recovered in the FAR DEEP cores: LA-ICP-MS U-Pb geochronology of detrital zircons and accompanying provenance analysis of siliciclastic sedimentary rocks

C. GÄRTNER[1], H. BAHLBURG[1], E. KOOIJMAN[2], J. BERNDT[2], H. STRAUSS, V. MELEZHIK[3], A. LEPLAND[3]

[1]Westfälische Wilhelms-Universität Münster, Geologisch-Paläontologisches Institut, Corrensstraße 24, 48149 Münster
[2]Westfälische Wilhelms-Universität Münster, Institut für Mineralogie, Corrensstraße 24, 48149 Münster
[3]Geological Survey of Norway, Leiv Eirikssons vei 39, 7491 Trondheim

During the transition from the Archean to the Proterozoic (c. 2500-2000 Ma), major changes in the *modus operandi* of the Earth system occurred. Plate tectonic reorganisations like the breakup of the supercontinent Kenorland coincided with major global environmental changes. These include the first global glaciation, known as the *Huronian Glaciation*, subsequently the first pronounced rise in atmospheric oxygen (*Great Oxidation Event)*, which conincided and was followed by the largest and longest duration positive excursion of carbon isotopic composition of sedimentary carbonates (*Lomagundi-Jatuli Event)*. Afterwards the deposition of sediments anomalously rich in organic carbon took place, leading to the formation of the shungite "coals" (*Shunga Event*). Associated with global changes these events mark the transition from the Archean to the Palaeoproterozoic, but represently geochronological constraints for these events are rather poor.

The aim of the study is to improve the time constraints of these environmental events by dating detrital zircons with U-Pb-geochronology using LA-ICP-MS. The youngest detrital zircon ages of each analysed formation reflect maximum depositional ages and yield information about the beginning and end of an event. Furthermore geochemical analyses of whole rock samples will supply related information about the provenance of the rocks providing the zircons. The Chemical Index of alteration (CIA) is used to constrain the weathering conditions and derive information on the climate change at that time. In a next step in situ-single grain geochemical analyses of rutiles and tourmalines will yield information about source rocks and the source area composition beyond the geochronological information from the detrital zircons. Tourmaline reflects in its composition the geochemical information from the rock in which it formed. The main geochemical variations are expressed by the Mg, Fe and Al content, hence the major element composition is a suitable provenance tool. Rutil is one of the most stable heavy minerals and therefore very useful to get primary information about the source area of the parent rock. The geochemical composition of rutile allows to distinguish between metapelitic and metamafic source rocks. Rutiles formed in metamafic rocks show low Cr and low Nb contents, whereas metapelitic rocks contain rutiles which are characterized by low Cr and high Nb contents. In addition the content of Zr in rutile enables estimations about the minimum temperature the parent rock experienced during metamorphism.

At the moment the first samples of sandstones and siltstone-shale from the Imandra/Varzuga area and the Pechenga Greenstone belt in Russia are in preparation for LA-ICP-MS analysis. Further samples are requested and will be delivered in the next few weeks. The zircons separated so far (100-140 per sample) mostly show brownish colours and are partially rounded. The shape of the grains is mostly elongated and of different sizes from 30 µm up to >150 µm. Preliminary geochronological results will be presented during the colloquium.

Seismic data reveal origin and evolution of the Laguna Potrok Aike maar (Patagonia, Southern Argentina)

A. CATALINA GEBHARDT[1], FRANK NIESSEN[1], MARC DE BATIST[2], FLAVIO S. ANSELMETTI[3], DANIEL ARIZTEGUI[4], CONRAD KOPSCH[5], CHRISTIAN OHLENDORF[6], BERND ZOLITSCHKA[6]

[1]Alfred Wegener Institute of Polar and Marine Research, Bremerhaven, Germany
[2]Renard Centre of Marine Geology, University of Gent, Belgium
[3]Swiss Federal Institute of Aquatic Science and Technology, Dübendorf, Switzerland
[4]Section of Earth Sciences, University of Geneva, Switzerland
[5]Alfred Wegener Institute of Polar and Marine Research, Potsdam, Germany
[6]Institute of Geography (Geopolar), University of Bremen, Germany

Laguna Potrok Aike is a maar lake located in southern-most Patagonia (~52°S and ~70°W), at about 110 m a.s.l. some 20 km north of the Strait of Magellan and approximately 90 km west of the city of Rio Gallegos. It is situated in the Pliocene to late Quaternary Pali Aike Volcanic Field (Santa Cruz, southern Patagonia, Argentina). The lake has an approximate diameter of 3.5 km and is almost circular and bowl-shaped with a 100 m deep, flat plain in its central part. Steep slopes separate the central plain from the lake shoulder at about 35 m water depth. At present, strong winds permanently mix the entire water column. The closed lake basin contains a sub saline water body and has only episodic inflows with the most important episodic tributary situated on the western shore. Discharge is restricted to major snowmelt events.

Laguna Potrok Aike is located at the present boundary between the Southern Hemispheric Westerlies and the Antarctic Polar Front. The sedimentary regime is thus influenced by climatic and hydrologic conditions related to the Antarctic Circumpolar Current, the Southern Hemispheric Westerlies and sporadic outbreaks of Antarctic polar air masses. Closed lakes in southern South America have been shown to be sensitive to variations in the evaporation/precipitation ratio and have experienced drastic lake level changes in the past causing for example the desiccation of the 75 m deep Lago Cardiel during

the Late Glacial (e. g. Gilli et al., 2001). Multiproxy environmental reconstruction of the last 16 ka documents that also Laguna Potrok Aike is highly sensitive to climate change.

Based on an Ar/Ar age determination, the phreatomagmatic tephra that is assumed to relate to the Potrok Aike maar eruption was formed around 770 ka ago (Zolitschka et al., 2006). Thus Laguna Potrok Aike sediments contain almost 0.8 million years of climate history spanning several past glacial-interglacial cycles. This makes it a unique archive for non-tropical and non-polar regions of the Southern Hemisphere. Laguna Potrok Aike has thus become a major focus of the International Continental Scientific Drilling Program. Drilling operations were carried out within PASADO (Potrok Aike Maar Lake Sediment Archive Drilling Project) in late 2008 and penetrated approximately 100 m of lacustrine sediments.

Laguna Potrok Aike is surrounded by a series of subaerial paleo-shorelines of modern to Holocene age (Zolitschka et al., 2006) that reach up to 21 m above the 2003 AD lake level. An erosional unconformity observed basin-wide along the lake shoulder at about -33 m marks the lowest lake level reached during Late Glacial to Holocene times (Anselmetti et al., in press). A high-resolution seismic survey revealed a series of buried, subaquatic paleo-shorelines that hold a record of the complex transgressional history of the past approximately 6800 years, which was temporarily interrupted by two regressional phases from approximately 5800 to 5400 and 4700 to 4000 cal BP (Anselmetti et al., 2009).

Seismic reflection and refraction data provide insights into the sedimentary infill and the underlying volcanic structure of Laguna Potrok Aike (Gebhardt et al., submitted). Reflection data show undisturbed, stratified lacustrine sediments at least in the upper ~100 m of the sedimentary infill. Two stratigraphic boundaries were identified in the seismic profiles (separating subunits I-ab, I-c and I-d) that are likely related to changes in lake level. Subunits I-ab and I-d are quite similar even though velocities are enhanced in subunit I-d. Subunit I-c is restricted to the central parts of the lake and thins out laterally.

A velocity-depth model calculated from seismic refraction data reveals a funnel-shaped structure embedded in the sandstone rocks of the surrounding Santa Cruz Formation. This funnel structure is filled by lacustrine sediments of up to 370 m in thickness. These can be separated into two distinct subunits with i) low acoustic velocities of 1500-1800 m s^{-1} in the upper part, and ii) enhanced velocities of 2000-2350 m s^{-1} in the lower part. Below the lacustrine sediments, a unit of probably volcanoclastic origin is observed (>2400 m s^{-1}). This sedimentary succession is perfectly comparable to other well-studied sequences (e.g. Messel and Baruth maars, Germany), confirming phreatomagmatic maar explosions as the origin of Laguna Potrok Aike.

Anselmetti, F. et al. (2009). Environmental history of southern Patagonia unravelled by the seismic stratigraphy of Laguna Potrok Aike. Sedimentology. doi: 10.1111/j.1365-3091.2008.01002.x

Gebhardt, A.C., et al. (subm). Origin and evolution of Laguna Potrok Aike Maar (Southern Patagonia, Argentina). Basin Research.

Gilli, A. et al. (2001). Tracking Abrupt Climate Change in the Southern Hemisphere: A Seismic Stratigraphic Study of Lago Cardiel, Argentina (49°S). Terra Nova, 13: 443-448.

Zolitschka, B. et al. (2006). Crater lakes of the Pali Aike Volcanic Field as key sites of paleoclimatic and paleoecological reconstructions in southern Patagonia, Argentina. Journal of South American Earth Sciences 21: 294-309.

Response of the Methane Cycle to Climate Changes in the Past and Present

J. GRIESS[1,2], K. MANGELSDORF[2], D. WAGNER[1]

[1]Alfred Wegener Institute, Research Unit Potsdam, Telegrafenberg A45, 14473 Potsdam, Germany
[2]Helmholtz Centre Potsdam, GFZ German Research Centre for Geosiences, Telegrafenberg B423, 14473 Potsdam, Germany

Arctic permafrost environments play an important role within the global methane cycle. Thawing of permafrost and the associated release of this climate relevant trace gas, due to an increased microbial turnover of organic carbon and from ancient methane reservoirs, represent a potential risk to global warming. For the prediction of a future development of the permafrost environment and its contribution to the global atmospheric carbon budget, it is important to understand how this system reacted to environmental changes in the past.

The El'gygytgyn lake region, Northeast Siberia, represents an ideal model system for studying the response of the methane cycle to climate change. It is supposed to be unglaciated since the time of a meteorite impact 3.6 Ma ago and since that time the permafrost went through four major climate-induced stages during the last 300,000 years. These changes in climate caused chemical and physical variations in sedimentary column and thus we expect changes in the composition of key microrganisms that were implicated in methane cycle.

A 140 m long permafrost core from El'gygytgyn lake region was recovered within the ICDP project "Scientific Drilling in El'gygytgyn Crater Lake" in November 2008. Our studies will be conducted on combining microbial biomarker analyses and rRNA gene analyses in a high stratigraphic resolution. While rRNA gene sequences provide detailed informations on taxonomy, the extraction and analyses of microbial marker molecules are quantitative and correlate to cellular biomass. These two approaches are independent and thus can verify each others results. In addition to these studies, methane concentrations as well as the methane production and oxidation activity will be determined in the deposits. The obtained data will be interpreted in context of the results on inorganic properties in permafrost deposits of the El'gygytgyn lake region and paleoclimate reconstructions in this area provided by cooperation partners of the ICDP project "Scientific Drilling at El'gygytgyn Crater Lake".

Magnetofabrics of ultrahigh-pressure gneisses from the Chinese Continental Scientific Drilling (CCSD) project: Evidence for a genetic link between ferromagnetic and paramagnetic gneisses

J.C. GRIMMER[1], X.X. QI[2], Z.Q. XU[2]

[1]Strukturgeologie & Tektonophysik, Geologisches Institut, Universität Karlsruhe (TH), Hertzstr. 16, 76187 Karlsruhe
[2]Institute of Geology, Chinese Academy of Geological Sciences, Baiwanzhuang Road 26, 10027 Beijing, China

Introduction

Quartzofeldspathic gneisses comprise the largest rock volumes in, but not limited to ultrahigh-pressure (UHP) orogens. Due to their uniform petrography and low- to medium-grade metamorphic conditions gneisses attract less interest than the volumetrically less abundant eclogites and ultramafic rocks, which commonly contain the evidence for UHP-metamorphism. Nevertheless gneisses play an important role during exhumation not only because they commonly host eclogites and ultramafic rocks, but also because of relatively low densities, a quartz-dominated weak rheology, and their potential for partial melting and crustal water recycling. We present data of the anisotropy of magnetic susceptibility (AMS) of UHP-gneisses from the uppermost 1750 m of the 5138 m deep CCSD-mainhole in the Sulu orogen of east-central China (Fig. 1) in order to improve our understanding of retrograde processes during exhumation of UHP-gneisses. AMS-studies are also helpful for interpreting susceptibility borehole logs. Based on geochemistry and petrography six units are distinguished for the uppermost 2 km by Zhang et al. (2006): Unit 1 (100-530 m) consists of quartz-rich eclogites, rutile-rich eclogites and thin gneiss layers. Unit 2 (530-600 m) consists of rutile- and ilmenite-rich eclogites. Unit 3 (600-680 m) consists of serpentinized ultramafic rocks with minor intercalations of eclogite and garnet pyroxenites. Unit 4 (680-1160 m) consists of interlayered paragneisses, eclogites, retrograde eclogites – i.e. amphibolites and greenschists – and a thin ultramafic layer at ca. 850 m. Unit 5 (1160-1600 m) consists of an orthogneiss body with thin layers of amphibolites and biotite-phengite-(±garnet)-gneisses. Unit 6 (1600-2050 m) consists of eclogites with minor gneiss layers. The Maobei eclogite body (units 1-3) represents a former lower crustal intrusive body with mafic-ultramafic cumulates (Zhang et al. 2006; Liu et al. 2008). The lithologies of unit 4 represent a supracrustal succession consisting of bimodal volcanic and (volcano-)clastic rocks (Zhang et al. 2006). Unit 5 represents a Neoproterozoic granitic intrusion whereas lithologies of unit 6 represent again a supracrustal succession. The UHP-gneisses of the CCSD-borehole are composed of variable proportions of quartz, K-feldspar, and plagioclase with variable contents of biotite, white mica, garnet, chlorite, epidote, amphibole, kyanite, jadeite – depending on bulk rock chemistry and the degree of retrograde metamorphism. Accessory phases comprise zircon, apatite, and Fe-Ti-oxides.

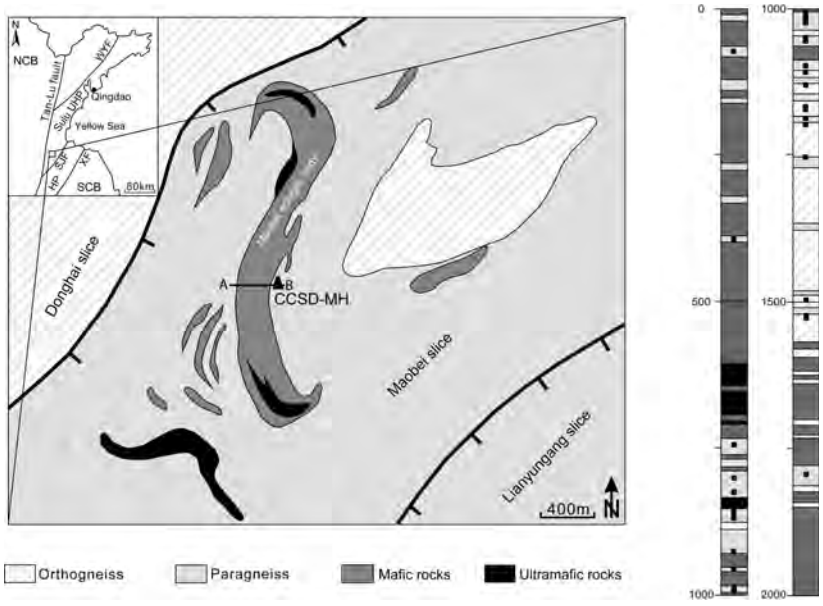

Figure 1: Left figure: Overview map (inset upper left) of the Sulu UHP metamorphic belt with bordering faults (XF: Xiangshui Fault; SJF: Shuyang-Jinping fault; WYF: Wulian-Yantai-Fault). Geologic overview map shows major mafic-ultramafic bodies in the UHP-gneisses and the presence of crystalline nappes (`slices´), which are separated by ductile shear zones with top to NW kinematics (barbs on hanging wall; Xu et al. 2006). Right figure: Lithologic section of the CCSD-mainhole showing the sampling (black squares).

Results

Bulk susceptibility

The mean susceptibilities (K_{mean}) of the felsic gneisses of unit 1 vary from 0.2×10^{-3} to 31.4×10^{-3} SI, of unit 4 from 0.1 to 38.8×10^{-3} SI, and of unit 5 from 0.2 to 22.9×10^{-3} SI. K_{mean} of the greenschists of unit 4 vary from 0.3 to 83.2×10^{-3} SI. Samples with $K_{mean} < 0.5 \times 10^{-3}$ SI are considered as paramagnetic whereas samples with $K_{mean} > 0.5 \times 10^{-3}$ SI may be already influenced by ferrimagnetic phases and thus may be treated as superposed para-/ferromagnetic fabric. Samples with $K_{mean} > 5 \times 10^{-3}$ SI

are commonly dominated by a ferromagnetic fabric. The gneisses and greenschists outline variable inter- and intra-sample variations of K_{mean} and thus variable contributions of para- and ferromagnetic subfabrics. Intra-sample variation of K_{mean} can be up to two orders of magnitude or rather insignificant. Variation diagram of K_{mean} versus density outlines a well-defined positive correlation for paramagnetic gneisses since higher contents of biotite augment both density and K_{mean} (Fig. 2). For the ferromagnetic gneisses the correlation is also well defined and again positive since higher contents of magnetite augment both density and K_{mean}. Cogenetic gneisses with a large intra-sample variation of K_{mean} are in particular suitable to assess possible genetic links between the para- and ferromagnetic gneisses. These particular samples outline diffuse, but nevertheless negative correlations between K_{mean} and the density implying the decomposition of magnetite and the concomitant formation of a paramagnetic Fe-silicate phase (Fig. 2). Variation of K_{mean} with depth is shown in Fig. 3. From 700 to 1000 m below surface K_{mean} appears to generally increase with depth: Paramagnetic gneisses appear to be more abundant in this depth interval than in the deeper levels. This depth interval roughly coincides with a seismic reflector, which is interpreted as a major ductile shear zone (Xu et al. 2006). In this shear zone eclogites are strongly retrogressed to greenschists implying that the paramagnetic gneisses may represent retrogressed ferromagnetic gneisses.

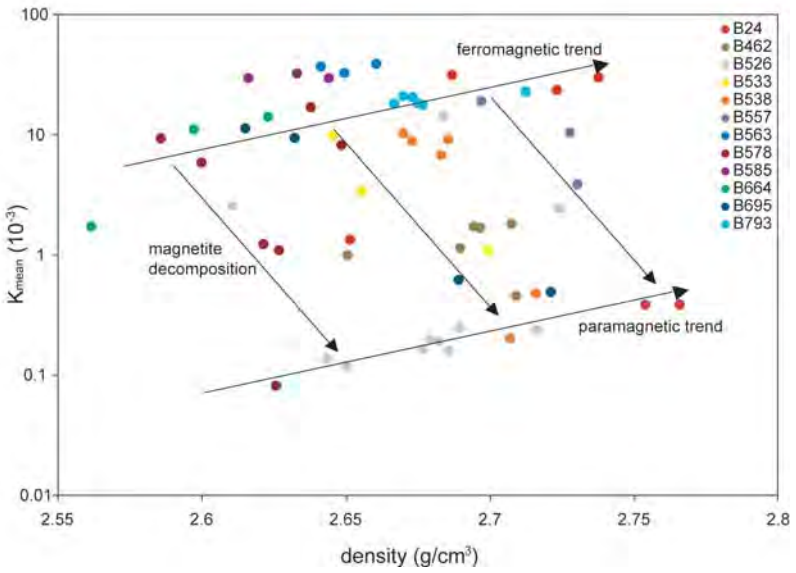

Figure 2: K_{mean}-density variation diagram of ferromagnetic gneisses and gnesses with a high intrasample variation of K_{mean} showing diffuse negative correlations for samples with large intrasample variation, which is interpreted to document magnetite decomposition of ferromagnetic gneisses and the formation of paramagnetic gneisses.

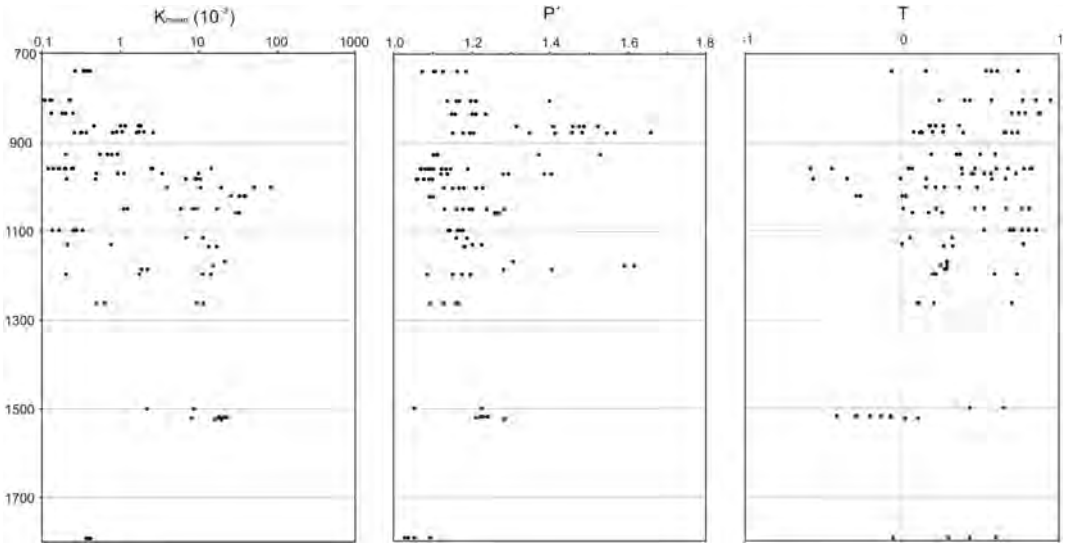

Figure 3: Depth-dependent variation of mean susceptibility (K_{mean}), corrected degree of anisotropy (P´), and shape factor (T) for the depth interval 700-1750 m below surface.

Magnetic anisotropy

The shape of the AMS ellipsoid and its degree of anisotropy in metamorphic rocks depend on the minerals that dominate both the magnetic susceptibility and shape- or lattice-preferred orientation acquired during their metamorphic history. The shape factor (T) and the corrected degree of anisotropy (P´) are plotted against each other in the Jelinek-Diagram in order to describe the shape of the AMS ellipsoids for the different felsic gneisses (Fig. 6). The corrected degrees of anisotropy (P´) of the gneisses of unit 1 vary from 1.07 to 1.35, of unit 4 from 1.06 to 1.53, and of unit 5 from 1.05 to 1.62. The majority of the samples have P´-values below 1.3. P´ of the greenschists of unit 4 vary from 1.03 to 1.66. The shape factors T of the gneisses of unit 1 vary from -0.74 to 0.83, of unit 4 from -0.59 to 0.95, and of unit 5 from -0.42 to 0.73. The shape factors T of the greenschists of unit 4 vary from 0.07 to 0.74. Except for a few samples anisotropies remain essentially constant or decrease slightly with decreasing susceptibilities. The decomposition of magnetite thus causes no major increase of P´.

Orientation of the principal susceptibility axes

Samples outlining significant intra-sample variations of K_{mean} are in particular suitable to assess the relative impact of ferrimagnetic phases onto magnetofabric evolution. These samples display coaxial AMS-ellipsoids that are almost independent of their susceptibility. Magnetic lineation of the majority of samples show some scatter due to the dominantly oblate shapes of the AMS ellipsoids and thus K_{max} may permute with the K_{int}-axes. The two samples of unit 1 show different fabrics: The shape of the AMS-ellipsoid of B24 is dominantly prolate whereas that of B164 is dominantly oblate. The magnetic lineation of B24 trends N-S and the bulk fabric is coaxial with the eclogites and ultramafic rocks of Qi et al. (in press). Magnetic foliation of B164 dips moderately to the E with an E-trending magnetic lineation and a N-S-trending K_{int}-axis probably mimicing the fabric of B24 and of the mafic-ultramafic rocks of units 1, 2, and 3 by axes permutation. Magnetic foliations of gneisses of unit 4 dip to the ENE with a large scatter of the dip angles and magnetic lineation trends due to axes permutation of K_{max} and K_{int}. Magnetic foliations of the gneisses of unit 5 (1160-1600 m) display shallow dip angles to the NE with strongly scattered orientations of the magnetic lineation. Magnetic foliations of the greenschists from unit 4 show moderate dip angles to the (E)NE with a NE-trending magnetic lineation.

Conclusions and discussion

Since no impact on the orientation of the AMS-ellipsoids is observed magnetite decomposition took place during or after the major ductile deformation phase – probably under greenschist facies conditions. This can be well documented by SEM imaging, which shows fractured magnetite with newly grown biotite and magnetite inclusions in biotite. AMS data may thus be better interpreted as tracing retrograde fluid-induced decomposition of magnetite and concomitant biotite growth rather than primary compositional variation. Fluid-induced retrogression and decomposition of magnetite may also explain the relatively low susceptibilities in the shear zone together with the occurrence of the greenschists as strongly retrogressed eclogites since ductile shear zones are considered as `fluid attractors´ in the middle and lower crust. Susceptibility borehole logging the CCSD-gneisses thus may serve as a first order tool to localize intense retrograde fluid-rock interaction zones and possible greenschist-grade ductile shear zones at various scales. The present data show that the measurement of the AMS appears to be insensitive to distinguish between para- and orthogneisses: There are no systematic petrographic or textural variations, which can be referred to a sedimentary or igneous origin and which are displayed by the AMS-data.

Acknowledgments

Support by the Deutsche Forschungsgemeinschaft (Project GR3193-1) and the Major State Basic Research Program of P.R. China (973; Grant No. 2003CB716504) is greatly acknowledged. Thanks to J. Hoefs and Y. Xiao (Göttingen), A. Gerdes (Frankfurt), R. Oberhänsli, and A. Riemann (Potsdam) for sample exchange and discussions.

Liu Y, Zong K, Kelemen PB, Gao S (2008) Geochemistry and magmatic history of eclogites from the Chinese continental scientific drill hole: Subduction and ultra-high pressure metamorphism of lower crustal cumulates. Chemical Geology 247, 133-153.

Qi XX, Grimmer JC, Xu ZQ (in press) Magnetofabrics of eclogites and ultramafic rocks from the Chinese Continental Scientific Drilling (CCSD) project: evidence for ultrahigh-pressure (UHP) texture inheritance throughout retrogression. Tectonophysics. doi: 10.1016/j.tecto.2008.09.015.

Xu Z, Zeng L, Liu F, Yang J, Zhang Z, McWilliams M, Liou J (2006) Polyphase subduction and exhumation of the Sulu high-pressure-ultrahigh-pressure metamorphic terrane. Geological Society of America, Special Paper 403, 93-113.

Zhang Z, Xiao Y, Hoefs J, Liou J, Simon K (2006) Ultrahigh pressure metamorphic rocks from the Chinese Continental Scientific Drilling Project: I. Petrology and geochemistry of the main hole (0-2,050 m). Contributions to Mineralogy and Petrology 152/4, 421-441, doi: 10.1007/s00410-006-0120-5.

Marine Isotope Stages (MIS) 100-101: The first modern glacial – interglacial cycle?

J. GROENEVELD[1,3] , H. DEBEY[2], E.C. HATHORNE[1], S. STEINKE[1]

[1]Institute of Marine Environmental Sciences (Marum), University Bremen, Leobener Str., D-28359 Bremen
[2]DeBey, H., University of California, Los Angeles, USA
[3]now at: Alfred Wegener Institute, Columbusstrasse D-27570 Bremerhaven

We present combined Mg/Ca and $\delta^{18}O$ measurements and sand content from ODP Site 1241 from the east Pacific and ODP Site 999 from the Caribbean. The studied time interval covers the first major glacial-interglacial cycle (MIS100-101) after intensification of Northern Hemisphere Glaciation. Analyses were performed on the planktic foraminifers *Neogloboquadrina dutertrei* and *Globigerinoides sacculifer*, representing water mass properties in the thermocline and the mixed layer respectively. Data resolution is aimed to be able to resolve millennial scale variations to constrain the changes in water mass conditions during MIS100-101.

Aim of the study is to test the theory that the Panamanian Gateway temporarily closed during glacial MIS 100 due to a drop in sea level of 50-80 m. This was first suggested in Groeneveld et al., (in prep.) and might have provided the necessary conditions to allow the Great American Biotic Interchange, the large scale migration of mammals from South to North America and vice versa. As this exchange would have required more arid conditions in Central America to allow the fauna, which was mainly adapted to a savannah-like environment, to cross, a glacial period would have provided the right conditions. Reconstruction of sea water temperatures can indicate if and when the gateway closed. With an open Panamanian Gateway relatively cold water flowed from the Pacific into the Caribbean. With the onset of glacial conditions sea surface temperatures (SST) expectedly would show a decrease in the east Pacific (Site 1241). But, SSTs in the Caribbean (Site 999) are expected to rise as no longer relatively cold Pacific water is entering the Caribbean, but rather the warmer waters from the Western Atlantic Warm Pool advanced from the north to the core location. Indeed, reconstructed SSTs from *G. sacculifer* show a decrease of 2.5°C at Site 1241 and an increase of 3°C at Site 999 suggesting that the Panamanian Gateway truly was closed during the glacial stage.

Additionally, the Mg/Ca-temperatures of *N. dutertrei*, a thermocline dweller, do not show any change in the east Pacific, but do show a 3°C cooling in the Caribbean. This suggest that the closing of the gateway only influenced surface water conditions. The decrease in *N. dutertrei* temperatures can be explained in two ways. With the closure the Western Atlantic Warm Pool extended towards the southern Caribbean, increasing sea surface temperatures as indicated by *G. sacculifer*. This resulted in an increase in mixed-layer thickness, pushing the thermocline to a larger water depth. As *N. dutertrei* is often characterized as following the nutrient maximum in the thermocline, it accordingly lived deeper during MIS100, and, hence, indicates lower temperatures. Alternatively, it was suggested that with the closure of the gateway slight upwelling conditions could have occurred in the Columbia Basin, resulting in colder temperatures in the thermocline and for *N. dutertrei*. Obviously in this case it would mean that upwelling was not very intense as sea surface temperatures meanwhile increased.

The sand fraction can give indications both on the preservation of the foraminifers, and therefore, on possible biases in the Mg/Ca reconstruction, and on changes in primary productivity. During interglacial MIS101 sand fraction is similar at both sites, again indicating an open Panamanian Gateway. Into glacial MIS100, however, sand fraction at Site 1241 shows a decrease, while an increase occurs in the Caribbean, again indicating closure of the gateway. It can be excluded that these changes represent significantly different preservation states and, therefore, did not have an effect on the Mg/Ca reconstructions. Reason is that at both Site 999 and Site 1241 the Mg/Ca records of *G. sacculifer* and *N. dutertrei* are not parallel, excluding a dissolution based bias. Therefore, it seems likely that the increase in the Caribbean is more likely to be related to an increase in primary productivity.

The next stage of this study will include stable isotope analyses on both species and extending the records to MIS96-99, so that all three major glacial-interglacial cycles around 2.5 Ma are covered.

PASADO deep drilling (southern Argentina) - first results reveal a climate record far back into the last glacial

A. HAHN, P. KLIEM, C. OHLENDORF, B. ZOLITSCHKA AND THE PASADO SCIENCE TEAM

University of Bremen, Institut of Geography (GEOPOLAR), 28359 Bremen, Germany

Laguna Potrok Aike is a 100m deep maar lake, located in the dry steppe of southern Patagonia 80km north of the Strait of Magellan. Although scarcely studied, paleoclimatic archives from this area are of special interest, as they permit insights into the variations of polar and mid latitude winds and pressure fields. During the 2008 PASADO international deep drilling campaign more than 500m of lacustrine sediments were recovered from Laguna Potrok Aike allowing climate and environmental reconstruction. In the onsite field laboratory analyses were done (1) on the core sections and (2) on samples taken from the core catchers.

Seven holes from two sites in the center of the lake were obtained, the maximum core depth being 100m. So far only samples that were taken in the field during the drilling operations have been analysed giving us an idea of the climate record that can be expected. These analyses are mainly based on core catcher sediment samples taken at the base of every core run at approximately 3 m intervals. The analyses done on site include grain size estimations, determinations of water content, smear slide analyses and the measurement of pH, conductivity, as well as chlorid and calcium concentrations in a sediment suspension..Additionally, magnetic susceptibility measurements were carried out on all cores in two centimeter increments

with the Geotek multi sensor core logger (MSCL). Magnetic susceptibility measurements show that cores from different holes of one site can be correlated to form a composite profile. Similarly, the composite profiles of both sites can also be correlated.

Core catcher sediment analyses reveal that the cores contain Holocene and Late Glacial sediments as well as sediments from large parts of the last glacial. The Holocene sediments can be distinguished by their higher calcium and chloride content, and a higher pH and conductivity. They form the topmost 10-15m of the sediment sequence. Smear slide analysis demonstrates that the increase in calcium results from autochthonous calcium carbonate precipitation. The magnetic susceptibility measurements agree with this finding, with relatively low and more variable values in the topmost ca.15 m of the record and higher values with decreased variability below 15m. The depth of 10-15 m is presumed to be the transition period between warm and cold climates and is marked by the increased appearance of organic macro remains in the sediments. As the topmost 15m seem to represent the Holocene and thus a time span of 11 600 years, it can be presumed that, if sedimentation rates remain relatively constant, the bottommost 85m could represent the last glacial including oxygene isotope stages 2 to 4 and maybe the end of stage 5.

Furthermore, volcanic ashes were identified by the appearance of pumice in smear slides. These light-coloured tephra layers which are also present on preserved subaereal terraces around the lakes not only document volcanic activity, but are also of importance for future linkages to marine sediment archives and ice cores. Moreover, volcanic ashes will be one of the main backbones for dating purposes - tephrochronology.

The PASADO deep drilling revealed coarse grained sands and fine gravel in several core sections which questions previous assumptions about the area's climatic past. The largest grain sizes (fine gravel) were found predominantly in a depth range of 70 to 100 m and may be the result of a low lake level or even a complete desiccation event of the lake, thus perhaps interrupting the continuity of the record.

These preliminary data collected during field-based analyses have given us a first impression about the composition of the sediments which will soon be substantiated. Sediment cores are currently on their way to Bremen where opening and sampling will start by the end of March 2009. The planned much more detailed analyses will allow high-resolution quantitative climate and environmental reconstructions from orbital and suborbital (multimillennial) down to decadal timescales supported by multiple dating (e.g. ^{14}C, OSL, Ar/Ar) and stratigraphic correlation (e.g. pollen, tephra, paleomagnetics). Finally, the aim is to work out linkages to marine archives and ice cores and to incorporate results from GCM climate simulations, thus enhancing the understanding and predictability of climate processes in the southern hemisphere.

Comparing the tropical vegetation distribution of a Heinrich-like climate to that of a pre-industrial one

DIAN N. HANDIANI, ANDRÉ PAUL, LYDIE M. DUPONT

MARUM - Center for Marine Environmental Sciences, University of Bremen, Leobener Strasse, 28359 Bremen

Abrupt climate change occurred in the ocean as well as on land during periods of Heinrich events. Heinrich events are associated with a slowdown of the Atlantic Meridional Overturning Circulation (AMOC), which in turn would lead to a cooling of the North Atlantic Ocean and a warming of the South Atlantic Ocean (the "bipolar seesaw" hypothesis). This also affected vegetation patterns in eastern South America and West Africa. Pollen data from the Angolan and Brazilian coasts indicated a retreat of the evergreen forest and an expansion of the coastal desert, while in north-east Brazil shrubs, dry forest and Atlantic rain forest thrived.

To understand the trans-Atlantic differences, we studied the vegetation response to Heinrich-like climate perturbations using a dynamic global vegetation model (TRIFFID), which is part of the University of Victoria (UVic) Earth System-Climate Model (ESCM). For a near-collapse of the AMOC, the model showed a clear bipolar seesaw in temperature and precipitation. A southward shift of the tropical rainbelt resulted in a strong decrease in precipitation in Northwest and West Africa and in northern South America, but an increase in precipitation in south-eastern South America. This caused a succession in plant-functional types (PFTs) from forest to shrubs to desert, with a spreading of desert in North Africa, a retreat of broadleaf trees in West Africa and northern South America, but an advance of broadleaf trees in southern South America.

To compare the model results with pollen data, we diagnosed the distribution of biomes from the distribution of PFTs and the simulated model climate. The biome distribution was computed for the simulation of Heinrich-like events and for a control-run using pre-industrial boundary conditions. They were then compared to available pollen data from Heinrich events (see abstract of Heßler et al., this volume) and the BIOME 6000 (v 4.2) vegetation reconstruction (http://www.bridge.bris.ac.uk/resources/Databases/BIOMES_data), respectively.

Flow Through cleaning and sequential dissolution of Neogene planktonic foraminifera for Mg/Ca analyses

ED C. HATHORNE[1], JEROEN GROENEVELD[1*], STEPHAN STEINKE[1], MARTIN KÖLLING[1]

[1]MARUM-Centre for Marine Environmental Sciences, University of Bremen, Leobener Strasse D-28359 Bremen
[*]Now at: Alfred Wegener Institute, Columbusstrasse D-27570 Bremerhaven

Much of what is known about the Cenozoic climate change comes from studies of the isotopic and elemental chemistry of the calcite tests of planktonic and benthic foraminifera preserved in marine sediments. However, there is no consensus concerning which cleaning methods to apply prior to trace element analysis, especially for samples from pre-Pleistocene sections. Here we demonstrate the application of a Flow Through (FT) cleaning device and sequential dissolution to conducting Mg/Ca measurements on foraminifera of Pliocene and Miocene age.

FT cleaning pumps water and other reagents in a constant flow over a sample to remove contaminants and then dissolves the sample calcite/aragonite while other contaminants remain on the sample holding filter (Klinkhammer et al., 2004). FT cleaning can be coupled directly to an ICP instrument and time resolved analysis enables data to be filtered for contaminants (Klinkhammer et al., 2004) providing a pure calcite/aragonite signal. We have developed a fully automated FT cleaning device at the MARUM, University of Bremen, and the initial results obtained by coupling the device to an Inductively Coupled Plasma Optical Emission Spectrometer (ICP-OES) are very promising. The stability of the element/Ca ratio of a standard solution while the Ca concentration is varied by dilution is remarkable and enables the element/Ca ratio of samples to be calculated with ease. The accuracy of the technique for the determination of Mg/Ca ratios is demonstrated by the repeated measurement of the limestone standard powder (ECRM 752-1) employed by a recent foraminiferal Mg/Ca interlaboratory study (Greaves et al., 2008).

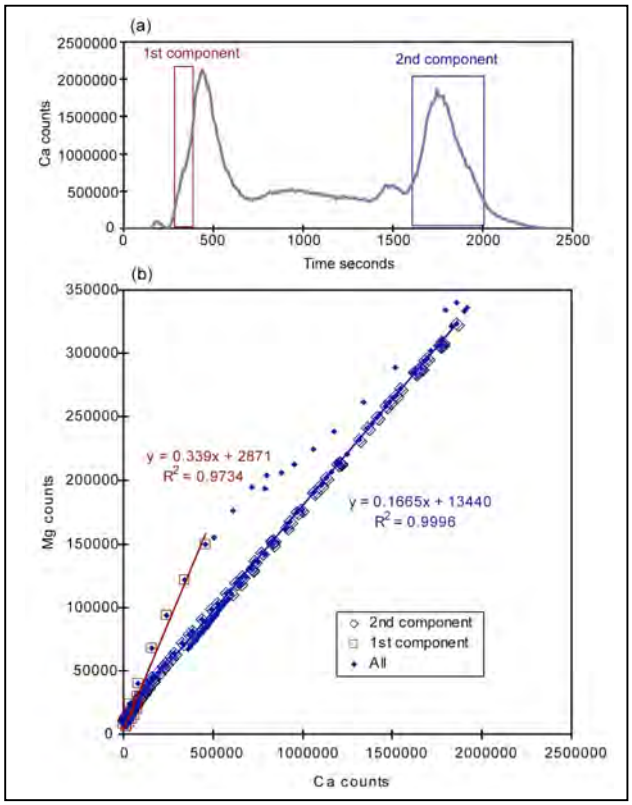

Figure 1. (a) Time resolved Ca signal resulting from the sequential dissolution of a *G. sacculifer* sample from ODP Site 999. (b) Mg versus Ca plot for the same sample showing the distinctive Mg/Ca ratios for two different components resolved by sequential dissolution.

Time resolved analysis of the sequential dissolution of a Miocene *G. sacculifer* sample from ODP Site 1146, not subjected to any cleaning, yields Mg/Ca ratios lying within the range of those obtained for the same sample following various traditional cleaning techniques. The same technique applied to *G. sacculifer* samples of Pliocene age, from ODP Site 999, reveals components with distinctive Mg/Ca (Figure 1) and Mn/Ca ratios, suggesting the technique has the potential to distinguish original calcite from secondary precipitates which can result from burial diagenesis.

Klinkhammer, G. P., et al. (2004) Paleoceanography 19, PA4030.
Greaves, M., et al. (2008) Geochem. Geophys. Geosyst.9(8), Q08010.

Investigations of the Heat Flow Density at the Chesapeake Bay Area, Virginia, USA

P. HEIDINGER[1], H. WILHELM[1], Y. POPOV[2], D. MIKLASHEVSKIY[2]

[1]Geophysical Institute, University of Karlsruhe, Hertzstrasse 16, 76187 Karlsruhe, Germany
[2]Russian State Geological Prospecting University, Miklukho-Maklai 23, Moscow 117997, Russia

The scientific well Eyreville-B drilled within the framework of the International Continental Deep Drilling Program (ICDP) penetrated the Chesapeake Bay impact structure ca. 9 km from its center. This deep structure is a late Eocene complex crater, which was excavated ~ 35 Ma ago in a continental shelf environment at the Atlantic margin, in Virginia. Petrophysical and geothermal studies of this borehole are in publication proccess (see papers by Mayr et al., 2009 and Heidinger et al., 2009). Boreholes drilled in impact structures are especially suited for investigations of the influence of lithological heterogeneities on petrophysical properties and the thermal field. A temperature measurement campaign in May 2006 and laboratory measurements of the thermal conductivity on 52 samples from this borehole yielded a depth profile of the vertical heat flow density (HFD). The total variation of the HFD is high and ranges from 40 to 80 mW/m^2 (Fig 1). The averaged result is identified as the terrestrial HFD, which was determined to a value of 65 ± 6 mW/m^2. This local terrestrial HFD is ~ 40% higher than the predicted values for this area (42 - 52 mW/m^2, Morgan and Gosnold, 1989). To investigate regional lateral heat flow variations within the central part of the impact zone by comparison of heat flow densities determined at different locations and local vertical heat flow variations within specific boreholes as an indication of regional thermal refraction, samples of other suitable boreholes (cores available and borehole still open and accessible) were collected in July 2008. Wells, number of samples and open depths are listed in table 1. The locations of these boreholes are shown in figure 2. The laboratory measurements of the thermal conductivity is in progress and the logging campaign to measure the temperature profiles of these boreholes is envisaged for summer 2009.

Name	Samples collected	Open depth
Kiptopeke	75	543 m
Newport News Park II	32	377 m
Fentress 61B 11	148	633 m
Jenkins Bridge 66M 23	40	402 m
North 59H 4	72	584 m
USGS STP 2	4	700 m
USGS Eyreville B	181 (in 2006)	1100 m

Table 1: Summary informations of the investigated boreholes and collected samples

References:
Heidinger P., Wilhelm H., Popov Y., Šafanda J., Burkhardt H., and Mayr S., 2009, First results of geothermal investigations, Chesapeake Bay impact structure, Eyreville boreholes, Geological Society of America Special Paper (preliminarily accepted).
Mayr S.I., Burkhardt H., Popov Y., Romushkevich R., Gorobtsov D., Heidinger P., and Wilhelm H., 2009, Physical rock properties (Eyreville coreholes) - Results and first interpretations of the laboratory measurements, Geological Society of America Special Paper (preliminarily accepted).
Morgan P., and Gosnold W., 1989, Heat flow and thermal regimes in the continental United States, in Pakiser L.C., and Mooney W.D., eds., Geophysical framework of the continental United States, Geological Society of America Memoir, Vol. 172, p. 493-522.

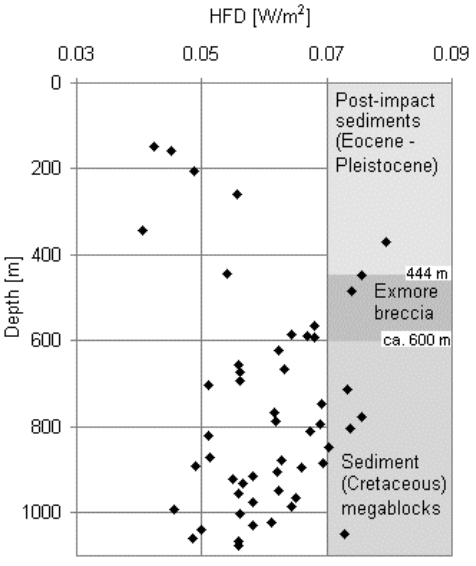

Fig. 1: Heat flow density data for borehole Eyreville.

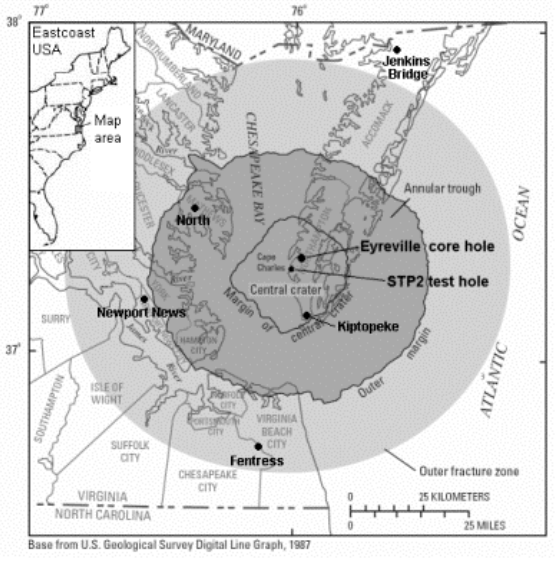

Fig. 2: Regional map showing the locations of wells. The geometry and structure of the Chesapeake Bay impact crater are based from the USGS professional paper 1688.

Magnetic susceptibility loss at glacial-interglacial transitions in the early Pliocene sedimentary record of ODP Site 1095

D. A. HEPP[1], T. MÖRZ[1], T. FREDERICHS[2], H.-J. BRUMSACK[3]

[1]MARUM – Center for Marine Environmental Sciences and Faculty of Geosciences, University of Bremen, P.O. Box 330440, 28334 Bremen, Germany
[2]Faculty of Geosciences, University of Bremen, P.O. Box 330440, 28334 Bremen, Germany
[3]Institute for Chemistry and Biology of the Marine Environment (ICBM), Carl von Ossietzky University of Oldenburg, P.O. Box 2503, 26111 Oldenburg, Germany

Ice has been present on Antarctica since the Eocene/Oligocene transition. Starting with the late Miocene (~10 Ma) the West Antarctica has been covered by a waxing and vanishing ice sheet that periodically extended to the shelf edge. The sedimentary response to Antarctic Peninsula ice sheet dynamics and changes in the regional oceanographic realm during the latest Miocene-early Pliocene warming phase is well documented in distal records from the Pacific continental rise off the Antarctic Peninsula (ODP Site 1095, Drift 7, Fig. 1). Such changes, especially enhanced primary productivity and accumulation of biogenic components, are reflected in paleoenvironmental proxies, e.g. the magnetic signal in the sedimentary record.

Prominent losses of the magnetic susceptibility signal have been reported in various studies. They may have a variety of reasons and characteristics, e.g. early diagenetic processes like iron reduction under suboxic to anoxic conditions and the anaerobe oxidation of methane, or sedimentary processes like dilution effects, changes in provenance of the of the source material and composition of the supplied sediments.

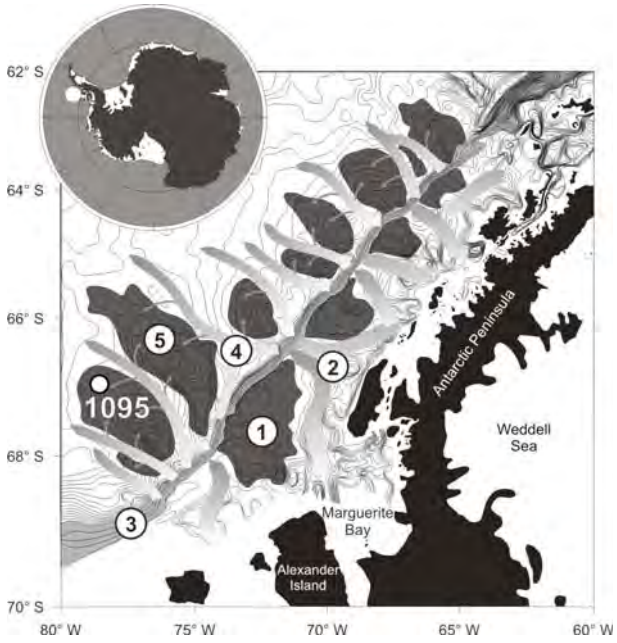

Fig. 1. Bathymetric map of the Pacific continental margin off the Antarctic Peninsula. The map shows a glacial driven sediment feeder system of (1) lobes and (2) troughs on the outer shelf, (3) an oversteepen slope, (4) deep-sea channels and (5) sediment drifts on the continental rise and the location of Site 1095, ODP Leg 178 on the distal part of Drift 7.

From ODP Site 1095 sediment cores, we have identified sixty-four zones with prominent losses of the magnetic susceptibility signal, which are comparable in shape, magnitude and value. These zones, in the following referred to as magnetic susceptibility minima zones (MSMZ), are characterized by a U-shaped decrease of about one order of magnitude in magnetic susceptibility and a lack of variance in the bottom part of the U-shape. MSMZ occur in ODP Site 1095 from 79.35 mcd (~3.17 Ma) to 382.97 mcd (~8.49 Ma). The 300 m long core sequence represents a period of ~5 m.y., from late Miocene to early Pliocene. In our study we analyze three shorter Pliocene sequences across this interval.

Magnetic susceptibility measurements of individual samples (Fig. 2d) containing hemipelagic sediment, silt or IRD from outside the MSMZ clearly show that the magnetic susceptibility of silt samples (solid circles) is about three times higher than in hemipelagic samples (open circles). High total magnetic susceptibility (between 104.30 and 103.66 mcd, Fig. 2c) is noticed in IRD dominated sections. The loss of magnetic susceptibility in the MSMZ is observed in hemipelagic and silt size samples independent of changes in grain size. Within the upper part of the MSMZ, coarse fraction samples with lithic fragments from IRD largely preserved their magnetic signal (Fig. 2d). Neither the onset of the MSMZ nor the termination coincide with changes in silt occurrence or IRD supply: (1) turbiditic silt layers are continuous across the sharp onset of the MSMZ, (2) the recovery of the magnetic signal in the fine fraction marks the end of the MSMZ during an episode of massive IRD supply. We conclude that mineral- and grain-size selective processes, largely independent from changes in the lithogenic flux, modified the magnetic susceptibility signal.

The onset of MSMZ is associated with an increase in diamagnetic $BSiO_2$ (Fig. 2f). This change is, however, insufficient to explain the abrupt drop in magnetic susceptibility by one order of magnitude. Dilution effects by diamagnetic and paramagnetic sediment compounds can be further ruled out since high opal contents continue across the upper termination of the MSMZ. The independence of MSMZ from sedimentary dilution effects is further confirmed by the Fe/κ_{nd} ratio (Fig. 2e). This ratio highlights diagenetic magnetic susceptibility loss decoupled from concentration changes of iron bearing mineral.

Low-temperature magnetic measurements and high-field magnetic hysteresis loops on samples across a glacial cycle were performed to detect the type of magnetic mineral species and possible provenance changes. The dominance of nonparamagnetic minerals and the relative contribution of para- and nonparamagnetic minerals are shown in Fig. 3. All samples show a drop in remanence intensity at temperatures ranging from 114 to 122 K (Fig. 4) indicating the presence of

nearly stoichiometric magnetite. Magnetite with cubic symmetry at room temperature shows a change to monoclinic symmetry below a temperature of 120 K. This phase transition is accompanied by higher remanent magnetizations towards lower temperatures. Deduced from field (FC) and zero-field (ZFC) cooling measurements, there is no indication for other remanence carrying minerals, e.g. monoclinic ferrimagnetic pyrrothite, hematite or greigite.

In addition to the findings from magnetic analysis we found no significant change in clay mineral composition. In general illite dominates, smectite and kaolinite are indifferent and below 10 wt.%. The chlorite concentration is slightly enhanced in glacials. Small variations in clay mineral concentration in the middle of the MSMZ are unrelated to the onset and termination of the MSMZ.

In summary, the FC, ZFC, hysteresis and clay mineral measurements demonstrate that the reduced signal of magnetic susceptibility is related to the decreased concentration of magnetominerals rather than to a dilution effect or a change in provenance of the source material. The decreased overall magnetic susceptibility in MSMZ between 105.38 and 104.44 mcd (Fig. 2) is best explained by a diagenetic process of sufficient strength and duration to dissolve small as well as large magnetite grains.

Diagenetic processes altering magnetic susceptibility signals in ODP Site 1095 sediments are found to act on long and short time scales with variable intensities and repeatability. Our repeated MSMZs are linked to short term changes on the glacial-interglacial scale that can not be explained by quasi stationary equilibrium conditions. Furthermore the diagenetic processes altering the magnetic susceptibility signal in the early Pliocene (and probably late Miocene) period differ clearly from magnetic mineralogy changes in late Pleistocene sedimentary sequences from the same drift site.

The most plausible cause for a near sysnsedimentary loss of sediment magnetic susceptibility in late Miocene-Pliocene at ODP Site 1095 is the degradation of organic matter in suboxic or anoxic conditions leading to a reduction of Fe^{3+} bearing mineral species. Diagenetic signatures of iron reduction fronts in otherwise well-ventilated open oceanic conditions have been observed at the tops of organic-rich turbidite deposits in the Madeira abyssal plain.

In modern high productivity margin settings more than 80% of the total sulfate reduction may occur in the uppermost first 30 cm of the sediment column. Those values are similar to a 15-25 cm paleo-depth estimate of sulfate depletion, deduced from the relative position of the diatom ooze layer and the onset of MSMZ (Fig. 2) in our West Antarctic cores. In modern outer continental margins sulfate reduction is commonly coupled to the process of the anaerobic oxidation of methane rather than to the remobilization of particulate sediment organic matter. Quasi longer term equilibrium conditions between downward sulfate flux and methane consumption is expressed in linear sulfate profiles. However, our glacially triggered Pliocene MSMZs are strongly linked to short term changes in organic matter fluxes, which likely prevent the establishment of equilibrium conditions.

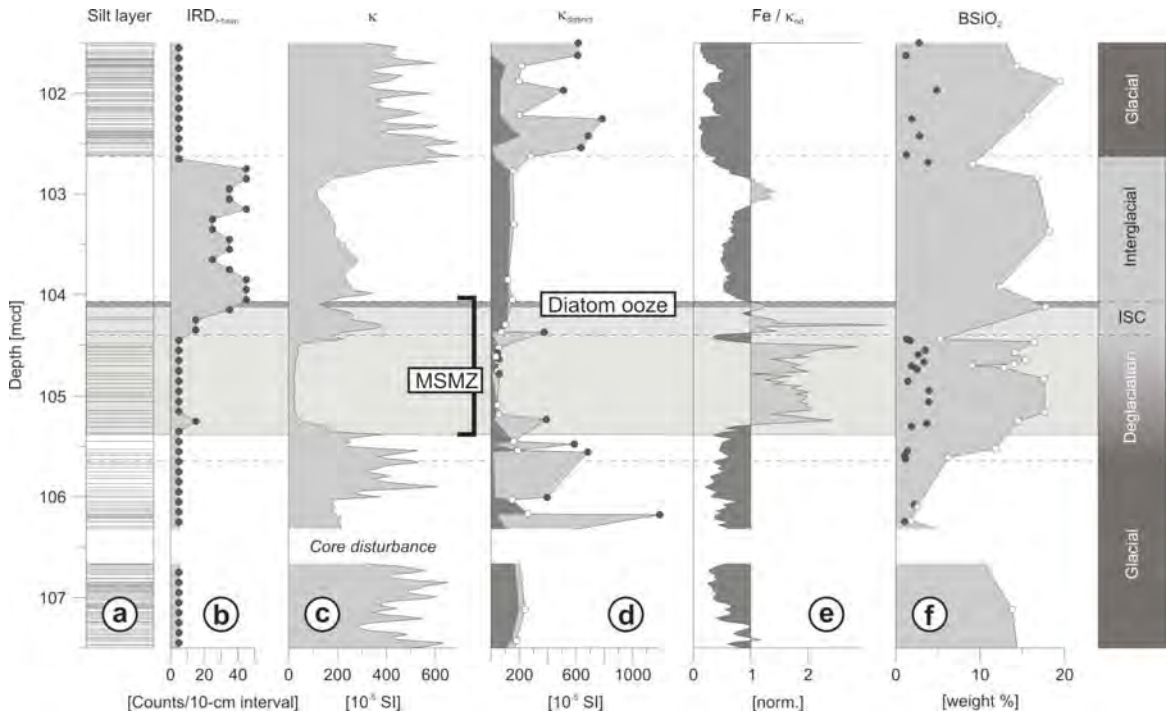

Fig. 2. Example of an early Pliocene MSMZ (105.28 and 104.48 mcd) in the context of a complete glacial-interglacial cycle: (a) absolute position of silt layers, (b) number of IRD pebbles (>1cm per 10-cm grid), magnetic susceptibility (κ) from (c) shipboard logging data and (d) individual measurements (light shading = grain-size coarse fraction >63 µm, dark shading = grain-size fine fraction <63 µm), (e) normalized Fe/κnd ratio, (f) biogenic silica (opal) from XRF logging (Open circles = samples from hemipelagic sediments, solid circles = samples from silt layers (<63 µm), dark bar = diatom ooze layer, shaded area = MSMZ, dashed lines = boundaries of glacial stages).

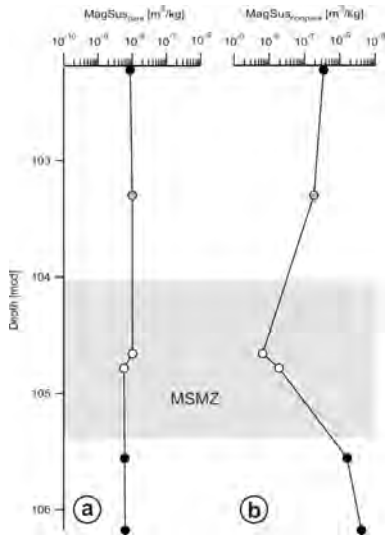

Fig. 3. Hysteresis parameters of a subset of six samples plotted against depth. The diagram shows the (a) paramagnetic and (b) non-paramagnetic magnetic susceptibility fraction deduced from magnetic hysteresis loops. While paramagnetic susceptibility shows no variation across the glacial-interglacial interval the non-paramagnetic susceptibility is reduced during the MSMZ (Solid circles = samples from glacial intervalls, grey circles = samples from interglacial interval, open circles = samples from MSMZ, shaded area).

Other aspects regarding the MSMZ termination are addressed in the following scenario that attempts to blend the suggested succession of diagenetic processes into a refined and integrated oceanographical-cryospherical and sedimentological conceptual model.

Diagenesis driven by organic matter re-mineralization is a complex function of organic carbon supply, sedimentation rate, intensity of bioturbation, ocean ventilation and deep water oxygen content. The Southern Ocean biological pump and coupled opal and organic carbon deposition are bound to winds, ocean circulation and sea ice. The modern Antarctic opal belt (~520 km north of ODP Site 1095) is located south of the APF and north of the winter sea ice edge. It is believed that the position of this opal depocentre was further north during the Last Glacial Maximum but kept its relation to the maximum winter sea ice edge. Late Miocene to early late Pliocene warm climate conditions and a reduction of 22% in sea ice cover at the continental rise, relative to modern conditions, are generally accepted for Antarctica. The late Miocene to early late Pliocene ice dynamics increased with frequent advances of the inland ice sheet to the shelf edge. This coincided with a rise in export $BSiO_2$ leading to suboxic, iron reducing conditions in the rise sediments confirmed by the onset of the MSMZ. We speculate that there was a rapid break down of the shelf ice sheet (massive IRD supply) at the end of the Eraly Pliocene deglaciation phases.

Nearly stagnant deep water conditions were required to preserve the current sensitive and easy to relocate diatom ooze on top of an elevated topographic feature like Drift 7. We conclude that an increased freshwater discharge at the end of the deglaciation phase and nutrient supply by fertilization of the ocean by terrigenous and dust-bound iron could have enhanced export productivity during relatively short time intervalls. At the same time a stratification of the ware column and weak bottom water currents resulted in a strong decrease of ventilation at the continental rise. This coincides with findings from Last glacial maximum core sections of Drift 7, where major meltwater discharge causes water stratification with less oxygenated and nutrient-enriched conditions at the sea bottom.

Studies on late Pleistocene-Holocene sedimentary sequences of Drift 7 draw scenarios of environmental conditions with prevented biological productivity, which cause minima in the rock magnetic signal during the deglaciation pase. These scenarios are in opposite to the scenario with diagenetic processes of sulfide formation in response to high paleoproductivity, proposed for the Pliocene sequences. In our study we found no indication for characteristic MSMZ above 79.35 mcd (~3.17 Ma). Our MSMZs differ significantly in shape and value from reduced magnetic susceptibility signals described for Pleistocene and LGM sediments along the Antarctic Peninsula continental rise. In our investigated Pliocene core section the magnetic susceptibility mean value from glacial to MSMZ is reduced about factor 16 and the signal of the MSMZ is nearly complete obliterated to a weak background noise. An explanation for the opposite biological productivity scenarios causing oxygene-reduced conditions in the late Miocene-early Pliocene and late Pleistocene-Holocene, respectively, could be seen in the drasticly altered environmental boundary condition between 5 and 2.7 m.y.

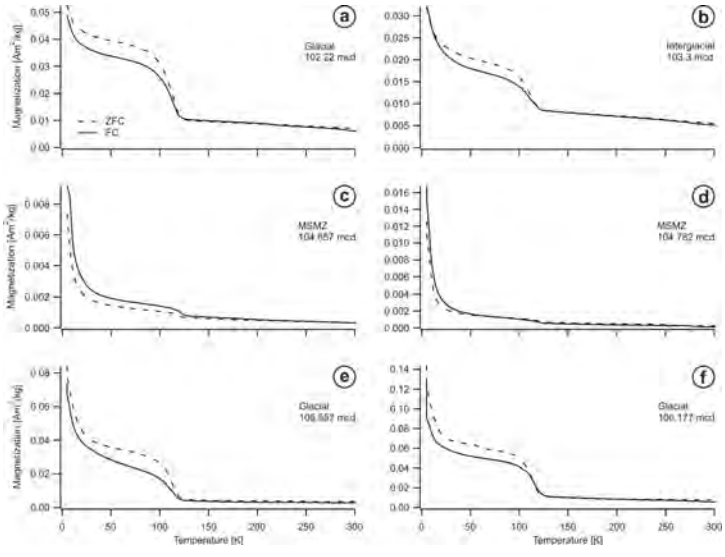

Fig. 4. Thermal demagnetization of a low-temperature remanence imparted in a magnetic field of 5 T at a temperature of 5 K after cooling the samples in zero field (ZFC, dotted line) and in presence of a 5 T field (FC, solid line). The ZFC curves for samples from glacial and interglacial intervals are higher than the respective FC curves. In contrast the ZFC curves from the MSMZ are lower than FC curves pointing to magnetite particles of smaller average grain sizes.

Preliminary Results of Vegetation Development in Tropical Africa during Heinrich Event 3 (ODP 1078, off Angola)

I. HEßLER, L.M. DUPONT, A. PAUL

MARUM – Center of Marine Environmental Sciences, University of Bremen, P.O. Box 330440, 28334 Bremen, Germany

Our objective is to gain insight in the interrelation between vegetation and climate of the African continent south of the equator with special emphasis on North Atlantic Heinrich events.

A high-resolution marine sediment record spanning the time period of North Atlantic Heinrich event 3 (H 3) has been obtained from Ocean Drilling Program Site 1078 (11°55'S, 13°24'E, 426 m water depth) off the coast of Angola. The distribution of pollen in these sediments is presented here to reconstruct the vegetation- and climate history of the adjacent continent during the H 3. Mountain and forest taxa percentages increase abruptly at the beginning of H 3 and decrease towards the end. The opposite development is observed for the curves of Poaceae and Cyperaceae. According to rising percentages of both desert and forest taxa we conclude that the environmental conditions in the inner mountainous part of southwestern Africa changed differently than those of the coastal regions.

At present, the Angolan vegetation ranges from dry and evergreen forest to savannah woodland forming a transition between the rain forest of the Congo basin and the *Acacia* savannah of the Kalahari. Previous work on ODP 1078 has shown that the pollen record is very diverse and represents large changes in continental vegetation, especially during H 1. Tree pollen percentages of Afromontane *Podocarpus* achieve maximum percentages during H 1 while percentages of Afroalpine elements like Ericaceae remain low. Percentages of *Podocarpus* are much higher during H 1 than H 3. Such differences in the vegetation between Heinrich events have prompted us to investigate other Heinrich events, namely H 4 and 5.

Nevertheless, a comparable impact of North Atlantic Heinrich events 1 and 3 on tropical vegetation south of the equator is observed. The tropical vegetation of southwestern Africa tends to become more lush with considerably higher percentages of forest and mountain taxa. As expected, dryforest/savannah elements and grasses showing short-term drops in their abundances during Heinrich event 3. This is in contrast to the situation in West Africa north of the equator where the vegetation cover during Heinrich events strongly reduces (Mulitza, Prange et al. 2008; Paleoceanography 23: 11).

The reconstruced vegetation based on marine pollen records will be compared with model output in the form of biomes and plant functional types (see abstract of Handiani et al., this volume).

The stable carbon isotope biogeochemistry of acetate in sediments from the NE Pacific: a synthesis

V.B. HEUER[1], J.W. POHLMAN[2], M.E. TORRES[3], M.A. LEVER[4,5], M. ELVERT[1], AND K.-U. HINRICHS[1]

[1]Fachbereich Geowissenschaften, Universität Bremen, 28359 Bremen, Germany
[2]U.S. Geological Survey, Woods Hole, USA
[3]College of Oceanic and Atmospheric Sciences, Oregon State University, Corvallis, OR, USA
[4]Department of Marine Sciences, University of North Carolina at Chapel Hill, Chapel Hill, NC, USA;
[5]Center for Geomikrobiologi – Biologisk Institut, Århus, Denmark

Ocean drilling has revealed the existence of vast microbial populations in the deep sub-seafloor, but to date little is known about their metabolic activities. To better understand the biogeochemical processes in the deep biosphere, we investigate the stable carbon isotope chemistry of acetate and other carbon-bearing compounds in sediment pore-waters.

Acetate is a key metabolite in the cycling of carbon in anoxic sediments. The water-soluble C_2-compound is produced by fermentation of organic matter as well as by acetogenic CO_2-reduction (acetogenesis), and it serves as an important substrate for a variety of microorganisms including methanogens. Rapid turnover typically maintains acetate concentrations at low levels, around 10 µM, in the pore-waters of near-surface sediments (e.g., Wellsbury and Parkes, 1995; Wu et al., 1997). However, in deeply-buried sediments acetate concentrations can reach levels of 10 mM and higher (Egeberg and Barth, 1998; Wellsbury et al., 1997). The stable carbon isotopic composition ($\delta^{13}C$) of acetate provides cultivation-independent information on the metabolic processes dominating acetate turnover in situ (eg., Blair et al., 1987; Gelwicks et al., 1989; Heuer et al., 2006; Heuer et al., submitted a). In particular, ^{13}C-depletions of acetate relative to bulk dissolved organic carbon (DOC) and total organic carbon (TOC) can be used to identify acetogenesis by CO_2 reduction while ^{13}C-enrichments point to the consumption of acetate by acetoclastic methanogenesis.

Expeditions 301 and 311 of the Integrated Ocean Drilling Program (IODP) established a series of sites at the eastern flank of the Juan de Fuca Ridge and across the gas-hydrate bearing accretionary prism of the northern Cascadia Margin (NE Pacific) (Fisher et al., 2005; Riedel et al., 2006) (Fig. 1). Along this transect, we observe distinct changes in the stable carbon isotopic composition of pore-water acetate (Fig. 2). At the ridge flank (Site U1301) and at the toe of the accretionary prism (Site U1326), $\delta^{13}C$-values of acetate are relatively uniform in the upper 265 m of sediment, averaging -29.5 ± 1.7‰ and -27.3 ± 1.4‰ vs VPDB, respectively. At both sites, acetate is slightly depleted in ^{13}C relative to TOC, which is assumed to represent the carbon isotopic composition of organic precursors, with mean $\Delta\delta^{13}C$ values of -4.2 ± 2.3‰ and -1.2 ± 1.4‰ at Site U1301 and U1326, respectively. Relative to DOC, which is assumed to represent the carbon isotopic composition of other fermentation products, acetate shows an even somewhat larger ^{13}C-depletion of -3.4 ± 1.6‰ at Site U1326 (for Site U1301, $\delta^{13}C$-DOC data are not available). The ^{13}C-depletion of acetate relative to TOC and DOC points to an acetogenic component in the pore-water acetate pool which is present throughout the upper 265 m of sediment at both sites.

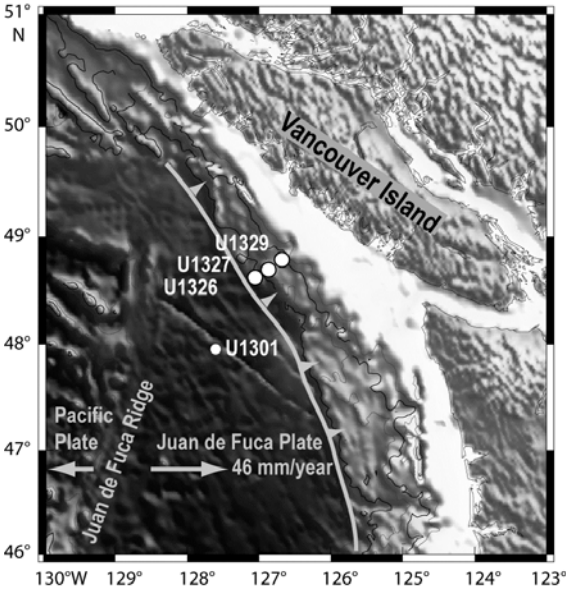

Fig. 1: This study investigates the carbon isotope chemistry of acetate along a transect of sites that were drilled during IODP Expeditions 301 and 311 at the eastern flank of the Juan de Fuca Ridge and across accretionary prism of the northern Cascadia Margin (NE Pacific) (modified after http://www.iodp.tamu.edu/scienceops/maps/exp/).

Moving upslope, $\delta^{13}C$-acetate gets increasingly variable (Fig. 2). At the midslope site U1327, $\delta^{13}C$ values of acetate range from -34.5 to -7.2‰. At the upslope site U1329 $\delta^{13}C$ values of acetate span an even wider range from -46.0 to -11.0‰. Relative to DOC, acetate is up to 23.1‰ depleted and up to 9.1‰ enriched in ^{13}C (Heuer et al., submitted b). At both sites, the carbon isotopic composition of acetate relative to DOC changes systematically with depth and suggests the existence of distinct sediment horizons with characteristic modes of acetate turnover. In the upper, suboxic, layer of sediment, $\delta^{13}C$ values of acetate are close to those of total organic matter (~-20‰). We consider this relationship as characteristic for production of acetate from sedimentary organic matter combined with a sink that leads to little or no isotopic fractionation in the residual acetate pool (zone I in Fig. 2). Below, production of acetate from H_2 and CO_2 results in acetate that is distinctly ^{13}C-depleted relative to DIC and usually also relative to dissolved organic carbon DOC (zone II in Fig. 2). Acetoclastic methanogenesis is associated with a strong isotopic fractionation creating ^{13}C-depleted CH_4 and a ^{13}C-enriched pore-water acetate pool. The gradual ^{13}C-enrichment of acetate points a relative increase in acetate flow to acetoclastic methanogenesis with depth (zone III in Fig. 2). For reasons

that are not clear yet, the gradual ^{13}C-enrichment of acetate comes to a halt in the deepest part of the cored sediment at Site U1329, and $\delta^{13}C$ values of acetate closely resemble those of DOC (zone IV in Fig. 2).

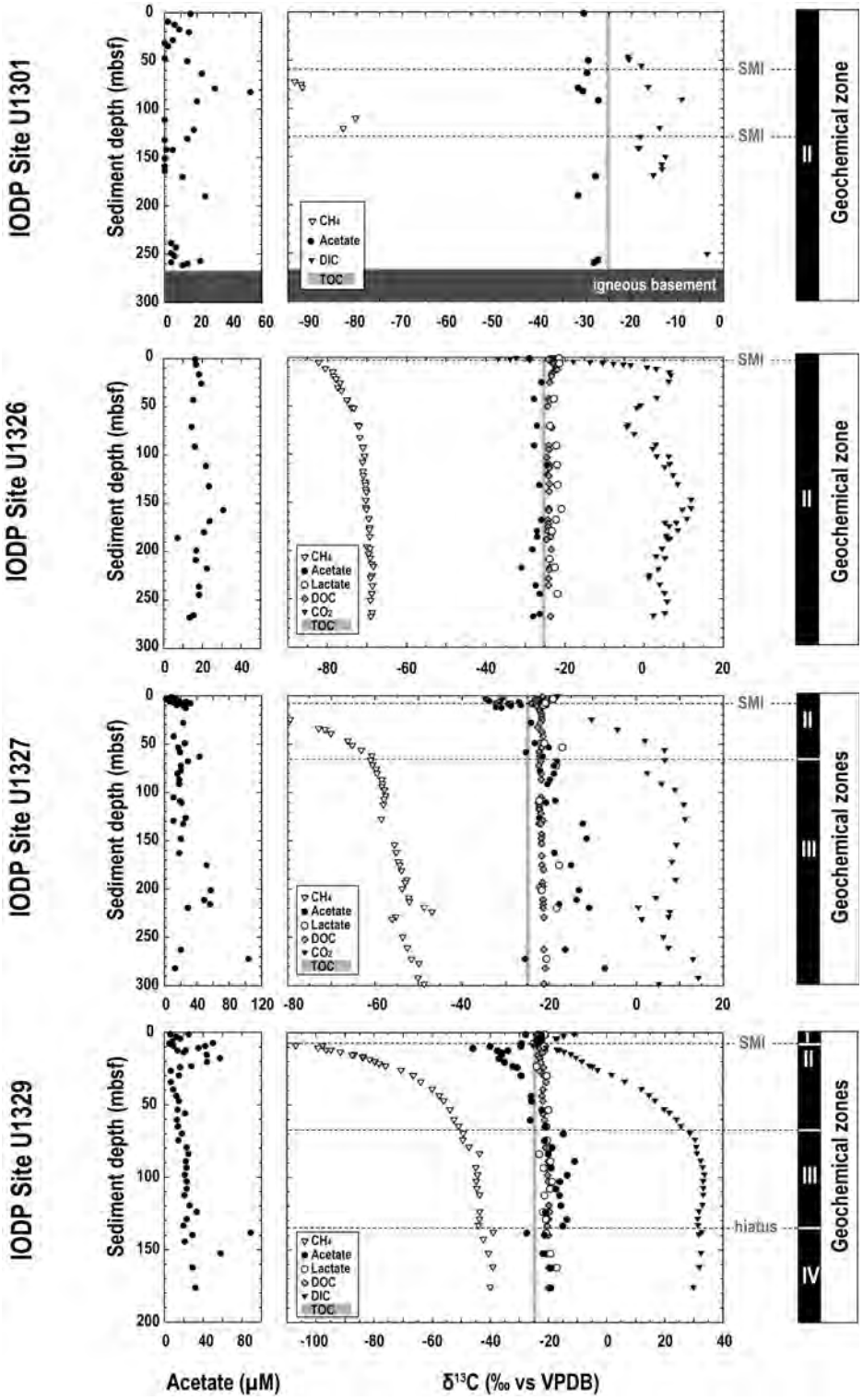

Fig. 2: Depth profiles fo the concentrations of acetate and carbon isotopic compositions of acetate, lactate, methane, DIC, DOC in pore-waters samples and CH_4 and CO_2 in void gas samples recovered from a transect of drill sites that were established during IODP Expeditions 301 and 311 in the NE Pacific. Grey line indicate average $\delta^{13}C$ of TOC in the solid phase (Kim and Lee, submitted). SMI indicates the depth of sulfate methane interfaces. Isotopic relationships suggest the presence of up to four distinct geochemical zones: Zone I, where the carbon isotope composition of acetate closely resembles $\delta^{13}C$-values of DOC and lactate; Zone II, where acetate is distinctly depleted in ^{13}C compared to lactate, DOC, and CO_2; Zone III, 65-135 mbsf, where acetate is enriched in ^{13}C relative to lactate and DOC, and Zone IV, a deep zone where $\delta^{13}C$ of acetate tracks that of lactate and DOC. Data for Site U1329 were taken from Heuer et al., (submitted).

Isotopic relationships between acetate and both dissolved organic carbon (DOC) and dissolved inorganic carbon (DIC) provide previously inaccessible information on the carbon flow. They suggest (a) the existence of distinct sediment horizons with characteristic modes of acetate turnover, (b) a widespread co-occurrence of methanogenic and acetogenic CO_2-reduction, (c) a relative increase in acetate flow to acetoclastic methanogenesis with depth, and (d) the presence and activity of specific functional prokaryotic communities which change systematically with sediment depth and with distance from shore. Our observations raise new questions regarding the factors controlling the expression of distinct modes of acetate turnover in different sedimentary units.

Blair N.E., Martens C.S., Des Marais D.J. (1987) Natural abundance of carbon isotopes in acetate from a coastal marine sediment. *Science*, 236, 66 - 68.
Egeberg P. K. and Barth T. (1998) Contribution of dissolved organic species to the carbon and energy budgets of hydrate bearing deep sea sediments (Ocean Drilling Program Site 997 Blake Ridge). *Chemical Geology* **149**(1-2), 25-35.
Fisher, A.T., Urabe, T., Klaus, A., and the Expedition 301 Scientists (2005) *Proc. IODP*, 301: College Station TX (Integrated Ocean Drilling Program Management International, Inc.). doi:10.2204/iodp.proc.301.2005
Gelwicks J.T., Risatti J.B., Hayes J.M. (1989) Carbon isotope effects associated with autotrophic acetogenesis. *Organic Geochemistry*, 14(4), 441 - 446.
Heuer V., Elvert M., Tille S., Krummen M., Prieto Mollar X., Hmelo L. R., and Hinrichs K.-U. (2006) Online $\delta^{13}C$ analysis of volatile fatty acids in sediment/porewater systems by liquid chromatography-isotope ratio-mass spectrometry. *Limnology and Oceanography: Methods* **4**, 346-357.
Heuer V.B., Krüger M., Elvert M., and Hinrichs K.-U. (submitted a) Experimental studies on the stable carbon isotope biogeochemistry of acetate in lake sediments. *Organic Geochemistry*.
Heuer V.B., Pohlman J.W., Torres M.E., Elvert M., and Hinrichs K.-U. (submitted b) The stable carbon isotope biogeochemistry of acetate and other dissolved carbon species in deep sub-seafloor sediments at the northern Cascadia Margin *Geochimica et Cosmochimica Acta*.
Kim, J.-H., and Lee, J.-Y. (submitted) Data report: elemental, rock-eval and isotopic compositions of bulk sediments in IODP Expedition 311. *In* Riedel M., Collett T.S., Malone M.J., and the Expedition 311 Scientists. *Proc. IODP*, 311: Washington, DC (Integrated Ocean Drilling Program Management International, Inc.).
Riedel, M., Collett, T.S., Malone, M.J., and the Expedition 311 Scientists (2006) Proc. IODP, 311: Washington, DC (Integrated Ocean Drilling Program Management International, Inc.). doi:10.2204/iodp.proc.311.2006
Wellsbury P. and Parkes R. J. (1995) Acetate Bioavailability and Turnover in an Estuarine Sediment. *FEMS Microbiology Ecology* **17**(2), 85-94.
Wellsbury P. and Parkes R. J. (1995) Acetate Bioavailability and Turnover in an Estuarine Sediment. *FEMS Microbiology Ecology* **17**(2), 85-94.
Wellsbury P., Goodman K., Barth T., Cragg B.A., Barnes S.P., and Parkes R.J. (1997) Deep marine biosphere fuelled by increasing organic matter availability during burial and heating. *Nature*, 388(6642), 573-576.
Wu H. G., Green M., and Scranton M. I. (1997) Acetate cycling in the water column and surface sediment of Long Island Sound following a bloom. *Limnology and Oceanography* **42**(4), 705-713.

Effects of orbital-scale fluctuations of the itcz on continental hydrology and marine carbon burial in the mid Cretaceous tropical Atlantic region

P. HOFMANN[1], B. BECKMANN[2], S. FLÖGEL[3], T. WAGNER[4]

[1]Institut für Geologie und Mineralogie, Universität zu Köln (peter.hofmann@uni-koeln.de)
[2]BGR, Hannover
[3]IFM-GEOMAR Leibnitz Institute of Marine Science, Kiel
[4]School of Civil Engineering, Newcastle University, UK

Organic carbon-rich stratigraphic intervals are well known to occur in the mid-Cretaceous Atlantic at several distinct time intervals. The equatorial Atlantic region was particularly prone to extensive anoxia/euxinia and black shale deposition during that time. In this study we explore the driving mechanisms for fluctuations on orbital time scales in ocean anoxia and organic carbon burial on both sides of the tropical Atlantic. We compare high resolution geochemical data from ODP Sites 1261 (off Surinam) and 959 (Ivory Coast), covering the the Coniacian to Santonian Oceanic Anoxic Event 3 (OAE3) and results from numeric climate simulations . The combined approach provides evidence to infer the roles of ITCZ dynamics, continental hydrology, and marine upwelling on the development of ocean anoxia/euxinia in the equatorial region.

Previous work on ODP Site 959 has shown that the formation of anoxia/euxinia and the deposition of organic rich sediments was directly linked to the moisture balance over Africa that controlled nutrient and freshwater supply to the ocean via continental runoff and hence triggered ocean anoxia/euxinia (Hofmann et al. 2003, Wagner et al. 2004, Beckmann et al. 2005, Flögel and Wagner 2006). Climate modeling and frequency analyses further indicated that cyclic formation of anoxia/euxinia at ODP Site 959 was primarily precession-controlled and best explained by fluctuations in episodic moisture transport from the mid latitude southern Atlantic to the tropical African region (Flögel and Wagner 2006), possibly linked to the northward migration of the ITCZ.

Geochemical records, frequency analyses and climate modeling from the continental margin of South America in contrast show distinctly different patterns of redox change and organic carbon burial. Precession apparently did not dominate the variability of ocean redox and carbon burial at Demerara Rise (Floegel et al, 2008), which was related to persistent high continental runoff from tropical South America (Floegel et al, 2008) maintaining the ocean redox system constantly perturbed in an anoxic and at times euxinic mode. Still, there is a clear lower-frequent cyclicity recognizable in synchronous fluctuations in oceanic productivity of calcareous and non-calcareous plankton, The Index of Chemical Weathering (CIA), and Zr/Al ratios (a commonly used grain size indicator) (Fig. 1) and the eccentricity cycles from ODP Site 1261 support a close link between enhanced carbonate production and burial (both organic and inorganic) with euxinia in the lower water column (Maerz et al., 2008) and coarsening of continental matter grain size as indicated by maxima in the Zr/Al ratios, coupled with less intense weathering conditions in northern South America, the source area of the clastic supply (Figs. 1 and

2). This data is best explained by periods of enhanced upwelling off Surinam during Coniacian to Santonian times (Villiamil et al. 1999) that re-occurred at short eccentricity time scales. Off tropical South America intense upwelling should have prevailed during strong westward blowing winds (NE trade winds, high Zr/Al ratios) because Ekman transport would have caused an increase in surface water productivity (high Ca/Al and TOC/Al ratios) and a switch in deep ocean redox from anoxic, non-sulfidic to sulfidic (euxinic) conditions (März et al. 2008). Periods of less intense upwelling with overall wetter climate conditions in tropical South America would then have been associated with finer grain sizes, weaker wind strength (Zr/Al ratios) and maxima in the chemical index of alteration (CIA*) in the sedimentary record.

Moisture transport in equatorial regions is closely linked to the position of the intertropical convergence zone (ITCZ) and its latitudinal fluctuations. We consequently interpret high values in CIA* and Zr/Al to reflect episodes when the ITCZ was shifted north, creating comparable climate conditions in tropical South America and tropical Africa. Under these conditions the influence of the NE trade wind would have weakened upwelling conditions off South America and created less intense oceanic redox conditions. With the ITCZ moving South the NE trade winds would have gained stronger influence on marine sedimentation off Surinam and climate on the adjacent continent.

The complementary geochemical records in combination with modeling suggest that organic matter production and deposition in the tropical Atlantic region was intimately linked to the dynamics of the ITCZ, although not necessarily responding at the same time frequencies and to the same forcing mechanisms.

One striking difference east and west of the tropical Atlantic is the frequency of ITCZ fluctuations recorded in the climate cycles at Site 959 and 1261. The reasons for these transatlantic differences in the frequency of the ITCZ movement are not yet completely understood, however, climate modeling has shown that tropical South America received distinctly more and constantly high precipitation than equatorial western Africa which is characterized by more distinct climate contrasts (Fig. 3), at least at precessional time scales. It is thought that the constantly high levels of precipitation in tropical South America were one critical reason why precession cycles are not recorded in the geochemical records at Site 1261 and why organic matter levels are higher at this site throughout the study interval.

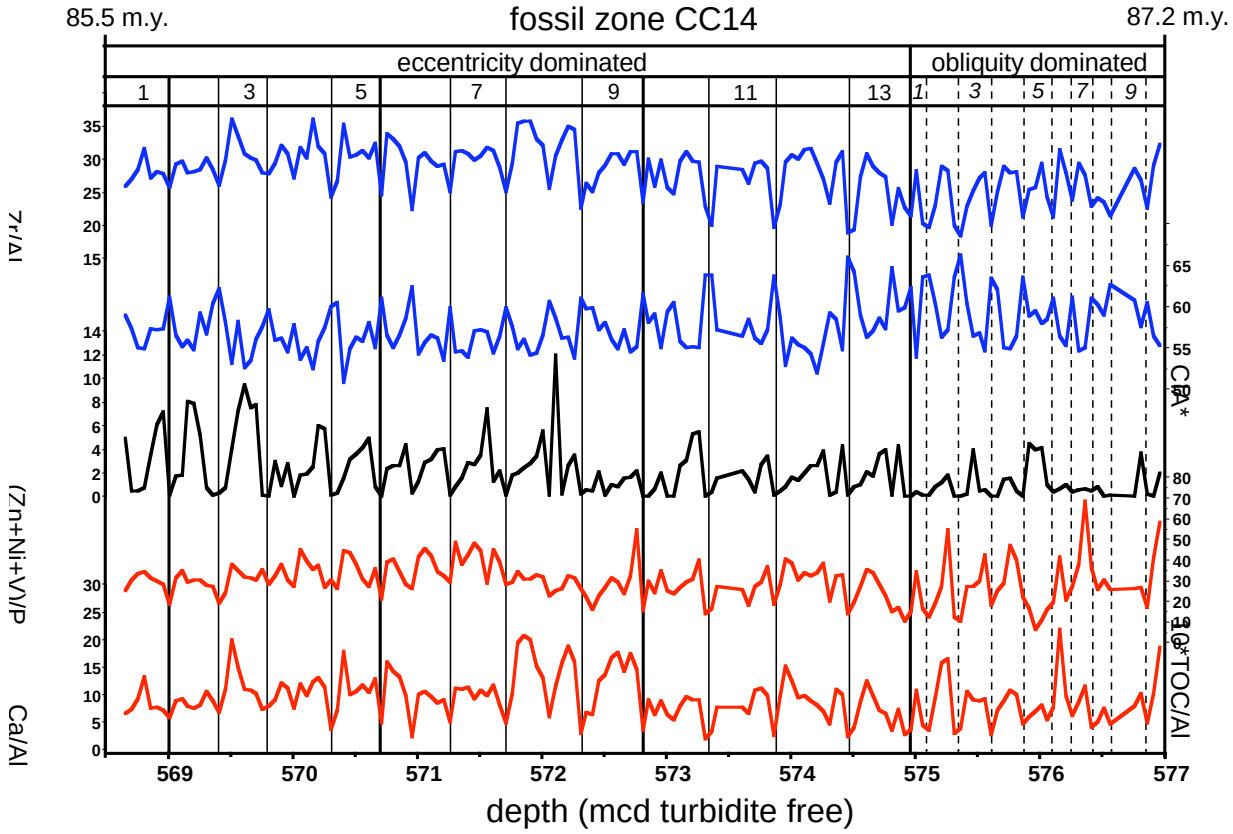

Fig. 1: Geochemical proxy record for ODP Site 1261. Zr/Al ratios are interpreted to reflect wind strength and grain size, CIA* represents weathering intensity and moisture, Zn+Ni+V/P is indicative fluctuations redox conditions from anoxic to euxinic (März et al. 2008). TOC/Al and Ca/Al reflect fluctuations in paleo-productivity.

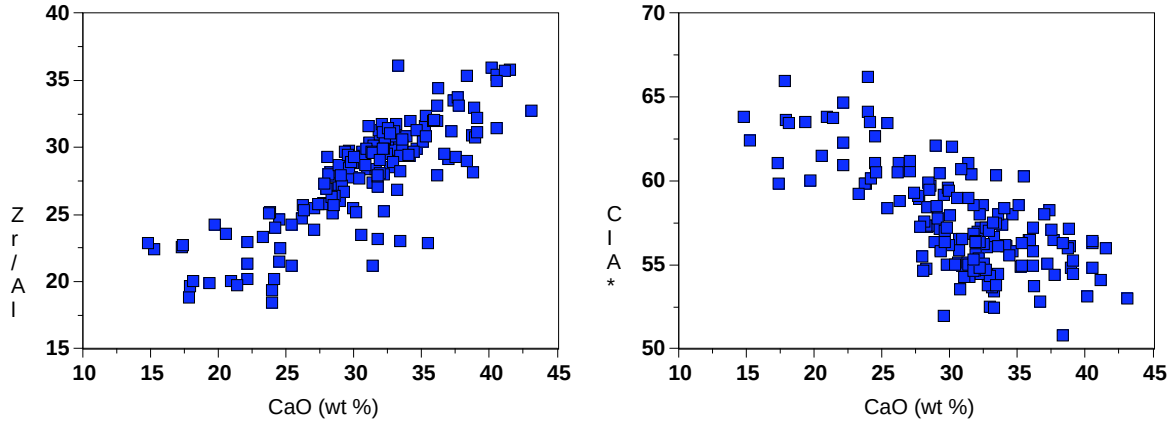

Fig. 2: Correlation of carbonate productivity and wind strength/grain size (Zr/Al) and weathering intensitiy/moisture (CIA* = Al/(Al+K+Na)).

Another reason for differences in the dynamics of the ITCZ at site 959 and 1261 may lie in their paleo-geographic position. Coniacian to Santonian plate reconstructions locate Site 959 south and Site 1261 north of the equator. I seems likely, that the southern site in west Africa was located in the corridor that was effected by precession forced shifts of the ITCZ, whereas in the northern Site 1261 was only reached by the ITCZ in orbital configurations that lead to excessive heating of northern South America.

We conclude, regardless of the timing of the observed cycle pattern and very similar to the Quaternary world, that the ITCZ has been a key player in the late Cretaceous tropical climate system, with strong regional impact on low latitude wind systems (Trades and Monsoon) and the associated distribution of moisture over the continents. More modeling work into the dynamics of the late Cretaceous ITCZ is necessary to place these far reaching results into a broader context.

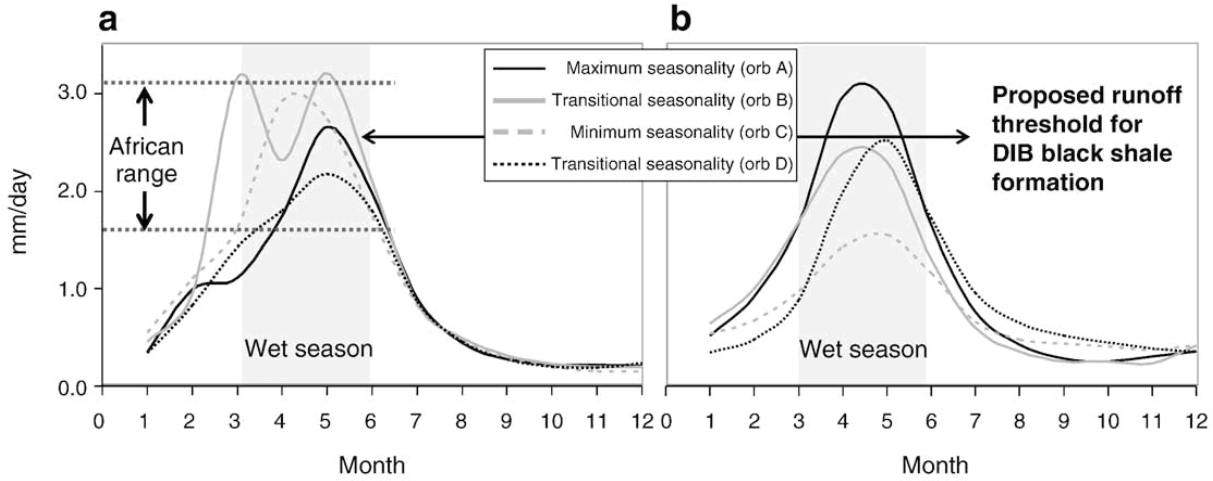

Fig. 3: Modeled precipitation differences between northern South America (a) and western Africa (b). Orb A to orb D reflect different orbital configurations across one precession cycle (Flögel et al. 2008).

Beckmann, B., Flögel, S., Hofmann, P., Schulz, M. and Wagner, T. (2005) Mid-Cretaceous African climate development and implications for the marine carbon cycle. Nature 437 (8), 241-244.

Flögel, S. Beckmann, B., Hofmann, P., Bornemann, A., Norris, R.D., Wagner, T.(2008). Evolution of tropical watersheds and continental hydrology during the Late Cretaceous greenhouse; marine carbon burial and possible implications for the future. Earth and Planetary Science Letters, 274, 1-13.

Hofmann P., Wagner T., Beckmann B. (2003) A millenial to centenial scale record of African climate variability and organic carbon accumulation in the Coniacian-Santonian eastern tropical Atlantic (ODP Site 959, off Ivory Coast/Ghana). Geology, 31, p. 135-138.

März C., S.W. Poulton, B. Beckmann, K. Küster, T. Wagner, S. Kasten (2008). Redox sensitivity of P- cycling during marine black shale formation. Geochimica Cosmochimical Acta 72, 3703-3717

Villimiamil, T., Arango, C., Hay W.W. (1999). Plate tectonic paleoceanographic hypothesis for cretaceous source rocks and cherts. In: Barrera E. and Johnson C. C. (eds.), Evolution of the Cretaceous Ocean-Climate System, Geological Society of America Special Paper 332, Boulder, 191-202,

Wagner T, Sinninghe Damsté J., Hofmann P., Beckmann B. (2004) Euxinia in Upper Cretaceous (Coniacian-Santonian) eastern equatorial Atlantic surface waters associated with climate-driven formation of marine black shales in the Deep Ivory Basin, ODP Site 959. Palaeocanography, 19, PA4099, doi:10.1029/2003 PA000898).

Development of sea surface temperature across the lower Aptian Oceanic Event 1a in the Subtropical North Atlantic, Galicia Margin

P. HOFMANN[1], C. L. HANDLY[2], H. TALBOT[2], T. WAGNER[2]

[1]Institut für Geologie und Mineralogie, Universität zu Köln (peter.hofmann@uni-koeln.de)

[2] School of Civil Engineering, Newcastle University, UK

Mesozoic Oceanic Anoxic Events (OAEs) represent major perturbations in the global climate system and are believed to have been caused by the liberation of large amounts of greenhouse gases such as CO_2 and CH_4. An intensification of greenhouse conditions is expected to result in an accelerated hydrological cycle: enhanced weathering conditions, an increase in nutrient export to the oceans and higher levels of bioproductivity and organic matter burial resulting in and oxygen depletion in the oceans. The globally recognized lower Aptian OAE 1a represents one of the most important OAEs of the Cretaceous and has been linked to oceanic plateau emplacement and methane release from gas hydrates.

Objectives

In this study we aim to reconstruct the chain of processes induced by a rapid injection of isotopically light CO_2 to the ocean-atmosphere system in order to elucidate the feedback mechanisms and time relationships of the ocean-continent-atmosphere system. Multi-proxy, high resolution records from the Galicia Margin (ODP Hole 614C) covering OAE 1a were generated to reconstruct the chronology of greenhouse gas release, and its relationships with changes in climate and ocean oxygen content in the subtropical North Atlantic.

Results

OAE 1a is marked by a distinct carbon isotope excursion recognizable both in carbonates and organic matter, and a distinct drop in carbonate content related to the global nannoconid crisis.

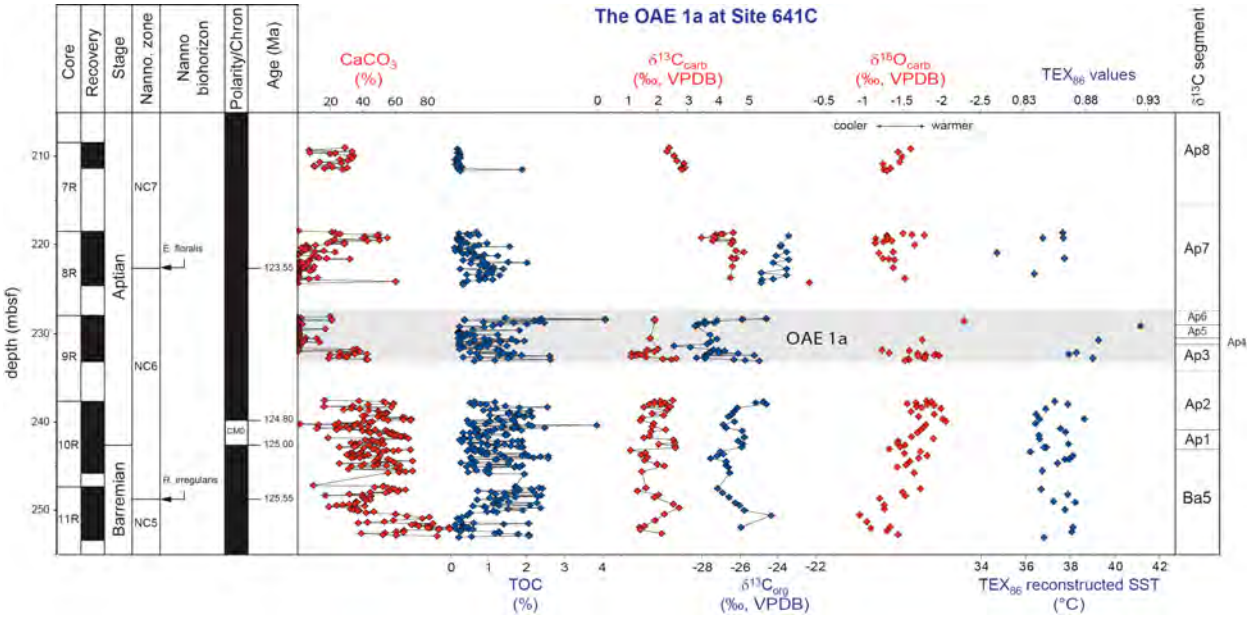

Fig. 1: $CaCO_3$ and TOC contents, isotopic profiles and sea surface temperature (SST) reconstruction across OAE 1a at ODP Site 614C. $\delta^{13}C$ segments are modified from Menegatti et al. (1998) and correlate to segments from the Cismon core. Core 9 contains the negative carbon isotope excursion diagnostic of the event. SSTs were reconstructed using the TEX86 proxy (Kim et al. 2008).

Notably, the base of OAE 1a at ODP 614C is characterized by a moderate negative carbon isotope shift of ca. -1‰ in carbonates and ca. -2‰ in bulk organic carbon, followed by positive shifts of ca. 3 and 4‰ in carbonates and organic carbon, respectively, recording the main period of globally enhanced marine carbon burial (Fig. 1). Similar trends in ^{13}C have been documented from other locations, however, in some cases with much larger amplitudes (Menegatti et al., 1998).

Sea surface temperatures

SSTs were very considerably warmer than 30°C in the lower Aptian tropical Atlantic, probably ranging from 36 to 41°C (note that the absolute values are not calibrated for the Tex_{86} temperature proxy in this interval). Carbonate $\delta^{18}O$ values shift to more negative values during OAE 1a and TEX_{86} values increase supporting a rise in surface ocean temperatures associated with the onset of the event. Although absolute temperature values must be considered with caution, this warming, on the

order of 3-4°C, was particularly pronounced in surface waters. Warming appears to be most extreme at the top of the anoxic event, approaching 41°C, before temperatures returned to near pre-OAE values.

Oceanic redox conditions

TOC-Fe-S relationships suggest normal marine conditions for most of the studied interval with the exception of the termination of OAE 1a (marked also by elevated sulfur values). Concentrations of redox sensitive element do not correlate with TOC or sulfur content. V/Al, Ni/Al and Zn/Al ratios fluctuate and are only moderately enriched compare to average shale throughout the studied interval suggesting variable, but possibly never suflidic bottom water oxygenation levels (Fig.2).

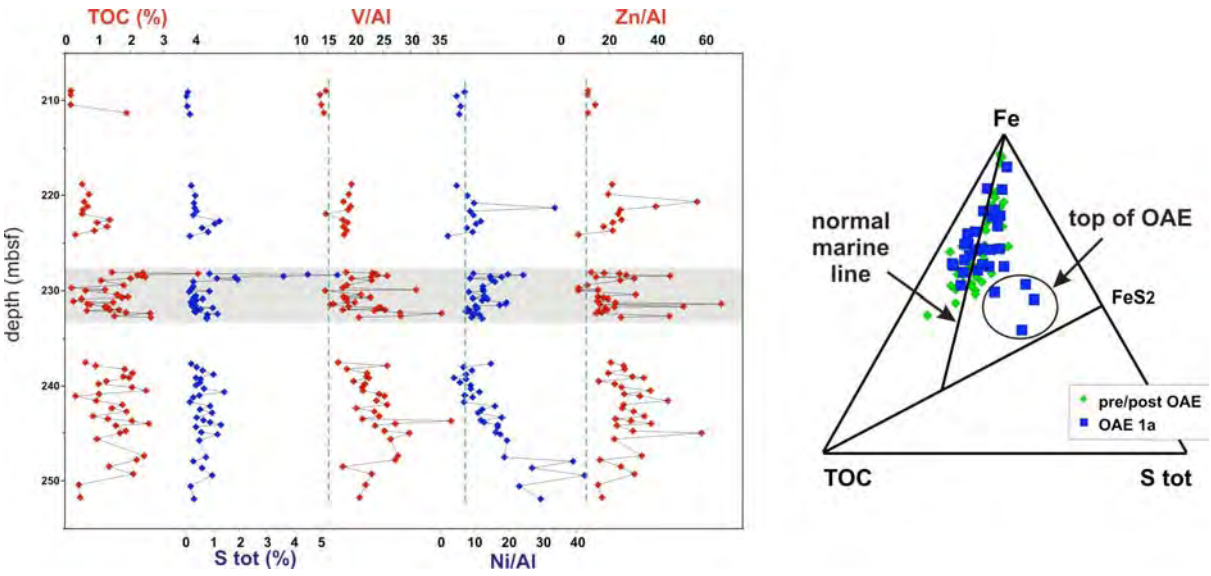

Fig. 2: Reconstruction of oceanic redox conditions. Moderate trace metal enrichments and TOC-Fe-S relationships suggest mostly normal marine conditions throughout the studied interval. Note broken lines indicate average shale values.

Productivity development

Carbonate productivity at site 641C started to decline at the base of chron M0 and reached a minimum during OAE 1b probably associated with the global nannoconid crisis. OAE 1a is characterized by an increase in biogenic silica production at the expense of calcareous plankton. Organic matter production/preservation (TOC) is not is not elevated compared to pre OAE values, but declined after the termination of the event.

Climatic effects

A minimum in Mg/Al and Na/Al and high CIA values (chemical index of alteration, Fig. 3) during OAE 1a suggest a contribution of more aluminum-rich clay minerals (e.g. kaolinite) and hence more intense weathering conditions in the source area (Iberia). A decreasing amplitudes of the Mg/Al, K/Al and Na/Al curves staring at the onset of OAE 1a support a reorganization towards less variable climate conditions.

Conclusions

The Barremian to lower Aptian record at ODP Site 641C indicates gradual warming of the tropical Atlantic which peaked during OAE 1a. Abrupt and massive methane emission from marine gas hydrates has been proposed as the cause for the negative excursion in δ13C values prior to the anoxic event. Such a global scale emission event is expected to have an almost instantaneous effect on global climate, and thus SST. However, both temperature proxy records at ODP 614C in fact show a gradual cooling of about 1°C associated with the initial negative isotope excursion, which does not support the proposed mechanism, at least not in this setting off the Galicia Margin. Further studies, in particular on the carbon isotopic composition of terrestrial leaf wax lipids and marine algal compounds, will help confirm the atmospheric and marine productivity responses to the proposed climate perturbation.

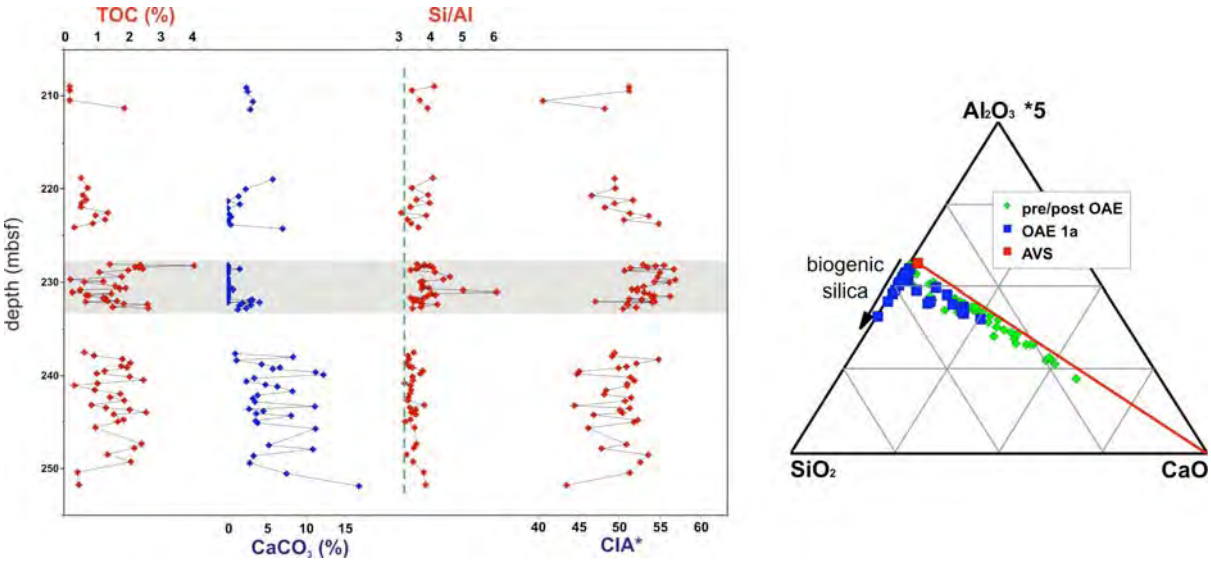

Fig. 3: Productivity indicators show a distinct decline in carbonate productivity associated with the global nannoconid cirisis, and an almost synchronous increase in biogenic silica production (indicated by elevated Si/Al values). Increasing values in the chemical index of alteration (CIA*) during the event is indicative for more moist conditions on the Iberian continental margin.

Kim, JH; Schouten, S; Hopmans, EC; Donner, B; Damste, JSS. "Global sediment core-top calibration of the TEX86 paleothermometer in the ocean." GEOCHIMICA ET COSMOCHIMICA ACTA 72: 1154, 2008.
Menegatti, A. P. et al. High-resolution $\delta^{13}C$ stratigraphy through the early Aptian "Livello Selli" of the Alpine Trias. Paleoceanography 13, 530-545 (1998)

Ramifications of high *insitu* temperatures for geotechnical testing at ambient temperature conditions – a case study from the Nankai margin

A. HÜPERS[1], S. KREITER[1], A.J. KOPF[1]

[1]MARUM - Center for Marine Environmental Sciences, University Bremen, P.O. Box 330440, 28334 Bremen, Germany
Email of corresponding author: ahuepers@uni-bremen.de

The recovery of drilling cores involves changes in pressure and temperature conditions, which alter the mechanical properties significantly. In particular, unlithified sediments are affected by these sampling artefacts. Pressure release during sampling causes an expansion due to elastic recovery, gas expansion or mechanical stretching. These effects are widely acknowledged (e.g. Blum, 1997) and can be estimated from loading behaviour under laboratory conditions known as consolidation tests. However, temperature induced artefacts are less accurately regarded. Temperature induced volume changes may have severe implications for geotechnical testing because in soil mechanics the pore space is directly linked to the applied load. Considering a sediment undergoing high temperatures with burial, the volume of the pore water increases significantly while the volume change of the solids is rather small. The excess volume to the original pore space is expelled by pore water outflow to maintain the equilibrium between pore space and load. Additionally, the temperature induces a decrease of interparticle friction, which may reduce the pore space at equilibrium. Upon core recovery, the sediment is subjected to cooling and the pore space is being reduced due to the volume decrease of the pore water. Such reduced pore space is equivalent to the pore space created by higher effective stresses. This may have substantial repercussion on maximum past effective stress estimates sediment experienced from consolidation tests. The proposed artefact would result in an overestimation of the determined effective stress. Although temperature differences between *insitu* and laboratory conditions are in most cases small due to limited coring depth and moderate geothermal gradients, a small number of sampled sediments from areas with high geothermal gradients may be affected. The central portion of the Nankai margin offshore Japan is such an area with high heat flow and temperatures up to 110°C due to an ancient spreading zone and adjacient seamount volcanism.

The proposed thermal hardening has been tested for the Lower Shikoku Basin (LSB) facies sediment at ODP Site 1173 which is located 11km seaward of the deformation front of the accretionary prism. The projected temperatures are ~ 65°C at the top and 105°C at the base of the strata. The observed strengthening during reconsolidation tests of samples from this stratum has been accounted to moderate cementation (Morgan et al., 2004). These results have lead to the suggestion that the decollement which separates the accreted from the underthrust sediments forms above this cemented section. In contrast, SEM investigations and p-wave velocity data support a normal consolidated state (Spinelli et al., 2007). We applied a thermal hardening model based on work of Picard (1994) to the shipboard data to estimated the expected maximum past effective stress (pre-consolidation stress) from consolidation tests which include the temperature effect. Regarding the uncertainties of the model and the laboratory pre-consolidation stress determination the modeled pre-consolidation stresses show a good agreement with published consolidation data. This implies that the LSB sequence is normally consolidated as proposed by

Spinelli et al. (2007). Thus, thermal hardening due to cooling during recovery may serve as an explanation for the observed high pre-consolidation stresses of the tested specimen at room-temperature testing conditions. Previously contradictory results based on seismic velocity data (Spinelli et al., 2007) and laboratory tests (Morgan and Ask, 2004) have here been mated for the first time by incorporating temperature effects on reconsolidation behaviour. The data argue against the hypothesis of a decollement location above a moderately cemented section. We propose that the low permeability and thus low drainage of the LSB leads to pore pressure formation due to the rapid loading of the overlying trench turbidites. The associated weakening makes the LSB the primary candidate for decollement formation along the central portion of the Nankai margin. In conclusion, we showed that temperature artefacts may have considerable implications for geotechnical testing and its interpretation. This may be important for IODP's NanTroSEIZE drilling project (Nankai Trough Seismogenic Zone Experiment) when samples will be recovered from seismogenic depth with equivalently high *insitu* temperatures.

Blum, P., 1997, Physical properties handbook: ODP Tech. Note, v. 26, p. doi:10.2973/odp.tn.26.1997.
Morgan, J.K., and Ask, M.V.S., 2004, Consolidation state and strength of underthrust sediments and evolution of the décollement at the Nankai accretionary margin: Results of uniaxial reconsolidation experiments: J. Geophys. Res., v. 109, p. B03102, doi:10.1029/2002JB002335.
Picard, J., 1994, Ecrouissage thermique des argiles saturées: application au stockage des déchets radioactifs: Thèse de Doctorat de l'Ecole Nationale des Ponts et Chaussées.
Spinelli, G.A., Mozley, P.S., Tobin, H.J., Underwood, M.B., Hoffman, N.W., and Bellew, G.M., 2007, Diagenesis, sediment strength, and pore collapse in sediment approaching the Nankai Trough subduction zone: GSA Bulletin, v. 119, p. 377–390.

Fault zone damage and chemical reactions at dept in the San Andreas Fault Zone – A study of SAFOD drill core samples

JANSSEN, C.

This project aims at detailed structural examinations of fault damage zone samples (cataclasites, fault breccias) combined with mineralogical and geochemical analyses of the same fault rocks taken during Phase 3 drilling at SAFOD. Core material has been made accessible to a selected international group of researchers after submission and evaluation of formal proposals. For our group, fault rocks from four core intervals at different depth and different distances to fault contacts are available for investigations. In particular, we will focus on:

- Characterization of damage and deformation mechanisms as a function of distance to the active fault trace. For the analysis we will mainly use optical microscopy (including cathodoluminescence microscopy), scanning and high-resolution transmission electron microscope techniques.
- Determination of preferred orientation patterns in shales and in quartz rock from different fault rock samples using advanced diffraction techniques particularly hard X-ray synchrotron and neutron diffraction.
- Development of a new method to determine residual stresses in strained rocks such as quartz veins in sandstones of the fault zone.
- Correlating mineralogical and geochemical fault rock variations with deformation mechanisms. The results will enable us to examine the coupling between chemical and mechanical evolution during faulting.
- Study of the distributions of minerals, elements and stable isotopes in fault rocks. These data will be used to elucidate the origin, timing and mechanism of fluid infiltration and the extent of fluid-rock interaction in the fault zone.

Melt-rock and fluid-rock interactions in serpentinized abyssal harzburgites (Mid-Atlantic Ridge, ODP Leg 209)

N. JÖNS[1], W. BACH[1], M. ROSNER[1,2], T. SCHROEDER[3]

[1]Fachbereich Geowissenschaften, Universität Bremen, Klagenfurter Straße, 28359 Bremen, Germany
[2]present address: Bundesanstalt für Materialforschung und -prüfung, 12205 Berlin, Germany
[3]Faculty of Science and Mathematics, Bennington College, Bennington VT05201, U. S. A.

At slow- and ultraslow-spreading mid-ocean ridges, abyssal peridotites are commonly exposed at the seafloor. Peridotite-seawater interaction leading to serpentinization influences the rheology, density and chemistry of the oceanic lithosphere. In addition, serpentinization reactions are the cause for increased methane and hydrogen concentrations, which fuel microbial activities at ultramafic-hosted hydrothermal systems. An almost complete lithological and hydrological history of the oceanic lithosphere can best be reconstructed by examination of different generations of veins. These veins are representative for an enormous spectrum of processes, from high-temperature melt impregnation in the deep lithosphere to seawater alteration at ambient pressures and temperatures.

We examined drillcore samples from the Mid-Atlantic Ridge (ODP Leg 209). The sample localities are north and south of the prominent 15°20'N Fracture Zone; Site 1270 is in proximity to the ultramafic-hosted Logatchev hydrothermal vent field. Here, abyssal peridotite is exposed along low-angle detachment faults. At Site 1270, four holes were drilled near the top of an exposed long-lived normal fault (Kelemen et al. 2004; Schroeder et al. 2007). Samples are strongly serpentinized peridotites with abundant gabbroic intrusions. Our study focuses on serpentinites that are crosscut by strongly deformed shear zones. These shear zones feature a distinct mineralogy and are of schistose appearance. Therefore, they are frequently referred to as "fault schists" (e. g., Boschi et al. 2006b).

Chlorite-amphibole-bearing veins are found within shear zones. There has been considerable debate about the formation mechanism of such chlorite- or, in other cases, talc-bearing fault schists. Some authors propose that these lithologies form from an ultramafic protolith under conditions of extremely high fluid/rock ratios, whereas others identify gabbroic melt impregnation veins as the likely protolith (e. g., Escartín et al. 2003; Bach et al. 2004; Boschi et al. 2006a, b). Veins examined in this study consist of porphyroclasts of brownish magnesiohornblende in a matrix of fibrous chlorite (X_{Mg}= 0.82–0.95). Hornblende (X_{Mg}= 0.86–0.96; TiO_2= 1.7–2.4 wt.%; Al_2O_3= 6.9–9.6 wt.%) crystals are slightly deformed with needles of actinolite/tremolite (X_{Mg}= 0.85–0.93; TiO_2= 0.00–0.08 wt.%; Al_2O_3= 0.8–2.9 wt.%) growing in pressure shadows (Figure 4). No talc has been identified. Zircon and apatite are common accessory mineral phases. From major and trace element geochemistry as well as mineralogy we conclude that the chlorite-amphibole veins represent alteration products of former plagiogranitic melt impregnations (Jöns et al., in press). Ti-in-Zircon thermometry (Watson and Harrison 2005; Ferry and Watson 2007) yields temperatures of ca. 820 °C for the crystallization of the precursor melt, which is in agreement with a plagiogranite. To provide a model for fluid flow through the detachment fault system and to examine the fluid-rock interactions necessary to produce the alteration assemblage observed, we performed reaction path modeling using the EQ3/6 software package. The model predicts rodigitization assemblages for hydrous alteration of a pure plagiogranite. In contrast, a mechanical mixture of plagiogranite and harzburgite, which is likely to be present on a shear zone, is able to act as a model protolith for the observed chlorite-amphibole assemblage. The model also shows that serpentine directly adjacent to altered plagiogranite veins as part of the equilibrium assemblage. To explain the co-occurrence of shear zones and chlorite-amphibole schists, we propose the following model: shear zones enable seawater to enter the oceanic crust. At greater depth and higher temperatures, the fluids might get in contact with gabbro intrusions, lower the gabbro solidus and allow partial melting and thus plagiogranite formation. During cooling under hydrous conditions, the original plagiogranite mineralogy breaks down to form a chlorite-bearing assemblage at temperatures of ca. 400–500 °C. At such temperatures olivine of the surrounding harzburgites and dunites is still stable, leading to strain localization around the altered melt veins. During further cooling, these shear zones act as effective fluid pathways for serpentinization of the host peridotites.

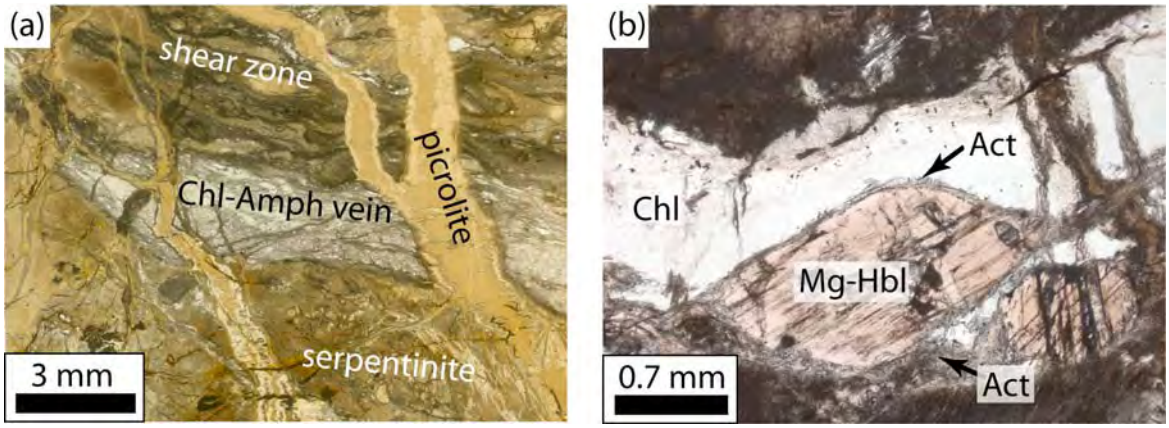

Figure 4: (a) Serpentinite showing the co-occurrence of chlorite-amphibole-bearing veins and shear zones. The latter is crosscut by picrolite veins. (b) Porphyroclast of magnesiohornblende in a matrix of chlorite. Fine-fibrous actinolite/tremolite is growing around magnesiohornblende.

Peridotite host rocks are almost completely serpentinized dunites or harzburgites, with less than 10 vol.% of the primary minerals being preserved. Relics of olivine are locally found in mesh textures, where they are largely replaced by secondary serpentine minerals; in shear zones, fine-grained recrystallized olivine is locally present. Both generations are Mg-rich with X_{Mg}= 0.87–0.90. Orthopyroxene is only rarely preserved. It is Mg-rich (X_{Mg}= 0.91–0.93), contains some aluminium (Al_2O_3= 1.2–3.8 wt.%) and mostly replaced by serpentine in bastite textures. Another primary mineral phase is chromium-bearing (Cr/[Cr+Al]= 0.47–0.55) spinel, which is generally rimmed by magnetite. By far the most common secondary mineral is serpentine. In mesh textures after olivine it is more magnesian (X_{Mg}= 0.93–0.97) than in bastite pseudomorphs after orthopyroxene (X_{Mg}= 0.88–0.92). Notably, brucite is not present as a secondary mineral phase after olivine, demonstrated by means of XRD, optical and electron microscopy. This is in accordance with reaction path modeling, which shows that high $aSiO_2$ values imposed to the fluid by the nearby plagiogranitic material inhibit brucite formation in the serpentinites. In addition, the whole-rock chemistry of serpentinites is changed in vicinity of melt veins: compared to an average peridotite, a strong enrichment in rare earth elements, strontium and potassium is found, whereas cobalt and nickel were apparently lost. These chemical changes can in part be explained by slight mechanical mixing of peridotite and plagiogranite on the shear zone, but must also result from fluid flow on the detachment fault. The latter is evidenced by whole-rock oxygen isotope data of altered plagiogranite veins ($\delta^{18}O$= +3.0–4.2 ‰ SMOW) and adjacent serpentinites ($\delta^{18}O$= +2.6–3.7 ‰ SMOW). Compared to values of unaltered peridotites ($\delta^{18}O\approx$ +5.5 ‰ SMOW) and serpentinites more distal from melt impregnations ($\delta^{18}O$= +3.2–5.2 ‰ SMOW; Alt et al. 2007), these comparatively low values indicate an intense influx of seawater-derived fluids in the detachment fault system.

Picrolite veins crosscut the chlorite-amphibole-bearing shear zones within the serpentinites and thus mark an even later stage of the alteration history. They are slightly more Fe-rich in composition (X_{Mg}= 0.85–0.87) than serpentine of the rock matrix. From textures, multiple opening and fluid transport stages can be derived; however, from mineral chemical data no clear distinction can be made between these growth stages.

Carbonate veins provide the latest and the lowest-temperature record of fluid-peridotite interaction. Some of these veins formed coeval with picrolite veins, but most of them even later. Four types of veins can be distinguished: calcite (X_{MgCO3}= 0.04–0.09) veins containing dolomite (X_{MgCO3}= 0.87–0.91), pure dolomite veins (X_{MgCO3}= 0.84–0.93), pure calcite veins, and aragonite veins. The latter two vein types have been examined in detail. Assuming a fluid $\delta^{18}O$ of +1.5 ‰ SMOW, formation temperatures of 90–185 °C can be derived from oxygen isotope analyses of calcite veins. This is contrasting the results from strontium and lithium isotopic analyses, which show similarities to 350 °C hot vent fluids from the nearby Logatchev hydrothermal field. If fluids on the detachment fault are equivalent to the Logatchev fluids, a significant amount of conductive cooling during upflow is thus required to explain these findings. Aragonite veins have been analysed by U-Th and radiocarbon dating as well as for oxygen isotopes. Formation ages for these veins are in the range of 2–130 kyrs. From oxygen isotope data of 8–12 kyrs old veins, a geothermal gradient of 100–150 °C can be deduced for Site 1274 (north of the 15°12'N Fracture Zone.

In summary, different types of veins in abyssal peridotites from ODP Leg 209 comprehensively record both melt-rock and fluid-rock interaction processes. Lithological inhomogeneities due to formation of plagiogranitic or gabbroic veins at high temperatures remain the locations of intense fluid flow even during cooling to greenschist- or subgreenschist-facies conditions. These major fluid pathways allow for initiation of serpentinization at different crustal levels and contribute to cooling of the oceanic crust.

Alt JC, Shanks WC III, Bach W, Paulick H, Garrido CJ, Beaudoin G (2007) Hydrothermal alteration and microbial sulfate reduction in peridotite and gabbro exposed by detachment faulting at the Mid-Atlantic Ridge, 15°20'N (ODP Leg 209): a sulfur and oxygen isotope study. Geochemistry Geophysics Geosystems 8:Q08002.

Bach W, Garrido CJ, Paulick H, Harvey J, Rosner M (2004) Seawater–peridotite interaction: first insights from ODP Leg 209, MAR 15°N. Geochemistry Geophysics Geosystems 5:Q09F26.

Boschi C, Früh-Green GL, Delacour A, Karson JA, Kelley DS (2006a) Mass transfer and fluid flow during detachment faulting and development of an oceanic core complex, Atlantis Massif (MAR 30°N). Geochemistry Geophysics Geosystems 7:Q01004 .

Boschi C, Früh-Green GL, Escartín J (2006b) Occurrence and significance of serpentinite-hosted, talc- and amphibole-rich fault rocks in modern oceanic settings and ophiolite complexes: an overview. Ofioliti 31:129–140.

Ferry JM, Watson EB (2007) New thermodynamic models and revised calibrations for the Ti-in-zircon and Zr-in-rutile thermometers. Contributions to Mineralogy and Petrology 154:429–437.

Jöns N, Bach W, Schroeder T (in press) Formation and alteration of plagiogranites in an ultramafic-hosted detachment fault at the Mid-Atlantic Ridge (ODP Leg 209). Contributions to Mineralogy and Petrology, doi: 10.1007/s00410-008-0357-2.

Kelemen PB, Kikawa E, Miller DJ et al (2004) Proceedings of the Ocean Drilling Program, initial reports, vol 209 [CD-ROM]. Ocean Drilling Program, Texas A&M University, College Station.

Schroeder T, Cheadle MJ, Dick HJB, Faul U, Casey JF, Kelemen PB (2007) Nonvolcanic seafloor spreading and corner-flow rotation accommodated by extensional faulting at 15°N on the Mid-Atlantic Ridge: a structural synthesis of ODP Leg 209. Geochemistry Geophysics Geosystems 8:Q06015.

Watson EB, Harrison TM (2005) Zircon thermometer reveals minimum melting conditions on earliest Earth. Science 308:841–844.

BUGLab – A new mobile geomicrobiology and biogeochemistry laboratory for exploring the deep biosphere

JENS KALLMEYER[1,2], KAI MANGELSDORF[1] AND BRIAN HORSFIELD[1]

[1]Helmholtz Centre Potsdam, GFZ German Research Centre for Geosciences, Telegrafenberg, 14473 Potsdam, Germany

[2] now with Universität Potsdam, Institut für Geowissenschaften, Karl-Liebknecht-Str. 24, 14476 Golm

Studies during the past two decades have demonstrated that the biosphere extends to great depths beneath the surface of the Earth's continents. This deep biosphere contains diverse and active microbial communities whose biomass may even exceed that of surface organisms. Progress in understanding life in the subsurface has been limited by available technology but also by funding. Knowledge of the deep biosphere is sparse, and while the marine realm has been well served by IODP, terrestrial systems are especially poorly understood because of the vanishingly small number of boreholes sunk to sample subterraneous life. In the recently published book "Continental Scientific Drilling – A decade of progress and challenges for the future" Horsfield et al. (2007) argued that the research of the "GeoBiosphere" should be an integrated part of the activities of the International Continental Scientific Drilling Program (ICDP) to correct the latter imbalance. We now have planned, built and basically equipped a portable field laboratory for geomicrobiology and biogeochemistry research, which can be transported to and deployed at terrestrial drill sites. The laboratory is composed of two portable standard 20 ft containers, which can be combined. According to requirements the "BugLab" containers can be fully equipped to conduct microbiological and biogeochemical sampling of diverse subsurface environments, on-site analysis of biologically significant transient properties, and on-site analysis of chemical and physical properties being useful to guide microbiological and biogeochemical sampling strategies.

Horsfield, B., Kieft, T.L., Kallmeyer, J., Mangelsdorf, K., et al., 2007. The GeoBiosphere. In: Harms, U., Koeberl, C., Zoback, M.D., Continental Scientific Drilling – A Decade of Progress, and Challenges for the Future. Springer Verlag Berlin Heidelberg, pp. 163-211.

Rapid switch in Indonesian subsurface throughflow triggering climate change across the mid-Pliocene

CYRUS KARAS[1], DIRK NÜRNBERG[1], ANIL K. GUPTA[2], KUPPUSAMY MOHAN[2], RALF TIEDEMANN[3], TORSTEN BICKERT[4]

[1] Leibniz Institute of Marine Sciences (IFM-GEOMAR), University of Kiel, Wischhofstrasse 1-3, D-24148 Kiel, Germany
[2] Department of Geology & Geophysics, Indian Institute of Technology, Kharagpur 721302, India
[3] Alfred Wegener Institute for Polar and Marine Research, Am Alten Hafen 26, D-27568 Bremerhaven, Germany
[4] Zentrum für Marine Umweltwissenschaften, Universität Bremen, D-28334 Bremen, Germany

The impact of the plate tectonic constriction of the Indonesian and the Central American Seaways on ocean circulation are crucial to understand Pliocene climate evolution, including the intensification of the Northern Hemisphere Glaciation and severe tropical climatic changes across the mid-Pliocene transition. Although the constriction history of the Indonesian Gateway is not well constrained by paleoceanographic data, plate tectonic reconstructions and model results point to a major reorganization of the Indonesian Throughflow at ~4-3 Ma. The hypothesis of Cane and Molnar (2001) suggests a switch in the source of the Indonesian Throughflow waters from warm/saline South Pacific towards cool/fresh North Pacific waters entering the Indian Ocean. Our reconstruction of tropical E-Indian Ocean (DSDP Site 214) surface and subsurface temperatures and $\delta^{18}O_{salinities}$ sheds new light on the hydrographic changes in the Indonesian Gateway and its implications for climate change across the mid-Pliocene. Our results partly contradict the assumptions of Cane and Molnar (2001) of a change in surface throughflow in line with the continuous plate tectonic narrowing in that area between 4 and 3 Ma. Our data rather reveal a pronounced cooling of ~4°C and freshening at the subsurface niveau (~300-450m) from ~3.5-2.95 Ma, pointing to the switch in ITF source waters from initially S-Pacific to N-Pacific subsurface waters (Figure 1). After 2.95 Ma, constantly low subsurface temperatures at gradually fresher conditions point to the prevailing throughflow of N-Pacific source waters through the Indonesian Gateway. The rapid changes in the thermocline might have preconditioned the cooling of the Benguela Upwelling system (ODP Site 1084) at ~3.2 Ma, amplifying the global cooling of the thermocline at that time (Figure 1). From both increasing productivity/upwelling events at equatorial E-Pacific Site 846 and the increasing gradient in ocean surface temperatures between the tropical E-Indian Ocean Site 214 and Site 846 evolving after 2.95 Ma (Figure 1), we suggest that the new plate tectonic constellation after 2.95 Ma was a viable mechanism to bring a larger portion of Subantarctic Mode Water via "ocean tunnels" into the Equatorial Undercurrent leading to the manifestation of the Equatorial E-Pacific Cold Tongue, in line with the intensification of Northern Hemisphere Glaciation.

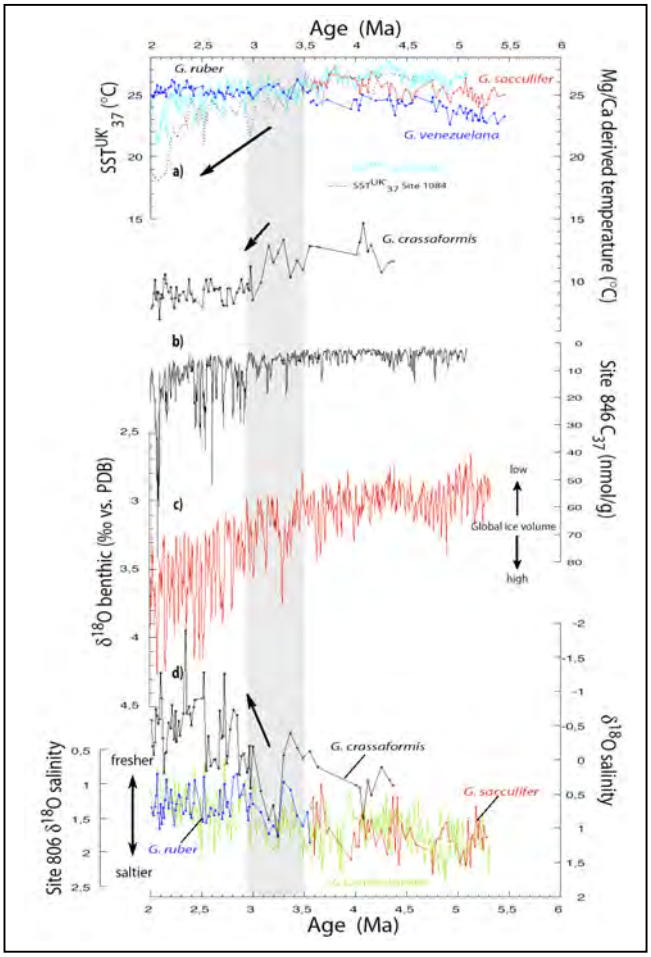

Figure 1. Proxy data from Site 214 in relation to other paleoclimatic records across 5.5-2 Ma. (a) Comparison between Mg/Ca derived temperatures of shallow dwelling *G. ruber/G. sacculifer*, *G. venezuelana* and the thermocline-dweller *G. crassaformis* of Site 214 and $SST^{UK'}_{37}$ records of Sites 846 and 1084 (Marlow et al. 2000; Lawrence et al. 2006). The age model of Site 1084 was revised by Johan Etourneau et al. (in prep.). (b) Concentration of C_{37} alkenones of Site 846 (Lawrence et al. 2006) indicating changes in paleoproductivity. (c) The LR04 global ice volume record (Lisiecki and Raymo 2005). (d) Surface and subsurface local seawater salinities at Site 214, expressed as $\delta^{18}O_{salinity}$, derived from *G. ruber/G. sacculifer* in comparison to Site 806 surface $\delta^{18}O_{salinity}$, ($SST_{Mg/Ca}$ and $\delta^{18}O$ values from Wara et al. 2005). The shaded time period from 3.5-2.95 Ma marks abrupt changes in subsurface waters at Site 214 that are accompanied by major changes in marine productivity and $SST^{UK'}_{37}$ at Sites 1084 and 846 contemporaneously with the intensification of the Northern Hemisphere Glaciation. Arrows clarify freshening and cooling trends.

Cane, M. & Molnar, P. Closing of the Indonesian seaway as a precursor to east African aridification around 3-4 million years ago. *Nature* **411**, 157-162 (2001).

Lawrence, K. T., Liu, Z. & Herbert, T. D. Evolution of the eastern tropical Pacific through Plio-Pleistocene glaciation. *Science* **312**, 79-83 (2006).
Lisiecki, L.E. & Raymo, M.E. A Pliocene-Pleistocene stack of 57 globally distributed benthic d18O records. *Paleoceanography* **20**, 1 PA1003, doi:10.1029/2004PA001071 (2005).
Marlow, J. R., Lange, C. B., Wefer, G., & Rosell-Melé, A. Upwelling intensification as part of the Pliocene-Pleistocene climate transition. *Science* **290**, 2288-2291 (2000).
Wara, M. W., Ravelo, A. C. & Delaney, M. L. Permanent El Niño-Like Conditions During the Pliocene Warm Period. *Science* **309**, 758-761 (2005).

Climatically induced spatial sedimentation dynamics of late Holocene sediment infill in Laguna Potrok Aike (southern Patagonia, Argentina) – a preliminary study in the framework of the ICDP project PASADO

STEPHANIE KASTNER[1], CHRISTIAN OHLENDORF[1], TORSTEN HABERZETTL[2], ANDREAS LÜCKE[3], NORA I. MAIDANA[4], CHRISTOPH MAYR[5], FRANK SCHÄBITZ[6], BERND ZOLITSCHKA[1]

[1] Institute of Geography (Geopolar), University of Bremen, Germany – steka@uni-bremen.de
[2] Institut des sciences de la mer de Rimouski (ISMER), Université du Québec à Rimouski (UQAR), Canada
[3] ICG 4, Energy & Environment, Research Center Jülich, Germany
[4] Department of Biodiversity and Experimental Biology, University of Buenos Aires, Argentina
[5] GeoBio-CenterLMU and Dept. of Earth & Environmental Sciences, University of Munich, Germany
[6] Seminar for Geography and Education, University of Cologne, Germany

The 100 m deep and max. 770 ka old maar lake Laguna Potrok Aike (51°58'S, 70°23'W; Fig. 1) has a high potential as a palaeolimnological key site for the reconstruction of terrestrial palaeoclimate conditions within a region of scarce palaeoenvironmental archives (Zolitschka et al., 2006). The strong influence of varying southern hemispheric wind and pressure systems on the lacustrine deposits was proven by several interdisciplinary multi-proxy studies of the lake´s sediments as well as a climate modelling approach (Wagner et al., 2007). Therefore, the lake holds a unique record of palaeoclimatic and palaeoecological variability within the dry steppe environment of south-eastern Patagonia. Hydrological variations of the lake are closley related to the fluctuations of the Southern Hemispheric Westerlies (Mayr et al., 2007) as it is shown from depositional changes inferred from the lacustrine sediment sequence as well as subaerial and subaquatic lake level terraces (Anselmetti et al., 2008). For this reason the lake was chosen as an ICDP drilling site in 2008 within the "Potrok Aike maar lake sediment archive drilling project" (PASADO).

Geochemical, palynological, diatomological and isotopic investigations were carried out with high temporal resolution on the 18.9 m long sediment record covering the last 16,000 years (Haberzettl et al., 2007; Mayr et al., 2009; Wille et al., 2007). Beyond this one point source of information the present study focuses on the understanding of internal depositional dynamics which control the characteristics and spatial distribution of the sediment infill of the lake. Furthermore, it provides information that can improve the accuracy of the interpretation of the long sediment record recovered within the PASADO project.

In 2005 46 gravity cores of up to 49 cm in length were recovered to survey the spatial sediment distribution. This grid of cores covers a range of water depths from 9 to 100 m (Fig. 2). All 46 cores were scanned with an X-ray fluorescence scanner and a scanner for magnetic susceptibility with 1 and 4 mm spatial resolution. Using Ca and Ti as well as magnetic susceptibility data the cores were correlated and linked to an existing depth/age model (Haberzettl et al., 2005). As these parameters vary considerably and not consistently within the suite of littoral cores, a correlation prior to the 2005 sediment surface is solely based on cores from water depths exceeding 45 m. Thus, samples of the surface sediments were taken from all 46 cores while sub-sampling of selected time intervals - AD 1960, 1800, 1610, 1500, 1380 - was only possible for up to 26 well correlated cores from the deep central basin. These time slices cover distinctive palaeoenvironmental intervals which represent different hydrological settings (i.e., different lake levels; Haberzettl et al., 2005). The sediment was further analysed geochemically (for element concentrations of C, N, S, and total phosphorus), sedimentologically (grain size), palynologically, diatomologically, and for stable isotopes of organic matter (C, N) and carbonates (C, O). Subsequently, distribution maps for all parameters and for each time slice were compiled by kriging methods. Additional 16 gravity cores and 40 shoreline sediment samples from all around the lake's perimeter were taken during the PASADO fieldwork in autumn 2008 to complement the existing grid.

First results of the surficial sediments, representing the last 20 years of the record, confirm pronounced differences between the littoral cores down to 45 m water depth and the lake's profundal cores separated from each other by steep slopes (Fig. 2; Kastner et al., in prep.). Modern sedimentation patterns of grain size, benthic diatoms, total inorganic carbon, Ti and Ca point to distinct internal depositional dynamics induced by the dominant westerly winds. At the eastern shore frequent erosion, resuspension and redistribution of littoral sediment is followed by transport to a profundal accumulation area (Fig. 3). Hence, sedimentation within this terminal lake is not only influenced by lake level changes, episodic inflows and the surrounding geology but also by wind driven wave action, resulting internal currents and shoreline erosion.

The sub-recent spatial sediment distribution is evaluated and interpreted in the context of the modern processes. Due to core correlation the interpretation is restricted to information of the deep central basin area. Changing wind patterns (Mayr et al. 2007; Meyer and Wagner, 2008) and varying lake levels (Haberzettl et al., 2005) are assumed to cause modifications of

depositional dynamics and affect the varying palaeo-shoreline proximity to the analysed sediment cores during the selected Holocene time sections (i.e., Little Ice Age, Medieval Climate Anomaly and transitional periods). To evaluate the mechanisms of the sediment distribution during different hydrological settings the grainsize data seem to be an important parameter as this data explicitly indicate sediment reworking from the lake margins as well as influences of the discontinuous tributaries (c.f. Fig. 3). The additional measured parameters complement and differentiate the underlying mechanisms. Distribution patterns in the deep basin reveal intensified sediment redistribution during lake level low stands and strengthened winds during post-Little Ice Age time (around AD 1960). In contrast, Little Ice Age (around AD 1800) conditions of a lake level high stand and less intense westerly winds result in a more homogeneous sediment distribution within the deep central basin. Furthermore, the spatial sediment distribution reveals distinct influences of the main western, the north-eastern and the south-eastern tributaries and a north-eastern outflow.

Acknowledgements

We are much obliged to Eva Hering (University of Cologne) for providing pollen data of her Diplom thesis and to Thomas Chwalek (University of Munich) for providing isotope data of his bachelor thesis. This research is supported by the International Continental Scientific Drilling Program (ICDP) in the framework of the "Potrok Aike Maar Lake Sediment Archive Drilling Project" (PASADO). Funding was provided by the ICDP, the German Science Foundation (DFG), the Swiss National Science Foundation (SNF), the Natural Sciences and Engineering Research Council of Canada (NSERC), the Swedish Vetenskapsradet (VR) and the University of Bremen

Anselmetti, F. et al. (2008). Environmental history of southern Patagonia unraveled by the seismic stratigraphy of Laguna Potrok Aike. Sedimentology. doi: 10.1111/j.1365-3091.2008.01002.x.

Haberzettl, T. et al. (2005). Climatically induced lake level changes during the last two millennia as reflected in sediments of Laguna Potrok Aike, southern Patagonia (Santa Cruz, Argentina). Journal of Paleolimnology 33: 283-302.

Haberzettl, T. et al. (2007). Lateglacial and Holocene wet-dry cycles in southern Patagonia: chronology, sedimentology and geochemistry of a lacustrine record from Laguna Potrok Aike, Argentina. The Holocene, 17: 297-310.

Kastner, S. et al. (in prep.). Southern Hemispheric Westerlies control the spatial variation of modern sediments at Laguna Potrok Aike (Argentina).

Mayr, C. et al. (2007). Holocene variability of the Southern Hemisphere westerlies in Argentinean Patagonia (52°S). Quaternary Science Reviews, 26: 579-584.

Mayr, C. et al. (2009). Isotopic and geochemical fingerprints of environmental changes during the last 16,000 years on lacustrine organic matter from Laguna Potrok Aike (southern Patagonia, Argentina). Journal of Paleolimnology. doi: 10.1007/s10933-008-9249-8.

Meyer, I. & Wagner, S. (2008). The Little Ice Age in southern Patagonia: Comparison between paleoecological reconstructions and downscaled model output of a GCM simulation. PAGES News 16: 12-13.

Wagner, S. et al. (2007). Transient simulations, empirical reconstructions and forcing mechanisms for the Mid-holocene hydrological climate in southern Patagonia. Climate Dynamics. doi: 10.1007/s00382-007-0229-x.

Wille, M. et al. (2007). Vegetation and climate dynamics in southern South America: The microfossil record of Laguna Potrok Aike, Santa Cruz, Argentina. Review of Palaeobotany and Palynology 146: 234-246.

Zolitschka, B. et al. (2006). Crater lakes of the Pali Aike Volcanic Field as key sites of paleoclimatic and paleoecological reconstructions in southern Patagonia, Argentina. Journal of South American Earth Sciences 21: 294-309.

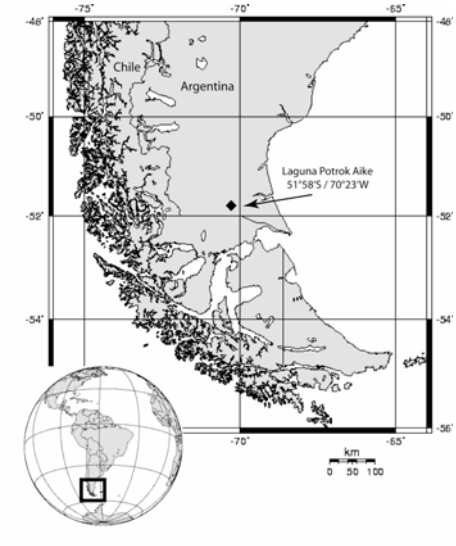

Fig. 1. Location of Laguna Potrok Aike in southern Patagonia, Argentina, southern South America.

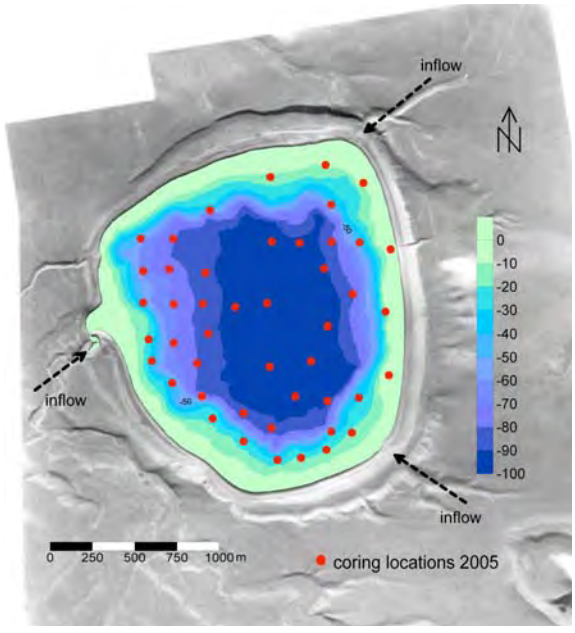

Fig. 2. Bathymetry and aerial photograph of Laguna Potrok Aike with positions of gravity cores (red dots) and main inflows.

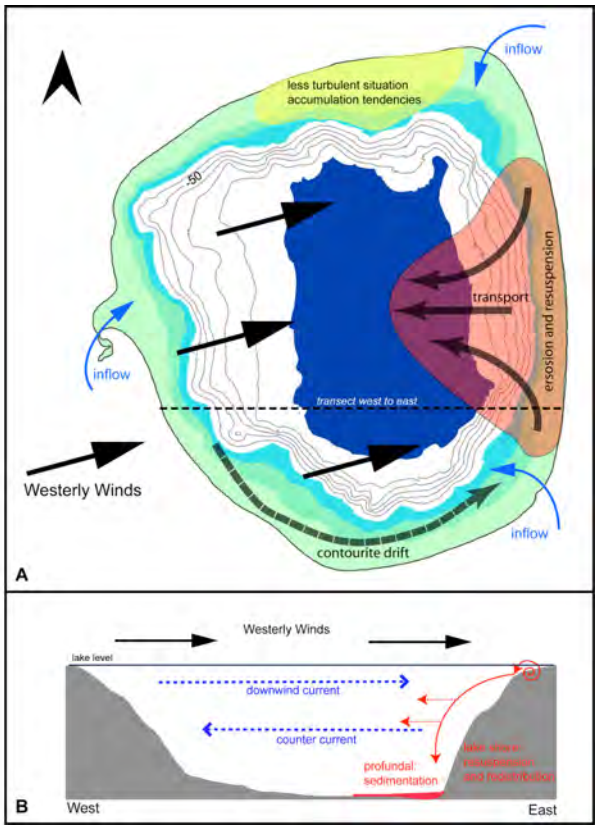

Fig. 3. Interpretation of areal sediment distribution data in terms of modern lake internal processes. (A) The littoral area is highlited in greenish colours, the deep basin area is coloured in blue, areas of high erosion dynamics and slope downward transport are coloured in red. An accumulation area is marked at the northern shore (coloured yellow). Wind direction and transport is indicated by arrows. (B) A west to east transect depicts lake internal currents and sediment transport pathways induced by westerly winds during modern climate and lake conditions.

Increased aridity in the Mediterranean Sea 3.55 – 3.35 Ma: a trend without climatic analogue in the ocean?

N. KHÉLIFI[1], AND M. SARNTHEIN[1]

[1]Institut für Geowissenschaften, University of Kiel, Germany (nk@gpi.uni-kiel.de and ms@gpi.uni-kiel.de)

ODP Site 978 (1930 m w.d.) provides a highly resolved record of surface waters and West Mediterranean Deep Water in the Alboran Sea for the period 3.62 – 2.72 Ma (Khélifi et al., submitted 2009). We found a ~4 psu increase in sea surface salinity from ~3.6 to 3.55 Ma, an event that occurred 100 kyr prior to a similar potential increase by ~1 psu in bottom water salinity from 3.5 to 3.45 Ma (if taking the Mg/Ca ratios of *Cibicidoides* spp. as face values of bottom water temperature). The joint salinity increase in surface and bottom waters records a significant aridification of Mediterranean summer climate, that was coeval with the onset of more “steppic” vegetation in the Gulf of Lion (Suc, 1984) and was also documented at the northeast Atlantic continental margin (DSDP 548; 1250 m w.d.) by an abrupt and persistent ~1-psu salinity rise of the Mediterranean outflow from 3.4 to 3.35 Ma. The aridification of the Mediterranean Sea near 3.55 Ma may present an early manifestation of the modern mode of Mediterranean climate (Suc, 1984). However, this mode was possibly still less seasonal than today (model simulation of Haywood et al., 2000). The early aridification was not paralleled by any pertinent changes in atmospheric and Atlantic ocean circulation (Kleiven et al., 2002). Accordingly, regional trends may have dominated over global climate trends in this region (Haywood et al., 2000).

Haywood, A.M., Sellwood, B.W., Valdes, P.J., 2000. Regional warming: Pliocene (3 Ma) paleoclimate of Europe and the Mediterranean. Geology, v. 28, p. 1063–1066.

Khélifi, N., Sarnthein, M., Andersen, N., Blanz, T., Frank, M., Garbe-Schönberg, D., Haley, B.A., Stumpf, R., Weinelt, M., 2009. A major and long-term Pliocene intensification of the Mediterranean Outflow (3.4 – 3.3 Ma). *submitted*.

Kleiven, H.F., Jansen, E., Fronval, T., Smith, T.M., 2002. Intensification of Northern Hemisphere glaciations in the circum Atlantic region (3.5 – 2.4 Ma), ice-rafted detritus evidence. Palaeogeography, Palaeoclimatology, Palaeoecology, v. 184, p. 213–223.

Suc, J.-P., 1984. Origin and evolution of the Mediterranean vegetation and climate in Europe. Nature, v. 307, p. 429–432.

Sediment deformation in accretionary prism toe: results from NanTroSEIZE Expedition 316, Sites C0006 and C0007

Y. KITAMURA[1], T. KANAMATSU[2], X. ZHAO[3]

[1] IFM-GEOMAR, Leibniz Institute of Marine Sciences at the University of Kiel, Wischhofstraße 1-3, 24149 Kiel
[2] Institute for Research on Earth Evolution, Japan Agency for Marine-Earth Science and Technology, 2-15 Natsushima-cho, Kanazawa-ku, Yokosuka, Kanagawa 237-0061, Japan
[3] Department of Earth and Planetary Sciences, University of California Santa Cruz, 1156 High Street, Santa Cruz CA 95064, USA

In this study, magnetic fabric analysis to examine internal structure of the accretionary wedge, especially at the toe of the prism was performed in the Nankai Trough, off Japan. Nankai Trough Seismogenic Zone Experiment (NanTroSEIZE) is a complex drilling project within a framework of Integrated Ocean Drilling Project (IODP) and aims to reveal insitu phenomena of seismogenic zone processes in subduction zone. This multi-stage, platform and expedition project has been started in 2007 with three expeditions as the first stage.

Two sites (C0006 and C0007) were drilled as a part of IODP Expedition 316, which penetrated the sediment section including in-sequence thrusts and the frontal thrust. Measurement of anisotropy of magnetic susceptibility (AMS) provides insight into recorded strain during sedimentary and tectonic processes. Results from the upper part of the wedge show sedimentary acquired compaction fabric in general. In the lower part, AMS fabrics occasionally rotate almost ninety degree and suggest horizontal compression. In contrast, magnetic fabric did not show any correspondence to in-sequence thrusts or minor faults, which implies that those faults have developed with concentrated shear deformation without disturbing surrounding sediments. Dense sampling from two adjacent drilling sites clearly figured out a change in strain field which is reported by previous ocean drilling studies. Based on the results, we propose a model of structural evolution at the toe of the prism. Plunging sediments induce horizontal stress in the lower part of the wedge, which reduces the effective stress and forms high pore pressure anomaly and fracture zone. The frontal thrust is bended geometrically and terminates its activity in response to increase of friction that triggers initiation of the next-generation frontal thrust. The upper part of the wedge tilts accordingly that results in unstable slope of the wedge surface. This model is only for ~1km scale tectonics at the deformation front but is very important to build up the “imbricate fold and thrust zone”. Since the region behind the prism toe is only dead structure unless they are cut by out-of-sequence thrusts later, deformation in the prism toe would be a key for whole accretionary wedge.

Messungen mit dem Göttinger Bohrlochmagnetometer (GBM) in der Bohrung Schotten/Sichenhausen im Vogelsberg

T. KLEIN[1], A. HÖRDT[1], M. LEVEN[2] , C. VIRGIL[1]

[1]Institut für Geophysik und extraterrestrische Physik, Technische Universität Braunschweig
[2]Institut für Geophysik, Georg-August Universität Göttingen

In Vorbereitung auf das ICDP-Projekt „ Three-component magnetic logging in Outokumpu deep drillhole“ wurden mit der Göttinger Bohrlochmagnetometer-Sonde Testmessungen in der Bohrung Schotten-Sichenhausen durchgeführt.

Das Göttinger Bohrlochmagnetometer (GBM) ist derzeit die einzige Sonde, die ihre Orientierung im Bohrloch unabhängig vom Magnetfeld bestimmen kann. Für diese Bestimmung werden drei orthogonal zueinander stehende Faserkreisel, fibre optic gyros (FOG), benutzt. Die Rotationsinformation der Bohrlochsonde wird verwendet, um mittels eines Algorithmus, der auf Euler-Matrizen beruht, die mit einer dreiachsigen Förstersonde gemessenen Magnetfelddaten in geographische Koordinaten (Nord, Ost, Vertikal) zu transformieren. Mit der 3-D-Information über das Magnetfeld im Bohrloch kann neben der Stärke auch die Inklination und Deklination der Gesteinsmagnetisierung bestimmt werden.

Mit der GBM-Sonde wurden mehrere Testmessungen in der 300 Meter tiefen Bohrung Schotten-Sichenhausen im Vogelsberg durchgeführt, um mit echten Messdaten Auswirkungen von Korrekturen und Datenauswertung zu untersuchen. Die Bohrung Schotten-Sichenhausen befindet sich an einem Waldweg am nordöstlichen Hang der Herchenhainer Höhe und ist ca. 1,5 km nordwestlich der Ortschaft Herchenhain zu finden.

Als Korrektur wurden unter anderem die Fehler der Magnetfeldsensoren (Verschiebung der Nullpunkte der Sensoren, unterschiedliche Skalenfaktoren der Sensoren und nicht exakte Orthogonalität der Sensoren zueinander) berücksichtigt, die erstmals mittels Kalibriermessungen im magnetischen Laboratorium Magnetsrode bestimmt werden konnten.

Das magnetische Laboratorium Magnetsrode des Instituts für Geophysik und extraterrestrische Physik befindet im abgelegenen Südwest-Zipfel des Geländes der ehemaligen Forschungsanstalt für Landwirtschaft in Braunschweig. Es zeichnet sich dadurch aus, dass es geringe zivilisatorische Störeinflüsse aufweist und frei von kleinräumigen magnetischen Anomalien ist. Es ist deswegen besonders gut für Kalibriermessungen von Magnetfeldsensoren geeignet. Magnetsrode verfügt über ein Braunbek-Spulensystem, in dessen Homogenitätsbereichs im Inneren das Magnetfeld um weniger als 1 nT abweicht.

Neben mehreren Messungen mit einer anderen Kalibriermethode zur Bestimmung der Fehler der Magnetfeld-sensoren, dem Drehverfahren, wurden auch Messungen im Braunbek-Spulensystem durchgeführt. Die ermittelten Fehlerparameter

(Nullpunktsverschiebungen, Skalenfaktoren und Orthogonalitäten) der Förstersonde konnten durch die zwei unterschiedlichen Bestimmungsverfahren bestätigt werden.

Die 4 gemessenen Logs in der Bohrung Schotten-Sichenhausen werden benutzt, um die Datenauswertung zu optimieren. So konnte durch Einbeziehung einer Fehlerkorrektur für die Magnetfeldsensoren in die Datenauswertung die Abweichung im magnetischen Totalfeld zwischen Up- und Downlog im Mittel um ca. 20 nT verbessert werden.

The Arctic Chronology Project – Academia meets Industry

J. KNIES[1], K. ANDREASSEN[2], K. FABIAN[1], K. GRØSFJELD[1], M. HALD, K. HUSUM[2]

[1]Geological Survey of Norway, N-7491 Trondheim, Norway
[2]University of Tromsø, N-9037 Tromsø, Norway

The Arctic is one of the few remaining petroleum frontiers of the world. Present estimates suggest that the potential recoverable hydrocarbon resources of the Russian offshore area alone are in excess of 100 billion toe, and the major part is within the Arctic shelf. During a recent assessment of the world's oil and gas resources the U.S. Geological Survey suggested that about 25 percent of the undiscovered oil and gas resources might be found in basins of the high northern latitudes. Hence, exploration is a keyword for future success in this remote area.

So far, the history of the late Cenozoic Arctic is so poorly known that scientists can look at the recovery of any material as a true exploration that will, by definition, increase the knowledge and understanding of this critical region for exploration purposes and climate change. As an important contribution to future planned exploration of Arctic frontiers including the Barents Sea, we propose to work out a refined stratigraphic framework for the Barents Sea over the last 3 Ma by working on existing ODP sites 910 and 911 from the marginal Arctic Ocean. This time period recently gained renewed interest due to the fact that StatoilHydro made a large gas discovery in Plio-Pleistocene sand stones capped glacial tills in the North Sea.

We chose the Yermak Plateau – the Atlantic/Arctic Ocean gateway – as key area for our study because, (1) here, rather than along the western Barents Sea or even the central Arctic Ocean, carbonate bearing sequences permit establishment of a relatively continuous stable oxygen isotope and foraminiferal stratigraphy, which is still the prerequisite for any subsequent application of chronological approaches, and (2) the site is characterized by a dynamic coupling between the northernmost branch of the Gulf Stream and the Arctic Ocean. We have selected two locations of high priority recovered during ODP Leg 151 (Sites 910, 911) (Fig. 1). At these sites, we will establish a reference stratigraphy for the Plio-Pleistocene sections along the Barents Sea continental margin which shall ultimately result in better integrating the seismic stratigraphic framework.

Three research tasks will address three crucial effects of successful exploration in Arctic frontier areas: 1) Consistent stratigraphic framework for Plio-Pleistocene sediment sequences, 2) expanded knowledge on coupled ice dynamics and paleoceanographic changes during the Plio-Pleistocene, and 3) improved spatio-temporal information on glacial erosion in the Barents Sea during the Plio-Pleistocene.

The project is fully funded by the petroleum industry for the next 3 year. We acknowledge Det Norske Oljeselskap, StatoilHydro and BG Norge for supporting the research.

Fig. 1. Bathymetry and borehole locations (red dots) in the European sector of the Arctic Ocean and Nordic seas. In- and outflow patterns of warm Atlantic derived water masses (red arrows) and polar water masses of the Transpolar Drift (TD) and East Greenland Current (EGC) are displayed (white arrows). Black arrows indicate postulated Arctic ice drift patterns during glacial intervals. Squares indicate the main sources of clay minerals and other detritus (I = illite, C = chlorite, S = smectite, K = kaolinite, Dol = dolomite). Small red arrows indicate the main transport pathways of smectite from the hinterland. Abbreviations are: Gr = Greenland, Sc = Scandinavia , BS = Barents Sea, FS = Fram Strait, YP = Yermak Plateau, KS = Kara Sea, Ys = Yenisei river, Kt = Kathanga river.

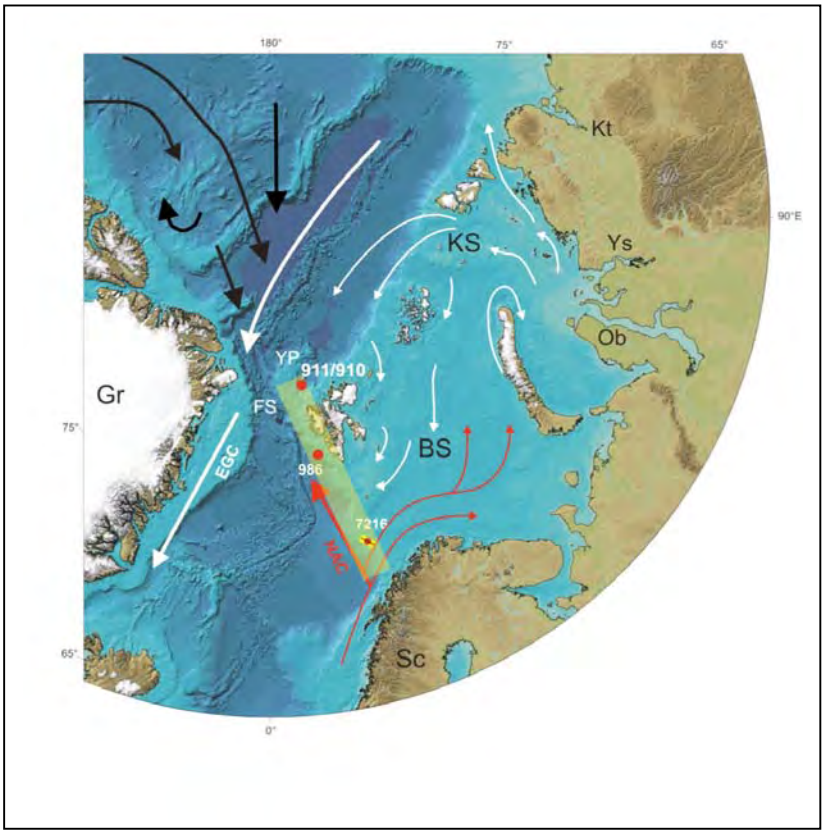

Why are some faults weak, some strong, and many seismogenic? Results from deformation tests in a combined ICDP – IODP study

A. KOPF

MARUM Research Centre, University of Bremen, Leobener Strasse, 28359 Bremen, Germany (akopf@uni-bremen.de)

There has been considerable controversy regarding the strength of fault rocks and how earthquake rupture and fault slip are accomplished mechanically. In addition to the intrinsic strength of geomaterials, pore pressure transients seem to play a major role in natural systems, in places compensating for the entire overburden stress. In natural faults, the interplay between the physical properties of fault rocks (most importantly the friction coefficient) and associated diagenetic and geochemical processes (pressure solution, mineral transformation, precipitation, frictional melting), the latter being complicated by fluids migrating through the fault zone, provide a poorly understood, complex scenario. Standard rock mechanical experiments often fail to simulate natural conditions such as high stress and elevated temperature convincingly. It is hence vital to run hydrothermal deformation experiments in addition to standard shear tests to get a comprehensive understanding.

Both the ICDP and the IODP have a significant number of projects that drilled, are drilling, or plan to drill fault zones all over the planet. Many of them are seismogenic, i.e. the fault gouge is capable of generating earthquakes. Most prominently, the ICDP recovered such materials in compressional (Chelungpu, Taiwan), strike-slip (San Andreas, USA) and extensional systems (Gulf of Corinth, Greece), with a series of other areas being the focus of future drilling projects. Similarly, the IODP flagship project NanTroSEIZE (Nankai Trough Seismogenic Zone Experiment) aims at penetrating a complex splay-fault system at several depth levels in the subduction zone off Japan. Some of the faults have successfully been drilled at shallow levels (<500 m below seafloor), and the deepest hole envisaged targets the plat boundary thrust and an overlying splay fault at a depth of 6000 and 5500 mbsf, respectively.

As the kick-off to a multi-phase rock deformation study, a series rotary shear experiments under water-saturated conditions (up to 25 MPa normal stress) has been carried out on materials from plate boundary faults and other major tectonic lineaments from both ICDP and IODP projects. Experiments served to solve the longstanding question whether low sediment friction is sufficient to explain movement along these sutures, or whether high transient pore-pressure is required to make the fault slip. Materials tested included (i) mineral standards, (ii) marine sediments and gouge material from deep-sea drilling off Costa Rica, Japan, Barbados, and Papua New Guinea, and (iii) fault gouge and country rock from continental drilling such as SAFOD/California, Chelungpu/Taiwan, or the Corinth rift/Greece as well as from associated onshore outcrops which were exhumed from seismogeneic depth (e.g. Nobeoka fault, Shimanto accretionary complex, Japan; Franciscan Complex, California). Initial results suggest that friction coefficients along major low-angle faults (decollements off Costa Rica, Nankai, Barbados; normal detachment in the Woodlark Basin; Chelungpu fault zone in Taiwan) are sufficiently low to explain movement along these faults, even at near-hydrostatic pore fluid pressures. Higher friction coefficients were encountered during shear tests of gouge from the San Andreas fault, or Nobeoka FZ/Japan, where alteration by fluids appears to have been less effective. Still, given the presence of considerable amounts of clay minerals, serpentine, and talc, aseismic movement (i.e. creep) is facilitated. Surprisingly high friction is encountered along the Aigeon FZ, Gulf of Corinth rift (ICDP AIG10 well). In this region, however, fault slip is possible because of the steep normal faults as well as high excess pore pressures owing to circulation of meteoric waters.

In the future, more sophisiticated testing is needed to simulate natural conditions more closely. At the MARUM geotechnical laboratory, we have developed two hydrothermal oedometer systems that allow 70-80 MPa normal stress and 150-200°C heat on the specimen. Fluid chemistry is monitored over the entire deformation tests, and sediment/rock is analysed prior and after the test to identify mineralogical transformations. Also, we currently build a heatable (up to 200-250°C), back-pressured direct shear apparatus where fault gouge and other geomaterials may be tested at up to 200 MPa normal stress. These setups will offer a wide range of opportunities to precisely measure thermal hardening effects, rate-dependent frictional strength of sediments and rocks, transients of pore pressure and permeability during loading, failure, and shear movement (with dilatancy versus shear-enhanced compaction and strengthening being monitored), and the physico-chemical interaction that governs the mechanical behaviour of the rocks.

Climate dynamics in the Aegean region from 17 to 7 ka BP deduced from combined marine and terrestrial palynological records

U. KOTTHOFF[1], J. PROSS[2], U. MÜLLER[2], G. SCHMIEDL[1] I. DORMOY[3], O. PEYRON[3], A. BORDON[3]

[1] Geological-Paleontological Institute, University of Hamburg, Bundesstraße 55, D-20146 Hamburg, Germany
[2] Institute of Geosciences, University of Frankfurt, Altenhöferallee 1, D-60438 Frankfurt, Germany
[3] Laboratoire de Chrono-Ecologie, UMR-CNRS 6565, University of Franche-Comté, 16 Route de Gray, F-25030 Besançon, France

The Lateglacial and the early Holocene are characterized by pronounced climate variability. The most prominent climate setbacks of these time intervals are the Younger Dryas (YD, ~12.7 to 11.7 ka BP) and the 8.2 ka event. There is still a lack of high-resolution vegetation and climate data to illustrate the impact of these setbacks on the eastern Mediterranean region, and to compare them with the glacial conditions preceding the Allerød-Bølling interstadial (~14.8 to 12.7 ka BP). We used a marine core from the Mount Athos Basin, northern Aegean Sea, and a terrestrial core from Tenaghi Philippon, NE Greece to carry out dinocyst- and pollen-based vegetation, oceanography and climate reconstructions. Pollen-based quantitative paleoclimatic reconstructions and dinocyst cold indicators suggest that low temperatures and precipitation prevailed in the

northern Aegean region until ~15.5 ka BP. Between ~15.5 and ~12.7 ka BP, temperatures were already comparable to Holocene levels, but low moisture availability appears to have controlled vegetation dynamics. The following Younger Dryas was almost as dry as and probably 3-5°C colder than the late Pleniglacial. A rapid temperature increase marks the onset of the Holocene. The early Holocene was punctuated by several short-term climate events. According to our data, the impact of these events was stronger in terrestrial ecosystems than in the marine realm. We propose that the most pronounced among these events (~11 ka BP) contributed to the delay of the Holocene reforestation in the Aegean region until ~10.4 kyr BP. From the late Pleniglacial until the early Holocene (~17 to ~9.5 ka BP), the relative abundances of deciduous tree pollen show a close correlation with Greenland ice core isotope records, indicating a teleconnection between the high and the lower latitudes. From ~9.5 to ~7 kyr BP, climate dynamics were more strongly affected by the monsoonally-influenced climate system of the lower latitudes, with the exception of the North-Atlantic-related 8.2 ka event. This event is strongly pronounced at Tenaghi Philippon, with winter temperatures declining by almost 4° C. In contrast, in the coastal areas of the Northern Aegean region, winter temperatures only dropped by ~1.5° C.

Pross, J., Kotthoff, U., Schmiedl, G., Müller, U.C., Peyron, O., Tzedakis, C., Christanis, K., Emeis, K.-C. (submitted): Massive perturbation in terrestrial ecosystems of the Eastern Mediterranean region associated with the 8.2 kyr climatic event. – Geology.

Dormoy, I., Peyron, O., Combourieu-Nebout, N., Goring, S., Kotthoff, U., Magny, M., Pross, J. (submitted): Terrestrial climate variability and seasonality changes in the Mediterranean region between 15,000 and 4,000 years B.P. deduced from marine pollen records. – Climate of the Past.

Kotthoff, U., Pross, J., Müller, U.C., Peyron, O., Schmiedl, G., Schulz, H., Bordon, A. (2008): Climate dynamics in the borderlands of the Aegean Sea during formation of Sapropel S1 deduced from a marine pollen record. – Quaternary Science Reviews 27, 832-845.

Kotthoff, U., Müller, U.C., Pross, J., van de Schootbrugge, B., Schmiedl, G., Schulz, H. (2008): Lateglacial and Holocene vegetation dynamics in the Aegean region: An integrated view based on pollen data from marine and terrestrial archives – The Holocene 18, 1019-1032.

Comparison of methods for the determination of total cell numbers in different sediments

G. KÖWEKER, C. HÖFT, A. SCHIPPERS

Federal Institute for Geosciences and Natural Resources (BGR), Hannover

The determination of total cell numbers is fundamental in microbial ecology and often builds the basis for further investigations. In recent years SYBR Green direct count (SGDC) has been proven to be superior to comparable methods using other cell stains (DAPI, Acridine Orange). The protocol from Weinbauer et al.(1998) is a common used instruction for SGDC of microorganisms in marine sediments which works well and solid for sediment samples bearing lots of cells. However, a detection limit of less than 10^6 cells in one mL sediment should not be undercut as the statistic uncertainness is getting too high and hardly any cell can be detected in the small volume used. To obtain more robust values even under this detection limit a lot of efforts were made to detach the cells from the sediment matrix. Many of the various methods tested turned out to be incapable or caused different problems depending on the sediment type used. Hence, the aim of this study was to check the efficiency of two different detachment protocols when employed to diverse sediments. Sediment samples from three different marine areas (Sumatra forearc basin, Benguela upwelling, Black Sea) and a terrestrial site (Chesapeake Bay, USA) were investigated using the standard (Weinbauer et al. 1998) and two detachement protocols (Lunau et al. 2005, Kallmeyer et al. 2008). The results were collected and compared to each other. The central step of the Kallmeyer protocol is a tenside-based detachment procedure followed by a density gradient centrifugation of the sample. It has already been successfully tested on sediments with very low cell densities. In contrast, the Lunau protocol uses an intensive ultrasonic treatment combined with warm methanol to release the cells from the sediment matrix. It has als been used before with Wadden Sea sediments. The results of this study clearly showed that the efficiency of the detachement process differed very strongly with the sediments used. Besides, in most cases the cell numbers obtained by the detachement protocols were much lower than those counted with the standard protocol. Obviously, the overall cell number and some sedimentological parameters that have not been further identified like the grain size, the density and the exact chemical composition of the sediment seem to determine the detachement efficiency to a high degree. It can also be suggested that the size as well the type and the vital state of the microorganisms play an important role in this. Especially in the sediment layers near the surface where high cell numbers prevailed, the loss of cells was high using the detachement protocols, while in the deeper layers the cell numbers converged. The Weinbauer protocol delivered the most reliable and comparable results showing a clear depth trend with decraesing cell numbers. The Lunau protocol overlooked many cells since in many samples the cell numbers were up to two orders of magnitude lower. The cell numbers obtained by the Kallmeyer protocol continiously confirmed the depth trend of the classic SGDC method. In sediment depths of more than one meter downwards the values often almost agreeded since the overall numbers were much lower in deeper sediment layers than at the sediment surface. Summed up, the detachement protocols as a single data basis is not advisable because too many unknown factors make these methods to unsteady. But nevertheless, detachement protocols like the one from Kallmeyer can be a reasonable addition to the standard SGDC method especially at low cell numbers. The clear advantage of this method is that one can work with bigger sample volumes and the statistic aberration of the cell counts is therefore lower. Thus, especially in deeper layers with less cells one can achieve robust and reliable results.

Kallmeyer, J., D.C. Smith, A.J. Spivack, and S. D'Hondt. 2008. New cell extraction procedure applied to deep subsurface sediments. Limnol. Oceanogr. Methods 6: 236–245.

Lunau, M., A. Lemke, K. Walther., W. Martens-Habbena, and M. Simon. 2005. An improved method for counting bacteria from sediments and turbid environments by epifluorescence microscopy. Environ. Microbiol. 7: 961-968.
Weinbauer, M.G., C. Beckmann, and M.G. Höfle. 1998. Utility of green fluorescent nucleic acid dyes and aluminum oxide membrane filters for rapid epifluorescence enumeration of soil and sediment bacteria. Appl. Environ. Microbiol. 64: 5000-5003.

Antarctic geological drilling ANDRILL results and plans

G. KUHN[1], F. NIESSEN[1]

[1]Alfred-Wegener-Institut für Polar- und Meeresforschung, Am Alten Hafen 26, 27568 Bremerhaven, Gerhard.Kuhn@awi.de

The ANtarctic geological DRILLing Program (ANDRILL) is an international collaboration between Germany, Italy, New Zealand, the United Kingdom and the United States. By drilling and pre-investigating a series of targeted sites ANDRILL recovers stratigraphic records from the Antarctic margin that are vital to address scientific questions regarding the past and future behavior of Antarctic ice sheets, the evolution of tectonic basins and related sedimentation, and in general the geological history of this continent. Two projects were undertaken during the International Polar Year. The McMurdo Ice Shelf (MIS) project was drilled 2006/07 and the Southern McMurdo Sound (SMS) project end of 2007.

With 1285 meters below the sea floor and a rock recovery of more than 98% the MIS drilling was record-breaking in Antarctica. The analyses of the core are exciting as well. Diatomites and diamictites indicate substancial glacial/interglacial climatic variation over the past ~14 million years, revealing the history and stability of the Ross Ice Shelf and the hereto related West Antarctic Ice Sheet. Volcanic components together with other parameters provide a relyable age control of the sequence.

The SMS project drilled 1138 meters of rock core with identical good recovery. The Mid-Miocene Climate Optimum (15 to 18 million years ago) a period much warmer than today is recorded with high sedimentation rates of 20 cm/k.y. between 200 and 800 mbsf. Sedimentary and geochemical cycles reveal changes in sedimentation processes related to past climate and sea level history.

A proposal for the most mature next ANDRILL project is under evaluation. Drilling from the edge of the Ross Ice Shelf on the Coulman High is planned to target earliest Miocene and older sections in the western Ross Sea. An ESF pre proposal for an EUROANDRILL project got positive reviews and a full proposal is written now. International collaboration is desired to develope and implement these campaigns.

Absolute healing of pyroclasts during rheomorphic welding of ignimbrites in the Snake River Plain, USA

YAN LAVALLÉE, DONALD B. DINGWELL, KAI-UWE HESS, GRAHAM ANDREWS, KELLY J. RUSSELL

The architectural description of ignimbrites often shows evidence for post-deposition development of a rheomorphic, ductile shear zone - a feature which may strongly affect the progression of pyroclastic flows; especially in large volcanic fields. Rheological experiments were performed on a welded rheomorphic unit from the Grey's Landing ignimbrite in the Snake River Plain to characterize its behaviour and assess the degree of welding.

The investigated sample contains 5 vol.% open pores and is made of approximately 5 vol.% crystals bathing in a relatively degassed, peraluminous glass containing 79 wt.% SiO_2. Pre-eruptive temperature determination from geothermometry on pyroxenes yielded values at around 900-1050 °C. Dilatometric measurements suggest a calorimetric glass transition temperature during deposition of approximately 845 °C and a H_2O content of approximately 0.04 wt.%. Repeated series of heating and cooling using an advanced dilatometric technique shows an increase of the glass transition temperature to 880 °C, which is in accordance with degassing of approximately 0.02 wt.% H_2O. Complementary investigation using a uniaxial press revealed an absence of strain rate dependence of the viscosity ($10^{10.78}$ Pa·s) at a temperature of 900 °C and at strain rates up to 2.5 x 10^{-4} s^{-1}. Under similar conditions, a fully degassed lava with an equivalent composition would yield a comparable viscosity of $10^{10.89}$ Pa·s.

Our findings may help constrain the flare up of the Grey's Landing ignimbrite. The presence of small amounts of water in the glass and the narrow temperature window between the residence in the reservoir and the transition to a glass (which would have mechanically locked this unit in place) in the flow indicates a high discharge rate and rapid post-fragmentation deposition, mass agglutination and welding. Moreover, the Newtonian character of this welded unit suggests that healing of the pyroclastic flow was absolute (that is, no thixotropic effects from the pores remain), and thus that the term 'lava-like' is adequate to rheologically describe rheomorphic pyroclastic flows.

Synthesis and Analysis of Antarctic Neogene Radiolaria

D. LAZARUS[1], J. RENAUDIE[1]

[1]Museum f. Naturkunde, Invalidenstrasse 43, 10115 Berlin, Germany. david.lazarus@rz.hu-berlin.de; johan.renaudie@museum.hu-berlin.de

In recent years large micropaleontology databases such as Neptune and new quantitative analysis methods based on these large datasets offer the promise of much higher resolution age-dating of deep-sea sediments and new insights into macroevolutionary mechanisms in pelagic organisms. Despite these developments our ability to effectively use the deep-sea microfossil record is still limited. Particularly for less intensively studied groups such as radiolaria, our knowledge of their taxonomy, biogeography and stratigraphic distribution is very incomplete. The large majority of known species of Neogene Antarctic deep-sea radiolarian fossils for example have been reported from one, or at most a few sites, despite their probable widespread presence in numerous sections possessing coeval Antarctic sediments. In most samples only a small fraction of the observable diversity has been recorded or analyzed. Recorded diversities are thus too low, and too incompletely recorded, to allow use of modern stratigraphic and evolutionary analytic tools. We have therefore recently begun a new study of these Antarctic Neogene radiolarian faunas with the goals of 1) building a much more complete picture of their taxonomy and stratigraphy; and 2) analyzing the new data set using modern quantitative methods to improve Antarctic Neogene geochronology, and to understand patterns of evolutionary change. Currently, in the first such review since the beginning of deep-sea drilling nearly 40 years ago, we are synthesizing the scattered taxonomic literature for these faunas and creating digital catalog records for each species at the global community website www.radiolaria.org. In a second phase we will collect detailed stratigraphic occurrence information for the majority of the ca 500 radiolarian species present in the Neogene Antarctic fossil record. Stratigraphic analysis will use CONOP and other quantitative biostratigraphic methods, and evolutionary analysis the Paleobiology Database and other software tools.

Quaternary Tertiary Tropics, Colônia Sediment Archive Project (QUE COISA)

M.-P. LEDRU[1], W.U. REIMOLD[2], I. BENTALEB[3], A. CROSTA[4], G. RAMSTEIN[5], C. RICCOMINI[6]

[1]Institut des Sciences de l'Evolution de Montpellier, Institut de Recherche pour le Développement, France (marie-pierre.ledru@ird.fr)
[2]Museum für Naturkunde – Leibniz-Institut at Humboldt University Berlin, Invalidenstrasse 43, 10115 Berlin, Germany (uwe.reimold@museum.hu-berlin.de)
[3]Université de Montpellier 2, France [4]University of Campinas, Brazil [5]CNRS, France [6]University of São Paulo, Brazil

Long continuous climate records provide unique knowledge on Earth's evolution. The American continents are characterized by continuous land surface from north to south, which allows to study interhemispheric linkage and the role of the tropical belt in global climate dynamics. However, such long-term records are still lacking in the Southern Tropics. Consequently, our global and regional climate reconstructions from orbital to millenial scales remain incomplete. The Colônia structure is located in southern Brazil, close to the city of São Paulo (23°52'S 46°42'20''W). It contains a bog deposited in a hilly circular structure of 3.6 km diameter with an outer rim elevated by up to 125 m. The structure is formed in Proterozoic crystalline rocks. New seismic surveys demonstrate that ~400 m of organic-rich, fine-grained lacustrine sediments fill the basin that could account for 2.5 Ma of sedimentation history. And, as it is located within the Atlantic rainforest domain, a biodiversity hotspot, this site has become a reference site for tropical paleoenvironmental and paleoclimatic research because the upper 8 m of sediments record 130 ka of paleoenvironmental history of the area. For instance, the pollen record shows specific responses of the tropical rainforest to global climatic changes in terms of moisture and biodiversity during the last glacial.

The drilling of Colônia will allow to study for the first time in the wet Tropics the evolution of biodiversity and climate through several glacial/interglacial cycles, which is unique to the tropical belt within the southern hemisphere. The location will allow to complete a transect of ICDP long-term records and shed new light on interhemispheric climate linkages and the role of the Tropics in the global climate dynamics. In addition, this record will contribute to the knowledge of the range of responses to climate changes that the tropical forest biodiversity is capable of. Our second objective is to study the formation and evolution of a basin/crater within a moist and weathered area. Although, there is a growing body of evidence that the basin is the product of a meteorite impact, up to now no obvious evidence for an impact has been discovered. An application for a planning workshop in 2009 has been submitted to ICDP.

Seismic pre-site survey for the SCOPSCO ICDP-campaign in ancient Lake Ohrid

K. LINDHORST[1], S. KRASTEL-GUDEGAST[1], T. SCHWENK[2], K. REICHERTER[3], G. DAUT[4], M. WESSELS[5], B. WAGNER[6]

[1] Leibniz-Institut für Meereswissenschaften (IFM-GEOMAR), Kiel, Germany, klindhorst@ifm-geomar.de
[2] Fachbereich Geowissenschaften, Universität Bremen, Germany
[3] Neotektonik und Georisiken, Universität Aachen, Germany
[4] Institut für Geographie, Friedrich Schiller Universität Jena, Germany
[5] Institut für Seenforschung, Langenargen, Germany
[6] Institute für Geologie und Mineralogie, Universität Köln, Germany

Lake Ohrid is a transboundary lake with approximately two thirds of its surface area belonging to the Former Yugoslav Republic of Macedonia and about one third belonging to the Republic of Albania. Lake Ohrid is considered to be the oldest, continuously existing lake in Europe, though the age and the origin are not completely unraveled to date. With more than 210 endemic species described, the lake is a unique aquatic ecosystem and a hotspot of biodiversity that is of worldwide importance.

An international group of scientists has recently submitted a full drilling proposal entitled SCOPSCO (Scientific Collaboration On Past Speciation Conditions in Lake Ohrid) to ICDP in order (i) to obtain more precise information about the age and origin of the lake, (ii) to unravel the seismotectonic history of the lake area including effects of major earthquakes and associated mass wasting events, (iii) to obtain a continuous record containing information on volcanic activities and climate changes in the central northern Mediterranean region, and (iv) to better understand the impact of major geological/environmental events on general evolutionary patterns and shaping an extraordinary degree of endemic biodiversity as a matter of global significance.

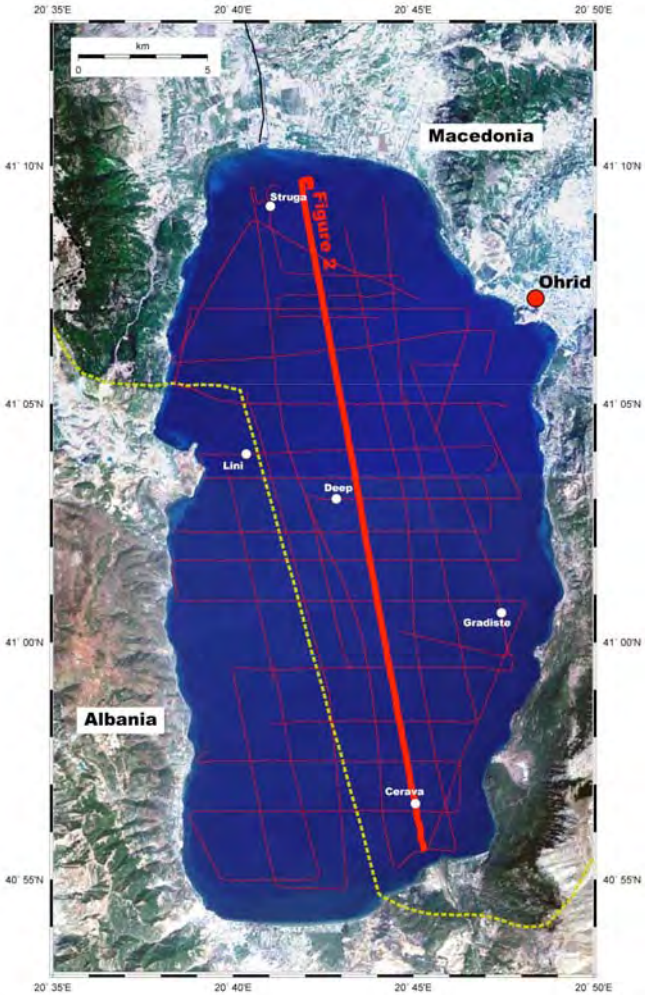

Figure 1: Map of ancient Lake Ohrid (Macedonia and Albania) with seismic lines from airgun surveys carried out in 2007 and 2008. Marked are the five primary drilling locations that have been proposed in January 2009 to ICDP. The bold line shows the location of the seismic profiles Figure 2.

Acoustic pre-site surveys started with a first shallow seismic campaign using a sediment echo sounder. Due to the limited penetration of the sediment echosounder (<50 m), Subsequently a first multichannel seismic pilot study followed in 2007 with a Mini-GI-Gun (0.25l) as seismic source and a 100m-long 16-channel streamer. To improve the coverage and resolution of seismic profiles significantly, a second multichannel seismic survey using a Mini-GI-Gun with reduced volume (0.1l) and the same 16 channel streamer as used in the previous year was carried out in June 2008. Now a profound grid of seismic lines (47 profiles, total length of 650 km) is available (Figure 1).

From the shallow seismic dataset a bathymetry grid was obtained showing the geometry of the lake resembles a bathtub shape with a large, deep (250m) central basin, steeply dipping slopes on the east and western sides, and a broad, shallow area in the northern part of the lake near the outflow, the Crni Drim River.

Seismic profiles show that the lake can be divided into slope areas and a large central basin (Figure 2). The slope areas are characterized by a dense net of faults, clinoforms, and slide deposits. The major faults are the eastern and western graben fault but numerous additional faults, especially in the northern part of Lake Ohrid, seem to be active, as we can trace them from the basement up to the lake floor. Clinoforms that are mainly found in the southern part of the lake, the main water supply area, indicate major lake level fluctuations. Additionally, slides are widespread and were mainly mapped based on the high resolution sediment echosounder data. In contrast the central basin shows widespread areas with a thick undisturbed sedimentary succession. No indications for a dry lake are found in this part of the lake, hence offering the possibility to recover long, continuous archives for the entire lifetime of Lake Ohrid.

Five primary drill sites were chosen based on the seismic data. First of all, an almost 700 m long core in the central basin (site: DEEP), at a water depth of 250 m, will provide substantial information to the age and origin of the lake, to the environmental history, to tephra deposition, and subsequently forms the basis to link evolutionary changes with geological events. The seismic line shows thick undisturbed sediments (up to 1.2 s TWT) filling up the entire central basin. Due to the fact that only one profile crosses the site, we have mapped the basement on all seismic lines crossing nearby to come up with a sediment isopach grid demonstrating that the proposed site is most likely located at the point with the thickest sediment succession.

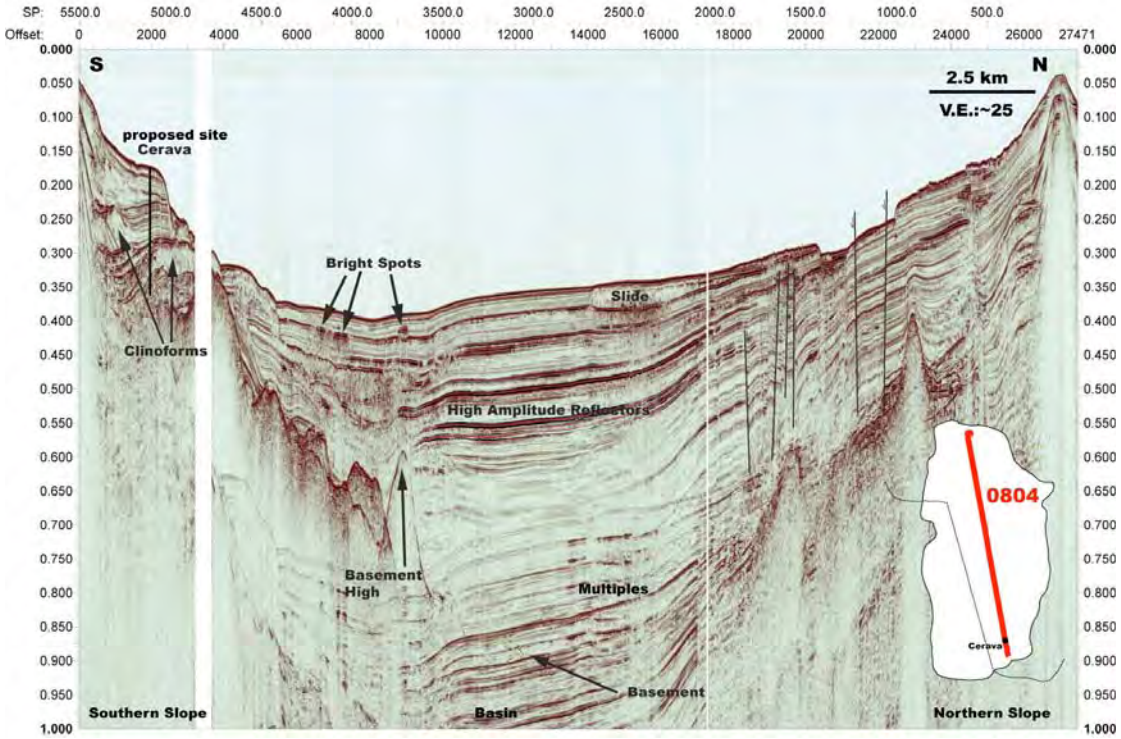

Figure 2: Stacked profile 0808 (N-S) showing the structure of ancient Lake Ohrid. In the south one proposed drill site The Cerava drilled site (see text for details) is located on this line.

The second proposed site (Cerava, see Figure 2) is located on a terrace close to the feeder spring area at Sveti Naum and Cerava River, the main tributary to Lake Ohrid. The seismic data show foresets overlain by thick package of well stratified sediments. Several of such foresets have been observed in the southern part of the lake suggesting that the lake underwent significant lake level fluctuations. Drilling will allow dating these foresets.

Two drill sites have been proposed that are located at active lake-bounding normal faults, one of them on the eastern part of the lake (Gradiste) and another on the Albanian side (Lini). Tectonic activity of Lake Ohrid can be seen in sediments that have undergone post depositional tilting. Interestingly, the individual mass wasting bodies are rotated antithetically by increasing angles downsection, which is interpreted as pulsed tectonic activity. On the Albanian side the location was depicted at an active half graben fault. Both sides can be compared to each other in terms of causes for mass wasting. Whereas at the eastern part an earthquake is more likely to have triggered a slide, on the western side yields two mass

wasting deposits of mainly undeformed sequences that are rotated antithetically towards the fault. These two vary significantly in thickness and extent, pointing to different magnitudes of seismogenic shocks.

Finally, one site was chosen in the northern part of Lake Ohrid close to the outflow, the Crni Drim River (Struga). Besides extensively normal faulting that can be observed on seismic lines crossing that region, buried foresets are one of the main drilling targets. The foresets indicate major sediment input from the north, with is in contrast to the present situation, hence suggesting that the hydrological regime changed significantly over time.

Lake Van Drilling Project 'PaleoVan' International Continental Scientific Drilling Program (ICDP): Upcoming Deep Drilling Campaign and Scientific Goals

T. LITT[1], S. KRASTEL[2], M. STURM[3] ,R. KIPFER[3], S. ÖRCEN[4], N. CAGATAY[5]

[1]University of Bonn, Germany, t.litt@uni-bonn.de
[2]IFM-GEOMAR Kiel, Germany
[3]Swiss Federal Institute of Aquatic Science and Technology, Switzerland
[4]University of Yüzüncü Yil, Van, Turkey
[5]Istanbul Technical University, Turkey

Lake Van on a high plateau in eastern Anatolia (Turkey) extends for 130 km WSW-ENE. It is the fourth largest terminal lake in the world by volume (volume 607 km^3, area 3570 km^2, maximum depth 460 m). It is situated in a collision zone where the Afro/Arabian Plate from the south meets the Eurasian Plate from the north and east. The lake fills a tectonic depression that is tectonically highly active and is characterized by voluminuous recent and active volcanism, earthquakes and hydrothermal activity. Evaporation, hydrothermal activity and chemical weathering of volcanic rocks are responsible for the extreme alkalinity of the lake water (alkalinity 155 $meql^{-1}$, pH 9.81, salinity 21.4‰). In fact, Lake Van is the largest soda-water lake in the world. Two active volcanoes rise in the immediate vicinity of the lake (1674 m a.s.l.): Nemrut Dag (3050 m a.s.l.) and Süphan Dag (3800 m a.s.l.).

The annually laminated sediments of Lake Van for at least the last 14 kyr (Wick et al. 2003) represent an exceptional high-resolution paleoclimate record. The lake is situated at a sensitive climate region of north-eastern Anatolia in a key climatic position, at the crossroad of the atmospheric south-western jet stream and the northern branch of the subtropical high pressure belt. It thus represents a first order continental climate archive between the Black Sea, the Arabian Sea and the Red Sea. The combination of this crucial climatic position with the varved sediment lithology makes Lake Van an outstanding candidate to disentangle processes and developments of former evolution of climate and environment. Size and depth of the lake suggest that the subsurface represents a continuous climate archive spanning multiple glacial-interglacial cycles. Recovering this long sedimentary record within the PaleoVan project will thus provide climatic and environmental data in eastern Anatolia and the Near East region of unprecedented duration and quality. Thus Lake Van is not only a key site for ICDP, but also for other international geoscience programs such as PAGES - Past Global Changes. PAGES, a core project of the International Geosphere-Biosphere Program, supports scientific foci related to past climate that perfectly match with the main goals of the proposed Lake Van Drilling Project 'PaleoVan' within ICDP.

The DFG (German Research Foundation) priority program ICDP funded a geophysical survey in combination with a coring campaign (financial support to T. Litt and S. Krastel). The seismic pre-site survey at Lake Van was carried out from June 1 to June 15, 2004. In total we collected 50 profiles with a length of ~850 km (Fig. 1) by means of a high-resolution multi channel seismic system and a GeoChirp system. Based on the seismic results we cored 10 different locations (Fig. 1) in water depths up to 420m (July 24 to August 10, 2004). Initially, we used a specially designed deep-water piston corer (UWITEC, Mondsee, Austria) to obtain cores longer than those obtained by the Kullenberg system. Our operation in water depths around 400m was a milestone in testing this new coring system for deep lakes such as Lake Van. Subsequently, a Kullenberg piston corer was used to recover a multiple set of cores along the seismic lines.

Multidisciplinary scientific work on the new cores including magnetic susceptibility, physical properties, stable isotopes, XRF scans, pollen and spores, composition of tephra layers has been carried out in the meantime (ongoing DFG projects). A major result is the clear evidence for a continuous sediment record back into the Last Glacial Maximum (LGM). The newly acquired seismic and core results thus show good evidence for a continuous sediment record in this part of Lake Van free of major gaps and hiatuses (Litt et al. 2009, accepted).

Based on a pre-proposal submitted to ICDP in 2005 and highly ranked by the ICDP Science Advisory Group (SAG), an international workshop took place in Van, Turkey, June 6-10, 2006 under the auspices of the ICDP (35 participants from 12 countries). Specific goals of the workshop were the discussion of the state of the art and the identification of an international group of scientists from different research fields who will become actively involved in the project and in the planning of drilling strategies using GLAD800 equipment (Litt et al. 2007).

A full proposal for an ICDP co-funded Lake Van Drilling Project "PaleoVan" in the Lake Van in eastern Anatolia was submitted by Litt, Krastel, Sturm, Kipfer, Örcen and Cagatay in 2007. We convinced the ICDP Executive Committee (EC) that our drilling project will address important scientific issues of global relevance. The EC emphasized that our full proposal is mature as it stands not only with respect to the science but also in terms of the planning and management status (letter by the EC Chairman from August 20, 2007). ICDP has decided to provide 750.000 USD for the PaleoVan project. This approval is intended to allow us to raise matching funds from other agencies. We were asked to plan for drilling in summer 2009. The exact schedule is under discussion.

Below we summarize the motivation and scientific goals of the drilling project as well as the proposed upcoming work:

Long continental paleoclimate record in a sensitive semiarid region

The controversial discussion of the nature of present and future global warming has shown that it is crucial to increase our knowledge of past climate change to better understand the dynamics and amplitudes of the global climate system in space and time. In continental regions, this information can be obtained from lacustrine sediments, where biotic and abiotic parameters (i.e. pollen and oxygen isotopes) provide proxy climate data. In this respect, Lake Van promises to be an excellent palaeoclimate archive because it has the potential to yield long continental records covering several glacial-interglacial cycles from annually-laminated sediments. This makes the lake a key site for the investigation of the Quaternary climate evolution in the Near East.

Dynamics of lake level fluctuations and hydrogeological development

The reconstruction of a long and continuous lake level curve of this closed basin is one of the major keys to reconstruct timing and amplitudes of past climate change as expressed in changes of P/E (precipitation/evaporation ratio). Previous studies on paleoshorelines and basinal sediments have shown that lake level fluctuated in the past between +90 m and -250 m (Lemcke & Sturm 1997). No erosional unconformity could be detected on seismic data below 250 m water depth, limiting the maximum lake level drop to that depth. These lake level changes are sensitively recorded in the lithological and geochemical composition of Lake Van sediments. In particular, the oxygen isotopic composition of the bulk carbonate, consisting almost purely of authigenic aragonite, provides a powerful proxy to track past lake level fluctuation. Such a dominance of authigenic carbonate precipitation is also expected in the older sedimentary succession, so that isotope studies will be the definitive tool in reconstructing past P/E.

Organic matter content and composition: proxies for macro- and microorganisms (biomarkers)

In this part we focus on three issues: (1) estimate of paleo pCO_2 calculated from paleoproductivity, (2) allochthonous/autochthonous production, and (3) microbial vs. algal productivity/nutrient utilization. Lake Van with its location between the Indian and Atlantic ocean and its exceptionally varved sediments is the hot spot to address all three questions. One of the main questions concerns the kind of material represented by the high organic matter (OM) content (12 %, found in a formerly taken 15.000 year old sediment core). Three different sources have to be considered: (1) phytoplankton productivity, (2) microbial productivity, and (3) terrestrial organic matter input. A first indication on the composition of the organic material (needed for pCO_2) can be revealed by the organic carbon isotopic composition. Possible processes include differentiation between allochthonous OM transported by rivers during snow melt and autochthonous OM (primary prodution) as well as a distinction between C3 and C4 plants, a prerequisite for paleo pCO_2 reconstructions in the atmosphere. Furthermore, the nitrogen isotopic composition of OM will allow us to determine the variability in nutrient utilization over time including nitrogen fixation during times of strong nutrient depletion. This will help to estimate productivity and the amount of carbon stored in the lake during glacial/interglacial times.

Noble gas concentration in pore water of the lake sediment

The equilibrium concentrations of (atmospheric) noble gases are given by the physical conditions prevailing gas/water partitioning during atmospheric gas exchange, i.e. the altitude of the lake surface and temperature and salinity of the exchanging water. The concentrations of chemically inert noble gases of the deep water in lakes are incorporated unchanged into the pore water of the growing lacustrine sediment column (Brennwald et al. 2003). New experimental tools allow the noble gas concentrations in pore waters of lacustrine sediments to be determined routinely. These new methods can be used to reconstruct the physical conditions of the overlying water body, e.g. water temperature and salinity, and lake levels. We intend to determine the concentrations of atmospheric noble gases in the pore waters of the long IDCP cores to geochemically reconstruct - for the first time - lake levels and salinity on time scales 1 - 100 kyr.

Temporal, spatial and compositional evolution of volcanism based on tephra layers in the sediments and on land

Tephra layers are the most suitable material to correlate geologically young terrestrial, lacustrine and marine records because they deposit instantaneously. Tephra layers, being composed mainly of highly unstable glass, are prone to fast reactions with pore solutions. They are significant sources of elements whose release into the water can supply critical elements to trigger and maintain biological activities such as terrestrial vegetation and diatom blooms. Tephra layers in the deep drill cores of Lake Van sediments will be studied structurally, texturally and compositionally for correlation between drill sites and with volcanic deposits on land. Analysis of equivalent deposits on the historically active caldera volcano Nemrut, probably the major supplier of tephra, will allow reconstructing larger volcanic events (Plinian fallout, pyroclastic flows and flank collapses), magma evolution and environmental impacts such as tsunamis. Time series of the frequency of tephra layers of various origins in the sediments will allow to reconstruct recurrence rates of volcanism in the area and thus contribute to regional hazard and risk assessments. A reconstruction of depositional fans of distinct tephra layers in the lake sediments and on land will provide important information on paleowind directions over the past 500 Ka. A synthesis of the dynamic evolution of the volcanism based on core and land deposits will help solve the problem of whether the deep subcircular Tatvan basin (40 km diameter) is purely of tectonic and/or volcanic origin (caldera).

Paleoseismic and earthquake activities

Lake sediments are sensitive recorders of past earthquake activity. Many paleoseismic studies have been performed on outcrops of lake sediments. New concepts and experiments on seismically-induced microdeformation of finely laminated varved sediments provide the basis for the successful use of lake sediment cores to establish chronologies of past earthquake activity. The Lake Van area is strongly affected by earthquakes that represent the major natural hazard in the region. No long paleoseismic record, however, exists to date that could document recurrence rates of strong earthquakes and past seismic activities for this tectonically active area. The newly collected cores from 2004 show strong evidence of earthquake-triggered

microfaults, which can be interpreted as seismites (Litt et al. 2008, submitted). Similar features, such as liquefaction structures (load casts, pseudonodules, sand dikes, mushroom structures), folded layers and 'mixed layers' are also expected to be found in the deeper sections.

Proposed drilling campaign

The GLAD800 drill rig, combined with the RV Kerry Kelts platform operated by DOSECC, provides a suitable drilling technology to drill and recover the sedimentary succession of Lake Van. We propose to drill five sites in water depths between 95 and 375 m starting in the northwestern area of the lake and moving in the course of the campaign towards the southeast. The drilling platform can be anchored at all sites (approved by DOSECC) eliminating the need for dynamic positioning. We propose to drill five primary sites (Fig. 1) based on the high-resolution seismic and coring data collected in 2004. The 'Ahlat Ridge'-Site (AR) is the most important site. It is the deepest site (water depth ~375 m) and we plan to recover a complete sedimentary section for paleoclimatic investigations. The 'Northern Basin' Site (NB) is located in a small basin close to the northern shore of Lake Van. The proximity to the Quaternary volcanoes will allow studies of major volcanic eruptions and associated volcanogenic hazards. Two sites in different water depths of the Erek Fan (LL-1 and LL-2) are planned to analyze lake level fluctuations and the evolution of Lake Van. Finally one site is proposed to examine the origin of widespread extrusions and intrusions (EX), which are important for the tectonic setting of the lake.

Brennwald, M.S., Hofer, M., Peeters, F., Aeschbach-Hertig, W., Strassmann, K., Kipfer, R., & Imboden, D.M. (2003): Analysis of dissolved noble gases in the pore water of lacustrine sediments. Limmnol. Oceanogr.: Methods, 1: 51-62.

Lemcke, G. & Sturm, M. (1997): $\delta^{18}O$ and trace element measurements as proxy for the reconstruction of climate changes at Lake Van (Turkey): preliminary results. NATO ASI Series, 149: 653-678.

Litt, T., Krastel, S., Örcen, S., Karabiyikoglu, M., 2007. Lake Van Drilling Project, Long Continental Record, Turkey. Scientific Drilling 4, 40-41.

Litt, T., Krastel, S., Sturm, M., Kipfer, R., Örcen, S., Heumann, G., Franz, S.O., Ülgen, U.B., Niessen, F., (2009). Lake Van Drilling Project "PALEOVAN", International Continental Scientific Drilling Program (ICDP): Results of a recent pre-site survey and perspectives. Quaternary Science Rewies (accepted).

Wick, L., Lemcke, G. & Sturm, M. (2003): Evidence of Lateglacial and Holocene climatic change and human impact in eastern Anatolia: high resolution pollen, charcoal, isotopic and geochemical records from the laminated sediments of Lake Van, Turkey. The Holocene, 13: 665–675.

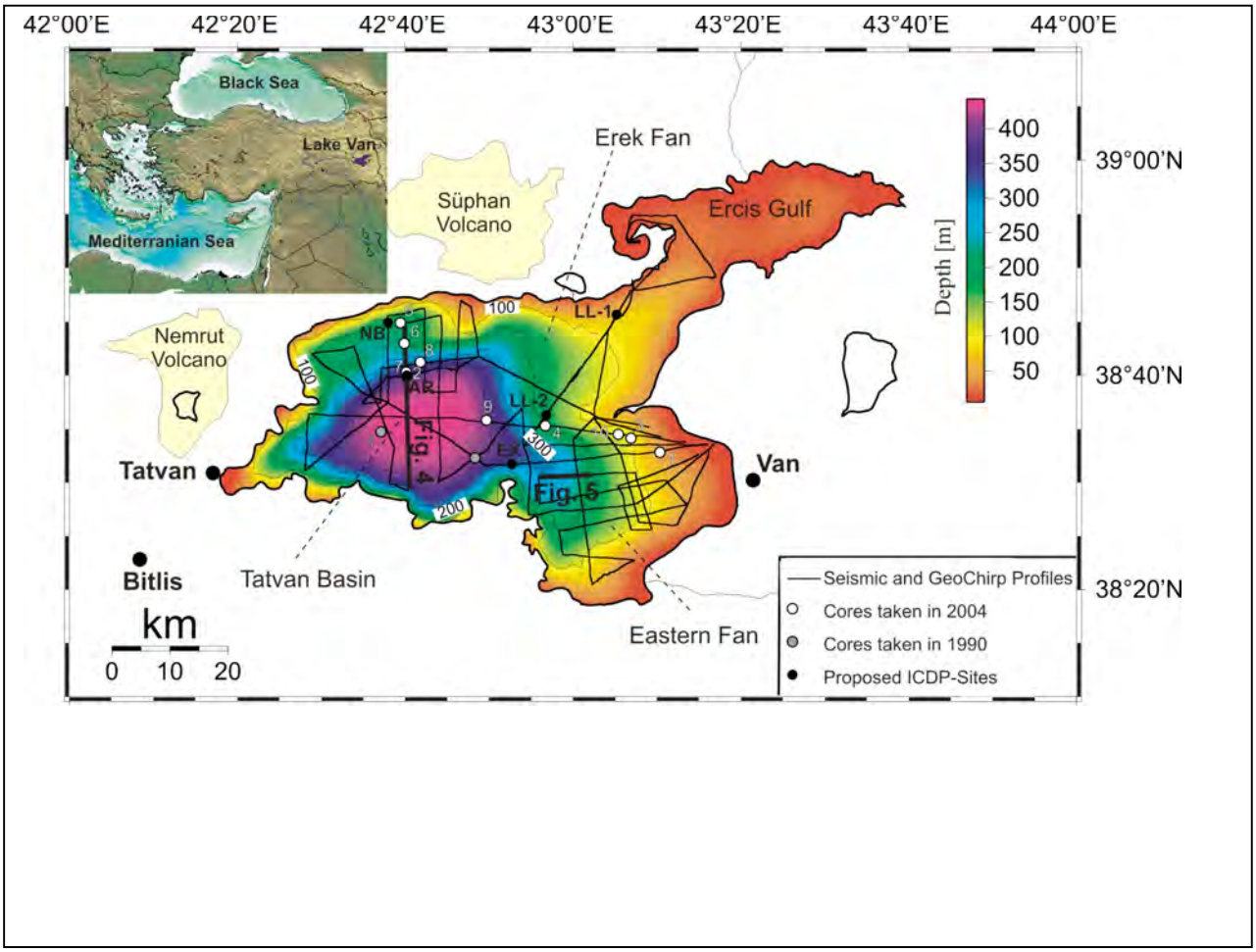

DIC and DOM (dissolved inorganic carbon and dissolved organic matter) in deep fluids. Preliminary results from the KTB-VB site

M. LODEMANN[1], H. ERLENKEUSER[2], M. WOLF[3], O. STÜCKRAD[1], P.M. GROOTES[2], P. SCHMITT-KOPPLIN[4], J. SCHWARZBAUER[5], N. HERTKORN[4], S.A. HUBER[6]

[1]Geowissenschaftliches Zentrum, Universität Göttingen, Goldschmidtstr. 3, D-37077 Göttingen
[2]Leibniz-Labor für Altersbestimmung und Isotopenforschung, Max-Eyth-Str. 11, D-24118 Kiel
[3]Institut für Grundwasserökologie, Helmholtz Zentrum München, Ingolstädter Landstr. 1, D-85764 Neuherberg
[4]Institut für Ökologische Chemie, Helmholtz Zentrum München, Ingolstädter Landstr. 1, D-85764 Neuherberg
[5]Institut für Geologie und Geochemie des Erdöls und der Kohle, RWTH Aachen, Lochnerstr. 4-20, D-52056 Aachen
[6]DOC-Labor Dr. Huber, Eisenbahnstr. 6, D-76229 Karlsruhe

Within the DFG project "Subsurface production of radioisotopes during the pumping test 2002-2003 in the KTB-VB" (ref. HA 1166/13-2), previous studies (Lodemann et al., 1998) were substantiated. ^{14}C analyses on DIC were performed continuously (Erlenkeuser et al., 2005) by AMS (Nadeau et al., 1997), followed by a first ^{14}C analysis on TOC (total organic carbon) in the deep fluids, analyses of compounds of the substance groups of TOC and DOC (dissolved organic carbon) and its molecular formulae and structures.

The 4000 m deep KTB pilot hole (KTB-VB) was cased down to a depth of 3850 m after drilling in 1989. Basement groundwaters in general contain DOC of around 0.5 mg/L (Thurman, 1996). At the end of the former pumping test in 1991 the DOC concentration of still 5.4 mg/L was suggested to be linked to possible residual contamination from the drilling mud additive Terradrill 451®, injected in the very last stage of the drilling activities into the borehole (Lodemann et al., 1998). During the pump test 2002-2003 DOC decreased rapidly from >50 mg/L at the very beginning to <10 mg/L after a couple of days.

Terradrill 451®, an organic ester based on rape oil, was designed by Henkel KG to be thermally stable up to 200 °C. Fatty acid methylester (FAME) related to Terradrill 451® was detected during the pump test 2002-2003 but in the range of only 0.01 to 0.04 $x10^{-6}$ mg/L (Stückrad, 2005), much too low to contribute essentially to the DOC content of KTB fluids. Terradrill 451 degrades to CH_4 and CO_2 through microorganisms (bacteria) or under appropriate conditions by hydrolysis. Short-chain fatty acids, which should have been produced if decomposition of Terradrill took place, were not found (Stückrad, 2005). Moreover, CH_4 as well as C_2H_6 is free of ^{14}C (Erlenkeuser et al, 2005). The high DOC content cannot be related to contamination with freshwater (residual layer above the pump, from previous hydraulic tests) or admixtures of (modern) groundwater during the pump test either. During the pump test delivered fluids were sampled for humic substances (HS) and immediately transported to the Helmholtz Zentrum München (formerly: GSF Research Center for Environmental and Health), Institute of Groundwater Ecology for analysis. No HS were detectable.

As DIC concentrations were less than 2 mg/L special caution and accuracy were required with respect to sampling and preparation techniques avoiding any contamination. Extraction of DIC as CO_2 for ^{14}C (AMS) and ^{13}C (IRMS) measurements was performed at the Helmholtz Zentrum München, Institute for Groundwater Ecology for samples of the first eight (of twelve) months. $^{13}C/^{12}C$ measured by Helmholtz-MS and Leibniz-IRMS agree well but differ essentially from those of the AMS-targets (at Leibniz lab). The extracted gases comprise CO_2, ethane and traces of propane.

With the sample gas composition quantified by mass spectrometry, a close negative correlation of ^{14}C and the ethane/CO_2 ratio showed up and revealed C_2H_6 to participate in the CO_2 reduction and graphite formation of the AMS ^{14}C target. From the established extraction lines for CO_2 from DIC, the collected gas comprises a mix of both CO_2 and C_2H_6 (and C_3H_8), a consequence of the cryogenic techniques applied (-196 °C). ^{14}C of CO_2 was calculated under the assumption that C of all gas fractions (CO_2, C_2H_6 and C_3H_8) was captured quantitative into the AMS target, and taking the C_3H_8/C_2H_6 ratio from additional GC analyses on three extracted gas samples. While C_2H_6 does not affect the $^{13}C/^{12}C$ analysis of CO_2 in the IRMS, the isotopic interference of CO_2 and the trace component C_3H_8 is significant and must not be neglected. It was corrected for after calibration measurements on artificial propane-CO_2-mixtures. Corrected ^{13}C and ^{14}C data of these samples (July 2002 – November 2002) are in the range of about –14 to –16 o/oo PDB and 6.4 to 10.7 pmC, respectively. Five samples from May and June 2003 were extracted at the Leibniz lab using advanced techniques to yield a high-purity CO_2. ^{13}C and ^{14}C data from June 2003 are in the range of -11,5 to -12.7 o/oo PDB and 3.1 to 9.1 pmC, respectively.

From a 50 l steel keg sampled on June 19, 2003 for ^{14}C on DIC 1 L fluid was evaporated under dust and gas protection at the Leibniz lab for ^{14}C and ^{13}C analysis on TOC. The salt evaporate was combusted under excess O_2 flow conditions in a 500 °C section leading into a 850 °C segment for afterburning. Further steps were necessary to remove chlorine, chloride and sulphur compounds to finally result in a high-purity CO_2 for AMS and IRMS. In total 4.4 mg/kg C was calculated from the final CO_2 yield representing TOC (DOC plus POC, particulate OC). The absolute yield of the total procedure is not known. Very surprising and yet not understood was the ^{14}C-result of 10 pmC on this TOC sample the more so as the ^{14}C of DIC (0.8 mg/kg C; 9 pmC) is nearly on the same level. The corresponding $\delta^{13}C$ values of TOC und DIC are about –30 o/oo and –12 o/oo PDB, respectively.

A 1 L-glass bottle sampled on the same day was passed to the DOC-Labor Dr. Huber, Karlsruhe for analysing the substance groups of DOC. The sample was analyzed by LC-OCD (Liquid Chromatogram – Organic Carbon Detection, Huber & Frimmel, 1991) additionally coupled with UV absorption (254 nm) for detection of HS. By LC-OCD 5.7 mg TOC was

analyzed (c.f. 4.4 mg/L at the Leibniz lab by O_2 combustion) including 35 ppb POC. The latter is in agreement with data of Stückrad (2005) who found 10-40 ppb methylester (POC) related to Terradrill-HT.

The DOC content of 5.6 mg consists of 4.5 hydrophilic organic carbon (CDOC, chromatographical DOC) and 1.1 mg hydrophobic organic carbon (HOC). The HOC fraction (possibly hydrocarbons), participating nearly 20 % of DOC yet was not identified in more detail as it was done for CDOC.

Noticeably the DOC concentration of 5.6 mg/L at the end of the pumping test 2003 agrees very well with that one from the end of the pumping test in 1991 (5.4 mg/L) and hence poses the question if these "final" DOC contents of the KTB fluids in both pump tests may represent the natural organic "background" load of the KTB fluids.

The CDOC solely consists of low molecular weight (LMW, <350 g/mol) neutral substances (2.4 mg/L), and (aliphatic) acids (2.2 mg/L). As LMW neutral substances alcohols, aldehydes, or ketons are possible either to be present primary or generated by hydrolysis from biopolymers. However, the absence of high molecular weight compounds suggests that the original organic content was strongly altered during the diagenesis of the KTB formation fluids (probably at high and/or altering pT-conditions), and hence point to very "old" KTB fluids. Moreover, the high fraction of acids may indicate that the original TOC content could have been much higher from which a bulk then had been mineralized to CO_2 (under appropriate conditions).

Based on LC-OCD data another KTB fluid sample of the same sampling date (June 19, 2003) as well as two further samples from December 2002 and April 2003 were analyzed on GC-MS at the RWTH Aachen aiming on advanced compound analyses (Schwarzbauer & Heim, 2005) of the detected spectrum of LMW neutral substances and LMW acids. With respect to (theoretically) possible hydrolysis products of Terradrill 451, it was important as well to determine the pattern of fatty acids (aliphatic mono carbon -COOH acids).

Considering the fatty acid composition, in particular the fractions of C_{12} to C_{16} acids, taking into account the fraction of the unsaturated C_{18} acids, contamination from the ester additive Terradrill 451 could not be established. In the KTB fluid samples di- and tricarboxyl acids are dominant but also oxocarbon (ketocarbon, C=O) acids were detected as well as some minor yet unknown compounds. The short-chain, solely linear structures of the LMW acids and neutral substances point to a diagenesis of the KTB fluids under varying pT-conditions.

Finally, a further KTB sample from June 19, 2003 was recently passed to the Helmholtz Zentrum München, Institute of Ecological Chemistry for a first experimental test applying ultrahigh-resolution FTICR-MS (Fourier Transform Ion Cyclotron Resonance-Mass Spectrometry, 12 Tesla magnet). With FTICR-MS at strong magnetic fields yet unknown compounds can be determined as molecular formulae. FT-mass spectra provide the most convincing direct experimental evidence for the extraordinary molecular diversity of complex organic materials at present. The complementarity of NMR spectroscopy (Nuclear Magnetic Resonance), also available in the same research department, optimizes the identification of complex structures (Hertkorn et al., 2007, 2008, Einsiedl et al., 2007). NMR and mass spectral data together can reconstruct chemical structures by empirical and mathematical back-projection.

Highly salted KTB samples were intensively desalted using solid phase extraction (C18 phase). Although the KTB sample after the (first) preparation for FT-MS consisted of many salt-clusters (Cl, Fe based), many typical and systematic CHO and CHOS compounds (less N-containing) within a very aliphatic field (fatty acids, mono- and dicarboxylic long chain aliphatic acids) were evident thus confirming the GC-MS analyses. Relating to ^{14}C-analyses on DOC (and DIC) and the question of subsurface ^{14}C production it is of interest to point to nitrogen bearing compounds which were detected as well. The profiles point to natural organic matter (NOM) yet not found in the typical distribution patterns of surface- or groundwaters, hydrothermal and sedimentary waters or seawater.

Because of the very interesting data on DOM (DOC) of the KTB fluids, so far the first detailed analyses in deep (basement) fluids worldwide, our working group is going to submit another DFG proposal for further DOM (and DIC) studies on KTB fluids, surroundings of KTB (Eger rift) and on deep fluids from other ICDP/IODP drilling sites.

Einsiedl F., Hertkorn N., Wolf M., Frommberger M., Schmitt-Kopplin P., Koch B.P. (2007): Rapid biotic molecular transformation of fulvic acids in a karst aquifer. *Geochim. Cosmochim. Acta* 71, 5474-5482.

Erlenkeuser H., Lodemann M., Grootes P.M., Wolf M., Hansen B.T. (2005): ^{14}C in gases from the KTB pilot hole pump test 2002/2003. *Joint Colloquium ICDP/IODP 2005*, Abstracts, pp 3.

Hertkorn N., Ruecker C., Meringer M., Gugisch R., Frommberger M., Perdue E.M., Witt M., Schmitt-Kopplin P. (2007): High precision frequency measurements: indispensable tools at the core of the molecular-level analysis of complex systems. *Anal. Bioanal. Chem.* 389, 1311-1327.

Hertkorn, N., Frommberger M., Schmitt-Kopplin Ph., Witt M., Koch B., Perdue E.M. (2008): Natural Organic Matter and the Event Horizon of Mass Spectrometry. *Anal Chem.* 80(23), 8908-8919.

Huber S.A., Frimmel F.H. (1991): A Liquid Chromatographic System with Multi-Detection for the Direct Analysis of Hydrophilic Organic Compounds in Natural Waters. Fresen. *J. Anal. Chem.* 342, 198-200.

Lodemann M., Fritz P., Wolf M., Ivanovich M., Hansen B.T., Nolte, E. (1998): On the origin of saline fluids in the KTB (Continental Deep Drilling Project of Germany). *Appl. Geochem.* 13, 651-670.

Nadeau M.J., Schleicher M., Grootes P.M., Erlenkeuser H., Gottdang A., Mous D.J.W., Sarnthein J.M., Willkomm H. (1997): The Leibniz-Labor AMS facility at the Christian-Albrechts-University, Kiel, Germany. *Nuclear Instruments and Methods in Physics Research* B 123, 22-30.

Schwarzbauer J., Heim S. (2005): Lipophilic organic contaminants in the Rhine river, Germany. *Water Research* 39,19, 4735-4748.

Stückrad O. (2005): Determination of fluid flow between the KTB main and pilot borehole by a unique fatty acid methyl ester tracer attached to zinc sulphide aggregates. *Joint Colloquium IODP/ICDP 2005*, Abstracts, pp.1.

Thurman, E.M. (1996): Organic geochemistry of natural waters. - 2. print., pp. 497, Nijhoff, Dordrecht.

Derivation and application of a simple transfer function for submarine gas hydrate quantification

M. MARQUARDT[1], T. HENKE[2], C. HENSEN[1], C. MÜLLER[2], R. GEHRMANN[1], K. WALLMANN[1]

[1] Leibniz-Institute of Marine Sciences, IFM-GEOMAR, Kiel
[2] Federal Institute for Geosciences and Natural Resources, BGR, Hannover

Introduction

The magnitude of marine gas hydrate (GH) inventories is usually estimated by the interpretation of seismic records or by the use of available pore water data (from ODP drill sites). Results derived from these two methods, however, very often reveal significant differences in terms of quantity and distribution. This can essentially be ascribed to inadequate data resolution or lack of key parameters and shortcomings regarding the conversion of proxy information into GH concentration. Within the project HYDRA a complementary approach has been developed, applying geochemical reactive-transport and geophysical rock physics modelling to quantify regional GH inventories. Here we present the results of a a simplified transfer function, which has been derived from various geochemical model runs and enables the estimation of the GH inventories based on easily accessable geological and geochmical parameters. 2-D GH distribution is shown along two seismic profiles (BGR99-39 and BGR99-44) across the Costa Rican forearc.

Model derivation

A geochemical transport-reaction model (according to Wallmann et al. 2006) has been applied to predict sub-seafloor gas hydrate distributions at various ODP and DSDP drill sites. In these cases, GH predictions are directly constrained by downwhole information of sensitive pore water and solid phase constituents.

In addition, systematic variations of potential control parameters (e.g. organic matter input, heat flow, etc.) have been performed in order to provide a robust sensitivity analysis. The motivation behind this stragety was to identify a set of easily accessable key parameters which can be used to predict GH concentrations. The most useful parameters in this regard are the sulphate-penetration depth (SPD), the sedimentation rate (SedRate), and the GH-stability zone (GHSZ) since they are sensitive and well correlated to the GH formation as it could be shown by systematic variations of these parameters in single model runs (Fig. 1). In general, GH concentrations increase with increasing sedimentation rate and the thickness of the GHSZ (Fig. 1a, b). However, in both cases the magnitude of POC degradation plays a important role and may even reverse the correlation for combinations of high sedimentation and low POC degradation rates. Because the direct correlation of POC degradation rates and GH formation is quite scattered, SPD has been chosen to serve as a proxy parameter for all processes related to POC degradation and the formation of CH_4 and GH (Fig. 1c). Since SPD is a model output Figure 1c represents a compilation of all model results, and hence displays higher data scatter.

All parameter combinations of Figure 1 a-c have been used to derive three single non-linear functions, which enable the calculation of GH concentrations in the sediment by inserting the respective parameter (SedRate, GHSZ and SPD). For the parameters SedRate and GHSZ, the functions consider the dependance on POC degradation. The results of these functions are compared to those of the numerical model in Figures 1d-f and show (although there is some scatter in case of SPD) the general validity of this approach.

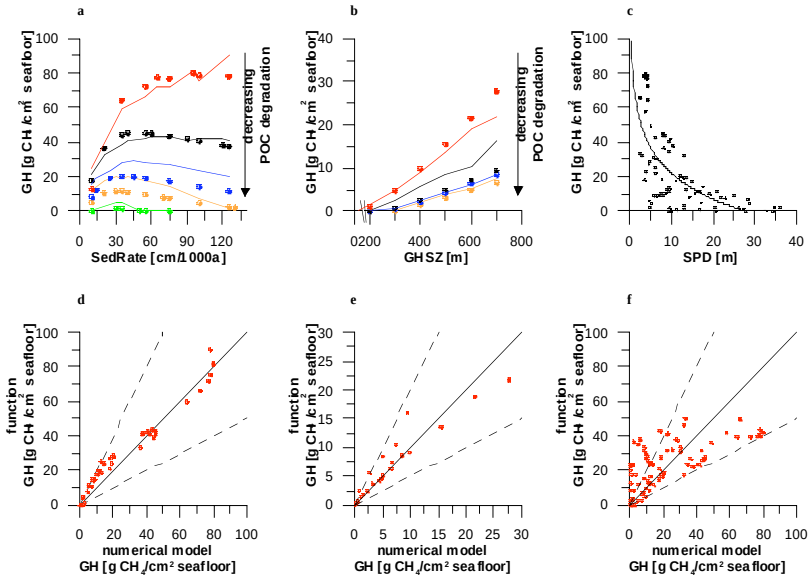

Figure 1: (Upper panel) Results of the sensitivity analysis of the numerical model showing the correlation of the control parameters SedRate, GHSZ, and SPD on GH formation. Specific model runs on SedRate and GHSZ are linked to POC degradation rates as well. Since SPD is an output of the numerical model numerous model runs have been compiled for the SPD-GH correlation. For each parameter a single analytical function has been derived. The application of the functions with the same data sets are plotted as solid lines in the same plots.
(Lower panel) Cross-plots of GH concentrations obtained by numerical model runs and application of the derived function. The solid line shows the 1:1 correlation, the dotted lines the 50% deviation interval.

In order to receive one general transfer function for the estimation of GH inventories the three single functions for SedRate, GHSZ, and SPD were combined into a non-linenear equation

system that has been solved by using the methods of least squares. Differences in the impact on GH formation for the three parameters were addressed by introduction of respective weighting coefficients so that the formation potential of GH can be expressed by

$$GH = a \cdot Ln(SedRate) \cdot SPD + b \cdot GHSZ^{(1+1/SPD)} + c \cdot EXP^{(1 + Ln(SPD))}$$

where GH is the potential amount of GH formed by CH_4 production (in g CH_4 / cm^2 seafloor), and a, b, c are weihting coefficients. In order to test the validity of the transfer function, results of the numerical model have been plotted against those of the transfer function (see Fig. 2). Most of the data plot within a 50% deviation interval.

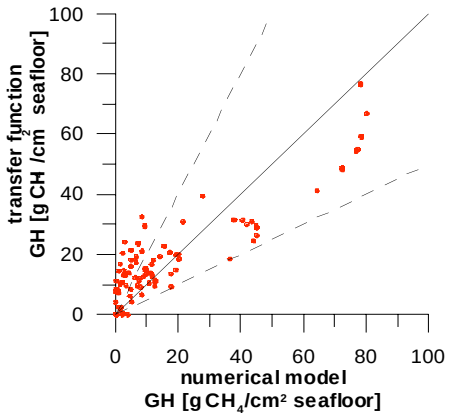

Figure 2: Results derived from numerical modeling and the transfer function. The solid line shows the 1:1 correlation, the dotted lines the 50% deviation interval. The standard deviation of the function compared to the model results is about 8.5 g CH_4 in GH/cm^2 seafloor.

Application of the transfer function

The transfer function has been applied to two seismic profiles BGR99-39 and -44 at the Pacific continental slope of Costa Rica close to Nicoya Peninsula (Fig. 3). Along these two profiles a dense data mesh exists, which has been acquired on cruises M54, SO173 and BGR99 and ODP Leg 170. In order to correctly apply the general function developed above, spatial information on SedRate, SPD and GHSZ is required along the profiles. Pore water data obtained from gravity cores have been used to determine the SPD by interpolation. The parameter SedRate has been determined as a general function of water depth derived from sedimentation rate data at ODP sites 1040, 1041, and 1043 (Kimura et al., 1997) as well as from gravity core analyes (Kutterolf et al., 2008; Marquardt, 2005). Seismic interpretation yields both the thermal gradient (derived from BSR information), which is necessary to calculate the GHSZ, and the overall sediment thickness above the basement. Where thermal information is not available because of larger gaps in the BSR distribution, the thermal gradient is determined based on data from Langseth and Silver (1996). The transfer function and, hence, all control parameters have been calculated in 625m intervals along the profiles.

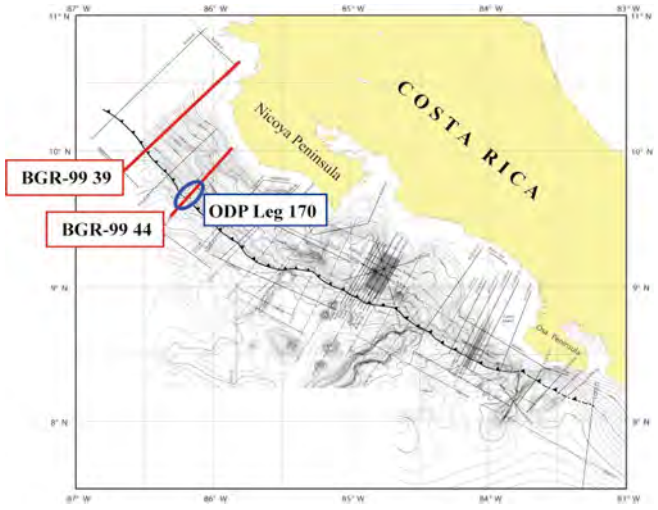

Figure 3: Location of the seismic profiles BGR99-39 and BGR99-44 (red lines) and the ODP Leg170 (blue circle) offshore Costa Rica.

Figure 4 shows the GH distribution along the two seismic profiles BGR99-39 and -44. In general GH concentrations varrying between 0 and 100 g CH_4 per cm^2 of seafloor area. Following our model predictions, highest concentrations of GH are to found at mid to upper slope depths where optimal conditions with respect to organic matter input, sediment thickness and stability conditions are met. Further downslope the input of organic matter, and hence, the methane and GH formation potential decreases as indicated by increasing SPD. At shallower depths the GHSZ thins out and does not allow for the accumulation of high amounts of GH.

Since one goal of the project is to accurately estimate margin-wide gas hydrate inventories we used the results displayed in Figure 4 to give a rough projection for the amount of GH stored along the Costa Rican forearc. Integration of the GH bearing sediments along the two seismic profiles and subsequent extrapolation to 1 km of continental margin length yield a potential of $13.9 \cdot 10^{12}$ g CH_4 per km for BGR99-39 and $23.6 \cdot 10^{12}$ g CH_4 per km for BGR99-44, respectively. Using this result

for an extrapolation to the entire continental margin length (~200 000km) would yield about $3.75 \cdot 10^{18}$ g CH_4 stored in submarine GH. This value is in the range of recently published data of $1.4 \cdot 10^{17}$ g CH_4 (Soloview, 2002) and $8.6 \cdot 10^{19}$ g CH_4 (Klauda and Sandler, 2005) and is in very good agreement with the amount of $4 \cdot 10^{18}$ g CH_4 estimated by Buffet and Archer (2004), which approves the applicabilty of the general approach.

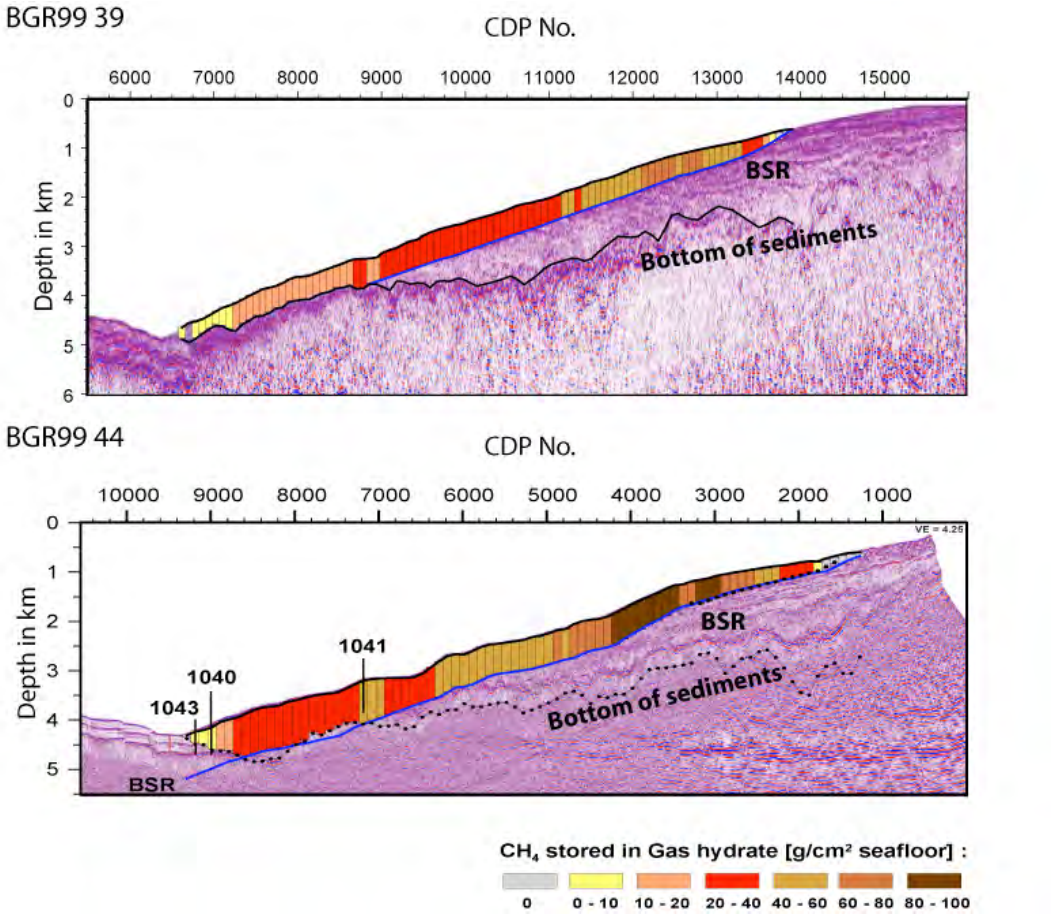

Figure 4: Formation potential of GH by the CH_4 degradation in g CH_4 /cm^2 seafloor for the seismic profiles BGR99-39 (upper plot) and BGR-99-44 (lower plot). The GH occurence zone begins at about 100m below the seafloor. The lower end is determined either by the BSR (blue line) or the sediment-basement boundary (black dotted line).

Acknowledgement

The project is funded by the German Research Foundation (DFG), grants HE 3512/1-2 and MU 2662/1-2.

Kimura G., Silver E., Blum P., et al., (1997): Proc. ODP, Init. Repts., 170: College Station, TX (Ocean Drilling Program).

Langseth and Silver (1996): The Nicoya convergent margin - a region of exceptionally low heat flow. Geophysical Research Letters, Vol 23, 891-894.

Kutterolf, S., Freundt, A., Schacht, U., Bürk, D., Harders, R., Mörz, T., Peréz, W. (2008): Pacific offshore record of plinian arc volcanism in Central America: 3. Application to forearc geology. Geochemistry Geophysics Geosystems (G3), Vol. 9, No. 2, Q02S03, doi:10.1029/2007GC001826.

Marquardt, M. (2005): Investigation of a submarine landslide off Costa Rica. Diploma thesis, unpublished.

Wallmann, K., Aloisi, G. Haeckel, M., Obzhirov, A., Pavlova, G., Tishchenko, P. (2006): Kinetics of organic matter degradation, microbial methane generation, and gas hydrate formation in anoxic marine sediments. Geochimica et Cosmochimica Acta, Vol. 70, S. 3905-3927.

Manganese diagenesis in Arctic Ocean sediments – Stratigraphic and paleoenvironmental implications

C. MÄRZ*, A. STRATMANN, S. ECKERT, B. SCHNETGER, H.-J. BRUMSACK

Microbiogeochemistry, ICBM, University of Oldenburg, 2503, 26111 Oldenburg
(*corresponding author: cmaerz@icbm.de, +49-441-798-3627)

Despite the fact that Arctic Ocean sediments have long been recognized as important archives of past climatic and environmental changes, their inorganic-geochemical composition and behaviour is poorly investigated. Marked light to dark brown layers are particularly well-known and widespread features of Quaternary Arctic sediments, and have been related to variable Mn contents. While brown layers are relatively rich in Mn (often > 1 wt.%), yellowish-greyish intervals are Mn-depleted. The ubiquity of these brown colour cycles in pelagic Quaternary Arctic Ocean sediments led to their use as stratigraphic, age-equivalent marker horizons genetically linked to global climate changes (e.g. Jakobsson et al., 2000; Löwemark et al., 2008). As in the Arctic Ocean conventional stratigraphic methods often fail, the use of Mn layers for chemostratigraphy seems to be a promising approach. However, several inorganic-geochemical and modelling studies of the Mn distribution in the Arctic as well as other oceans have shown that multiple Mn layers in marine sediments can be created by diagenetic processes, i.e. Mn redistribution due to microbially mediated dissolution-reprecipitation reactions (e.g. Li et al., 1969; Gobeil et al., 1997; Burdige, 2006; Katsev et al., 2006). Such biogeochemical processes can lead to rapid migration or fixation of redox boundaries in the sediment, resulting in the (partial) dissolution and re-precipitation of metal-rich layers long after sediment deposition. Another potentially important mechanism is the transformation of primary or diagenetic amorphous Mn (oxyhydr)oxides to well-crystallized Mn oxides, and ultimately to Mn carbonates upon progressive sediment burial. This does not change the location of Mn-rich layers, but sediment properties like colour (from brown to whitish), porosity and permeability. As such diagenetic processes clearly would alter primary paleoenvironmental signals recorded in the sediments in the Arctic Ocean, we see an urgent need to unravel their real stratigraphic and paleoenvironmental potential before they are readily established as standard tools. For this purpose, we will study Mn cycles in Arctic Ocean sediments recovered during IODP Expedition 302 (ACEX) from the Central Arctic Lomonosov Ridge (Backman, Moran, McInroy, Mayer, et al., 2006). As indicated by quantitative single sample XRF analyses, Mn layers occur in the ACEX record down to a depth of about 55 mcd. Thus, the ACEX sediments are ideal for studying various processes related to potential Mn diagenesis in Arctic Ocean deposits. The only limitation for unravelling biogeochemical processes in the sediments is the lack of high-resolution pore water data from the ACEX cores. We will close this gap by a parallel investigation of a high resolution pore water set we obtained during R/V *Polarstern* expedition ARK XXIII/3 to the Mendeleev Ridge (East Siberian Sea). First results of pore water and sediment composition (analysed by ICP-OES and XRF) indicate that certain Mn-rich layers are currently dissolving, while others are forming. This internal Mn re-distribution, while being more pronounced in some locations than in others, also has an impact on related trace metal distributions (e.g. Co, Cu, Ni, Mo). This additional geochemical data set will hopefully allow us to establish a conceptual model of biogeochemical processes in Arctic sediments, and to develop diagnostic criteria for or against diagenetic Mn redistribution. In addition to more sensitive geochemical analyses (acid digestions and HR-ICP-MS measurements) of the ACEX and *Polarstern* samples, we will apply methods like sequential Mn extraction, X-ray diffraction and electron microscopy to study Mn-rich layers. These data will be put into a broader context by comparing them to records of, e.g., magnetic susceptibility, grain size distribution, sediment colour or porosity. This will presumably result in a better understanding of Mn biogeochemistry in the Arctic Ocean, including its application as a paleoenvironmental proxy.

Burdige, D.J. (2006) Geochemistry of marine sediments. Princeton University Press, 609 pp.

Gobeil, C., Macdonald, R.W., Sundby, B. (1997) Diagenetic separation of cadmium and manganese in suboxic continental margin sediments. Geochim. Cosmochim. Acta 61, 4647-4654.

Jakobsson, M., Løvlie, R., Al-Hanbali, H., Arnold, E.M., Backman, J., Mörth, M. (2000) Manganese and color cycles in Artic Ocean sediments constrain Pleistocene chronology. Geology 8, 23-26.

Katsev, S., Sundby, B., Mucci, A. (2006) Modeling vertical excursions of the redox boundary in sediments: Application to deep basins of the Arctic Ocean. Limnol. Oceanogr. 51, 1581-1593.

Li, Y.-H., Bischoff, J. Mathieu, G. (1969) Migration of manganese in Arctic Basin sediments. Earth Planet. Sci. Lett. 7, 265-270.

Löwemark, L., Jakobsson, M., Mörth, M., Backman, J. (2008) Arctic Ocean manganese contents and sediment colour cycles. Polar. Res. 27, 105-113.

Major and minor element signatures and their paleoenvironmental significance in Central Arctic Ocean sediments (Lomonosov Ridge, IODP Leg 302)

C. MÄRZ*, B. SCHNETGER, H.-J. BRUMSACK

Microbiogeochemistry, ICBM, Oldenburg University, POB 2503, 26111 Oldenburg
(*corresponding author: cmaerz@icbm.de, +49-441-798-3627)

The Arctic environment is not only affected most directly and rapidly by present-day global warming – it also has a great potential for recording comparable climate fluctuation that happened in the past. However, although the paleoenvironmental development of the Arctic Ocean during the late Quaternary is comparably well studied, its early Cenozoic- Mesozoic history is still unexplored. Recently, a major step ahead in our understanding of the long-term history of the Arctic was taken when IODP Expedition 302 (Arctic Coring Expedition, ACEX) drilled ~428 m of sediment on the Lomonosov Ridge close to the North Pole (Backman et al., 2006; Backman, Moran, McInroy, Mayer et al., 2006; Moran et al., 2006). Despite moderate core recovery, this expedition recovered the most continuous record of the last ~60 Ma of sedimentation in the central Arctic so far. A number of astonishing findings from this unique paleoenvironmental archive have already been published. However, a fundamental, comprehensive and quantitative bulk inorganic-geochemical study covering the record in high resolution is missing to date. Some spatially limited records of certain elements determined by quantitative X-Ray Fluorescence (XRF) and Inductively Coupled Plasma Mass Spectrometry (ICP-MS) at our lab were published in Knies et al. (2008), O´Regan et al. (2008), Sangiorgi et al. (2008), Sluijs et al. (2008), and Stickley et al. (2008). Spofforth et al. (2008) presented an XRF scanner record of the lithological Units 2 and 1/6. However, these data sets are fragmentary, and XRF scanning of drill cores is doubtful in terms of quantitative results. Recently, Martinez et al. (in press) published a comprehensive and quantitative, but low-resolution geochemical data set for the whole ACEX record based on single sample powder XRF, ICP-OES and ICP-MS analyses. The conclusions drawn from the chemical and statistical data are, however, largely limited to the discrimination of terrigenous sediment sources. Here we will present high-resolution elemental data of the recovered sediments obtained by single-sample quantitative XRF analysis using borate glass beads. Our aim is a basic inorganic-geochemical description and characterisation of the different lithological units, to provide information on provenance, paleoenvironmental conditions, and diagenesis.

Sediment samples from cooperating institutes (AWI Bremerhaven, R. Stein; Utrecht University, H. Brinkhuis; Bremen University, C. Vogt) were combind to construct the most complete geochemical data set possible. After sample preparation, we performed elemental analysis by XRF for major and minor elements (Fig. 1). To correct for variable dilution by biogenic (e.g. carbonate, opal) or diagenetic (e.g. pyrite, barite, apatite) components, elemental records are normalized to Al. This element is generally abundant in marine sediments, stable during diagenesis, and largely unaffected by biogenic processes. The results of this quantitative single sample XRF analyses (Fig. 1) of the complete ACEX record are shown for some selected elements. These records lead to a number of implications for the depositional environment on the Central Arctic Lomonosov Ridge, from the Late Cretaceous to the Holocene. These implications comprise the detrital sediment sources and their variations through time, depositional processes, the reconstruction of paleoproductivity and organic matter deposition, the geochemical conditions in the water column, and early diagenetic alterations of elemental records.

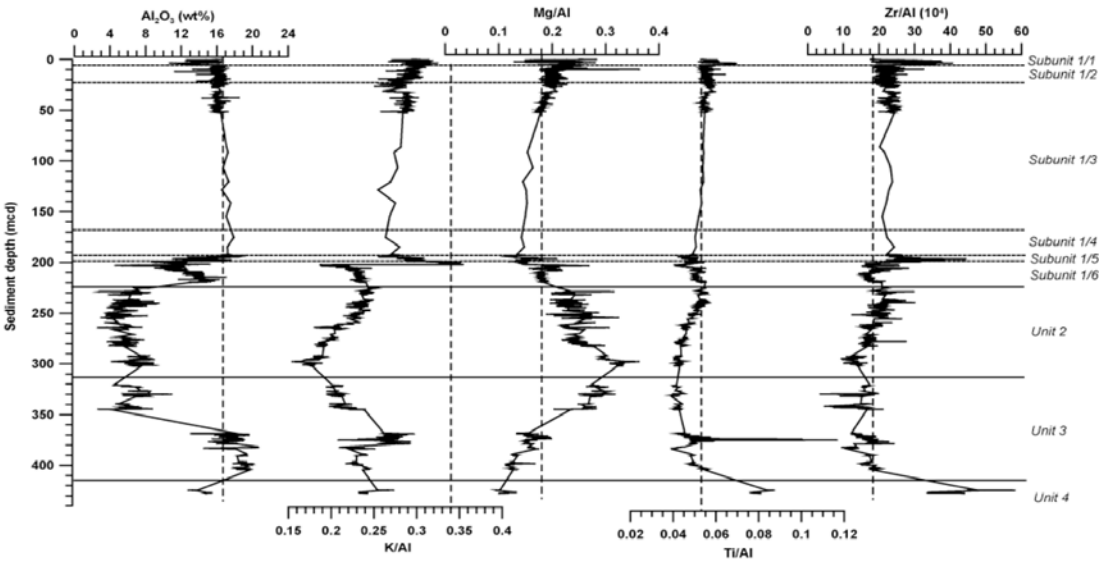

a)

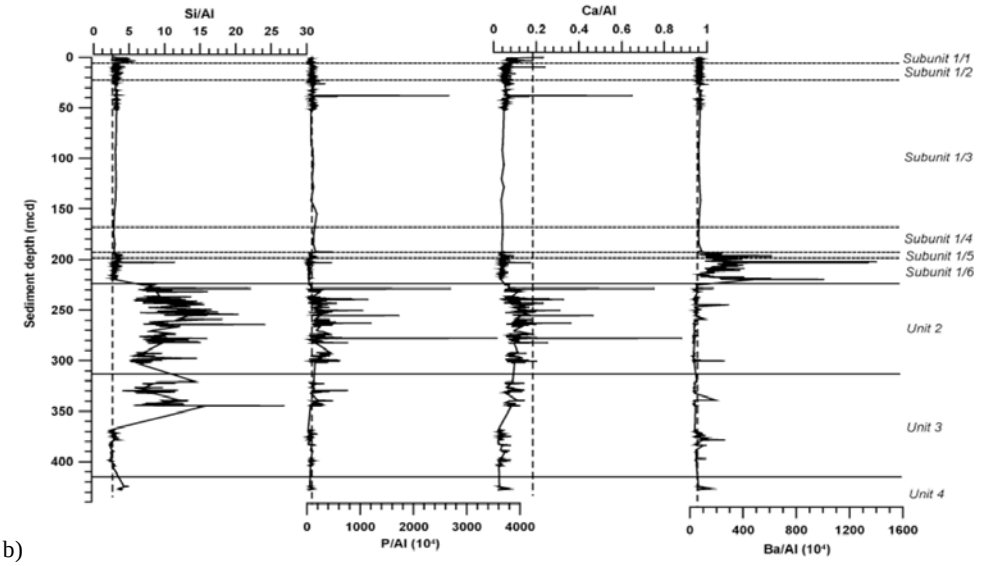

b)

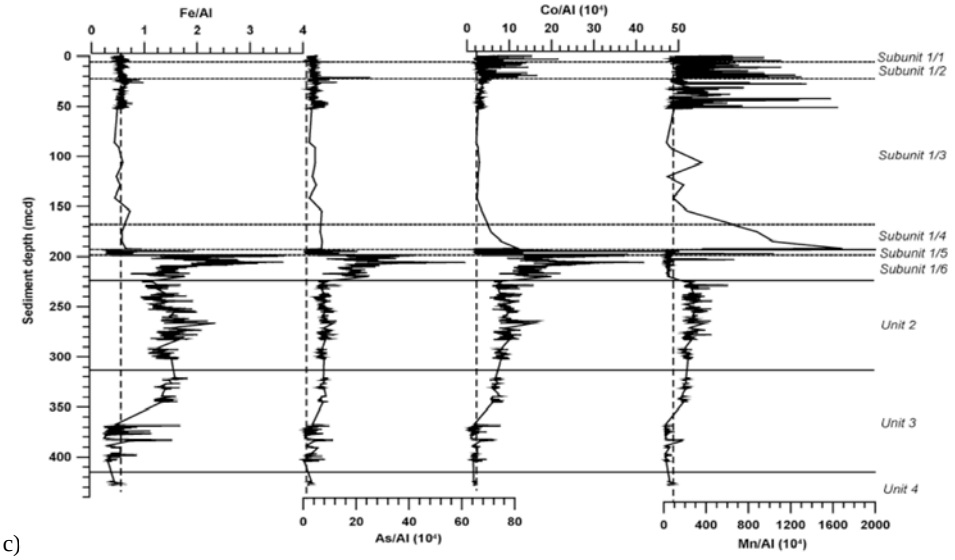

c)

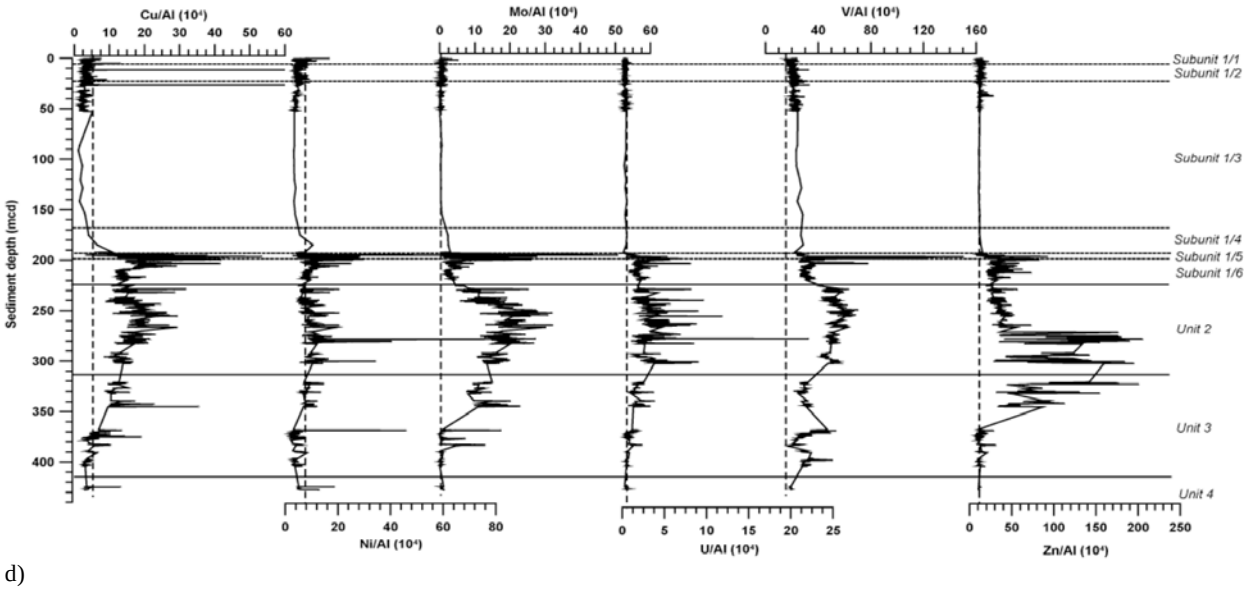

d)

Figure 1: Element/Al ratios versus core depth (meters composite depth) of the ACEX record. a) Al_2O_3, K/Al, Mg/Al, Ti/Al, Zr/Al; b) Si/Al, P/Al, Ba/Al, Ca/Al; c) Fe/Al, As/Al, Co/Al, Mn/Al; d) Cu/Al, Ni/Al, Mo/Al, U/Al, V/Al, Zn/Al.

Unit 4, although poorly recovered, was most probably deposited relatively close to the paleo-coastline in a shallow high-energy environment (elevated Si/Al, Ti/Al and Zr/Al ratios). During the Late Cretaceous, Lomonosov Ridge was still attached to the Siberian shelf. Primary productivity and the resulting organic matter export to the sea floor were supposedly elevated, most probably due to nutrient input through riverine input (as indicated by elevated Ba/Al, Cu/Al, Ni/Al and P/Al ratios). Decomposition of this organic matter, despite relatively well-mixed shallow waters, led to at least episodically anoxic conditions in the sediments and minor enrichment of various redox-related trace elements (e.g. As, Mo).

Deposition of Unit 3 can be subdivided into two episodes. Throughout the unit, the records of detrital elements indicate a gradual change in the detrital source area and/or the distance to the paleo-coastline (increasing Al_2O_3, Mg/Al; decreasing Si/Al, Ti/Al, Zr/Al), most probably documenting the progressive drifting of Lomonosov Ridge away from the Siberian margin due to rifting at Gakkel Ridge. However, as deepening of the water column was obviously not a constant process (derived from variable element/Al profiles), the rifting process probably occurred in pulses as well. Periods of enhanced paleoproductivity (PETM, Elmo) developed under low energy conditions, i.e. below the wave base or in a sheltered environment (higher P/Al, Ba/Al, Cu/Al, Ni/Al). During these periods, anoxic to sulfidic conditions persisted within the sediments, and at least episodically in the ocean as well (enrichments of Mo, U). However, these relatively short-termed intervals were interrupted by times of more vigorous water motion (peaks in Ti/Al and Zr/Al) and well-oxygenated conditions. In the upper part of Unit 3, there was a strong increase in productivity of biosiliceous organisms (drastic increase in P/Al, Si/Al), resulting in the accumulation of organic matter on the sea floor. Bottom water anoxia and euxinia developed frequently due to extensive sulfate reduction and sulfide production, leading to the accumulation of As, Cu, Mo, Ni, and U. However, progressive burial and organic matter decomposition resulted in dissolution and redistribution of biogenic silica.

During deposition of the lowest part of Unit 2, biosiliceous organisms became even more dominant, as documented by the Si/Al record. This high productivity was accompanied by a high availability of P (extreme peaks of P/Al) and other nutrients (Cu, Ni), and well-stratified “Black Sea”-type conditions resulted in extensive accumulation of organic matter on the sea floor. Anoxic to sulfidic conditions prevailed episodically on the sea floor, creating enrichments of As, Cu, Fe, Mo, Ni, U, V and Zn. Enrichments of Co and Mn are caused by trapping of dissolved Mn that is mobilised in the sediment under anoxic conditions and re-precipitated (probably as mixed Ca-Mn carbonates) in the high-porosity biosiliceous deposits. The detrital elements indicate that most terrigenous material within Unit 2 was derived from the Siberian Putoran flood basalt province (with low Al_2O_3 contents, low Mg/Al and high K/Al) most probably transported to the Lomonosov Ridge by high river discharge. The middle to upper section of Unit 2 was obviously dominated by even more pronounced anoxic to sulfidic conditions in the water column and related trace metal enrichments. In addition, there are first indications for episodic sea ice formation and cold climate conditions, derived from the detrital element records (pulsed input of Ti and Zr associated to a coarse grained fraction) and extremely high Fe/Al ratios that require the occurrence of peat bogs in the hinterland as sources of dissolved Fe.

The lower part of Subunit 1/6 probably reflects the most intense anoxic/sulfidic conditions of the whole ACEX record, with maximum enrichments of As, Cu, Co, Fe, Mo, Ni and V. However, the tentative 26 Ma hiatus within Subunit 1/6 also marks a shift to better oxygenated conditions in the water column, indicated by a drastic decrease in redox-related trace elements. The geochemical fingerprint of the Putoran trap basalts is still pronounced in the detrital element records, probably due to intensified sea ice transport from the Siberian shelf. In addition, the elemental records indicate high-energetic conditions on Lomonosov Ridge above and below the hiatus (extreme Zr/Al ratios), probably due to shallow-water conditions. However, there is a dramatic change in sediment source that significantly predates the palynologically defined hiatus, most obvious in an abrupt positive shift in K/Al. In any case, the formation of a diagenetic front (enriched in Ba, Ca, Co, Fe, Mn, Mo, P) within Subunit 1/6 below the hiatus is most probably related to the supposed period of non-sedimentation.

The onset of Subunit 1/5 marks a distinct shift in the depositional regime on Lomonosov Ridge. Anoxic conditions only prevailed during deposition of the lower Subunit 1/5 (“Zebra Layer”), accompanied by only minor biosilica deposition. The colour cycles in the sediment are paralleled by only minor variations in both detrital and redox-related elemental composition. Probably diagenetic overprint altered the original sediment composition and largely destroyed the primary redox-influenced element record. In any case, the upper boundary of the Zebra Layer marks the onset of well-oxygenated conditions in the deep Arctic Ocean.

Subunits 1/4 to 1/2 mark the onset and persistence of current depositional conditions in the Arctic Ocean. Detrital elements indicate a relatively stable sediment source with a composition close to average shale and to modern Arctic Ocean deposits, and the frequent influence of sea ice transport. Long-term changes in detrital elements most probably reflect gradual geodynamic changes in the Arctic realm, e.g. opening of the Fram Strait or progressive drifting of the Lomonosov Ridge. Redox conditions in bottom waters were mostly oxic, and euxinic conditions did not reach the sediment surface. Geogenic background contents of redox-related elements and low TOC contents indicate a drastic reduction of primary production and organic matter export compared to the underlying sediments. This change probably resulted from increasing sea ice cover, establishment of different circulation patterns due to progressive opening of the Fram Strait, or a combination of both. However, cyclic Mn-rich layers still indicate slight changes of organic matter export and/or variation of sedimentation rates.

Subunit 1/1 is the only interval of the ACEX record with slightly higher preservation of calcium carbonate. The records of detrital elements bound to coarser grain sizes (Si/Al, Ti/Al, Zr/Al) are anti-correlated with those of feldspar- and clay-bound elements (Al, K/Al). This mutual dilution was most probably related to winnowing, deposition of turbidites or IRD. Redox conditions were mostly oxic in the bottom waters, sometimes suboxic in the sediments.

Knies, J. et al. (2008) Paleoceanography 23, doi:10.1029/2007PA001455
O´Regan, M. et al. (2008) Paleoceanography 23, doi:10.1029/2007PA001559
Sangiorgi, F. et al. (2008) Paleoceanography 23, doi:10/1029/2007PA001477
Sluijs, A. et al. (2008) Paleoceanography 23, doi:10.1029/2007PA001495
Stickley, C.E. et al. (2008) Paleoceanography 23, doi:10.1029/2007PA001485

Spofforth, D.J.A. et al. (2008) Paleoceanography 23, doi:10.1029/2007PA001489
Martinez, N. C. et al. (in press) Paleoceanography, doi:10.1029/2007PA001567

The Arctic Ocean Sea-Ice Cover in the Neogene: Evidence from Marine Palynomorphs

J. MATTHIESSEN, M. SCHRECK

Alfred Wegener Institute for Polar and Marine Research, Bremerhaven, Germany

The presence or absence of a sea-ice cover in the Neogene Arctic Ocean has been debated for a long time. Since IODP Exp. 302 drilled for the first time in the Central Arctic Ocean (CAO) on the Lomonosov Ridge, an increasing number of studies (sedimentology, mineralogy, radiogenic and cosmogenic isotopes) indicate that a sea-ice cover has been present at least since the Middle Miocene (Cronin et al. 2008; Darby 2008; Frank et al. 2008; Haley et al. 2008; Krylov et al. 2008; St. John 2008). It has been suggested by most studies that the CAO was ice-covered year-round since that time but benthic foraminifera provide evidence rather for a seasonal than a permanent sea-ice cover in the Pleistocene (Cronin et al. 2008). Moreover, Frank et al. (2008) stated that two ^{10}Be maxima in the Late Miocene may be attributed to increased fluxes to the seafloor during short warmer periods with a reduced sea-ice cover. In contrast to the Central Arctic, the marginal Arctic Ocean and adjacent seas experienced strong fluctuations in the ice cover since the Middle Miocene and an extensive sea-ice cover similar to today might have been established first in the Late Pliocene (Polyakova 2001, Matthiessen et al. 2008 and references therein).

To test the hypothesis of a perennial ice covered CAO since the Middle Miocene, a detailed palynological study will be conducted on IODP Exp. 302 Hole M0002A. Initial shipboard biostratigraphic studies already revealed that marine palynomorphs (dinoflagellate cysts, acritarchs, chlorophycean algae) are the only microfossil group in Neogene sediments (Backman et al. 2006) and thus may provide additional information on surface water conditions. Based on these initial results the whole Neogene will be sampled to obtain a palynomorph record at a relatively high resolution. Preliminary results based on an initial low resolution study show that the occurrence of marine palynomorphs is quite variable and the abundances are generally increasing with increasing age. In the late Miocene, most samples are productive and quantitative analysis on a selected number of samples revealed a predominance of few taxa (Fig. 1). The ecology of the extant genera *Impagidinium* spp. and *Nematosphaeropsis* spp. implies a relation to a seasonal but definitely not a permanent sea-ice cover (Matthiessen et al. in press). Additionally, a year-round sea-ice cover would have caused an extremely low production as in the modern Arctic Ocean leading to low abundances or absence of aquatic palynomorphs in the sediments. The extinct marine acritarch *Decahedrella martinheadii* has its maximum concentrations in the Late Miocene (Fig.1) comparable to sites in the western Nordic Seas pointing to somewhat similar ecological conditions at these locations, possibly due to an extensive exchange of water masses between these regions.

The reconstruction of a seasonal rather than a permanent sea-ice cover in the Late Miocene CAO is in stark contrast to previous reconstructions. This discrepancy may be explained on the one hand by the low temporal resolution of the proxy records leading to a under-representation of warmer climate phases. The study by Darby (2008) has with a average sampling interval of about 0.17 Ma a much higher resolution than those by Krylov et al. (2008), Frank et al. (2008) and Healy et al. (2008) but we used only samples at an average sample interval of 500cm in the selected Late Miocene interval (Fig. 1) corresponding to a temporal resolution of approximately 0.32 Ma according to the age model of Frank et al. (2008).

On the other hand, interpretations were partly based on reconstructions of transport pathways of terrigenous sediments from their source regions by sea ice, assuming certain drift rates, to the Lomonosov Ridge. Darby (2008) and Krylov et al. (2008) suggested that, if transit times of sea ice from source areas to the Lomonosov Ridge have exceeded one year, a perennial ice cover is required as transport agent. The applied drift rates of sea ice on the order of 3cm/s, however, may underestimate the potential pronounced variability as recorded from historical measurements. Drift rates frequently exceeded 5cm/s in the past 50 years (Hakkinen et al. 2008). Thus, the CAO might have been easily reached by sea ice from most potential sediment source areas in less than a year.

Apart from these objections to certain assumptions, all studies agree that the Central Actic Ocean was covered by sea-ice but the timing of the formation of a permanent sea-ice cover and the development of the seasonal extent with time is still an open question. We suggest that these discrepancies between reconstructions may first of all be explained by the low temporal resolution of the records and the accidental sampling of different climate states. Periods with a reduced seasonal extent of the sea-ice cover (interglacials?) may have been preferentially sampled for palynological analysis whereas the other studies sampled the periods with an extensively and possibly year-round sea-ice cover (glacials?). Therefore, the CAO might have been characterized by a strong (cyclic?) variability in sea-ice conditions between a more open and a more closed state in the Late Miocene.

To address this hypothesis a high-resolution study at millenial time-scales is required using various proxies. In the frame of an ongoing project (DFG MA3913/2) a continuous palynological record at a 1500 kyr resolution will be additionally established in a selected Late Neogene time interval to provide basic information on the short-term variability of sea-surface conditions. The long-term changes (eg. intensification of sea-ice cover, formation of a permanent ice cover) will be addressed at approximately 100ka resolution for the whole Middle Miocene to Early Pliocene. The correlation to records from the adjacent Nordic Seas (Site 909, 907) will enable us to study spatial gradients in sea-ice cover.

Backman, J., Moran, K., McInroy, D. B., Mayer, L. A. and Expedition 302 Scientists, 2006. *Proceedings of the Integrated Ocean Drilling Program*. College Station, TX, IODP Management International, Inc., **302**, doi:10.2204/ iodp.proc.2302.2101.

Cronin, T. M., Smith, S. A., Eynaud, F., O'Regan, M. & King, J. 2008. Quaternary paleoceanography of the central Arctic based on Integrated Ocean Drilling Program Arctic Coring Expedition 302 foraminiferal assemblages. *Paleoceanography* **23**, PA1S18.

Darby, D. A. 2008 The Arctic perennial ice cover over the last 14 million years. *Paleoceanography* **23**, PA1S07.

Krylov, A., Andreeva, I., Vogt, C., Backman, J., Krupskaya, V. V., Grikurov, G. E., Moran, K. & Shoji, H. 2008. A shift in heavy and clay mineral provenance indicates a middle Miocene onset of a perennial sea-ice cover in the Arctic Ocean. *Paleoceanography* **23**, PA1S06.

Frank, M., Backman, J., Jakobsson, M., Moran, K., O'Regan, M., King, J., Haley, B., Kubik, P. and Garbe-Schöenenberg, D., 2008. Beryllium isotopes in central Arctic Ocean sediments over the past 12.3 million years: Stratigraphic and paleoclimatic implications. *Paleoceanography*, **23**, PA1S01.

Hakkinen, S., Proshutinsky, A., Ashik, I., 2008. Sea ice drift in the Arctic since the 1950s. Geophysical Research Letters, 35, L19704.

Haley, B. A., Frank, M., Spielhagen, R. F. & Eisenhauer, A. 2008. Influence of brine formation on Arctic Ocean circulation over the past 15 million years. *Nature Geosci.* **1**, 68-72.

St. John, K. 2008. Cenozoic Ice-rafting history of the Central Arctic Ocean: Terrigenous sands on the Lomonosov Ridge. *Paleoceanography* **23**, PA1S05.

Matthiessen, J., Knies, J., Vogt, C., Stein, R. 2009. Pliocene palaeoceanography of the Arctic Ocean and subarctic seas Phil.Trans.R.Soc London A, **367**(1886), 21-48.

Matthiessen, J., Brinkhuis, H., Poulsen, N., Smelror, M.(in press). Decahedrella martinheadii - a stratigraphic and paleoenvironmental acritarch indicator species for the high northern latitude Late Miocene, Micropaleontology.

Polyakova, Y. I. 2001 Late Cenozoic evolution of northern Eurasian marginal seas based on the diatom record. *Polarforsch*. **69**, 211-220.

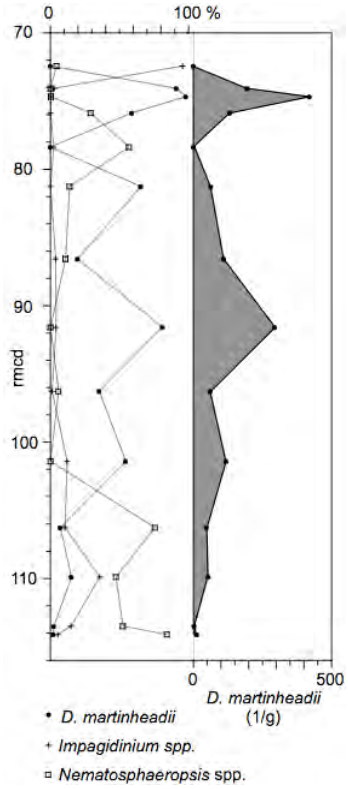

Fig. 1 Distribution of the abundant aquatic palynomorphs in a selected number of samples from the Late Miocene of IODP Exp. 302 Hole M0002A (Matthiessen et al. in press).

Millenial and shorter scale slowdown of North Atlantic Meridional Overturn Circulation over the last 20,000 years

H. MEGGERS[1], C. VOGT[1], K.-H. BAUMANN[1], T. WAGNER[2]

[1] MARUM and Geosciences Department, Bremen University, 28359 Bremen, Germany
[2] School of Civil Engineering and Geosciences, Newcastle University, Newcastle upon Tyne, NE1 7RU, United Kingdom

Direct linkages between deep-water mass characteristic, meltwater input and the meridional overturning circulation within the northern North Atlantic are sparse. Drift sediment bodies as excellent recorders of climatic change from the northern North Atlantic were used as high accumulation rate sites, where processes as lateral advection were visualized. The nature of the drift sediments however also implies that they are influenced by lateral transport of re-suspended material potentially providing important information on changes in bottom water currents and pathways of particulate matter transport. Lateral sediment displacement plays a conspicuous role for the accurate interpretation of geochemical and micropaleontological marine records. Mineralogical and sedimentological data sets from ODP sites 980 and 984 within the Feni and Björn Drift reveal a strong modulation of the deep-water properties in the northern North Atlantic. Clay mineral and grain size data indicate that the last 20,000 years within the subpolar North Atlantic were punctuated by several abrupt events in the deep-water circulation activity. Especially during the Holocene high frequency changes within an overall decreasing trend in the clay mineral distribution support previously not recognized short term changes in the deep ocean circulation of the North Atlantic.

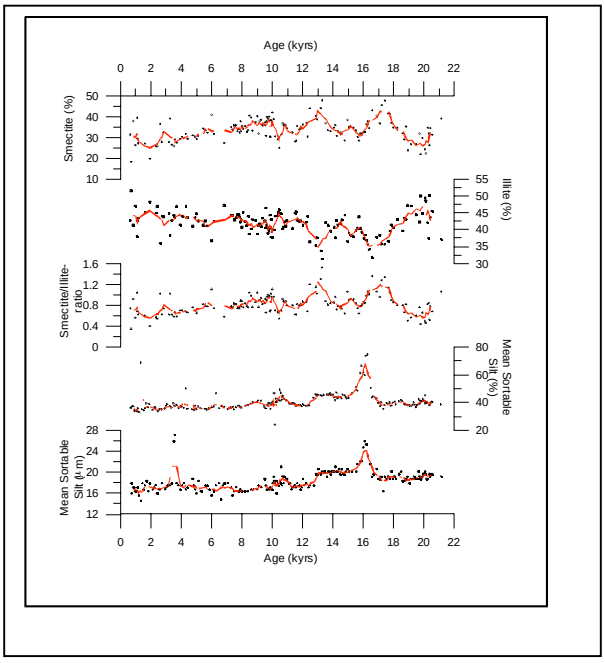

Fig. 1: Running averages (in red) of smectite, illite and the smectite/illite-ratio in North Atlantic sediment core ODP 980 in comparison to the mean sortable silt (in % and in µm).

To assess temporal fluctuation in bottom water flows and main directions of sediment supply we combine at ODP 980 granulometric records with source-specific clay mineral data (Fig.1). We consider smectite as an indicator for the origin from the north (Island) whereas illite serves as an indicator for the origin from the east (British Islands/Ireland). Using the illite/smectite record we differentiate several phases in the deep-water characteristic during the past 20 kyrs (Fig.1). We assume that preferential supply from northern directions, represented by high illite/smectite ratios corresponded with a strong MOC (Fagel et al., 2001), and vice versa. The illite/smectite record at 980 reveals a pronounced cycle pattern, best documented in the deglacial section with a wavelength of about 5 kyrs. Strongest supply from a northern direction is suggested around 17 ka, within the H1 event, and at the transition from the BA to the YD around 13 ka. More subtle increases in the illite/smectite ratio are recognized by secondary peaks centered ~19.5 ka, 15.ka, and 11 ka. The symmetric shape of all illite/smectite maxima and their apparent relationship to orbital frequencies (i.e. quarter precession of about 5 kyrs) argues for more gradual changes in flow direction during the glacial-deglacial period rather than abrupt switches. This principal pattern changed in the Holocene where a series of abrupt maxima in illite/smectite ratios at ~9.5 ka, 6.5 ka, between 3.5-2.5 ka, and at 1 ka suggest preferential supply from the north followed by gradual admixture from eastern sources, resulting in a saw-tooth pattern.

Fagel, N., Robert, C., Preda, M. & Thorez, J. (2001) Smectite composition as a tracer of deep circulation: the case of the Northern North Atlantic. Marine Geology 172, 309-330.

Degree of pyritization and δ^{34}S-values record suboxic conditions in sediments of the Eastern Equatorial Pacific, ODP Site 1226

PATRICK MEISTER[1], SARAH FREUND[2], LAURA M. WEHRMANN[1], BENJAMIN BRUNNER[1] AND TIMOTHY G. FERDELMAN[1]

[1]Max Planck Institute for Marine Microbiology, Celsiusstr. 1, D-28359 Bremen, Germany, e-mail: pmeister@mpi-bremen.de

[2]Institute for Paleoontology, University of Erlangen-Nürnberg, Loewenichstr. 28, D-91054 Erlangen, Germany

The reductive dissolution of solid phase Fe- and Mn-oxides is considered an important process in ocean sediments, however the particular role of reactive Fe- and Mn-oxides as electron acceptors remains poorly understood. Reactions involving solid phase substrates are limited by dissolution kinetics but can be an important factor to drive metabolic activity in the deep biosphere over geological time scales. Since dissimilatory Fe- and Mn-reduction often overlap with other redox processes such as microbial SO_4^{2-} reduction, the relative contribution of these redox processes can not simply be derived from porewater chemistry.

We report results from sequential Fe extraction and solid phase S distillation from a sedimentary sequence drilled in the Eastern Equatorial Pacific (ODP Site 1126). High contents of hydrothermally derived Fe/Mn-oxides are deposited in proximity to the East Pacific Rise. Total Fe(III) concentrations are in the order of 1 wt.% (based on X-ray fluorescence) and mainly consist of Fe-silicate (HCl leachate). All Fe-fractions correlate well with intervals of organic C-rich Late Miocene and Pleistocene diatom ooze. Only about 0.1 wt.% of the total solid phase Fe-pool can be considered as "reactive Fe" (ferrihydrite and lepidocrocite; hydoxylamine leachate) at this site. A linear correlation between reactive Fe and Fe-silicate is probably the effect of variable dilution with pelagic carbonate. Deviation at the high end of concentrations could reflect some loss of reactive Fe due to pyrite precipitation. Indeed the degree of pyritization (DOP) with respect to reactive Fe is around 0.8 in the Fe-rich vs. 0.5 in the Fe-poor layers. Apparently, under low Fe concentrations Fe-sulfide formation was limited by the production of S^{2-}, whereas in Fe-rich layers Fe-limitation occurred. This paradox can be explained by the co-variation of organic C and Fe content in these stratigraphic sequence, which imposes a strong control on the Fe-S system. Furthermore, the δ^{34}S of pyrite shows values as negative as -50‰ in the microbially active, organic C-rich Late Miocene and Pleistocene sediments, which is the result of intense microbial sulfate reduction and S-disproportionation. In the Pliocene low activity zones δ^{34}S-values are 10 ‰ to 15 ‰ more positive. These more positive values, in correlation with lower DOP values, indicate that S^{2-}-free, suboxic conditions prevailed for a long time which is expressed in the colorful mottling. Small amounts of pyrite are forming in these sediment layers only because of the downward diffusion of isotopically heavier S^{2-} from stratigraphically higher intervals with greater SO_4^{2-} reducing activity.

The presented results demonstrate that the combined analysis of reactive Fe minerals, reduced Fe-sulphide phases and S-isotopes can be used to reconstruct the diagenetic history and paleo-deep biosphere activity of sedimentary sequences with variable lithologies such as at Site 1226. This approach also helps to resolve the question if solid phase electron acceptors or organic reductants limit and control microbial activity in the deep biosphere through time.

Lake El´gygytgyn Drilling under way: state of the operation and first results

M. MELLES[1], J. BRIGHAM-GRETTE[2], P. MINYUK[3], C. KOEBERL[4], B. WAGNER[1], AND ELGYGYTGYN SCIENTIFIC PARTY

[1]University of Cologne, Institute of Geology and Mineralogy, Zuelpicher Str. 49a, 50674 Koeln, Germany, mmelles@uni-koeln.de
[2]University of Massachusetts, USA
[3]Northeast Interdisciplinary Scientific Research Institute Magadan, Russia
[2]University of Vienna, Austria

Lake El´gygytgyn, located in central Chukotka, NE Siberia, was formed 3.6 million years ago by a meteorite impact and has never been glaciated or desiccated. This makes Lake El´gygytgyn a unique target of an interdisciplinary, multi-national drilling campaign, which currently is carried out as part of the International Continental Drilling Program (ICDP).

Drilling operations started in Nov./Dec. 2008, when a 142 m long sediment core was retrieved from the permafrost deposits in the western lake catchment by the local drilling company Chaun Mine Geological Company (CGE). The core penetrated coarse-grained, ice-rich alluvial sediments with variable contents of fine-grained material. It will be investigated for the environmental history, including potential lake-level changes, and the permafrost history and characteristics, in order to learn more about the influences of catchment changes on the lake sedimentation. Besides, the hole was permanently instrumented for future ground temperature monitoring as part of the Global Terrestrial Network for Permafrost (www.gtnp.org/index_e.html).

The major drilling effort will commence in Febr. 2009, when two sites in the central part of Lake Elgygytgyn shall be drilled down to 630 m below the lake floor. Drilling will be carried out by DOSECC, using a new GLAD 800 system that will be operated from a sheltered platform on the lake ice. Drilling objectives include replicate overlapping cores from the up

to 420 m thick lake sediment fill. The cores promise to yield the longest, most continuous record of climate change in the terrestrial Arctic. The record will extend back one million years prior to the intensification of the Northern Hemisphere Glaciation at the Pliocene/Pleistocene boundary, thus offering unique insight into the climatic and environmental history of the Arctic and its comparison with records from lower latitude marine and terrestrial sites to better understand hemispheric and global climate change. Coring shall be continued up to 300 m into the underlying impact breccia and brecciated bedrock in order to investigate the impact process and the response of the volcanic bedrock to the impact event.

The field season will continue into May, when surface melting on the lake will push to start evacuation of the drill rig. In summer 2009, the cores will be flown by chartered cargo plane to St. Petersburg. Later they will be trucked to the University of Cologne, Germany, for sub-sampling starting in September by the international team and their students; the archive core halves will be shipped to the University of Minnesota LacCore Facility in the US for post-moratorium studies.

This talk will provide an introduction into the drilling objectives, summarize the first conclusions that can be drawn from the field data, and outline the next steps towards multidisciplinary investigation of the core material by the international science team.

Serpentinite schists in an intraoceanic island arc: exhumation by extension?

MARTIN MESCHEDE[1], HAYATO UEDA, YUJIRO OGAWA, AND SHIPBOARD SCIENTIFIC PARTY OF YK08-05

[1]Institut für Geographie und Geologie, Universität Greifswald, Friedrich-Ludwig-Jahn-Str. 17A, 17487 Greifswald

Serpentinite outcrops exist at the base of the Ohmachi Seamount in the Bonin island arc south of Japan in a depth of more than 3200 mbsf. They are overlain by volcanic rock and sediment material of probably Oligocene to Eocene age. The serpentinite schists have been exhumed and transported to the surface by tectonic processes. The process of exhumation in this intraoceanic environment, however, is unclear. Diving cruise Yk08-05 with R/V Yokosuka and the research submersible Shinkai 6500 performed five dives at the western slope of the Ohmachi Seamount to get new samples from the base of this structure where serpentinitic materials occur. The morphology of the seafloor in the surroundings of the Ohmachi Seamount displays a number of scarps including the prominent Sofugan tectonic line which are related to the plate tectonic pattern of the Parece-Vela basin west of the Izu-Bonin-Marianas island arc system. The plate tectonic evolution of this area has two stages, one related to the Eocene E-W oriented spreading system in the Western Philippine Basin and a second one related to the younger Shikoku- and Parece-Vela basins. Spreading direction of the presently inactive oceanic ridge of the Shikoku- and Parece-Vela basins, however, was not orthogonal to the N-S to NNW-SSE curved orientation of the spreading axis but more or less in NE-SW direction. The bent course of the spreading axis causes extensional deformation on the concave eastern side of the axis by stretching the oceanic lithosphere in particular in the area of the Sofugan tectonic line and around the Ohmachi Seamount. It is assumed that extensional tectonic processes along the prolongation of a transform fault of the Parece-Vela basin play an important role in the uplift history of the Ohmachi Seamount.

Lake Karakul in the Pamirs and its potential as a long-term climate archive

S. MISCHKE[1], I. RAJABOV[2], N. MUSTAEVA[2], C. ZHANG[3], I. BOOMER[4], S.C. SHERLOCK[5], E.T. BROWN[6], A. MYRBO[7], A. NOREN[7], K. BRADY[7], U. HERZSCHUH[8], M.E. SCHUDACK[1], E. ITO[7]

[1]Institute of Geological Sciences, Freie Universität Berlin, Malteserstr. 74-100, 12249 Berlin, Germany
[2]State Administration for Hydrometeorology of the Committee for Environmental Protection under the Government of the Republic of Tajikistan, 47 Shevchenko Str., Dushanbe 734025, Tajikistan
[3]Institute of Environmental Sciences, Lanzhou University, Gansu 730000, PR China
[4]Stable Isotope and Luminescence Laboratory, University of Birmingham, Edgbaston, Birmingham, B15 2TT, UK
[5]Department of Earth and Environmental Sciences, Centre for Earth, Planetary, Space & Astronomical Research, The Open University, Walton Hall, Milton Keynes, UK
[6]Large Lakes Observatory, University of Minnesota, 2205 E. 5th St., Duluth, MN 55812, USA
[7]Limnological Research Center, University of Minnesota, 310 Pillsbury Dr. SE, Minneapolis 55455, USA
[8]Alfred Wegener Institute for Polar and Marine Research, Research Unit Potsdam, Telegrafenberg A43, 14473 Potsdam, Germany

Lake Karakul is a large closed-basin lake in the eastern Pamirs (NE Tajikistan) at an altitude of 3930 m. The lake fills a basin about 45 km in diameter which may originate from a meteorite impact in the late Neogene. A field survey of the Lake Karakul region was conducted in July 2008 as a first attempt to evaluate the potential of the lake as a long-term climate archive in Central Asia. Sediment samples from the lake's bottom, water samples from the lake and inflowing streams, aquatic and terrestrial plant samples, and rock samples were collected to enable an interdisciplinary investigation of the lake and its catchment. Exposed lake sediments at the northwestern shore 20 m above the lake display an ususual Yardang relief indicating higher water levels in the past. Eroded remnants of lake, playa and fluvial sediments can be found on the northeastern slopes of the basin 200 m above the lake but their depositional age remains unknown. However, well-preserved shells of freshwater ostracods within these sediments indicate different hydrological conditions in comparison to the present status of Lake Karakul. This lake has a high pH (9.1), a high electrical conductivity (10.3 mS/cm), and SO_4>Cl>HCO_3/Mg>Na+K>Ca water due to the lack of an outlet. Corresponding with the brackish water of Lake Karakul, only five ostracod species were recorded in numerous surface sediment samples and three short cores. The two species *Candona* sp. 1 and *Candona* sp. 2 have not been recorded elsewhere so far, indicating that the lake may have existed for a significant period of time. A short (~1 m) sediment core was obtained near the centre of the more shallow and flat eastern sub-basin of the lake at 19 m water depth. Fine aragonite needles constitute most of the sediments. Additionally, abundant ostracod shells, aquatic plant fragments, detrital grains and *Radix* (Gastropoda) shells were recorded in the core which covers the last 3000 years. TOC, $\delta^{18}O$ and $\delta^{13}C$ of authigenic aragonite, $\delta^{13}C_{org}$, bulk magnetic susceptibility and XRF-derived element abundances show relative large variations over the late Holocene and demonstrate that Lake Karakul responded sensitively to climatic, hydrologic and environmental changes.

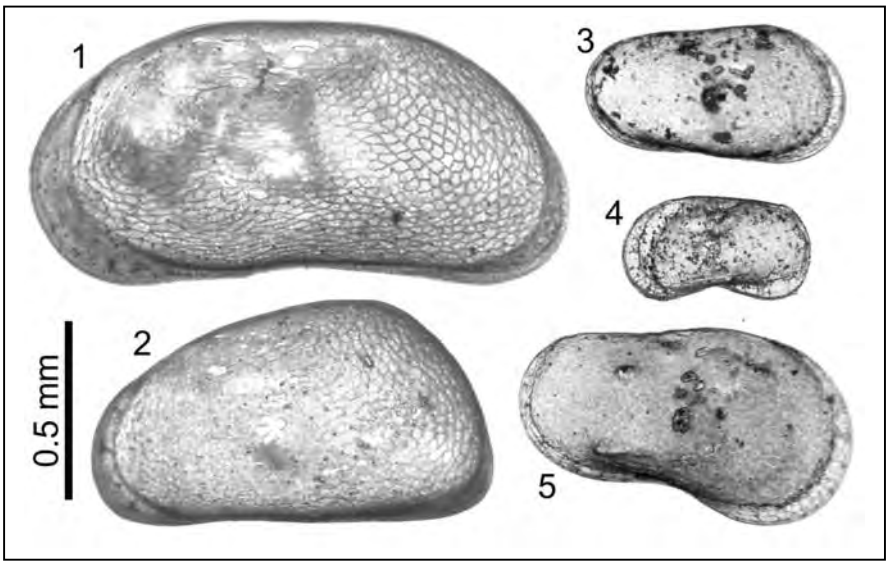

Ostracod shells found in surface samples from Lake Karakul (Pamirs, Tajikistan) and recorded in short cores. 1 *Candona* sp. 1, 2 *Candona* sp. 2, 3 *Leucocytherella sinensis*, 4 *Limnocythere inopinata*, 5 *Leucocythere dorsotuberosa* (1, 2, 4 are left shells, 3 and 5 are right shells, external views)

Global versus regional ocean anoxia during OAE-2 and the T-OAE

C. MONTOYA PINO[1], S. WEYER[1], B. VAN DE SCHOOTBRUGGE[1], A.D. ANBAR[2], H.W. ARZ[3], W. OSCHMANN[1], J. PROSS[1]

[1]Institut für Geowissenschaften, Goethe Universität, Frankfurt am Main 60438, Germany
[2]School of Earth and Space Exploration, Arizona State University, USA
[3]Deutsches Geoforschungszentrum GFZ, Potsdam, Germany

Introduction

Though oceans were generally oxidized throughout the Phanerozoic, some periods, e.g. the Mesozoic oceanic anoxic events (OAE), are characterized by extensive black shale formation, indicating a potentially global enhancement of oceanic anoxia. The goal of this study is to find suitable proxies to characterize the redox conditions and to quantify the spatial extent of oceanic anoxia during such OAEs. We are using the isotope composition of the redox sensitive trace metals Mo and additionally, that of the newly defined redox proxy U (i.e. variations in $^{238}U/^{235}U$) for this task. Both elements are enriched in anoxic/euxinic environments and show systematic isotope variations between seawater, oxic- and anoxic sinks. They are thus sensitive to a redox-driven change in their oceanic budget. Additionally, we are using trace element compositions for characterization and comparison of the redox conditions of the anoxic basins that were investigated during this study. We focused our study on Mesozoic black shales from two well-recognized OAEs; the Early Jurassic T-OAE (ca. 183 Ma) and the Late Cretaceous (Cenomanian–Turonian) OAE-2 (ca. 93 Ma). Both OAEs are regarded as widespread events (*Pearce et al., 2008; Erbacher et al., 2005*) and their duration was long enough that a global oceanic redox change should have affected the oceanic U and Mo isotope budget. In order to evaluate the oceanic redox state during these OAEs, we compared the U and Mo isotope composition of OAE-2 (ODP Leg 207 Demerara Rise, Site 1261A) and T-OAE black shales (Western and Central Europe) with that of their modern equivalents (Black Sea sapropels) and black shales that were deposited prior to - and post OAE-2 at Demerara Rise.

Results

Overall, redox proxies such as Fe_T/Al, Mn/Al and [Mo]/TOC ratios, indicate low oxygen levels during the deposition of black shales of all studied localities. Euxinic conditions are recognized for the Black Sea, T-OAE and OAE-2 samples. In contrast, samples from above and below OAE-2 were likely deposited under anoxic relative non-euxinic conditions compared to the strong euxinia during OAE-2, as indicated by their low Fe/Al ratios and increased Mn/Al of some samples.

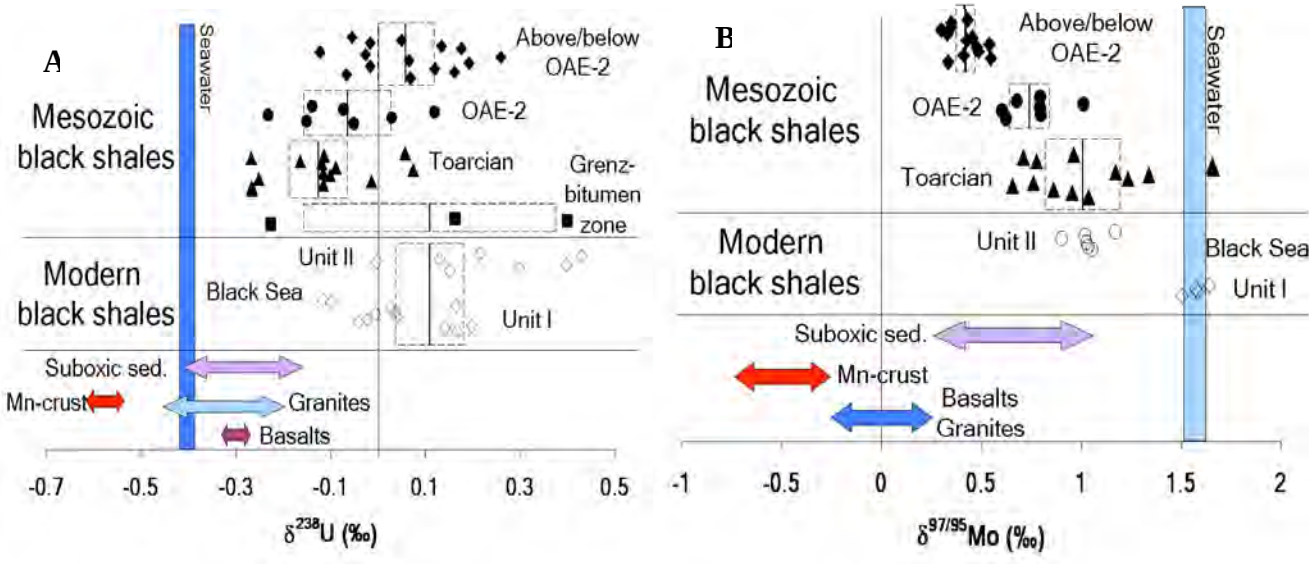

Fig. 1) Summary of U- (A) and Mo- (B) isotope compositions analysed in this study. Open symbols represent modern black shales from the Black Sea unit I and II. Solid symbols correspond to Mesozoic black shales from the Middle Triassic Grenzbitumen zone (squares), the early Jurassic – T-OAE (triangles), the Cretaceous, Cenomanian/Turonian OAE-2 (circles) as well as samples from the intervals above and below the OAE-2 (diamonds). The U isotopic compositions of basalts, granites, suboxic sediments, manganese crusts (shown as colored arrows), seawater (blue rectangle) and 6 Black Sea black shales (open diamonds and circles) were taken from Weyer et al. (2008), Arnold et al. (2004); Siebert et al. (2003) and Barling et al. (2001), respectively. The mean U and Mo isotope compositions and 2 standard errors for each group of samples are displayed as solid lines and dashed rectangles.

For the first time, U isotopes, in addition to Mo isotopes (Fig. 1A and B), were used for a quantitative approach to model the extent of anoxic environments by applying mass balance constraints. We observed a systematic shift (≈ 0.2‰) of average $\delta^{238}U$ towards lighter values for black shales deposited during both, the OAE-2 and the T-OAE compared to their modern

equivalents (Black Sea) and to Mesozoic black shales from outside the OAEs (Fig. 1). Relative to their TOC values, which crudly correlate with U isotopic composition, both OAEs display even a slightly larger shift toward lower $\delta^{238}U$ relative to the Black Sea samples (by 0.3‰). A shift of both OAEs towards lower U-isotope compositions and/or U concentrations is also evident in a plot of $\delta^{238}U$ versus U/Al (Fig.2). In this plot black shales from the Black Sea and OAE-2 show a negative-, while those from the T-OAE show a positive correlation. Molybdenum isotopes compositions of black shales from the Black Sea unit I samples display Mo isotope compositions that are indistinguishable from that of modern seawater ($\delta^{97/95}Mo$ = 1.56‰, in agreement with Barling et al., 2001 and Siebert et al., 2003). Both the OAE-2 and the T-OAE black shales display lighter compositions as those from the Black Sea. However, in contrast to U, Mo isotopes of black shales from above and below OAE-2 are even lighter than those that were deposited during OAE-2.

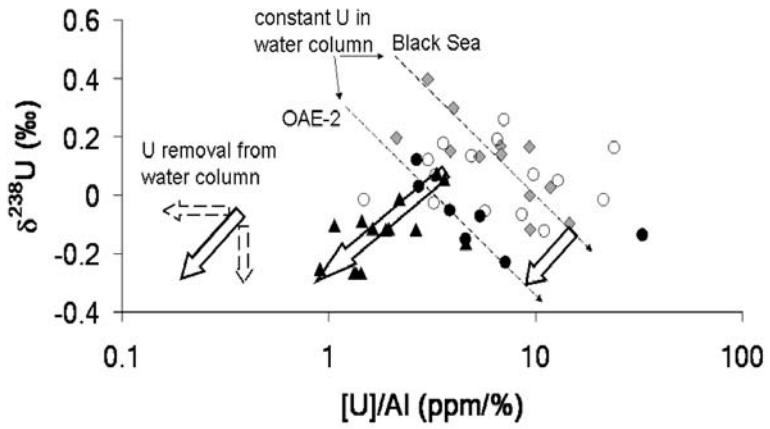

Fig.2) Plot of $\delta^{238}U$ (‰) versus U/Al (ppm/%). Toarcian OAE samples yield a positive-, while Black Sea and OAE-2 black shales yield a negative correlation.

Toarcian: Triangles
OAE2: solid circles
Above/below OAE2: open circles
Black Sea: diamonds

Discussion and Conclusions

The shift of U and Mo isotope compositions between black shales from the OAEs and modern black shales implies a light U and Mo isotopic composition of seawater during the OAE periods, if assuming a constant fractionation factor between seawater and black shales. For U isotopes, this shift can also be observed between OAE-2 black shales and those above and below OAE-2 at Demerara Rise. In contrast, Mo-isotope compositions of the latter black shales are even lighter than OAE-2 black shales. However, as Mo isotopes are very sensitive to local redox conditions (Poulson et al., 2006) and low Fe_T/Al ratios indicate less euxinic conditions during black shale deposition above and below OAE-2 compared to those during OAE-2, this shift was likely produced by a local redox change at the onset of OAE-2. The heavy isotope composition of above/below OAE-2 black shales indicates that U isotopes appear to be less sensitive to such local redox changes. Nevertheless, the shift at Demerara Rise between OAE-2 and above/below OAE-2 black shales may be cosidered as a minimum shift.

We used these findings to model the increase of anoxic sinks for U during the OAE periods using U isotope data of this study and Weyer et al. (2008) and applying mass balance constraints. According to this model, we obtained enhanced U removal into anoxic sinks during the investigated OAEs to about 60 -20/+30% compared to 10% at present day. This enhancement was on a global scale, if assuming an unrestricted connection of the sample localities to the world ocean at the time of black shale deposition. The seawater U concentration and the U ocean residence time were also affected during the OAEs, the latter decreasing to about 220 kyr compared to ~0.5 Ma (modern U residence time).

Additionally to an isotopic offset in U and Mo, T-OAE black shales show a positive-, while Black Sea and Demerara rise OAE-2 black shales a negative correlation between U isotopes and U/Al. The negative correlation was likely produced by a reservoir effect during black shale deposition. The positive correlation displayed by the T-OAE black shales may reflect coupled U depletion and isotope fractionation in the water column, which is not seen for other localities. This may be best explained if the enhancement of U burial during the T-OAE into anoxic environments occurred in an almost isolated basins, such as the European epicontinental seaway. In fact, low Mo/TOC indicate very high water mass restriction for this basin (McArthur et al., 2009). Hence, we conclude that the enhancement of anoxic environments during OAE-2, as modeled with black shale U isotope compositions, represents a global event, while that of the T-OAE more likely represents a regional event.

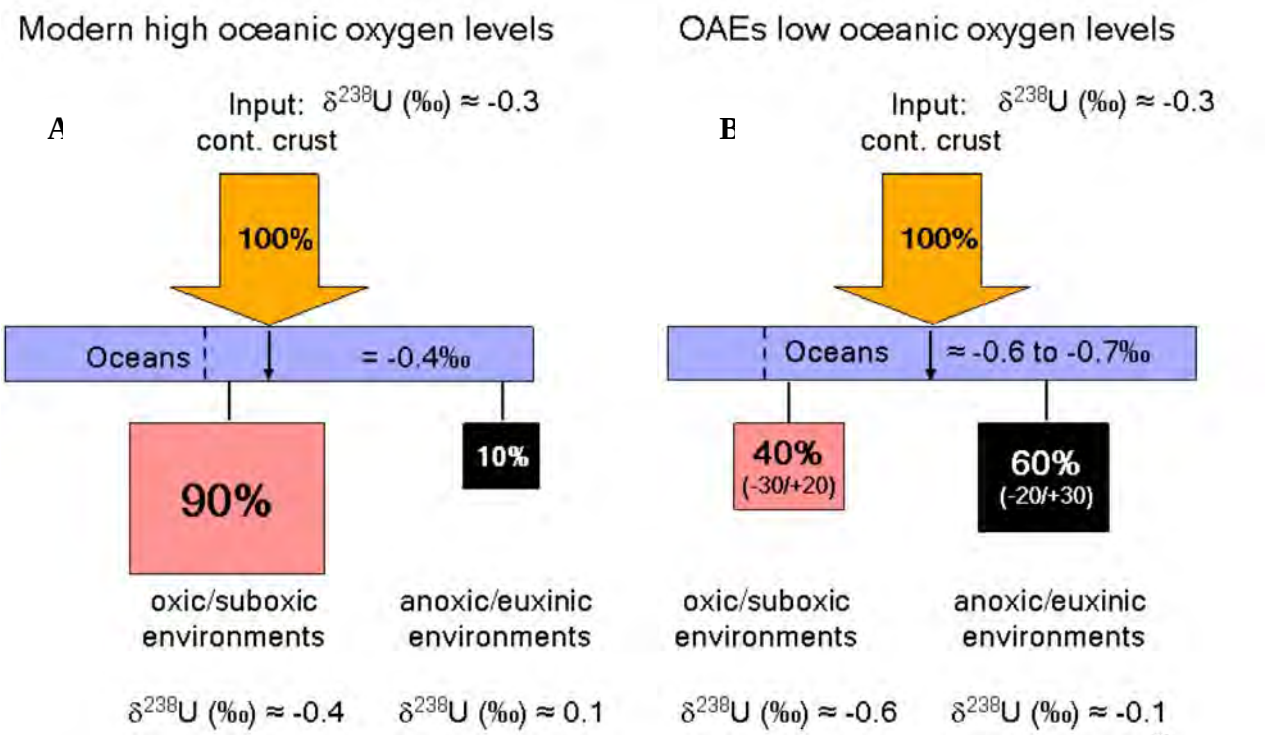

Fig. 3) Oceanic U mass balance for **(A)** modern oceans (little anoxia) and **(B)** oceans during the OAEs (enhanced anoxia). Low $\delta^{238}U$ of OAEs compared to modern black shales indicate enhancement of anoxic/euxinic sinks during the Toarcian OAE and the OAE-2 if applying mass balance constrains. $\delta^{238}U$ from seawater and oxic/suboxic settings during OAE periods were estimated assuming a constant fractionation factor between black shales and seawater (of ≈ 0.5‰) and little fractionation between seawater and suboxic sediments. $\delta^{238}U$ (‰) for the U input (continental crust; Weyer et al., 2008) was assumed to be invariant with time.

Arnold G. L., Anbar A. D., Barling J. and Lyons T. W. (2004) Molybdenum isotope evidence for widespread anoxia in Mid-Proterozoic oceans. *Science* **304**, 87-90.

Barling J., Arnold G. L. and Anbar A. D. (2001) Natural mass dependent variations in the isotope compositions of molybdenum. *Earth Planet. Sci. Lett.* **193**, 447-457.

Erbacher J., Friedrich O., Wilson P. A., Birch H. and Mutterlose J. (2005) Stable organic carbon isotope stratigraphy across oceanic anoxic event 2 of Demerara Rise, western tropical Atlantic. *Geochemistry Geophysics Geosystems* **6**, doi: 10.1029/2004PA001102.

McArthur J. M., Algeo T. J., van de Shootbrugge B., Li Q. and Howarth R. J. (2009) Basinal restriction, black shales, Re-Os dating and the Early Toarcian (Jurassic) Oceanic Anoxic Event. *Paleoceanography* (in press).

Pearce C. R., Cohen A. S., Coe A. L. and Burton K. W. (2008) Molybdenum isotope evidence for global ocean anoxia couple with perturbations to the carbon cycle during the Early Jurassic. *Geology* **36**, 231-234..

Poulson R. L., Siebert C., McManus J. and Berelson W. (2006) Authigenic molybdenum isotope signatures in marine sediments. *Geology* **34**, 617-620.

Siebert C., Nägler T. F., von Blanckenburg F. and Kramers J. (2003) Molybdenum isotope records as a potential new proxy for paleoceanography. Earth Planet. Sci. Lett. 211, 159-171.

Weyer S., Anbar A. D., Gerdes A., Gordon G. W., Algeo T. J. and Boyle E. A. (2008) Natural fractionation of 238U/235U. *Geochim. Cosmochim. Acta* **72**, 345-359.

Omphacite and other minerals in the eclogites from the Chinese Continental Scientific Drilling project (CCSD): A TEM study

W.F. MÜLLER[1], Z.Q. XU[2], F.E. BRENKER[3]

[1]Geomaterialwissenschaft, Fachbereich 11, Technische Universität Darmstadt, Schnittspahnstr. 9, 64287 Darmstadt, Germany; wmueller@geo.tu-darmstadt.de
[2]Institute of Geology, Chinese Academy of Geological Science, Bejing 100037
[3]Geozentrum der Goethe-Universität Frankfurt, Altenhöferallee 1, 60438 Frankfurt am Main, Germany

The locality of the Chinese Continental Scientific Drilling Project (CCSD) is situated at Donghai in the Sulu segment of the Dabie-Sulu ultrahigh pressure metamorphic belt (cf. Xu et al. 2005). The drill cores consist of orthogneiss, paragneiss, eclogite, ultramafic rock and minor schist. The geological setting of the area, petrography, mineral assemblages and compositions of the rocks and minerals have been described and discussed, e.g., in Xu et al. (2005), Xuexiang Qi et al. (2009), Zhang et al. (2006) and Zhu et al. (2007).

We have studied the minerals of seven eclogite samples from the main hole of the CCSD by methods of transmission electron microscopy (TEM) in order to characterise their microstructures. The goal is to contribute to the knowledge of the formation and exhumation of ultrahigh pressure eclogites, with special attention to deformation features. The samples investigated stem from 223, 318, 331, 397, 448, 452 and 584 m depths of the drilling hole. The first four samples belong to the lithologic unit 1 of Zhang et al. (2006), the last to unit 2. About 20 TEM-specimens were examined. In our TEM-study we found omphacite, amphibole, garnet, Na-rich plagioclase, quartz, K-feldspar, and phengite. The investigations concentrated on omphacite. There are three minerals in the Earth Crust and the Upper Mantle which largely control the rheological properties of their crystalline rocks: Quartz, olivine, and omphacite. The Na-Ca clinopyroxene omphacite and garnet are the defining minerals and main phases of the eclogites. The rheological properties of the eclogites are dominated by the mechanical behaviour of omphacite (Zhang & Green, 2007, and literature therein). Therefore, the plastic behaviour of omphacite is most important for the geodynamic processes of subduction and exhumation of oceanic and continental crust.

Experimental

Most of the TEM studies were carried out on a Philips CM 12 transmission electron microscope at Darmstadt, a few were made at Bayreuth with a Philips CM 20, equipped with a field emission gun. Specimens suitably thin for TEM were chiefly prepared by Ar^+ ion milling, a few by focused ion beam (FIB) and Ion Slicer. Mineral compositions were usually determined by energy dispersive X-ray spectrometry (EDX) with an EDAX Genesis system attached to the CM 12 electron microscope. The microstructures were studied by conventional bright field, dark field and weak beam imaging modes, high-resolution transmission electron microscopy and selected area electron diffraction.

TEM observations

Omphacite

The TEM-observations on omphacite of the present study are summarised in Table 1. The metamorphic peak temperatures are taken from Zhang et al. (2006). Antiphase domains (APDs) occurred in all specimens with omphacite. The APDs are a consequence of the convergent ordering of Al (Fe3+) and Mg (Fe2+) which leads to the diffusion-controlled transition of the disordered omphacite with space group C2/c to ordered omphacite with space group P2/n, which takes place below about 800 °C (depending on composition). The presence of APDs shows that the omphacites crystallised first in the disordered structure with the C2/c-lattice and the crystallisation of most, if not all omphacites took place within the phase regime of the P-phase according to the estimated peak metamorphic temperatures (e.g. Zhang et al. 2006). The chemical composition of omphacites is variable what is in agreement with Zhang et al. (2006) and Zhu et al. (2007). All EDX spectra of the omphacites contained Fe peaks. However, we refrained from calculations of the aegirine component NaFe3+Si2O6 (Ae), because we did not measure the Fe2+/Fe3+ ratio by EELS, and arbitrary partitioning would not have improved the substance of the results. The effect of adding Ae to the system is broadly similar to increasing temperature in that the substitution of Fe 3+, with an ionic radius between the radii of Al and Mg, should reduce the drive both for ordering and exsolution (Carpenter 1980). This was confirmed by Cámara et al. (1998), and they could demonstrate that the size of the APDs decreased with the Ae contents. We found that omphacites with intermediate compositions between the end-members jadeite and diopside have electron diffraction patterns with sharp and intense superstructure reflections of the type h + k odd. TEM-images, especially in dark field, show large APDs on the order of 1 µm and more (Fig. 1). Their displacement vector is **R** = 1/2[110] (Champness 1973; Phakey & Ghose 1973). Omphacites rich in the component NaAlSi2O6 (Jd) or in the component CaMgSi2O6 (Di) display small APDs on the order of about 20 to 50 nm, or less (Fig. 1). Correlation of the Jd and Di contents with the size of the APDs may suggest that the exsolution gap in the system Jd – Di (see Fig. 7 in Carpenter 1980) is slightly asymmetric, i.e., the C2/c stability field of the Di-rich pyroxenes is wider than that of the Jd-rich pyroxenes.

Indications of plastic deformation of the omphacites of our samples are not pervasive. All microstructures listed in Table 1, with exception of the APDs, are due to deformation. Faults parallel to (010), which are chain multiplicity faults (Müller et al. 2004), and deformation twin lamellae on (100) have been found only in the sample 584 m. This sample differs from the other samples also in the composition of the omphacitic pyroxenes which are richer in the Di component. It should be mentioned that faults parallel to (010) have been found in two grains, one of them had a composition rich in Di and poor in Jd and did not show reflections of the type h + k odd, i.e. it had the space group C2/c. Small angle grain boundaries (SAGBs) as observed in samples 318 m and 397 m are the result of recovery effects: dislocations reorganise by diffusion processes into arrangements with lower energy. Interesting are interactions of dislocations in SAGBs and antiphase domain boundaries (APBs) (Fig. 2). The dislocations at which the APBs end have probably the Burgers vector **b** = 1/2[110] (Fig. 3). Recrystallising grains and non-crystallographic faults (see Müller & Franz 2008) have not been seen in the CCSD omphacites.

Amphibole grains show occasionally CMFs parallel to (010) and free dislocations and SAGBs. Noteworthy are semi-coherent interfaces between amphibole and omphacite, which are made up by dislocations.

Garnet is mainly free of dislocations. However, there is one case of a SAGB formed by two sets of dislocations.

Quartz and K-feldspar: Quartz associated with K-feldspar was observed in the samples from 223 m and from 318 m. No coesite was seen. The quartz typically contains free dislocations or dislocations organised into SAGBs.

Na-rich plagioclase of a composition within the peristerite gap (≈ An12) was observed in the sample from 331 m and 584 m. It shows modulated structures with a preferential orientation about 5° tilted against (010). The wavelengths are around 20 to 25 nm. A faint tweed structure is visible in some areas of the grains.

Concluding remarks

The distinction of the lithological units according to Zhang et al. (2006) is reflected in the microstructures of their omphacites. Sample 584 m of the lithological unit 2 shows deformation twinning on (100) and planar faults parallel to (010). These defects have not been seen in the specimens from lithological unit 1. Microstructures due to deformation are not abundant in the CCSD samples from the lithological unit 1. This is especially evident for omphacite which usually carries the deformation of eclogites and shows a wealth of deformation-induced crystal defects, e.g., in the eclogites from the Lower Schist Cover and the Eclogite Zone of the Tauern Window, Eastern Alps (Müller et al., 2004; Müller & Franz 2008). The omphacites from the ultrahigh pressure metamorphic unit of Lago di Cignana, Valtournenche, Western Alps, did not show deformation twinning and CMFs are very rare, but they often contained SAGBs as indication of recovery of deformed omphacites (Müller & Compagnoni 2009). Nature and concentration of deformation-induced microstructures in samples recovered from geologic units with complex formation, subduction and exhumation histories are obviously different.

Cámara F, Nieto F, Oberti R (1998) Effects of Fe2+ and Fe3+ contents on cation ordering in omphacite. Eur. J. Mineral. 10, 889-906

Carpenter MA (1980) Mechanisms of exsolution in sodic pyroxenes. Contrib. Mineral. Petrol. 71, 289-300

Champness PE (1973) Speculation on an order-disorder transformation in omphacite. Am. Mineral. 58, 540-542

Müller WF, Compagnoni R (2009) Eclogite from the ultrahigh pressure metamorphic unit at Lago di Cignana, Western Alps: a process-oriented transmission electron microscope study. Lithos (in press), doi-10.1016/j.lithos.2008.07.013

Müller WF, Franz G (2008) TEM-microstructures in omphacite and other minerals from eclogite near to thrust zone; the Eclogite Zone – Venediger nappe area, Tauern Window, Austria. N. Jahrb. Mineral. Abh. 184/3, 285-298

Müller WF, Brenker FE, Barnert EB, Franz G. (2004) Chain multiplicity faults in deformed omphacite from eclogite. Eur. J. Mineral. 16, 37-48

Phakey PP, Ghose S (1973) Direct observation of anti-phase domain structure in omphacite. Contr. Mineral. Petrol. 39, 239-245

Xu ZQ, Yang J, Robinson PT (2005) Deep drilling in the Dabie-Sulu ultrahigh pressure metamorphic belt, China. EOS 86 (8), 77-78

Xuexiang Qi, Grimmer JC, Xu ZQ (2009) Ultrahigh-pressure texture inheritance during retrogression: Evidence from magnetofabrics in eclogites and ultramafic rocks (Chinese Continental Scientific Drilling project). Tectonophysics (in press), doi:10.1016/j.tecto.2008.09.015

Zhang J, Green HW (2007) Experimental investigation of eclogite rheology and its fabrics at high temperature and pressure. J. metamorphic Geol., 25, 97-115

Zhang Z, Xiao Y, Hoefs J, Liou JG, Simon K (2006) Ultrahigh pressure metamorphic rocks from the Chinese Continental Scientific Drilling project: I. Petrology and geochemistry of the main hole (0-2,050 m). Contr. Mineral. Petrol. 152, 421-458

Zhu Y-F, Massonne H-J, Theye T (2007) Eclogites from the Chinese continental scientific drilling borehole, their petrology and different *P-T* evolutions. Island Arc 16,508-535

Table 1. Microstructures in omphacites from the CSSD project at Donghai at different depths.

Depth of the sample Sample number	318 m B 131R	397 m B 178R	452 m B 210R	584 m B 294R
Metamorphic peak conditions	621 °C	698 °C	615 °C	726 °C
Antiphase domains: size; Jd-component	~ 50 nm; Jd69 ~ 0.5 μm; Jd57	~ 0.5 – 2 μm Jd51 – Jd55	~ 0.5 – 1 μm	~ 5 – 10 nm Jd37 – Jd42
Faults ‖ (010)	–	–	–	+
Faults ‖ (110)	–	–	–	–
Dislocations	+	+	–	+
Deformation twins on (100)	–	–	–	+
Deformation twins on (001)	–	–	–	–
Small-angle grain boundaries (SAGB)	+	+	–	–
Interaction APBs–SAGB	–	+	–	–
Recrystallising grains	–	–	–	–
Non-crystallographic faults	–	–	–	–

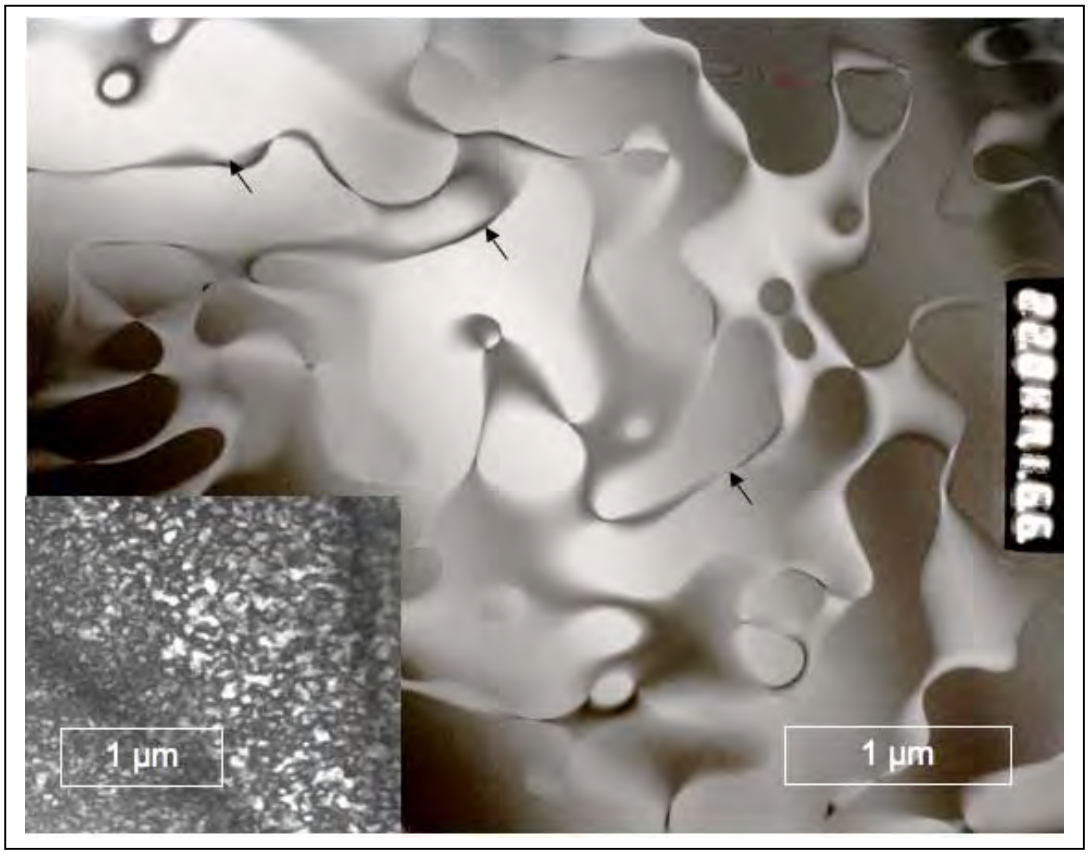

Fig. 1. Antiphase domains (APDs) and antiphase domain boundaries (arrows) in omphacite (Jd 57). TEM dark field micrograph with g = 101 as operating beam. Insert: Small APDs (~ 50 nm) in Jd-rich area (Jd 69) of the same grain. Sample 318.

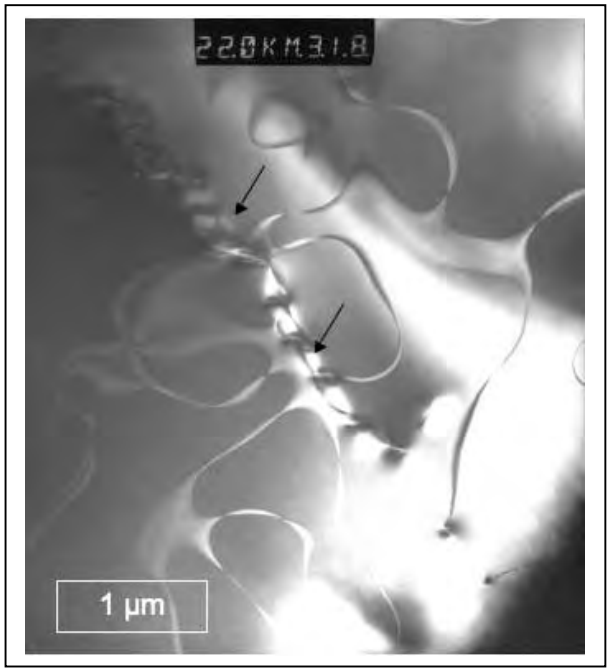

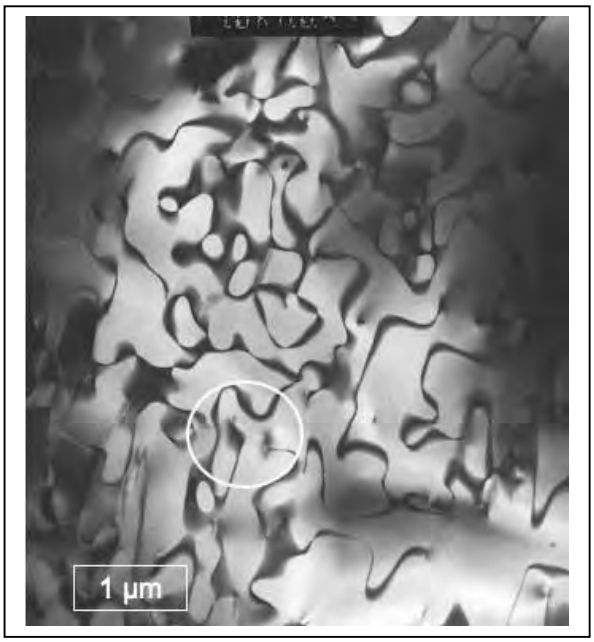

Fig. 2 (left) and Fig. 3 (right). Omphacites from sample 397 m. Fig.2: Small-angle grain boundary (arrow) and interaction of its dislocations with the antiphase domain boundaries. Dark field with g = 050. Fig. 3: A few antiphase domain boundaries end at dislocations (circled). Dark field with g = 10-1.

WI Sea surface characteristics in the North Atlantic during the Pleistocene and Pliocene; a biomarker approach

B. DAVID. A. NAAFS[1,2]*, RUEDIGER STEIN[1], GERALD H. HAUG[2,3]

[1]Alfred-Wegener-Institute for Polar and Marine Research, Columbusstrasse, 27568 Bremerhaven, Germany (*corresponding author: david.naafs@awi.de)
[2] Universität Potsdam, Institut für Geowissenschaften, 14476 Golm, Germany
[3] ETH Zürich, Geologisches Institut, Universitätstrasse 6, 8092, Zürich, Switzerland

During the last few glacial cycles, the region of the North Atlantic Ocean was sensitive to changes in Northern Hemisphere ice sheet dynamics [e.g., McManus et al., 1999]. An important feature in North Atlantic climate was the location of the Polar Front, which changed over time and might have had a different location during different glacial periods [Calvo et al., 2001], because across and directly south of the Polar Front a sharp gradient in sea surface temperature (SST) was present. We used material from IODP Sites U1308, U1313 and U1314 to make a high-resolution (~ 4 kyr) reconstruction of sea surface characteristics in the North Atlantic during the last 1 Myr. To reconstruct SSTs we made use of the organic biomarker proxy $U^{k'}_{37}$, analyzed by a newly developed method using GC/TOF-MS suited for large sample batches [Hefter, 2008]. Besides reconstructing SSTs, total alkenone and long-chain n-alkane abundance provided information about marine productivity and terrestrial input, respectively. Sites U1308 and 1313 are re-drills of the old DSDP Sites 609 and 607, respectively, and together with the more northern located Site U1314 gave us the possibility to reconstruct a transect in sea surface characteristics between 41°N and 56 °N.

Results from Site U1313 show that SSTs varied at a regular glacial/interglacial pattern during the last 1 Myr with typical glacial SSTs of around 12 °C, compared to interglacial temperatures of 18 °C. At Site U1313 glacial periods are characterized by increased TOC values and long-chain n-alkanes and alkenone abundance, suggesting an increase in (marine) productivity as well as terrestrial input. In addition, SSTs at Site U1313 during MIS 16 show an interesting pattern of gradual warming by 9 °C between 611 and 670 ka, resembling the behaviour of mid-latitude $U^{k'}_{37}$ based SSTs during MIS 6 [Schneider et al., 1999]. This while MIS 16 is the period when the first true “100-kyr” glacial cycle led to an expansion of ice sheets in the Northern Hemisphere. We suggest that this warming during ice sheets expansion is affiliated to a change in position of the Polar Front during MIS 16 and ongoing research will provide information about the SST patterns of the two other IODP Sites during MIS 16. First results from the other two IODP Sites show that the location of the Polar Front, determined as the place where a strong gradient in SSTs between the three Sites existed, changed significantly over time during the last 0.5 Myr. At the same time, the timing of marine productivity maxima followed the northward migration of the Polar Front at the end of each glacial cycle. In addition, a low-resolution SST record spanning the last 3 Myrs from Site 1313 shows that surface waters in the North Atlantic cooled by around 5 °C between 3 and 1.4 Ma and remained stable afterwards. At last, glacial/interglacial variability during MIS G6/G7 at 2.7 Ma, meaning; before the intensification of Northern Hemisphere glaciation [Haug et al., 2005], was 5 °C.

[1] McManus, J.F., D.W. Oppo and J.L. Cullen, 1999. A 0.5-Million-Year record of millennial-scale climate variability in the North Atlantic. Science, 283, pp 971-974
[2] Calvo, E., J. Villanueva, J.O. Grimalt, A. Boelaert and L. Labeyrie, 2001. New insights into the glacial latitudinal temperature gradients in the North Atlantic. Results from $U^{k'}_{37}$ sea surface temperatures and terrigenous inputs. EPSL, 188, pp. 509-519
[3] Hefter, J., 2008. Analysis of Alkenone Unsaturation Indices with Fast Gas Chromatography/Time-of-Flight Mass Spectrometry. Anal. Chem., 2008, *80* (6), pp 2161–2170
[4] Schneider, R.R., P.J. Müller and R. Acheson, 1999. Atlantic alkenone sea-surface temperature records. In: F. Abrantes, A.C. Mix (eds.), Reconstructing Ocean History: A Window into the Future, Plenum, New York, pp. 33-55
[5] Haug, G.H., et al., 2005. North Pacific seasonality and the glaciation of North America 2.7 million years ago. Nature, 433, pp. 821-825

Constraints on rhyolite magma genesis, Yellowstone hotspot: evidence from mineral thermometry, Nd and O isotopes, and U-Th-Pb zircon geochronology

B. NASH[1], H. CATHEY[1], J.VALLEY[2], C. ALLEN[3], R. ALMEEV[4], AND F. HOLTZ[4]

[1]Department of Geology, University of Utah
[2]Department of Geosciences, University of Wisconsin
[3]Research School of Earth Sciences, Australian National University
[4]Institute of Mineralogy, Leibniz University of Hannover

Over the past 16 Ma the Yellowstone hotspot has produced an enormous volume of rhyolite. The silicic magmas originate from the interaction of mantle basalt with Precambrian continental crust. However, the precise nature of the crustal source material, depth of magma formation, volatile content, and the complex evolution of individual eruptive centers are not well understood. The proposed ICDP drilling program for the central Snake River Plain is designed to provide critical information on the origin and evolution of these large volume silicic systems.

The Bruneau-Jarbidge eruptive center of the central Snake River Plain produced at least 10 large volume "supereruptions" between 12.7 and 10.5 Ma that constitute the Cougar Point Tuff (Cathey and Nash, 2004). The explosive episode was followed from ~11.2 to 8.1 Ma by multiple rhyolite lava flows with volumes of <10 km^3 to 200 km^3 each that represent the waning stages of silicic volcanism at a major eruptive center of the hotspot track. Estimates of the cumulative volume of the multiple members of the Cougar Point Tuff and subsequent rhyolite lava flows range from $7x10^3$ km^3 to more than $1x10^4$ km^3.

Pyroxene and quartz thermometry yield temperatures in the range 900-1000ºC, with a trend towards increasing temperature as the system evolves through time. This trend is consistent with whole rock compositions becoming generally less differentiated as the system evolves. Neodymium isotopes in glass (Nash et al., 2006) and whole rock samples (Bonnichsen et al., 2008) indicate an increase in the contribution of the mantle component to the magmas over the interval from 12.7 to 8 Ma (ε_{Nd} -8.0 to -6.3), consistent with the trend towards the highest ε_{Nd} values recorded in hotspot rhyolite in contemporaneous ashflow eruptions in the Twin Falls region more than 100 km to the east (ε_{Nd}= -5.9, -5.7) (Nash et al., 2006). These isotopic ratios preclude significant contributions from Archean basement material to the magma source (ε_{Nd} = -25 to –50) consistent with an upper crustal protolith. However, the trends are not unidirectional, thus providing evidence for open system behavior in the complex magma reservoir sysem.

Oxygen isotopes in quartz (laser fluorination) and from *in situ* analyses by ion microprobe of 111 zircons indicate that the quartz and 96 % of the zircons grew in low $\delta^{18}O$ melts. U-Th-Pb dating of the same individual zircons yield crystallization ages similar to eruption ages for all but two zircons, indicating they are not inherited from earlier low $\delta^{18}O$ environments. More than half the zircons are zoned by $\geq$ 0.5‰ and indicate that multiple discrete low $\delta^{18}O$ sources were involved in magma generation for most units. Average zircon rim values track those measured in quartz, and are consistent with quartz-zircon isotopic equilibrium at pre-eruptive magma temperatures. First order estimates of the average $\delta^{18}O$ of the total eruptive volume range from 2.7 to 3.2 ‰. These values confirm the discovery of the largest low $\delta^{18}O$ silicic volcanic province yet known (Boroughs et al., 2005), and require very large volumes (>10^4 km^3) of hydrothermally altered upper crustal source material for magma generation. The experimental investigations of Almeev et al. (2009) will help to resolve critical questions about the pre-eruptive conditions of pressure, temperature and volatile content of these large volume, low $\delta^{18}O$ magmas.

Almeev, T., Holtz, F., Kuschel, L., Cathey, H., and Nash, B. (2009) Pre-eruptive conditions of the Bruneau-Jarbidge Rhyolite, Snake River Plain-Yellowstone hotspot track. (This program).

Bonnichsen, B., Leeman, W., Honjo, N., McIntosh, W., and Godchaux, M., (2008) Miocene silicic volcanism in southwestern Idaho: geochronology, geochemistry, and evolution of the central Snake River Plain. Bulletin of Volcanology, 70, 315-342.

Boroughs, S., Wolff, J., Bonnichsen, B., Godchaux, M., Larson, P. (2005) Large volume, low-$\delta^{18}O$ rhyolites of the central Snake River Plain, Idaho, USA. Geology, 33, 821-824.

Cathey, H., and Nash, B. (2004) The Cougar Point Tuff: Implications for thermochemical zonation and longevity of high-temperature, large-volume silicic magmas of the Miocene Yellowstone hotspot. *J. Petrology*, 45, 27-58.

Nash, B., Perkins, M., Christensen, J., Lee, D-C., and Halliday, A., (2006) The Yellowstone hotspot in space and time: Nd and Hf isotopes in silicic magmas. Earth and Planetary Science Letters, 247, 143-156.

Fractionation processes of Ca isotopes in interstitial waters of marine sediments

C. OCKERT[1], B.M.A. TEICHERT[2], S. KAUFHOLD[3], N. GUSSONE[1]

[1]Institut für Mineralogie, Corrensstraße 24, 48149 Münster
[2]Geologisch-Paläontologisches Institut, Corrensstraße 24, 48149 Münster
[3]Bundesanstalt für Geowissenschaften und Rohstoffe, Stilleweg 2, 30655 Hannover

Isotope ratios of the element Calcium (Ca) have attracted the attention of the paleoceanographic community since their use as paleo-thermometer and as reconstruction tool for the oceanic Ca-budget have been demonstrated (cf. Skulan et al 1997, Zhu and MacDougall 1998). But until now it has not been investigated in detail in which way processes during fluid-solid interactions in the sediments potentially affect the proxy signal. Diagenetic processes like dissolution of calcareous nannofossils, release of organically bound Ca, ion exchange processes with clay minerals, Ca-complexation with carbonate or sulfate ions as well as Ca release from volcanic material might affect the Ca isotope signature in the pore fluids and thus have the potential to alter the proxy signals of carbonate shells in the sediment.

To investigate Calcium geochemistry in pore waters of marine sediments, sites from Expedition 303 were chosen because here different diagenetic processes influence Ca concentration patterns. Site U1308 is the first site investigated in this study. This site is located in the North Atlantic, south-east of the Charlie Gibbs Fracture Zone, and reveals a lithology composed of mainly nannofossil ooze (88 %) and silty clay (12 %). The terrestrial clay component decreases with depth and is entirely absent below 255 mbsf (Channell et al., 2006). This implies that below this depth the sediment is entirely composed of nannofossil ooze with an average calcium carbonate content of 91 wt%. On-board interstitial water analyses revealed a distinct Ca concentration profile with depth, with seawater concentration at the top of the core decreasing to a minimum of about 7 mmol/l at 114 mbsf and then again increasing to about 16 mmol/l at the bottom of the core (Channell et al., 2006). The increase in Ca concentration at the bottom of the core could be caused by reaction with the underlying oceanic crust or by extensive dissolution of calcareous nannofossils.

In contrast to the Ca concentration, the $\delta^{44/40}$Ca (normalized to SRM NIST 915a) shows a steady decrease from 1.62 ‰ at the top of the core to 0.46 ‰ at the bottom. A mixing diagram (Ca isotopy versus 1/Ca concentration) reveals that at least two different fluid sources are present. The pore fluid at intermediate depth is characterised by a Ca concentration of about 7 mmol/l and a Ca isotopy of 0.77 ‰. This fluid mixes with seawater in the shallow part of the core. From below a deep sourced fluid characterised by high Ca concentration (16 mmol/l) and light Ca isotopy (0.46 ‰) rises upwards. Another important observation is the negative correlation of ammonium concentration and Ca isotopy with depth. Teichert et al. (accepted) have observed the same relationship and attributed it to the displacement of isotopically light Ca from sediment-particle surfaces by ammonium that is released during organic matter remineralization.

In addition to Ca isotope measurements of porewater samples from Site U1308, first experiments on Ca isotope fractionation during adsorption of Ca on pure clay minerals have been conducted. Montmorillonite was cleaned from adsorbed Ca and then loaded with Ca of a known isotopic composition.

Channell, J.E.T., Kanamatsu, T., Sato, T., Stein, R., Alvarez Zarikian, C.A., Malone, M.J., and the Expedition 303/306 Scientists (2006) Proceedings of the Integrated Ocean Drilling Program, 303/306: College Station TX (Integrated Ocean Drilling Program Management International, Inc.). doi:10.2204/iodp.proc.303306.2006

Teichert, B.M.A., Gussone, N., Torres, M.E. (accepted) Controls on Calcium Isotope Fractionation in Sedimentary Porewaters. Earth and Planetary Science Letters.

Skulan, J., DePaolo D. J., and Owens T. L. (1997) Biological control of calcium isotopic abundances in the global calcium cycle. Geochim.Cosmochim. Acta 61(12), 2505-2510.

Zhu, P. and Macdougall D. (1998) Calcium isotopes in the marine environment and the oceanic calcium cycle. Geochimica et Cosmochimica Acta 62(10), 1691-1698.

Living and fossil ostracode species assemblages from the Yucatán Península as indicators of environmental change

-a contribution to the Lago Petén Itzá Drilling Project-

L. PÉREZ [1], B. SCHARF [1], A. SCHWALB [1]

[1] Institut für Umweltgeologie, Technische Universität Braunschweig, Braunschweig, Germany

Ostracodes (microscopic bivalved crustaceans, usually 0.4 to 3 mm long, with low-Mg calcite valves) are being used as a proxy for paleoenvironmental and paleoclimate reconstruction from Lago Petén Itzá, Guatemala, sediment cores covering the past approximately 85 kyr (Hodell et al., 2008, Pérez et al. 2008). Ostracodes are powerful tools for paleoenvironmental reconstructions because they are sensitive to environmental parameters such as conductivity, pH, temperature, water depth and sediment types. Because the ecology of individual species is poorly known but crucial for the interpretation of fossil species assemblages, we have established a modern data set in addition to the analysis of fossil species from Lago Petén Itzá (Pérez et al. 2009a). Lago Petén Itzá is 20 km long and 3-4 km wide, located ~ 110 m above sea level, and it is the deepest lake in the Yucatán Península with a maximum depth of 165 m (Anselmetti et al., 2006; Hodell et al., 2008).

In order to cover a maximum of individual species, we sampled a total of 63 aquatic environments across a south-northwest precipitation gradient in the Yucatán Península. Sampled sites included lakes, sinkholes, brackish water lagoons, rivers, and lakes in the Guatemalan highlands (Figure 1A).

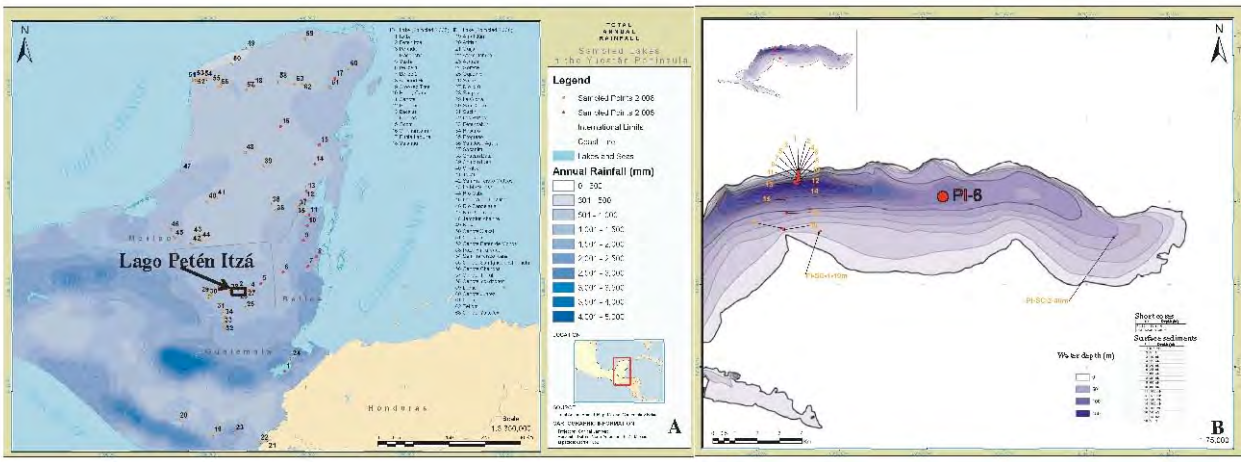

Figure 1. A. Precipitation map of the Yucat‡n Pen'nsula showing the 63 sampling sites; B. Bathymetry of Lago PetŽn Itz‡ and location of surface sediments samples, short cores and long core PI-6.

Water samples and surface sediments were analyzed for geochemistry. Ostracodes from each locality were selected from sediments and identified. In Lago Petén Itzá, surface sediment samples were retrieved at different water depths from the northern to the southern littoral zone. Samples were collected every 5 m from 5 to 30 m water depth, and every 20 m to a max. depth of 160 m (Figure 1B). For the reconstruction of the recent environmental history of the lake we retrieved two short cores (PI-SC-1-10m and PI-SC-2-40m) at 10 and 40 m water depth. Long core PI-6 (70 m long) was collected with the the drilling platform GLAD 800 from a water depth of ~ 70 m. One cm-thick slices of sediment were taken for analysis of ostracode species assemblages every 20 cm. Here we present first results for the period of the Deglacial and Last Glacial Maximum.

Our data set includes mostly oligotrophic to mesotrophic lakes and one eutrophic lake, Lago de Amatitlán, Guatemala (Bugja, 2009). Lake waters are slightly basic and dominated by HCO_3^-, SO_4^{-2}, and Cl^-. Conductivity shows an overall trend with highest values in the north, and lower values in the south, reflecting the latitudinal precipitation-evaporation gradient. Lakes close to the coast showed high Cl^- values, and lakes in the central and northern Yucatán were dominated by sulfates. Lake waters in southern Yucatán and close to the coast have low $\delta^{18}O$ values typical of areas with high effective moisture (precipitation-evaporation). $\delta^{18}O$ range from -4.13 to +4.35 and the $\delta^{13}C$ values from -22.06 ‰ to +2.38 ‰ (Pérez et al. 2009a).

Eighteen ostracodes species were identified. Overall, the fauna of Yucatán is similar to the fauna of southwestern Florida. Results show that the distribution of ostracodes in the region is influenced by the lake water chemistry (Table 1). Lakes waters dominated by sulfate and chlorides show the highest ostracode diversity. *Physocypria globula* shows a tolerance for anoxic waters and was collected living at a maximum water depth of 40 m. *Heterocypris punctata* and *Strandesia intrepida* were only found in shallow water and vegetated areas. *Fabaeformiscandona* sp. is characteristic of organic rich sediments. *C.*

okeechobei and *D. stevensoni* are typical freshwater ostracodes but were also found in brackish waters.

Table 1. Lake water types in the Yucat‡n Pen'nsula and modern fresh and brackishwater ostracode species. Cosmopolitan species comprise the most widely distributed species with high hydrochemical tolerance.

$Ca\text{-}Mg\text{-}SO_4$	Na-Cl	Na-Cl Ca-Mg-SO_4	$Ca\text{-}Na\text{-}HCO_3$	$Ca\text{-}HCO_3$ Ca-Mg-SO_4 Ca-Mg-HCO3-SO_4	$Ca\text{-}HCO_3\text{-}SO_4$	Ca-Mg-HCO_3 Ca-HCO_3 Ca-Mg-HCO_3-SO_4	Ca-Mg-HCO_3-SO_4	Cosmopolitan species
-Cyprideis salebrosa - Perissocytheridea cribosa	*-Eucypris serrato-marginata - Loxoconcha matagordensis* cf.	*- Thalassocypria vavrai*	*-Physocypria xanabanica - Stenocypris malcolmsoni*	*-Strandesia intrepida*	*-Potamocypris* sp.	*-Physocypria globula*	*-Cypretta brevisaepta* cf.	*-Cytheridella ilosvayi - Cypridopsis okeechobei -Darwinula stevensoni - Fabaeformiscandona* sp. *-Heterocypris punctata - Limnocythere opesta - Physocypria gibbera*
Brackishwater ostracodes			Freshwater ostracodes					

Guatemalan Highland lakes are characterized by *Chlamydotheca colombiensis*, *C. okeechobei*, *C. ilosvayi*, *D. stevensoni*, *Eucypris* sp., *Fabaeformiscandona* sp., *Ilyocypris* sp., *Limnocythere* sp., *Metacypris* sp., *P. globula*, *S. malcolmsoni*, *Thalassocypria* sp. 1 and sp. 2. First results show that the ostracode fauna of the Guatemalan and Colombian Highland lakes share similar species (Lorenschat 2009).

Sediment surface samples collected along the water-depth transect in Lago Petén Itzá show higher abundance and diversity of ostracodes down to a depth of 40 m. This correlates with the position of the thermocline and a decrease in oxygen concentration below 40 m. *H. punctata* and *S. intrepida* were only found in the littoral zone. Thus, they are characteristic of shallow waters with abundant macrophytes and serve as indicators for lake level low stands (Pérez et al. 2009b). Short cores from Lago Petén Itzá reveal that ostracodes have been abundant and diverse in the last ~ 455 years. Seven species were found in short core PI-SC-1-10m (Figure 2). Adult carapaces that represent a living fauna are more abundant since ~ 1750 A.D. Higher contents of organic matter (characterized by darker sediments from 0 to 6 cm and 20 to 24 cm) as result of human population growth and heavy rains in the 1940's in Flores, Petén, correlate well with an increase in ostracode abundance. Six species were found in short core PI-SC-2-40m. Sediments are homogeneous and consist of dark olive gray silty clays. The most abundant species in the last ~ 145 years has been *P. globula*. First results show ostracode abundance to be related to both water depth and Total Organic Carbon (TOC)(Bugja, 2009; Pérez et al. 2009a).

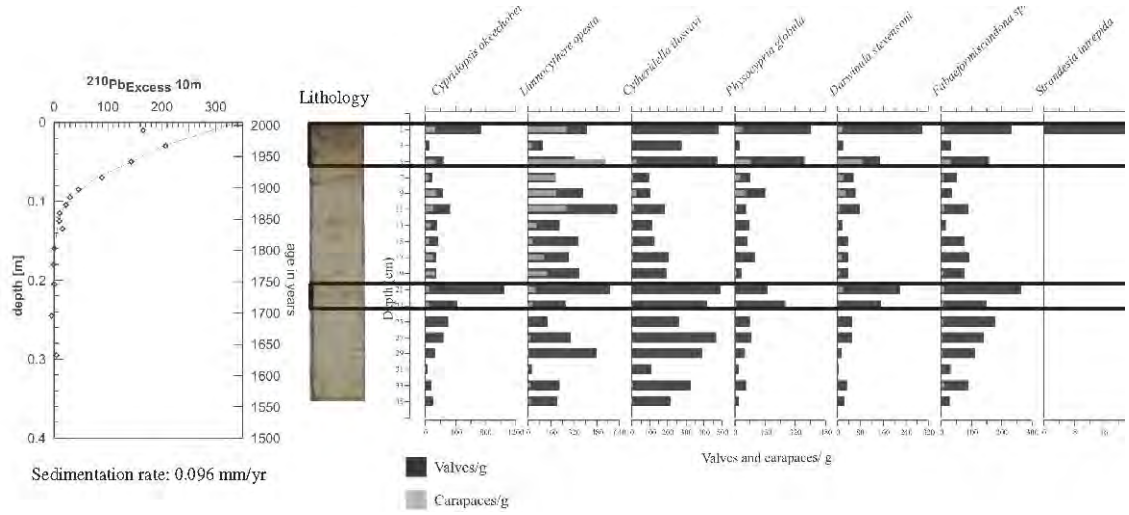

Figure 2. Ostracodes species assemblages in short core PI-SC-10m-1 retrieved from Lago PetŽn Itz‡, Guatemala. Sediments consists of light olive gray and yellowish silty clays (bars 0-6 cm and 20-24 cm).

Seven species were identified in the long core PI-6 (section from 1481 to 2532.2 cm). This section includes the Last Glacial Maximum (between ~23 and 18 ka) and the early Deglacial (Figure 3). The fossil ostracode species assemblages can be divided into three zones. Zone 1 (Last Glacial Maximum, LGM) is characterized by only two benthic ostracodes species (*Fabaeformiscandona* sp. and *D. stevensoni*) that seem to prefer sediments without macrophytes. According to Hodell et al. 2008, the LGM was a cold and wet period characterized by the deposition of clay rich sediments. Pollen analysis indicates that the vegetation consisted of a montane pine-oak forest typical of relatively cool and moist conditions. Zones 2 and 3 (Deglacial, 18 to 11.6 ka) are characterized by ostracode species that are known to prefer habitats with macrophytes indicating lake level low stands. Species include *H. punctata*, *S. intrepida* and *L. opesta*. This is consistent with the presence of gypsum layers suggesting recurrence of drier periods. The highest abundances of ostracodes are found in the early Deglacial (1950 cm depth). Zone 4 represents the living ostracodes at a water depth of 60 m for comparison. Today, *P.*

globula is the dominant species that tolerates anoxic waters. These preliminary results from the long core show that ostracodes have a high potential and can be use to reconstruct lake level changes in Lago Petén Itzá.

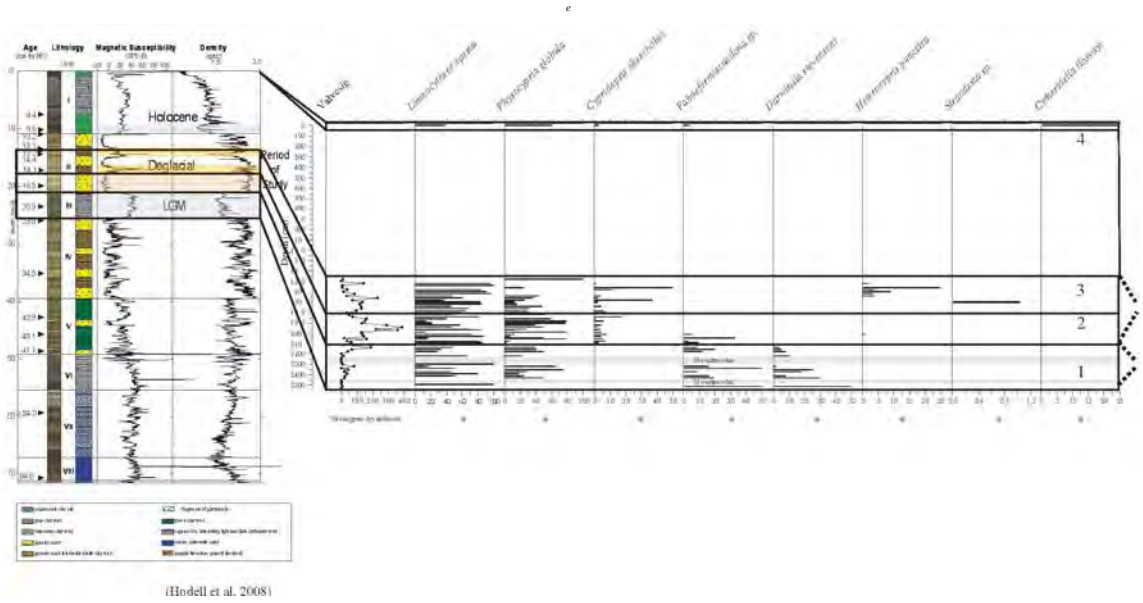

Figure 3. Sedimentology, magnetic susceptibility and density (Hodell et al., 2008) and Ostracodes species assemblages from the LGM and Deglacial of core PI-6.

Acknowledgements:
We would like to thank D. Hodell, M. Brenner, F. Anselmetti, J. Curtis, the PISDP sampling party, R. v. Geldern, M. Palmieri, M. Dix, CONAP, SRE, CONAPESCA, G. Islebe (ECOSUR-Chetumal), and the Universidad del Valle de Guatemala for their support during our field trip.

Anselmetti, F.S., D. Ariztegui, D. A. Hodell, M. B. Hillesheim, M. Brenner, A. Gilli, J. A. McKenzie, and A. D. Mueller, 2006. Late Quaternary climate-induce lake level variations in Lake Petén Itzá, Guatemala, inferred from seismic stratigraphic analysis. Palaeogeography, palaeoclimatology, palaeoecology, 230: 52-69.

Bugja, R., 2009. Hydro-und Sedimentchemie aquatischer Habitate auf der Halbinsel Yucatán. Diplomarbeit. Institut für Umweltgeologie, Technische Universität Braunschweig, Germany (in prep.)

Hodell, D. A., F. S. Anselmetti, D. Ariztegui, M. Brenner, J. H. Curtis, A. Gilli, D. A. Grzesik, J. Guilderson, A. D. Müller, M. B. Bush, A. Correa-Metrio, J. Escobar, S. Kutterolf, 2008. A 85-ka record of climate change in lowland Central America. Quaternary Science Reviews, 27: 1152-1165.

Lorenschat, J., 2009. Artenvergesellschaftungen von Ostracoden moderner aquatischer Habitate im südlichen Guatemala als Indikatoren rezenter Umweltänderungen. Diplomarbeit. Institut für Umweltgeologie, Technische Universität Braunschweig, Germany (in prep.)

Pérez, L., G. Alfaro, M. Palmieri, M. Dix, M. Maldonado, G. Islebe, B. Scharf, and A. Schwalb, 2008. Paleoclima y Paleoecología de las tierras bajas del norte de los neotrópicos: Investigación limnológica y extracción de sedimentos del lago Petén Itzá (Guatemala). Revista de la Universidad del Valle de Guatemala, 18: 65-83

Pérez, L., B. Scharf, and A. Schwalb, 2009a. Modern Ostracoda (Crustacea) from lacustrine surface sediments and aquatic environments of the Yucatán Península (Guatemala, Mexico and Belize). (In prep.) Pérez, L., B. Scharf, and A. Schwalb, 2009b. The ecology of the ostracodes (Crustacea) from Lago Petén Itzá, Guatemala. (In prep.)

Fluid composition and Palaeofluid evolution in veins of the Outokumpu drilling site, Finland

C. PIRIBAUER[1], F. M. MEYER[1], S. SINDERN[1], T. W. VENNEMANN[2], W. PROCHASK[3]

[1]Institute of Mineralogy and Economic Geology, RWTH Aachen University, Wüllnerstraße 2, D-52056 Aachen, piribauer@iml.rwth-aachen.de
[2]Institut de Minéralogie et Géochimie, Université de Lausanne, BFSH-2, CH-1015 Lausanne
[3]Department Angewandte Geowissenschaften und Geophysik, Montanuniversität Leoben, 8700 Leoben

Paleofluids in the Outokumpu Deep Drill core are characterized by high salinities and high homogenization temperatures in excess of 330 °C. Fluid inclusions in addition to an aqueous phase contain also gaseous phases such as CO_2 und CH_4. Cationic radii of the dissolved salts are higher than seawater with Li/Na ratios in deeper parts of the hole indicating the influence of magmatic water. Stable isotope (δD, $\delta^{18}O$) signatures point to a metamorphic origin of the paleofluids. Deep ground waters in the Outokumpu crystalline basement deviate significantly in their stable isotope ratios from fluid inclusions plotting to the left of the global meteoric water line in a δD - $\delta^{18}O$ diagram. This suggests that they may have formed as a mixture of meteoric and saline waters. In addition, Cl/Br and Na/Br ratios point to chemical exchange with serpentinite host rocks of the Outokumpu Formation. Many models have been proposed to account for the enhanced salinity of deep ground waters and the shift in the stable isotopes, but our data gathered so far indicate that the saline fluids are derived primarily through water–rock interaction. The role of fluid inclusions as important contributors to the saline fluids is unsupported so far.

Geologically, the drill site is located within the Outokumpu allochthon in eastern Finland which represents a 1 - 5 km thick remnant of folded and imbricated overthrust terrane, dominated by 1.92 - 1.90 Ga old metaturbitites, emplaced over a basement complex consisting of late Archean gneisses and a thin Palaeoproterozoic cover. The lithologies comprise (1) metasediments, now metamorphosed to amphibolite facies mica schists and black schists; and (2) serpentinites, skarns and sulphide rich black schists, commonly referred to as the Outokumpu Rock Association (ORA) (Gaál et al., 1975; Koistinen, 1981; Park, 1988).

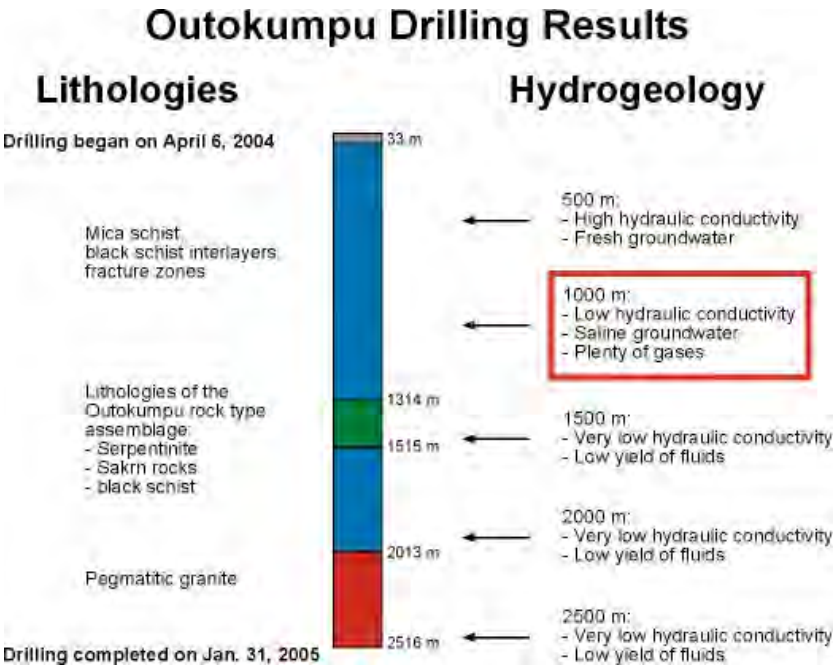

Fig. 1: Schematic illustration of the drill core (source GTK)

The base of the sequence (2516 - 1515 m) is composed of amphibolite facies metasediments, which are locally intruded and crosscut by pegmatite dykes. The metasediments are overlain by serpentinites, skarns and black schists of the Outokumpu Rock Association (ORA), which can be detected until 1314 m. This is followed by a sequence of metasediments, which mainly consists of biotite-mucovite schists, biotite schists, black schists and biotite-rich gneisses. The uppermost 33 m of the drill core are made up of sand and silt.

In all lithologies, except the black schists, fluid inclusion-bearing quartz and carbonate veins can be found. The primary, pseudosecondary and secondary fluid inclusions contain up to three different phases: vapour phase and/or liquid phase and partly a solid phase as accidentally trapped crystals. Within the veins fluid inclusions occur on intragranular trails, on

transgranular trails, in clusters, or as single inclusions in the veins. Fluid inclusions within the carbonate veins are smaller than 5 µm and cannot be analysed with microthermometry or LA-ICP-MS.

Three different types of fluid inclusions can be distinguished within the quartz veins:

Typ 1: LV → H_2O-NaCl
Typ 3: LV → H_2O-$CaCl_2$-NaCl
Typ 2: L → CO_2

CO_2 bearing, type 3, inclusions show a T_m(ice) between -57° and -60°C, which suggests the presence of another gas phase, most likely CH_4. They show different homogenisation Temperatures T_h(CO_2 LV→L) between -11°C and +6°C. The homogenisation carries out into the liquid phase.

Type 1 fluid inclusions show a T_m between -2 and -22°C, which corresponds to a salinity of 2 – 22 mass% NaCl equiv.. The size of the inclusions differs between <2 µm and maximum 40 µm. The T_h(LV→L) of the type 1 fluid inclusions plot between 100 and 400 °C. More detailed information about the compositions provides the analysis with the LA-ICP-MS. The measurements show, in addition to Na also the presence of minor quantities of Ca and Mg. The trend shown in Figure 2 suggests the mixing of a colder NaCl-poor fluid with a hotter higher saline fluid.

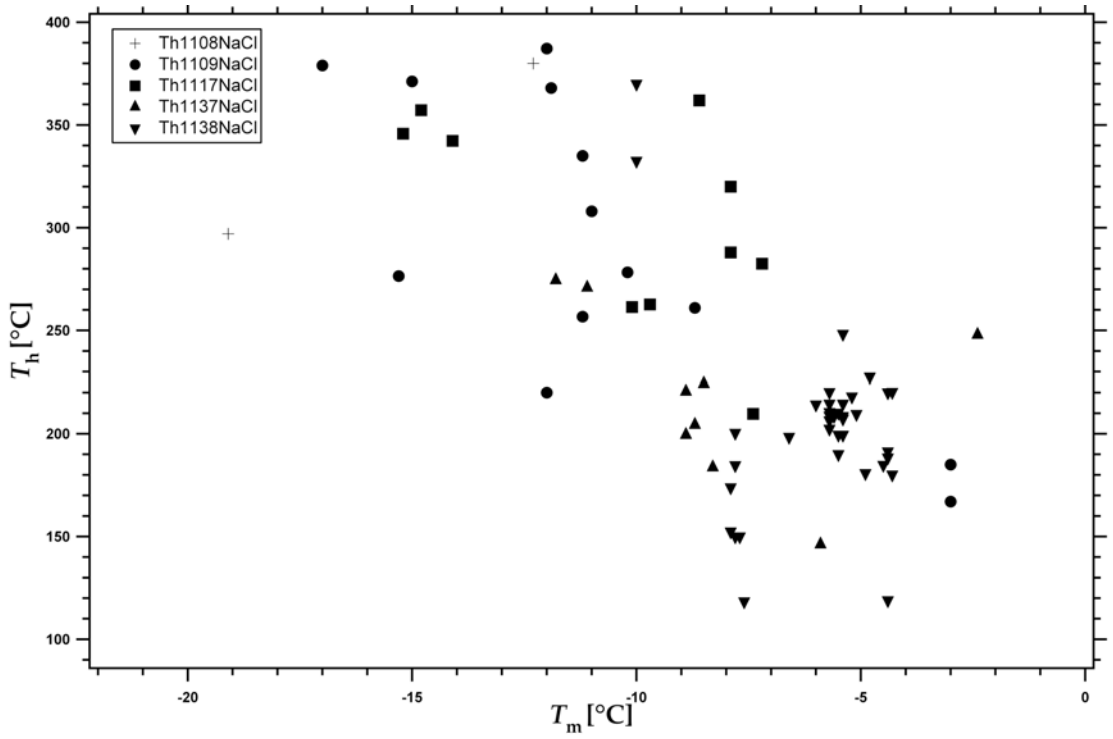

Fig. 2: T_m versus T_h of type 1 fluid inclusions

Type 3 fluid inclusions show a lower eutectic melting (T_E) than type 1 fluid inclusions. T_E is around -60 °C, which suggests the presence of $CaCl_2$. The analyses with the LA-ICP-MS show the presence of Ca, Na and K within the fluid. The Ca/Na ration is 3,18 and the K/Na ration show a value of 0,16.

The results of the crush-leach analyses show cation ratios of Ca/Na (0,2551 – 0,9484 molar), K/Na (0,0968 – 0,2044 molar) Li/Na (0,0007 – 0,0847 molar) und Mg/Na (0,0241 – 0,3438 molar) which are partly higher than seawater (Ca/Na 0,0218; K/Na 0,0213; Li/Na 0,0001; Mg/Na 0,1130). The Li/Na ratio rises in the vicinity to the deeper pegmatites, which suggests an influence of magmatic water.

Within the Cl/Br-Na/Br Diagram, most of the crush-leach samples differ significantly from the seawater evaporation trajectory (SET, Fig. 3). They also plot mainly below the 1:1 line, which shows the change of the Cl/Br-Na/Br ratios during halite precipitation and halite dissolution. The molar Cl/Br ratios range between 100 and 400 and are significantly lower than seawater, which suggests a higher Br concentration than in seawater. The molar Na/Br ratios are between 80 and 580 and reach nearly seawater ratios.

The oxygen isotopes within the fluid inclusions were calculated under the assumption of isotopic balance between the fluid phase and the host mineral (quartz) (Hu and Clayton, 2003). The δD values of the fluid inclusions show a broad scatter,

however, all values plot in the field for metamorphic fluids. The isotopic composition of the groundwater at Outokumpu is situated left of the meteoric water line (Fig. 4). The deviation of the values from the MWL corresponds to the salinity and is interpreted as 2 component mixing of meteoric and water of high salinity (Frape et al., 1984).

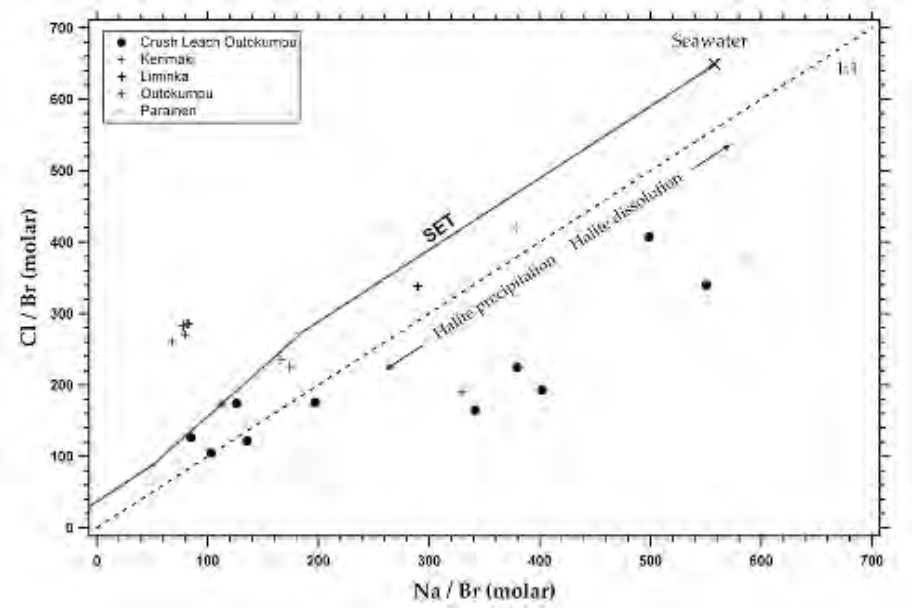

Fig. 3: Cl/Br-Na/Br ratios from crush-leach measurements

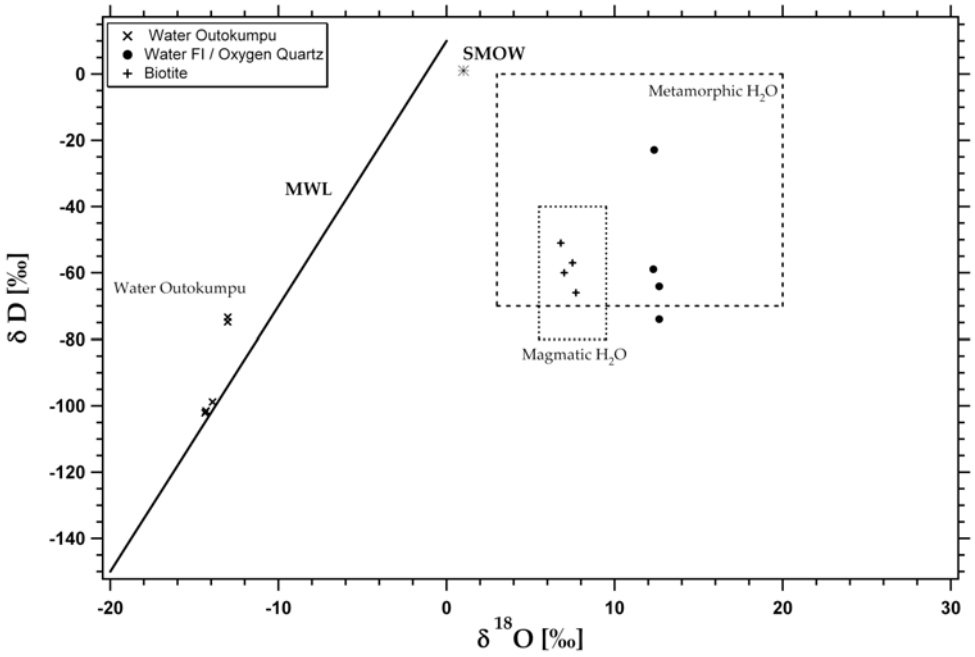

Fig. 4: δD - δ^{18}O Diagram

Frape SK, Fritz P, McNutt RH (1984) Water — rock interaction and chemistry of groundwaters from the Canadian Shield. Geochim Cosmochim Acta 48:1617–1627

Gaál, G., Koistinen, T., and Mattila, E. (1975): Tectonics and stratigraphy of the vicinity of Outokumpu, North Karelia, Finland: Including a structural analysis of the Outokumpu deposit. Geological Survey of Finland, Bulletin 271, 67 p.

Hu and Clayton, 2003 G.-X. Hu and R.N. Clayton, Oxygen isotope salt effects at high pressure and high temperature, and the calibration of oxygen isotope geothermometers, Geochim. Cosmochim. Acta 67 (2003), pp. 3227–3246.

Koistinen, T.J. (1981): Structural evolution of an early Proterozoic stratabound Cu-Co-Zn deposit, Outokumpu, Finland. Transactions of the Royal Society of Edinburgh: Earth Sciences 72, 115-158.

Park, A.F. (1988): Nature of the early Proterozoic Outokumpu assemblage, Eastern Finland. – Precambrian Research, 38: 131 – 146.

Drilling into dewatering sites along the Costa Rica and Nicaragua margin (IODP proposal 633-Full2): first results from pre-site survey seismic data evaluation

L. PLANERT[1], D. KLAESCHEN[1], C. BERNDT[1], W. BRUECKMANN[1], C. HENSEN[1]

[1] IFM-GEOMAR, Leibniz Institute of Marine Sciences at the University of Kiel , Wischhofstr. 1-3, D-24148 Kiel, Germany.

Mound structures and large-scale slides related to the subduction of seamounts are manifestations of dewatering pathways that control and balance the overall fluid budget at the erosive convergent margin of Costa Rica and Nicaragua. Two mound locations (Mound Culebra, Mound 11/12) and one seamount site (Jaco Scarp) are proposed for drilling (IODP proposal 633-Full2) in order to clearly identify (1) the processes of mud and fluid mobilization and mud volcano/diapir formation, (2) the controls of fluid geochemistry and heat flow, and (3) the geologic time-space variability of mud and fluid flow.

In spring 2008, new pre-site survey seismic data was collected during a cruise of R/V Marcus Langseth at the proposed sites of Mound Culebra and Mounds 11&12. These new data – together with the reprocessed pre-existing geophysical data - is a crucial part of the site survey data for the IODP safety panel. The new seismic profiles were acquired using a 36-gun, four-string linear gun array up to 240 Hz, and a 240 channel streamer with 3000 m active length. MCS seismic data processing included cmp crooked line binning with 6.25 m, bandpass filtering 4/8-180/240 Hz, resampling from 0.5 ms to 2 ms, spherical divergence correction using the smoothed depth migration velocity field, and a shot gather consistent predictive deconvolution. The seismic lines were prestack depth migrated, in which the velocity model is iteratively improved from top to bottom using depth focussing analysis and residual moveout correction on common image point gathers. Additionally, a true amplitude prestack time migration was applied to the data. In general, the available seismic data is of very good quality and it is currently screened for a systematic evaluation of the different types of fluid escape features and their geospatial distribution along the lines.

The selected mound sites at Mound Culebra and Mound 11 are both clearly related to deep-reaching fault systems, corroborating preliminary estimates of the source depth of fluids and extruded material. In addition, the new seismic data show differences in terms of the mounds' activity and stage of development. A continuous bottom simulating reflector (BSR), i.e. the base of the gas hydrate stability zone, is visible in the vicinity of the mounds, but seems to vanish directly beneath their surface expression (Fig. 1). The selected drill sites are chosen to penetrate deeper than BSR depth in order to record changes in fluid geochemistry and microbiology along the flow path where it transgresses into the hydrate stability field.

At Jaco Scar, which is the target site selected for studying seamount subduction, there is evidence for fluid flow as detected by geochemical anomalies in scar sediments and prominent methane plumes in the water column. Drilling of the seamount site at Jaco Scar will test the hypothesis that seamount subduction creates deep-reaching conduits between the upper plate sediments and the continental basement wedge.

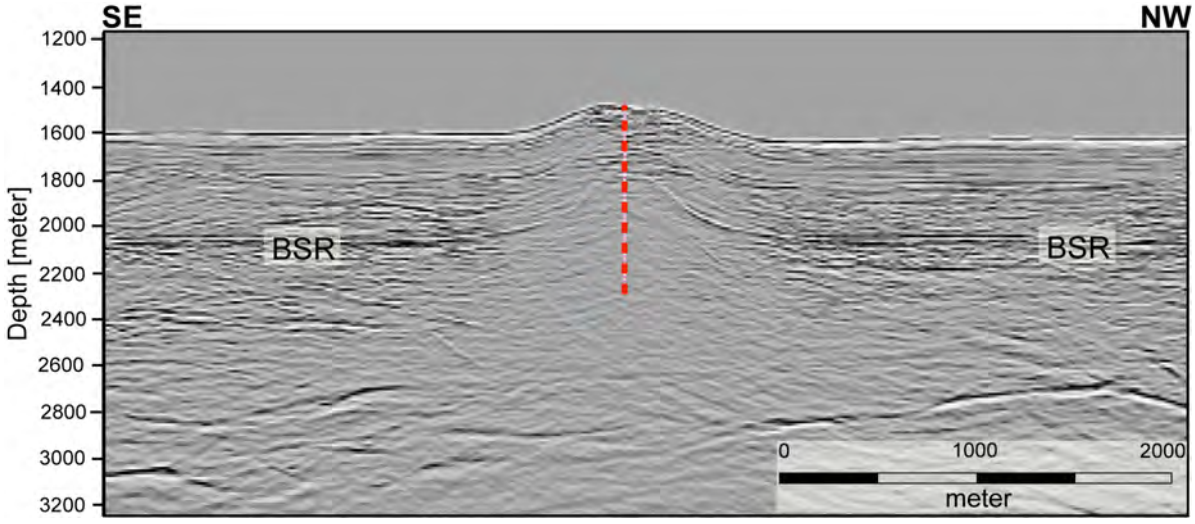

Fig. 1: Closeup of MCS line Cul9 together with proposed drill location CRMD-04A at Mound Culebra. A continuous BSR at ~400 m depth below seafloor is visible away from the mound but seems to vanish beneath the crest.

Observation of high-frequency seismic events (100 Hz to 170,000Hz) in a deep gold mine, South Africa

PLENKERS, KATRIN[1]; KWIATEK, G[1]; NAKATANI, M.[2]; DRESEN, G.[1]; PHILIPP, J.[3]; YABE, Y.[4]; JAGUARS-GROUP

[1]GFZ German Research Centre for Geoscience, Potsdam/Germany
[2]University of Tokyo, Japan
[3]GMu GmbH, Germany
[4]Tohoku University, JapanMu GmbH, Germany

In the Earth crust deep mines provide a unique opportunity by giving access to the focal depth of earthquakes. To investigate the physics of earthquakes and link laboratory and seismological observations, the JAGUARS (Japanese-German Acoustic Emission and Microseismicity Research in South Africa) Working Group was established. The JAGUARS project continuously monitors high- frequency seismic activity at 3.5km depth in Mponeng gold mine, Republic of South Africa.

JAGUARS' network is focused on monitoring the Pink Green Dyke (width=30m), which is used as a support pillar in the mining process. Active mining is ongoing 90m above JAGUARS' network and an increased seismic activity is observed due to stress concentrations on the dyke.

The major components of the network are currently 8 acoustic emission sensors, one 3C accelerometer, three 1C accelerometers and two strainmeters. The sampling frequency of the acquisition system is 500 kHz and the total frequency range recorded is between 50Hz and 170 000Hz.

Here data recorded in the time period end of May, 2007 to beginning of June, 2008 are presented. More than 400,000 events were successfully recorded with Mw=-0.5 to Mw=-4.5. Events are successfully located using an automatic localisation algorithm. Of special interest is an aftershock sequence, containing more than 25,000 events, which were recorded after the occurrence of an M=1.9 event, which happened 20m from JAGUARS' network. Additionally preliminary results of spectral analysis are shown, which estimate the source radii in cm to m scale.

Paleo-environment of cold-water coral initiation in the NE Atlantic: Implications from a deep-water carbonate mound drilling core

J. RADDATZ[1], A. RÜGGEBERG[1], S. MARGRETH[2], W.-CHR. DULLO[1], AND IODP EXP. 307 SCIENTIFIC PARTY

[1] Leibniz-Institute of Marine Sciences (IFM-GEOMAR), Wischhofstrasse 1-3, D-24148 Kiel, Germany
[2] University of Fribourg, Department of Geosciences, Ch. du Musée 6, Fribourg, Switzerland

The understanding of the paleo-environment during initiation and early development of deep-water carbonate mounds in the NE Atlantic is still under debate. The Integrated Ocean Drilling Program Expedition 307 sailed in 2005 to the Porcupine Seabight in order to investigate for the first time sediments from the base of a giant carbonate mound (Challenger Mound, 155 m). These results indicate that the initiation and start-up phase of this carbonate mound coincides with the beginning of the Northern Hemisphere Glaciation (NHG) at around 2.6 Ma (Kano et al. 2007). Further carbonate mound development seems to be strongly dependent on rapid changes in paleo-oceanographic and climatic conditions around the Pliocene-Pleistocene boundary, especially characterized and caused by intermediate water masses.

To characterise the paleo-environmental and paleo-ecological setting favourable for the initial coral colonization at ~2.6 Ma, we use well-developed proxies such as δ18O and δ13C of planktonic (Globigerina bulloides) and of a collection of benthic foraminifera (Cibicidoides wuellerstorfi, Discanomalina coronata, Cibicides lobatulus, Lobatulua antarctica, Planulina ariminensis), benthic foraminiferal assemblages, as well as grain size analysis. These proxies indicate variability in seawater temperature, salinity and density of intermediate water masses from southern origin (Mediterranean, Bay of Biscay) supporting cold-water coral settlement and initial development in the Porcupine Seabight.

Kano et al. (2007) Age constraints on the origin and growth history of a deep-water coral mound in the northeast Atlantic drilled during Integrated Ocean Drilling Program Expedition 307. Geology, 35(11):1051–1054.

Timing and magnitude of CO_2 uptake by ocean crust through seawater interaction and carbonate veining

S. RAUSCH[1], F. BÖHM[2], A. KLÜGEL[1], W. BACH[1]

[1] Geoscience Department, University of Bremen, Petrology of the Oceanic Crust, Klagenfurter Str.2, 28359 Bremen, Germany, srausch@uni-bremen.de
[2]IfM-GEOMAR, Wischhofstr. 1-3, 24148 Kiel, Germany, fboehm@ifm-geomar.de

Seawater circulation within mid-ocean ridge flanks plays a major role in global chemical budgets of crust-seawater interaction (STAUDIGEL ET AL., 1996, ALT AND TEAGLE, 2000). In particular, the importance of the ocean crust as a sink for CO_2 caused increasing interest in this topic. In general it is assumed that about two thirds of convective heat loss in the ocean crust takes place at mid-oceanic ridge flanks due to seawater circulation at low temperatures. To cool the crust at these relatively low temperatures the fluid flux must be orders of magnitude higher than in axial high temperature (black smokers) systems (e.g. ELDERFIELD AND SCHULTZ, 1996). In addition to an increased elemental flux at ridge flanks, the direction of flux is often opposite to that of axial systems. Potassium and other alkali metals for instance, are leached from the rocks during high-temperature alteration in axial systems, but are taken up by the crust in low-temperature off-axis settings. The off-axis uptake flux usually overwhelms the axial leaching flux, and therefore the altered ocean crust provides a net sink for alkalis. The net oceanic crustal CO_2 sink is comparable to the total atmospheric CO_2 input by subaerial volcanism and subaerial hydrothermalism in subduction zone settings. The budget is based on global oceanic uptake fluxes of 2–4 * 10^{12} mol CO_2/yr (STAUDIGEL ET AL., 1989, ALT AND TEAGLE, 1999) estimated for Mesozoic crust. Younger ridge flanks in the East Pacific, however, indicate CO_2 uptake-fluxes that are an order of magnitude smaller (SANSONE ET AL., 1998, BACH ET AL., 2003). The discrepancy between the two datasets is puzzling. One hypothesis states that the crustal uptake of CO_2 increases continuously with age and distance from the ridge axis (ALT AND TEAGLE, 1999). Testing this hypothesis requires knowledge of CO_2 uptake budgets for a large number of drill holes from a representative range of global ridge flanks. We examine drillcore samples from basement of crust of different age and spreading rates and to develop a comprehensive picture of the importance of carbonate veining. To examine the processes occurring during carbonate veining and their temporal evolution, we integrate oxygen and strontium isotope analyses with trace element concentrations at high spatial resolution by laser-ablation ICP-MS to gather information about the evolution of circulating seawater composition of single carbonate veins.

Twenty-three cores from the North Atlantic and the Pacific (Fig.1) were examined and the carbonate occurrences of each core was logged including carbonate vein characteristics such as length, width, shape and connectivity as well as crystal habit and differences in mineral composition. Carbonate proportion was calculated using the exposed area of carbonate referenced to the area the cut surface of the core. Our results confirm that carbonate abundance principally increases with increasing basement age. The oldest samples are of Jurassic to Cretaceous age, e. g. Holes 417A, 417D, 418A, 801C, and 1149D, and show a carbonate proportion of 2.3 to 5.5 vol.%. In contrast, younger samples, e. g. from Holes 332A, 332B, 334, 395, 396, 396B, 407, 409, 504B, 553A, 597C, 896A, 1032A, 1027C, and 1224F, show significantly lower carbonate percentages between 0.1 and 1.2 vol.%. Exceptions are Holes 333A and 335, which show very high abundances of carbonate vein (~5 vol.%), most of which are micritic and apparently not precipitates. In the case of Hole 801C the carbonate abundance increases with depth. Shallow holes (e.g. 801B) may hence provide only minimum estimates of carbonate vein abundance. Except for these holes, the visual core logging data show a general trend of intensification of carbonate veining with increasing basement age (Fig.2).

Carbonate formation temperatures (see companion paper by Böhm et al.) indicate that younger samples precipitated from colder water while for older samples higher formation temperatures are found (Fig.3). These relatively high temperatures can either be explained by warmer deep-sea water during the Cretaceous or by carbonate recrystallisation at greater depths after initial formation. Also, some sites show a weak correlation between calculated temperatures and thickness of sediment cover. A similar trend of sediment thickness vs. basement-sediment interface temperature is found in the eastern Juan de Fuca Ridge flank (e.g. ELDERFIELD ET AL. 1999) and is indicative of conductive reheating due to a thermal-blanket effect of the accumulating sediment (e.g. FISHER ET AL. 2003). It is possible that our data reflect the complex development of fluid and heat transport in the course of progressive lithospheric cooling and sediment accumulation (Fig.3a).

$^{87}Sr/^{86}Sr$ ratio of seawater has strongly increased during the past 40 Ma and notable isotopic exchange between circulating fluid and basement rocks has been proposed to be unlikely, making the $^{87}Sr/^{86}Sr$ ratio in carbonate veins useful geochronometers (e.g. HART AND STAUDIGEL 1978, HART ET AL. 1994). Sr isotopic ratios of the analysed samples (see companion paper by Böhm et al.) indicate that carbonate veins in some sites (335, 395, 396, 407, and 1224) formed much later than the basement which suggests prolonged (<20 Ma) open circulating of seawater. In contrast, samples with $^{87}Sr/^{86}Sr$ ratio lower than contemporaneous seawater indicates hydrothermal uptake of ^{86}Sr from the basaltic basement (Sites: 332, 333, 409, 418, 801, and 1149) and impair their use as a chronometer.

In general, the Sr/Ca and Mg/Ca ratios of the investigated calcites decrease with increasing temperature of formation. U/Ca ratios seem to show a similar trend. This negative correlation may reveal that Mg and U contents of the fluid decrease as they are taken up by the basalt. Calcium, on the other hand, becomes enriched in the fluid. COGGON ET AL. (2004) showed that carbonate veins from the Juan de Fuca Ridge flank reveal a systematic trend in Mg/Ca vs. Sr/Ca plots that is distinct from the diagenetic trend seen in the abiotic calcite cements (CICERO AND LOHMANN, 2001). There, Mg/Ca ratios of carbonate veins correlate with formation temperature and hence the temperature-dependent intensity of exchange with basement (COGGON ET AL. 2004). Our data show that low-temperature carbonate veins from open circulation sites do not show any sign of seawater exchange with basement in Mg/Ca and Sr/Ca. Some of the veins that have unradiogenetic Sr isotope ratios,

however, do deviate from the diagenetic trend in a Mg/Ca vs. Sr/Ca diagram (Fig.4). Overall, the intensity of basement exchange recorded in the vein composition is fairly minor. Carbonate veins, for which exchange with basement can be ruled out, can therefore be used to reconstruct the Mg/Sr evolution of seawater.

Rare earth element (REE) concentrations of the investigated carbonate veins show two distinct groups: one with a pronounced Ce depletion and one without a Ce depletion (Fig.5). Ce is typically depleted in oxic seawater, hence the Ce depltetion in the carbonates are an indication of oxidative conditions during carbonate precipitation. Remarkably, Ce depletions are exclusively observed in carbonates from veins with excess ^{87}Sr (i.e., sites with open circulation). In contrast, all sites where Sr isotope compositions indicate exchange with basement show no Ce depletion, suggesting that conditions at those sites are far less oxidizing than seawater. Suboxic to anoxic conditions are to be expected for a case of isolated circulation where exchange with the ocean is strongly limited.

The Y/Ho relationship is a sensitive indicator for low-intensity seawater-basement interaction. Unlike Mg/Sr, it responds to trivial extents of exchange with basement, because the concentrations of REE and Y concentrations of seawater are 5-6 orders of magnitude lower than those of basalt. Moreover, the Y/Ho ratio of seawater is about twice that of basalt. The Y/Ho ratios of the carbonate samples lie in the range between MORB and seawater (Fig. 6) indicating variable extents of basement-seawater exchange.

Many carbonate veins are strongly zoned with respect to trace elements as indicated by compositional profiles. In chondrite-normalized trace element diagrams, the samples are generally enriched in U and Sr and are depleted in Zr. Some veins show rare earth element concentrations near the contact to the host basalt that are similar to MORB, whereas the vein centers show distinctly lower values and seawater-like Y/Ho ratios. Apparently these changes represent a systematic variation of seawater-basement interaction during the formation of the veins. The reason for this transition during the development of the veins is unclear, but the solid-state diffusion between calcite and wall-rock appears unlikely. Perhaps early carbonate formation along fracture walls imposes an obstacle to basement exchange during subsequent carbonate precipitation.

More trace element analyses are underway, and our working hypotheses will be tested rigorously once the complete data set for all drill holes is available. In addition, we will carry out Sr-isotope spot analysis along vein transects and into the vein halos in basalt to further our understanding of the interaction between basalt and water recorded in the carbonate veins.

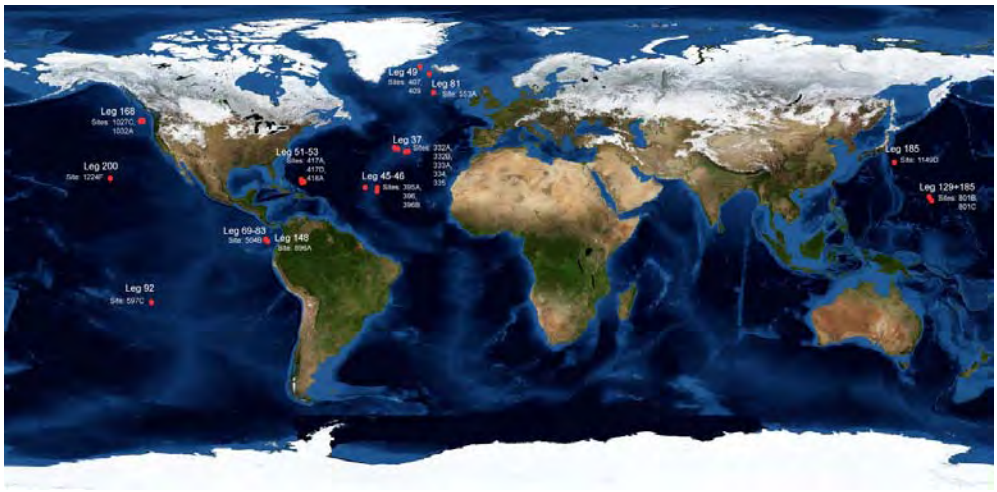

Fig.1: Map showing the earthand locations of examined DSDP and ODP drill sites (red dots). (www.visibleearth.nasa.gov)

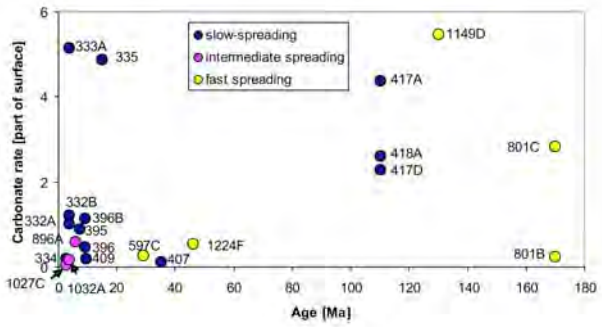

Fig.2: Percentage of carbonate in veins and vesicles of ocean basement rocks (using the exposed area of carbonate referenced to the area of the cut surface of the core).

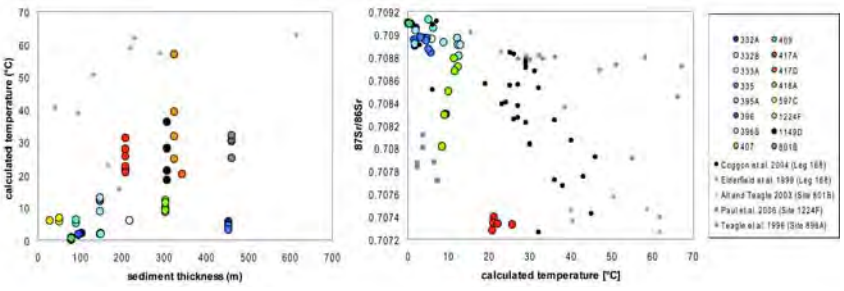

Fig. 3: (a) calculated formation temperatures of carbonate veins plotted against the sediment thickness show temperature increases with overlaying sediment thickness. (b) Sr-isotope compositions of carbonates against calculated for-mation temperatures.

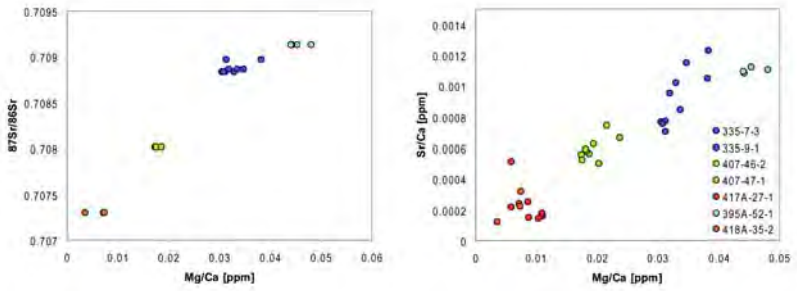

Fig.4: (a) Sr-isotope compositions of carbonate veins versus their Mg/Ca ratios. (b) Sr/Ca versus Mg/Ca ratios of calcites. Carbonates with higher formation temperatures show the lowest Sr/Ca and Mg/Ca ratios. Related to this, carbonates with lower formation temperature accordingly show higher Sr/Ca and Mg/Ca ratios.

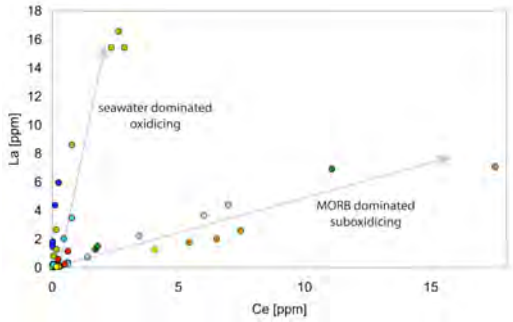

Fig.5: La versus Ce diagram showing two trends of carbonate veins. The samples with a more seawater dominated trend also show a Ce-anomaly. The samples are the same as those described in the legend of Fig.3.

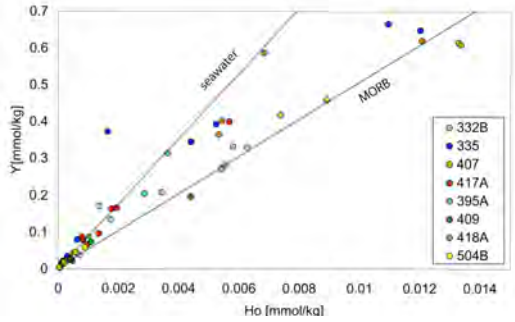

Fig.6: Y against Ho concentration in carbonate vein samples. The black curves are either an average seawater (after Nozaki et al. 1997) or MORB correlation.

Alt, J. C. and D. A. H. Teagle (2000). "Hydrothermal alteration and fluid fluxes in ophiolites and the ocean crust." Geological Society of America, Special Paper 349: 273-282.

Alt, J. C. and D. A. H. Teagle (1999). "The uptake of carbon during alteration of the ocean crust." Geochimica et Cosmochimica Acta 63(10): 1527-1535.

Bach, W., Peucker-Ehrenbrink, B., Hart, S.R., Blusztajn, J.S. (2003). Geochemistry of hydrothermally altered oceanic crust: DSDP/ODP Hole 504B – Implications for seawater-crust exchange budgets and Sr- and Pb-isotopic evolution of the mantle. Geochem. Geophys. Geosys. 4, 10.1029/2002GC000419.

Cicero, A. D. and K. C. Lohmann (2001). "Sr/Mg variation during rock-water interaction:Iplications for secular changes in the elemental chemistry of ancient seawater." Geochimica et Cosmochimica Acta 65(5): 741-761.

Coggon, R. M., D. A. H. Teagle, et al. (2004). "Linking basement carbonate vein compositions to porewater geochemistry across the eastern flank of the Juan de Fuca Ridge, ODP Leg 168." Earth and Planetary Science Letters 219: 111-128.

Elderfield, H., C. G. Wheat, et al. (1999). "Fluid and geochemical transport through oceanic crust: a transect across the eastern flank of the Juan de Fuca Ridge." Earth and Planetary Science Letters 172: 151-165.

Elderfield, H. and A. Schulz (1996). "Mid-Ocean Ridge Hydrothermal Fluxes and the chemical Composition of the Ocean." Annual Rev. Earth Planet. Sci. 24: 191-224.

Fischer, A. T., E. E. Davis, et al. (2003). "Hydrothermal recharge and discharge across 50 km guided by seamounts on a young ridge flank." Nature 421: 618-821.

Friedman, I. and J. R. O´Neil (1977). "Data of geochemistry. Compilation of stable isotope fractionation factors of geochemical interest." U.S. Geological Survey Professional Paper: 440-KK.

Hart, S. R. and H. Staudigel (1978). "Oceanic crust: age of hydrothermal alteration." Geophys. Res. Lett. 5: 1009-1012.

Hart, S. R., J. Blusztajn, et al. (1994). "fluid circulation in the oceanic crust: Contrast beween volcanic and plutonic regimes." Journal of Geophysical Research 99: 3163-3173.

McArthur, J. M., R. J. Howarth, et al. (2001). "Strontium Isotope Stratigraphy: LOWESS Version 3: Best Fit to the Marine Sr-Isotope Curve for 0–509 Ma and Accompanying Look-up Table for Deriving Numerical Age" The Journal of Geology 109: 155-170.

Sansone, F. J., M. J. Mottl, et al. (1998). "CO2-depleted fluids mid-ocean ridge-flank hydrothermal springs." Geochimica et Cosmochimica Acta 62(13): 2247-2252.

Staudigel, H., T. Plank, et al. (1996). "Geochemical fluxes during seafloor alteration of the basaltic upper crust: DSDP Sites 417 and 418." Geophysical Monograph 96: 19-38.

Staudigel, H., S. R. Hart, et al. (1989). "Cretaceous ocean crust at DSDP Sites 417 and 418: Carbon uptake from weathering versus loss by magmatic outgassing." Geochimica et Cosmochimica Acta 53: 3091-3094.

Tectonic Evolution of the Ohrid Basin (Macedonia/Albania): preliminary results for a future ICDP deep drilling site

K.REICHERTER[1], T. FERNÁNDEZ-STEEGER[2], N.HOFFMANN[1]

[1] Institute of Neotectonics and Natural Hazards, RWTH Aachen University, Lochnerstr. 4-20, 52056 Aachen, Germany; contact: k.reicherter@nug.rwth-aachen.de
[2] Chair of Engineering Geology and Hydrogeology, RWTH Aachen University, Germany

In the frame of the planned Lake Ohrid ICDP deep drilling site (Macedonia/Albania, SCOPSCO initiative), we are focusing on the tectonic framework of the basin. The Ohrid basin is an important N-S trending graben structure in Macedonia/Albania and located within the Afro-European Convergence Zone a region with dispersed active seismicity. In contrast to the compressive coastal part of Albania the central and eastern part are presently subject to extension. The general geodynamic setting of the Lake Ohrid area can be described with a "basin and range" situation.

Within the basin an "ancient lake" developed since the Late Miocene/Pliocene with almost 290 m water depth. Since the beginning of basin formation around 700 m of sediment accumulated in the lake, the initial stage of subsidence is triggered either by extension or strike-slip movements.

Several pronounced scarps testify to an active, seismogenic landscape as revealed also from DEM data. Paleozoic metamorphic and magmatic rocks form the country rock of the Western Macedonian Zone around Lake Ohrid. Triassic carbonates and clastics are widely exposed to the southeast and northwest of the lake. These rocks bear the imprints of several deformation phases that affected the basin system since the Late Cretaceous to present.

The central mountain chain, especially the intramontane basins of Late Neogene age, form one of the most active seismic zones in Albania/Macedonia with several moderate earthquakes reported during the last few centuries (Muço 1998; NEIC database, USGS). Major earthquakes occurred during historical times. The last prominent earthquake took place in on 18th February 1911 at 21.35 close to Lake Ohrid Basin, (M 6.7, corresponding to EMS X; 15 km depth, N 40.9°, E 20,8°). The last earthquake occurred on Jan 8th 2009 with a magnitude of 4.9 close to the lake. Hypocenter depths scatter between 10 and 25 km but some deeper earthquakes occur between 25 and 50 km depth. Therefore the Ohrid-Korça Zone is considered to be the region of the highest seismic hazard in the Albanian-Macedonian Corridor based on present-day seismicity (Aliaj et al., 2004).

However, until today the different steps in the tectonic evolution of the graben are not clear. Therefore, we started to investigate the (neo)tectonic evolution of Lake Ohrid with a field campaign focusing on the collection of structural data, like paleostress data (fault-slip data) and mapping of folds, joints and fractures. Up to now, we studied a total of 24 sites along the steep flanks and the mountains surrounding Lake Ohrid, with suitable fault-slip data for stress inversion. At each location we measured a representative number of fault planes concerning the spatial orientation of fault plane (dip direction, dip) and striae (azimuth, plunge) and additional the sense of slip (reverse, normal, dextral or sinistral).

After separation and classification of the data the preliminary results already show a tendency of three major deformation phases affecting the surroundings of Ohrid Basin: NW-SE, NE-SW horizontal contraction and later an almost vertical uplift with E-W extension. The multiple inverse method of Yamaji (2000) was applied on datasets with a polyphase stress history and to investigate the spatial and temporal variations of paleostresses in the Ohrid Basin. The applied methods led us to the following preliminary results:

- Three main phases of deformation can be assumed NW-SE shortening, NE-SW shortening and a present-day extension
- Morphological lineations, which are directed NNE-SSW, NW-SE, and E-W fit in the observed pattern of faults
- Earthquake focal solutions and data of the world stress map data point to SW-NE directed extension and normal faulting acting presently

The origin of the lake formation is possibly initiated by an older tectonic transtensional phase or reactivation of inherited faults led to a pull-apart like opening of the basin, followed by E-W directed extension.

The Ohrid Basin meets all criteria of an active, seismogenic landscape: linear step-like fault scarps in the landscape and under water in the lake. Post-glacial (or Late Pleistocene) bedrock fault scarps at Lake Ohrid are long-lived expressions of repeated surface faulting in tectonically active regions, where erosion cannot outpace the fault slip. Other morphotectonic features are wineglass-shaped valleys and triangular facets, which are well preserved. Generally, the faults and fault scarps are getting younger towards the basin center, as depicted on seismic and hydroacoustic profiles. Additionally, mass movement bodies within the lake and also onshore (rockfalls, landslides, sub-aqueous slides, homogenites, turbidites) are likely to be seismically triggered, eventually damming the outflow of Lake Ohrid temporarily.

Aliaj, S., Adams, J., Halchuk, S., Sulstarova, E., Peci, V., Muco, B., 2004. Probabilistic seismic hazard maps for Albania. 13th World Conf. Earthquake Engineering, Vancouver, B.C., Canada, paper no. 2469, 14 pp.
Muço, B., 1998. Catalogue of ML 3,0 earthquakes in Albania from 1976 to 1995 and distribution of seismic energy released. Tectonophysics, 292, 311–319.
Yamaji, A., 2000. The multiple inverse method: a new technique to separate stresses from heterogeneous fault-slip data. J. Struct. Geol. 22, 441-452.

Active seismic imaging using microseismic events – results from the San-Andreas-Fault system at SAFOD

A. RESHETNIKOV[1], S. BUSKE[1], S. SHAPIRO[1]

[1]Institut für Geologische Wissenschaften, Freie Universität Berlin, Malteserstrasse 74-100, 12249 Berlin

The analysis and interpretation of microseismic data sets are receiving increased attention, both in the exploration industry for the characterization of hydrocarbon and geothermal reservoirs as well as in academia for the general understanding of seismogenic processes at plate boundaries. The gain in data quality due to e.g. the deployment of borehole-receiver-arrays and the meanwhile common practice of recording the full waveform of the seismic events allows the processing of these data sets using modern seismic imaging and inversion algorithms. We have developed a passive seismic imaging approach which consists of two steps. Firstly, the hypocenter of the microseismic event is precisely located. Secondly, this event is treated as pseudo-active seismic source and we process the reflections within the recorded wavefield using a directional migration algorithm in order to construct a high-resolution image in the close vicinity of the located hypocenter. Here we describe this approach and demonstrate the application to several microseismic events recorded by a borehole array in the SAFOD (San-Andreas-Fault-Observatory-at-Depth) main hole. The results are high-resolution images of different fault branches related to the San-Andreas-Fault (SAF) system in the close vicinity of the borehole. The comparison of these findings with existing surface seismic reflection images as well as additional borehole information demonstrates some interesting features. In summary our results allow a spatial characterization of the complex internal structure of the SAF and can certainly be helpful for other studies which rely on this knowledge.

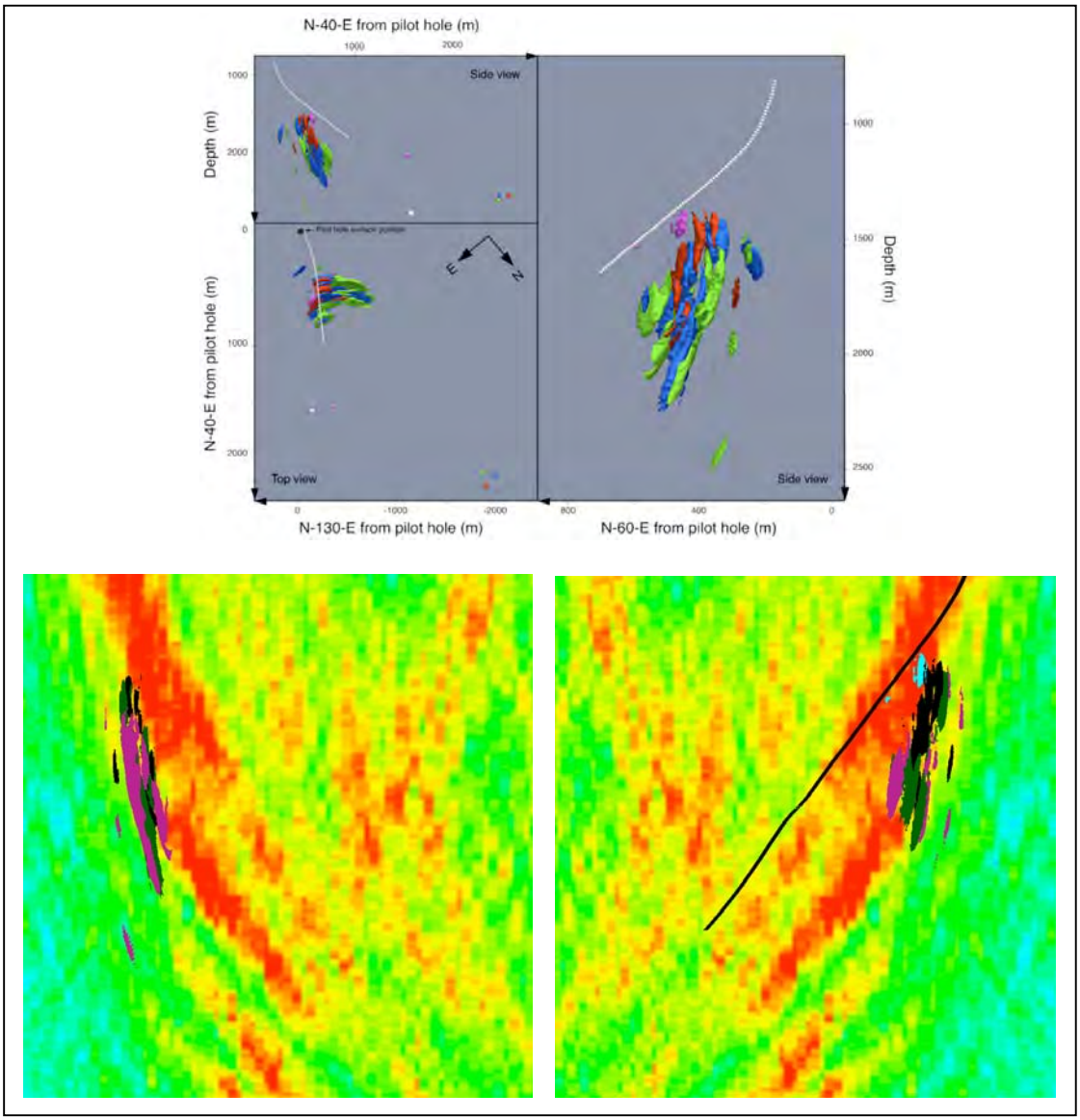

Fig. 1: Top: perspective views of imaged fault branches; bottom: overlay on active seismic reflection image.

Sulphur isotope variation in Paleoproterozoic strata from Fennoscandia

M. REUSCHEL[1], H. STRAUSS[1], V.A. MELEZHIK[2], A. LEPLAND[2]

[1]Westfälische Wilhelms-Universität Münster (Germany)
[2]Geological Survey of Norway (Norway)

The objective of the ICDP drilling project "FAR-DEEP" was the acquisition of an unweathered representative and continuous stratigraphic section through the Archean-Proterozoic transition on the Fennoscandian shield in Arctic Russia (Melezhik et al., 2005). Three main areas were selected: the Pechenga and Imandra/Varzuga Greenstone Belts in northern Russia and the Onega Paleobasin in Karelia (Fig.1).

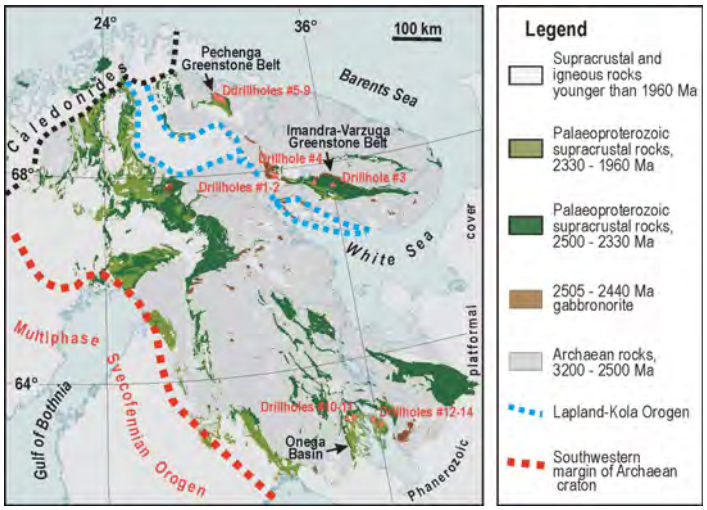

Fig.1: Geological map of eastern Fennoscandia with emphasis on the Palaeoproterozoic rocks (modified from Koistinen et al., 2001).

The drilling operations took place from May to October 2007. 15 holes were drilled, generally with more than 90% core recovery. A total of 3650 m of drill core, now available for multidisciplinary research, is being stored at the Norwegian Geological Survey (NGU) in Trondheim. Initial curation and archiving, involving visual documentation and selection of 500 archive and substantially more research samples, started in late January 2008.

An initial set of 107 samples from different FAR-DEEP cores was analyzed for their TS, TC and TIC contents. Sulphur was wet chemically extracted as acid volatile sulphur (AVS, sulphur from monosulphides) and as chromium reducible sulphur (CRS, sulphur from pyrite and elemental sulphur).

This initial selection of samples were based on archive samples in order to obtain a general overview of chemical variations across stratigraphy.

The 2.4 Ga old Seidorechka Sedimentary Formation within the Imadra Varzuga Greenstone Belt should still capture the oxygenation of Earth's surface environments. Hence, 16 siliciclastic and carbonatic samples were selected between 100 m and 180 m of core 1A. The $\delta^{34}S$ values should be compared with already existing $\delta^{34}S$ data from outcrop samples. Both of the successions show comparable temporal variations but the drillcore section seems to be more condensed or partly eroded in the lower part. $\delta^{34}S$ ranges between +3.3 and -15.1 ‰ with a deviation to positive values between 114 and 131 m (Fig. 2.). This deviation correlates with a change in lithology from siliciclastic facies to a carbonate unit. Additional work on this unit is planned. $\Delta^{33}S$ measurements are available for samples from the outcrop succession and these show in part mass independent fractionation (MIF). Additional ^{36}S measurements are planned to verify the mass independent fractionations.

Another set of 13 samples was taken from the 2.3 Ga old Umba Sedimentary Formation. The silicilclastic rocks are characterized by low sulphur contents (0.00 to 0.26%) and $\delta^{34}S$ ranges from +13.8 to +31.9‰ with a shift from 13.8 ‰ to more than 30‰ between 218 and 185 m.

38 samples from a preliminary drilling operation in the 2.0 Ga old Pilgujärvi Sedimentary Formation within Pechenga Greenstone Belt were analyzed for their sulfur isotopic composition and for their TS, TC, TIC and Fe contents.

This siliciclastic formation is characterized by low C_{org} and high S_{pyr} abundances and high S/C ratios. This could suggest an euxinic depositional environment. $\delta^{34}S$ varies between -9.5 and 18.7 ‰, AVS and CRS display mainly the same variations with AVS being enriched in ^{32}S by 3.6 ‰ (Fig.3). A distinct stratigraphic variation exists with larger variations in $\delta^{34}S$ for the lower 300 m of the succession. Seawater sulphate at that time had an isotopic composition of 15 to 21 ‰ (Schröder et al 2008). A maximum isotopic difference between sulphate and sulphide ($\Delta^{34}S$) of 25 - 30 ‰ is consistent with

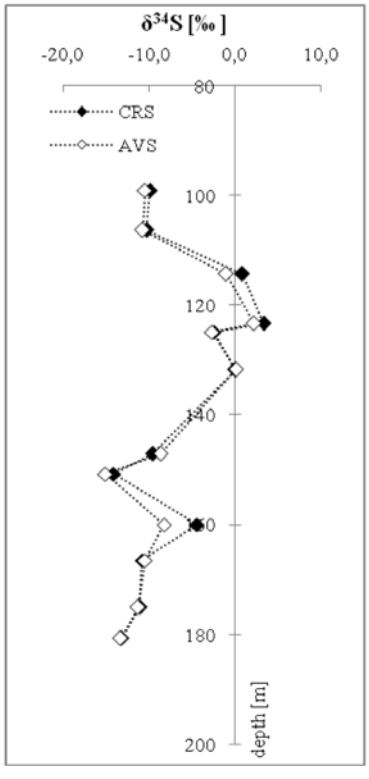

Fig. 2: $\delta^{34}S$ variation within the Seidorechka Formation (1A)

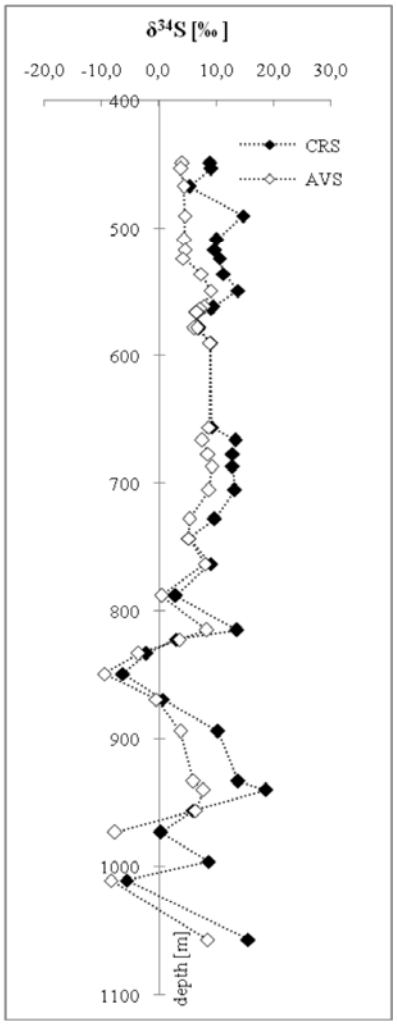

Fig.3: $\delta^{34}S$ variation within the Pilgujärvi Sedimentary Formation

the range commonly observed for bacterial sulphate reduction. The degree of pyritization (DOP) is lower in the upper part of the section. But the total iron content remains stable throughout the succession (10.6±3.4 %). In the upper part, S_{pyr} correlates weakly with C_{org} (r^2=0,22) and DOP remains stable with variing C_{org} concentrations. This is in contrast to the upper part where S_{pyr} and C_{org} are correlated (r^2=0,51) and DOP increases with higher C_{org} concentrations (r^2=0,34). These relationships could indicate the iron limited formation of syngenetic pyrite in the upper part of the section due to enhanced association of organic matter with iron oxide particles (Raiswell&Berner 1985).

The third region of interest on the Fennoscandian Shield are the strata in the Onega Paleobasin. 77 samples were obtained from three cores in this area. Core 11A represents the upper part of the carbonatic Tulomozero Formation (2.09 Ga). 16 siliciclastic samples were selected from the uppermost 400 m. The sulphur contents are generally very low (0.02-0.27%) and $\delta^{34}S$ ranges between -0.1 and 6.0‰ in the upper 55 m of the succession. The underlying samples had too less S for extraction. There is just one measurement with a very negative $\delta^{34}S$ value of -37.7 ‰. The explanation for this shift is yet unclear. Further study of trace sulphates in carbonate rocks is planned to quantify the $\delta^{34}S$ of seawater-sulphate at 2.0 Ga and occurring fractionation processes between seawater sulphate and sulphide. Drillcores 10A and 10B cover the rest of the Tulomozero Formation, but archive samples aren't available yet.

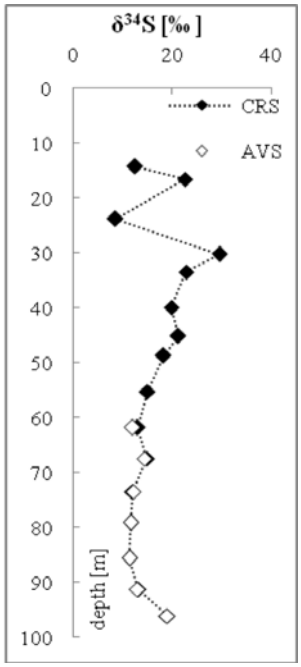

Fig.4a: $\delta^{34}S$ variation within the Zaonega Formation (12A)

Cores 12A and 12B were drilled in an organo-siliceous diapir within the Zaonega Formation (~2.0 Ga). These organic carbon rich rocks are called "shungite" and represent the first major enrichment in C_{org} in Earth history. The accumulation took place in the aftermath of the ca. 2330–2060 Ma Lomagundi-Jatuli Event (Melezhik et al., 1999, 2004). They are considered to be one of the oldest and best preserved petrified oil-fields. Core 12A covers the top of the diapir with a gabbroitic intrusion and siliciclastic rocks surrounding the diapir. 16 samples were selected. $\delta^{34}S$ varies from +8.5 to 29.6 ‰ (Fig.4a). The upper part of the section does not contain an AVS fraction which could suggest a complete conversion of the monosulfides to pyrite. The lower part consists mainly of gabbroitic rocks; they hold AVS and CRS with almost equal $\delta^{34}S$ compositions.

Drillcore 12B comprises mostly organo-siliceous rocks of the diapir but also siliciclastics, carbonates and a gabbroitic intrusion. The shungite rocks contain up to 40,6 % C_{org} and the sulphur content varies between 0,05 to 9,09%. $\delta^{34}S$ displays strong stratigraphic variations between -22.6 and +19.4‰. Several samples do not contain AVS but those who do, AVS displays the same isotopic composition as CRS (Fig.4b). There is also a strong positive correlation between the very low $\delta^{34}S$ values (lower than -12.5 ‰) and the organic carbon content (r^2=0,89). This strong coherence does not appear with the higher $\delta^{34}S$ values and is independent of lithology.

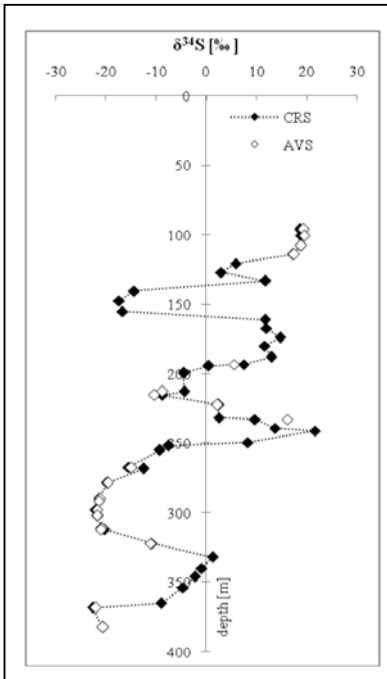

Fig.4b: $\delta^{34}S$ variation within the Zaonega Formation (12B)

Koistinen, T., Stephens, M., Bogatchev, V., Nordgulen, O., Wennerstrom, M., Korhonen, J.V. 2004: Geological map of the Fennoscandian Shield 1:2,000,000. International Geological Congress, Abstracts; Congres Geologique International, Resumes 32, Part 1: 565-565.

Melezhik, V .A., Fallick, A.E., Filippov, M .M., and Larsen, O. 1999: Karelian shungite—an indication of 2000 Ma-year-old metamorphosed oil-shale and generation of petroleum: geology, lithology and geochemistry: Earth-Science Reviews, 47, 1–40.

Melezhik, V .A., Filippov, M .M., and Romashkin, A.E. 2004: A giant Palaeoproterozoic

deposit of shungite in NW Russia: genesis and practical applications: Ore Geology Reviews, 24, 135–154.
Melezhik, V.A., Fallick, A.E., Hanski, E.J., Lepland, A., Prave, A.R., Strauss, H. 2005: Emergence og the aerobic biosphere during the Archean-Proterozoic transition: Challenges of future research. GSA Today,15,4.
Raiswell, R., Berner, R.A. 1985: Pyrite formation in euxinic ans semi-euxinic sediments. American Journal of Science, 285, 710.
Schroeder, S., Bekker, A., Beukes, N. J., Strauss, H., van Niekerk, H. S. 2008: Rise in sea water sulphate concentration associated with the Paleoproterozoic positive carbon isotope excursion; evidence from sulphate evaporites in the approximately 2.2-2.1 Gyr shallow-marine Lucknow Formation, South Africa. Terra Nova 20,108.

Iron and sulfur cycling in sediments from the Nankai Trough, Japan

N. RIEDINGER[1], B. BRUNNER[1], E. SOLOMON[2], L. CLAESSON LILJEDAHL[3], S. KASTEN[4], T.G. FERDELMAN[1], AND IODP EXPEDITION 314/315/316 SCIENTIFIC PARTY

[1]Max Planck Institute for Marine Microbiology, Celsiusstraße 1, 28359 Bremen, Germany
[2]Scripps Institution of Oceanography, University of California, San Diego, 9500 Gilman Drive #0212, La Jolla CA 92037-0212, USA
[3]Department of Geology and Geochemistry, Stockholm University, Svante Arrhenius väg 8C, 10691 Stockholm, Sweden
[4]Alfred-Wegener-Institute of Polar and Marine Research, Am Handelshafen 12,
27570 Bremerhaven, Germany

We present results of iron and sulfur geochemistry of sediments from the shallow mega splay fault and frontal thrust system at the Nankai Trough, collected during the IODP 316 Expedition. The objective of this research is to better understand the impact of dynamic systems on biogeochemical processes, specifically sulfur and iron cycling, as well as microbiological signals in deep subsurface sediments. For this purpose, we measured the concentrations of acid volatile sulfur (AVS) as well as chromium reducible sulfur (CRS), and determined the speciation of reactive ferric iron. The sediments at the investigated stations are characterized by shallow sulfate/methane transition zones where released hydrogen sulfide reacts with reactive iron minerals to form iron sulfides. Exceptional settings were found at Site C0007 where sulfate in the pore water is present in the approximately upper 160 mbsf. The analyzed AVS and CRS data reflect the alteration of iron oxides and their primary signals. The amount of AVS is rather low in the sediments while the CRS concentration profiles mirror the total sulfur concentration. This indicates that the main sulfur-bearing phase in the investigated sediments is pyrite.

Furthermore, we determined the sulfur isotope composition of AVS and CRS and measured the sulfur and oxygen isotopes of pore water sulfate. In the upper 33 mbsf sediments at Hole C0007C the isotope data of sulfate show an enrichment in heavier sulfur isotopes with decreasing sulfate concentration in the pore water. In the deeper sediments no direct trend is observable. This indicates a mixing of sulfate by diffusion from different sources where the upward diffusing sulfate has seawater isotope values. The sulfur isotope composition data of CRS at Site C00004 show strong variations, with ratios ranging from -45 to +47 ‰VCDT, while at Site C0008 the values are more or less constant.

Overall, our data show a high variability, that may be caused by different sulfur sources and biochemical sulfur cycling, which relate to the tectonic and sedimentary complexity of the Nankai Trough.

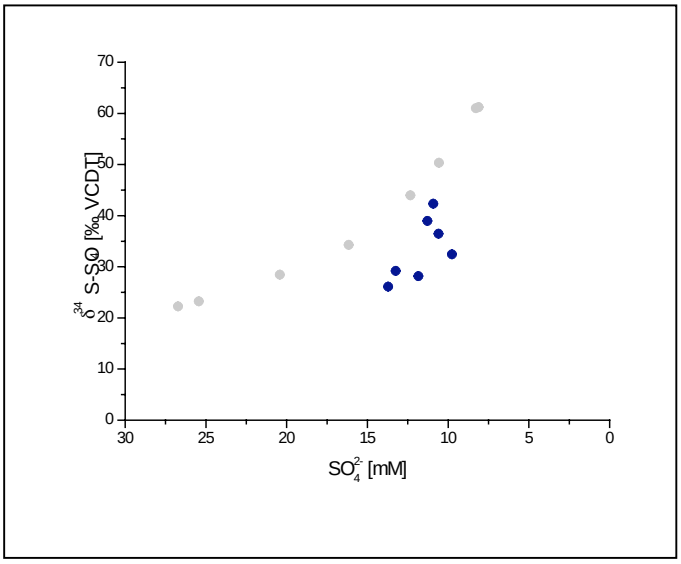

Fig. 1. The sulfate-sulfate isotope plot shows an enrichment in heavier isotopes with decreasing sulfate concentration for the first 33 mbsf (grey dots), indicating sulfate isotope fractionation due to Rayleigh processes. The deeper sediment display no direct trend which indicates mixing by diffusion (black dots).

In situ dating of metasomatically controlled zircon growth during retrogression: a LA-SF-ICP-MS study of zircon from UHP eclogites (Sulu deep drill hole, CCSD)

A. RIEMANN[1], R. OBERHÄNSLI[1], A. MÖLLER[2] A. GERDES[3]

[1]Universität Potsdam, Institut für Geowissenschaften, Karl-Liebknechtstrasse 24, Haus 27, D-14476 Potsdam, Germany
[2]University of Kansas, Department of Geology, 1475 Jayhawk Boulevard,Lawrence, Kansas 66045,USA
[3]Institut für Geowissenschaften, Mineralogie, Altenhoeferallee 1, D-60438 Frankfurt am Main, Germany

Introduction

The Dabie-Sulu region in east-central China is one of the largest and most coherent ultrahigh pressure (UHP) and high pressure (HP) metamorphic belts in the world, and has attracted a great deal of worldwide attention. A large number of contributions concerning the petrology, geochemistry, geochronology, metamorphic P-T paths, and large-scale conceptual tectonic evolution models for the creation and exhumation of the UHP and HP metamorphic rocks in the region. Central to resolving the physical and chemical processes involved in the genesis and exhumation of UHP terranes is constraining the sequence of events. Simple questions like the following remain poorly answered: ‘‘How rapid was continental subduction?’’ ‘‘How many metamorphic events were recorded?’’ ‘‘How long did these events last?’’ In the specific case of the giant Qinling-Dabie-Sulu UHP terrane, we know that it developed during northward subduction of the Yangtze Craton beneath the Sino-Korean Craton in the Triassic (Hacker et al., 2000), but important controversies include the following: Were UHP subduction and exhumation coeval everywhere along the length of the orogen, implying a short-lived subduction and exhumation event of regional extent, or were they diachronous? Are some of the eclogites assumed to be Triassic actually remnants of early (U)HP metamorphic events? (Hacker et al 2006)

The drill site of the Chinese Continental Scientific Drilling (CCSD) is located near Maobei village (N34° 25’, E118° 40’), about 17 km southwest of Donghai in the southern segment of the Sulu UHP terrane. The drill core obtained from the main hole of CCSD consists mainly of eclogites, ortho- and paragneisses, ultramafics, and some schists and quartzite. A number of petrographic and isotopic studies have shown that all of the Dabie-Sulu UHP rocks underwent prograde metamorphism related to plate subduction, with subsequent decompression-recrystallization related to exhumation of the subducted plate and consequent amphibolite-facies retrograde metamorphism (Zhang et al. 1995; Wawrzenitz et al 2006, Romer et al 2003). Three different metamorphic events were determined: A 244-236 Ma “precursor” UHP event, was followed by a 230-220 Ma “main” UHP event, which was itself terminated by a 220-205 Ma amphibolite facies overprint (Hacker et al. 2006,). Although there are many studies about inclusions in zircon and their relevance for the PT-path, little is known about the zircon growth itself and the main driving forces.

This study reports a detailed microstructural analysis and inductively coupled plasma mass spectrometry (ICP*) in-situ* experiments on zircon in a fluid influenced shear zone. This research is aimed to: (1) document the petrological evolution of distinct zones in eclogite, (2) link the appearance of *fluid and zircons* in the Sulu region, (3) get a better resolution of the post peak evolution.

Results

The sample for this investigation was taken from an UHP-eclogite at 382 m drill hole depth. Within fifteen centimetres, the sample shows macroscopic zoning with intense retrogression by the conspicious occurrence of white bands (quartz) and very dark-blue green amphibole. This zone can be subdivided to: 1. non-retrogressed coesite-bearing eclogite 2. transition zone and 3. retrogression zone. Four thin sections were cut from this core sample and used for detailed petrographic observations and in situ measurements. On both sides of this reaction zone described, the eclogite is poorly retrogressed and shows a marked UHP foliation defined by omphacite and garnet. The retrograde zone cuts this foliation at a low angle. Contacts between UHP and lower grade regions are gradual. In the retrogression zone the foliation is lost due to recrystallisation.

Applying the Theriak-Domino Gibbs-energy minimization program (De Capitani, 2000) for the measured bulk composition we reproduce the analysed mineral compositions show equilibrium textures at 735 ± 5 °C and 3.4 ± 0.5 GPa. Fluid saturation mineral composition are approximated at conditions of ca. 700°C at 1.4 GPa. Based on the breakdown of phengite to biotite, allanite and aegirine component in pyroxene we estimate conditions similar to the ones given by Tong et al. (2007)of ca. 530-560 $^\circ$C and 0.7-0.9 GPa.

In this study zircon in polished thin sections was investigated using CL imaging in polished to distinguish between different generations. Spot sites for LA-SF-ICPMS U-Th-Pb analyses were selected on the base of these observations. Zircon (I) from UHP eclogite differs from the retrogression zone zircons (II)) by host minerals, morphology, size, luminescence, presence of metamorphic rims and by quantity.

Ninety-two spots on zircons typ zircon II in the retrogression zone were analysed.. Cores and rims were analysed in situ in a single thin section. The U-Th-Pb zircon analyses show a cluster of concordant triassic ages (201 - 246 Ma) and a trend of discordant ages that intersects at 784 ± 21 Ma and 208 ± 7 Ma with a MSWD of 1.4. Thirtysix analyses of the overgrowth rims gave concordant ages and can be splitted in two concordant groups. The first group range from 201 to 214 Ma with a weighted mean age (MSWD) of 207 ± 1.4 Ma. With respect to the textural position of zircon, this age is interpreted as a post peak metamorphic age. Concordant analysis of the second zircon II group between 221 to 246 Ma yield a weighted mean age of 233.1 ± 5.3 Ma in the range of UHP metamorphism.

Conclusion

In situ dating of petrologically and texturally well constrained zircon rims in a thin section from retrogressed UHP elclogite of the CCSD hole shows an age pattern that is in agreement with the previous published U-Pb datas obtained from mineral separates. However, the correlation with retrograde textures by texture controlled analysis we can show that retrogression along discrete fluid-induced retrogression zones within the UHP eclogites initiated at deeper levels and earlier than reported from coherent amphibolite bodies in the Sulu drill core. This investigation documents the onset of exhumation during the UHP metamorphic event along preexisting zones.

Hacker, B. R., Wallis, S. R., Ratschbacher, L., Grove, M. \& Gehrels, G. (2006): High-temperature geochronology constraints on the tectonic history and architecture of the ultrahigh-pressure Dabie-Sulu Orogen. Tectonics, 25, TC5006, doi: 10.1029/2005TC001937.

Hacker, B. R.; Ratschbacher, L.; Webb, L.; McWilliams, M. O.; Ireland, T.; Calvert, A.; Dong S.; Wenk, H.-R.; Chateigner, D. (2000): Exhumation of ultrahigh-pressure continental crust in east central China; Late Triassic-Early Jurassic tectonic unroofing, Journal of Geophysical Research, Vol. 105, Issue B6, pp. 13,339-13,364.

Southeast Atlantic upwelling intensity changes influencing late Miocene C_4 plant expansion?

FLORIAN ROMMERSKIRCHEN[1], LYDIE DUPONT[1], TEGAN CONDON[2], GESINE MOLLENHAUER[3], ENNO SCHEFUß[1]

[1]Marum - Center for Marine Environmental Sciences, University of Bremen, P.O. Box 330 440, D-28334 Bremen, Germany
[2]Department of Earth & Planetary Sciences, Havard University, 20 Oxford Street, Cambidge, MA 02138 USA
[3]Alfred Wegener Institute for Polar and Marine Research, D-27570 Bremerhaven, Germany

The Late Miocene epoch (about 15 to 5 Myrs BP) is characterised by fundamental changes in Earth's climate system: turnovers in marine and terrestrial biota, sea-level variability, changes in surface- und deep-water circulations, and increase in upwelling intensities along the coasts [1,2]. During the transition period the Antarctic ice sheets expanded and were permanently established, while additionally ice volumes began to fluctuate [1]. Plants acting with the C_4 concentrating mechanism of CO_2 fixation for photosynthesis expanded nearly simultaneous at different places in the world, whereas the global CO_2 levels exhibit no corresponding change [1,3]. However, C_4 plants are also known to have a competitive advantage in habitats of higher temperature, light and fire intensities as well as of limited water supply, compared to the almost ubiquitous C_3 plants. This study tries to give insights to Miocene climatic conditions in Southwest Africa and how these conditions may be linked to the C_4 plant expansion.

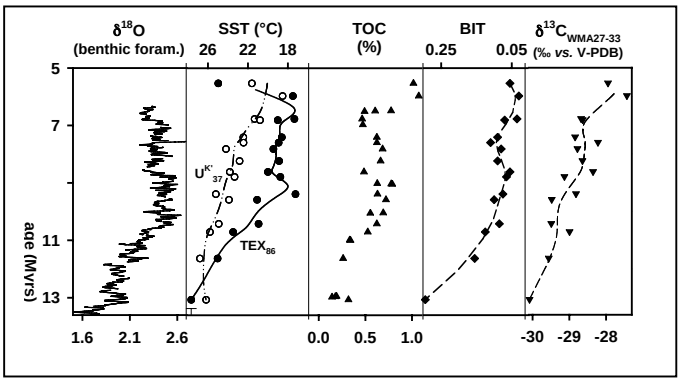

Fig. 1. Late Miocene data of core ODP 1085A: displayed are a 51-kyr moving average of $\delta^{18}O$ values of benthic foraminifera [4], SSTs (calculated via TEX_{86} and $U^{K'}_{37}$ indices), TOC, BIT and weighted mean averages of *n*-alkane $\delta^{13}C$ values in the odd carbon number range 27 to 33 (‰ vs. V-PDB). Dashed and straight lines represent an estimated trend of data.

We focused on data from a sediment core of the Ocean Drilling Program (Leg 175, ODP 1085A), which span about 10 Myrs of the late Miocene. The core is situated in the Cape basin at the south-western African continental margin in the upwelling zone of the Benguela coastal current. The current brings cold, nutrient-rich waters from South Atlantic and the Antarctic circumpolar current to the surface water along the coast of Southwest Africa. Miocene sea surface temperatures (SST) were reconstructed by two indices, tetraether index (TEX86) and an alkenone based index ($U^{K'}_{37}$). Both trends exhibit a shift to cooler temperatures from around 27 to 18°C, but are different in rate and timing (Fig.1). Especially by TEX86 reconstructed SSTs exhibit a similar trend as found for ice volume changes shown by the $\delta^{18}O$ curve (cf. Fig. 1) [4]. These findings may reflect an intensification of the Benguela upwelling current during the late Miocene, probably in association with the formation of West Antarctic ice sheet. The increased upwelling enhances the marine primary production shown by a small overall shift in the total organic carbon (TOC) content (<1%, Fig. 1).

Terrestrial organic material is supplied to Cape basin by the Orange River and by airborne dust. The branched and isoprenoid tetraether (BIT) index correlates with the relative fluvial input of terrestrial organic material delivered to the ocean. The decline in BIT to almost negligible levels (<0.1, Fig.1) indicates a decrease in river runoff and continental humidity and/or an increase of upwelling, eliminating the river discharge contribution to the studied sediments. The C_4 plant contribution to the vegetation is ascertainable by stable carbon isotopic composition of sedimentary wax *n*-alkanes ($\delta^{13}C_{WMA27-33}$). The shift to heavier values indicates an increased contribution of C_4 plants to the continental vegetation (Fig. 1). We want to discuss these findings with pollen counts of grasses and of other taxa of the same sediments.

Upwelling supported cold SSTs are linked with continent to ocean heat transfer, which favours an increase in aridity on the adjacent continent. It is believed that these conditions enhance biomass burning driving the Miocene C_4 plant expansion on continents [5], probably driven by climatic changes due to the formation of polar ice sheet.

[1] Zachos, J. et al. (2001) Science 292, 686-693.
[2] Diester-Haass, L.D., et al. (1990) Paleoceanogr. 5, 685-707.
[3] Tipple, B.J., Pagani, M. (2007) Annu. Rev. Earth Planet. Sci. 35, 435-461.
[4] Westerhold, T., Bickert, T., Röhl, U. (2005) Palaeogeogr. Palaeoclimat. Palaeoecol., 217, 205-222.
[5] Keeley, J.E., Rundel, P. W. (2005) Ecol. Lett. 8, 683-690.

Cold-water coral reef development on carbonate mounds in relation to paleo-density estimates

A. RÜGGEBERG, V. LIEBETRAU, J. RADDATZ, S. FLÖGEL, W.-CHR. DULLO, AND THE IODP EXP. 307 SCIENTIFIC PARTY

Leibniz-Institute of Marine Sciences (IFM-GEOMAR), Wischhofstrasse 1-3, D-24148 Kiel, Germany

Cold-water coral reefs are very abundant along the European continental margin in intermediate water depths and are able to build up large mound structures. These carbonate mounds particularly occur in distinct mound provinces on the Irish and British continental margins. Previous investigations resulted in a better understanding of the cold-water coral ecology and the development of conceptual models to explain carbonate mound build-up. Two different hypotheses were evoked to explain the origin and development of carbonate mounds, external versus internal control (e.g., Freiwald et al. 2004 versus e.g. Hovland 1990). Several short sediment cores have been obtained from Propeller Mound, Northern Porcupine Seabight, indicating that cold-water corals grew during interglacial and warm interstadial periods of the Late Pleistocene controlled by environmental and climatic variability supporting the external control hypothesis (e.g. Dorschel et al. 2005, Rüggeberg et al. 2007).

The recent discovery of Dullo et al. (2008) highlights the impact and importance of the external (environmental) control hypothesis with coral growth and distribution following the structure of seawater density, i.e. the potential density anomaly sigma-theta. This study evidences that all studied living coral reef sites of the NE Atlantic are occurring in water masses with a specific density window of sigma-theta = 27.5 ± 0.15 kg m^{-3}, whereas dead reefs are outside this density range. In order to transfer this idea to the paleo-record, we used the method of Lynch-Stieglitz (2001) and others for the determination of paleo-densities using stable oxygen isotope measurements ($\delta^{18}O$) on benthic foraminifera. The accuracy of the density reconstruction is well known for the Holocene, the Last Glacial Maximum, and past interglacials.

With this knowledge we tested whether paleo-densities might be an important prerequisite for growth and development of cold-water coral reefs during the past interglacials and during mound initiation. $\delta^{18}O$ records of benthic foraminifera from sediment cores of Propeller Mound indicate that paleo-density values have a similar range during interglacials and interstadials of the past 300 kyr as for the present-day settings. However, the method is only valid for temperatures between 5° and 30°C. Therefore, mean glacial values of 27.8 kg m^{-3} are minimum estimates considering possible glacial temperatures below 5°C, but are clearly offset to the living-coral-reef-density-range of 27.35–27.65 kg m^{-3}. We also tested this application on sediments from IODP Exp. 307 core 1317 C indicating that seawater densities are in a similar range during mound initiation at 2.6 Ma (Kano et al. 2007) as today.

Dorschel et al. (2005) Earth and Planetary Science Letters, 233: 33– 44.
Dullo et al. (2008) Marine Ecology Progress Series, 371:165–176.
Freiwald et al. (2004) UNEP-WCMC, p. 84.
Hovland (1990) Terra Nova, 2: 8–18.
Kano et al. (2007) Geology, 35(11):1051–1054.
Lynch-Stieglitz (2001) Geochemistry Geophysics Geosystems, 2, doi: 10.1029/2001GC000208.
Rüggeberg et al. (2007) International Journal of Earth Sciences, 96: 57–72.

Chalcophile element budget in the oceanic crust: First results from the complete section of upper oceanic crust at borehole 1256D (ODP-Leg 206, Exp 309 and Exp 313)

B. SCHEIBNER[1], H.-G. STOSCH[2]

[1]Forschungszentrum Jülich, Abteilung Neue Materialien und Chemie, 52525 Jülich
[2]Universität Karlsruhe, Geologisches Institut, Kaiserstr. 12, 76131 Karlsruhe

Hydrothermal processes in the oceanic crust at ridges causes significant changes in the budget of chalcophile elements. Circulation of mobilised chalcophile elements (e.g. copper and zinc) have, under appropriate conditions, the potential to form stockwork sulphide mineralisation. Pronounced massive sulphide deposits in the oceanic crust are often located in the Transition Zone between the Lava Flows and the Sheeted Dike Complex. The root zones for these ore-forming deposits are probably located at the transition between the Sheeted Dike Complex and the Gabbros. Although in previous studies (e.g. Alt 1995, Peucker-Ehrenbrink et al. 2003) calculations on the mass transport during hydrothermal processes in the crust were presented, a complete budget of the geochemical flux of the chalcophile elements in the upper crust is still lacking. For performing such a calculation, a sample suite is required, which probes a complete in situ section of upper oceanic crust. Such a section of oceanic basalts and gabbros was drilled during ODP-Leg 206, Expedition 309 and Expedition 313 at borehole 1256 in the eastern equatorial Pacific on 15 Ma oceanic crust of the Cocos plate. A detailed description and dicussion on the petrogenesis of the section is given in Wilson et al. (2006) and Koepke et al. (2007).

Selected samples from each stratigraphic unit (Lava Pond, Transition Zone, Sheeted Dike Complex, Gabbro) of borehole 1256 were analysed during this study – amongst others – for their major and trace elements by XRF at the Steinmann Institut, Bonn University. We find copper concentrations to be highly variable in the Gabbro and Granoblastic Dikes, whereas zinc shows no significant variation in these units (Figure 1). In contrast, zinc is highly variable in the upper parts of the Upper Dikes, where the concentration of copper is fairly constant. Both, copper and zinc, show slight enrichments in the Transition Zone and uniform concentrations in the parts above the Transition Zone. The enrichments in the Transition Zone are significantly lower than enrichments found in the Transition Zone at other places (e.g. Bach et al. 2003).

The variation of copper in the Gabbro and the Granoblastic Dikes can be explained by oxidation of primary (magmatic) sulphides during hydrothermal alteration (Bach et al. 2003). Inspection of thin sections has shown secondary pyrite and chalcopyrite to occur in the Sheeted Dike Complex of borehole 1256 as recrystallised igneous sulphide globules, inclusions in moderately altered plagioclase or in interstitial areas. Furthermore it appears that the mobilised copper from the Gabbro and Granoblastic Dikes has not precipitated in the upper parts of the Upper Dikes but in the Transition Zone and possibly in stockworks above the Transition Zone.

The variation of zinc at borehole 1256 may have been produced during the formation of secondary oxides, because mobilisation of zinc is ascribed to the replacement of primary Ti-magnetite by sphene and secondary magnetite (Bach et al. 2003).

In summary, the geochemical patterns of copper and zinc in the downhole variation diagram of borehole 1256 indicate that mobilisation of these elements was caused by different processes and/or under the influence of different kinds of fluids under different temperatures.

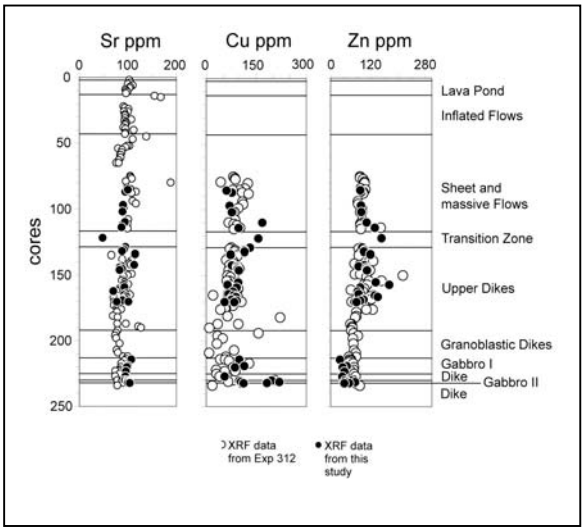

Figure 1. Downhole variation of Sr, Cu and Zn in borehole 1256D. Samples were measured by XRD during Leg 206, Expedition 309 and 312 (open circles) and during this study (filled circles). Strontium – as a fluid-mobile element – was not significantly affected by hydrothermal alteration, except being slightly depleted in the Transition Zone. This observation is consistent with previous studies about strontium fractionation in basalts. Further explanations about copper and zinc see text.

Alt, J.C. (1995) Geology 23, 585-588
Peucker-Ehrenbrink, B., Bach, W., Hart, S. R., Blusztajn, J. S., Abbruzzese, T. (2003) Geochemistry, Geophysics, Geosystems 4 (7)
Bach, W., Peucker-Ehrenbrink, B., Hart, S. R. and Blusztajn, J. S. (2003) Geochemistry, Geophysics, Geosystems 4 (3)
Wilson et al. (2006) Science 312 (5776) 1016-1020
Koepke, J., Christie, D., Dziony, W., Holtz, F., Lattard, D., Maclennan, J., Park, S., Scheibner, B., Yamasaki, T., Yamasaki, S. (2008) G^3 9

Clay nano-coatings and their role in fault-creep activity in the San Andreas Fault

A.M. SCHLEICHER[1,2], B.A. VAN DER PLUIJM[2], L.N. WARR[3]

[1]*Friedrich-Alexander Universitaet Nuernberg-Erlangen, Geozentrum Nordbayern, Schlossgarten 5, 91054 Erlangen, Germany*
[2]*University of Michigan, Department of Geological Sciences, 1100 University Ave, C.C.Little Building, Ann Arbor, MI 48109, U.S.*
[3]*Ernst-Moritz-Arndt-Universitaet Greifswald, Institut für Geographie und Geologie, Friedrich-Ludwig-Jahn-Str. 17, 17487 Greifswald, Germany*

The San Andreas Fault Observatory at Depth (SAFOD) drill-site situated near Parkfield, California offers the opportunity to investigate the role of in-situ, fault-related mineralization along an active strike-slip plate boundary (Hickman et al. 2004). During summer 2005, drilling successfully crossed the active trace of the San Andreas Fault at ~3300 m measured depths; in 2007 core material was obtained across the active deformation zones at 3194 and 3301 m, and from just outside the geologically defined San Andreas Fault Zone (Hickman et al. 2008; Fig, 1). Many investigations have show that phyllosilicates contribute to a mechanically weak San Andreas Fault (e.g. Wu et al. 1974), but there are contrasting opinions as to which minerals are responsible for low frictional coefficients and fault creep behavior along the active section of the Fault. One recent hypothesis proposes that talc and serpentine are responsible for the apparent weakness of the fault rock in the SAFOD drillhole (Moore and Rymer 2007). However, in our study of mineral phases from mineralized slip planes at ca. 3.0-3.4 km measured depths, we have not been able to identify these minerals in big amounts or on displacement surfaces.

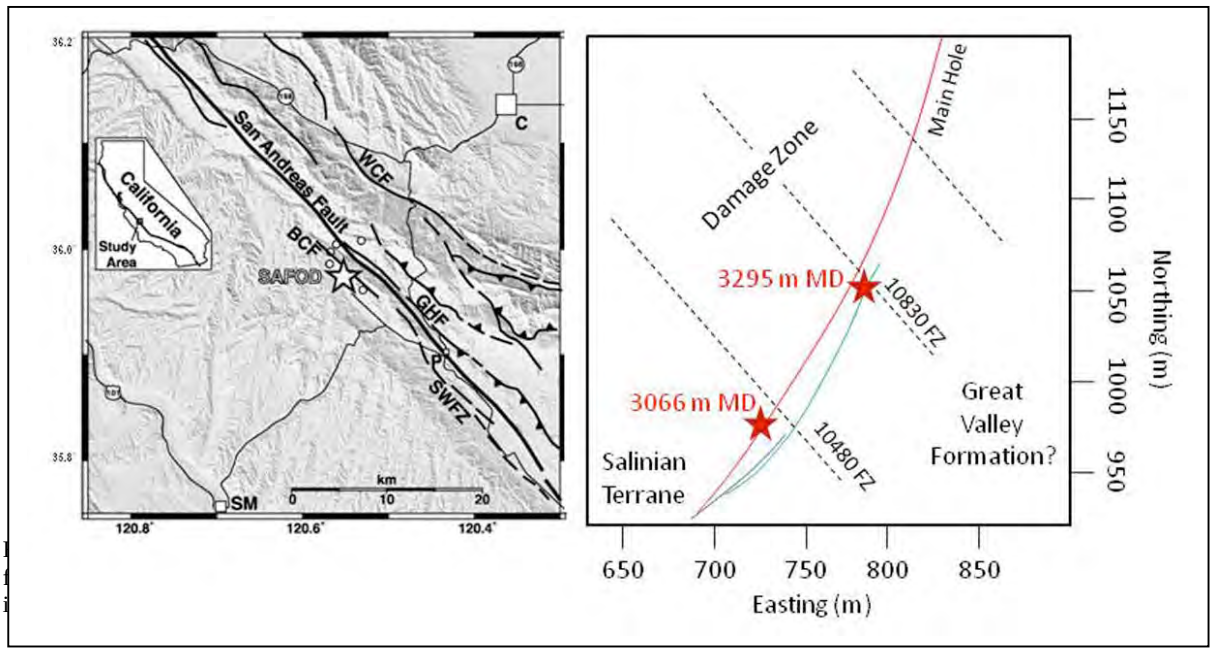

We investigated samples from two distinct shear zones at ~3066 m and ~3300 m measured depth, using X-ray diffraction (XRD), secondary–and transmission electron microscopy (SEM/TEM), as well as $^{40}A/^{39}Ar$ dating analysis (Fig. 2). The deeper rocks belong to the sedimentary rocks of the Great Valley Sequence (K Mc Dougall in Bradbury et al. 2007), and are close to an area of active casing deformation (Zoback et al. 2005). They contain dark greenish-gray, thinly bedded siltstone and very fine-to medium-grained sandstone that are disrupted by offset along discrete mesoscale faults and by more distributed shearing in the finer-grained layers. The upper samples are situated outside the actively deforming traces of the fault and derived from a ~ 30 cm broad, clay-rich shear zone positioned in the lowest part of a fine-grained arkosic and lithic arenite containing siltstones and mudstones (Bradbury et al. 2007, Solum et al. 2006, Schleicher et al. 2009).

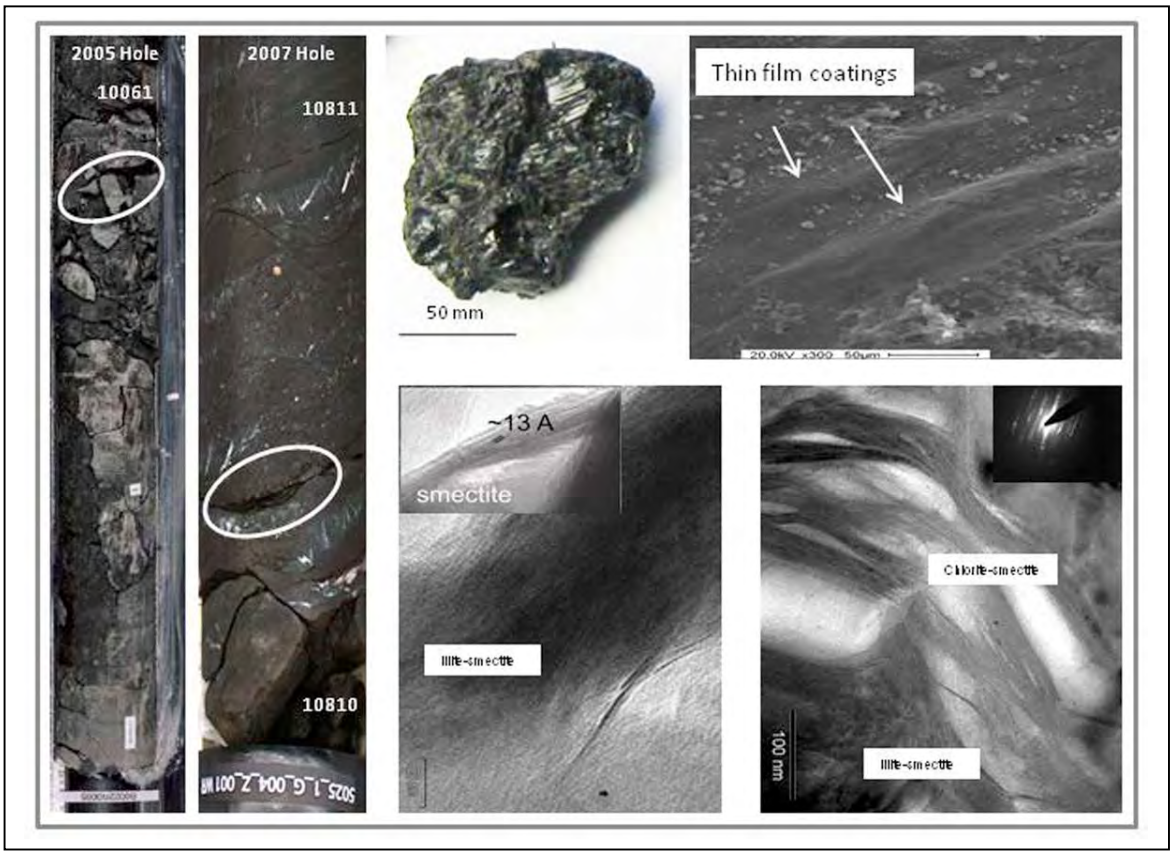

Fig. 2: core material from the SAFOD borehole at 3066 m MD and 3295 m MD, b,c) rock chips and SEM pictures show polished surfaces and thin film slickensides, d,e) TEM pictures show thin layers of illite-smectite and chlorite-smectite crystals with wavy layers and irregular crystal boundaries

A detailed mineralogical study of both shear zones show illite and illite-smectite (I-S) clay minerals, with additional chlorite and chlorite-smectite (C-S) in the deeper sample. The characteristics of some authigenic I-S and C-S indicate a deep diagenetic origin. Randomly ordered C-S with up to 50% smectite layers, and I-S with ca. 20-25 % smectite layers are the dominant authigenic clay species across the fault zone (Schleicher et al. 2009). However, the most smectite-rich mixed-layered assemblage with the highest water content occurs in the actively deforming creep zone at ca. 3300 – 3350 m measured depth. Adopting available kinetic models for the crystallization of I-S in burial sedimentary environments and the current borehole depths and thermal structure, the conditions and timing of I-S growth can be evaluated. Assuming a typical K+ concentration of 100-200 ppm for sedimentary brines, a present day geothermal gradient of 35°C/km and a borehole temperature of ca. 112°C for the sampled depths, most of the I-S minerals can be predicted to have formed over the last 4-11 Ma and are probably still in equilibrium with circulating fluids. The exception to this simple burial pattern is the occurrence of the mixed-layered phases with higher smectite content than predicted by the burial model. These minerals, which characterize the actively creeping section of the fault and local thin film clay coating on polished brittle slip surfaces, can be explained by the influence of either cooler fluids circulating along this segment of the fault or the flow of K+ depleted brines in the fault.

We also investigated in detail localized, thin precipitations of hydrous mixed-layered clay minerals in both fault rocks, which grow preferentially on polished fracture clasts at occasionally slickensided displacement surfaces (Schleicher et al. 2006, Fig. 2). These heterogeneously distributed nano-coatings are of particular interest due to their specific localization, large surface areas, cation exchange possibilities, clay hydration state, and preferred orientation produced by substrate-controlled growth. TEM analysis of the separated minerals shows a random arrangement of ~5-10 layers of illite-smectite and chlorite-smectite crystals, with an average lattice thickness of 1.0 to ~1.4 nm (Fig. 2). The crystal boundaries are irregular and wavy.

Determining the formation of illite in relation to fault activity, the $^{40}Ar/^{39}Ar$ ages of different grain sizes reveal an “older” fault strand (8 Ma) at 3066 m measured depth, and a “younger” fault strand (5 Ma) at 3295 m measured depth. These ages imply that the fault zone initiation is at least 5 Ma and 8 Ma old and that the recent creep activity at ca.3300 m measured depth reflects a stage of fault reactivation. We propose that the majority of the slow creep occurs on such nano-coatings, accommodated by a combination of 1) slip along particle surfaces, 2) displacement along hydrated smectitic phases (primarily illite-smectite and chlorite-smectite), and 3) intracrystalline deformation of the clay lattice, associated with repeated dissolution and growth. The presence of enhanced concentrations of smectite in both illite-smectite and chlorite-smectite phases is proposed to contribute to fault weakening, with renewed cataclasis creating nucleation sites for neomineralization on grain surfaces during faulting. Our observations reveal the ultrathin hydrous clay coatings along displacement surfaces of the Parkfield section of the San Andreas Fault play a key role in influencing weak fault and creep behavior as opposed to talc/serpentine phases at these depths.

Bradbury K.K, Barton D.C., Solum J.G., Draper S.D., Evans J.P. (2007) Mineralogic and textural analyses of drill cuttings from the San Andreas Fault Observatory at Depth (SAFOD) boreholes: Initial interpetations of fault zone composition and constraints on geologic models, Geosphere, 3, 5, 299-318

Hickman S., Zoback M., Ellsworth W. (2004) Introduction to special section: Preparing for the San Andreas Fault Observatory at Depth, Geophysical Research Letters, 31, LI2SO

Hickman S., Zoback M., Ellsworth W., Chester J., Chester F., Evans J., Moore D., Kirschner D., Schleicher A., van der Pluijm B., Solum J. (2008) Structure and composition of the San Andreas Fault in central California: recent results from the SAFOD sample analysis, EOS 89 (Fall Meet.Suppl.) abstr.

Moore and Rymer (2007) Talc-bearing serpentinite and the creeping section of the San Andreas Fault, Nature, 448, 16,

Schleicher A.M., van der Pluijm B.A., Solum J.G., Warr L.N. (2006): The origin and significance of clay-coated fractures in mudrock fragments of the SAFOD borehole (Parkfield, California); *Geophysical Research Letters DOI* 10.1029/2006GL026505

Schleicher A.M., Warr L.N., van der Pluijm B.A. (2009) On the origin of mixed-layered clay minerals form the San Andreas Fault at 2.5-3 km vertical depth (SAFOD drillhole at Parkfield, California), Contributions to Mineralogy and Petrology, 157, 2

Solum J.G., Hickman S., Lockner D., Moore D., van der Pluijm B., Schleicher A.M**.,** Evans, J.P. (2006): Mineralogical characterization of protolith and fault rocks from the SAFOD main hole; *Geophysical Research Letters 34, DOI* 10.1029/2006GL027285, 2006

Wu F.T., Blatter L., Roberson H. (1975) Clay gouges in the San Andreas fault system and their possible implications, *Pure Applied Geophysics, 113: 87-96*

Zoback M.D., Hickman S., Ellsworth W. (2005) Overview of SAFOD Phases 1 and 2: Drilling, sampling and measurements of the San Andreas Fault zone at seismogenic depth, EOS 86 (Fall Meet.Suppl.) abstr. T23E-01

Preliminary heat flow results from NanTroSeize Expeditions 314/315/316 Nankai Trough, Japan

F.SCHMIDT-SCHIERHORN[1], R. HARRIS[2], M. KINOSHITA[3]

[1] University of Bremen, Postfach 330 440, Bremen, D-28334, Germany
[2] COAS, Oregon State University, 104 COAS Administration Building, Corvallis, OR 97331, United States
[3] IFREE, Japan Agency for Marine-Earth Science and Technology, 2-15 Natsushima, Yokosuka, 237-0061, Germany

Knowledge of the temperature distribution of the frontal thrust and shallow portion of the megasplay system off shore the Kii Peninsula is important for understanding the geodynamics of active plate boundaries and processes influencing the nature of the seismic/aseismic transition. During Integrated Ocean Drilling Program (IODP) Expeditions 315 and 316 temperature measurements were made at seven sites using both the APCT-3 and DVTP temperature tools. These data are of high quality and are internally consistent. The deepest measurement at each site varied from ~80 to ~243 mbsf. In addition, extensive thermal conductivity measurements were made on the recovered cores allowing thermal gradients to be reliably converted to heat flow. Thermal conductivities are combined with temperature data to form thermal resistance plots. In general temperature increases linearly with thermal resistance suggesting that a constant heat flow characterizes the data at each site. Heat flow values show relatively large spatial variations consistent with an accretionary prism undergoing active faulting and dewatering. Computed values of heat flow are anomalously low with respect to other values of heat flow along the Nankai Trough and in the vicinity of the Kii transect (Yamano et al., 2003, Phys. Chem. Earth, 28, 487-497). Reconciling these lower values obtained deeper in the section with shallow probe measurements requires a decreasing thermal gradient with depth.

Palecology and Paleoenvironment of the Neogene Nordic Seas based on Dinocyst Assemblages

M. SCHRECK, J. MATTHIESSEN

Alfred Wegener Institute for Polar and Marine Research (AWI), Bremerhaven, Germany

The Cenozoic is a period of considerable climatic changes when the Earth finally went from the „Greenhouse World“ into the fully glaciated, so called „Icehouse World“ (e.g. Zachos et al. 2001). Superimposed on the long-term cooling trend frequent short-term climate changes occured leading to rather variable climate conditions during the Neogene and finally to the pronounced glacial-interglacial cycles in the Pleistocene (e.g. Flower and Kennett 1994). Despite being a sensitive region for climate change on various timescales, marine paleontological proxy records played a subordinate role in reconstructing the Northern High Latitude climate evolution in the Neogene. Most of our knowledge is based on the North Atlantic, and although Neogene sequences were succesfully drilled during ODP Legs 104, 105, 151 and 162, the long-term paleoenvironmental evolution of the Nordic Seas is still virtually unknown due to the low biogenic carbonate and opal content in the hemipelagic sediments.

Despite marine palynomorphs (e.g. dinoflagellate cysts, acritarchs etc.) have been proven as a useful tool for biostratigraphy as well as for paleoecological and paleoenvironmental reconstructions in the High Northern Latitudes in the past two decades (e.g. Head et al. 1989, Manum et al. 1989, Matthiessen and Brenner 1996) a consistent palynostratigraphy is not available. This is mainly due to a inconsistent Neogene chronostratigraphic framework of ODP holes which hampered the comparison of numerous potentially valuable dinocyst datums identified at the severel sites. To overcome this obstacle, a transect from the seasonally ice-covered Nordic Seas to the perennial ice-coverd Arctic Ocean consisting of Sites 907, 909 and M0002A is studied within the project „Palynomorphs in the Northern High Latitude Cold Water Domain: A Neogene Stratigraphic and Paleoenvironmental Transect across the Fram Strait” (DFG-MA3913/2). Site 907A in the Icelandic Sea,

with a almost continous Neogene sequence recovered, is the standard reference section for the past 15-17 Ma. Its revised high-resolution magnetic polarity stratigraphy (Channel et al. 1999) based on the composite section of three holes is well-dated and additionally tied to an independent diatom biostratigraphy (Koç and Scherer 1996). Therefore it provides one of the best Neogene high northern latitude chronostratigraphic records and will be used to calibrate our palynomorph datums to the polarity time scale.

In a initial study Poulsen et al. (1996) established a informal dinocyst zonation for ODP Leg 151 Sites 907-909 with an average resolution of 60-300kyr consisting of three dinocyst zones for Site 907. Based on the established age-model and in order to improve the temporal resolution Hole 907A was initially sampled at 100kyr intervals. A first overview suggested a suddivision into two intervals from 50-110mbsf and 110-216mbsf.

With the study on the 50-100 mbsf interval we are able to extend the dinocyst record of Poulsen et al. (1996) up to the Piacenzian/Gelasian boundary. Generally dinoflagellate cyst concentration is low in this interval with only a few species recorded in most samples possibly reflecting the cold environment in the Late Miocene to Middle Pliocene. The distribution of dinocysts is apparently related to hydrographic conditions of the surface water layer (temperature, salinity, nutrients) and the temporal and spatial distribution of extant species (e.g. *Nematosphaeropsis labyrinthus*, *Impagidinium* spp.) is used to infer palecological preferences (e.g Matthiessen et al. 2005). Since the Neogene comprises a considerable number of extinct species (e.g. *Decahedrella martinheadii*, *Habibacysta tectata*), their palecological affinities cannot be simply inferred from a modern distribution. Therefore a different approach using the relationship between their paleogeographic distribution and the known paleoclimate evolution is additionally applied. Preliminary semiquantitative estimates of abundances are indicating substantial changes in assemblage composition that will be utilized in a high latitude reconstruction of Neogene paleoenvironments. We identified different assemblages and distinctive suites of acmes possibly reflecting considerable variations in the physical characteristics of water masses due to the long-term global cooling. Six dinocyst assemblages often dominated by a few species were tentatively defined for the 50-100 mbsf interval, showing a broad variation and changes on short intervals possibly indicating a cold (*Spiniferites* cf. *elongatus*, *Impagidinium* spp.) and oceanic (*N. labyrinthus*) setting. Assemblages dominated by the cold water species *D. martinheadii* are centered around an acme in the middle Late Miocene which is similar to its maximum concentration in the Arctic Ocean (Matthiessen et al. in press). Based on the magnetostratigraphy the last appearance datum (LAD) is tentatively fixed at approx. 6.2 Ma. at Site 907A. Although *D. martinheadii* is accepted to be a good stratigraphic marker (Matthiessen et al. in press) its still difficult to define the first appearance datum (FAD) because of too few holes covering the total stratigraphic range. Due to the good age control and the complete early Middle-Late Miocene sequence of 907A the precise FAD and LAD will be adressed in the future work by resampling the specific intervals at higher resolution. A barren interval between 99-103 mbsf, representing approx. 700kyr is also designated for resampling at higher resolution to detect short term changes in productivity probably related to sea-ice cover.

Within the 110-216mbsf interval dinocyst diversity starts to increase downcore reflecting changes in water mass properties. Higher abundances of *Protoperidinium* spp. may indicate a increased productivity and nutrient-rich surface water conditions. The assemblages in most of the samples between 110-216 mbsf show high proportions of small to medium sized spherical morphotypes such as *Baticasphaera* spp., *H. tectata*, *Filisphaera filisphaera* s.l., *Cymatiosphaera* spp. and other acritarchs. We found several intervals partly dominated by the *Cymatiosphaera* complex which Poulsen et al. (1996) reported from two samples only (as *Cymatiosphaera*? *invaginata*). Due to its restricted stratigraphic range this group might be a good biostratigraphic marker. Its also reported in the Labrador Sea (De Vernal and Mudie 1989) from a possibly time-equivalent interval. Besides *C.*? *invaginata* we recorded several other *Cymatiosphaera* species as well as spinose palynomorphs with unclear biological affinity (acritarchs) not described by Poulsen et al. (1996).

A careful study of 907A dinocysts and comparison with Poulsen et al. (1996) revealed several other discrepancies in the taxonomy, and estimates of abundances are partly not reproducible. As an example of problematic taxonomic assignments, we only found *Baticasphaera minuta* sensu Matsuoka and Head (1992) while Poulsen et al. (1996) recorded 5 different species of *Baticasphaera*. The concept for the genus *Baticasphaera* Drugg is questionable due to slight variations in cyst surface ornamentation that were not clearly documented in the first descriptions possibly reflecting morphological transitions within a species rather then different species. This genus might be of stratigraphic importance in the Central Arctic Ocean and therfore needs a careful reexamination. As a result of our study on Site 907A it is evident that taxonomic concepts of more high latitude dinocyst taxa must be reevaluated than expected in order to make reliable interpretations on their stratigraphic value and paleoenvironmental significance.

Smelror et al. (unpubl. manuscript) proposed several marker species for a Norwegian-Greenland Sea Zonation (NGSZ) which are often rare in 907A and only two of them (*D. martinheadii* and *F. filifera*) are recorded in IODP Site M0002A so far (Matthiessen et al. in press). This is partly due to the more temperate-warm water affinities of the stratigraphic markers proposed by Smelror et al. (unpubl. manuscript). We attempt to incorperate as many zonal markers of the NGSZ into our coldwater zonation to allow correlation between the Nordic Seas and Arctic Ocean but nevertheless it displays that new marker species are required to establish a high resolution biostratigraphy including the Central Arctic Ocean realm. The broad and often undescribed group of acritarchs recognized in Hole 907A might be useful groups to establish a Neogene palynostratigraphic framework in the High Northern Latitudes.

On the poster we present a tentative definition of dinocyst assemblages throughout the complete 907A record as well as a initial compilation of stratigraphic useful species and their paleogeographic distribution indicating (paleo-) environmental preferences.

Channell, J. E. T., Amigo, A. E., Fronval, T., Rack, F. and Lehman, B. 1999. Magnetic stratigraphy at Sites 907 and 985 in the Norwegian-Greenland Sea and a revision of the Site 907 Composite section. In: M.E. Raymo, E. Jansen, P. Blum and T.D. Herbert (Editors), *Proceedings of the Ocean Drilling Program, Scientific Results*. 131-148.

De Vernal, A. and Mudie, P.J. 1989a. Late Pliocene to Holocene palynostratigraphy at ODP Site 645, Baffin Bay. In: S.P. Srivastava, M. Arthur, B. Clement et al. (Editors*), Proceedings of the Ocean Drilling Program, Scientific Results.* 105, 387-399.

Flower, B.O. and Kennett, J. P. 1994. The middle Miocene climate transition: East Antarctic ice sheet develoopment, deep ocean circulation and global carbon cycling. *Palaeogeography, Palaeoclimatology, Palaeoecology*. 108: 537-555.

Head, M.J., Norris, G. and Mudie, P.J. 1989a. Palynology and dinocyst stratigraphy of the upper Miocene and lowermost Pliocene, ODP Leg 105, Site 646, Labrador Sea. In: S.P. Srivastava, Arthur, M.A., Clement, B., et al. (Editors), *Proceedings of the Ocean Drilling Program, Scientific Results*, 105, 423-451.

Koç, N. and Scherer, R.P. 1996. Neogene diatom biostratigraphy of the Icelandic Sea Site 907. In: J. Thiede, A. Myhre, J.V. Firth, G.L. Johnson and W.F. Ruddiman (Editors), *Proceedings of the Ocean Drilling Program, Scientific Results.* 151, 61-74.

Manum, S.B., Boulter, M.C., Gunnarsdottir, H., Rangnes, K. and Scholze, A. 1989. Eocene to Miocene Palynology of the Norwegian Sea (ODP Leg 104). In: O. Eldholm, J. Thiede and E. Taylor (Editors), *Proceedings of the Ocean Drilling Program, Scientific Results* 104, 611-662.

Matthiessen, J. and Brenner, W. 1996. Dinoflagellate cyst ecostratigraphy of Pliocene/Pleistocene sediments from Yermak Plateau, Arctic Ocean (ODP Leg 151,Site 911A). In: J. Thiede, A. Myhre, J.V. Firth, G.L. Johnson and W.F. Ruddiman (Editors), *Proceedings of the Ocean Drilling Program, Scientific Results*. 151, 243-253.

Matthiessen, J., de Vernal, A., Head, M.J., Okolodkov, Y., Zonneveld, K., Harland, R. 2005. Modern organic-walled dinoflagellate cysts in Arctic marine environments and their (paleo-) environmental significance. *Paläontologische Zeitschrift* 79(1), 3-51

Matthiessen, J., Brinkhuis, H., Poulsen, N., Smelror, M. in press. Decahedrella martinheadii – a stratigraphic and paleoenvironmental acritarch indicator species for the high norther latitude Late Miocene. *Micropaleontology*

Matsuoka, K. and Head, M.J. 1992. Taxonomic revision of the Neogene palynomorphs *Cyclopsiella granosa* (Matsuoka), *Baticasphaera minuta* (Matsuoka) , and a new species of *Pyxidinopsis* Habib (Dinophyceae) from the Miocene of the Labrador Sea. In: M.J. Head and J.H. Wrenn (Editors), *Neogene and Quarternary dinoflagellate cysts and acritarchs*. 165-180.

Poulsen, N.E., Manum, S.B., Williams, G.L. and Ellegard, M. 1996. Tertiary dinoflagellate biostratigraphy of Site 907, 908, and 909 in the Norwegian-Greenland Sea. In: J. Thiede, A. Myhre, J.V. Firth, G.L. Johnson and W.F. Ruddiman (Editors*), Proceedings of the Ocean Drilling Program, Scientific Results.* 151, 243-253.

Smelror, M. and Anthonissen, E.: A Neogene dinoflagellate cyst biozonation for the Norwegian-Greenland Sea. (unpubl. manuscript)

Zachos, J., Pagani, M., Sloan, L.,Thomas, E. and Billups, K. 2001. Trends, rhythms, and aberrations in global climate 65 Ma to present. *Science* 292: 662-667.

Pelagic red beds in ODP Leg 207 (Demerara Rise): Evidence for an Early Paleogene oxic event in the Western Atlantic?

P. SCHULTE[1], A. KONTNY[2], M. JOACHIMSKI[1]

1 GeoZentrum Nordbayern, Universität Erlangen, D-91054 Erlangen, Germany (schulte@geol.uni-erlangen.de)
2 Geologisches Institut der Universität Karlsruhe, Strukturgeologie und Tektonophysik, D-76187 Karlsruhe, Germany

Introduction: The early Paleogene is associated with prominent environmental changes, including the recovery from the global mass extinction at the Cretaceous-Paleogene (K-Pg) boundary [1], a second phase of Deccan Trap flood basalt volcanism [2], as well as with the possible occurrence of a hyperthermal event about 200 kyr post K-Pg [3]. To understand the effects of these events, we combined high-resolution mineralogical and isotope geochemical analysis with shipboard geophysical data to determine climate and paleoceanographic changes from the Cretaceous-Paleogene (K-Pg) boundary up to the Danian-Selandian boundary (about 60 Ma) in the western tropical Atlantic. The ODP Leg 207 from the Demerara Rise, western Atlantic occupies a central position for understanding the post-K-Pg evolution for the low latitude Paleogene deepwater record [4-6]. Moreover, ODP Leg 207 shows several prominent red-stained intervals during the Paleocene that may indicate significant oceanographic changes [6].

Methodology: The investigated cores 1258A and 1259C recovered a biostratigraphically complete K-Pg succession including latest Maastrichtian (Zones CF1-CF2) and Danian (P0 to P3a) clayey chalks, separated by the spherule-rich K-Pg event deposit [4, 5]. We used the geophysical log data from the ODP Janus database (measured on the working core halves with the multi sensor track instrument). For $\delta^{13}C$ and $\delta^{18}O$ analysis, samples were washed over a 36 µm sieve. Subsequently, the fine fraction <36 µm was powdered and analyzed at the University of Erlangen. The mineral content was determined at the University of Erlangen on wet powdered samples (grain size <10 µm obtained with a McCrone Micromill) with a Siemens D5000 X-ray diffractometer and evaluated by quantitative Rietveld analysis with the BGMN software. The magnetic susceptibility as function of temperature was measured at the University of Karlsruhe for the temperature range between –192 and 700 °C using KLY-4 S Kappabridge (300 A/m, 875 Hz), combined with the CS-L/CS-3 furnace of AGICO.

Results (see Fig. 1 and 2): Stable isotopes and mineral abundances revealed quite stable late Maastrichtian (Biozones CF2 and CF1) environments without evidence for oceanographic and climate changes. The K-Pg boundary is associated with the spherule-bearing event deposit [see details in 5] as well as with a prominent drop in carbonate content (from >75 wt% to <15 wt%) and a –2.5 per mil shift in $\delta^{13}C$. The K-Pg boundary also correlates with the iridium anomaly [4 and Deutsch et al. this volume], providing further support for the K-P boundary event – Chicxulub impact link.

There is a rapid recovery of the carbonate content following the K-P boundary productivity crash to quite stable values around 30 wt% already during Biozone Pα. During Biozone P0, $\delta^{18}O$ values show a brief, 1 per mil positive excursion, that may correspond to a short-term cooling event following the K-Pg boundary [1]. Moreover, our results confirm the rapid recovery of $\delta^{13}C$ values during Biozone P0 and Pα, followed by a second long-term negative shift up to Biozone P1a as also observed by [7] at ODP Leg 208, eastern South Atlantic. The significance and cause for the second $\delta^{13}C$ minimum, however, is not yet constrained. Pre-K-Pg $\delta^{13}C$ were not reached during the interval studied (Biozones P0 to P3a), though carbonate contents recovered to pre-K-Pg values of >75 wt% during Biozone P3a, about 2.5-3 My following the K-Pg boundary.

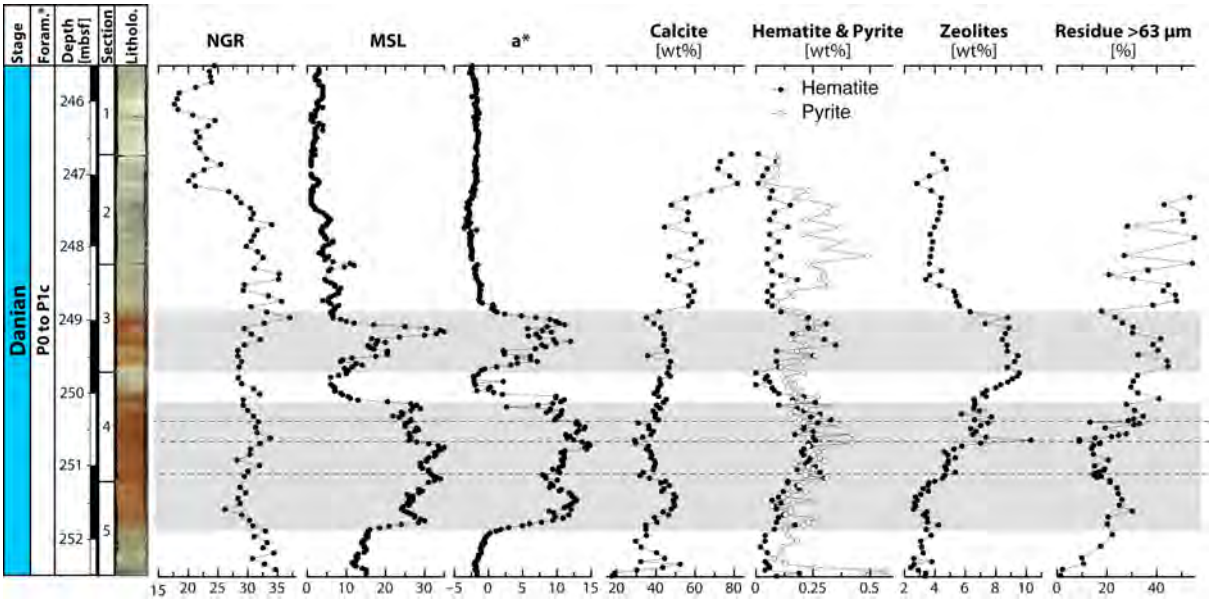

Fig. 1. Compilation of stratigraphy, lithology, geophysical logs (natural gamma ray, magnetic susceptibility, color reflectance) and mineralogy of Danian sediments from Hole 1258A Core 27R.

Major oceanographic perturbations associated with rapid $\delta^{13}C$ fluctuations, carbonate dissolution and onset of prominent red-staining occur during Biozone P1a, about 200 ky post-K-Pg. The red stained intervals during Biozone P1a are present in cores 1258A, B, 1259A, B, C, and 1260A. The onset is generally gradual and occurs always at 20-40 cm above the K-Pg boundary over several cm followed by several maxima in red color intensity associated with low-carbonate layers. The top of the red intervals is sharp, well defined, sometimes with light grey burrows from the overlying grey chalks. Red coloration is not linked to specific lithological changes, but the onset correlates with sharp increase in calcite abundance. Surprisingly, the color parameters a* and b* allow for further subdividing the red-stained intervals into parts with modest and extreme high a* and b* values that are, however, anti-correlated with the MSL values. That means, the highest a* and b* values do not correspond necessarily to peak MSL or NGR values. The late Maastrichtian red stained intervals (only found in cores 1260A, B) are of less intense coloration compared to the early Danian intervals and obviously associated with intense faulting. Along with the increase of the hematite contents, there is a prominent increase of the neoformed zeolites associated with the red stained intervals, whereas minerals characteristic for detritus input show no change in composition or abundance. Rietveld refinement, however, reveals improved calcite crystallinity during the red stained intervals that may result from the preferential removal of weakly crystallized carbonate phases during dissolution episodes. The temperature-dependent magnetic susceptibility shows that the red intervals are characterized by a prominent wide peak of the heating curve between 200-600 °C. This broad peak may be caused by the presence of ultrafine hematite particles. Considering stable isotope trends, the lowermost of the red intervals, up to three, short-lived –0.5 per mil $\delta^{13}C$ shifts occur that are associated with a 1 per mil lowering of $\delta^{18}O$ values and a 50 % reduction of the carbonate content, whereas generally, the red intervals are associated with strongly scattered, but a distinctly positive shift of the $\delta^{18}O$ values.

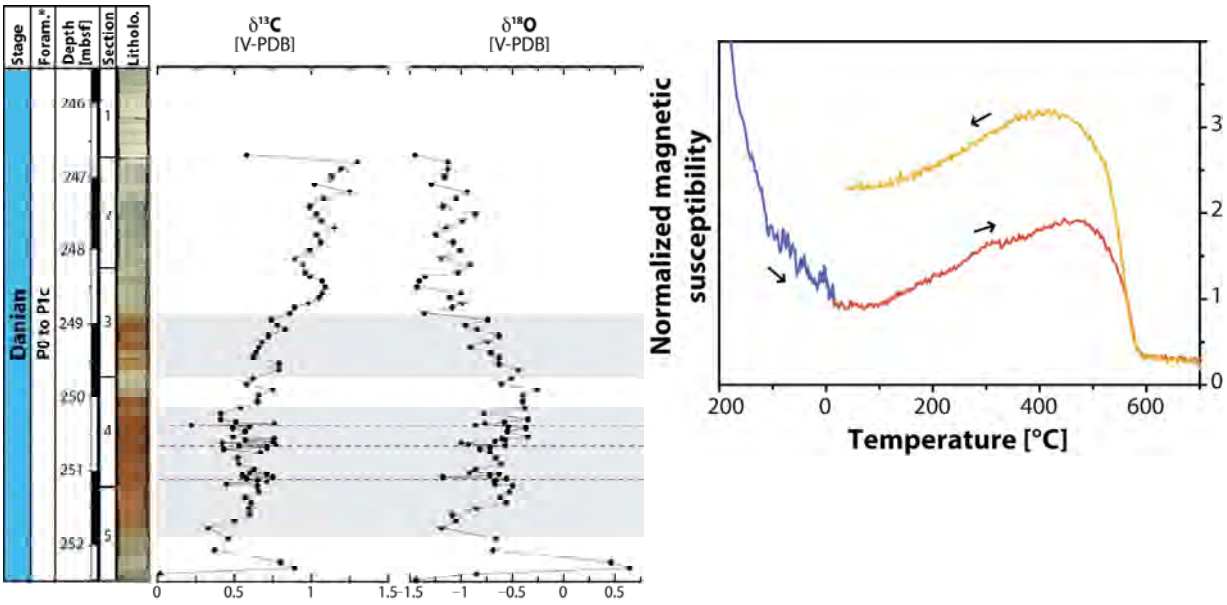

Fig. 2. Left: Compilation of stratigraphy, lithology, and stable isotopes from Danian sediments in Hole 1258A Core 27R. **Right:** Temperature-dependent magnetic susceptibility for a sample from the lowermost red interval.

Conclusions and Outlook: Mineralogical and rock magnetic as well as the stable isotope characteristics of the red intervals are very similar to Cretaceous red beds from the Tethyan realm [8]. Therefore, we tentatively suggest formation (redox boundary burn down) due to oceanographic changes (pulsed influx of cool oxygen-rich water masses?). The short-term negative $\delta^{13}C$ and carbonate content fluctuations may reflect a perturbation of the global C cycle and carbonate dissolution intervals that are correlative to the "DAN-C2 hyperthermal event" in the northern (ODP Site 1049C) and southern Atlantic (DSDP Site 527 and 528) [3]. The oceanographic implication of these findings are currently investigated by incorporating data from other Atlantic DSDP and ODP sites. The Nd isotope evolution during the Paleocene at ODP Leg 207 sites – which could provide data for changes in the oceanic current system – is currently analyzed by the group of Kenneth G. MacLeod (University of Missouri). In addition, a cyclostratigraphic framework for the K-Pg transition is established by Thomas Westerholt (Universität Bremen) to provide solid ground for correlating the succession of environmental changes at ODP Leg 207 to other Paleocene localities

[1] Koeberl, C., and MacLeod, K.G., eds., 2002, GSA Special Paper 356, 746 p.
[2] Chenet, A.-L., et al., JGR 113, B04101.
[3] Quillévéré, F., et al., EPSL 265, 600-615.
[4] MacLeod, K.G., et al., GSA Bulletin, 119, 101-115.
[5] Schulte, P., et al., 2009, GCA, (in press), doi: 10.1016/j.gca.2008.11.011.
[6] Schulte, P., et al., 2009, Geochemistry, Geophysics, Geosystems – G3 (submitted).
[7] Kroon, D., et al., eds., Proceedings of the Ocean Drilling Program: Scientific Results 208 1–55.
[8] Hu, X. et al., 2005, Cretaceous Research 26, 3-20.

Research study for a geoelectrical pre-site survey of the drilling location within the Eger Rift / NW-Bohemia: Investigation of the subsurface electrical conductivity distribution

C. SCHÜTZE, C. RÜCKER, CH. FLECHSIG

Institut für Geophysik und Geologie, Universität Leipzig, Talstraße 35, D-04103 Leipzig, Germany

The epicentral area in the Eger Rift near Nový Kostel/NW-Bohemia is favorised as location for a deep drilling project. The north-eastern part of the Cheb Basin is one of the most seismically active regions of Central Europe. Seismicity has a mainly swarm-like character. Most of the micro-earthquakes are located near to the northern limit of the basin and follow a N-S- striking fault zone. The numerous CO_2 emanations at the surface of the Cheb Basin are supposed to be generally connected to seismicity and to stem from the upper mantle.

Despite an intensive and complex geological-geophysical research in this area, many questions about the settings for the fluid regime and the generation of the earthquake swarms are unanswered. Geoelectrical methods could make a contribution to clarify the structural configuration of the region by an image of the resistivity distribution and to outline regions/zones of anomalous electrical resistivity as well as to delineate prominent geoelectric structures associated with seismological and fluid related features. Variations of the electrical conductivity structure may reflect structural changes in the upper crust which control the uprise of magmatic fluids in the geodynamic active area.

The results will assist the selection of adequate ICDP drilling locations in the Eger Rift from the sight of geoelectric rock properties.

The key parts of the research study were DC field experiments (injection test profiles and self-potential determination) and the development of a measurement strategy for a large-scale DC experiment in the region under investigation. Aware of the known high level of electrical noise and the industrial disturbances in the Eger Rift/Cheb Basin it was essential to clarify, whether artificial electrical signals are detectable over distances of approximately 15 km to enable a target depth of investigation of 4-5 km. The field tests aimed to the determination of signal quality, noise level and the kinds of noise sources, maximum transmitter – receiver distances, the influence by topography and the natural electrical field. The electrical resistivity tomography (ERT) measurement strategy has to adapted to the investigation of the conductivity distribution within the western part of the Eger Rift (DC configuration, transmitter power, dipole lengths, etc.). The DC data processing routines were adapted to the noisy signal in term of time domain filter techniques (despiking, treatment of sharp signal steps). After extracting the significant injection time sections from the whole time series, a low pass filtering and drift correction using a Savitzky-Golay filter was performed to smooth the data and to minimize the cultural noise influences. The selective stacking was applied to improve the DC signal quality.

The most remarkable outcome of the DC test is the large signal tracing up to 15 km distance in spite of the strong industrial noise level in that area.

In collaboration with the MT research group of the Geophysical Institute (GFU) Prague combined DC/MT measurements were carried out. In addition to the DC dipoles two magnetotelluric stations were installed during the DC experiment with the aim to detect the DC signal and check the influence of the cultural noise on MT measurements in that area. The DC signal was verified over a distance of 7 km on the registrations of the MT stations. The DC investigations of the conductivity distribution are very promising in comparison to former MT measurements due to the strong industrial noise in the Cheb region.

The second part of the project is the modeling of DC-geoelectrical responses of the 3-D geological and topographical settings of the Eger Rift/Cheb Basin region. Theoretical modeling should include a priori information of the target area (from geology, tectonics, seismology, gas-geochemistry, hydrogeology, etc.) to assess expected electrical measuring effects and to optimize the future field work.

A record of permafrost conditions for Arctic Siberia from El'gygytgyn Impact Crater

G. SCHWAMBORN[1], G. FEDOROV[2], B. DIEKMANN[1], L. SCHIRRMEISTER[1], H.-W. HUBBERTEN[1]

[1]Alfred Wegener Institute for Polar and Marine Research, D-14473 Potsdam
[2]Arctic and Antarctic Research Institute, RUS-199937 St. Petersburg

El'gygytgyn Impact Crater in the terrestrial Arctic holds the unique opportunity to trace back frozen ground conditions to the Pliocene/Pleistocene boundary. A meteor hit the Chukotkian mountain belt 3.6 Myr ago and created a basin in Cretaceous volcanic bedrock. Its geological composition produces a fairly uniform provenance signal in the lake sediments, which presumably start to accumulate soon after the impact event. It makes the archive suitable to test variations of sediment-mineralogical properties as proxy data reflecting the strength of cryogenic weathering in the catchment. The production of (a) silt size debris, (b) a peculiar single grain morphometry, and (c) the enrichment of quartz grains in the silt fraction with respect to feldspar occurrence and to the sand fraction serve as indicators of frozen ground conditions in near surface deposits. They result from thaw and freeze dynamics in the active layer and cause a selective grain break-up. Around the Crater Lake deposits also accumulate at piedmont settings. A set of surface samples and two five-meter-sections extracted from slope deposits serve as a reference for the modern and the Holocene permafrost situation.

Recent ICDP drilling into the permafrost margin of El'gygytgyn Crater has recovered a core 140 m in length and ongoing deep drilling into the lake basin extends beyond 300.000 years, the time our study covers up to now. The presentation sums up current results of both permafrost and lake sediment records when displaying the sediment-mineralogical properties. They illustrate the persistence of cryogenic weathering even in warm periods such as the Eemian and the Holocene.

Storage conditions and degassing processes of low-K and high-Al tholeiitic island-arc magmas: Experimental constraints for Mutnovsky volcano, Kamchatka

T. SHISHKINA[1], R. BOTCHARNIKOV[1], R. ALMEEV[1], F. HOLTZ[1]

[1]Institut für Mineralogie, Universität Hannover, Callinstrasse 3, 30167 Hannover, Germany

Mutnovsky volcano (Kamchatka, Russia) is the object of the proposed ICDP drilling project which is focused on the investigation of the interaction between active magmatic and adjacent hydrothermal systems. This project has two central scientific issues: the identification of magmatic component in fluids proximal to conduits and the determination of the overall volatile and thermal budget of the volcano.

The experimental data and natural observations provided in the frame of this DFG - project should contribute new constraints on the pre-eruptive conditions, especially on the pressures (depths), temperatures and volatile contents in the magma chamber of Mutnovsky volcano. These constraints will be obtained from high pressure - high temperature experimental investigations on phase relations and volatile solubilities in basaltic magmas and from the studies of natural samples, in particular melt inclusions in olivines, collected from the erupted rocks and drilled by the ICDP. The data obtained for Mutnovsky volcano have a broad application and can be used to constrain a general genetic model for the formation of island arc tholeiitic series and will provide estimates on the budget and contribution of magmatic volatiles to the magmatic-hydrothermal volcanic systems.

The project consists of three main parts: (1) experimental study of the H_2O-CO_2 solubilities in basaltic melts relevant to Mutnovsky primitive magmas, since H_2O and CO_2 contents in magmas can be used as indexes of magma storage conditions; (2) determination of pre-eruptive conditions and depths of basaltic magma chamber beneath Mutnovsky volcano based on crystallization experiments and petrological data on natural samples; and (3) the study of natural samples, in particular compositions and volatile contents of glass inclusions.

The part (1) of the project is devoted to the quantitative determination of H_2O-CO_2 solubility in basaltic melts in the pressure range from 50 to 500 MPa, simulating pre-eruptive conditions of basaltic magmas at Mutnovsky volcano. The variations in experimental P-T parameters and composition of fluid coexisting with the silicate melt will be used to investigate the partitioning of H_2O and CO_2 between fluid and melt phases. The preliminary experimental data obtained at 50, 100, 200, and 500 MPa show that basaltic melts can dissolve up to 8.8 wt.% H_2O (X^{fluid}_{H2O}=1) and up to 0.25 wt% CO_2 (X^{fluid}_{CO2} =0.82) at 500 MPa. The solubilities of both H_2O and CO_2 in the melt show non-linear dependences on pressure, and non-ideal solubility behavior. The obtained solubility data can be used to develop an empirically-based model, predicting the P-T conditions in the magmatic chamber at which the magma was saturated with the fluid phase of a given composition.

In the second subproject, phase relationships of the Mutnovsky parental magmas (an example of typical island-arc tholeiite) will be investigated as a function of pressure, fO_2 and aH_2O. The experimental results will be used to constrain phase diagrams at different pressures and temperatures for basaltic magma, coexisting with H_2O-CO_2 fluid phase. Different water activities (aH_2O=0-1) in the system will be controlled by varying the composition of the H_2O-CO_2 fluid phase. The

obtained experimental data will provide quantitative information on the influence of pressure, aH_2O and fO_2 on differentiation trends of Mutnovsky parental magma. Phase compositions and mineral assemblages will be compared to natural samples (including samples from ICDP drilling), giving insights into pre-eruptive conditions and general petrochemical trend of Mutnovsky magmas. The successful experimental reproduction of Mutnovsky liquid lines of descent will indicate a genetic link between parental basaltic compositions and more silicic derivatives. A combination of the experimental data on phase equilibria and C-O-H fluid solubility in the melt will provide model constraints on the degassing and evolution of Mutnovsky magmas prior to eruption.

The direct measurements of volatile concentrations in melt inclusions (subproject 3) will be compared with experimentally calibrated H_2O-CO_2 saturation pressures, providing quantitative estimates on the depth(s) at which Mutnovsky magmas started to degas. In addition, the data on magma degassing at depth combined with the estimates on the magma production during eruptions (Melekestsev *et al.*, 1987; Selyangin, 1993), emission of volcanic gases (e.g., Taran et al., 1992) and information obtained in the framework of the ICDP drilling project are needed to constrain the budget and contribution of magmatic volatiles to the magmatic-hydrothermal system of Mutnovsky volcano.

Melekestsev I. V., Braizeva O. A. & Ponomareva, V. V. (1987). The activity dynamics of Mutnovsky and Gorely volcanoes in Holocene and volcanic hazards for surrounding areas. Volcanology and Seismology, 3-18 (in Russian).

Selyangin O. B. (1993). New data on Mutnovsky volcano: Structure, evolution and prediction. Volcanology and Seismology 1, 17-35 (in Russian).

Taran, Y. A., Pilipenko, V. P., Rozhkov, A. M. & Vakin, E. A. (1992). A geochemical model for fumaroles of the Mutnovsky volcano, Kamchatka, USSR. Journal of Volcanology and Geothermal Research 49, 269-283.

Determination of porosity and diffusion transport in differently altered basalts of the oceanic crust

A.V.SIMONYAN[1,2], S. DULTZ[1], H. BEHRENS[2], J. PASTRANA[3], U. SCHWARZ-SCHAMPERA[4]

[1]Institute of Soil Science, Leibniz University of Hannover, Herrenhäuser Str. 2, D-30419 Hannover
[2]Institute of Mineralogy, Leibniz University of Hannover, Callinstr. 3, D-30167 Hannover
[3]Institute of Bioproduction Systems, Biosystems and Horticultural Engineering Section, Leibniz University of Hannover, Herrenhäuser Str.2, D-30419 Hannover
[4]Federal Institute of Geosciences and Natural Resources, Stilleweg 2, D-30655 Hannover

Introduction

Studying diffusion transport in porous rocks is of fundamental importance in understanding a variety of geochemical processes including mineral dissolution and precipitation kinetics and cementation (clogging, narrowing) of pores by secondary minerals. For element budgets also ion transport, occurring for many elements during seawater-rock interactions in the oceanic crust, is of interest. The rate of seawater/rock interaction and alteration of the oceanic crust depends on the rock permeability and on the accessible specific surfaces. This, in turn, is mainly controlled by the fraction of total pore space that forms a connected network in rock matrices. The scope of our project is to investigate systematically the role of pores and rock permeability on element turnover in oceanic hydrothermal systems. Samples from ODP leg 169 at Middle Valley, Juan de Fuca Ridge and dredged basalts from the East Pacific Rise are used to capture a wide range of rock types from strongly altered sediments to nearly unchanged basement rocks. In order to correlate results of diffusion transport with material properties of the rocks, various methods were applied for the characterization of textures and porosity.

Pore Volume, pore size distribution and connectivity of the pore system

Volume fractions of connected pores in representative basalt samples were determined by three independent methods: (1) mercury intrusion porosimetry (MIP); (2) intrusion with an alloy called Wood's metal (WMI) and subsequent image analyses of back-scattered electron (BSE) images, and (3) NIR spectroscopy on water-saturated basalt sections. In a WMI method, Wood`s metal (an alloy which solidifies below 78°C, 50 % Bi, 25 % Pb, 12.5 % Zn and 12.5 % Cd) was intruded in porous basalts. Thus, pore structures can be visualized in polished sections using BSE images and enhanced topographical images.

Pore volumes of basalts determined by MIP vary from 0.5 vol.% for a dredged basalt to 17.1 vol.% for strongly altered basalt from ODP drilling hole 856H.. In pore size distribution broad maxima are found in the sub-micrometer range. The most frequent pore sizes are observed in the range between 15 and 200 nm. In back-scattered electron images, pores intruded with Wood`s metal are shown in white (Fig. 1a, b). Interconnected porosity is observed within the whole fragment of porphyritic basalt, which has a porosity of 6.3 vol.%. A marked tortuosity of the pore system is visible.

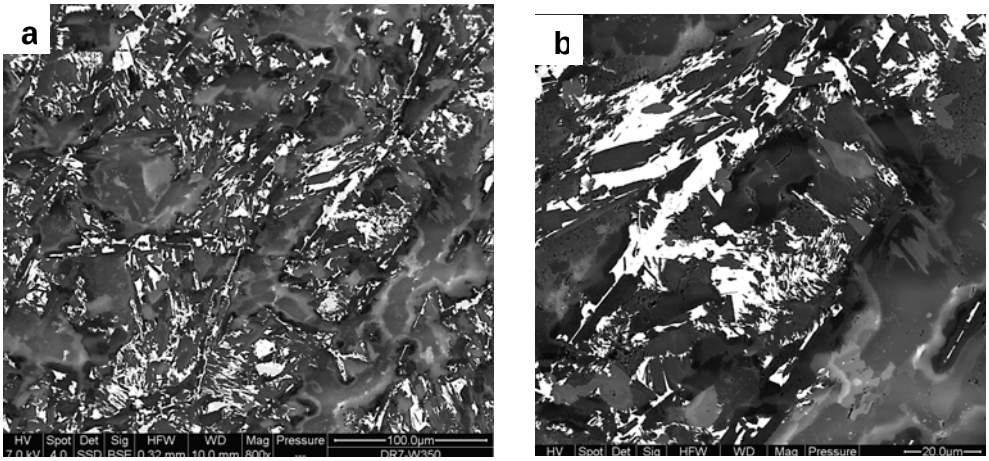

Figure1. Back-scattered electron images showing the tortuosity of pore networks in basalt (sample *DR7*, W350) from Juan de Fuca Ridge after intrusion with Wood`s metal. (a) magnification 800x; (b) 2000x. White: Wood`s metal.

3D pore structure

Cylindrical sections (∅: 2.1 mm) were sampled from the basalt samples with a corer. X-ray tomography was performed at a synchrotron light source (Paul Scherrer Institute, Villigen, Switzerland). A series of projection images (typically 1,024 with a pixel size of 0.7 μm) was recorded. The thickness of each "layer" represents the pixel size, and there is basically no distance between the layers. The voxel size is therefore 0.7 μm x 0.7 μm x 0.7 μm. The images were digitized in 256 grey levels in arrays of 1,024 pixels edge length. The grey values in the images depend on chemical composition and the presence of voids in the sample. All regions in the images were infiltrated with noise caused by the physical property of the X-ray tomography apparatus. Therefore, a Gaussian filter (21 x 21 pixels) was used for pre-processing and smoothing of the images (Fig. 2). To image and quantify the voids, the grey-scale histogram was segmented by a threshold interval ranging from 0 to 110. The 3D images were calculated with circular arrays having a diameter of 1000 pixels. Three-dimensional images were

created by displaying the area pixels or the border pixels of the separated regions. Only objects having a volume greater than 9.261 µm³ (27 neighbor voxels) were used for visualization (Fig. 3a). The anisotropy of the pore orientation is given by the red line in Fig. 3b.

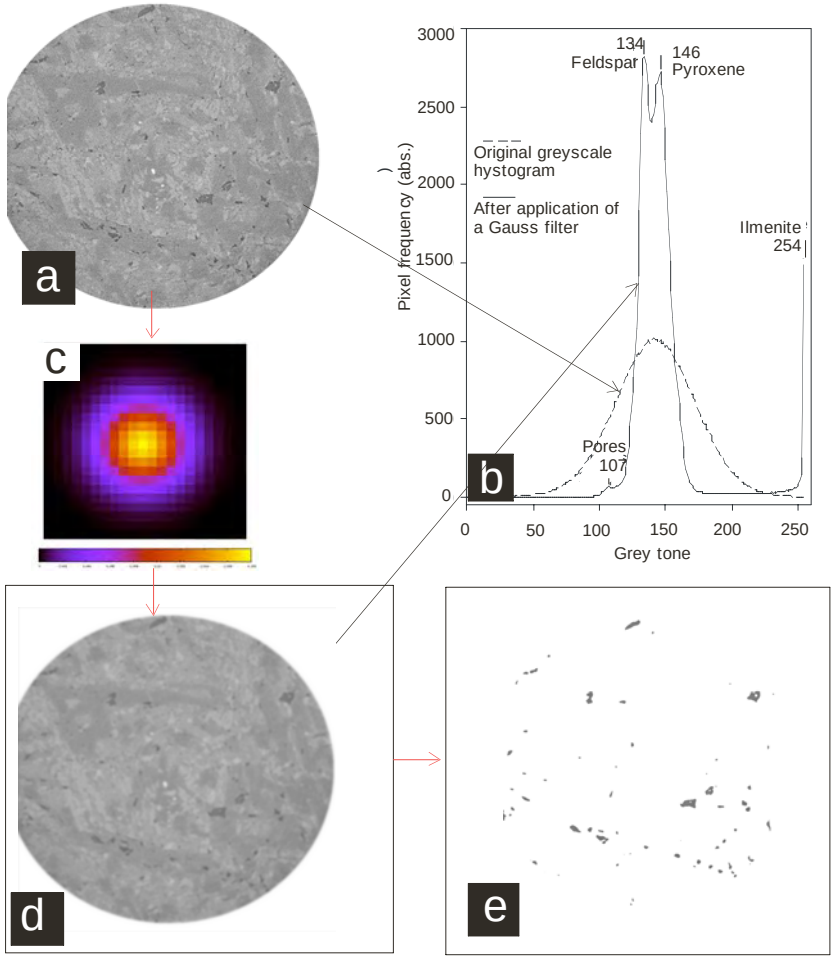

Figure 2 a-e: Image analysis with a Gauss filter of diabase 0856H 55R1. Image of a layer obtained by X-ray microtomography (a) and corresponding greyscale histogram (b). Gauss filter mask (21*21 Pixel) (c) and the resulting image (d) with the corresponding greyscale histogram (b). By application of a threshold (greytone 0-110) the pores are obtained (e).

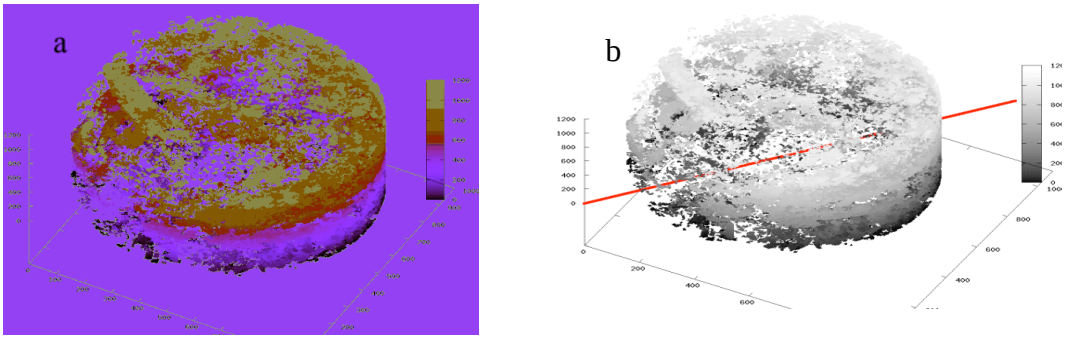

Figure 3. Three dimensional image of pore distribution in a cylindrical section (∅: 700 µm) of diabase 0856H 055R (a) and main vector of pore orientation (b).

Diffusion transport

Diffusion processes of solutions within the porous basalts were studied *in situ*, using a novel experimental cell attached to a *FTIR*-microscope. $H_2O \rightarrow D_2O$ exchange at *T* from 5 to 50°C at ambient pressure was performed with strongly and partially altered basalt from ODP drilling (0856H55R and 0856H65R) and fresh dredged basalt (43DS9-C) from Juan de Fuca Ridge.

For the experiment a basaltic rock sample with typical diameter of ~ 5 mm is polished on one side and fixed with UV-glue in the center of a silica glass plate. After that, the sample is polished from the upper side to a thickness of about 0.1-0.15 mm. Then, the sample is covered with a second thin silica glass plate, providing a complete sealing of the sample. After that, one side of the sample plate was carefully re-opened by cutting the upper glass plate and the sample with a diamond band saw. The sample assemblage is inserted into a cell which can be placed in a *FTIR*-microscope to collect infrared absorption spectra. The solution can be continuously pumped through the cell using a peristaltic pump. Constant temperature in the cell is adjusted by a flux of tempered water which passes through the sample holder.

For the study of diffusion at elevated temperatures and pressures we designed a spectroscopic cell (Fig. 4 a) which operates at *T* up to 150°C and *P* up to 200 bar. Limiting is mostly the glue which is used to connect the different parts of the cell and to seal the system with respect to pressure.

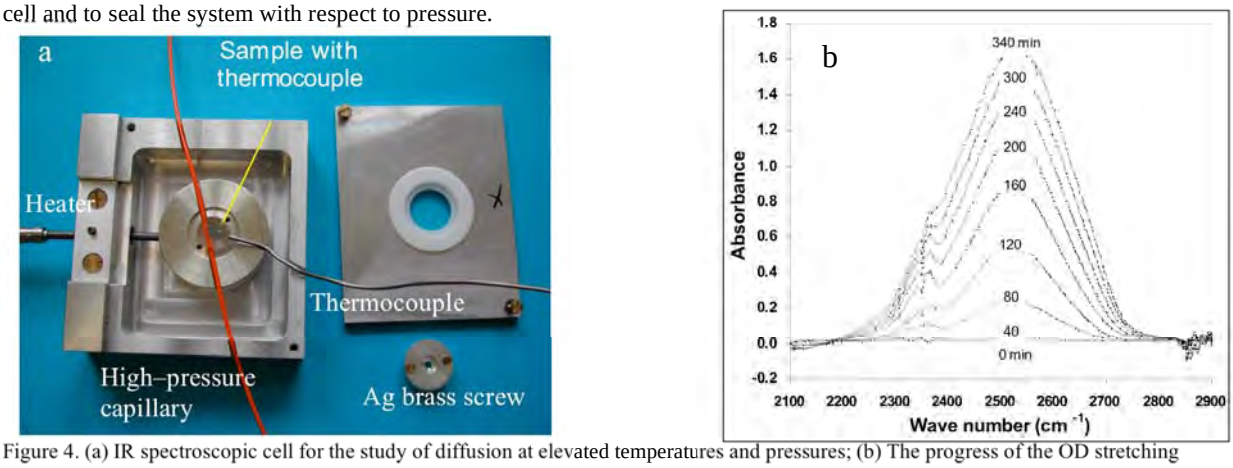

Figure 4. (a) IR spectroscopic cell for the study of diffusion at elevated temperatures and pressures; (b) The progress of the OD stretching vibration band during the diffusion experiments.

The progress of the exchange reaction was determined *in situ* using the OD stretching vibration band in the infrared at 2520 cm^{-1} (Fig. 4b). Concentrations of D_2O were calculated from baseline-corrected peak heights by the Lambert-Beer law. Effective diffusivities of water in the porous medium D_{eff} were derived by fitting time-absorbance curves to the appropriate solution of Fick's 2nd law. The calculated effective diffusion coefficients D_{eff} for water diffusion in the oceanic basaltic rocks vary in the range from 10^{-9} to 10^{-11} m^2/s (Fig.5a). That is one-two orders of magnitude smaller than the diffusion coefficients D_{H2O} for H_2O in liquid water (Mills, 1973). The diffusion data were used to estimate the activation energies (E_a) of diffusion by the Arrhenius equation. The calculated E_a values for water diffusion in completely altered rock is slightly higher than in fresh and partly altered basalts (14.5 kJ/mole vs. 13.1 kJ/mole). The tortuosity factors X (D_{H2O}/D_{eff}) basaltic samples are plotted in Fig. 5b as a function of volume porosity Φ determined by fitting. Our results indicate that the morphology and structure of pore network may have a strong influence on the diffusivity of aqueous solutions. Sample 0856H55R with the largest amount of pores has the highest values of X up to 80. This basalt exhibits disconnected pores with a large proportion of secondary phases. The presence of precipitated minerals inside the pore system affects the transport ways for water molecules by bound H2O layers and an increased tortuosity (Nakashima, 2003).

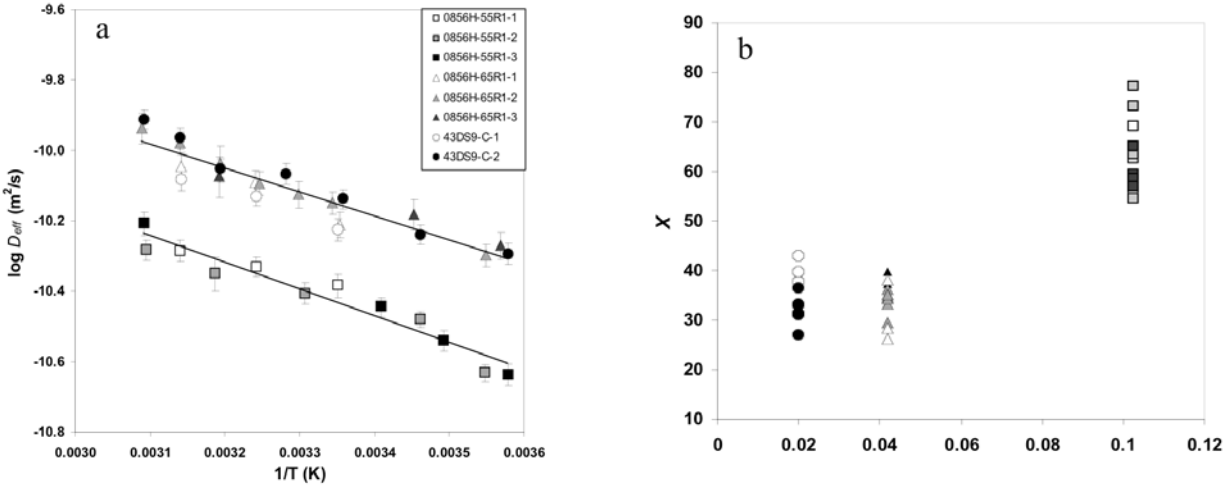

Figure 5. (a) Arrhenius-plot for water diffusion in porous basaltic rocks; (b) Tortuosity factor as a function of porosity.

Mills R.: Self-diffusion in normal and heavy water in the range 1-45°C. J. Phys. Chem. 77, 685-689 (1973).
Nakashima Y. : Diffusion of H_2O in smectite gels: obstruction effects of bound H_2O layers. Clay and Clay Min. 51.2-22, (2003).

The Greenland–Scotland–Ridge needs to be revisited

PETER P. SMOLKA

Postanschrift: Isolde–Kurz–Str. 85, 48161 Münster

The Greenland–Scotland-Ridge (GSR) is a prominent submarine feature that sets boundary–conditions for exchange of water between the North Atlantic and the Norwegian Sea.

Its importance caused a series of DSDP drillsites as early as Leg 38 and Leg 49 (the sites on the Reykjanes Ridge).

The Norwegian Sea was later visited by several ODP Legs that addressed, amongst others, the Voering Plateau, the Yermak Plateau, the East Greenland Current (such as by Legs 151 and 162). All these expeditions provided a wealth of important data. The location of the drillsites shows that several questions Leg 38 could not address due to the technology of that time are still open.

Faunal/Floral maps of all available Diatoms, Radiolaria, Forams and Coccoliths (DSDP/ODP data plus extensions), e.g. both, siliceous(!) and calcareous biota, show extreme faunal/floral differences between North Atlantic and Norwegian Sea during the Miocene and preglacial Pliocene (now: 2.6 Ma) and little or no faunal/floral gradients post 2.6 Ma and during the Oligocene. The maps integrate over large stratigraphic intervals and large coring gaps. Appearing gradients are thus robust against technical disturbances.

A subsidence-pattern: Water exchange (WE) in the Oligocene, inhibited WE until 2.6 Ma, reestablished WE post 2.6 Ma appeared to be inconsistent with known plate–tectonic concepts, such as "sclater curves". The extraordinary thickness of the Icelandic crust and the unspecified but "non oceanic" crust beneath the Faeroe–Basalts (Faeroe Block) had not been included in respective models ("sclater curves").

Recently the movements of the continents over the Iceland Hot Spot (IHS) had been addressed. Dated volcanics show a consistent trace of the IHS from about the Tamyr Region (Siberia) through West Greenland, East Greenland to Iceland. Hot spots impact the overlying crust thermally. An early opening of the GSR, a later closing (impact of the IHS plus thickness of Icelandic and Faeroese crust) followed by a reopening from 2.6 Ma on appears thus a plausible way to interpret early DSDP data. Such interpretations lead to different circulation patterns both in the Norwegian Sea and the North Atlantic. Middle Miocene temperature drops, visible as early as in DSDP Site 407 can easily be explained by ice buildup. They do not require overflow through the Denmark Straits. Old seismic data show that overflow in the Denmark Straits occurred "not too much" before 2.6 Ma. Across other sections of the GSR it is, with difficulties, around 2.6 Ma. In the Faeroe Shetland Channel the data that are available to the author do not permit a conclusion.

To arrive at datasets that are suitable for coupled atmosphere/ocean models redrills of DSDP sites 336, 337 and 352 are needed. New sites are needed directly in the Denmark Straits (two shallow, one deep) and in the Faeroe Shetland Channel.

Numerical model of evolution of the San Andreas Fault system constrained by geo-observations and SAFOD-drilling data

STEPHAN V. SOBOLEV, ANTON POPOV, (GFZ) AND M.D. ZOBACK (STANFORD UNI.)

The San Andreas Fault System formed in response to collision of the Farallon ridge with North America plate margin during the Oligocene. At present the system accommodates the relative motion between the Pacific plate and the North American plate along the complex network of sub-parallel faults. Using the 3D thermo-mechanical numerical models we study the major factors controlling simultaneous activity of these sub-parallel faults and the overall landward migration of the plate boundary (accretion of the North America terranes to Pacific plate).

The typical model starts at ~20 Ma and spans ~1000 km laterally and ~100 km in depth. It includes the subducting and migrating Gorda slab on the northern part, and the Great Valley block in the eastern part. We focus at the influence of the strength of major faults on the strain localization in the crust. In doing that we make no assumptions about the spatial styles of the deformation; our models are completely three-dimensional and thermo-mechanically coupled.

The models suggest that a series of microplate capture events has been the most likely reason of the inland migration of the San Andreas plate boundary over the recent 20 Ma. We demonstrate that a lack of the slip weakening (which implies strong major faults) fails to predict the distinct zones of strain localization in the brittle crust. Our best-fit model requires the friction coefficient on major faults to be about 0.1, which is far less than typical values 0.6 – 0.8 obtained by variety of borehole stress measurements and laboratory data. Therefore, we side with a “weak fault” theory, and favor importance of the slip-related weakening. Our models imply that low strength at San Andreas Fault reported by analysis of cores collected during SAFOD drilling must remain also at depth of 10-15 km, which will require lowering of effective friction coefficient to about 0.1.

Experience with a Shallow Water Seismic Pre-Site Survey for combined IODP and ICDP Drilling Campaigns in the Gulf of Naples and Gulf of Pozzuoli, Tyrrhenian Sea

[1] V. SPIESS, [1] J. METZEN, [1] N. FEKETE, [1] L. PALAMENGHI, [2] M. SACCHI

[1] Department of Geosciences, University of Bremen, Klagenfurter Strasse, D-28359 Bremen, Germany
[2] Institute for Coastal Marine Environment (IAMC), Italian Research Council (CNR), Calata P.ta di Massa, Porto di Napoli, 80133 - Napoli, Italy

The Gulf of Naples receives particular attention due to its proximity to major volcanic features, as the Somma-Vesuvius stratovolcano and the Campi Flegrei Volcanic Fields, both being viewed to bear extreme hazard potential in the highly populated area. Accordingly, a better understanding of the geologic history of the region and its volcanic activity is of high value for predictive approaches.

In January 2008, a dedicated shallow water multichannel seismic survey on R/V URANIA was carried out by the Institute for Coastal Marine Environment in cooperation with the University of Bremen in Pozzuoli Bay as well as in its surroundings to image subseafloor volcanic features as well as the neotectonic framework, as it is documented in Holocene sediments. Furthermore, volcanoclastic events, volcanic edifices, pyroclastic flows and lava flows were identified complicating the stratigraphic interpretation. Major units as the Campanian Ignimbrite and the Neapoltian Yellow Tuff could be traced on regional scales.

Particular focus was put on the nearshore surveys, to connect the onland future ICDP drilling results with the marine deposits and planned IODP drill sites in the vicinity of the survey area. It turned out particularly difficult to collect seismic data in the coastal zone due to intense usage and protected areas.

The equipment used was optimized to collect multichannel seismic data in shallow and very shallow environments. A 50 m long streamer with 48 single hydrophone channels allowed to record undistorted seismic response in waters shallower than 10 meters, and high shot rates – 2 to 4 seconds – provide high coverage and a lateral resolution as good as 1 meter. A modified mini-GI Gun with a reduced volume of only 0.1 L, called micro-GI Gun, generated a frequency spectrum up to 1000 Hz, optimizing also the vertical resolution to less than 1 meter.

Examples will be shown to demonstrate the capability of the equipment for use in amphibic projects, where ICDP and IODP cross the borders of land and sea, and where quality and seismic resolution play a major role to achieve goals of proper site surveys and stratigraphic interpretation.

Drilling in Current-Controlled Sedimentary Environments on the Southeast African Margin - The SAFARI Pre-Site Survey Challenges on the Madagascar, Mozambique and the South African Margin

[1] V. SPIESS, [1] B. PREU, [1]T. SCHWENK, [1] L. PALAMENGHI, [2] R. SCHNEIDER, [3]I. HALL, [4]R. ZAHN

[1]Universität Bremen, Fachbereich Geowissenschaften, Bremen, Germany
[2]Christian Albrecht Universität, Institut für Geowissenschaften, Kiel, Germany
[3]Institució Catalana de Recerca i Estudis Avançats, ICREA; Universitat Autònoma de Barcelona, Institut de Ciència i Tecnologia Ambientals and Depto. de Geologia, Campus UAB, E-08193 Bellaterra (Cerdanyola)
[4]Cardiff School of Earth and Ocean Sciences, Cardiff, UK

As part of the global conveyer belt circulation, the Agulhas, Mozambique and Madagascar Currents are guided southward along the Southeast African margin as strong contour currents, affecting local sediment mobilization, redistribution and deposition. To gain a better understanding of their evolution through time, a transect of drill sites ranging from the southern tip of Africa to Madagascar was proposed by Hall et al. (SAFARI, IODP proposal 702).

As contour currents become erosive in their vicinity, deposition may be inhibited and incoming sediment will be redistributed. To find suitable drill sites, they must be positioned strategically to provide continuous depositional records on the one hand by not not being located in the core of the current, and to record variations in current activity and strength, which requires a certain proximity to the mean current position. Furthermore, sources of sediment and their spatial and temporal variability play a role for the interpretation of accumulation rates, provenance of particles, reconstruction of current velocities and terrestrial input, which can be compared as climate indicators with marine geochemical tracers.

Six different working areas, West of Capetown, Natal Valley, Limpopo Cone, Zambezi margin, Davie Ridge and N-Madagascar margin, were visited during R/V Meteor Cruises M63/1 (2005) and M75/3 (2008) to gain an understanding of sediment deposition and to select sites for the drilling proposal.

Main observations of both cruises were, in contrast to the expectation of margins being predominantly shaped by fan deposition and mass wasting processes, the widespread occurrences of large scales contourite bodies, which were situated between 100 and 1500 m water depth. They appear to be independent of the mechanisms and volume of sediment input, revealing a close relationship to the acting contour currents. Accordingly, the drift bodies appear to be suitable deposits which record the activity of the currents by sedimentologic properties.

For the preparation of the drilling proposal we started to develop a regional stratigraphy to estimate accumulation rates and to reconstruct the shift of depocenters in space and time. Examples are shown for different working areas with a focus on the Limpopo and Zambezi, where extended drift deposits tell the story of onset and variation of the regional current systems.

East Asian summer monsoon evolution and variability during the Late Miocene

S. STEINKE[1], J. GROENEVELD[2], H.J.H. JOHNSTONE[1]

[1]MARUM – Center for Marine Environmental Sciences and Faculty of Geosciences, University of Bremen, Bremen, Germany
[2]Alfred Wegener Institute for Polar and Marine Research, Bremerhaven, Germany

The monsoon system represents one of the basic elements of the global atmospheric circulation that controls the redistribution of latent and sensible heat and its evolution and variability play a significant role in our understanding of global climate (Webster et al., 1998). One of the central questions in this context is how the monsoon has evolved over long periods of geologic time. In this study, we focus on the Late Miocene time interval from 10 to 6 Ma, a period of postulated profound ecological, environmental and climatic shifts in East Asia (e.g. Molnar et al., 2005).

Here, we used combined measurements of Mg/Ca and stable oxygen isotopes in tests of the planktonic foraminifera *G. quadrilobatus-sacculifer* from Ocean Drilling Program (ODP) Site 1146A (19°27.40'N; 116°16.37'E; water depth of 2092 m) to reconstruct the hydrographic and thermal history of the northern South China Sea (SCS), and hence changes in East Asian monsoon climate during the Late Miocene. Located offshore of the Pearl (Zhujiang) River, or its predecessor, the location of Site 1146A is considered as providing record most sensitive for detecting potential changes in freshwater input/river-run off as a result of changes in continental humidity/aridity. ODP Site 1146A provides a continuous middle to late Miocene sediment section of relatively carbonate rich ($CaCO_3$ content ranges from 20 to 50% throughout the Miocene period), hemipelagic nannofossil clays. The chronology for ODP Site 1146A is based on a combination of planktonic foraminiferal and calcareous nannofossil first occurrence (FO) and last occurrence (LO) datums, and magnetostratigraphic datums (Nathan and Leckie, 2003; Su et al., 2004).

In order to evaluate the carbonate preservation state of the planktonic foraminifera used for trace element and stable oxygen analyses, tests were examined using computer tomography (CT; Johnstone et al., in prep.). The presence of clear pore structures and smallest (juvenile) chambers of scanned *G. quadrilobatus-sacculifer* specimens indicates well preserved individuals Thus, the Mg/Ca estimates should not be affected by post-depositional selective dissolution.

Approximately 15 *G. sacculifer-quadrilobatus* specimens of the 315-400 µm size fraction are used for stable oxygen isotope analyses. Prior to trace elemental analyses, approximately 20-30 foraminiferal tests of *G. sacculifer-quadrilobatus* were cleaned in successive steps according the cleaning protocol of Barker et al. (2003) with the modification that samples were centrifuged (10 min. at 6000 rpm) after dissolution of the samples in ultra-pure HNO_3 (%) in order to remove any insoluble impurities. To assess possible contamination by clays, Fe/Ca and Al/Ca were analyzed simultaneous with Mg/Ca. Mn/Ca and Fe/Ca ratios are further monitored as indicator of Mn-Fe-oxyhydroxides and Mn-Fe carbonate coatings. Trace elements were analysed on a Perkin-Elmer Optima 3300R ICP-OES at the Department of Geosciences, University of Bremen.

Mn/Ca and Fe/Ca ratios of the analyzed samples vary between 0.71 and 1.39 mmol/mol and 0.38 and 0.82 mmol/mol, respectively, and are significantly higher than the 0.1 mmol/mol Mn/Ca and Fe/Ca ratios given by Barker et al. (2003) for clean, uncontaminated foraminiferal tests. Although high Fe/Ca ratios (up to 0.82 mmol/mol) have been detected, it is assumed that the Mg/Ca analyses are unaffected by contaminant clay particles since Al has been found to be under the detection limit of the ICP-OES technique. High Fe/Ca and Mn/Ca ratios may result from Mn-Fe-oxyhydroxides present on the foraminiferal shells (e.g. Boyle and Keigwin, 1985), which might exert a significant control on the Mg/Ca ratios, resulting in elevated Mg/Ca ratios and thus by inference in overestimated SSTs. Due to high Mn/Ca and Fe/Ca ratios in non-reductively cleaned samples, reductive cleaning tests were performed in order to remove these contaminants following the standard procedure according the Barker et al. (2003) cleaning protocol. As reductive cleaning reagents, hydroxylamine and hydrazine have been used, detailed in Shen et al., 2001 and Martin and Lea (2002), respectively. Results using an additional reductive cleaning step revealed a 20% to 50% decrease in Mn/Ca and Fe/Ca compared to the non-reductive cleaned samples. More importantly, Mg/Ca ratios of both cleaning methods show constant Mg/Ca ratios, indicating no Mg contributions from Mn-Fe-oxyhydroxides or Mn-rich carbonates. Therefore, there is no a priori reason to include an additional reductive cleaning step for these samples.

G. quadrilobatus-sacculifer Mg/Ca ratios for site 1146A vary between 2.5 and 4.0 mmol/mol (Fig. 1). Translating the Mg/Ca ratios into surface water temperatures using the calibration of Nürnberg et al. (2000) and taking into account lower seawater Mg/Ca (4.5 mol/mol according to Wilkinson and Algeo, 1989) during the Late Miocene, Mg/Ca-SST estimates vary between 23.5°C and 29°C in the investigated time interval. The Mg/Ca SST estimates suggest a distinct cooling trend from 10 Ma (~29°C) to ~7.5 Ma (~26°C) that is followed by an abrupt increase in SSTs around 7.5 Ma. Lower temperatures around 26°C are recorded for the time interval 7 to 6 Ma.

The combined approach of measuring foraminiferal Mg/Ca and stable oxygen isotopes on *G. quadrilobatus-sacculifer* enables us to reconstruct temperature independent $\delta^{18}O_{seawater}$ variations, which may be related to changes in monsoonal intensity. $\delta^{18}O_{seawater}$ are estimated by removing the temperature driven component of changes in the planktonic foraminiferal $\delta^{18}O$ record using the palaeotemperature equation given by Shackleton (1974). An estimate of the Late Miocene ice volume signal is subtracted from the $\delta^{18}O_{seawater}$ record, leaving a local $\delta^{18}O_{seawater}$ record, which provides an approximation of relative changes in local surface water $\delta^{18}O$. Local $\delta^{18}O_{seawater}$ estimates imply increased (heavier) local $\delta^{18}O_{seawater}$ estimates after ~7.5 Ma that are most likely attributed to a decrease in summer monsoon precipitation (continental humidity), and hence decreased river run-off from the Pearl River (Zhujiang) River, or its predecessor (Fig. 1). Lighter local $\delta^{18}O_{seawater}$ estimates before ~7.5 Ma may indicate a period of wetter conditions. Compared to micropalaeontological and sedimentological winter monsoon proxy records of the same site (Wan et al., 2007), an intensification of the winter monsoon around 7.5 Ma can be interpreted to reflect a profound shift in the intensity of the East Asian winter monsoon relative to the summer monsoon, as well as more arid conditions on the Asian continent after 7.5 Ma. The decrease in the intensity of the East Asian summer monsoon as deduced from our local $\delta^{18}O_{seawater}$ estimates around 7.5 Ma is consistent with the notion of an overall shift towards more drier conditions in East and South Asia during the Late Miocene (Molnar et al, 2005; Clift and Plumb, 2008; Clift et al., 2008). In the last phase of our project, our aim will be to extent our monsoon proxy record to 12.5 Ma.

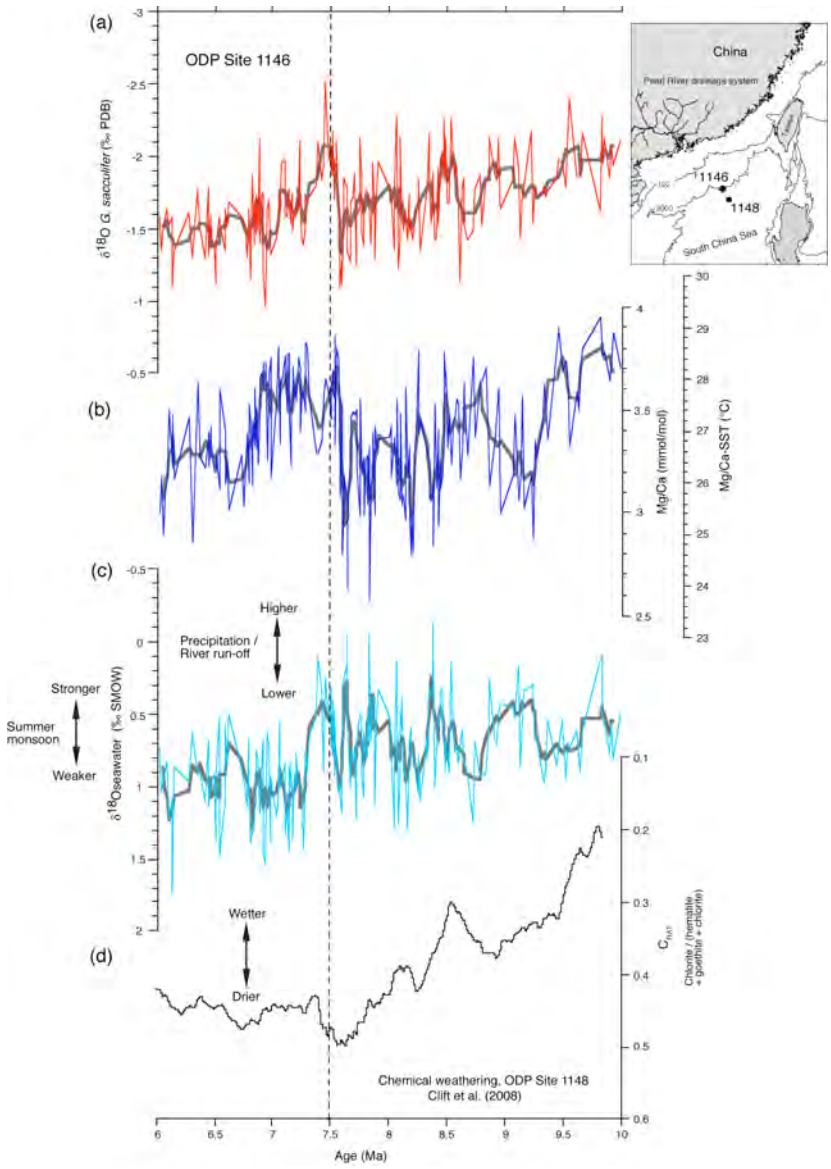

Figure 1. (a) Oxygen isotope record of *G. quadrilobatus-sacculifer* of ODP Site 1146A; (b) Mg/Ca ratios (mmol/mol) and Mg/Ca-SST estimates at ODP Site 1146A. Mg/Ca ratios were transformed to surface water temperatures by using the calibration equation for *G. sacculifer* of Nürnberg et al. (2000). The Nürnberg et al. (2000) calibration were modified in order to account for differences in seawater Mg/Ca ratios between the Late Miocene (4.5 mol/mol; Wilkinson and Algeo, 1989) and present (5.1 mol/mol; Broecker and Peng, 1982); (c) Local $\delta^{18}O_{seawater}$ estimates at ODP Site 1146A. Local $\delta^{18}O_{seawater}$ were derived by removing the temperature driven component of changes in the planktonic foraminiferal $\delta^{18}O$ using the Shackleton (1974) palaeotemperature equation and changes in global ice volume; (d) Chemical weathering index C_{RAT} of ODP Site 1148 (Clift et al., 2008).

Barker, S., Greaves, M., Elderfield, H., 2003. A study of cleaning procedures used for foraminiferal Mg/Ca paleothermometry. Geochemistry Geophysics Geosystems 4, doi: 10.1029/2003GC000559.

Boyle, E.A., Keigwin, L.D., 1985. Comparison of Atlantic and Pacific paleochemical records for the last 215,000 years: changes in deep ocean circulation and chemical inventories. Earth and Planetary Science Letters 76, 135-150.

Broecker, W., Peng, T., 1982. Tracers in the sea. Columbia Univ. Press. New York.

Clift, P.D. and Plumb, R. A., 2008. The Asian monsoon: causes, history and effects, Cambridge University Press, Cambridge, UK.

Clift, P.D., Hodges, K.V., Heslop, D., Hannigan, R., Van Long, H., Calves, G., 2008. Correlation of Himalayan ehumination rates and Asian monsoon intensity. Nature Geoscience, (875-880).

Johnstone H.J.H., Schulz, M., Yu, J., Elderfield, H., in prep. Inside story: An X-ray microtomography method for assessing dissolution in foraminifera tests.

Molnar, P., 2005. Mio-Pliocene growth of the Tibetan Plateau and evolution of East Asian Climate. Palaeontologia Electronica Vol. 8, http://palaeo-electronica.org/paleo/2005_1/molnar2/issue1_05.htm

Nathan, S.A., Leckie, R.M., 2003. Miocene Planktonic foraminiferal biostratigraphy of Sites 1143 and 1146, ODP Leg 184, South China Sea. In: Prell, W.L., Wang, P., Plum, P., Rea, D.K., Clemens, S.C. (Eds.) Proc. ODP. Sci. Res. 184, 1-43 (online).

Nürnberg, D., Müller, A., Schneider, R. R., 2000. Paleo-sea surface temperature calculations in the equatorial east Atlantic from Mg/Ca ratios in planktic foraminifera: A comparison to sea surface temperatures from $U^{k'}_{37}$, oxygen isotopes, and foraminiferal transfer function. Paleoceanography 15, 124-134.

Shackleton, N.J., 1974. Attainment of isotopic equilibrium between ocean water and benthonic genus *Uvigerina*: Isotopic changes in the ocean during the last glacial. In: Les methodes quantitative detude des varations du climat au cours du Pleistocene, Colloq. Int. C.N.R.S., 219, 203-209.

Su, X., Xu, Y., Tu, Q., 2004. Early Oligocene-Pleistocene calcareous nannofossil biostratigraphy of the northern South Shian Sea (Leg 184, Sites 1146-1148). In: Prell, W.L., Wang, P., Plum, P., Rea, D.K., Clemens, S.C. (Eds.) Proc. ODP. Sci. Res. 184, 1-24 (online).
Wan, S., Li, A., Clift, P.D., and Stuut, J.-B.W., 2007, Development of the East Asian monsoon: Mineralogical and sedimentologic records in the northern South China Sea since 20 Ma: Palaeogeography, Palaeoclimatology, Palaeoecology, v. 254, p. 561-582.
Webster, P.J., Magana, V.O., Palmer, T.N., Shukla, J., Tomas, R.A., Yanai, M., and Yasunari, T., 1998, Monsoons: Processes predictability, and the prospects for prediction, in the TOGA decade: Journal of Geophysical Research, v. 103, p. 14451-14510.
Wilkinson, B., Algeo, T., 1989. Sedimentary carbonate record of calcium-magnesium cycling. American Journal of Science 289, 1158-1194.

Nankai Trough submarine landslide history: Results from IODP NanTroSEIZE drilling and presentation of a new IODP APL-proposal

M. STRASSER[1], G.F. MOORE[2], A.J. KOPF[1],

& IODP EXPEDITIONS 314/315/316 SCIENTISTS & IODP PROPOSAL 738-APL CO-PROPONENTS

[1]MARUM – Centre for Marine Environmetal Sciences, University of Bremen (mstrasser@marum.de)
[2]Dept. Of Geology & Geophysics, University of Hawaii, USA

Nankai Trough Seismogenic Zone Experiment (NanTroSEIZE) stage 1a operations of the Integrated Ocean Drilling Program (IODP) coring the Nankai accretionary prism offshore SW Japan yielded discoveries about gravitational slope-failure processes and subsequent mass-movement deposition in a slope basin seaward of a prominent out-of-sequence thrust (megasplay fault). Late Pliocene to early Pleistocene mass-transport deposits (MTDs) in the lowermost part of the slope-basin stratigraphic succession (Site C0008) are characterized by poorly sorted, subangular to rounded mudclasts floating in a sandy, clayey silt matrix. Systematic comparison between clasts, matrix and interbedded background sediments on the basis of lithofacies, biostratigraphy and clay mineralogy reveal that the clasts derived from accreted strata and not from a slope apron source. Furthermore, biostratigraphic and magnetostratigarphic data show that the time period of MTD deposition is time-correlative with a prominent stratigraphic hiatus between overlying Pleistocene slope sediments and underlying accreted strata in the hanginwall block of the megasplay fault (Site C0004). Core observations and X-CT images show mineralization along this stratigraphic unconformity suggesting seafloor exposure. Hence, the angular unconformity is interpreted to represent a buried landslide scar.

A conceptual splay-fault development model, constructed on the basis of seismic reflection data, seismic-to-core correlation and bio- and magnetostratigraphy age constraints allows for investigation of the genetical link between sediment mass-transport processes and the early tectonic evolution of the fault system. Results document the time period between 1.95 Ma and 1.8 Ma to be a high activity phase during an early stage of splay fault activity. It resulted in gravitational mass movements along the upthrusted and uplifted prism and in subsequent deposition of MTDs in the adjacent slope basin.

Apart from the deepest section, the drilled slope basin (Site C0008) lacks clear evidence for MTDs, potentially due to a significant hiatus in its upper part, suggesting erosion or non-deposition likely related to a prominent slope collapse structure seaward of the mega splay fault. New 3D seismic data interpretation of a lower slope basin seaward of that collapse structure reveal a peculiar sedimentary succession that is composed of stacked Pleistocene-to-recent MTDs. It includes one exceptionally large MTD of up to 150 m in thickness. This succession has been proposed for future IODP drilling (IODP Proposal 738-APL), as it is ideally suited to constrain timing, causes and consequences of submarine landslides in one of the worldwide best studied accretionary complexes. The proposed project aims to catalog a detailed submarine landslide event history along with clues on the depositional dynamics of each MTD as they relate to tsunamigenic potential. High-resolution data on the spatial and temporal distribution of mass movements and clues on their tsunamigenic potential will provide a solid base for determining the relation of sediment remobilization to the tectonic evolution and seismicity of the margin and for assessing geohazards from submarine slide, respectively.

Geochemical surface patterns and the structure of mantle plumes – news from Ne isotopes and noble gas abundance ratios from Hawaii

N. A. STRONCIK, T. KRÜSMANN, S. NIEDERMANN, J. ERZINGER

Helmholtz-Zentrum Potsdam, Deutsches GeoForschungsZentrum, Telegrafenberg, D-14473 Potsdam, Germany

Mid-ocean ridge and ocean island basalts provide access to one of the largest geochemical reservoirs on Earth – the mantle. Whereas mid-ocean ridges are thought to sample the upper mantle, oceanic islands are thought to represent surface manifestations of localized mantle upwellings that may originate as deep as the core/mantle boundary. Detailed chemical and especially isotopic studies of oceanic basalts have put fundamental constraints not only on the geochemical and isotopic composition of the mantle but also on mantle geodynamic processes, formation of the continental crust, mantle-crust-atmosphere interaction and so on. In this context, it has almost become a truism that ocean island basalts (OIBs) exhibt a high degree of compositional heterogeneity and that much of this heterogeneity can be found even within individual settings. Generally, the isotopic signatures observed at those settings are not only considered to reflect the composition of the mantle source at depth but are interpreted to mirror spatial patterns of compositional variations of the solid mantle.

At Hawaii, for example, the shift during the late shield or post-shield stage from isotopic compositions typical for an enriched source to those typical for a more depleted source has been interpreted to be caused by a concentrically zoned mantle plume, with enriched material from the deep mantle in the centre and a shell of depleted material around it. The depleted material is thought to be derived from entrainment of shallower mantle (e.g. Kurz and Kammer 1991; Frey and Rhodes 1993). In addition to this isotopic shift with time, lateral isotopic differences can be observed, dividing the Hawaiian Islands into the subparallel "Loa" and "Kea" chains. The Loa chain volcanoes sample a source that has a larger longterm enrichment of incompatible elements than the source sampled by the Kea chain volcanoes. These observations can easily be explained by the concentrically zoned plume model if the volcanoes of the two subchains move over the plume at different distances from the centre. An alternative explanation is that the plume has a NE-SW asymmetry in composition (Abouchami et al. 2005). Similar ideas of a compositionally zoned plume have been proposed for e.g. the Galápagos and the Easter plume.

Surely this concept of surface chemical patterns emulating mantle chemical patterns is an intriguing and in its simplicity an elegant concept. However, evaluation of the entire chemical record (e.g. Sr, Pb, Nd and noble gas isotopes) available for a plume setting such as Hawaii as well as recent modelling results (Bianco et al. 2008) indicate that the complex processes operating during melt generation in conjunction with mantle dynamic processes can lead to surface compositional patterns deviating from any intrinsic pattern within the source region. In this context we present, besides He and Ar data, Ne isotope data from the islands of Hawaii and Maui which are at odds with any type of zoning or heterogeneity of the Hawaiian plume at all.

The studied sample set consists of olivine seperates obtained from lava flows cored during the Hawaiian Scientific Drilling Project (HSDP) and from subaerial lava flows of the five volcanoes of the island of Hawaii and of Haleakala, Maui. The olivines are mainly derived from a primitive to very mildly evolved magma since the Fo content of 75% of the analysed olivines ranges between Fo80 and Fo90, corresponding to melt Mg#s of 55 to 73, which translates to melt MgO contents of roughly 7 to 14 wt.%. Generally, the He isotopic ratios of the studied samples vary from 7 to 18 R_A (Fig. 1), and thus they range from ratios typical for the upper mantle to ratios more typical for a primitive mantle source. Interestingly they never reach values as high as those measured at Loihi (35 R_A). In addition, the He isotope ratio in the Mauna Kea section of the HSDP core shows a slight positive correlation with sample depth and thus age. This correlation with depth is interrupted by spikes reaching $^3He/^4He$ ratios being significantly higher (up to 25 R_A) than the ratios located on the "age trend". In contrast to this, the Ne isotope data show no correlation with sample age and they all plot along the Loihi-Kilauea line (being typical for a primitive mantle source) in a Ne-three isotope plot (Fig. 2).

Even though the observed He isotopic patterns are consistent with the zoned plume model described above, the Ne isotopic signatures neither can be interpreted in terms of a zoned plume nor in terms of a heterogeneous mantle. These contrasting He/Ne isotope signatures confront us with a serious problem since one of the fundamental concepts in noble gas geochemistry is that He and Ne isotopic systematics should be coupled. The reason is that primordial He and Ne isotopic ratios in terrestrial samples are solar-like, with the deviation from those solar-like ratios having increased during Earth's history due to the coupled production of radiogenic ^4He and ^{21}Ne. ^4He is produced in the radioactive decay chains of ^{238}U, ^{235}U and ^{232}Th, whereas ^{21}Ne is mainly produced by nuclear reactions of α particles with ^{18}O. As the α particles needed for these reactions are derived from U and Th decay and O is thought to be homogeneously distributed within the Earth's mantle, the production of radiogenic ^4He and nucleogenic ^{21}Ne has to be coupled. Since mantle ^3He, ^{20}Ne and ^{22}Ne are dominantly primordial in origin, mantle He and Ne isotopic ratios are controlled by the ratios of [primordial ^3He]/[U+Th] and [primordial Ne]/[U+Th], respectively. Thus high $^3He/^4He$ ratios denote high ratios of [primordial ^3He]/[U+Th] and solar-like Ne isotopic compositions imply high ratios of [primordial Ne]/[U+Th]. As a consequence, the Ne isotopic patterns in the studied olivines should resemble those of the He isotopes and thus should range from compositions typical for the upper mantle to compositins more typical for an enriched source, but should never become as primitive as those observed at Loihi or Kilauea. The only logical explanation for this observation is that the isotopic patterns observed in the surface samples derived from Hawaiian volcanoes are not controlled by source intrinsic spatial distributions of isotopic signatures but by melt generation and evolution processes.

I this context the relative elemental abundances of e.g. He and Ne can be used as tracers to assess the processes responsible for the observed He and Ne isotopic patterns. Ne is variably affected by atmospheric contamination, thus its

measured abundance cannot be used directly. In the following discussion, the calculated amounts of nucleogenic (Ne*) and solar Ne (Ne_S) of each sample will be related to the measured ^{4}He abundances. As shown in Fig. 3, He and Ne interelement ratios correlate positively and almost exclusively stay below the corresponding production and primordial ratios. Whereas ratios below current estimates of solar composition and the theoretical production ratios indicate that He has been fractionated from Ne the positive correlation might either denote a mixing process or magmatic degassing subsequent to the fractionation process. As magmatic degassing results in a preferential enrichment of He in the melt compared to Ne, resulting in He/Ne interelement ratios higher than the primitive and theoretical production ratios, the He depletion must be caused by a predegassing process, leaving melt formation as such as the only process. This at the same time implies that He is more compatible during mantle melting than Ne. However, a preferential retention of He in the solid residue results in a He deficit compared to Ne in the produced melt, making the initial ^{3}He/^{4}He ratio more susceptible to changes caused by e.g. mixing of melts than the Ne isotopic ratios. Thus the He and Ne isotope signatures observed at Hawaii are consistent with a model in which the isotopic patterns observed at the surface are generated by mixing of low degree plume melts carrying a fractionated He/Ne abundance signal, with melts being derived from a more depleted source carring a He isotope signal characteristic for the upper mantle but probably no fractionated He/Ne abundance signal. Mixing then results in a range of He isotope signals but leaves the Ne isotopic signal basically uneffected. This model is also supported by melting and mixing models combining the He isotope data with Pb and Nd isotope data. Whereas the Nd/Pb systematics of the measured samples can be explained by a more or less simple linear binary mixing model, the He/Pb systematics cannot be explained by such a model. Whereas the He isotope data following the "increase with age trend" show a positive correlation with ^{206}Pb/^{204}Pb the high ^{3}He/^{4}He spikes are combined with intermediate ^{206}Pb/^{204}Pb ratios. To explain these He/Pb isotope systematics we could either assume that the Hawaii plume is isotopically extremely heterogeneous (consisting of more than three endmembers) or that the different trends are produced by variations in melting and mixing processes. Considering the quite homogeneous Ne isotopic composition and the fact that the He and Ne isotopes should show a coupled behaviour in long term evolution a source having a highly heterogeneous He isotopic composition is not very logical and likely. However, the varying He/Pb abundances required to explain the full He/Pb isotope record by mixing processes can be produced by variations in the melting process. Thus, all of these observations in He/Pb and Nd/Pb isotope space in conjunction with the Ne isotopes can best be explained with processes occuring during melt formation and evolution and not by a zoned plume model.

This finding is also supported by a recent numerical model published by Bianco et al. (2008). That model includes a hot plume of upwelling, isotopically heterogeneous mantle that is interacting with, and melting beneath a moving lithospheric plate. And even though the plume used in their model is compositionally unzoned, with the isotopic heterogeneities of enriched (low Nd isotopes) and depleted (high Nd isotopes) material statistically distributed in the plume, a geographical zoning in Nd isotopes similar to the zoning oberseved at Hawaii is predicted. In their opinion the observed surface patterns are caused by the differences in melting depth of the distinct source components and plume-lithosphere interaction. Such a model can also explain the noble gas isotope patterns observed at Hawaii.

To conclude, while we certainly do not negate that different components contribute to the formation of Hawaiian lavas, our data clearly show that observed surface geochemical patterns do not emulate mantle geochemical patterns and that the geographical distribution of isotopic signatures at the surface is produced by melting and mantle dynamic processes.

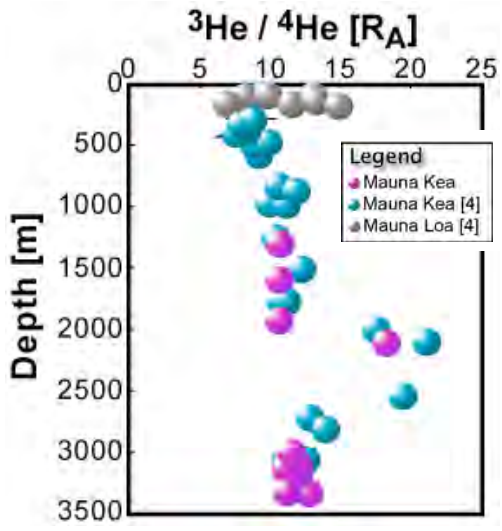

Fig. 1: Distribution of He isotopes with depth of HSDP core.

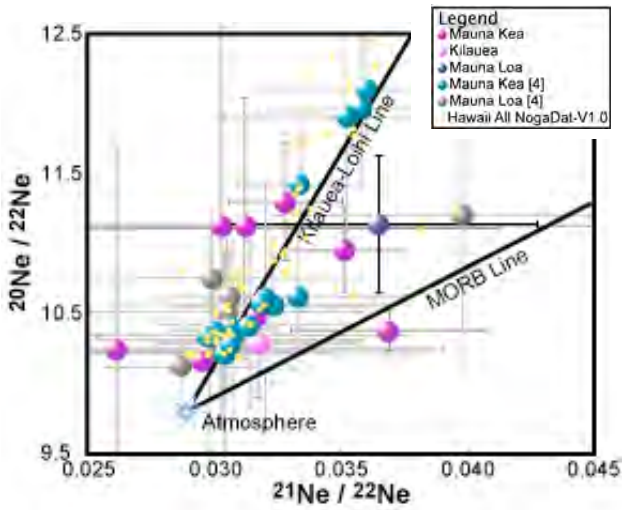

Fig. 2: Ne-three isotope plot of all measured surface and HSDP samples. The small dots are Hawaii data taken from NogaDat-V1.0.

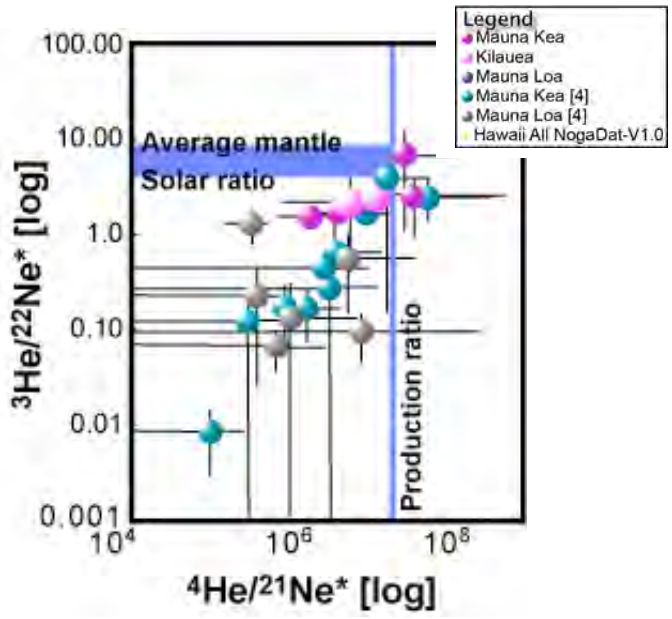

Fig. 3: He/Ne interlement plot showing that He has been fractionated from Ne during the melting process resulting in a He depletion of the produced melts.

Abouchami, W. W H, Galer SJG, A FF, J E, Feigenson M (2005)Lead isotopes reveal bilateral asymmetry and vertical continuity in the Hawaiian mantle plume. Nature 434:851-856
Bianco TA, Ito G, van Hunen J, Ballmer MD, Mahoney JJ (2008) Geochemical variation at the Hawaiian hot spot caused by upper mantle dynamics and melting of a heterogeneous plume. Geochemistry Geophysics Geosystems 9(11)
Frey FA, Rhodes JM (1993) Intershield geochemical differences among Hawaiian volcanoes: implications for source compositions, melting processes and magma ascent paths. Philosophical Transactions of the Royal Society of London A342:121-136
Kurz MD, Kammer DP (1991) Isotopic evolution of Mauna Loa volcano. Earth and Planetary Science Letters 103:257-269.

Explosive volcanism during evolution of Lake Van

M. SUMITA[1], H-U. SCHMINCKE[1]

[1]Research Division 4, Leibniz-Institute of Marine Science, IFM-GEOMAR, Wischhofstr.1 24148 Kiel, Germany

Active Nemrut and Süphan stratovolcanoes (Eastern Anatolia) have supplied abundant tephra into alkaline Lake Van, site of a major ICDP drilling project to be implemented in 2010. Thick tephra deposits on land, previously almost unstudied, comprise numerous huge fallout deposits, several ignimbrites and debris avalanche deposits. Some pumice lapilli fallout units near Ahlat, close to the lake shore, exceed 10 m in thickness. Depositional tephra fans of Nemrut and Süphan volcanoes overlap in space and time. Initial results suggest that both sources can be distinguished chemically and mineralogically. Sixteen rhyolitic fallout and pyroclastic flows (represented as syn-ignimbrite turbidites) in the cores drilled during the exploratory phase (2004) (T1~T16) fall into two compositionally distinct groups: alkaline and sub-alkaline rhyolites. The alkaline differ from sub-alkaline rhyolites by significantly higher Fe, Ti, total alkalis and halogens (F, Cl) and lower-Al, Mg, Ca, K and are characterized by green hedenbergitic cpx and fayalite. They are sourced in Nemrut volcano. The subalkaline tephras are characterized by biotite, hypersthene and minor amphibole and some by accessory chevkinite. Their source is Süphan volcano based on comparison with tephras studied on land. Both types of rhyolites are clearly separated in time with tephras (T 8-15) recording closely-spaced eruptions from Süphan. The oldest tephra cored (T16), however, is compositionally identical to Nemrut tephras. Alkaline rhyolites are also represented by the major Subrecent hydroclastic tephra (surge and fallout deposits) blanketing the caldera rim and interpreted as resulting from a phreatomagmatic eruption through the caldera lake. The twofold clear change in composition greatly facilitates correlation between cores.

Apart from six tephra layers (T1, T6, T7, T11, T12 and T13) of mixed lithology interpreted as representing reworking following an eruption, primary tephra layers represent both fallout and turbidites. The latter show clear grain size contrast between the coarse-grained basal and fine-grained top layers. Because of the abundance of fine ash in the strongly graded layers, turbidites are interpreted to reflect entry of pyroclastic/hydroclastic density currents into Lake Van.

Contrary to our expectation, all Holocene tephra glass shards are extremely fresh. Zeolites inside shards occur in tephra layers older than T13 although glass in comenditic T16 is fresh. Whether or not glass alteration is correlated with a drastic increase in alkalinity of pore waters downward is unclear.

The abundance of angular and non- or only slightly vesicular vitric shards in most tephra layers – and their dominance in some – indicates that hydroclastic fragmentation by thermal shock resulting from magma-water interaction was common. The textural resemblance of glass shards to those of the sub-recent base surge tephra mantling the caldera rim suggests that the

younger tephra layers may reflect eruption of rhyolite magma through Nemrut caldera lake that may therefore have existed for some time. Magma-groundwater interaction and/or subaqueous eruptions cannot be excluded, however. Occurrence of highly vesicular pumice in most tephra layers – and their dominance in a few - indicates plinian/sub-plinian pyroclastic/hydroclastic eruption.

The tephra layers represent slightly more than one major explosive eruption/1ka. As is common in volcanic systems, however, explosive eruptions were not evenly spaced in time. The last historic eruption of Nemrut (1440 AD) was minor (lava flow). Further large explosive eruptions could be expected in the foreseeable future. Future eruptions could produce fallout or pyroclastic flows or both, making the town of Tatvan at the shore of Lake Van highly vulnerable. Moreover, Holocene (?) debris avalanche deposits sourced in Nemrut discovered on the outskirts of Tatvan close to the lake shore and major debris avalanche deposits east of Ahlat are major volcanic hazards, are likely to have generated tsunamis during entry into the lake and should be recorded in the seismic reflectors. Monitoring of both volcanoes should be implemented.

Controls on Calcium Isotope Fractionation in Sedimentary Porewaters of ODP Expedition 204

BARBARA M.A.TEICHERT[1,2], NIKOLAUS GUSSONE[3,4] AND MARTA E. TORRES[5]

[1]Geologisch-Paläontologisches Institut, Universität Münster, Corrensstr. 24, 48149 Münster, Germany
[2]Bundesanstalt für Geowissenschaften und Rohstoffe, Stilleweg 2, 30655 Hannover, Germany
[3]Institut für Mineralogie, Universität Münster, Corrensstr. 24, 48149 Münster, Germany
[4]Forschungszentrum Ozeanränder, Universität Bremen, Postfach 330440, 28334 Bremen, Germany
[5]College of Oceanic and Atmospheric Sciences, Oregon State University, Corvallis, Oregon, USA

The calcium isotopic composition of porewaters and authigenic carbonates in the anoxic sediments of a convergent continental margin drilled during the Ocean Drilling Program (ODP) provides first insight into the different processes that control Ca geochemistry in clastic marine, organic-rich sedimentary environments. In 4 sites drilled during Leg 204 at Hydrate Ridge (Cascadia Margin, offshore Oregon/USA), sulfate is consumed during anaerobic oxidation of methane and of organic matter via sulfate reduction within the upper meters of the sedimentary section. These reactions promote the precipitation of authigenic carbonates through the generation of bicarbonate, which is reflected in a pronounced decrease in calcium concentration. Although Ca isotope fractionation is observed during carbonate precipitation, Ca concentration in the pore fluids from ODP Leg 204 is decoupled from Ca isotopy, which seems to be mainly controlled by the release of light Ca isotopes that completely overprint the carbonate formation effect. Different processes, such as the release of organically bound Ca, ion exchange and ion pair formation may be responsible for the released light Ca. Deeper within the sedimentary section, additional processes such as ash alteration influence the Ca isotopic composition of the porewater. Two sites, drilled into the deeper core of the accretionary prism, reveal the nature of fluids which have reacted with the oceanic basement. These deep fluids are characterized by relatively high Ca concentrations and low $\delta^{44/40}$Ca ratios.

The missing link to understand Plio-Pleistocene changes in southeast Pacific oceanography, productivity, and El Niño behavior – SE trade wind strength and its dust transport.

R. TIEDEMANN[1], D. RINCON-MARTINEZ[1], C. SAUKEL[1] , F. LAMY[1] ,S. STEPH[1], A. STURM[1]

[1]Alfred-Wegener-Institute for Polar and Marine Research, Am Alten Hafen 26, 27568 Bremerhaven (Ralf.Tiedemann@awi.de)

One of the fundamental missing links in understanding the Neogene climate evolution is the interaction and variability between SE trade wind strength, SE Pacific upwelling intensity, dust transport and continental climate evolution of S-America. This, however, is currently a significant issue with regard to global warming and its impact on long-term El Niño behaviour.

In this respect, we examined two ODP Sites from offshore subtropical and tropical South America (ODP Sites 1237 and 1239) to reconstruct Plio-Pleistocene continent-ocean-atmosphere climate linkages on orbital and tectonic time-scales. These changes are thought to be influenced by latitudinal shifts of the Intertropical Convergence Zone (ITCZ) and and long-term variability in the El Niño-Southern Oscillation (ENSO) and are related to major variations in global ice-volume and long-term tectonic reorganisations (central American gateway and Andean uplift). Multi-proxy analyses indicative of changes in dust input and wind strength, river discharge, sea-surface temperature, and productivity provide important insights into these interactions.

ODP Site 1237 is located 140 km off the coast of Peru (~16°S) at 3212 m water depth on the eastern flank of Nazca Ridge. The area is characterized by high biological productivity, connected to upwelling, and lies underneath the modern path of eolian dust transport from the Atacama Desert. Site 1239 was drilled further north, on Carnegie Ridge at 1414 m water depth, 120 km off the coast of Ecuador (~1°S). At this latitude, the continental climate and its vegetation are marked by a strong gradients. Arid conditions expand from the Atacama to southernmost Ecuador at ~3°S (Golfo de Guayaquil). Further north, the coastal regions are under the influence of tropical rainfall related to the ITCZ. Therfore, Site 1239 presumably contains signals of fluvial sediment discharge from the Guayas River, the largest river of tropical South America draining into the Pacific.

At Site 1237, long-term changes in eolian sediment supply, SST, and productivity suggest a strong relationship to major changes in global ice-volume that are linked to intensifications of northern hemisphere glaciations during the Pliocene and Pleistocene. On orbital time-scales, maxima in iron input and siliciclastic grain-size are generally related to SST minima and maxima in biogenic opal productivity during cold stages. This is interpreted to reflect enhanced trade-winds during cold stages leading to colder SSTs and stronger upwelling (productivity).

At Site 1239, the long-term history of terrigenous supply is more complex and largely controlled by Andean uplift in the Pliocene and regional tectonic processes in the early Pleistocene (development of basins in the drainage area). However, orbital-scale variability in terrigenous supply is more closely linked to global climate. Here, we observe a clear relationship between maxima in iron contents and biomarkers indicative of fluvial sediment supply during interglacials particularily well developed after the Mid-Pleistocene climate revolution (MPR). These data suggest more humid conditions probably controlled by a southward shift of the tropical rainbelt (ITCZ) and the Equatorial Front. In addition, these wetter conditions may be partly related to ocean-atmosphere interactions which favoured more frequent El Niño-like conditions during interglacials as coastal Ecuador presently receives significantly higher rainfall during the warm phase of ENSO events. Before the MPR, orbital-scale variability in our terrigenous input proxy is more complex with iron maxima partly occurring during glacials (as at Site 1237) and partly during interglacials. This more complex pattern may be induced a mixture of fluvial and eolian sediment input.

Surprisingly, we also found higher interglacial terrigenous input at Site 1237 after the MPR. Assuming that the general increase of trade-wind strength during glacials as suggested by our data before the MPR is likewise valid in the Late Pleistocene (as e.g. evidenced by furthe offshore records (Winkler et al., 2008)), this higher interglacial supply off Peru may mirror stronger fluvial supply in the generally arid environments. Such rain events are presently occuring during El Niño years. This may argue for strengthened El Niño-like conditions during late Pleistocene interglacials, consistent with our results from Site 1239.

Winckler, G., Anderson, R.F., Fleisher, M.Q., McGee, D. and Mahowald, N., 2008. Covariant Glacial-Interglacial Dust Fluxes in the Equatorial Pacific and Antarctica. Science, 320(5872): 93-96.

The quaternary depositional history of Anholt Loch Kattegat and Hanø Bay / Bornholm Basin: Results of a high resolution seismic IODP Pre-Site Survey

A. F. TRAMPE[1], V. SPIESS[1], S. KRASTEL[2], T. ANDRÈN[3], R. ENDLER[4], J.HARFF[4]

[1]Department of Geosciences, University of Bremen, Klagenfurter Str., 28359 Bremen, Germany
[2]Leibniz Institute of Marine Sciences (IFM-GEOMAR), Wischofstr. 1-3, 24148 Kiel, Germany
[3] Department of Geology and Geochemistry, Stockholm University, SE-106 91 Stockholm, Sweden
[4] Marine Geology Section, Baltic Sea Research Institute, Seestraße 15, Warnemuende 18119 Roststock, Germany

The Baltic Sea Basin (BSB) is one of the world's largest intra-continental basins. The BSB has served as depositional sink throughout its geological history. The accumulated sediments comprise a unique high-resolution paleoenvironmental archive where the history of the drainage area and the basin itself is preserved. Present knowledge of the development of the BSB is based on results from short cores (up to 20 m long), but seismic data and onshore drillings indicate much thicker apparently undisturbed sediment sequences (EIRIKSSON ET AL., 2005; JENSEN ET AL., 2002; LYKKE-ANDERSEN ET AL., 1993; KRISTENSEN ET AL., 2005).

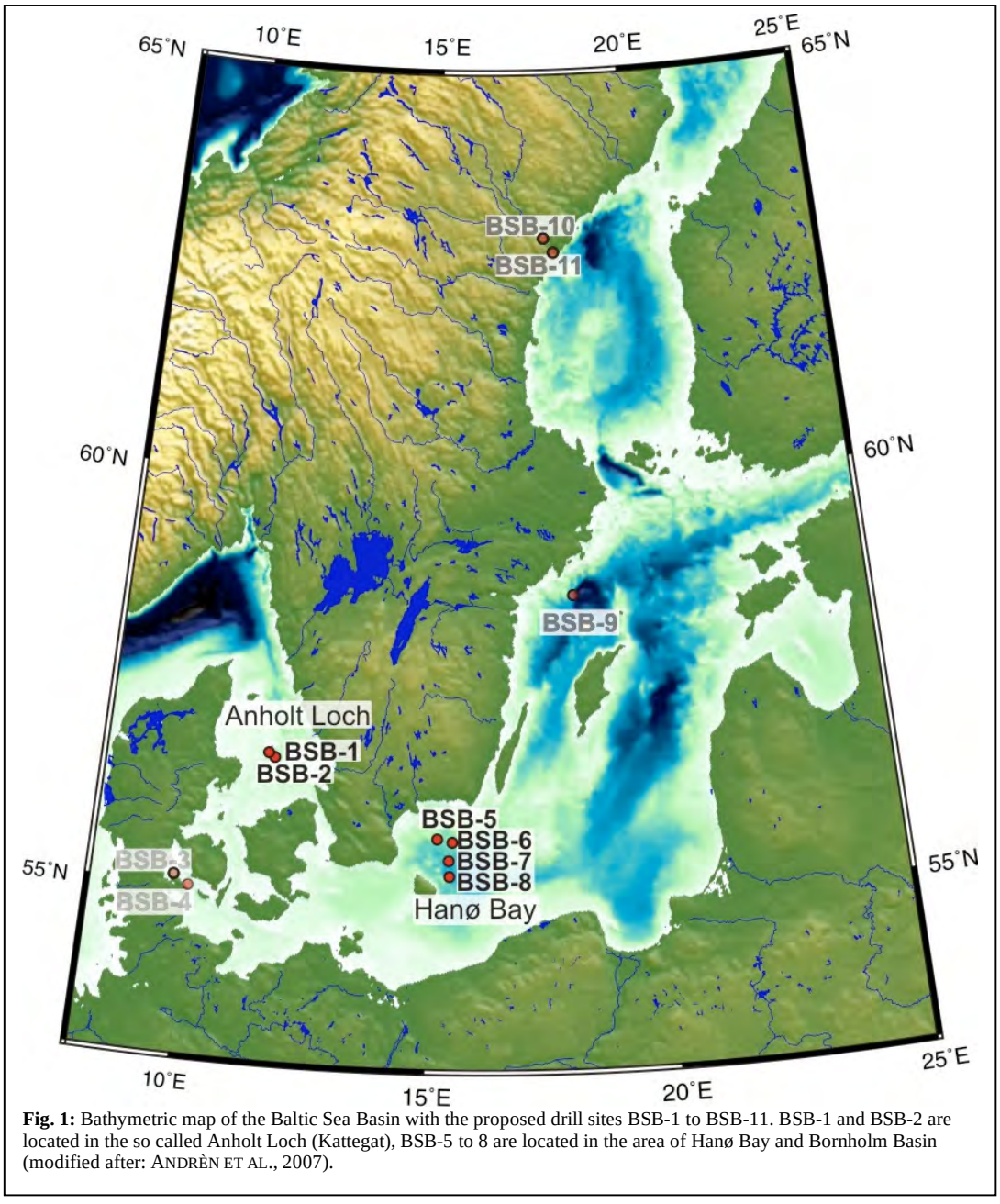

Fig. 1: Bathymetric map of the Baltic Sea Basin with the proposed drill sites BSB-1 to BSB-11. BSB-1 and BSB-2 are located in the so called Anholt Loch (Kattegat), BSB-5 to 8 are located in the area of Hanø Bay and Bornholm Basin (modified after: ANDRÈN ET AL., 2007).

In 2004 the IODP Pre-Proposal "Paleoenvironmental evolution of the Baltic Sea Basin trough the last glacial cycle" was submitted by ANDRÈN ET AL. (2004). The general aim of the project is to reconstruct the climatic response of Northern Europe to the forcing of the Northern Atlantic atmospheric and oceanic circulation system during the last glacial cycle (Holocene, Weichselian and Eemian) by using the sedimentary record of the BSB. During a seismic Pre-Site Survey in February 2006 with the RV Heincke, high-resolution seismic data and sediment echo sounder data were collected in the south-western Baltic Sea. This Pre-Site Survey was an important step for submitting a Full-Proposal in October 2007 (ANDRÈN ET AL., 2007). In total 11 sites are proposed based on our and other seismic data (Fig. 1). Our data were collected around Sites BSB 1 and 2 (Anholt Loch) and BSB 5 to 8 (Hanø Bay / Bornholm Basin) with the Bremen high-resolution seismic system. Two different streamer systems were used simultaneously during data acquisition: a 300 m long 48 channel streamer and a 50 m long 48 channel shallow water streamer. The long streamer was mainly used for velocity analysis, which is crucial for distinguishing between Quaternary and older sediments. Figure 2 shows an example of a velocity model, which is the result of velocity analysis for Profile GeoB06-003. The sharp increase in seismic velocity to >2000 m/s between the lowermost and the overlying facies, suggest this to be the boundary of Pre-Quaternary and Quaternary sediments (Fig. 2). The high resolution data of the shallow water streamer were used for a structural and seismic attribute analysis. The objectives of our investigations are to reconstruct the quaternary history of the Anholt Loch and of Hanø Bay / Bornholm Basin in order to verify these proposed sites for potential drilling sites.

The Anholt Loch is located in the Kattegat, the westernmost area of the Baltic Sea. The elongated depression is incised into the lowermost facies A, characterized by tilted reflectors and a sharp increase in seismic velocity (Fig. 2). Facies A is interpreted as Pre-Quaternary sediments. A drilling on the island of Anholt shows that the Pre-Quaternary sediments are Jurassic in age (LYKKE-ANDERSEN ET AL., 1993). The detection of the boundary of the Pre-Quaternary and Quaternary sediments is based on a facies analysis and a detailed velocity analysis (Fig. 2). South-western of the valley Anholt Loch an angular unconformity between facies A and B could be detected (Fig. 2). At the base of this unconformity, the boundary between Pre-Quaternary and Quaternary sediments could be clearly identified. This boundary does not only show a change in facies, but also a distinct increase in seismic velocity. The facies analysis was not in the whole area a suitable parameter for the identification of the boundary between Pre-Quaternary and Quaternary sediments. If the results of the facies analysis were equivocal, as for example in the valley, the sharp increase of seismic velocity was used for identification of this boundary.

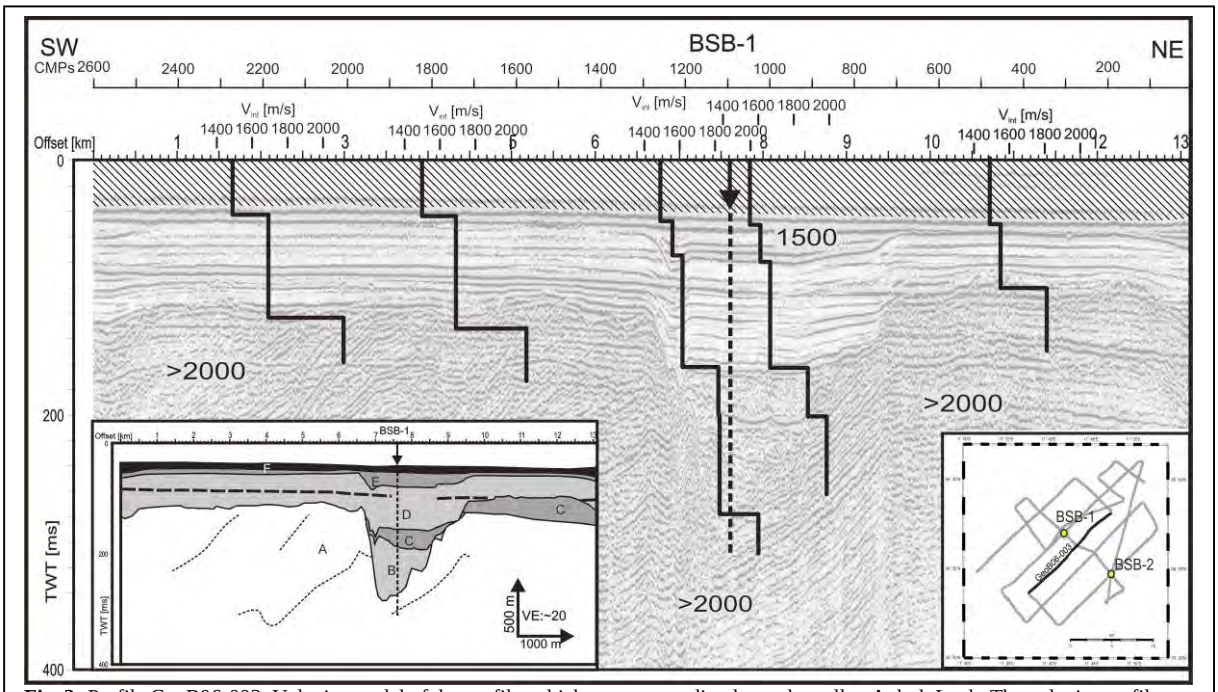

Fig. 2: Profile GeoB06-003: Velocity model of the profile, which runs perpendictular to the valley Anholt Loch. The velocity profiles are embedded over the migrated seismic data. The box in the bottom left corner of the velocity model shows the interpretation of this profile.The location of the profiles is shown in the inserted map. BSB-1 and BSB-2 are the proposed drill sites. BSB-1 is located north-west of profile 003 and is projected on this profile. **III:** A: Jurassic, B: Saalian and Eemian C: Weichselian till, D: Weichselian, glacio-marine sediments, E: late Weichselian, F: Holocene. (hier fehlt der hinweis, dass das für III gilt)Dashed line: Multiple of the seafloor reflector, dotted lines: tilted reflectors in facies A. For location of the study area and the proposed drill sites see Fig. 1

The erosional valley, which is interpreted as a sub glacial melt water valley, is filled with a more than 250 m thick sedimentary succession, in which five different facies (B-F) could be identified (Fig. 2). Facies B to F are interpreted as Quaternary sediments, which were deposited during Saalian to Holocene times. The interpretation of stratigraphic analysis, the drilling on Anholt (LYKKE-ANDERSEN ET AL., 1993) and dated vibrocores, which covered Weichselian to Holocene sediments (JENSENS ET AL., 2002), suggest that sediments of the complete last glacial cycle can be found at this site.

The areas of Hanø Bay and Bornholm basin are located in the southern Baltic Sea, east of the area of Anholt Loch (Fig. 1). For the reconstruction of the Quaternary depositional history, it is necessary to distinguish between Pre-Quaternary and Quaternary sediments, which is a complicated task because older reflectors are running nearly parallel to the upper reflectors representing the Quaternary sediments. As already discussed for Anholt Loch, however, the velocity analysis allows a precise detection of the boundary between Pre-Quaternary and Quaternary sediments (Fig. 2).

The whole area is characterized by a ~10 m thick top layer, which is interpreted as Holocene Mud and Clay (Fig. 3). Below these sediments, a relative thin till layer of late Weichselian age is presumed. The relative thick transparent layer with some internal reflectors beneath would then be of Eemian or early to mid Weichselian age. In the deeper part of the Bornholm Basin, some sediment pockets below the Weichselian till were discovered. These sediments were probably deposited in the lake that occupied the southern Baltic Basin from Eemian up to the last Weichselian ice advance. This will give the opportunity to study the lake development both in littoral phases in Hanø Bay and in deep lake phases in the Bornholm Basin. The four sites in Hanø Bay and Bornholm Basin are located in sediment pockets (Fig. 3), because these locations offer the possibility to recover sediments, which were not severely altered by glacial processes. Sites were chosen close to the shore in the area of Hanø Bay and also in the deeper Bornholm basin along a transect in order to compare records in environments with different glacial influence. The sequences should vary in respect to the relative amount of terrestrial input and also with respect to the impact of glacial load and glacial deformation. Furthermore, the locations of these sites provide the possibility to study glacial retreat in this area.

ANDRÈN T., BITINAS A., BJÖRK S., EMELYANOV E., HARFF J., JAKOBSON M., JENSEN J. B., KNUDSEN K. L., KOTILAINEN A., LEMKE W., USCINOWICZ S., VESKI S., and ZELCHS V. (2004) Paleoenvironmental evolution of the Baltic sea basin through the Last Glacial Cycle (Pre-Proposal).

ANDRÈN T., BJÖRCK S., JØRGENSEN B. B., KNUDSEN K. L., HARFF J., BITINAS A., EMELYANOV E., JAKOBSON M., JENSEN J. B., KOTILAINEN A., SPIESS V., USCINOWICZ S., VESKI S., and ZELCHS V. (2007) Paleoenvironmental evolution of the Baltic sea basin through the Last Glacial Cycle (Full-Proposal).

EIRIKSSON J., KRISTENSEN P.-H., LYKKE-ANDERSEN H., BROOKS K., MURRAY A., KNUDSEN K. L., and GLAISTER C. (2005) A Sedimentary record from a deep Quarternary valley in the southern Lillebaelt area, Denmark: Eemian and Early Weiselian lithology and chronology at Mommark. Boreas 35, 320-331.

JENSEN J. B., PETERSEN K. S., KONRADI P., KUIJPERS A., BENNIKE O., LEMKE W., and ENDLER R. (2002) Neotectonics, sea-level changes and biological evolution in the Fennoscandian Border Zone of the southern Kattegat Sea. Boreas 31, 133-150.

KRISTENSEN P.-H. and KNUDSEN K. L. (2005) Palaeoenvironments of a complete Eemian sequence at Mommark, South Denmark: foraminifera, ostracods and stable Isotopes. Boreas 35, 349-366.

LYKKE-ANDERSEN H., SEIDENKRANTZ M.-S., and KNUDSEN K. L. (1993) Quarternary sequences and their relation to the pre-Quarternary in the vicinity of Anholt, Kattegat, Skandinavia. Boreas 22, 291-298.

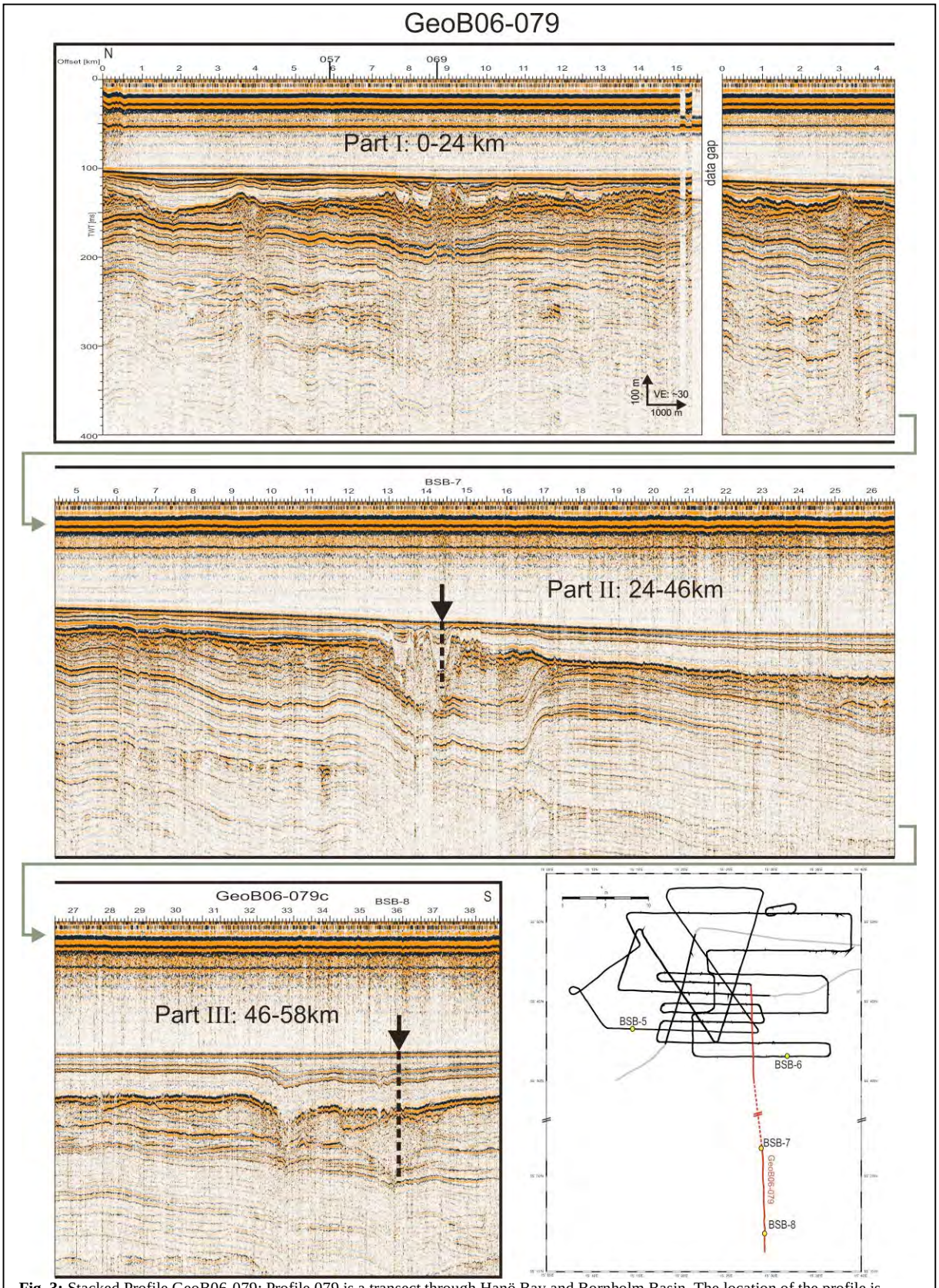

Fig. 3: Stacked Profile GeoB06-079: Profile 079 is a transect through Hanö Bay and Bornholm Basin. The location of the profile is shown in red in the inserted map. BSB 5 to 8 are the proposed drill sites. BSB – 7 and 8 were shown in detail in the inserted close- ups. The study area and the proposed drill sites are shown in Fig. 1.

Proposal to drill for the Cretaceous and Paleogene high latitude climate history, James Ross Basin, Antarctic Peninsula.

L. VIERECK-GOETTE[1], J. FRANCIS[2], A. VAUGHAN[3], S. MARENSSI[4], B. MOHR[5], AND THE D-ANDRILL MEMBERS

[1]Institut fuer Geowissenschaften, Friedrich-Schiller-Universitaet Jena, Burgweg 11, D-07749 Jena, Germany
[2]School of Earth and Environment, Leeds University, Leeds, LS2 9JT, United Kingdom
[3]British Antarctic Survey, Natural Environment Research Council, High Cross, Madingley Road, Cambridge CB3 0ET, United Kingdom
[4]Instituto Antártico Argentino, Universidad de Buenos Aires, Cerrito 1248, Ar-C1010AAZ Buenos Aires, Argentina
[5]Museum fuer Naturkunde, Institut für Palaeontologie, Invalidenstrasse 43, D-10115 Berlin, Germany

This proposal is for drilling a key geological section in the Antarctic Peninsula region. The James Ross Basin, east of the Antarctic Peninsula, contains the best high-latitude section in the world that spans more than 40 million years of geological history from the mid-Cretaceous through the Paleogene (~80-34Ma). More than 5000m of marine and estuarine sediments were deposited during the filling of the James Ross back-arc basin. The sedimentary succession is extremely fossiliferous, yielding diverse invertebrate, vertebrate and plant fossil assemblages, allowing detailed reconstructions and integration of both terrestrial and marine systems. The sequence also contains a key global reference section for the Cretaceous-Tertiary extinction event at high latitudes.

The sequence contains several key intervals that provide details about past polar climates: a) the mid-Cretaceous Thermal Maximum (~80Ma) when tropical floras grew at ~65°S and greenhouse temperatures reached their peak across the globe; b) a possible phase of high-latitude glaciation within greenhouse times during the latest Cretaceous; c) the Cretaceous-Tertiary extinction event at 65Ma; d) the Paleocene-Eocene Thermal Maximum episode of rapid global warming at 55Ma (possibly an unconformity in Seymour Island but this can be better established in a drill core); e) a cooling phase during the Eocene, and f) the first signs of glaciation in the latest Eocene/earliest Oligocene.

Although the sedimentary sequence is reasonably well known from surface outcrop and a stratigraphy has been established, the unconsolidated and weathered nature of the outcrop prohibits high resolution studies. Drill cores will provide more consolidated sediments that can be logged and sampled at high resolution and provide an extremely detailed picture of environmental and climate evolution through this transition from greenhouse to icehouse climates. The outcomes of drilling and science projects will be a detailed record of climate change at southern high latitudes that can be matched to global events. These new data will be used to test climate models and evaluate climate simulations. In addition, new information about marine and terrestrial ecosystem extinctions and recovery at major events, such as Cretaceous Tertiary boundary and the mid-Cretaceous Thermal Maximum, will be obtained to add a high-latitude perspective to these global events.

Several sites are planned on the Islands of Seymour (Marambio), Snow Hill, and James Ross to drill this time span using a land-based rig. Seymour (Marambio) Island is suggested as base for the project as it is home of the Argentinian Marambio Station and an airfield with a runway 1260m in length.

Three-Component Magnetic Logging in the Outokumpu Borehole

C.VIRGIL[1], F. DIETZE[2], A.HÖRDT[1], T.KLEIN[1], M. LEVEN[3], E. STEVELING[3]

[1] Institut für Geophysik und Extraterrestrische Physik, Technische Universität Braunschweig, Germany (c.virgil@tu-bs.de)
[2] Geologisches Institut der Universität Karlsruhe, Karlsruhe, Germany
[3] Institut für Geophysik, Universität Göttingen, Germany

Magnetic measurements in boreholes are normally used for the interpretation of total field anomalies or for tool orientation. Some more sophisticated tools may use inclinometers to obtain the vertical and the horizontal field components and estimate magnetic field inclination. However, in particular in ore exploration, the declination of the magnetic field is of interest for reducing the ambiguity of the interpretation. Another possible application is the reorientation of borehole cores. With the knowledge of the declination one can easily combine the results of magnetic laboratory measurements with other logging results.

To determine the declination of the rock magnetization, it is critical to obtain the inclination as well as the azimuthal position with a high accuracy. In our tool, the “Göttinger Bohrloch Magnetometer” (GBM), the rotation along the x-, y- and z-axis is recorded by three fibre-optic gyros (FOG’s). These instruments have the benefit of a very small drift per hour (approx. 1 °/h) in combination with a high resolution ($9 \cdot 10^{-5}$ degree per increment). The small drift is critical due to the measuring time of several hours in deep boreholes. The magnetic field is measured by a three-component Fluxgate sensor with a resolution of 6.1 nT in x- and y-direction and 8.5 nT in z-direction.

The hardware and processing schemes of the GBM are continuously being modified and tested to improve the accuracy of the reorientation. The declination of magnetization was successfully determined in the HSDP borehole, but a systematic evaluation of the accuracy was not carried out. Here, we discuss data from the Outokumpu borehole in Finland, acquired in September 2008.

The aim was to obtain an understanding of the deep structure of the Cu-Co-Zn ore deposits as well as their formation process. The ore is hosted in the so-called Outokumpu assemblage, consisting of black shales, serpentinite and skarn rock. The total depth of the Outokumpu borehole is 2500 m with a maximum tilt of 9.6 °. We carried out six measurements at

different spatial resolutions, varying from 5 cm to 20 cm. The resolution is controlled by the logging speed, which varied between 6 m/min and 20 m/min at a logging frequency of 0.5 Hz. After various steps of data processing we obtained several down- and uplogs of the magnetic field in three components.

The most important step in data processing is the reorientation of the magnetic field data from the tool coordinate system to the geographical coordinate system. A very high accuracy of the orientation with errors below 0.1 degrees is required, because small orientation errors may cause large errors in the magnetic field components. Therefore, all system parameters, such as the orthogonality of the 3-component Fluxgate sensors and gyros, as well as the temperature dependent drift of the gyros, need to be measured with great care. We measured these calibration parameters in the magnetic laboratory "Magnetsrode" in Braunschweig, where magnetic fields in all three directions can be generated in a Braunbek coil system.

To compute the magnetization from the magnetic field we used an inversion algorithm which is based on a 2D-Model of homogeneously magnetized layers. This constitutes a simplification of the real situation, but permits a first estimate and quality check of the computed rock magnetization along the borehole. The repeatability of the inclination of the rock magnetization is about 5°, the repeatability of the declination between the individual measurements lies between 10 ° - 20 °. This accuracy might be sufficient for some applications, e.g. ore exploration. Further improvement is expected from refined processing schemes and remeasuring of calibration parameters, e.g. the orientation of the sensors with respect to the housing. We will also develop an inversion algorithm for more complex geological structures to obtain a better model of the ore deposit crossing the borehole.

The integrated interpretation of our results with data from core samples and other well logging datasets will enable us to test various hypotheses on the tectonic evolution of the Outokumpu assemblage.

A paleoclimate record with tephrochronological age control for the last climatic cycle from Lake Ohrid, Albania and Macedonia

H. VOGEL[1], B. WAGNER[1], G. ZANCHETTA[2], R. SULPIZIO[3], S. SCHOUTEN[4], M.J. LENG[5]

[1] Institute for Geology and Mineralogy, University of Cologne, Cologne, Germany
[2] Dipartimento di Scienze della Terra, Universita di Pisa, Pisa, Italy
[3] CIRISIVU c/o Dipartimento Geomineralogico, Universita di Bari, Bari, Italy
[4] Royal Netherlands Institute for Sea Research (NIOZ), Den Burg - Texel, The Netherlands
[5] NERC Isotope Geosciences Laboratory, British Geological Survey, Nottingham, United Kingdom

Lake Ohrid, a transboundary lake situated on the border of Macedonia and Albania in the central-northern Mediterranean with an age of approximately 3-5 Ma, is considered to be the oldest lake in Europe. With a sediment fill of more than 600 m it provides a unique record in a region responding sensitively to climate change.

Here we present first results from a sediment record (Co1202) recovered from Lake Ohrid in autumn 2007. The c. 15m long sediment sequence was taken from 145 m water depth in the north-eastern part of the lake, where the sediment succession is widely undisturbed according to a shallow seismic pre-site survey. The identification of nine tephra and cryptotephra layers (Fig. 1) and their geochemical correlation to well dated eruptions of Italian volcanoes as well as seven additional radiocarbon dates (Fig. 1) allowed the establishment of a relatively reliable chronology for core Co1202. According to our age-depth model core Co1202 covers the last-glacial interglacial cycle and reaches back to marine isotope stage (MIS) 6. The sediment succession is, however, not continuous and comprises a hiatus of approximately 16,000 yrs. between c. 82,000 and 98,000 yrs. BP.

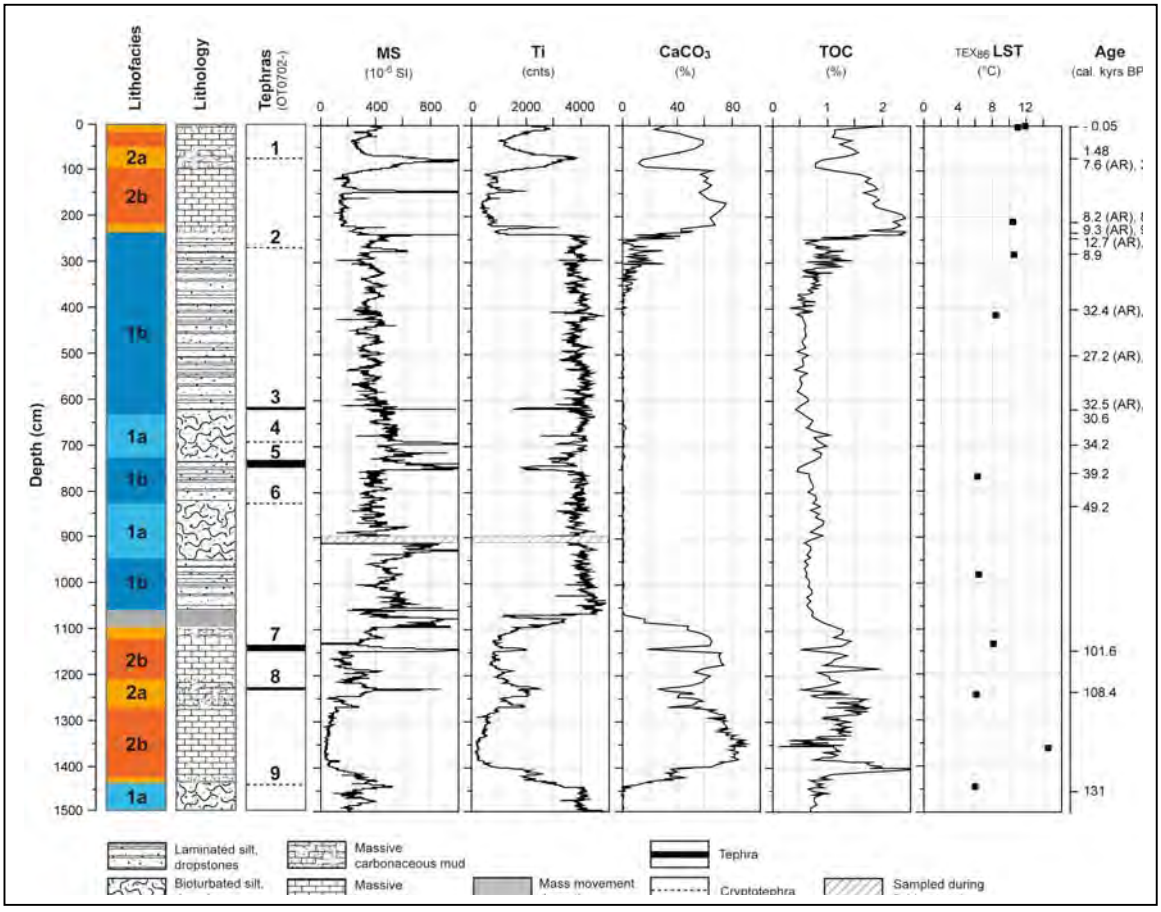

Fig. 1: Major lithofacies, lithology, occurrence of tephras, and selected physical and geochemical properties of core Co1202 from the northeastern part of Lake Ohrid. Test measurements of TEX_{86} reveal a temperature anomaly of ca. 5-6°C between glacial and interglacial periods. The warmest temperature is reconstructed for the Eemian. Ages are based on radiocarbon dating (asterisks) and on tephrostratigraphy.

The sediment composition of core Co1202 varies strongly showing two clearly distinguishable lithofacies. Massive sediments with high amounts of $CaCO_3$, TOC, and low amounts of detrital clastic material as indicated by low Ti and low magnetic susceptibility values (Fig. 1) correlate well with interglacial stages MIS 5 and the Holocene. Partly laminated sediments, dominated by high amounts of detrital clastic material as indicated by high Ti and magnetic susceptibility values,

frequent occurrences of dropstones, and low $CaCO_3$ concentrations (Fig. 1), correlate well with glacial stages MIS 6, 4, 3 and 2.

Despite these general sedimentation patterns reflecting glacial and interglacial climate conditions, short termed climatic fluctuations probably representing Dansgaard/Oeschger, Heinrich, and Mediterranean sapropel events are recorded by proxies sensitive to hydrological changes. Initial results on changes in past lake surface temperature, obtained by application of the recently proposed TEX_{86} paleothermometer, indicate temperature differences of c. 5-6°C between the Last Glacial Maximum and the Holocene, as well as 2°C warmer temperatures during the Eemian if compared to the Holocene (Fig. 1). These initial results on the variation of past lake surface temperature using the TEX_{86} paleothermometer will be extended within the scope of a DFG (SPP ICDP) funded PostDoc project starting in October 2009.

Climate Cycles and Events in the Plio-/Pleistocene of the Yermak Plateau, Arctic Ocean: Causes and Consequences based on validated X-ray Fluorescence Scanner Data of ODP Sites 910 and 911: Towards Millenial Scale Resolution

CHRISTOPH VOGT[1], JENS MATTHIESSEN[2], CHRISTIAN MÄRZ[3], HANS-J. BRUMSACK[3], REINHARD X. FISCHER[1]

[1]Crystallography, Geosciences, University of Bremen, Klagenfurter Str. 2, 28359 Bremen, cvogt@uni-bremen.de
[2]Geosciences, Alfred Wegener Institute for Polar and Marine Research, Am Handelshafen 26, 27568 Bremerhaven
[3]Geochemistry, Institute for Chemistry and Biology of the Marine Environment (ICBM), Carl-von-Ossietzky-University, PO Box 2503, 26111 Oldenburg

New high resolution elemental analysis (discrete samples and XRF-Scanning) data combined with grain-size and mineralogical data of ODP Sites 910 and 911 will be presented for the last 1 Ma. Validation of XRF scanning data vs. discrete sample chemistry, lithological and mineralogical changes is highly emphasized.

Based on a revised chronostratigraphy, data from this project (Fi442/13-1,2), and a compilation of borehole data from the Barents Sea continental margin, we proposed for the first time a coherent general glaciation model for the Barents Sea ice sheet over the past 3.5 million years (Ma) Knies et al. (in press). Three principal phases of ice growth were suggested: (1) The initial build-up phase, covering mountainous regions and reaching the coastline/shelf edge in the northern Barents Sea during shortterm glacial intensification, is concomitant with the onset of the Northern Hemisphere Glaciation (3.6–2.4 Ma). (2) A transitional growth phase (2.4–1.0 Ma), during which the ice sheet expanded towards the southern Barents Sea and reached the northwestern Kara Sea. This is inferred from step-wise decrease of Siberian river-supplied smectite-rich sediments, likely caused by ice sheet blockade and possibly reduced sea ice formation in the Kara Sea as well as glacigenic wedge growth along the northwestern Barents Sea margin hampering entrainment and transport of sea ice sediments to the Arctic–Atlantic gateway (see Vogt & Knies 2008 for a detailed sedimentation process description and Krylov et al., 2008 for the general Tertiary to Quaternary trends). (3) Finally, large-scale glaciation in the Barents Sea occurred after 1 Ma with repeated advances to the shelf edge. The timing is inferred from ice grounding on the Yermak Plateau at about 0.95 Ma, and higher frequencies of gravity-driven mass movements along the western Barents Sea margin associated with expansive glacial growth.

Long-term climate changes on Earth and in particular the Northern Hemisphere glaciations are related to Milankovich cycles. Despite large obstacles to prepare a high resolution chronostratigraphy in Arctic Ocean sediments beyond 300,000 years (see Knies et al., 2007; Matthiessen et al., 2009), we are now able to identify paleoenvironmental changes down to milenial scale resolution and back to 3.5 Ma in the Yermak Plateau and Fram Strait region. As show in Figure 1, the sedimentary record in the Fram Strait Gateway region yields a rather high complexity, in particular during deglaciations, due to multiple short time meltwater events from the Svalbard-Barents Sea (SBIS) and Kara Sea Ice Sheets and related sedimentation changes. This suggests a pronounced instability of the Arctic climate system, with major consequences for the environment.

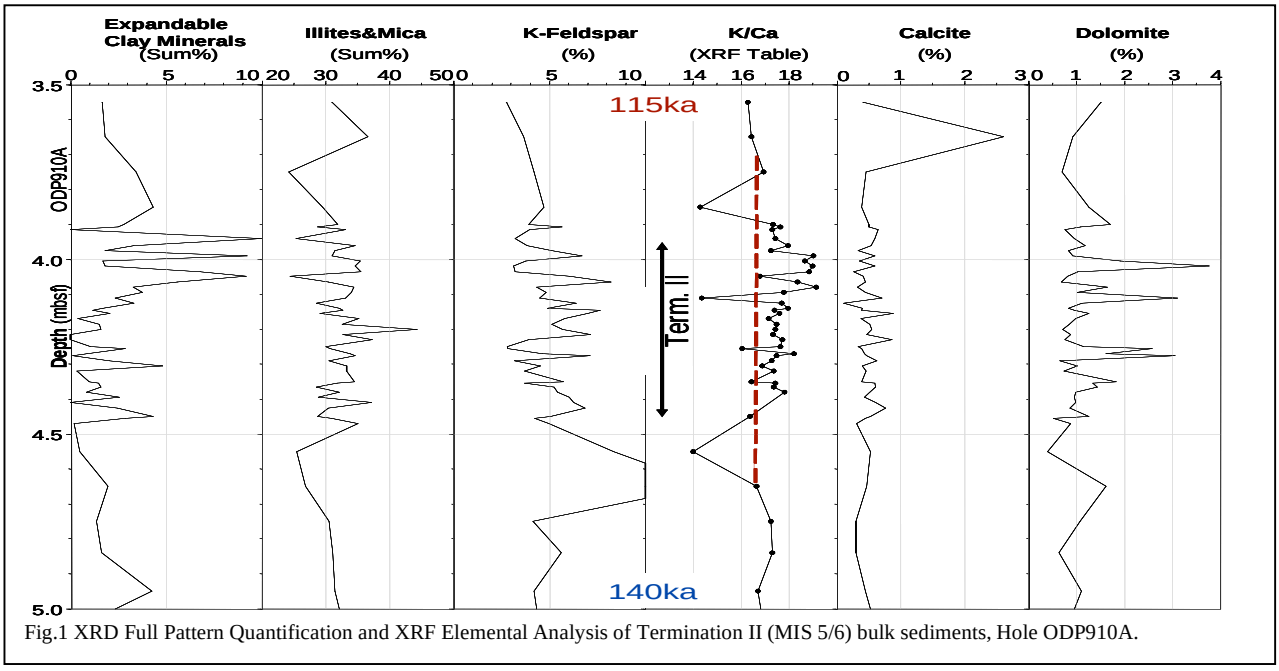

Fig.1 XRD Full Pattern Quantification and XRF Elemental Analysis of Termination II (MIS 5/6) bulk sediments, Hole ODP910A.

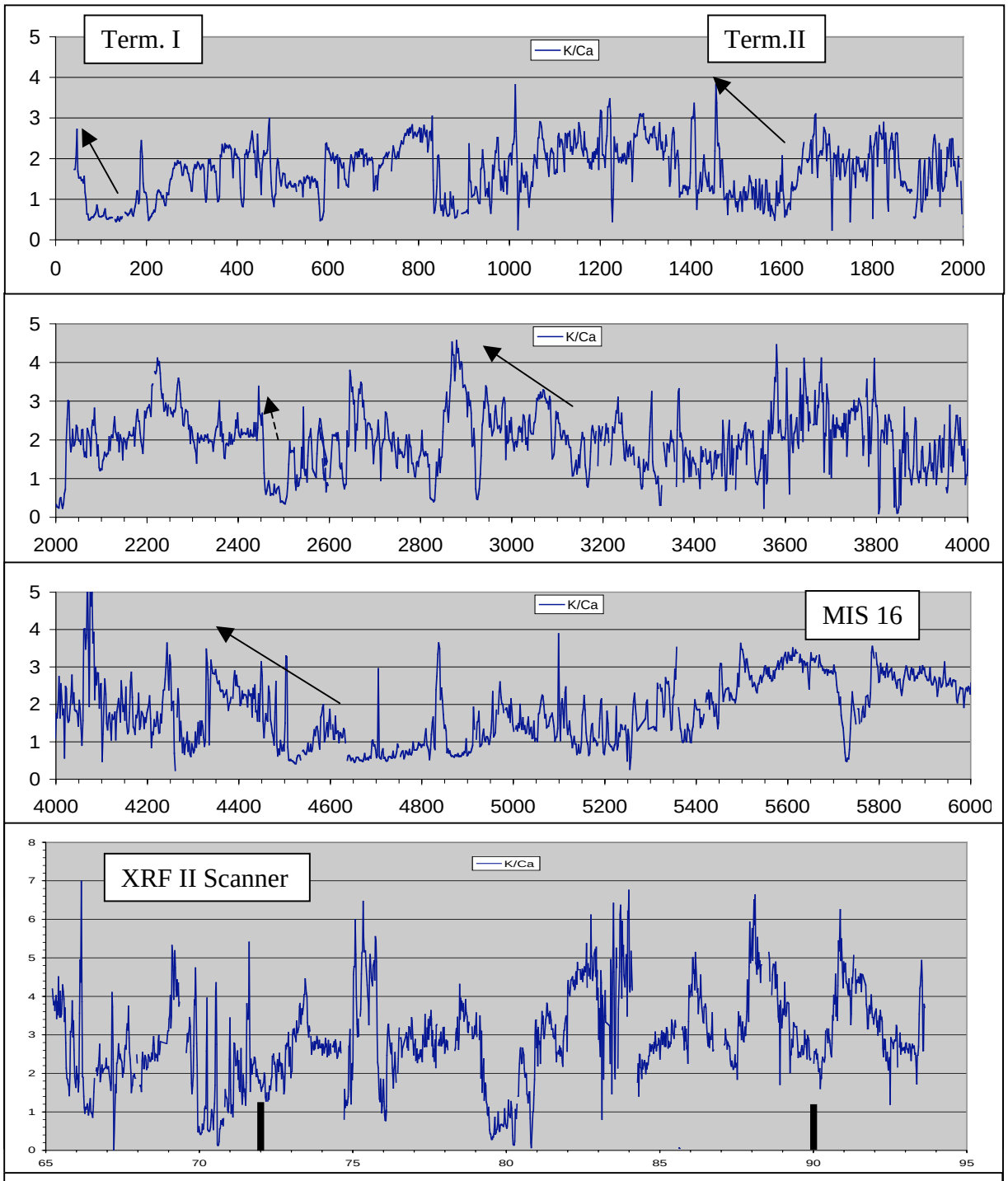

Fig.2 XRF scannning data of Hole ODP 911A measured with the Bremen AVAATECH XRF I and II Scanner (>65 m). B/M Paleomagnetic Boundary (781 ka) at aprrox. 72 mbsf, top of the Jaramillo subchron (988ka at 90 mbsf black lines). Some MIS Stages are indicated by numbers. A comparison of the good compareability of XRF Scanner I and II records will be presented at the Meeting.

Figure 1 illustrates how high K/Ca-ratios are linked to complex changes in K-feldspar and K-rich clay minerals vs. carbonate in aprox. 70 cm of Termination II sediments. Marine Isotope Stage (MIS) 6 was the youngest very large glaciation of the Barents-Kara Sea region. The Kara Sea outlet was completely blocked and very small amounts of its typical mineral assemblage incl. expandable smectites/montmorillonites and mixed layer clays could reach the Yermak Plateau (c.f. Knies & Vogt 2003). Local sources with very high illite/mica content and detrital carbonates (dolomite) dominate (c.f. Vogt et al., 2001). These are usually combined with indicators of warmer Atlantic Water influx including biogenic carbonates (mainly calcite, Vogt et al., 2001 and references therein). But during Term. II and in older sediments many phases of calcite dissolution are observed in the Fram Strait and around the Yermak Plateau desturbing the record of the so called “high productive events” (c.f. Hebbeln et al., 1998; Vogt et al., 2001 and references therein). K-feldspars are derived from Triassic sandstone-rich rocks of Franz-Josef-Land and Svalbard and are typical indicators of iceberg ice-rafted debris in the region of the Yermak Plateau (Vogt et al., 2001).

Only in the late phase of Termination II after the major breakup of the Svalbard Barents Sea Ice Sheet, a secound freshwater pulse from the Kara Sea deglaciation is recorded in the Yermak Plateau records (Fig. 1) compare the Expandable Clay Mineral content increase to Vogt et al., 2001).

In general, a deglacial sequence in the K/Ca ratio at the Yermak Plateau is characterized by a extraordinary high values intercalated between 2 extreme lows. The later are typically fuelled by reduced deposition of local abrasional products and increased calcite contents which could indicate stronger Atlantic Water flux to the Arctic Ocean. By tracing this outlined sequence and despite the complications from carbonate/ calcite dissolution effects we can find plenty of large deglacial sequences in the ODP 911A Hole records (Fig.2).

Termination I and II are well described in other cores of the Yermak Plateau, the southwestern Eurasian Basin and the Fram Strait. Ice rafted debris (sand, gravel), carbonate content and isotope records support the recognition of these sediment sequences in the high sedimentation and high resolution ODP 911A record. While Termination II sediments are at about 4 mbsf in ODP 910A and many other sediments core of the Yermak Plateau we find Term. II at roughly 14.5 to 15 mbsf in Hole ODP 911A (compare Fig.1 & 2). The Brunshes Matuyama Magnetic Boundary is at about 72 mbsf compared to 19.45 mbsf in Hole ODP 910A (Knies et al, in press and references therein). Frequent changes in the K/Ca-ratio between Term. I and II in Hole ODP 911A could indicate rather fast sedimentation changes on the millenial scale. Fast fluctuations of the of the SBIS northern rim have allready been document for MIS 2 & 3 and 5 (e.g. Knies & Vogt, 2003). Below Term. II several large scale K/Ca-ratios might indicate strong deglacial events at approx. 25, 30 and 45 mbsf. Large sedimentation rate changes are typical in Hole 911A and we are currently improving the age model between 20 and 72 mbsf. Besides the well investigated paleomagnetic events the XRF scanning data helps us to find sediment horizons containing carbonates and calcitic foraminifera.

Based on our latest publication (Knies et al., in press) and in cooperation with us a Norwegian mainly stratigraphic research project was initiated to better understand the age of three phases of Northern Hemisphere glacation and in particular the correlation of certain distinc regional seismic unconformaties to the ODP holes of the Yermak Plateau and the western Barents Sea slope. See the presentation of Knies, Vogt, Andreassen, Hald, Husum, Fabian & Grøsfjeld.

Hebbeln D, Henrich R, Baumann K-H (1998) Paleoceanography of the last interglacial/glacial cycle in the Polar North Atlantic. Quaternary Science Reviews 17, 125-153.

Knies J, Vogt C (2003) Freshwater pulses in the Eastern Arctic Ocean during Saalian and Early Weichselian ice-sheet collapse. Quaternary Research 60,243-251.

Knies J, Matthiessen J, Mackensen A, Stein R, Vogt C, Frederichs T, Nam S-I (2007) Effects of Arctic freshwater forcing on thermohaline circulation during the Pleistocene. Geology 35, 1075-1078.

Knies, J., Matthiessen J., Vogt C., Laberg, J.S., Hjelstuen, B.O., Smelror, M., Larsen, E., Andreassen, K., Eidvin, T., Vorren, T.O. (in press). The Plio-Pleistocene glaciation of the Barents Sea-Svalbard region: A new model based on revised chronostratigraphy. Quaternary Science Reviews: (2009),doi:10.1016/j.quascirev.2008.12.002.

Krylov A, Andreeva I, Vogt C, Backman J, Krupskaya VV, Grikurov GE, Moran K, Shoji H (2008) A shift in heavy and clay mineral provenance indicates a middle Miocene onset of a perennial sea-ice cover in the Arctic Ocean. Paleoceanography 23, PA1S06, doi:10.1029/2007PA001497, ACEX Spec. Sect.

Matthiessen, J., Knies, J., Vogt, C., Stein, R., (2009). Pliocene palaeoceanography of the Arctic Ocean and subarctic seas. Philosophical Transactions of the Royal Society A: Mathematical, Physical and Engineering Sciences, 367(1886): 21-48, doi:10.1098/rsta.2008.0203, online since 16. Oct. 2008.

Vogt, C., Knies, J. (2008). Sediment dynamics in the Eurasian Arctic Ocean during the last deglaciation -- The clay mineral group smectite perspective. Marine Geology, 250(3-4): 211-222, doi:10.1016/j.margeo.2008.01.006

Vogt C, Knies J, Spielhagen RF, Stein R (2001) Detailed mineralogical evidence for two nearly identical glacial/deglacial cycles and Atlantic water advection to the Arctic Ocean during the last 90,000 years. Global and Planetary Change 31, 23-44.

SCOPSCO – Scientific Collaboration On Past Speciation Condition in Lake Ohrid

B. WAGNER[1], T. WILKE[2], A. GRAZHDANI[3], G. KOSTOSKI[4], S. KRASTEL-GUDEGAST[5], K. REICHERTER[6], G. ZANCHETTA[7]

[1]University of Cologne, Institute of Geology and Mineralogy, Cologne, Germany
[2]Institute of Animal Ecology and Systematics, Justus Liebig University Giessen, Germany
[3]Universiteti Politeknik, Fakulteti i Gjeologjise dhe Minierave, Tirane, Albania
[4]Hydrobiological Institute Ohrid, Republic of Macedonia
[5]Institute Cluster of Excellence: The Future Ocean, Leibniz Institute of Marine Sciences (IFM-GEOMAR), Kiel, Germany
[6]Institute of Neotectonics and Natural Hazards, RWTH Aachen University, Germany
[7]Dipartimento di Scienze della Terra, Università di Pisa, Italy

Lake Ohrid is a transboundary lake with approximately two thirds of its surface area belonging to the Former Yugoslav Republic of Macedonia and about one third belonging to the Republic of Albania. With more than 210 endemic species described, the lake is a unique aquatic ecosystem and a hotspot of biodiversity. This importance was emphasized, when the lake was declared a UNESCO World Heritage Site in 1979, and included as a target area of the International Continental Scientific Drilling Program (ICDP) already in 1993.

Though the lake is considered to be the oldest, continuously existing lake in Europe, the age and the origin of Lake Ohrid are not completely unravelled to date. Age estimations vary between one and ten million years and concentrate around two to five million years, and both marine and limnic origin is proposed. Extant sedimentary records from Lake Ohrid cover the last

glacial/interglacial cycle and reveal that Lake Ohrid is a valuable archive of volcanic ash dispersal and climate change in the central northern Mediterranean region. These records, however, are too short to provide information about the age and origin of the lake and to unravel the mechanisms controlling the evolutionary development leading to the extraordinary high degree of endemism. Concurrent genetic brakes in several invertebrate groups indicate that major geological and/or environmental events must have shaped the evolutionary history of endemic faunal elements in Lake Ohrid.

High-resolution hydroacoustic profiles (INNOMAR SES-96 light and INNOMAR SES-2000 compact) taken between 2004 and 2008, and multichannel seismic (Mini-GI-Gun) studies in 2007 and 2008 demonstrate well the interplay between sedimentation and active tectonics and impressively prove the potential of Lake Ohrid for an ICDP drilling campaign. The maximal sediment thickness is ˜680 m in the central basin, where unconformities or erosional features are absent. Thus the complete history of the lake is likely recorded.

A deep drilling in Lake Ohrid would help

(i) to obtain more precise information about the age and origin of the lake,

(ii) to unravel the seismotectonic history of the lake area including effects of major earthquakes and associated mass wasting events,

(iii) to obtain a continuous record containing information on volcanic activities and climate changes in the central northern Mediterranean region, and

(iv) to better understand the impact of major geological/environmental events on general evolutionary patterns and shaping an extraordinary degree of endemic biodiversity as a matter of global significance. For this purpose, five primary drill sites were selected based on the results obtained from sedimentological studies, tectonic mapping in the catchment and detailed seismic surveys conducted between 2004 and 2008. For the recovery of the up to ca. 680 m long sediment sequences the GLAD800 shall be used. The drilling operation is planned to take place in 2011.

Millennial-to-centennial scale fluctuations in marine organic carbon export and burial since the Last Glacial Maximum in the Northeast Atlantic

T. WAGNER[A], H. MEGGERS[B], K.-H. BAUMANN[B], T. EGLINTON[C], J. HOLTVOETH[C/D], G. MOLLENHAUER[B/E]

[a] *School of Civil Engineering and Geosciences, Newcastle University, Newcastle upon Tyne (UK)*
[b] *MARUM and Department of Geosciences, University of Bremen (Germany)*
[c] *Marine Chemistry and Geochemistry Department, Woods Hole Oceanographic Institution (USA)*
[d] *Department of Earth & Ocean Sciences, University of Liverpool (UK)*
[e] *Alfred Wegener Institute for Polar and Marine Research, Bremerhaven (Germany)*

The nature of deep ocean drift sediments implies that they are influenced by lateral transport of re-suspended material. This suggests that they may hold information on past variations in the trajectory and vigor of particulate matter transport which, in turn, may be linked to changes in bottom water flows, surface ocean processes, and ultimately climate. Drift deposits are well known to exhibit exceptionally high rates of sedimentation for deep ocean settings, sometimes in excess of 100 cm ka^{-1} (e.g., Bianchi and McCave, 2000), providing rare opportunities to explore the combined effects of lateral and vertical particle supply on deep sea sedimentation at high temporal resolution. Mechanisms of organic matter (OM) transport and burial is of particular interest as laterally advected (allochthonous) and vertical-sourced (autochthonous) OM may be markedly different in its respective composition and reactivity, with implications for carbon turnover in the deep ocean and for interpretation of the geological sedimentary record.

Radiocarbon (^{14}C) measurements on sedimentary carbon (total organic and inorganic) and on individual organic compounds can provide information on the mechanisms and effects of the various types of sediment supply on the marine paleoclimate record (Pearson et al., 2001, Inthorn et al., 2006, Mollenhauer et al., 2007), and it has been demonstrated that temporal offsets between different proxy records in deep-sea sediment drifts can be substantial (Ohkouchi et al., 2002). While there is growing recognition from ^{14}C work that lateral advection is of importance for regional carbon burial and for interpretation of paleoclimate records, far less is known about fluctuations in organic carbon (OC) content and composition within the different size fractions of drift deposits. Information embedded in different size fractions, however, may hold important clues on hydrodynamic sorting and on the sources and preservation of OM that can inform about connections between surface and bottom water currents, and their fluctuations through time.

In this study we examine the ^{14}C content of planktonic foraminiferal carbonate, phytoplankton-derived alkenones, and OC in bulk sediment and silt and clay size fractions from sediments deposited on the Feni Drift in at ODP Site 980 since the Last Glacial Maximum (LGM). ^{14}C ages, combined with bulk and size-fraction specific (silt and clay) concentrations of total organic and inorganic carbon, stable carbon isotopic compositions of OM ($\delta^{13}Corg$), and molecular evidence suggest that OM in the clay fraction, like the alkenones and foraminifera, derives from surface waters, and therefore can be used to reconstruct the history of productivity since the LGM. In contrast, OM in the silt fraction of pre-Holocene sediments is significantly older (>3.4 kyrs) than that in corresponding clay fractions, arguing for stronger resuspension possibly related to enhanced bottom water currents during that time period.

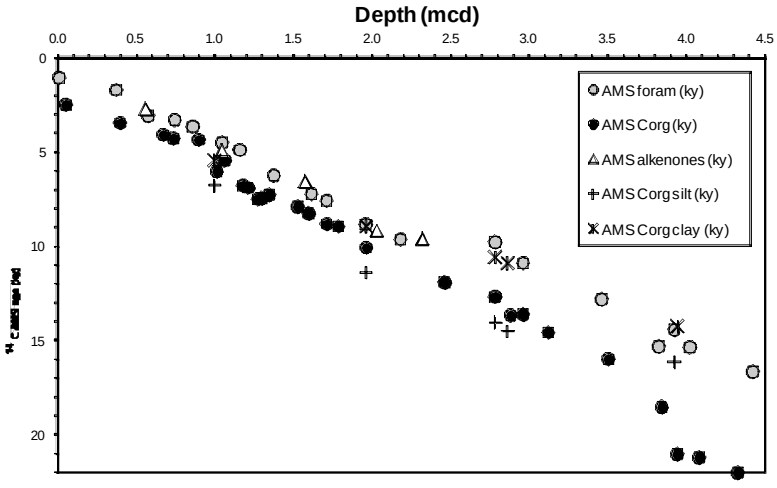

Fig. 1. Foraminiferal carbonate, bulk organic matter, size fraction (silt and clay) and biomarker-specific (alkenone) AMS ^{14}C of LGM to modern sediments from ODP 980. Ages are expressed as converted calendar ages.

Maximum age differences are observed between OC in corresponding silt and clay fractions, while the total OC from bulk sediment shows intermediate ^{14}C ages (Figure 1). Notably, the age of foraminiferal shells from the coarse (sand) fraction show a strong similarity to OC in the clay fraction and also with the alkenones, whereas the OC in the silt fraction was systematically older for the same sample depths. Due to low abundances or absence of alkenones in the pre-Holocene sections, alkenone ^{14}C data are limited to the Holocene. The age offset between OC in the silt and clay fractions ranges between 1350- 3610 ^{14}C years in the pre-Holocene interval, and reaches a maximum (>3400 yrs) between about 15-10 ka. In contrast, much smaller age differences are observed for the Holocene silt and clay fractions.

Abundances of bulk carbonate and TOC (TOC_{bulk} and TOC on a carbonate-free basis, $TOC_{bulk\text{-}kf}$), and OC of the silt (OC_{silt}) and clay (OC_{clay}) fractions document both general climate trends from the LGM to the present as well as a series of millennial-to-centennial time-scale variations (Figure 2a and 3a). To better illustrate difference in TOC between the bulk sample and the silt and clay fractions we show the relative differences in OC_{silt} and OC_{clay} compared to TOC_{bulk} for the entire record (Figure 2b). TOC_{silt} follows TOC_{bulk} in the lower part of the record but starts to diverge after ~11 ka with a second phase starting ~6 ka. The TOC_{clay} record is remarkably different, with higher average values and larger amplitude fluctuations that occur at millennial-centennial scale.

Stable carbon isotopic composition of organic matter was analysed on a subset of the samples to obtain insights into OM sources. $\delta^{13}Corg_{silt}$ is offset by about 1-1.5‰ from $\delta^{13}Corg_{bulk}$ to more negative values, whereas $\delta^{13}Corg_{clay}$ allover follows $\delta^{13}Corg_{bulk}$. A series of millennial-to-centennial time scale variations with amplitudes ranging between 1-3‰ is recognized in the grain size specific $\delta^{13}Corg$ records. $\delta^{13}Corg_{silt}$ and $\delta^{13}Corg_{clay}$ show some co-variation (r^2=0.46) and a series of millennial scale swings that tend to parallel each other, although not necessarily at the same amplitude and in any single case. Also, weak to moderate co-variation exists between TOC and $\delta^{13}Corg$ for both size fractions (clay r^2 = 0.28, silt r^2 = 0.47) supporting at least some common depositional controls. Co-variations are also apparent between the abundances of marine biomarkers (alkenones and short-chain $C_{16,18}$ fatty acids) with $\delta^{13}Corg$. Co-variation between alkenones and $\delta^{13}Corg$ is best for the silt fraction (r^2 = 0.52) but also exists for the clay fraction (r^2 = 0.36). Notably, terrigenous fatty acid abundances ($C_{26,28,30}$) show no relationship to either isotopic signal nor to variations in TOC.

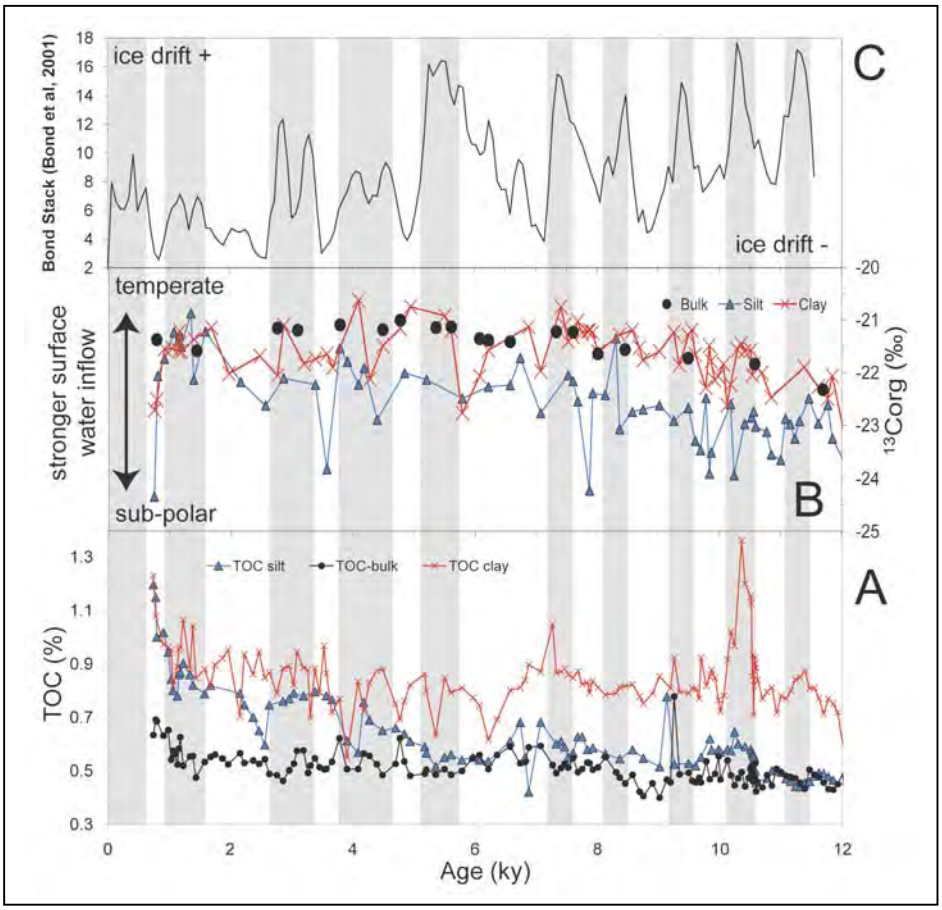

Fig. 2. Carbon and $\delta^{13}Corg$ records of LGM to modern sediments from ODP 980. (A) Abundances of bulk carbonate and TOC (TOC_{bulk} and TOC on a carbonate-free basis, $TOC_{bulk\text{-}kf}$); (B) Differences in OC_{silt} and OC_{clay} compared to TOC_{bulk}; (C) $\delta^{13}Corg$ in bulk sediment and the silt and clay fractions. 10 point moving average records for silt and clay in bold lines.

We infer that the observed high amplitude variations in OC content and $\delta^{13}Corg$ of clay reveal previously unrecognized millennial-to-centennial scale fluctuations in primary productivity and/or export flux. Enriched ^{13}C signatures and elevated OC are of particular interest as they may document intervals of enhanced productivity and marine organic matter flux. It is known that surface ocean ^{13}C of particulate OC varies significantly with latitude, resulting in more negative/depleted carbon isotope values at high latitudes, i.e. in cooler (sub-polar) waters (Goericke & Fry, 1994; Rau et al., 1991). Interpretation of $\delta^{13}C_{org}$ in terms of marine versus terrestrial inputs is therefore problematic at OPD 980. Uniformly low abundances of terrigenous biomarkers also support the conclusion that variations in $\delta^{13}Corg$ are not due to changes in admixture of terrestrial OM but primarily changes in surface ocean properties. If variable influx of surface water masses caused variations in $\delta^{13}C_{org}$, the records suggest that differences between silt and clay $\delta^{13}C_{org}$ largely document lateral supply of silt that contains marine OC produced in more northern polar waters. Following from that, millennial-to-centennial scale variations in

both records would document relative changes in the inflow of water masses from different latitudes, with more depleted $\delta^{13}C_{org}$ values indicating enhanced supply of OM from sub-polar sources (Figure 3b). Interestingly, higher $\delta^{13}C_{org}$ signatures correlate with maxima in sea ice debris in the North Atlantic (Bond et al., 2001) (Fig. 3c). This may suggest repetitive but focused inflows of Gulf Stream waters into the northeast Atlantic which would have shifted the $\delta^{13}C$ signature of primary producers to heavier (more `temperate surface water`) values while large parts of the North Atlantic remained under sub-polar surface water influence with widespread release of sea ice debris, as evidenced by sea ice debris.

We conclude that OM in the clay fraction is particularly sensitive to changes in surface ocean conditions, whereas OM in the silt fraction is more strongly influenced by lateral transport. These findings require further validation. In particular, studies on the sources of OM in the different grain size fractions and paired alkenone SST estimates from the bulk sediment and clay fraction are needed. If confirmed, similar records from other drift deposits may provide new information into subtle but significant short-term changes of the climate-ocean system.

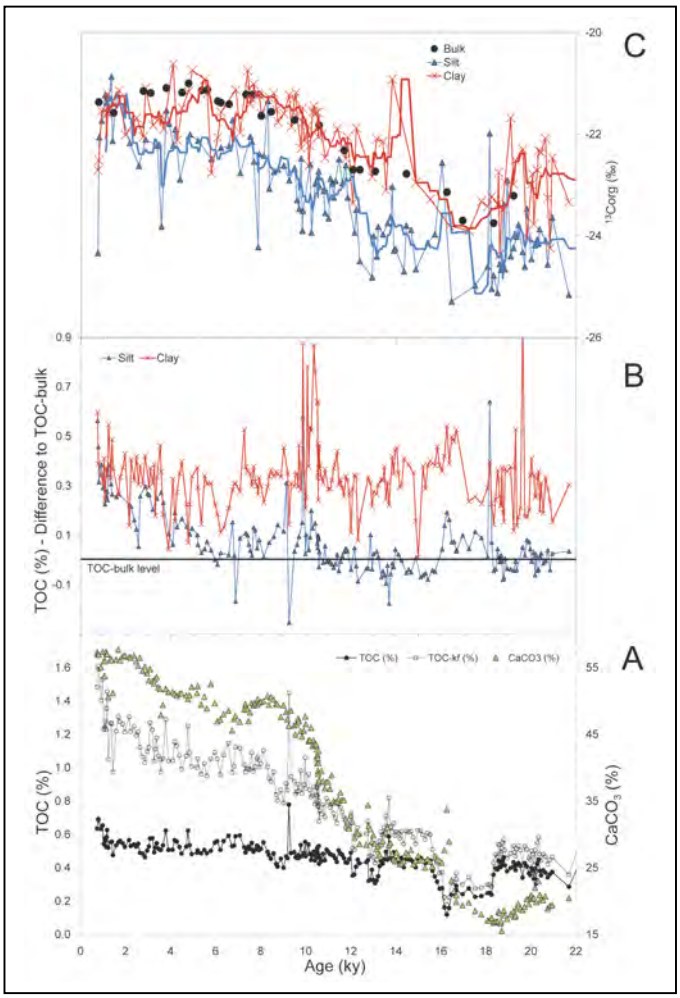

Fig. 3. Bulk and size-fraction specific TOC and δ^{13}Corg records from ODP 980 over the past 12 kyrs compared to the stacked record of sea ice debris (Bond et al., 2001). (A) Abundances of TOC (bulk sediment, silt and clay fraction) at OPD 980; (B) δ^{13}Corg of bulk sediment and the silt and clay fractions with indication of proposed fluctuations in stronger inflow of surface water masses with different temperatures; (C). Stacked record of sea ice debris according to Bond et al. (2001) with indication of ice drift intensity. Grey bars show intervals of enhanced deposition of sea ice debris in the North Atlantic.

Bianchi, G.G., and McCave, I.N., 2000. Marine Geology, v. 165, p. 137-169.
Bond, G., Kromer, B., Beer, J., Muscheler, R., Evans, M.N., Showers, W., Hoffman, S., Lotti-Bond, R., Hajdas, I., and Bonani, G., 2001. Science, v. 294, p. 2130-2136.
Goericke, R., and Fry, B., 1994. Glob.Biogeochem.Cycles, v. 8, p. 85–90.
Inthorn, M., Wagner, T., Scheeder, G., and M., Z., 2006, Geology, v. 34, p. 205-208.
Mollenhauer, G., Inthorn, M., Vogt, T., Zabel, M., Sinninghe Damsté, J.S., and Eglinton, T.I., 2007. Geochemistry, Geophysics, Geosystems, v. Q09004.
Okhkouchi, N., Eglinton, T.I., Keigwin, L.D., and Hayes, J.M., 2002. Science, v. 289, p. 1224-1227.
Pearson, A., McNichol, A.P., Benitez-Nelson, B.C., Hayes, J.M., and Eglinton, T.I., 2001. GCA, v. 65, p. 3123-3137.
Rau, G.H., Takahashi, T., and Des Marais, D.J., 1989. Nature, v. 341, p. 516-518.

Deformation and stress transfer at Vesuvius and Campi Flegrei

TR WALTER (1), A MANCONI (1,2), M SHIRZAEI (1), R LANARI (3), B. LÜHR (1), H. WOITH (1), J. ZSCHAU (1), T. WIERSBERG (1), J. ERZINGER (1)

[1]Dept. Physics of the Earth, Helmholtz Centre Potsdam, GFZ German Research Centre for Geosciences, Potsdam, Germany
[2] now at: Istituto per il Rilevamento Elettromagnetico dell'Ambiente IREA, Consiglio Nazionale delle Ricerche, Napoli, Italy
[3] Istituto per il Rilevamento Elettromagnetico dell'Ambiente IREA, Consiglio Nazionale delle Ricerche, Napoli, Italy

Historical reports suggest that major volcanic unrests are spatially and temporally clustered, meaning that volcanoes located adjacent to each other tend to become active synchronously. This was observed for Andean volcanoes in Chile, for volcanoes in Kamchatka or Alaska, and for adjacent volcanic centers on Hawaii Island. While in some cases, simultaneous eruptions occur, in other cases eruptions take place at one volcano while the neighboring centers collapse or merely deform. As summarized in this presentation, the reasons of such interaction may be different including triggering by faulting, large tectonic earthquakes and associated stress changes within the crust or common reservoirs. However, eruptions are considered to be the final stage of a long chain of magmatic and crustal processes, and volcano interactions may occur largely non-eruptive as suggested by new observations from the Italian volcanoes. As this work suggests, the non-eruptive deformation at Campi Flegrei and Vesuvius is correlated and also provides new insights into the location and geometry of their pressurized reservoirs beneath. Important implications arise for the planned Campi Flegrei ICDP project and associated hazards in the Bay of Naples.

Weddell Sea bottom-water production and ice-sheet dynamics during the Last Glacial Maximum – seasonal- to centennial-scale variability

M. E. WEBER[1], G. KUHN[2], W. RICKEN[1], L. REICHELT[1]

[1] Institute for Geology and Mineralogy, Zuelpicher Str. 49a, 50935 Cologne, Germany (michael.weber@uni-koeln.de)
[2] Alfred-Wegener-Institute for Polar and Marine Research, Columbusstr., 27568 Bremerhaven, Germany

The Southern Ocean and the adjacent Weddell Sea are key areas for Earth's climate variability because they influence the global thermohaline circulation as major sites of bottom and intermediate water formation. With respect to suborbital climate change, Antarctica is becoming increasingly interesting, because the Southern Ocean and specifically the Weddell Sea, may have acted as a major supplier of deep water (Antarctic Bottom Water) during stadials, when production of North Atlantic Deep Water was sluggish or even terminated. Unfortunately, there is a lack of high-resolution Antarctic sediment cores that could provide detailed and continuous insight into Antarctic climate variability during the last glacial.

To fill in that gap, we re-examined AMS^{14}C-dated gravity cores that were retrieved in the late eighties to early nineties with RV Polarstern in the southern to eastern Weddell Sea, using high-resolution non-destructive methods. The sites are mostly located on sediment ridges of the Antarctic continental margin north and east of Crary Fan and contain ultrahigh-resolution records of bottom-water production and glacial ice-sheet dynamics with sedimentation rates of up to 4 m/ka! during the last glacial maximum (LGM; 25-19 ka as deduced by AMS^{14}C dating).

The most intriguing characteristic is the abundant mm-scale lamination of relatively coarse (silty, bright) and fine (muddy, dark) layers of detrital composition. We developed software-based tools to identify the layers in gray-scale curves, and to count them semi-automatically. As a result, there is strong evidence that layer couplets represent varves and therefore the sites from the ridges contain an extremely valuable climate archive for ultrahigh-resolution studies of glacial climate variability in high southern latitudes.

Our preliminary interpretation is that a seasonally variable bottom-water production was induced by brine injection, which again, initiated density currents that were canalized within the channels. They overspilled the NW levee shoulder and deposited a coarser-grained (siltier) layer during glacial winter, when brine injection was probably enhanced, and a finer-grained (muddier) layer during glacial summer, when brine injection was likely reduced. Apparently, this mechanism operated consistently, producing intense bottom-water in the channels, and creating fine-scale lamination on the ridges over thousands of years during the LGM. Accordingly, we see evidence for a bipolar see-saw, i. e., the sluggish NADW production during the LGM in the North Atlantic might have been at least partially compensated by intense bottom-water production in the southern Weddell Sea.

However, bioturbated sections that dominate the post glacial record, are also scarcely intercalated into LGM sections with a 1 to 1.5 kyr spacing. Bioturbated sediment contains clear evidence of at least partly open water above the site and occasionally intensified iceberg calving and transport. Therefore, it represents warmer periods with likely enhanced paleoproductivity. As a working hypothesis we assume that these intervals correspond to Antarctic Isotopic Maxima (AIM) -like intervals, representing times of diminished bottom-water production in the Weddell Sea. Unfortunately, the currently available core material does not reach beyond the LGM so that the AIM of Marine Isotopic Stage 3 could not be analyzed.

Spectral analyses of laminae thickness, magnetic susceptibility, and Lab color indicate a novel finding: prominent cycles at periods of 80 – 90 years (Gleisberg cycle) and 200 – 220 years (de Vries cycle), revealing a dominant linear response to solar forcing. Our multiproxy records will allow for detailed comparison to the neighboring EPICA-DML ice core at seasonal resolution over several millennia during the LGM. This will put our results into a larger-scale perspective, which includes the

potential correlation of several (IRD-rich) marker horizons and the potentially asynchronous retreat of the East and West Antarctic Ice Sheets.

Latest on the absolute age of the Paleocene – Eocene Thermal Maximum (PETM): new insights from exact stratigraphic position of key ash layers +19 and -17

T. WESTERHOLD[1], U. RÖHL[1], H. K. MCCARREN[2], J. C. ZACHOS[2]

[1]Marum – Zentrum für Marine Umweltwissenschaften, Universität Bremen, Leobener Strasse, 28359Bremen, Germany, tho@uni-bremen.de
[2]Earth & Planetary Sciences Department, University of California, Santa Cruz, CA 95064, USA

During the late Paleocene and early Eocene the opening of the North Atlantic was accompanied by enormous effusive and explosive volcanism (Eldholm and Thomas, 1993; Rea et al., 1990) which induced the deposition of widespread layers of volcanic ash in northern Europe (Knox and Morton, 1988). Single-crystal (sanidine) 40Ar/39Ar dates from Early Eocene ash layers +19 and -17 in the Fur Formation of Denmark (Bøggild, 1918) have played an important role in constructing the Geomagnetic Polarity Time Scale (GPTS) (Cande and Kent, 1992, 1995; Ogg and Smith, 2004) and for deciphering potential trigger mechanisms of the transient global warming event known as the Paleocene - Eocene Thermal Maximum (PETM) (Storey et al., 2007; Zachos et al., 2008).

Because at this stage no datable ash layer has been found in the PETM itself, the absolute age of the PETM is based on interpolations of the relative position of the PETM and the radiometric dated ash -17 within magnetochron C24r (for discussion see Westerhold et al., 2007). Two factors are critical in this context: 1) the exact distance between the PETM and ash -17 is not known due to a hiatus in the reference record from Site 550 (Aubry et al., 1996), and 2) the accuracy of this radiometric age depends on the correct absolute age of the Fish Canyon Tuff (FCT, ~28.02 Ma) sanidine reference standard (Villeneuve, 2004). Recently, the age of the FCT standard has been recalibrated and the uncertainty of the methods was reduced to 0.25% (Kuiper et al., 2008). Moreover, a astronomically calibrated floating time scale for the Paleocene based on the identification of the stable long eccentricity cycle (405-ka) result into proposing three options for the absolute age of the PETM (Westerhold et al., 2008). The “third option” given therein would be consistent with the new calibrated age for FCT but results in a relatively old age of 56.33 Ma for the PETM, an age that would be in strong conflict with existing radioisotopic constraints. In addition, there seems to be a discrepancy in the number of 405-ka eccentricity cycles in early Paleocene records (Hilgen et al., 2008; Kuiper et al., 2008) making the definition of the correct age of the PETM even more difficult.

Here we present a new cyclostratigraphy for DSDP Site 550 (Leg 80, Goban Spur) obtained from high resolution X-ray fluorescence (XRF) data in order to establish the exact relative timely distance between the onset of the PETM and the prominent ash layers +19 and -17. Both ashes have been found in Site 550 and were correlated to the Danish ash series of the Fur Formation (Knox, 1984; Knox, 1985). Incorporating the latest radiometric dates for ash -17 we then have estimated the absolute age range of the PETM to assess the effect on the GPTS and test the astronomically calibrated Paleocene time scale.

We analyzed 50 meter of sediment cores retrieved at the Northeastern Atlantic (Goban Spur) DSDP Site 550* (Leg 80) using the non-destructive Super-slit X-Ray Fluorescence (XRF) Core Scanner at the MARUM - Marine Center for Marine Environmental Sciences, Bremen University, supported by the DFG-Leibniz Center for Surface Process and Climate Studies at the University of Potsdam. The interval spanning DSDP Cores 550-29X to -34X encompass the characteristic carbon isotope excursions (CIEs) of the early Eocene transient warming events PETM and Elmo (Cramer et al., 2003; Lourens et al., 2005). Two runs on archive halves at 2cm resolution with 10kV and 50kV energy were carried out to determine the elemental intensities of Calcium (Ca), Titanium (Ti), Iron (Fe), Zirconium (Zr) and Barium (Ba).

High resolution late Paleocene to early Eocene records from the South Atlantic Ocean show pronounced evidence of Milancovitch related orbital cyclicity in Ca, Fe, and Ba which have been successfully utilized to construct a detailed cyclostratigraphy for magnetochron C24r including the PETM (Röhl et al., 2007; Westerhold et al., 2007). Similar variation in Ca, Fe, and Ba content were expected from sediments drilled in the Goban Spur area and therefore provided high potential to also construct a cyclostratigraphy for DSDP Site 550 between PETM and Elmo mainly based on XRF core scanner data. Prerequisite for the subsequent, unambiguous spectral analysis was the recognition and the successive removal of ash layers from the data presenting the pelagic background sediments. Especially the XRF counts for Ti and Zr were used to identify ash layers.

XRF data for DSDP Site 550 show a diverse elemental pattern through time. The record is characterized by nannofossil chalk with high carbonate contents of up to 70% (Shipboard Scientific Party, 1985) expressed as generally high Ca values. Lower Ca values are present prior to the PETM due to the more siliceous marly composition as well as stronger dissolution (Aubry et al., 1996) and during the carbon isotope excursions from which F, G, H1 (equivalent of Elmo or ETM-2, Lourens et al., 2005), H2, and I1 were labeled according to the system, introduced by Cramer et al., (2003). Fe and Ca intensities are anti-correlated with lowest Ca values in the carbonate dissolution interval from 411.7 to 409.8 mbsf (Raffi et al., 2005). A stratigraphic unconformity (Aubry et al., 1996; Shipboard Scientific Party, 1985) at 407.38 mbsf is characterized by a switch from green to red sediments. However, the XRF data (e.g., analyzing the total Fe rather than Fe2+ versus Fe3+) do not reflect

any change supporting the assumption of a redox front at this horizon (Fig. DR1). Intriguingly the Ba intensity data show extremely well developed cycles especially in Cores 30X to 33X (365 - 401 mbsf) which encompass both ash layers +19 (392.99 mbsf) and -17 (399.76 mbsf).Ti values are generally low except for the ash rich horizons in Cores 32X and 33X (384 to 401 mbsf). Apart from several significant Zr peaks in a few distinct ash layers the acquired Zr data are below detection limit.

We use the well developed precession cycles in the Ba intensity record of Site 550 to develop a cyclostratigraphy. The accuracy was checked by comparing the bulk d13C record of Site 550 (Cramer et al., 2003; Raffi et al., 2005) with the high-resolution bulk d 13C record of ODP Site 1262 (McCarren and Zachos, in prep). The two d 13C curves match excellently (Fig. 2) and verify that the cyclostratigraphy of Site 550 is robust. Between the unconformity (407.38 mbsf) and the PETM carbon isotope values at Site 550 are stretched because the condensation of sediment allows no reliable age tie point other than in the center of the CIE. The relative distance of ashes +19 and -17 to the onset of the PETM and the relative position with respect to magnetochron C24r based on the new cyclostratigraphy is shown in Table 1. We estimate that the precision of the cyclostratigraphy is less than two precession cycles.

We constructed a precise Early Eocene cyclostratigraphy for DSDP Site 550 (Leg 80, Goban Spur, North Atlantic) counting orbital precession related cycles in Barium intensity data obtained from high resolution X-Ray Fluorescence core scanning of archive halves. Based on the cyclostratigraphy the exact timely position of two volcanic ash layers in Site 550 which correlate to ashes +19 and -17 of the Fur Formation in Denmark was defined. The ashes have a relative distance to the onset of the Paleocene/Eocene Thermal Maximum (PETM) of 862 ka and 672 ka, respectively.

When combined with published absolute ages for ash -17 the absolute age for the onset of the PETM is consistent with astronomically calibrated ages regardless of the age of the Fish Canyon Tuff (FCT) standard. The new results clearly demonstrate that the recalibrated FCT standard age of 28.201 Ma is consistent with tuning option 3 in the astronomically calibrated Paleocene time scale.

Aubry, M.-P., Berggren, W.A., Stott, L.D., and Sinha, A., 1996, The upper Paleocene-lower Eocene stratigraphic record and the Paleocene-Eocene boundary carbon isotope excursion: implications for geochronology, in Knox, R.W.O.B., Corfield, R.M., and Dunay, R.E., eds., Correlation of the Early Paleogene in Northwest Europe, Volume 101, Geological Society Special Publication, p. 353-380.

Bøggild, O.B., 1918, Den vulkanske Aske i Moleret samt en Oversigt over Danmarks ældre Tertiærbjærgarter.

Cande, S.C., and Kent, D.V., 1992, A New Geomagnetic Polarity Time Scale for the late Cretaceous and Cenozoic: Journal of Geophysical Research, v. 97, p. 13,917-13,951.

—, 1995, Revised calibration of the geomagnetic polarity timescale for the Late Cretaceous and Cenozoic: Journal of Geophysical Research, v. 100, p. 6093-6095.

Cramer, B.S., Wright, J.D., Kent, D.V., and Aubry, M.-P., 2003, Orbital climate forcing of _13C excursions in the late Paleocene - Eocene (chrons C24n-C25n): Paleoceanography, v. 18, p. 1097, doi:10.1029/2003PA000909.

Eldholm, O., and Thomas, E., 1993, Environmental impact of volcanic margin formation: Earth and Planetary Science Letters, v. 117, p. 319-329.

Hilgen, F.J., 2008, Recent progress in the standardization and calibration of the Cenozoic Time Scale: Newsletters on Stratigraphy, v. 43, p. 15-22.

Knox, R.W.O.B., 1984, Nannoplankton zonation and the Palaeocene/Eocene boundary beds of NW Europe: an indirect correlation by means of volcanic ash layers: Journal of the Geological Society, v. 141, p. 993-999.

—, 1985, Stratigraphic significance of volcanic ash in Paleocene and Eocene sediments at Sites 549 and 550, in Graciansky, P.C.d., Poag, C.W., and et al., eds., Initial Reports DSDP, 80: Washington (U.S. Government Printing Office), p. 845-850.

Knox, R.W.O.B., and Morton, A.C., 1988, The record of early Tertiary N Atlantic volcanism in sediments of the North Sea Basin, in Morton, A.C., and Parson, L.M., eds., Early Tertiary Volcanism and the Opening of the NE Atlantic, Volume 39: Special Publications: London, Geological Society, p. 407-419.

Kuiper, K.F., Deino, A., Hilgen, F.J., Krijgsman, W., Renne, P.R., and Wijbrans, J.R., 2008, Synchronizing Rock Clocks of Earth History: Science, v. 320, p. 500-504.

Lourens, L.J., Sluijs, A., Kroon, D., Zachos, J.C., Thomas, E., Röhl, U., Bowles, J., and Raffi, I., 2005, Astronomical pacing of late Palaeocene to early Eocene global warming events: Nature, v. 435, p. 1083-1087.

Ogg, J.G., and Smith, A.G., 2004, The geomagnetic polarity time scale, in Gradstein, F., Ogg, J., and Smith, A., eds., A Geological Timescale 2004, Cambridge University Press, p. 63-86.

Raffi, I., Backman, J., and Pälike, H., 2005, Changes in calcareous nannofossil assemblages across the Paleocene/Eocene transition from the paleo-equatorial Pacific Ocean: Palaeogeography, Palaeoclimatology, Palaeoecology, v. 226, p. 93-126.

Rea, D.K., Zachos, J.C., Owen, R.M., and Gingerich, P.D., 1990, Global change at the Paleocene-Eocene boundary: climatic and evolutionary consequences of tectonic events: Palaeogeography, Palaeoclimatology, Palaeoecology, v. 79, p. 117-128.

Röhl, U., Westerhold, T., Bralower, T.J., and Zachos, J.C., 2007, On the duration of the Paleocene-Eocene thermal maximum (PETM): Geochemistry, Geophysics, Geosystems, v. 8, p. doi:10.1029/2007GC001784.

Shipboard Scientific Party, 1985, Site 550, in Graciansky, P.C.d., Poag, C.W., and et al., eds., Initial Reports DSDP, 80: Washington (U.S. Government Printing Office), p. 251-355.

Storey, M., Duncan, R.A., and Swisher, C.C., III, 2007, Paleocene-Eocene Thermal Maximum and the Opening of the Northeast Atlantic: Science, v. 316, p. 587-589.

Villeneuve, M., 2004, Radiogenic isotope geochronology, in Gradstein, F., Ogg, J., and Smith, A., eds., A Geological Timescale 2004, Cambridge University Press, p. 87-95.

Westerhold, T., Röhl, U., Laskar, J., Bowles, J., Raffi, I., Lourens, L.J., and Zachos, J.C., 2007, On the duration of magnetochrons C24r and C25n and the timing of early Eocene global warming events: Implications from the Ocean Drilling Program Leg 208 Walvis Ridge depth transect: Paleoceanography, v. 22.

Westerhold, T., Röhl, U., Raffi, I., Fornaciari, E., Monechi, S., Reale, V., Bowles, J., and Evans, H.F., 2008, Astronomical calibration of the Paleocene time: Palaeogeography, Palaeoclimatology, Palaeoecology, v. 257, p. 377-403.

Zachos, J.C., Dickens, G.R., and Zeebe, R.E., 2008, An early Cenozoic perspective on greenhouse warming and carbon-cycle dynamics: Nature, v. 451, p. 279-283.

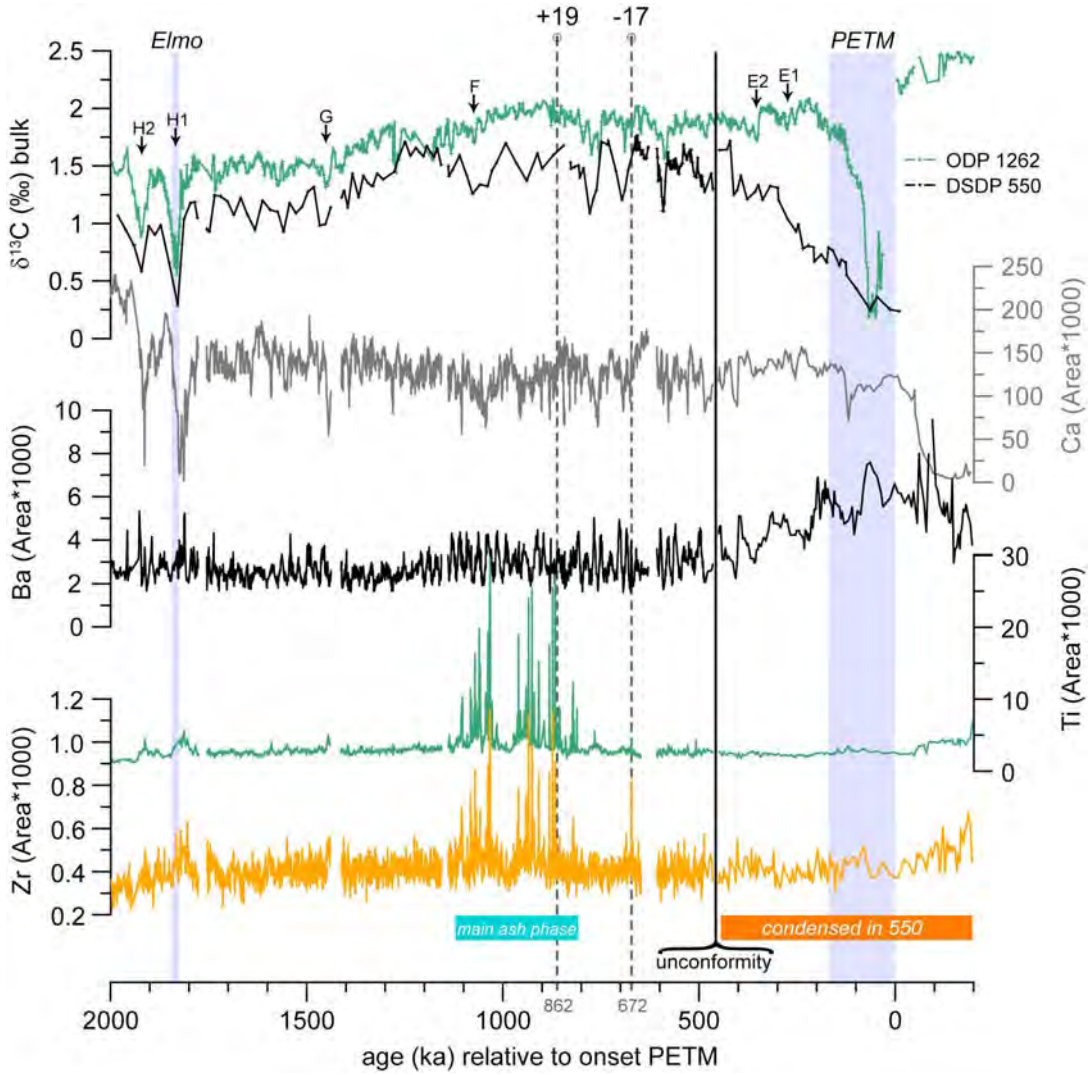

Figure 1. Bulk carbon isotope data from ODP Site 1262 (green; McCarren et al. in prep.) and DSDP Site 550 (black; Cramer et al. 2003, Raffi et al. 2005), and XRF data from Site 550 (Calcium in gray, Barium in black, Titanium in green, Zirconium in orange) potted relative to the onset of the PETM. The age model for 550 is based on the cyclostratigraphy developed in this study, the age model for 1262 is from Westerhold et al. (2007). Data from ash layers have been removed from the Calcium and Barium data. Blue bars mark the transient global warming events PETM and Elmo, the turquoise bar marks the main ash deposits, the gray dashed lines mark the positions of ash layers +19 and -17, and the solid black line marks the unconformity at Site 550. Note that the interval prior to the unconformity in Site 550 is condensed. The lettering of carbon isotope transient decreases is after Cramer et al (2003).

Gas migration and permeability structure of the San Andreas Fault at SAFOD deduced from drill-mud gas monitoring data

THOMAS WIERSBERG AND JÖRG ERZINGER

[1]Deutsches GeoForschungsZentrum, 14473 Potsdam, Germany

Outlook and aim

The San Andreas Fault Observatory at Depth (SAFOD), a component of the U.S. research initiative EarthScope with support by the ICDP (International Continental Drilling Program), was drilled in several phases between 2002 and 2007. SAFOD consists of a straight Pilot Hole (PH), drilled in 2002 and a deviated Main Hole (MH), drilled 2004 and deepend 2005. In 2007 three side tracks were drilled out of the MH (SAFOD-III) to obtain drill core samples and for downhole monitoring instrumentation, including the holes D (3137m-3262m), E (2952m-3182m) and G (3125m-3356m). The sidetracks are almost parallel to the MH and penetrate the SAF nearly orthogonal. The holes D and G intersect two active moving tracks of the SAF, identified by casing deformation in the MH at 3194m and 3301m depth. Drill core samples were obtained in Hole E from 3141m to 3153m and in Hole G from 3187m to 3199m and 3295m to 3312m, respectively.

The drill site is situated on the Coast Range of central California, in close vicinity to Parkfield, 1.8 km southwest of the surface trace of the San Andreas Fault (SAF) on the Pacific plate. This location was choosen for drilling because of the simultaneous occurrence of creep and repetitive seismicity at drillable depths, several historical M6 earthquakes and an expected change in lithology when crossing the SAF at depth (Hickman et al., 2004). The MH traverses the SAF between approx. 3100–3450m bore hole depth and penetrates into the North American Plate. Although the PH drilled only crystalline rocks below 768m, Erzinger et al. (2004) found evidence for sedimentary gas at the bottom of the hole (BOH) at 2168 m. These sediments were probably in close vicinity to the PH, as the MH encounters sedimentary strata below 1930 m that persist to the bottom at 3987 m depth.

During all drilling phases of SAFOD, gas was continuously extracted from drill mud and analyzed in real-time for its composition. Off-line gas samples were investigated in the laboratory for selected isotopes (noble gases, ^{13}C, H/D). The aim of this study is to determine the origin and distribution of gaseous fluids within the SAF in order to understand the permeability structure of an active moving plate-bondering fault and possible links between apparent fluids in fault zones and the processes occurring there. The role of fluids in particular with pressure more than hydrostatic in fault zone processes is yet not fully understood.

Results and discussion

The MH drilling revealed hydrocarbons, CO_2 and H_2 as principal formation gases at SAFOD. During SAFOD-III, CO_2 was found only in traces in drill mud. Most likely, CO_2 was consumed during drill mud return by $CaCl_2$ that was used to adjust the drill mud weight during phase III, others than during drilling the MH. Apparent H_2 in SAFOD-III is probably artificial due to the use of diamond-coated drill bits.

The MH and all sidetracks show enhanced concentrations of hydrocarbons between approx. 3150-3190m and also below 3310m (if reached), but distinctly lower contents of hydrocarbons in the section enclosed by both active moving tracks at 3194m and 3301m (inner section, IS). Moreover the molcular, but not the isotopic composition of hydrocarbons in the IS is clearly different from above and below (Fig. 1). The ratio C1/(C2+C3) in the IS shows values of up to 60, distinctly higher then at shallower and greater depth [C1/(C2+C3)<10 between 3150-3190m and ≤20 below 3310m, respectively].

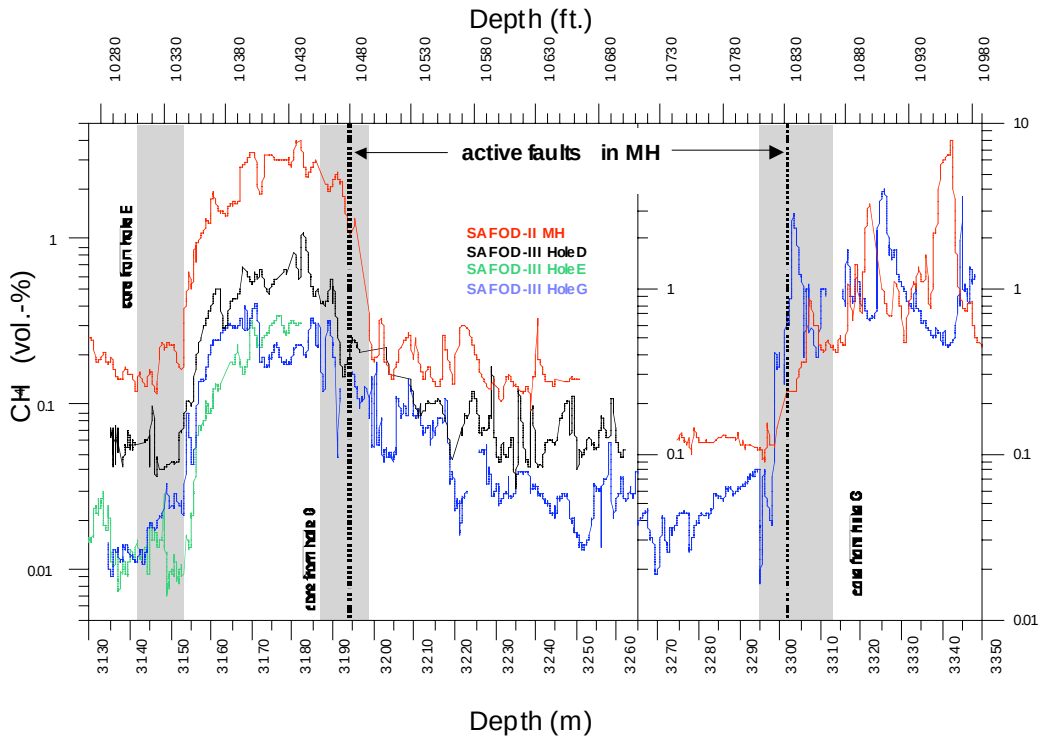

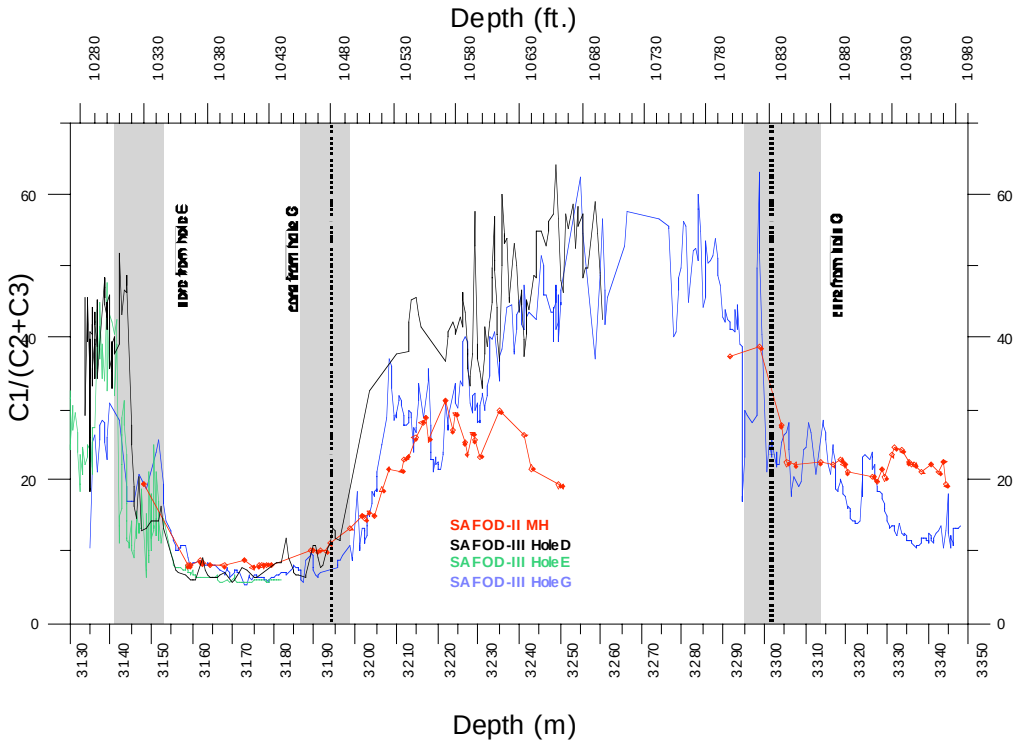

Fig 1: methane concentration (up) and molecular composition of hydrocarbons (down) in drill mud gas from the SAFOD MH and sidetracks between 3130m and 3350m depth. Active creep was identified in the MH at 3194m and 3301m depth.

In contrast to the molecular composition, the carbon isotope composition of hydrocarbons between 3147m and 3326m is relativly homogenous, showing $\delta^{13}C$ values of CH_4 between –29.7‰ and -33.5‰ (PDB). This indicates a common source of hydrocarbons in this interval. Both the molecular composition and carbon isotopes suggest that hydrocarbons derive from thermal decomposition of kerogen. The differences in the carbon isotopic composition between C1 and C4 enables estimation of the initial $\delta^{13}C$ value from the source kerogen, which is in a range between –22‰ and –25‰.

Elevated hydrocarbon concentrations in drill mud coincide with the occurrence of (partly shared) shale at approx. 3150-3200m and 3310-3340m depth. It is, however, not clear weather shale is the source rock of kerogen or if hydrocarbons generated at greater depth have migrated towards the surface and became trapped in low-permeable shaley rock. The gas maturities estimated from the carbon isotope composition of hydrocarbons are in a range between approx. 1.4 to 1.8% R_0 assuming a type-II kerogen. These maturity values correspond to maximum burial temperatures higher than actual formation temperatures at given depths. The wet gas composition also suggests a relatively marture type-II kerogen.

The discrepancy between recent formation temperatures (approx. 100°C) and estimated maximum burial temperatures can be explained either by gas migration from a deeper source or by higher formation temperatures in the past. Comparision between the thermal maturities of the shale from rock-eval pyrolysis experiments and the gas maturities from corresponding depths will help us to distinguish between both processes.

Helium isotopes

Wiersberg and Erzinger (2007) report a relatively constant helium isotope composition on the Pacific Plate ($0.354\pm0.021R_a$ at 3051m) but increasing contribution of mantle-derived helium below 3196m on the North American Plate with maximum air-corrected R_a values at 3903m depth ($0.938\pm0.097R_a$). Evidence for an even higher contribution of mantle-derived helium on the North American Plate with greater distance from the center of the SAF issued from Kennedy et al. (1997). The authors report 1.5 R_a from a borehole about 1500m away from the surface trace of the SAF (Phillips-Varian well). This observations suggests that the SAF is probably not the principal conduit for mantle-derived fluids at the SAFZ, however, only one sample from Wiersberg and Erzinger (2007) derived from the IS ($0.46\pm0.26R_a$ at 3196m).

When drilling the sidetracks in 2007, R_a values of ≥0.85 were found in two samples from hole D in 3203m and 3262m depth, indicating somewhat enhanced flow of mantle-derived fluids in the IS. In contrast, very low R_a values were observed outside of this interval but in closest vicinity at 3147m ($0.26\pm0.12R_a$) and 3312m ($0.22\pm0.12R_a$).

The considerable variations in R_a values on short spatial scale imply that the SAF consists of strata with different permeability parallel to the fault direction, from which low-permeable rocks hamper the fluid flow orthogonal to the fault. Separation of two individual hydrogelogical systems by a low-permeable fault core was already suggested by Wiersberg and Erzinger (2008). It is, however, not clear weather the elevated R_a values within the IS reflect temporal variation in the fluid flow, i.e. recharging of the fault with fluids from the mantle after depletion e.g. by the earthquake from 09/28/2004, or continuous uplift of mantle-derived fluids through the fault.

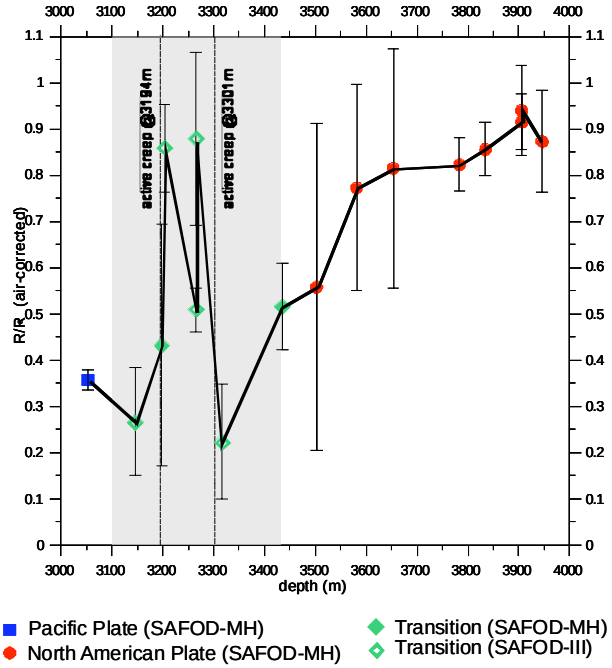

Fig. 2: air-corrected $^{3}He/^{4}He$ values (R_a) versus depth. MH data taken from Wiersberg and Erzinger, 2007.

Erzinger J., Wiersberg T. and Dahms E. (2004) Real-time mud gas logging during drilling of the SAFOD Pilot Hole in Parkfield, CA, Geophys. Res. Lett. 31, L15S18, doi:10.1029/2003GL019395.

Kennedy B.M., Kharaka Y.H., Evans W.C., Ellwood A., DePaolo D.J., Thordsen J., Ambats G. and Mariner R.H. (1997) Mantle fluids in the San Andreas Fault system, California, Science 278, 1278-1281

Wiersberg T. and Erzinger J. (2007) A helium isotope cross-section study through the San Andreas Fault at seismogenic depths, G-cubed 8, No.1, doi: 10.1029/2006GC001388

Wiersberg T. and Erzinger J. (2008) On the origin and spatial distribution of gas at seismogenic depths of the San Andreas Fault from drill mud gas analysis, Applied Geochemistry 23, 1675-1690, doi:10.1016/j.apgeochem.2008.01.012

PASADO: Report about the ICDP lake drilling at Laguna Potrok Aike, Argentina

BERND ZOLITSCHKA[1], FLAVIO ANSELMETTI[2], DANIEL ARIZTEGUI[3], HUGO CORBELLA[4], PIERRE FRANCUS[5], CATALINA GEBHARDT[6], ANNETTE HAHN[1], PIERRE KLIEM[1], ANDREAS LÜCKE[7], CHRISTIAN OHLENDORF[1], FRANK SCHÄBITZ[8], AND THE PASADO SCIENCE TEAM

[1] Institute of Geography (Geopolar), University of Bremen, 28359 Bremen, Germany – zoli@uni-bremen.de
[2] Swiss Federal Institute of Aquatic Science & Technology (Eawag), Ueberlandstrasse 133, 8600 Dübendorf, Switzerland
[3] University of Geneva, Section of Earth Sciences, Rue des Maraîchers 13, 1205 Geneva, Switzerland
[4] Argentine Museum of Natural History, Av. A. Gallardo 470, 1007 Buenos Aires, Argentina
[5] INRS, 490 rue de la couronne, Québec, Québec G1K 9A9, Canada
[6] Alfred Wegener Institute for Polar and Marine Research, 27576 Bremerhaven, Germany
[7] ICG 4, Energy & Environment, Research Center Jülich, 52425 Jülich, Germany
[8] Seminar for Geography and Education, University of Cologne, Gronewaldstr. 2, 50931 Cologne, Germany

Within the framework of the ICDP-funded "Potrok Aike maar lake sediment archive drilling project" (PASADO) an international team of scientists carried out interdisciplinary research at the unique mid-Pleistocene (770 ka) maar lake of Laguna Potrok Aike (Fig. 1) in southern Patagonia, Province of Santa Cruz, Argentina (Zolitschka et al., 2006a, 2008). This lake is very sensitive to variations in southern hemispheric wind and pressure systems and thus holds a unique lacustrine record of climatic and ecological variability of global significance (Mayr et al., 2007; Wille et al., 2007; Zolitschka et al., 2006b). Moreover, Southern Patagonia with its many active volcanoes is an ideal location to better understand the regional history of volcanism. These are two challenging geo-scientific themes that need to be tackled, especially as both of them have an increasing socio-economic relevance.

Three months of drilling activities that finished last November 2008 were carried out by DOSECC and an international team of 34 scientists from 10 countries from the drilling platform R/V "Kerry Kelts" (Fig. 2). More than 500 m of lacustrine sediments were recovered. This sedimentary archive will provide (1) new insights into the processes of regional back arc volcanism within the Pali Aike Volcanic Field itself as well as the more distant explosive volcanism of the Andean mountain chains; and, (2) high-resolution (decadal) quantitative climate and environmental reconstructions supported by multiple dating and stratigraphic correlations. Marine – ice core – terrestrial linkages will be emphasized as well as the incorporation of results from global climate modelling simulations (Meyer & Wagner, 2008; Wagner et al., 2007).

Fig. 2. The drilling platform R/V "Kerry Kelts" with the GLAD800 drill rig in the centre of Laguna Potrok Aike in southern Patagonia.

The two drilled sites in the central deep basin of Laguna Potrok Aike have been selected based on four seismic surveys carried out between 2003 and 2005 (Anselmetti et al., 2008; Gebhardt et al., subm.). Slightly more than 100 m of sediments were recovered at each of the drilled sites using the GLAD800 drill rig with the hydraulic piston corer tool (HPC) at water depths varying between 95 and 100 m. Sites were cored in quadruplicate (Site 1) and triplicate (Site 2) with a total core recovery of 94%. On-site core logging with the multi sensor core logger (MSCL) documents an excellent correlation between the four recovered holes drilled at Site 1 as well as with the three holes obtained from Site 2 which is located ca. 700 m south of Site 1. Additionally, a variety of sedimentological, physical and geochemical analyses were carried out on the core catcher samples in the field laboratory. Preliminary interpretation of all data that is available before core opening indicates that the record may go back in time as far as to the end of oxygen isotope stage 5.

Acknowledgements
This research is supported by the International Continental Scientific Drilling Program (ICDP) in the framework of the "Potrok Aike Maar Lake Sediment Archive Drilling Project" (PASADO). Funding was provided by the ICDP, the German Science Foundation (DFG), the Swiss National Science Foundation (SNF), the Natural Sciences and Engineering Research Council of Canada (NSERC), the Swedish Vetenskapsradet (VR) and the University of Bremen.

Anselmetti, F., Ariztegui, D., De Batist, M., Gebhardt, C., Haberzettl, T., Niessen, F., Ohlendorf, C., Zolitschka, B. (2008). Environmental history of southern Patagonia unraveled by the seismic stratigraphy of Laguna Potrok Aike. Sedimentology. doi: 10.1111/j.1365-3091.2008.01002.x.

Gebhardt, A.C., M. De Batist, F. Niessen, F.S. Anselmetti, D. Ariztegui, C. Kopsch, C. Ohlendorf, B. Zolitschka (subm.). Origin and evolution of the Laguna Potrok Aike maar, Southern Patagonia. Basin Research.

Mayr, C., M. Wille, T. Haberzettl, M. Fey, S. Janssen, A. Lücke, C. Ohlendorf, G. Oliva, F. Schäbitz, G.-H. Schleser, B. Zolitschka (2007). Holocene variability of the Southern Hemisphere westerlies in Argentinean Patagonia (52°S). Quaternary Science Reviews, 26: 579-584.

Meyer, I. & Wagner, S. (2008). The Little Ice Age in southern Patagonia: Comparison between paleoecological reconstructions and downscaled model output of a GCM simulation. PAGES News 16: 12-13.

Wagner, S., M. Widmann, J. Jones, T. Haberzettl, A. Lücke, C. Mayr, C. Ohlendorf, F. Schäbitz, B. Zolitschka (2007). Transient simulations, empirical reconstructions and forcing mechanisms for the Mid-holocene hydrological climate in southern Patagonia. Climate Dynamics. doi: 10.1007/s00382-007-0229-x.

Wille, M., N.I. Maidana, F. Schäbitz, M. Fey, T. Haberzettl, S. Janssen, A. Lücke, C. Mayr, C. Ohlendorf, G. H. Schleser, B. Zolitschka (2007). Vegetation and climate dynamics in southern South America: The microfossil record of Laguna Potrok Aike, Santa Cruz, Argentina. Review of Palaeobotany and Palynology 146: 234-246.

Zolitschka, B., Corbella, H., Maidana, N., Ohlendorf, C. (2006a). Investigating Maar Formation and the Climate History of Southern Argentina – the Potrok Aike Maar Lake Sediment Archive Drilling Project (PASADO) Scientific Drilling 3: 54-55.

Zolitschka, B., Schäbitz, F., Lücke, A., Clifton, G., Corbella, H., Ercolano, B., Haberzettl, T., Maidana, N., Mayr, C., Ohlendorf, C., Oliva, G., Paez, M.M., Schleser, G.H., Soto, J., Tiberi, P., Wille, M. (2006b). Crater lakes of the Pali Aike Volcanic Field as key sites of paleoclimatic and paleoecological reconstructions in southern Patagonia, Argentina. J. of South American Earth Sciences 21: 294-309.

Zolitschka, B, Corbella, H., Ohlendorf, C., 2008. Deep lake drilling at Laguna Potrok Aike, southern Argentina. DOSECC News, 6: 1-4.